



Core, Giulia (2024) *User-friendly and robust paper-based device for DNA diagnostic of infectious diseases in resource-poor settings*. PhD thesis.

<https://theses.gla.ac.uk/84414/>

Copyright and moral rights for this work are retained by the author

A copy can be downloaded for personal non-commercial research or study, without prior permission or charge

This work cannot be reproduced or quoted extensively from without first obtaining permission in writing from the author

The content must not be changed in any way or sold commercially in any format or medium without the formal permission of the author

When referring to this work, full bibliographic details including the author, title, awarding institution and date of the thesis must be given

Enlighten: Theses

<https://theses.gla.ac.uk/>
research-enlighten@glasgow.ac.uk

User-friendly and Robust Paper-Based Device for DNA Diagnostic of Infectious Diseases in Resource-Poor Settings

Giulia Core

Submitted in fulfilment of the requirements for the
Degree of Doctor of Philosophy

Division of Biomedical Engineering
School of Engineering
College of Science and Engineering
University of Glasgow



University
of Glasgow

January 2024

Ken: Yeah, because actually, my job... it's just beach.

Barbie: And what a great job you do at beach!

Barbie (2023) by Greta Gerwig

Abstract

Communicable diseases, such as malaria, viral and bacteria infections, which are still widely spread in low- and middle-income countries, cause high morbidity and mortality rates. Elimination of infectious disease reservoirs requires rapid, and highly sensitive molecular diagnostic platforms that can be effectively used outside laboratory settings. The integration of nucleic acid amplification tests (NAATs) in paper-based microfluidic devices has represented a remarkable turning-point in the context of point-of-care (POC) diagnostics, as they combine NAATs' high sensitivity and specificity with the advantages of low-cost, easy-to-use paper-based microfluidics. Various configurations of low-cost single-use POC diagnostic devices have been developed. However, none of those thoroughly fulfil the ASSURED criteria for effective POC testing provided by the World Health Organisation in 2003 (Affordable, Sensitive, Specific, User-friendly, Rapid and robust, Equipment-free and Deliverable to end-users). Even if current tests can successfully detect very low concentrations of infectious organisms, the degradation of essential reagents restricts their practical use in challenging field conditions where refrigerators, external equipment and trained personnel might not be easily accessible. Increasing attention has been paid to achieving "reassURED" aspects in the recent years, but further investigations are still required to face the real challenges that in-field testing entails.

My PhD research aims at addressing some of the major limitations of paper-based POC NAATs in terms of user-friendliness and robustness in resource-poor settings. First of all, I have developed a new paper-based procedure to extract nucleic acid (NA) material from bacteria present in large volumes which reduces user intervention. Secondly, I have stored reagents in a ready-to-use solid format and "on-board" to incorporate NAATs inside a POC diagnostic platform for easy shipment and long-term storage. Moreover, a simple device that combines sample pretreatment and NA amplification in one chamber was investigated. Such a device will incredibly facilitate access to low-cost, accessible, and accurate diagnosis, thus delivering all the ASSURED aspects.

Contents

Abstract	iii
Publications and Conferences	viii
Acknowledgements	ix
Author's Declaration	xii
Disruptions	xiii
Thesis Outline	xiv
Abbreviations	xvii
List of Figures	xxii
List of Tables	xxiv
1 Introduction	1
1.1 Motivation of Study	2
1.2 Aim and Objectives	4
1.3 Point-Of-Care Diagnostic Devices for Infectious Diseases	5
1.3.1 Immunological Tests	6
1.3.2 Nucleic Acid Amplification Based Tests	7
1.3.3 Biomarkers	9
1.4 Paper-Based Microfluidics	10
1.4.1 Fluid Transport in Paper	11
1.4.2 Paper for Diagnostics and μ PADs	12
1.4.3 Beyond Paper-Based Diagnostic Devices	19
1.5 Storing Reagents for DNA Detection	20
1.5.1 Techniques to Store Reagents in Extreme Environmental Condi- tions	22
1.5.2 Enzyme-Free Amplification Strategies	26
2 Materials and Methods	29
2.1 Bacterial Culture	29
2.2 Lysis Buffers	30
2.3 Filter Papers	30
2.4 LAMP and qPCR reagents	33

2.4.1	Master mixes	33
2.4.2	Synthetic and genomic DNA	33
2.4.3	Primers	34
2.5	Real-Time LAMP Conditions	37
2.6	Real-Time PCR Conditions	38
2.7	Computation of Time-to-Positive Values in Real-Time LAMP and Cycle Threshold Values in qPCR	38
2.8	Analytical Sensitivity of the Real-Time LAMP and qPCR Assays . . .	40
2.9	Statistical Analysis for Real Time LAMP and qPCR results	40
2.10	Conversion of DNA Concentration from ng/ μ L to copies/reaction . . .	41
2.11	Lateral Flow DNA Detection Assay and Interpretation of Results . . .	41
2.12	Colour Intensity of Test Bands on Lateral Flow Strips	43
2.13	Plastic Cassettes for Point-of-care Devices	44
2.14	Paper-Based Protocol to Extract Genomic Material from Bacteria Present in Large Volumes	44
2.14.1	DNA Binding Investigation	45
2.14.2	DNA Extraction Procedures and Use of Different Papers	46
2.14.3	DNA Extraction Using Lysis Buffer Air-Dried on Paper Discs . . .	50
2.14.4	Chitosan-Functionalised Paper	51
2.15	Techniques for easy on-board-storage of molecular reagents at room tem- perature	53
2.15.1	Molecular Reagents Stored in Pullulan and Trehalose Tablets . . .	54
2.15.2	Storage of Molecular Reagents In-the-field and in a Paper-Based Device.	60
2.16	Modular Paper- and Plastic-Based Device Design, Assembly, and Fab- rication	71
2.16.1	Overview of Point-Of-Care Molecular Device	71
2.16.2	Device Design and Fabrication	73
2.16.3	Pullulan Tablets as Delay Layers for Fluids Control	77
2.16.4	Microfluidic Device Testing and Development	84
2.16.5	Sample Processing and DNA Extraction On The Device Cassette . . .	87

3 Paper-based Protocol to Extract Genomic Material from Bacteria in Large Volumes 91

3.1	Results	92
3.1.1	Optimization of the Concentration of Primers for the Detection of <i>E. coli malB</i> Gene with LAMP	92
3.1.2	LAMP and qPCR Assays for the Detection of <i>E. coli malB</i> Gene . . .	94
3.1.3	Ability of Filter Paper to Capture DNA	97
3.1.4	Reduction of Initial Number of Steps and Procedure Optimiza- tion of the Paper-Based DNA Extraction Method Based on Zou <i>et al.</i> (2017)	101
3.1.5	Introduction of an Additional Elution Step for Quantitative Com- parative Analysis Using qPCR of the Paper-Based DNA Extrac- tion Method	107

3.1.6	Lysis Buffer Optimization in the Paper-Based DNA Extraction Procedure	110
3.1.7	Use of Different Papers in DNA Extraction Based on Zou <i>et al.</i> (2017)	116
3.1.8	Paper-based DNA Extraction Based on Magazorb [®] Kit	120
3.1.9	Paper-based DNA Extraction Using Lysis Buffer Air-Dried on Paper Discs	124
3.1.10	Chitosan-Functionalised Paper	128
3.2	Discussions	130
3.3	Contribution to Knowledge	135
4	Easy-on-board-storage of Molecular Reagents for the Long-Term and at Room Temperature Using Pullulan	136
4.1	Results	137
4.1.1	Molecular Reagents Stored in 10% (w/v) Pullulan Solutions	137
4.1.2	Optimization of LAMP Master Mix Concentrations (New England Biolabs)	139
4.1.3	Molecular Reagents Stored in 10% (w/v) Pullulan and 0.5 M Trehalose	142
4.1.4	Reagents Stored in 5% (w/v) Pullulan and 0.5 M Trehalose or 10% (w/v) Pullulan and 0.5 M Trehalose	154
4.1.5	Storage of Molecular Reagents Returned from the Field	156
4.1.6	Summary of Results about Molecular Reagents Stored in Pullulan	160
4.1.7	Modified DNA Extraction from Blood for Use on the Point-of-Care Device	161
4.1.8	Paper Device and Storage of Molecular Reagents In-The-Field	163
4.2	Discussions	182
4.2.1	Tablet-Based Storage of Reagents	182
4.2.2	Paper Device and Storage of Molecular Reagents In-The-Field	185
4.3	Contribution to Knowledge	189
5	Modular Paper- and Plastic-Based Device Design, Assembly, And Fabrication	190
5.1	Results	191
5.1.1	Dissolution rate of pullulan tablets at different concentrations	191
5.1.2	Microfluidic Device Development	195
5.1.3	Sample Processing and DNA Extraction On The Device Cassette	214
5.2	Discussions	220
5.3	Contribution to Knowledge	225
6	Enzyme-free Amplification Strategies	226
6.1	Results	228
6.1.1	Optimisation of catalytic hairpin assembly (CHA) reaction for result visualisation on lateral flow strips	228
6.1.2	Optimisation of the assembly-mediated strand release reaction (ASR) and 4-way junction (4WJ)	237

6.1.3	DNA-zyme mediated RNA cleavage	238
6.1.4	Enzyme-free biosensor for <i>Clostridioides Difficile</i> detection . . .	239
6.2	Discussions and Conclusions	241
6.3	Contribution to knowledge	243
7	Conclusions and Future Works	244
7.1	Summary of Findings and Conclusions	244
7.2	Future Works	247
	Bibliography	265
A	Appendices	266
A.1	Sample Size Calculator	266
A.1.1	Motivation	266
A.1.2	Objectives and Contribution	267
A.1.3	Theory Background	267
A.1.4	Methodology	270
A.1.5	Formulas Used in the Sample Size Calculator	271
A.1.6	Results and Discussion	273
A.2	Pressure Applied to the PMMA Stack to Create the 3D Structure of Point-Of-Care Device	275
A.3	Enzyme-free Amplification Strategies Materials and Methods	276
A.3.1	Oligonucleotide Sequences	276
A.3.2	Polyacrylamide Gel Electrophoresis (PAGE)	276
A.3.3	Preparation of Crude Extracellular Matrix and Crude Intracel- lular Mixture from <i>E. coli</i> K12	276
A.3.4	Cleavage Reactions and Activity	277
A.3.5	Conditions for DNazyme Mediated Enzyme-Free Amplification Method	277
A.4	Hairpins details for CHA	278
A.5	Proof of Copyright Permissions	285
B	MATLAB[®] Scripts	287
B.1	MATLAB [®] Script Used to Compute Time-to-Positive Values in Real Time LAMP	287
B.2	MATLAB [®] Script Used to Compute ANOVA	292
B.3	MATLAB [®] Script Used to Study Pullulan Tablets Dissolution Rate . .	293
B.3.1	Script Used to Identify the Colour Difference detected by the Camera	293
B.3.2	Script Used for Image and Statistical Analysis of Pullulan Tablets Dissolution Rate	295

Publications and Conferences

Journal Papers

G. Core, “Lab-on-a-chip - fostering a sustainable future”. *Frontiers in Lab on a Chip Technologies*, 2, 1239134 (2023).

Conferences

G. Core, J. M. Cooper. and J. Reboud, “Long-term storage of ready-to-use reagents for point-of-care isothermal nucleic acid testing in resource-poor settings”, *MicroTAS 2023*, Katowice, Poland. - Poster presenter.

G. Core, J. Reboud and J. M. Cooper, “Detecting low abundance bacterial pathogens using a paper-based sample-to-answer point-of-care device for nucleic acid tests”, *Biosensors 2023*, Busan, South Korea. - Poster presenter.

G. Core, G. Xin, P. Jajesniak, X. Yan, W. McConnel, A. Garrett, J. Reboud, J. M. Cooper, “Paper-based sample-to-answer point-of-care device for nucleic acid detection of infectious diseases with ready-to-use reagents”, *Lister Lecture and Lister Medal presentation 2022*, Society of Chemical Industry and Royal Society of Edinburgh, Edinburgh, UK. - Poster presenter.

Acknowledgements

Fortunately (for me) and unfortunately (for the readers), I have a long list of thanks to give. I have been incredibly lucky to have a great community that supported and listened to me at every stage of this PhD rollercoaster.

I would like to express my deepest gratitude to my supervisors, Prof. Julien Reboud and Prof. Jonathan M. Cooper, who have guided me throughout my PhD journey and during the challenging times of the pandemic. Thank you, Julien, for always having faith in me and supporting my wild ideas and last minute applications. You helped me access some amazing opportunities.

A great thank you to Prof. Yingfu Li for hosting me in his Li Lab at McMaster University (Hamilton, ON, Canada), and to Jimmy Gu for teaching me everything about PAGE gels and DNAszymes.

I would also like to thank all the people in the research group who have supported me during the development of this project. A great thank to Alice, Shantimoy, Weronika, Xiaoxiang and Pawel for their punctual provision of materials, supervision, and endless helpfulness. I am very grateful to Marcia for helping me navigate the first months of PhD. You have been an amazing mentor, and you helped me unveil the mysteries of microbiology and pipetting with your patience and wisdom. A great thank to my other colleagues, Maha (my rock) for the deep and encouraging chats early in the mornings, Menghan for the laughs and cries at failed experiments. A huge shout out to Olivia and Rory for implementing the most robust manufacturing chain of point-of-care devices that has ever existed, and to always remind me that, eventually, everything will always be fine. Thank you also to all those who helped in making my trip to Uganda possible, and those who always listened to my ‘lab’ dramas: Mieszko, Ella, Yana, Becky, Kenny, Ollie, Xin, Zhuoer, Jiaying, and Yunus. Last but not least, I would like to thank the ‘Power team’ (Becky, Kenny, Xin, Elias, Victor) for the great work and collaboration. Even when we faced challenges like the lockdowns, we managed to stay connected.

The University of Glasgow made me find a family of kind and brilliant people both within and outside the lab.

I would like to start with the wonderful experience in the PhD society that has lighten the darkest days of lockdown and through which I met invaluable friends. Thank you Laura, Federica, Sofia, Valentina, Hannah, for brightening up my days during lockdown and supporting me with your kindness and humour. I am so grateful for your friendship and the incredible memories we shared.

Another amazing experience during the PhD was taking part in the Glasgow Science

Festival (GSF). Thanks to Debbie for always understanding immediately and acting upon uncomfortable situations. But most importantly, GSF introduced me to Kathrin. Whose energy sweeps you away and always makes you feel that anything is always possible.

Without GSF, and in turns Kathrin, ‘The Bards’ would not exist. Thanks to the ‘The Bards’ and Zumba pals (Laura E., Ella, Silvia, Laura C., Antonia, Robert, Danko, Lucia), with whom the lunches at the ARC, the music and the laughter made the last year of the PhD fantastic, and the writing less tragic than expected! I wish everyone to experience the end of the PhD to the fullest, one ‘pem pem’ at a time.

A huge thank you to Sara, Natale, Mara and Mash, for their support, their resilience and the endless conversations about the challenges of our society, which helped us survive and overcome the lockdown. Thanks also to Sissy for tricking me into the PhD, and for being so supportive from the first day I set foot in Glasgow. Thanks to rest of the Italian gang, Marta, Iacopo, Manuela, Eugenio, Francesca, Vincenzo for being the most wonderful support and fun group. I hope we will keep sharing tasty food, hiking and... weddings.

I am grateful for the fun (and too short) time spent with Rosalia, a lovely dark soul, with whom I squeezed in many adventures between one experiment and the other.

I would like to express my gratitude to my friends Letizia, SoYeon and Enàs at McMaster University, who are brilliant scientists and engineers. We had such a fun time chatting about food and the latest innovations in science. I also appreciate Peter for being a great flatmate and showing me the fun world of Drag Race. I look forward to seeing you all again soon and giving you a warm hug.

A special mention to Laura, for having listened to me, and listened to me again, and listened to me again... But for never having stopped being there.

To Silvia because your arrival in Glasgow made everything light up with laughter.

To Chicco, without whom Glasgow would always have remained a mystery and without whom everything would have been unnecessarily complicated and less fun... Thank you for always being unconditionally at my side, e grazie per avermi fatto trovare casa.

A huge thank you to my lifelong friends. That there have been, are and always will be. To Shaineze and Leonardo, who always cracked me up with their hilarious videos and brought me back down to earth... Cheers to our (always unclear) goals! (Don’t worry, you don’t have to read this boring thesis!)

To my loyal buddies Chiara and Andrea (Uccia). Thank you, Chiara, for teaching me that our differences are our strength, they help us see things differently but also bond us together. Thanks Uccia for the instant connection and empathy that sometimes leaves me speechless, I miss you.

To my sister, my mom and dad who listened to me cry and laugh from afar. We did it again... And as always, ‘contenti e baldanzosi’, we will continue to move forward! And, again, to my ‘patata’ because you don’t have to be a genius to do a PhD (as you have now well understood)... You have to be resilient and love yourself.

All this, all of you, even those who I might have missed to mention... you have contributed day by day to making this PhD special, fantastic, and worth doing again! Ok, maybe not 'doing again'... But I am extremely grateful, because your love and courage brought me here today too.

Author's Declaration

Name: GIULIA CORE

Registration Number: xxxxxxxx

I certify that the thesis presented here for examination for a PhD degree of the University of Glasgow is solely my own work other than where I have clearly indicated that it is the work of others (in which case the extent of any work carried out jointly by me and any other person is clearly identified in it) and that the thesis has not been edited by a third party beyond what is permitted by the University's PGR Code of Practice.

The copyright of this thesis rests with the author. No quotation from it is permitted without full acknowledgement.

I declare that the thesis does not include work forming part of a thesis presented successfully for another degree.

I declare that this thesis has been produced in accordance with the University of Glasgow's Code of Good Practice in Research.

I acknowledge that if any issues are raised regarding good research practice based on review of the thesis, the examination may be postponed pending the outcome of any investigation of the issues.

Date: 9th January 2024

Signature:

Disruptions

My research topic is significantly experimental, having to prototype devices to diagnose infectious diseases and involving molecular biology and biochemistry studies. Therefore, having access to the laboratory facilities was vital for the success of the project. The COVID-19 pandemic caused a high level of disruption. In fact, since the beginning of the pandemic (23rd March 2020) I was not able to access lab-facilities for about 9 months. I had limited access (at 30%) for 4.5 months. However, when access to the laboratory was possible, some key experiments needed to be repeated to recreate the optimal and consistent conditions to carry on the work left half-way before the lockdown, thus taking up time for the possibility of doing new research. Not to mention the delays in reagents /components delivery that have slowed further progression. As a mitigation approach, a team-group side-project has been carried out during the months of disruptions and it is described in Appendix A.1. Moreover, the Graduate School of Science and Engineering of the University of Glasgow granted a 6-months funded extension.

Furthermore, in February 2022 my research group and its equipment have moved to a different building on campus, disrupting laboratory activities for 2 extra months. During that time my efforts focussed on helping in ensuring that consumables and reagents were properly packed, unpacked and displaced appropriately in the new facility.

Detailed dates of COVID-19 disruption

- From 23rd March 2020 to 6th July 2020 – 3 months and a half with 100% disruption of my lab-work due to complete lack of access to the lab. This affected my ability to progress all experimental aspects of the project.
- From 6th July 2020 to 22nd November 2020 – 4 months and a half with 70% disruption of my lab-work due to limited access to the lab (1 day and a half per week). This affected my ability to progress many experimental aspects of my project.
- From 23rd November 2020 to 14th December 2020 – 3 weeks with 100% disruption due to complete lack of access to the lab. This affected my ability to progress all experimental aspects of the project.
- From 26th December 2021 to 26th of April 2021 – 4 months and a half with 100% disruption of my lab-work due to complete lack of access to the lab. This is still affecting my ability to progress all experimental aspects of the project.

Thesis Outline

This thesis is divided into six chapters.

Chapter 1: Overview of point-of-care devices for the diagnosis of infectious diseases. The focus is given to paper-based point-of-care devices that detect genomic pathogenic material and integrate nucleic acid amplification methods. Strategies used to modify paper and control fluid flow are also briefly summarised.

Chapter 2: Materials and methods common to each result chapter. The chapter describes the paper-based methods for extracting nucleic acids and the fabrication techniques for developing devices based on paper and plastic. The strategies for storing molecular reagents at ambient temperature are also presented in detail.

Chapter 3: Optimisation of paper-based nucleic acid extraction methods. The chapter presents the steps followed to optimise sample pretreatment methods that use paper to capture and release DNA. The performance of different lysis buffers, types of papers, dimensions of paper and paper-functionalisation are analysed.

Chapter 4: Strategies to store loop-mediated amplification (LAMP) reagents for molecular diagnostics at room temperature to eliminate the need for cold-chain. The chapter investigates the role of pullulan (polysaccharide) in preserving LAMP reagents reactivity over time. Pullulan and trehalose (a common disaccharide) have been used to create tablets containing different reagents and they have been tested after shipping in uncontrolled temperature conditions. Moreover, the chapter introduces a proof-of-concept point-of-care device for the detection of malaria that was shipped with dried LAMP reagents stored ‘on-board’ to Uganda. The design and fabrication of the device are presented, along with the challenges of field testing in a low-resource setting.

Chapter 5: Modular paper- and plastic-based point-of-care device that integrates sample pretreatment and nucleic acid amplification in a single chamber. The device was developed for the detection of the bacteria *Escherichia coli* in large samples. The chapter describes the device design, fabrication processes, and limitations.

Chapter 6: Enzyme-free amplification strategies. The chapter explores catalytic hairpin assembly (CHA), as an alternative to LAMP, combined with lateral flow assays to investigate the deployability of CHA at the point-of-use. The work was mostly carried out during a 12-month placement at McMaster University (Ontario, Canada), and preliminary results are given.

Chapter 7: Conclusions and future works. The chapter offers a summary of findings and future works, including preliminary results about the integration of enzyme-free amplification method with result visualisation on lateral flow assays.

Nomenclature

2D - Two dimensional

3D - Three dimensional

C. - *Clostridioides*

E. - *Escherichia*

P. - *Plasmodium*

ANOVA - Analysis of variance

BSA - Bovine serum albumin

CHA - Catalytic hairpin assembly

DNA - Deoxyribonucleic acid

EDTA - Ethylenediaminetetraacetic acid

FAM - Fluorescein amidites

FIND - Foundation for Innovative Diagnostics

FITC - Fluorescein isothiocyanate

GuHCl - Guanidine hydrochloride

IDT - Integrated DNA Technologies

ISPf - International Standard for *Plasmodium falciparum*

LAMP - Loop-mediated isothermal amplification

LB - Lysis buffer

LFS - Lateral flow strip

LMICs - Low- and middle-income countries

LOD - Limit of detection

NA - Nucleic acid

NAAT - Nucleic acid amplification test

NEB - New England Biolabs

NFW - Nuclease free water

NTC - No template control

PAGE - Polyacrylamide gel electrophoresis

PBS - Phosphate buffered saline

PC - Positive controls

PCR - Polymerase chain reaction

PDMS - Polydimethylsiloxane

PK - Proteinase K

PMMA - Poly(methyl methacrylate)

POC - Point-of-care

qPCR - Quantitative polymerase chain reaction, real-time polymerase chain reaction

RDT - Rapid diagnostic test

RT - Room temperature

SDS - Sodium dodecyl sulphate

TBE - Tris-boric-EDTA

TBS - TRIS buffered saline

TE - Tris-EDTA

TTP - Time-to-positive

UV - Ultraviolet light

w/v - Weight per volume

WHO - World Health Organization

List of Figures

1.1	Steps involved in nucleic acid amplification tests (NAATs).	3
1.2	Time line of paper-based diagnostic devices	12
1.3	Strategies for fluid and analyte handling in paper substrates.	14
1.4	Schematic of pH dependent capturing and releasing of DNA on chitosan-functionalised paper.	17
1.5	Examples of low-cost plastic-based microfluidic chips that integrate nucleic-acid amplification tests and lateral flow assays.	21
1.6	Schematics of freeze-drying and drying of nucleic acid amplification tests reagents.	23
1.7	Structural formulas of trehalose and pullulan in Haworth projection.	25
1.8	Example of a RNA-cleaving DNAzyme.	26
1.9	Enzyme-free amplification methods.	27
2.1	Computation of time-to-positive values in real time LAMP.	39
2.2	Interpretation of test results on lateral flow strips.	43
2.3	Schematic of the nucleic acid purification method performed by Zou <i>et al.</i> (2017).	45
2.4	Procedures to investigate DNA-paper binding properties.	46
2.5	Schematic of paper-based sample pretreatment procedure.	47
2.6	Schematic of the reduction of steps for the paper-based DNA extraction from <i>Escherichia coli</i> bacterial sample.	48
2.7	Schematic for the addition of the elution step in the paper-based DNA extraction procedure.	49
2.8	Schematic of paper-based DNA extraction using MagaZorb [®] reagents.	50
2.9	Schematic of the paper-based DNA extraction with lysis buffer air-dried on the paper disc.	51
2.10	Disc-shaped pullulan films.	53
2.11	Schematic of the ‘two-pill method’ to store LAMP reagents in pullulan-trehalose tablets.	57
2.12	Two-pill method used to ship LAMP reagents to Uganda under uncontrolled temperature conditions.	60
2.13	Modified DNA extraction from blood finger prick.	62
2.14	Schematic of the point-of-care device for the detection of malaria from blood.	63
2.15	Schematic of the functioning of the point-of-care device for the detection of malaria from blood.	65
2.16	Results interpretation on diagnostic cassette for detection of malaria.	66

2.17	Assembly of the point-of-care malaria cassette.	68
2.18	Field testing.	71
2.19	Schematic of the diagnostic device for <i>E. coli</i> detection.	72
2.20	Overview of the working mechanism of the diagnostic device for <i>E. coli</i> detection.	73
2.21	Poly(methyl methacrylate) (PMMA) layers used to create the 3D structure of the point-of-care device.	74
2.22	Bonding process of three PMMA layers.	75
2.23	<i>E. coli</i> point-of-care device sealing process using adhesive film.	77
2.24	Pullulan tablets drying on glass slides for dimension control.	78
2.25	Different combinations of Allura Red and Xylene Cyanol for pullulan tablets dissolution analysis.	81
2.26	PMMA mould for pullulan tablets dissolution measurements.	82
2.27	Schematic of PDMS position to seal central chamber in POC device.	85
2.28	Incubation time on the device determined by pullulan discs.	86
2.29	Materials to test the full operation of the <i>E. coli</i> point-of-care device.	87
2.30	Schematic of the sample pretreatment on the point-of-care device.	89
3.1	Time-to-positive values and melting curve plots of LAMP reaction for the detection of <i>E. coli malB</i> gene using three different concentrations of primers.	93
3.2	Analytical sensitivity and standard curves of the LAMP assay for the detection of <i>E. coli malB</i> gene.	94
3.3	Analytical sensitivity and standard curves of the qPCR assay for the detection of <i>E. coli malB</i> gene.	96
3.4	DNA-paper incubation time comparison when using the first paper-based DNA extraction procedure.	98
3.5	Comparison between the first and “in tube” paper-based DNA extraction procedures.	99
3.6	Sensitivity of the paper-based DNA extraction “in tube” procedure.	100
3.7	Time-to-positive values of paper-based extraction when changing lysis step conditions.	102
3.8	Time-to-positive values of paper-based extraction performed using the 9-steps or 7-steps methods.	104
3.9	Analytical sensitivity experiment of the paper-based sample pretreatment for the detection of <i>E. coli malB</i> gene from a sample, using LAMP.	105
3.10	Time-to-positive values of the 7-steps paper-based DNA extraction procedure performed using different paper substrates.	106
3.11	Amplification plot of the 7-steps method when proteinase K is added to the sample.	107
3.12	Interaction of paper disc with fluorescence reading in qPCR.	109
3.13	Time-to-positive values of paper-based extraction performed using the 7-steps methods with and without an additional elution step.	110
3.14	Cycle threshold values of the paper-based DNA extraction performed with different volumes of lysis buffers.	111
3.15	Structural formula of ethylenediaminetetraacetic acid (EDTA).	112

3.16	Cycle threshold values of the paper-based DNA extraction performed with different lysis buffers having different EDTA concentrations.	113
3.17	Structural formula of Guanidine hydrochloride (GuHCl).	113
3.18	Cycle threshold values of the paper-based DNA extraction performed with lysis buffers having different GuHCl concentrations.	114
3.19	Cycle threshold values of the paper-based DNA extraction performed with lysis buffers having different pH.	115
3.20	Cycle threshold values of the paper-based DNA extraction performed with different sizes of Whatman [®] Grade 1 paper discs.	117
3.21	Cycle threshold values of the paper-based DNA extraction performed with one or two paper discs of Whatman [®] Grade 1, or one disc of Whatman [®] Grade 3 paper.	118
3.22	Cycle threshold values of the paper-based DNA extraction performed with one, two or three paper discs of Whatman [®] Grade 3, compared to one disc of Whatman [®] Grade 1 paper.	119
3.23	Cycle threshold values of the paper-based DNA extraction performed using Whatman [®] Grade 3, Grade 470, CF4, CF5.	120
3.24	qPCR results when proteinase K is added to the paper-based DNA extraction methods.	122
3.25	Cycle threshold values of the Magazorb Kit paper-based DNA extraction performed with different types of paper.	123
3.26	Cycle threshold values of the Magazorb Kit paper-based DNA extraction performed with two different lysis buffers.	124
3.27	Cycle threshold values of the 7-steps method with elution performed with air-dried lysis buffer.	126
3.28	Cycle threshold (Ct) values of the 7-steps method with elution performed with air-dried lysis buffer when the dilution step is not performed.	127
3.29	Cycle threshold (Ct) values of the two paper-based DNA extraction methods developed performed with air-dried lysis buffer.	128
3.30	Amplification plot and time-to-positive values of paper-based extraction procedure performed using chitosan-functionalised Whatman [®] Grade 1 paper discs.	129
3.31	Time-to-positive values of paper-based extraction procedure performed using chitosan-functionalised Fusion 5 paper discs.	130
4.1	Master mix ISO004-LYO stored in 10% (w/t) pullulan tablets at 35 °C over time.	138
4.2	Primer mix stored in 10% (w/t) pullulan tablets at 35 °C over time.	139
4.3	Performance of LAMP assay carried out using the master mix provided by New England Biolabs or by Optigene Ltd. (ISO-004).	140
4.4	Optimisation of MgSO ₄ and betaine concentration in LAMP master mix (New England Biolabs, NEB).	141
4.5	Analytical sensitivity and standard curves of the optimised LAMP assay with New England Biolabs reagents.	142
4.6	Simplified schematic of loop-mediated isothermal amplification (LAMP).	144

4.7	Gibbs free energy change (ΔG) of labelled primers for the detection of <i>E. coli malB</i> gene.	145
4.8	Lateral flow assay results obtained with a primer mix made of only loop primers for the detection of <i>E. coli malB</i> gene.	146
4.9	5X labelled primer mix stored in 10% (w/v) pullulan tablets at 35 °C and tested after 10 ,30, and 60 days.	147
4.10	LAMP assay with different primer mixes concentrations.	148
4.11	25X labelled primer mix stored in 10% (w/v) pullulan and 0.5 M trehalose tablets at 35 °C and tested after 10 , 30 days.	149
4.12	LAMP amplification plots of reagents stored in separate 10% (w/v) pullulan and 0.5 M trehalose tablets, compared to reagents stored at -20 °C.	150
4.13	LAMP reagents stored in two 10% (w/v) pullulan and 0.5 M trehalose tablets for 10 and 30 days.	152
4.14	Amplification plot of tablet-based LAMP assays with different concentrations of WarmStart [®] Bst 2.0 (New England Biolabs).	153
4.15	Limit-of-detection of LAMP reagents stored in two separate 5% or 10% (w/v) pullulan and 0.5 M trehalose tablets for 10 days at 35 °C.	155
4.16	LAMP assays for the detection of <i>Plasmodium falciparum</i>	157
4.17	LAMP assays validation of dried reagents brought back from the field for the detection of <i>Plasmodium</i> species.	158
4.18	LAMP assays validation of dried reagents brought back from the field for the detection of <i>BRCA1</i> gene.	158
4.19	Tablet-based LAMP reagents brought back from the field.	159
4.20	Schematic of simplified DNA extraction methods from whole blood.	161
4.21	Results of simplified DNA extraction methods from whole blood.	162
4.22	Comparison of simplified DNA extraction methods from whole blood.	162
4.23	Dimensions of the point-of-care device for the detection of malaria: designs a	164
4.24	Dimensions of the point-of-care device for the detection of malaria: designs b	165
4.25	Heating process of the malaria diagnostic cassette; design b - 1	166
4.26	Different types of walls and thicknesses between chambers (5)-(6), (6)-(7) and (8)-(6).	167
4.27	Dimensions of the point-of-care device for the detection of malaria and magnetic beads handling: designs c	168
4.28	Results of liquid and magnetic beads handling in the device: design c - 1	169
4.29	Heat block and aluminium bands used to perform LAMP on the point-of-care device for malaria.	170
4.30	Results of liquid manipulation and heating of the point-of-care device for the detection of malaria with different wall thicknesses between the reaction and LFS chambers: design b = 1	171
4.31	Results of full DNA extraction from blood and LAMP assay performed on the point-of-care device.	172
4.32	Results of full DNA extraction from blood and LAMP assay performed on the point-of-care device.	173
4.33	LAMP reaction set-up in the field.	174

4.34	Example 1 of issues encountered during the field-trial.	176
4.35	Results of devices sealed with or without the use of super glue.	177
4.36	Results of a device whose resuspension chambers are sealed from the adjacent oil chambers with parafilm.	178
4.37	New batch of lateral flow strips run with proprietary runnin buffer and water.	179
4.38	DNA extraction from whole blood performed with reagents brought back from the field.	180
4.39	Plastic cassettes for malaria diagnostics shipped to Uganda and tested in the laboratory in UK.	181
5.1	Table of content figure of the modular paper- and plastic-based point-of-care device.	191
5.2	Colour change detected by the camera.	192
5.3	Mean ΔE of each well compared to the well controls.	193
5.4	Time-to-plateau values of pullulan tablets with different dimensions and concentrations.	194
5.5	Mean ΔE curves of 6-mm pullulan discs with concentrations between 2% and 3%.	195
5.6	Dimensions of the first and second layer of the point-of-care device. . .	196
5.7	Dimensions of the third layer of the point-of-care device: designs a and b.	198
5.8	Results of drying pullulan inside the point-of-care device.	199
5.9	Results of incubation time provided by pullulan discs on point-of-care device.	200
5.10	Pictures of paper-discs soon after the fluid front in the absorbent pad stops and after washing.	201
5.11	Examples of liquids overflowing in adjacent channels inside the point-of-care device.	203
5.12	Results of incubation time provided by a 2% pullulan disc on point-of-care device with pre-wetted central chamber or additional glue in sample inlet.	204
5.13	Dimensions of the second layer of the point-of-care device that reduces overlap between central chamber and waste container.	205
5.14	Pictures of full device operation. Design b - 3	207
5.15	Dimensions of the third layer of the point-of-care device: designs c. . .	208
5.16	Pictures of design c - 1 and c - 3 testing.	208
5.17	Pictures of design c - 2 and c - 4 testing.	210
5.18	Dimensions of the third layer of the point-of-care device: designs d and e.	211
5.19	Pictures of the waste container of the point-of-care device sealed. . . .	212
5.20	Ct values of the 7-steps paper-based DNA extraction procedure performed with lysis buffer dried on the paper discs at room temperature or at 70 °C.	215
5.21	Results of the paper-based DNA extraction procedure performed on the point-of-care device.	216

5.22	Results of the paper-based DNA extraction procedure performed on the point-of-care device compared with the paper-based 7-steps method performed in tube and the gold standard.	218
5.23	Lateral flow strips result of the 7-steps paper-based DNA extraction procedure with lysis buffer already dried on paper discs and directly inserted in LAMP mix.	219
6.1	Enzyme-free DNA biosensing system.	227
6.2	Performance assessment of catalytic hairpin assembly (CHA) on nPAGE.	229
6.3	Performance assessment of catalytic hairpin assembly (CHA) on nPAGE for different incubation times.	230
6.4	Performance assessment of different catalytic hairpin assembly (CHA) on nPAGE.	232
6.5	Labelling options of hairpins for CHA and lateral flow assay integration.	233
6.6	Assessment of hairpins stability on nPAGE and lateral flow strips.	234
6.7	Assessment of CHA leakage on lateral flow strips.	236
6.8	Assessment of hairpins stability on lateral flow strips.	237
6.9	Assessment of four-way junction formation on nPAGE.	238
6.10	Assessment of DNAzyme-mediated RNA cleavage for the recognition of <i>E. coli</i> bacteria on denaturing PAGE.	239
6.11	Schematic of a fully paper-based device that integrates a DNAzyme biosensor with lateral flow assay.	242
A.2	10% dPAGE analysis of the DNAzyme cleavage reaction.	277
B.1	Wells identification in PMMA mould for pullulan dissolution rate study.	296

List of Tables

1.1	Summary of paper-based point-of-care nucleic acid amplification tests. . .	18
2.1	Properties of different types of paper tested.	32
2.2	Volumes and concentrations used to create master mix using reagents from New England Biolabs (NEB).	33
2.3	Conversion table from international units (IU) per milliliter (WHO International Standard for <i>P. falciparum</i>) to parasites/ μ L.	34
2.4	Primers sequences of LAMP assays.	35
2.5	LAMP primer mixes for the detection of <i>E. coli malB</i> gene, <i>Plasmodium</i> species, and <i>BRCA1</i> gene.	36
2.6	PCR primer mix for the detection of <i>E. coli malB</i> gene.	37
2.7	Graphical symbols for p-values.	41
2.8	Optimised formulation of the stored dry Tablet 1 and 2 for LAMP test.	58
2.9	Volumes of chambers incorporated in the plastic cassette to perform the nucleic acid amplification test for <i>Plasmodium Falciparum</i> detection.	67
2.10	Pullulan tablets of different (w/v) concentrations tested inside the point-of-care device.	79
2.11	Pullulan tablets of different (w/v) concentrations tested inside the point-of-care device.	80
3.1	Three different concentrations of primers tested in the final LAMP reaction for the detection of <i>E. coli malB</i> gene.	92
3.2	Conversion table for 204 bp long <i>E. coli malB</i> gene synthetic DNA from ng/ μ L to copy number per LAMP reaction.	95
3.3	Conversion table for 4,639,675 bp long <i>E. coli</i> genomic DNA from ng/ μ L to copy number per LAMP reaction.	95
3.4	Conversion table for 204 bp long <i>E. coli malB</i> gene synthetic DNA from ng/ μ L to copy number per reaction in qPCR.	97
3.5	Conversion table for 4,639,675 bp long <i>E. coli</i> genomic DNA from ng/ μ L to copy number per reaction in qPCR.	97
4.1	Conversion table from ng/ μ L to copy number per reaction in LAMP for 204 bp long <i>E. coli malB</i> gene synthetic DNA with 5 μ L template in final reaction.	142
4.2	Volumes to prepare a primer mix containing only labelled loop primers for <i>E. coli malB</i> gene detection.	146

4.3	Primer mix concentrations used to understand the lowest concentrations that allowed to detect the target DNA on the lateral flow assay.	149
4.4	Volumes of reagents to create 10% (w/v) pullulan and 0.5M trehalose tablets containing dNTPs and different concentrations of Bst 2.0 DNA polymerase.	153
4.5	Summary of the results of LAMP reagents stored in pullulan solutions.	160
4.6	Number of point-of-care malaria cassettes used during in-field testing. .	173
5.1	Cost analysis per point-of-care device and assay (<i>E. coli</i>).	223
6.1	Gibbs free energy of hairpins in kcal/mol.	231
A.1	Accuracy indices for diagnostic tests and their definitions.	268
A.2	Factors affecting sample size calculation for diagnostic studies.	269
A.3	Oligonucleotide sequences used in the CHA biosensors developed by Zhou <i>et al.</i> (2020)	276
A.4	Volumes used in DNAzyme mediated RNA cleavage (DRC) reactions. .	278
A.5	Volumes used in CHA reactions.	278
A.6	Copyright permissions.	285
A.7	Copyright permissions.	286

Chapter 1

Introduction

Communicable diseases, such as malaria, diarrhoeal diseases and tuberculosis, are widespread globally and cause high morbidity and mortality rates [1]. As illustrated in the current COVID-19 pandemic, early detection of infections is essential to prevent further spread of pathogens amongst populations, increased severity, and death by facilitating rapid treatment and prompt isolation. To halt epidemics and fight the global threat of antimicrobial resistance, rapid, point-of-care (POC), highly sensitive and specific molecular diagnostic platforms need to go beyond the current centralised testing approach that relies on costly, complex procedures and significant infrastructure, often not available at the community level and in rural areas. The World Health Organisation (WHO) has established the ASSURED criteria for endorsing effective POC devices: Affordable, Sensitive, Specific, User-friendly, Rapid and robust, Equipment free and Deliverable to end-users [2]. To overcome data collection and interpretation difficulties, and tackle complicated specimen acquisition, the ASSURED criteria have been adjusted to REASSURED by Land *et al.* [3], where R addresses real-time connectivity, and E refers to both the ease of specimen collection and environmental friendliness.

This thesis project focuses on developing new strategies to secure the user-friendliness, rapidity and robustness, and equipment free (“reassURED”) in paper-based POC molecular diagnostic devices, since “reaSSured” features have already been extensively addressed in the literature.

1.1 Motivation of Study

Accurate disease diagnosis is a critical component of healthcare to guide patient management by identifying the appropriate treatment, and to take broader public health actions, such as control and surveillance measures. Laboratory-based molecular diagnostic techniques have rapidly progressed in the past decades with the development of robust nucleic acid (NA) approaches to achieve rapid, highly sensitive and specific diagnosis. The first laboratory-based nucleic acid amplification test (NAAT) was based on polymerase chain reaction (PCR) which requires repeated cycles at different temperatures. To overcome the complexity and long running times of this approach, different types of isothermal NA amplification procedures have been developed during the last 10 years, including loop-mediated amplification (LAMP) [4], helicase-dependent amplification (HDA) [5], recombinase polymerase amplification (RPA) [6] and rolling circle amplification (RCA) [7]. These techniques can detect very low levels of the target NA sequences, having a great impact in detecting infections at a very early stage. However, laboratory-based NAATs require very expensive equipment and trained personnel to be performed, thus, making access to such tests prohibitive in high-incidence regions. For instance, in low-income countries, where infectious diseases still represent the leading cause of death [8], about 60% of the population lives in rural-areas with limited access to healthcare or laboratory facilities. Therefore, there is a dire need for diagnostic tests that can be performed outside laboratory settings, at the point-of-need, and that are affordable, user-friendly, rapid, robust and deliverable [3]. NA-based tests offer a more sensitive and specific option over other types of POC devices for infectious diseases, *i.e.*, diagnostics tests based on antigens, antibodies or biomarkers [3]. In general, NAATs require three main steps: (a) sample pretreatment to extract the NAs from cells, (b) DNA/RNA amplification and (c) detection (Fig. 1.1).

There are already many commercially available POC NAATs [9] that come in the form of closed automated devices and that use single-use integrated cartridges with pre-measured dried reagents ready for hydration. However, the cartridges manufacturing costs are very expensive and usually not affordable to most developing countries without subsidies [3]. The increasing need for field-deployable POC devices has turned the attention to paper-based disposable devices to fill the gap on several counts. In fact, paper has advantages stretching from being low-cost and abundant to relying on capillary flow and having the potential to form batteries. The recent translation of isothermal

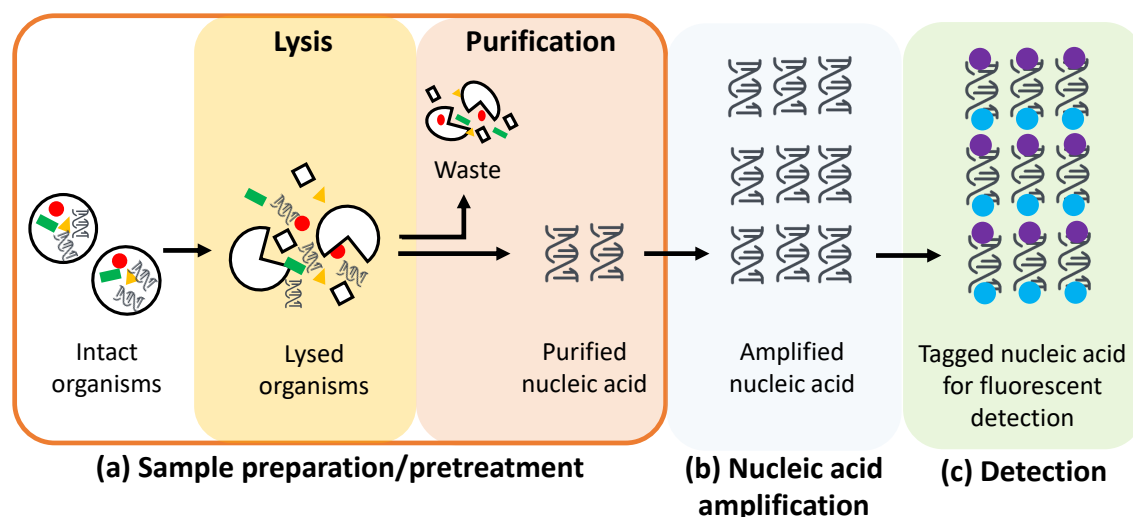


Figure 1.1: **Steps involved in nucleic acid amplification tests (NAATs).** NAATs involve three main steps. (a) Sample pretreatment consists in the lysis of the intact organisms and the following purification of the DNA from the cellular debris. (b) Amplification of the purified DNA. (c) Detection of the amplified DNA.

NAATs to a paper-based format has combined the advantages of paper with the high accuracy of NAATs, thus having a great potential for the development of affordable and accessible POC devices that are portable, reduce reaction volumes and lower the risk of sample contamination when fully enclosed. Only a few configurations of paper-based molecular tests have been developed to incorporate all the steps of NAATs with minimal user's intervention [10–13], and another few have been validated with clinical samples for the detection of a variety of diseases stretching from SARS-CoV-2 and influenza viruses, to *Plasmodium falciparum*, *Mycobacterium tuberculosis* and *Staphylococcus aureus* [13–19]. To the best of our knowledge only one of these paper-based POC NAATs has been tested in a resource-poor setting and this was presented by Reboud *et al.* [17] (University of Glasgow). Therefore, most of the paper-based NAATs have been limited to proof-of-concept and they have not been tested outside laboratory settings where adverse environmental conditions could affect the diagnostic results. More generally, when referring to application in-field, paper-based NAATs devices show some major challenges: (i) complicated manual operations in sample pretreatment, sample processing and control of application volume, (ii) cross-contamination, (iii) need for an external incubator, (iv) long-term reagent stability affected by temperature and humidity, as well as (v) reagents evaporation [17,20]. To have an impactful progress in diagnosing communicable diseases, in future, paper-based POC NAATs need to show adequate performance under adverse field conditions, along with improved accuracy. Thus, attention must be focused in new strategies to secure “assURED” aspects and

not only “aSSured” criteria [2].

1.2 Aim and Objectives

My research aims at increasing paper-based POC NAATs access in low-resource settings by addressing two main challenges: reduce the number of steps necessary for sample pretreatment, and find an effective pre-load and storing strategy for NAATs reagents. The ultimate goal of this research work was to create the basis for a LAMP POC diagnostic device that provides pipetting-free sample preparation, amplification and detection of pathogens with NAATs reagents stored dry “on-board”. The idea was that the specimen introduction alone led to the reagent hydration, with the addition of only one additional buffer.

The achievement of this goal builds around the development of two main strategies:

1. **Paper-based protocol to extract genomic material from bacteria present**

in large volumes. The use of a paper-based DNA extraction protocol reduces the number of handling steps in the sample pretreatment phase compared to the use of magnetic beads-based DNA extraction method that was originally implemented by Reboud *et al.* [17] and previous laboratory group members. The use of paper in the extraction procedure holds promise for an easy integration in a fully enclosed paper-based POC device as it reduces the number of buffers to be used and facilitates the use of the device by unskilled healthcare personnel.

A paper-based DNA extraction procedure similar to the one introduced by Zou *et al.* [21] was optimised and investigated using different lysis buffers and types of paper. *Escherichia coli* K12 was used as a proof-of-concept pathogen, and *E. coli malB* gene as DNA target.

2. **Easy-on-board-storage technique that also allows for long-term stor-**

age of reagents at room temperature. The limited shelf-life of reagents at ambient temperature represents one of the major barriers for the effective deployment of POC NAAT devices outside laboratory settings. Creating simple and inexpensive tablet-based assays to stabilise labile bioreagents over the long term and in extreme environmental conditions would significantly improve diagnostic support in resource-limited settings, by lowering devices costs, facilitating shipping and manual operations. One of the main challenges in reagent stabil-

ity is the susceptibility of enzymes to degradation by water. To preserve the activity of such protein-based reagents for long-term use, dry storage is preferable over liquid conditions, especially for POC devices that require simple design and manufacturing. Existing dry storage of pre-mixed LAMP reagents, such as freeze-drying [22–24] and drying by concentration/desiccation [25], is experimentally laborious and requires sophisticated equipment.

I have developed and validated a novel method for storing dry LAMP reagents in a ready-to-use format without compromising sensitivity, based on the use of pullulan and trehalose, following the approach of Leung *et al.* [26]. Pullulan-trehalose tablets preserves the reactivity of the reagents and allows for their on-board storage, facilitating the future integration of all the steps involved in NAATs in a fully enclosed device.

My research has the potential to transform the POC diagnostic landscape for a whole range of infectious diseases that pose a serious risk to a huge proportion of the world population. More specifically, by developing a sample-in-answer-out POC diagnostic device that can operate with minimal infrastructure, energy, high temperatures and untrained personnel, my PhD research aligns with the United Nations' Sustainable Development Agenda (SDGs) 3.3 [27], which aims to end the epidemics of AIDS, tuberculosis, malaria, neglected tropical diseases and other infectious diseases. The goal is to improve health outcomes in general and reduce health inequalities, especially for the young (<5 years) and minorities in low- and middle-income countries (LMICs), who are disproportionately affected by these diseases and face barriers to education and social mobility. Thus my work also supports SDG 1 (no poverty) and SDG 10 (reduced inequalities) by addressing the root causes of poverty and exclusion.

1.3 Point-Of-Care Diagnostic Devices for Infectious Diseases

Point-of-care (POC) testing is a broad term that covers many medical tests that are performed outside the central laboratory, where the patient is receiving care or treatment [28]. The location of the testing, rather than the type of tests, is what defines point-of-care testing [29], that can also be referred to as remote testing, bedside testing, near-patient testing, or rapid diagnostics. The main advantage of POC testing is that

the results are available in a short time and can be used to make immediate clinical decisions.

POC tests need to be accurate, reliable and have a short turn-around-time in order to rapidly inform appropriate clinical actions and improve patient outcomes. The ASSURED criteria were introduced as general guidelines to evaluate the quality of POC tests by the WHO in 2003 for tropical and sexually transmitted diseases [2]. However, these criteria are not absolute, and trade-offs are necessary depending on the context and the level of the health care system [3,29]. For instance, at the community and primary care level, that is the lowest level of the healthcare system, the limited access to infrastructure and skilled personnel requires POC tests to be simple to use, fast so that patients do not have to travel far to get their results, equipment-free, and portable with stable reagents that can function in different environmental conditions. In addition, when it comes to infectious diseases that demand elimination or eradication, tailored solutions are necessary to address the specific challenges and needs of the patients and the health care providers, such as mental well-being and lack of resources. Therefore, POC tests should not only be patient-centric and context-specific, but also aligned with the treatment strategies and the health care system as a whole [30].

Broadly, POC diagnostics for infectious diseases can be classified in immunological, molecular (NA-based), and biomarker-based tests, which are described in the sections below.

1.3.1 Immunological Tests

Immunological POC tests detect either antigens or antibodies that are associated with the immune response to a specific infection. An antibody or an antigen is usually immobilised on a solid substrate, such as a paper strip or a microfluidic chip, and when a sample containing the target analyte is applied, it forms an immune-complex with the immobilised molecule. The complex then produces a visible signal, such as a color change or a fluorescence emission, that can be read by the naked eye or by an optical device [28]. Immunological POC tests rely on the ability of antigens/antibodies to bind to a particular target, such as a protein, a drug, or a pathogen, with high sensitivity and specificity; and they can provide both qualitative and quantitative results.

Immunological POC tests offer many benefits and are widely used for the detection of infectious diseases. They are robust, they provide results rapidly (in approx. 15 min-

utes), and they are cost effective compared to other types of diagnostic tests, thus being accessible in various healthcare settings. Moreover, this type of test does not need sample preparation and the clinical sample can be directly applied to the test pads. Therefore, immunological POC tests can be easily used by untrained operators in remote areas where complex equipment is not available [30]. Immunoassay-based POC tests have some limitations that affect their performance and reliability [30]. First, they rely on the detection of antibodies/antigens in the patient's blood or other body fluids, which may not be present at the early stages of infection or may vary depending on the immune response of the individual. For instance, the immune response is affected by pathogens' growth cycle: fast-growing pathogens can trigger an immune response within days of infection, slow-growing pathogens can take weeks before enough antibody is produced in the body fluid, resulting in false negative results. In some cases, pathogens can evade the immune system and remain in the body for weeks/months without generating a detectable immune response. Moreover, a weakened immune systems due to co-morbidities or malnourishment can affect the immune response of individuals [30]. Second, temperature and humidity may compromise the functionality of the test kits or reagents. In addition, antibody-based tests cannot be used to verify the presence of a disease or to evaluate the effectiveness of a treatment because antibodies persist after infection and can cause false positive results. Therefore, in many scenarios, immunological POC tests should be complemented by other diagnostic methods, such as molecular or microbiological tests, to confirm diagnoses and guide patient management.

Immunological POC tests can provide multiplexed and rapid results, but they can have lower sensitivity and specificity than nucleic acid-based testing methods, resulting in incorrect diagnosis and unsuitable treatment [28]. Rapid antigen- or antibody-based diagnostic tests are the preferred choice in in-field testing where infectious diseases, such as malaria and dengue, are endemic [31], however, for the reasons highlighted in this section, more sensitive POC tests would be crucial.

1.3.2 Nucleic Acid Amplification Based Tests

Nucleic acid-based POC tests detect the genetic material (DNA or RNA) of the pathogen to identify the diseases of interest. The high sensitivity of these tests is usually achieved by the specific amplification of the targeted nucleic acid (NA) se-

quence, thus the name of nucleic acid amplification tests (NAATs).

In general, NAATs are the most sensitive tests for infectious disease diagnosis with excellent specificity [32]. Indeed, they can detect very low levels of the target NA sequences from low-volume clinical samples, *e.g.*, 10 copies/reaction of *Escherichia coli malB* gene [33] and below 1 parasite/ μL of malaria infections [31], which might become reservoirs for future disease emergence. Moreover, NAATs can test multiple pathogens in one single assay (multiplexing), thus accelerating the best treatment choice, and identify the severity of the infection (virulence). The main drawback associated with POC NAATs is the need for sample preparation that increases complexity and running times. NA contamination is a common problem for POC NAATs, so they need a closed automated system to prevent false positives [30]. However, automation may increase the costs because of the hardware required for system management. Furthermore, the design of NAATs for specific NA sequences that are unique and do not match any other genomes in the sample could be a challenge.

Initially, the vast majority of miniaturized and POC NAATs diagnostics exploited the polymerase chain reaction (PCR) amplification procedure which requires repeated thermal cycles [34]. However, PCR-based NAATs are not feasible in resource-constrained areas because they need expensive instruments and they have a high-energy consumption [35]. Therefore, different types of isothermal NA amplification procedures, which work at a single temperature, have been developed. These methods would require simpler instrumentation than their PCR counterpart as a single contact temperature is needed. Not only are the whole process and test run times significantly shorter, but the instrumentation is also simpler, since the method only aims at reaching one constant temperature. Isothermal NAATs have equivalent or higher sensitivity in clinical diagnosis than PCR-based systems, and have shorter test run times [36]. Some examples are loop-mediated amplification (LAMP) [4], helicase-dependent amplification (HDA) [5], recombinase polymerase amplification (RPA) [6] and rolling circle amplification (RCA) [7]. LAMP operates at 60 - 65 °C and it shows interesting performances in terms of amplification rates, sensitivity and stability, thus being the most popular procedure at present for innovative POC applications [37]. On the other hand, RPA and RCA have the advantage of allowing nucleic acid amplification at lower temperatures than LAMP and HDA.

Currently commercially available NAATs that can be used near the patient bedside

are still dominated by PCR-based assays [36]. However, the recent COVID pandemic has stimulated more investment in POC diagnostics, leading to the development of LAMP-based tests. A new COVID-19 test, developed by Anavasi Diagnostics (Washington, United States) and branded as AscencioDx, has entered the market recently. However, this test is not suitable for home testing or for most LMICs, because its high costs require a detection unit for US\$ 250 and each test kit costs US\$ 34. The increased demand for low-cost and accessible testing platforms, either at home or at the primary healthcare settings, has seen an increased interest in exploring paper-based POC NAATs, as described in Sections 1.4.2, and 1.4.3.

1.3.3 Biomarkers

Biomarkers are biological molecules found in body fluids or tissues of living organisms that can signal a disease condition when their levels differ from the ‘normal range’ [30]. For clarity, in this section, the term biomarker is used for any molecule, *e.g.*, proteins, other than antigens and antibodies produced in immunological reactions (Section 1.3.1) or pathogenic genomic material (Section 1.3.2). Infectious diseases can be detected by various biomarkers, such as those related to inflammation, acute phase response, and specific proteins such as C-reactive protein, procalcitonin, and SARS-CoV-2-S spike glycoprotein [38]. Another type of biomarkers is metabolites, which are the final products of the metabolic processes of the pathogens [39]. Among these, C-reactive protein is the only biomarker used in a POC test to direct anti-microbial therapy in acute respiratory-tract infections [30]. The most widely used detection techniques for biomarkers are colorimetric, fluorescent and electrochemical detection, but also chemiluminescence, and electrochemiluminescence are implemented [40,41]. Aptamers, which are single-stranded DNA or RNA sequences that bind to specific targets, are a promising alternative to antibodies for the detection of infectious diseases and POC devices development [30,42]. Aptamers have high sensitivity and selectivity, and they can be quickly produced through simple chemical synthesis, making them promising for rapid diagnostic approaches during epidemics or pandemics [43]. Aptamers have been developed for various infectious diseases, including cholera, tuberculosis, anthrax, malaria, viral hepatitis, AIDS, and COVID-19 . The aptamer-based detection technologies have been recently reviewed by Wang *et al.* [43] and among others they include enzyme-linked oligonucleotide assay, and aptasensors.

Biomarkers play a significant role in different stages of a disease [44]. They can help with screening and risk evaluation before a diagnosis is made, or with determining the stage, grade, and optimal primary treatment of a disease at the time of diagnosis. Furthermore, they can be useful for tracking therapy responses to choose additional interventions. Therefore, they play a crucial role in personalised medicine. However, biomarkers have some limitations that could lead to wrong measurements or interpretation and, in turn, to false associations with diseases [44]. The development and screening of biomarkers can be expensive and time-consuming. For example, the selective expansion of ligands by exponential enrichment (SELEX) used to develop highly specific aptamers can take up to several months [42]. Complex diseases may involve multiple biomarkers that are hard to identify and understand how they relate to the disease pathophysiology. Moreover, not all biomarkers are equally reliable or useful for making critical decisions, so they need to be distinguished from potential or exploratory ones. Thus, biomarkers are important tools in healthcare, but they also need rigorous evaluation and validation. Despite the potential benefits of biomarker-based POC devices, there are some major challenges around low sample volumes, skilled personnel, long optimisation times, mass production incompatibility that need to be addressed before this type of devices can be applied as clinical POC testing [41]. Another significant obstacle is the higher cost associated with the creation and distribution of biomarker-based POC tests compared to rapid immunological methods [30].

1.4 Paper-Based Microfluidics

Paper substrates play a crucial role in sensing applications due to their unique properties, driving their widespread adoption in clinical diagnostics, food/environmental analysis, and wearable devices [45]. First and foremost, the global abundance of paper facilitates the production of low-cost disposable devices across various regions. Additionally, its biocompatibility and fibrous structure - providing an ideal three-dimensional matrix for sample interactions and analyte capture - make it suitable for diagnostic assays and reactions. Moreover, paper's chemical stability allows it to withstand exposure to commonly used reagents. Lastly, the ease of production and modification renders paper an attractive substrate for creating cost-effective sensing platforms [?].

Therefore, compared to other microfluidic detection platforms, paper substrates of-

fer distinct advantages in terms of cost-effectiveness, flexibility, and passive fluidic transport [?]. Understanding fluid transport characteristics within paper (see Section 1.4.1) and its property for functionalisation is crucial to unlock its full diagnostic potential (Sections 1.4.2). Additionally, paper’s properties, such as thickness, porosity, roughness, and wettability, allow precise regulation of microfluidic behavior to meet diverse requirements [46]. As demand grows for accessible and affordable diagnostic testing platforms - whether at home or in primary healthcare settings - researchers have increasingly explored paper-based POC NAATs to leverage diagnostic sensors in low-income areas. In diagnostic applications paper serves the essential functions of transporting and measuring samples and analytes, providing reaction support, and visualising results [45].

1.4.1 Fluid Transport in Paper

Fluid transport in paper is passive and driven by capillary forces, thus no external pumping sources are required. In paper, wicking is the result of the interplay between surface tension, that is generated by the cohesive forces between fluid molecules at the liquid-air interface, and the Van der Waals force (adhesion) between the fluid and the fibers. The surface characteristics of the paper determine how much adhesion there is, and thus paper wetting which can be described by the contact angle between the fluid and the fiber. The fluid transport can be modelled using the Lucas-Washburn’s equation which shows how the wetted length depends on the wicking time [47]:

$$l(t) = \sqrt{\frac{\gamma r \cos\theta}{2\mu} t} \quad (1.1)$$

where $l(t)$ is the distance moved by the fluid front under capillary pressure, t is the wicking time, γ is the effective liquid-air surface tension, r is the average pore radius of the paper matrix, θ is the liquid-fiber contact angle, and μ is the fluid viscosity. The main limitation of the Lucas-Washburn’s equation is that pores are assumed to be uniform and have a constant cross-sectional area, thus being significantly far from real paper conditions [47]. Equation 1.1 has been expanded in several ways to describe that the imbibition speed of paper is also affected by the presence of hydrophobic barriers [48], non-uniform channels cross-sections [49], and evaporation [50]. Moreover, experimental results have shown that wicking is affected by not only the pore size and

specific surface area of paper, but also by the temperature and fiber alignment [47,51]. Most recently, Chang *et al.* [52] proposed a mathematical model that combines the fluid transport within the network of fibers (inter-fiber voids) with cellulose-paper swelling caused by flow through intra-fiber pores. Through the integration of fibers swelling that also alters the pores' size and shape between the fibers, Chang *et al.*'s model can accurately estimate the flow rate in various types of cellulose-based filter papers.

1.4.2 Paper for Diagnostics and μ PADs

Paper-based diagnostic systems have a very long history [53,54] and significant milestones have been set in the twentieth century (Fig. 1.2), such as the development of lateral flow tests and the first microfluidic paper-based analytical device (μ PAD) introduced a bit more than a decade ago [55].

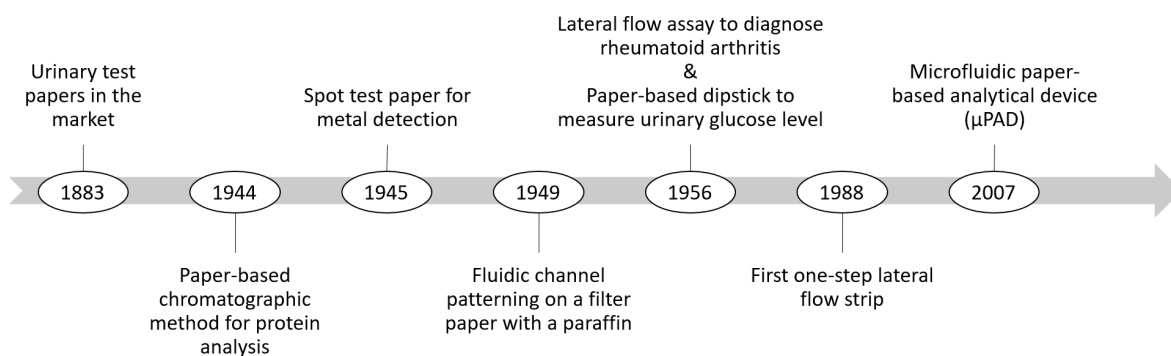


Figure 1.2: **Time line of paper-based diagnostic devices [53,54].**

Cellulose-based paper has found its application as a substrate for the development of POC diagnostic tests thanks to several factors: paper is cheap, abundant, mass-producible, safely disposable and it can be easily modified *i.e.*, folded, cut, chemically modified [47,56]. Another advantage of using paper relies on the passive fluid transport driven by capillary forces, that does not require external pumping sources (as explained in Section 1.4.1).

1.4.2.1 Fluids and Analytes Handling

Different strategies for fluid and analyte handling have been adopted in paper-based microfluidic devices based on geometry and use of physical or chemical barriers. Fluids direction on paper can be controlled by patterning paper with hydrophobic materials, such as wax [57], polydimethylsiloxane (PDMS) [58], inkjet printing/etching [59],

plasma or laser treatment [60,61], however, some bioassays (immunoassays and NAATs) need different reagents or buffers to be applied at specific times. Flow control and the associated time delays indeed become very important in timing the onset and offset of reactions, and in the process of automating multistep paper networks [47,62]. Fig. 1.3 shows some examples of how fluid and analytes have been handled in paper-based devices. For example, imbibition can be controlled geometrically using channels with expanding and contracting widths (Fig. 1.3A) [63,64], delayed shunt (Fig. 1.3B) [65] or by paper folding (principle of paper origami) to allow the flow across different layers (Fig. 1.3C) [66]. Physical delays, instead, can be introduced, *e.g.*, by compressing specific regions in the channel so that the porosity is reduced and the fluidic resistance increased (Fig. 1.3D) [67,68]. Alternatively, paper matrix permeability can be altered through deposition of sugar [69], wax [70] or water-insoluble ink [71] to chemically control the flow.

Valving systems have also found their application in stopping and actuating the flow in paper. Examples are erodible porous or polymeric bridges between two paper strips that are based on the dissolution of a solid component [72,73]. Wax with high melting temperatures has also been used to fully stop liquid flow and small resistive heaters have been integrated to restore the flow by melting the wax [12]. Mechanical displacement and paper deformability represents alternative valving techniques. For instance, a fluid-triggered expanding element, when wicked, can expand and move the main channel thus creating an on-switch, off-switch or diversion switch [74]. A multi-layered paper structure with fluidic connectivity interrupted by air spacers can be used to control fluid flow by pressing the paper in those positions and restore the liquid continuity [75]. Other valving systems use fluidic diodes, electromagnets, and volume-metered actuation [71]. Most of these valving methods, however, have large dead volumes that limit their use with small sample volumes, require unscalable fabrication processes, or are not as effective in fluid control as claimed. Therefore their practical use is limited. A few methods have also been developed for the control of flow rate of fluids in paper, based on printable porous media. The printable porous media based on colloidal, precipitated calcium carbonate developed by Li *et al.* [76] bring the advantage of producing sensors with different shapes without using hydrophobic barriers, changing the media porosity along the sensor length, and the potential to fabricate a fully printed biosensor in a continuous production line. However, this preliminary study needs to overcome challenges surrounding unwanted binding, bioconjugation, and the small working pH

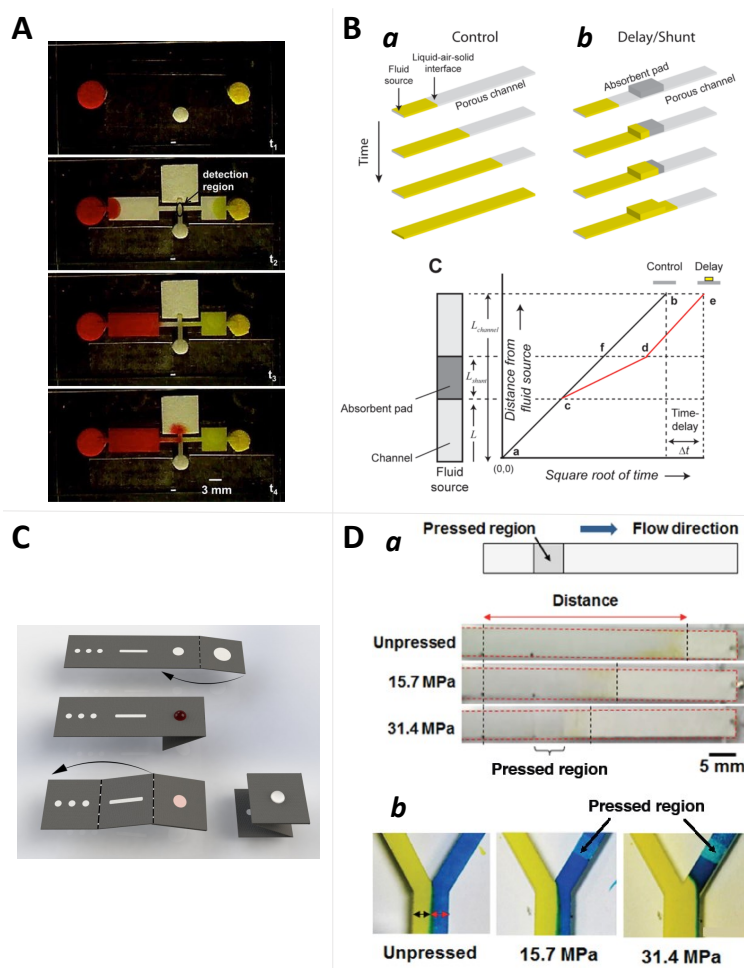


Figure 1.3: **Strategies for fluid and analyte handling in paper substrates.** **A.** Sequential delivery of reagents to a detection region. Input legs of different dimensions are used. In t_1 the source pads are filled with fluids. The clear fluid in the center leg is the first one to reach the detection region (at t_2), next yellow fluid arrives (t_3), and finally red fluid reaches the detection region (t_4). Reproduced from [64], with permission of the rightsholder Springer-Verlag (Appendix A.5). **B.** Delay shunt. *a*) Flow of fluid through a channel of a porous membrane in the absence and in the presence of a shunt. *b*) Idealised plot of the distance travelled by the fluid front as a function of square root of time. Reprinted with permission from [65]. Copyright 2013 American Chemical Society. **C.** Three-dimensional (3D) paper-based device in which four panels are shown. A few paper-folding steps are performed for fluidic manipulation. The arrows indicate the direction of folding. The fluid flows vertically when paper is folded. Reproduced from [17], with permission of the rights holder, PNAS (CC BY). **D.** Paper strip with a pressed region. *a*) Schematic and pictures of water flowing through strips that are pressed with different pressures. Varying amounts of pressure are applied to specific paper regions to modify the physical properties of the paper strip. *b*) Laminar flow profile of dyes when pressure increases. Adapted from [67], with permission of the rights holder, AIP Publishing (Appendix A.5).

range. Another recent development in paper-based assays is the use of synthetic paper [77], which has a uniform and controlled microstructure that can improve the prediction of fluid dynamics. However, the lithographic fabrication method makes synthetic paper expensive. A cheaper approach to control flow rate of fluids in paper strips is based on deploying flexible films (with different contact angles) to sandwich them [78].

1.4.2.2 Paper and Bioconjunction

The types of paper used as support in POC tests normally include cellulose, cotton fiber, glass fiber, nitrocellulose membrane and thread. Their physicochemical properties, such as hydrophilicity/hydrophobicity, pore size, and specific surface area, have been exploited for developing sample pretreatment strategies that aim at reducing, or even eliminating, the use of sophisticated instrumentation and need for skilled workers [79]. These strategies improve the in-field deployability of POC tests. Sample pretreatment, in general, aims at purifying the target from other components, and its implementation on paper enables a significant reduction of handling steps compared to the widely used solid phase DNA extraction methods.

In general, paper surfaces have different chemical groups, such as hydroxyl and carboxyl groups, that can bind chemical reagents and biomolecules. There are various methods to immobilise molecules on paper, that Pelton *et al.* has summarised in four categories: (1) physical and (2) chemical immobilisation, (3) biochemical coupling and (4) bioactive pigments [80]. To contextualize this thesis, the following paragraphs offer a concise overview of (1) and (2). Physical immobilisation is represented by biomolecules adhering to the paper surface due to van der Waals and electrostatic forces [80]. Pure cellulose is a slightly anionic (with a low negative charge on its surface) and very hydrophilic material. Water-soluble cationic polymers can easily bind to cellulose, while anionic ones usually do not. Protein adsorption onto paper also depends on electrostatic interactions between cationic regions on proteins and anionic cellulose. Most filter papers used in laboratories are made of pure cellulose, however, some paper products that need to work when wet, *e.g.*, kitchen towels and coffee filters, are treated with wet-strength resins, such as PAE or polyvinylamine. PAE gives paper a net positive charge and can make both antibodies and DNA aptamers bind to cellulose. Therefore, pure cellulose weakly binds DNA aptamers and proteins, whereas paper with wet-strength resin might be a good substrate for biosensor immobilization. The fact that the cationic surface of treated cellulose can bind most biomolecules might make it necessary to use something to block non-specific binding, such as Tween 20 (non-ionic surfactant), albumin bovine serum (BSA), or casein. Due to the weak attachment of biomolecule, the simple physical immobilisation is not a reliable method. Chemical immobilization can also be used to bind biomolecules to paper surfaces through covalent bonds [80]. However, pure cellulose has limited options for direct bioconjugation, because its hy-

droxyl groups are not very reactive in water at low temperature. Therefore, to make cellulose substrates available for biomolecule immobilisation, paper activation might be necessary using small molecules or polymer that adds surface functional groups. This process is not very appealing for mass production of paper products with low-cost pathogen detection, because it involves several chemical steps.

In paper-based NAATs, for instance, NA extraction has been performed using untreated Whatman[®] Grade 1 filter paper (cellulose) [21] and Fusion 5 membranes (glass fibers) from Whatman[®] [81] exploiting the affinity of different charges between the membranes and DNA. Detection of proteins, NAs and chemical molecules is mainly based on the physicochemical features of nitrocellulose (NC) membranes, adsorption paper and glass fibers that are generally used to fabricate lateral flow assay (LFA) test strips [79]. Furthermore, various paper modification approaches have been developed to improve extraction efficiency, detection sensitivity and specificity [79]. For example, the efficiency of nucleic acid extraction using Whatman[®] Grade 1 filter paper was increased by treating the paper with cationic polymers, such as polyethylenimine (PEI) and chitosan [21]. DNA adsorption in Fusion 5 membranes was improved by modifying Fusion 5 fibers with chitosan polymer [82, 83].

Chitosan-functionalised paper. Chitosan is a non-toxic cationic polysaccharide, with an amino group pKa of 6.3-6.4. It is positively charged and soluble in weakly acidic solutions (for pH lower than 6.3-6.4) and negatively charged in alkaline solutions (pH above 6.3-6.4) [84]. Chitosan has a series of characteristic that makes it a promising polymer for functionalisation of paper in DNA extraction application (as also confirmed in [82, 85, 86]). Firstly, chitosan has shown to strongly interact with DNA through electrostatic forces while having a weak binding with protein in different applications [87,88]. This advantage facilitates, *e.g.*, the purification of DNA from other components in biological samples. Secondly, chitosan can rapidly release adsorbed DNA through the pH-induced deprotonation of an amine. Lastly, the pH of the charge change is low enough to not interfere with downstream processes. Therefore, when paper is functionalised with chitosan, DNA can be trapped in the presence of a weakly acid solution thanks to the interaction of opposite charges between the polysaccharide and DNA, and its release can be induced using a pH in the 8.5-9.0 range (as schematically indicated in Fig. 1.4) [85]. The so released DNA is in a PCR-ready state that can be further processed [87].

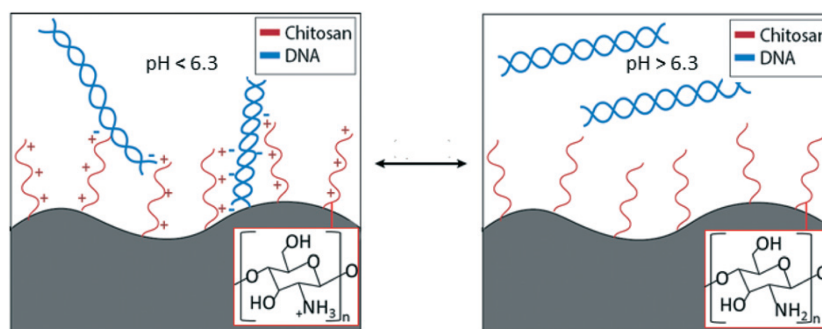


Figure 1.4: **Schematic of pH dependent capturing and releasing of DNA on chitosan-functionalised paper.** Chitosan is positively charged in weakly acidic solutions ($\text{pH} < 6.3$) and creates a high electrostatic interaction with the negatively charge DNA, facilitating its capture of functionalised paper. A pH above 6.3 induces a change of charges in chitosan that promotes the realise of DNA. Reproduced from [85], with permission of the rightsholder, Royal Society of Chemistry (Appendix A.5).

Studies demonstrated that cellulose paper strongly retains chitosan due to the opposite surface charges of the chitosan and cellulose [89]. Moreover, it has been studied that nitrocellulose adsorbs more chitosan than glass fiber [85], probably due to nitrocellulose higher surface area per unit volume. However, chitosan has a higher capacity for DNA in glass fiber than in nitrocellulose meaning that if a type of paper has a good chitosan binding ability, it does not necessarily facilitate DNA binding to the functionalised membrane. Lastly, DNA binding capacity of chitosan has shown to be equally good as other cationic polymers such as PEI and 3-aminopropyl trimethoxysilane (APTMS) in Grade 1 filter paper, but better than spermine. However, chitosan was the only one able to rapidly release the adsorbed DNA at pH 8.5-9, while the other polymers did not show the same characteristic [21].

Given the great potential of chitosan in binding DNA, future efforts will move towards understanding the role of chitosan in a paper-based extraction process and how this could be exploited in a potentially enclosed device.

1.4.2.3 Paper-Based POC NAATs

After the introduction of μPADs , various configurations of paper-based NAATs have been developed which incorporate in the device either NA purification, amplification and detection [15, 17, 18, 90], lysis and purification [91, 92], purification alone [85, 93], amplification and detection [19, 94, 95], or lysis, purification, amplification and detection [10–13]. A summary of the paper-based POC NAATs discussed is given in Table 1.1. It is worth mentioning that sample preparation is performed in all the devices presented in [10–13], but while in [10, 12] some auxiliary equipment is still required, such as

pipettes, incubators and heat blocks, the devices introduced by Tang *et al.* [11] and Lafluer *et al.* [13] need sample deposition only to run the assay. However, none of these sample-in-answer-out devices have been evaluated at the point-of-need with the potential final end-user.

Table 1.1: Summary of paper-based point-of-care nucleic acid amplification tests (NAATs) discussed in this chapter. The target pathogen, the type of amplification and paper membranes included in the devices are provided. The NAATs steps integrated inside the device (‘on-chip’) are also indicated. Abbreviations: PES, Polyethersulfone; LFS, Lateral flow strips; iSDA, Isothermal strand displacement amplification; LAMP, Loop-mediated amplification; HDA, Helicase-dependent amplification.

Target	Type of amplification	Types of paper	NAAT steps ‘on-chip’				Ref.
			Lysis	Purification	Amplification	Detection	
Methicillin-sensitive <i>Staphylococcus aureus</i>	-	Chitosan treated glass fiber		X			Byrnes <i>et al.</i> [85]
<i>Plasmodium falciparum</i>	-	Glass fiber, Chromatography paper		X			Kolluri <i>et al.</i> [14]
Amelogenin marker from human genomic DNA	-	Fusion 5	X	X			Gan <i>et al.</i> [91]
Hepatitis B virus (HBV)	-	Fusion 5, Whatman Grade 1	X	X			Tang <i>et al.</i> [92]
Human papillomavirus (HPV) 16	LAMP	PES, LFS		X	X	X	Rodriguez <i>et al.</i> [18]
Rotavirus A	LAMP	Glass fiber		X	X	X	Ye <i>et al.</i> [16]
<i>Plasmodium</i> species		Glass fiber, LFS		X	X	X	Reboud <i>et al.</i> [17]
<i>Escherichia coli</i> , and <i>Salmonella</i>	LAMP	Chitosan treated Whatman Grade 2		X	X	X	Trieu <i>et al.</i> [90]
SARS-CoV-2, and influenza A (H1N1)	LAMP	Whatman Grade 1		X	X	X	Manzanas <i>et al.</i> [15]
<i>Plasmodium</i> species	RPA	Whatman 1 Chromatography paper, blotter paper, glass fiber, LFS			X	X	Cordray <i>et al.</i> [94]
<i>Mycobacterium tuberculosis</i>	LAMP	Glass fiber			X	X	Kaur <i>et al.</i> [19]
<i>Streptococcus agalactiae</i> , <i>Streptococcus pneumoniae</i> , and <i>Staphylococcus aureus</i>	LAMP	PES, Glass fiber, cellulose fiber			X	X	Seok <i>et al.</i> [95]
<i>Escherichia coli</i>	LAMP	FTA, Ahlstromm Grade 226	X	X	X	X	Connelly <i>et al.</i> [10]
Methicillin-resistant <i>Staphylococcus aureus</i>	iSDA	Whatman Standard 17, LFS	X	X	X	X	Lafluer <i>et al.</i> [13]
<i>Salmonella typhimurium</i>	HDA	Fusion 5, Whatman Grade 1, LFS	X	X	X	X	Tang <i>et al.</i> [11]
HIV	LAMP	Whatman MF1, PES, LFS	X	X	X	X	Phillips <i>et al.</i> [12]

All these devices use different types of paper to perform NAATs and a thorough critical review of paper-based POC NAATs is available in the literature [96]. Paper-based NAATs have the potential to offer fast, simple, low-cost, and accurate diagnosis at the point-of-care, without requiring specialized facilities or equipment. However, the challenges of scaling up and distributing these technologies, as well as developing and validating new assays for emerging pathogens, remain significant [96]. To make these technologies ready for real-world applications, it is essential to design and develop them

with clear objectives, and collaborate with local stakeholders. A paper-based POC NAAT that is commercially viable and field-deployable is not yet available [32,96].

1.4.3 Beyond Paper-Based Diagnostic Devices

Paper is a very convenient platform, but it has some challenges in fluid manipulation and predictability compared to other microfluidic devices. Therefore, fully paper-based devices able to perform all the steps of NAATs are limited in number [37]. Thermoplastic materials have been used to translate conventional microfluidics from laboratory prototyping to industrial production and commercialization, as they offer good compatibility with manufacturing processes. In addition, their low-cost and fast fabrication processes can provide diagnostic access to low- and middle-income countries (LMICs). Some common thermoplastics used for microfluidic chips or cartridges are polymethylmethacrylate (PMMA) [97], cyclo olefin copolymer (COC) [98], polycarbonate (PC) and polystyrene (PS) [99], which can be processed by milling, laser-cutting and moulding techniques. Ongaro *et al.* [99] have also proposed a biodegradable thermoplastic, polylactic acid (PLA), as a more environmentally friendly alternative to the petroleum-based plastics usually employed for POC applications.

Hybrid devices that combines paper and microchips or paper and plastic-casings have been used to perform NAATs since the dawn of μ PAD studies [37]. This is shown also in the paper-based POC NAATs mentioned in Section 1.4.2.3, that mostly use the time flexible plastic films or plastic supports. In addition to the paper-based POC NAATs included in the most recent reviews by Magro *et al.* [37], Kaur *et al.* [32], and Sritong *et al.* [96], there are some interesting low-cost plastic-based microfluidic chips that integrate NAATs and visualise the results on LFSs [100–102]. NATflow is a novel test that can detect two types of HPV DNA (HPV16 and HPV18) in 45 minutes using LAMP [101] (Fig. 1.5A). The estimated cost of the test is less than US\$ 5 per sample and US\$ 1000 for the equipment, which includes a NATflow heater and a minicentrifuge. The test is still expensive and requires many manual handling steps, but it could be feasible at the district care level where technicians can perform the test [3]. It is unsuitable for use at the community level. Lu *et al.* [100] introduced an automated POC NAAT controlled with an Arduino board designed for the detection of tuberculosis in sputum samples (Fig. 1.5B). The device consists of a disposable cartridge that incorporates special pumps for fluid control, water electrolysis for pumping, ce-

ramic beads for sample pretreatment, and LFSs for result visualisation. To prevent the reaction chamber from being affected by external factors before and during the amplification process, the system employs a venting chamber and check valves that only allow one-way flow as effective mechanisms of isolation. Even though the cartridge is produced using injection moulding that is a scalable manufacturing method, the assembly of the device is far from being easily automatised. Another disadvantage of this system is that it is not fully automated as the sputum is disinfected and filtered outside the device itself, thus limiting its use by untrained personnel. A POC NAAT device that is easy to operate and only requires loading the sample on the chip and moving magnetic particles before visualising the results was introduced by Rodrigues-Mateos *et al.* [102] (Fig. 1.5C). The device was designed for the detection of SARS-CoV-2 infection and it was produced by machine milling of PMMA. The NAAT exploits the IFAST (Immiscible Filtration Assisted by Surface Tension) method, and uses magnetic particles that bind to NA molecules to lyse and purify the sample. The magnetic beads are dragged across aqueous-organic liquid interfaces in microchannels, thus transporting NA molecules, while unwanted substances are blocked by the immiscible phase. This technique eliminates the need for multiple washing steps and simplifies the extraction process. Once the magnetic beads have reached the last amplification chamber, reverse transcription LAMP is performed and a color change is produced that indicates the presence or absence of the targeted infection. The user-friendliness and rapidity of this device (1 hour turnaround) makes it suitable for low-resource settings at the primary healthcare where unskilled personnel might perform the tests. However, a possible limitation of the device is the difficulty in discerning the colour change. In a later iteration of the device, the results have been displayed on LFSs [103], but they were not yet incorporated into the device and required additional manual handling steps to open the amplification chamber and transfer the sample on LFSs. Moreover, the integration of dried LAMP reagents inside the device would enhance the effectiveness of the device at the point-of-care. Strategies for storing dry molecular reagents are discussed in Section 1.5.1.

1.5 Storing Reagents for DNA Detection

The limited shelf-life of reagents at ambient temperature represents one of the major barriers for the application of paper-based POC NAATs in low resource settings. The

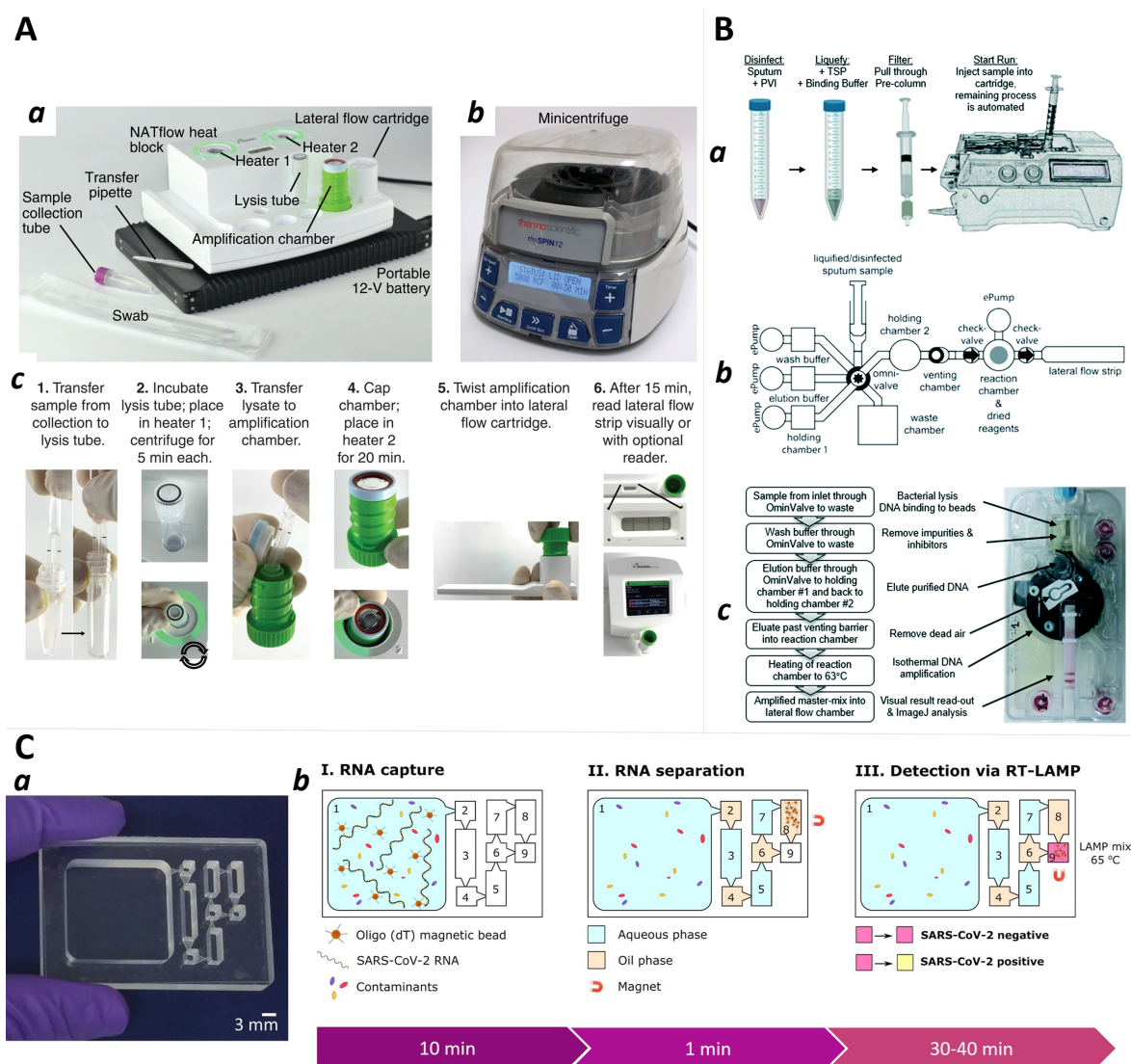


Figure 1.5: **Overview of low-cost plastic-based microfluidic chips that integrate nucleic-acid amplification tests (NAATs) and lateral flow strips result visualisation.** **A.** NATflow for the detection of HPV16 and HPV18. **a)** NATflow components and accessories. **b)** External equipment (minicentrifuge). **c)** Schematic of NATflow workflow. Reproduced from [101], with permission of the rightholder, American Association for the Advancement of Science (Appendix A.5). **B.** Automated diagnostic device for detection of tuberculosis in sputum samples. **a)** Overview of sample preparation. **b)** Schematic of the cartridge that includes pumps and valves. **c)** Schematic of NAATs inside the device. Reproduced from [100], with permission of the rightholder, Royal Society of Chemistry (Appendix A.5). **C.** IFAST reverse transcription LAMP device for SARS-CoV-2RNA detection. **a)** Photograph of the device. **b)** Schematic of testing workflow. Reproduced from [102], with permission of the rightholder, Elsevier (Appendix A.5).

instability of reagents is mainly associated with the presence of enzymes that are prone to denaturation and non-specific proteins binding. Processes facilitated by water are believed to promote enzyme denaturation and decrease their thermostability [104]. For instance, the presence of water increases the mobility of enzyme molecules and their unfolding rate [105].

To overcome the limitations of NA amplification methods associated with fragile biological enzymes, two main approaches have been adopted:

- Strategies to retain the original structural integrity and the activity of enzymes for an extended period of time in extreme environmental conditions, pH and detergents. Examples of these strategies are lyophilization and drying [19, 25, 106, 107] (Section 1.5.1), enzyme encapsulation in golden cages [108] and enzyme conjugation with polymers [109].
- Enzyme-free strategies for NA amplification, such as catalyzed hairpin assembly (CHA) [110], hybridization chain reaction (HCR) [111] and DNAzymes [112, 113] (Section 1.5.2).

1.5.1 Techniques to Store Reagents in Extreme Environmental Conditions

Several techniques have been investigated to stabilise reagents containing proteins over the long term and these storage strategies can vary substantially [114]. However, for the majority of NA amplification reagents, dry storage is preferred to liquid storage because of the negative effects of water. Furthermore, dry storage is advantageous in terms of in-field applicability of POC devices because it simplifies their design and fabrication procedures. Therefore, one of the main challenges in developing POC NAAT devices is to find strategies to store reagents in a ready-to-use format, where reagents are rehydrated directly at the time of use, that can ensure robust and reproducible device function over the long term and in different environmental conditions.

Several techniques to store-dry reagents have been used in POC NAATs application, but the two most common ones to stabilise pre-mixed LAMP reagents are freeze-drying and drying by concentration or desiccation (Fig. 1.6). All strategies utilise additives like sugars to stabilise enzymes during the drying process and successive storage. Indeed, sugars have been proven to stabilise proteins by hindering denaturing conformational movements [115]. Generally, disaccharides are better at forming tight molecular packing around proteins and restrict local mobility, whilst polysaccharides can reduce global mobility more efficiently [115]. Trehalose is the most common disaccharide used to store-dry LAMP reagents because it preserves the three-dimensional conformations of the reagents during drying by acting as a substitute of water around biomolecules thus preventing it from affecting the reagents [116].

However, freeze-drying strategies and drying procedures that involve centrifuges are experimentally laborious and require sophisticated equipment [19, 25]. In addition,

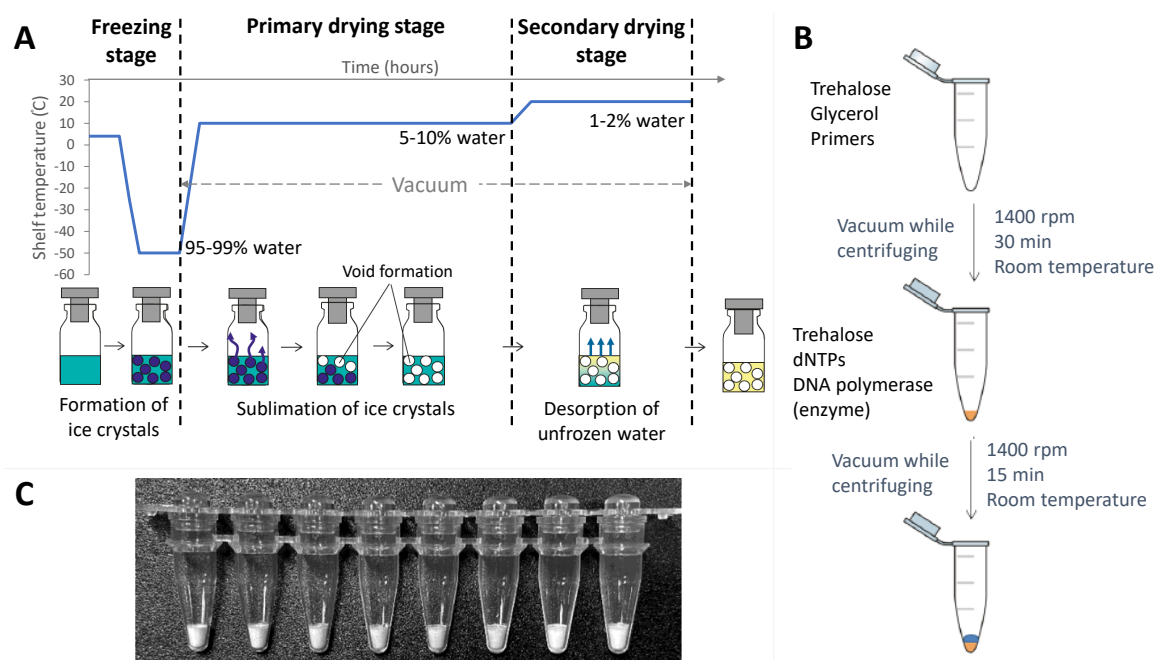


Figure 1.6: **Schematics of freeze-drying and drying of nucleic acid amplification tests reagents.** **A.** Schematic of freeze-drying. Freeze-drying removes water from a frozen material by sublimation of ice crystals. It consists of three main steps: freezing of the reagents, primary drying (sublimation) under vacuum and secondary drying (desorption) under vacuum. Adapted with permission from [117]. Copyright 2019, Hidenori Kawasaki et al. **B.** Drying by concentration in two steps [25]. A mix containing primers, trehalose (sugar) and glycerol was concentrated for 30 min. On top of this dried pellet, a mix containing dNTPs, DNA polymerase and trehalose was added and concentrated for 15 min. Adapted with permission from [25]. Copyright 2019, J. García-Bernalt Diego et al. **C.** Dried pellets that are obtained both by freeze-drying or by drying. These stored dry reagents can be rehydrated at the time of need. Reprinted with permission from [118]. Copyright 2021, American Chemical Society.

freeze-drying is extremely costly due to the freezing procedure and variation of temperatures [106]. Therefore, other solutions for the preservation of LAMP reagents are recommended to ensure easy manufacturing of the devices and affordability to low-income countries.

Quite recently, pullulan has been used as a polysaccharide to encapsulate biomolecules and retain reagents reactivity. Pullulan is a natural polysaccharides from a yeast-like fungus [119] that is non-hygroscopic, thermally stable and biodegradable, and it forms oxygen impermeable solid films upon drying [119]. The film-forming property of pullulan has been used in diverse applications in the pharmaceutical and food industries [120, 121], and it was used for the first time as simple and inexpensive method for long-term stabilisation of enzymes by Jahanshahi-Anbuhi *et al.* [119] in 2014. The enhanced stability at room temperature provided by the pullulan-bioassay tablets was hypothesised to be due to the reduction of the molecular motion of proteins and the impermeability to molecular oxygen given by the tablets [122]. This way of encapsulating

reagents facilitates shipping and guarantees protection against chemical modification and thermal denaturation of reagents during shipping and storage [122]. Moreover, the ability of pullulan tablets to dissolve in aqueous solutions in seconds, without interfering with the final assay, makes it a valuable preservative to store reagents ‘on-board’, in a ready-to-use format. Creating pullulan tablets is easy, and it only requires to dissolve a pre-measured quantity of reagents in a solution containing pullulan and let the solution air-dry. Different pullulan solutions (5%, 10%, 15% and 20% w/t) have been investigated in their ability to preserve Taq DNA Polymerase (a commonly used enzyme in NAATs) and it was shown that concentrations of pullulan up to 10-12% provide better protection of the cast enzyme. On the other hand, concentrations of pullulan equal or higher than 20% increase the risk of losing samples during pipetting due to the high viscosity. Pullulan tablets protect labile reagents better than other sugar-glasses, such as dextran, and polymers, like polyethylene glycol (PEG) [122]. However, to increase the long-term stability of reagents that might be affected by oxidation processes, the production of pullulan tablets should be performed under nitrogen and dried under vacuum [122].

Successive studies have shown the possibility of using pullulan as a timing element that can spatio-temporally control events [123] if different reagents are premeasured and stored in a layered format. When creating layers, it is important to consider the fact that the thickness of pullulan films is directly correlated to the concentration of pullulan, and that the velocity of the releasing process is connected both to the films thickness and the concentration of pullulan [123].

A two-pills method that combines trehalose and pullulan has been recently suggested to store reagents for NAATs [26] (the chemical structure of trehalose and pullulan is provided in Fig. 1.7). The method for LAMP reaction consisted in creating two separate pills by mixing 10% w/t pullulan solution and 0.5 M trehalose with primers, deoxynucleotide triphosphates (dNTP) and DNA polymerase enzyme in one pill, and with amplification buffer and salts in the other pill. The two pills were rehydrated with water, fluorescent dye and the sample before performing the LAMP reaction. The results were promising and they showed no activity loss after 4 weeks of storage at room temperature. Moreover, two important observations from the study lead by Leung *et al.* [26] should be highlighted. Firstly, two separate pills were created in order to separate the DNA polymerase from salts because the salt in the pullulan film could be detrimental to the stability of molecules dried in it. Secondly, the application of a

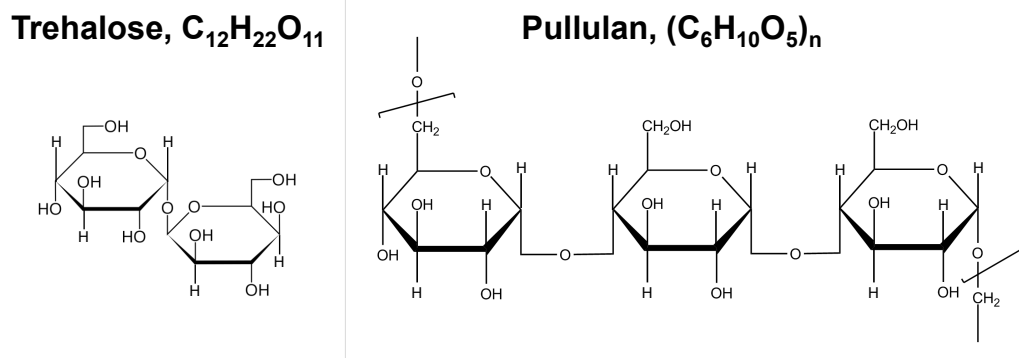


Figure 1.7: **Structural formulas of trehalose and pullulan in Haworth projection.** Trehalose is a homodisaccharide that consists of two glucose units linked together via an α -1,1-glycosidic linkage [124]. Pullulan is a natural polysaccharides derived from starch by *Aureobasidium pullulans* fungus. Pullulan consists of α -(1 \rightarrow 6) d-glucopyranose and α -(1 \rightarrow 4) d-glucopyranose monomers, forming a water-soluble, neutral linear polysaccharide with α -1,6-linked maltotriose residues [125]. Modified and reproduced with permission under public domain.

mixture consisting of trehalose (small disaccharide) and pullulan (large polysaccharide) combined the advantages of both a tight molecular packing (by the disaccharide) and a high physical stability (from the polysaccharide) [126].

The possibility of creating in a simple and inexpensive way, tablet-based assays able to stabilise labile bioreagents over the long term and in extreme environmental conditions could significantly improve diagnostic support in resource-limited settings. All the advantages and characteristics aforementioned of pullulan make it a valuable alternative to current freeze-drying techniques and a good preservative to investigate further for the creation of ready-to-use and thermally stable assay tablets. The use of pullulan opens the route for the development of a device where reagents for both sample preparation and amplification are stored in stacking layers. The layers containing reagents could be alternated with layers acting as delays, and the sequential dissolution of the layers would be triggered by the deposition of the biological sample. This strategy would reduce the user intervention in performing the NAAT and it could become accessible to resource limited settings. Future efforts will focus on developing effective strategies to store in pullulan-tablets those reagents that are currently used in the assay for the detection of *E. coli malB* gene, and on integrating the entire NAAT into an enclosed sample-to-answer device.

1.5.2 Enzyme-Free Amplification Strategies

The limitations associated with fragile biological enzymes surrounding the use of NAATs in POC devices and in low-resource settings could be overcome by enzyme-free amplification methods. These methods rely on single stranded NA networks that can be programmed to self-assemble and disassemble using the simple rules governing NA hybridization to cause signal amplification [127]. Example of NA circuits for molecular amplification are catalyzed hairpin assembly (CHA) [110] and hybridization chain reaction (HCR) [111], whereas DNazymes are an example of functional NAs able to catalyse signal-amplification reactions [112, 113]. These strategies have the great advantage of not requiring any perishable protein enzymes and, thus, the preservation of reagents under ambient storage condition is guaranteed by the enhanced thermal stability exhibited by oligonucleotides as opposed to enzymes. Other advantages of enzyme-free amplification methods are associated with their intrinsic modularity and scalability [127], and the easiness with which they can be concatenated [128, 129] and conjugated with different amplification procedures to improve sensing performance [130]. These methods have been used for NA detection [131, 132] and DNzyme- and CHA-based strategies have proven to be rapid and have equivalent sensitivity to NAATs in detecting bacterial pathogens [128]. More in detail, DNazymes are single-stranded DNA sequences with catalytic properties that have been extensively used in biosensing applications [133]. DNazymes mimic functions of protein enzymes and they can catalyze a diverse range of reactions such as RNA/DNA cleavage (an example is given in Fig. 1.8), RNA/DNA ligation and activities as peroxidases [134].

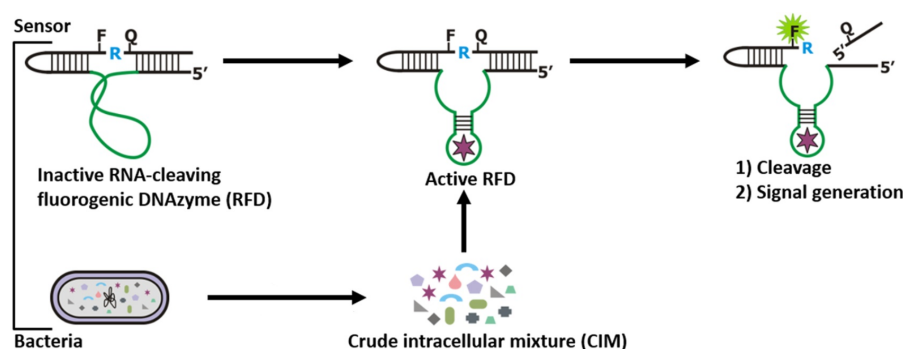


Figure 1.8: **Example of a RNA-cleaving DNzyme.** Schematic illustration of the action of a RNA-cleaving fluorescent DNzyme (RFD). The DNzyme fluoresces upon contact with the target(s) present in CIM that are released from the lysed bacteria. Once the inactive DNzyme comes in contact with the target(s), it cleaves the fluorogenic substrate to produce a fluorescent signal. Reproduced with permission from [135]. Copyright 2017, M. Monsur Ali et al.

CHA and HCR amplification methods rely on autonomous hybridization and strand-

displacement reactions. In particular, the basic principle behind CHA shows the target DNA (initiator) acting as a key that cyclically opens the corresponding hairpins without consuming the target (Fig. 1.9A). The generated double-stranded DNA (dsDNA) sequences are encoded with functional NA that promotes further reactions, e.g., fluorescent readout [132]. On the other hand, in HCR, the target initiates a serial autonomous cross-opening of hairpins that produce very long dsDNA nanowires [129] (Fig. 1.9B). For all the techniques, several different readouts have been applied for the visualisation

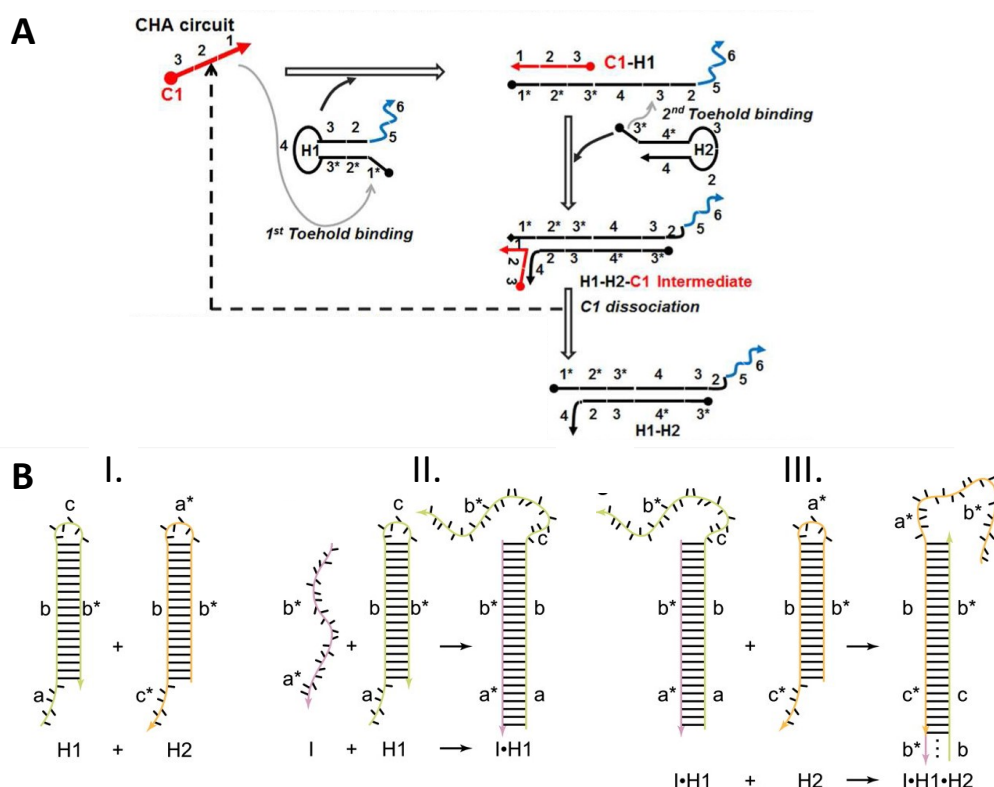


Figure 1.9: **Enzyme-free amplification methods.** H1 and H2 are harpins whose structure is always toehold-stem-loop. Numbers/Letters marked with asterisks are complementary to the corresponding toehold-unmarked number/letter. **A.** Mechanisms of catalytic hairpin assembly (CHA). Reprinted with permission from [136]. Copyright 2013, American Chemical Society. **B.** Schematic of linear of hybridization chain reaction (HCR). Reproduced with permission from [111]. Copyright 2004, National Academy of Sciences.

of the detected target including, for example, fluorescence, colorimetry, and chemiluminescence [132, 133, 137].

The translation of these methods onto paper devices is possible, however, most of the published paper sensors do not fulfil the “ASSURED” criteria [133]. Future efforts should focus on the integration of all the reaction modules into a single paper-based device, stretching from the raw sample pretreatment to the easy visualisation of the results, that is also able to detect multiple pathogens.

Given the advantages of enzyme-free amplification methods and of paper, future works could focus on the combination of the strengths of the two for the creation of POC diagnostic devices for low-resource settings. DNazymes have been integrated on paper for the detection of several diseases and by several groups [133], while works to visualise CHA results on lateral flow assays have been recently introduced by a few groups [138–140]. For instance, a biosensor that integrates a DNazyme and CHA reaction for the recognition of *E. coli* (as a model non-pathogenic organism) and signal amplification, such as the one introduced by Zhou *et al.* [128] could be investigated for full incorporation on paper. The possibility of integration of a paper-based DNA extraction method with ready-to-use dried reagents and an enzyme-free detection method has a great potential to become the future POC diagnostic device that fulfils “rEAS-SURED” criteria.

Chapter 2

Materials and Methods

In this chapter, the materials, methods and equipment used throughout the experiments are provided along with a description of the experimental procedure.

2.1 Bacterial Culture

Escherichia coli strain K12 was anaerobically grown in Luria-Bertani broth (Merck, Darmstadt, Germany) using a shaking incubator (Stuart[®], Cole-palmer Ltd., Eaton Socon, England) at 250 rpm for 20 hours at 30 °C. The bacteria culture concentration was measured using a Synergy[™] HT Multi-Mode Microplate Reader (BioTek[®] Instruments, Inc., Agilent, Santa Clara, California, United States).

The bacterial culture for the paper-based DNA extraction experiments was stored as follows: the bacterial culture was pipetted in 200 µL, 300 µL, 400 µL aliquots and the cells precipitated by centrifugation at 8000 g for 3 min at room temperature (RT); the supernatant was discarded and the formed pellets were stored at -20 °C until required. Upon use, the cells were suspended in either 200 µL, 300 µL, or 400 µL of 1X Phosphate buffer saline (PBS) depending on their initial aliquot.

When referring to ‘already purified DNA’ in the text, *E. coli* DNA was extracted using a magnetic-bead based method, MagaZorb[®] DNA Mini-Prep Kit (Promega Corporation, Madison, Wisconsin, United States), following the manufacturer’s instructions, and the DNA concentration was measured using NanoDrop[™] Lite Spectrophotometer (Thermo Fisher Scientific Inc., Waltham, Massachusetts, United States). Already purified DNA was used for comparative analysis and is considered the gold standard for the investigated applications.

2.2 Lysis Buffers

Nuclease-free water (NFW) was used to prepare all aqueous solutions. All reagents were purchased from Sigma-Aldrich (Sigma-Aldrich, Merck KGaA, Darmstadt, Germany) unless otherwise specified.

Different lysis buffers were used to lyse *E. coli K12* bacterial cells.

Extraction buffer # 2 taken from Zou *et al.* [21] with components: 800 mM Guanidine HCl (GuHCl), 50 mM Tris-HCl (pH 8), 0.5% Triton X100 and 1% Tween-20. A 2X concentration of extraction buffer # 2 was also used with components: 1.6 M GuHCl, 100 mM Tris-HCl (pH 8), 1% Triton X100, and 2% Tween-20.

An acidic version of extraction buffer # 2 was made for applications where chitosan is involved: 800 mM GuHCl, 50 mM MES (pH 5.5), 0.5% Triton X100 and 1% Tween-20. The final lysis buffer used was the one provided with the MagaZorb[®] DNA Mini-Prep Kit (Promega Corporation), further referred to as ‘Lysis buffer by the Magazorb kit’. The components of this proprietary buffer are not known. However, a patent associated to the beads-based extraction kit [141] suggests that the buffer contains: 50 mM Tris-HCl (pH 6.3), 50 mM EDTA, 6 M GuHCl, 6 M Urea, 10 mM Calcium Chloride, and 10% Tween-20. The safety data sheet provided with the kit further suggests the presence of sodium dodecyl sulphate (SDS) in the lysis buffer, however, the quantities are not specified.

2.3 Filter Papers

Various filter papers were purchased from Cytiva (GE Life sciences, Chalfont St Giles, Buckinghamshire, UK): Whatman[®] Grade 1, Grade 3, and Grade 470 filter paper; glass microfiber filters (GF/DVA); cotton linter filters (CF4, CF5); and Fusion 5. Silica membranes were obtained from Biocomma Ltd (Biocomma Ltd, Longgang Dist, Shenzhen, China).

The properties of each type of paper are listed in Table 2.1. Grade 1 and 3 have different particles retention sizes (11 μm for Grade 1, 6 μm for Grade 3), thicknesses (180 μm Grade 1, 290 μm Grade 3), and wet strengths (higher in Grade 3 than in Grade 1), but they both have negative surface charges [21]. Glass microfibers have positive surface charges [21].

Before use, all filter paper variants were cut with different diameter dimensions, ranging

from 3 mm to 6 mm, using a hole puncher (Biopsy punch, Kai Medical, Kai Corporation and Kai Industries co., ltd., Manchester, England).

Table 2.1: **Properties of different types of paper tested [142].**

Product	Material	Thickness (μm @ 53 kPA)	Wicking rate (s/4 cm)	Water ab- sorption (mg/cm^2)	Suggested use and properties	Particle reten- tion size * (μm)	Nominal basis weight (g/m^2)	Price** (USD/ cm^2)
CF4	100% cotton liners	482	67.3	49.9	Blood separator/sample pad, absorbent pad.		Medium weight	0.0038
Grade 470	100% cotton liners	840	77	78	Blood separator/sample pad.			0.0031
CF5	100% cotton liners	954	63.3	99.2	Blood separator/sample pad.		Medium Weight	1.557
GF/DVA	Bound glass fiber	785	28.2	93	Blood separator/sample pad. Works well with saliva samples and can act as a blood separator.			1.713
Fusion 5	Not speci- fied	370	43.9	42.3	Blood separator/sample pad, conjugate re- lease.	2.3 [91]		1.496
Grade 1	Cellulose	180			Applications requiring medium retention and flow rate.	11	87	0.0009
Grade 3	Cellulose	390			Well suited for sample transport after collection. Increased wet strength compared to Grade 1.	6	185	0.0020

* At 98% efficiency, in liquid.

** Based on USD prices on 6 October 2022.

2.4 LAMP and qPCR reagents

2.4.1 Master mixes

Loop-mediated isothermal amplification (LAMP) experiments were performed using three types of master mixes. Two isothermal master mixes were purchased from OptiGene Ltd., ISO-004 and ISO-004-LYO (OptiGene Ltd., Horsham, England), and the second one from New England BioLabs (NEB, Ipswich, Massachusetts, United States). LAMP experiments using reagents purchased from NEB contained the following final concentrations: 1X Isothermal Amplification Buffer (20 mM Tris-HCl, 10 mM $(\text{NH}_4)_2\text{SO}_4$, 50 mM KCl, 2 mM MgSO_4 , 0.1% Tween-20 (pH 8.8 at 25 °C)), additional 4 mM MgSO_4 , 0.32 U/ μL Bst 2.0 WarmStart[®] DNA Polymerase, 1.4 mM Deoxynucleotide (dNTPs) Solution Mix and 0.5X LAMP Fluorescent Dye (Table 2.2). The concentration of these reagents have been optimised as shown in Chapter 4, Section 4.1.2. PCR experiments used Brilliant II SYBR[®] Green QPCR Master Mix from Agilent technologies (Agilent, Santa Clara, California, United States).

Table 2.2: **Volumes used to create 15 μL of master mix using reagents from New England Biolabs (NEB).** The concentration of reagents provided is the one in the final 25 μL LAMP reaction.

Component	Concentration in final LAMP reaction	Volume from stock [μL]
10X Isothermal Amplification Buffer	1X	2.5
dNTPs (10 mM)	1.4 mM	3.5
MgSO_4 (100 mM)	4 mM	1
Bst 2.0 (8000 U/mL)	0.32 U/ μL	1
50X LAMP Fluorescent Dye	0.5X	0.25
Nuclease-free water		6.75
Final volume		15

2.4.2 Synthetic and genomic DNA

Synthetic *E. coli malB* gene DNA (204 bp) was purchased from Eurofins Scientific (Eurofins Scientific, Luxembourg). Jurkat Genomic DNA for the detection of *BRCA1* gene was purchased from ThermoFisher Scientific (Thermo Fisher Scientific Inc.). The WHO International Standard for *P. falciparum* DNA [143] was purchased from the National Institute for Biological Standards and Control (NIBSC, UK's National Control Laboratory, South Mimms, UK).

The limit of detection (LOD) of rapid diagnostic tests (RDTs) and nucleic acid amplification assays for the detection of malaria is commonly expressed in parasites per microliter of blood (parasites/ μL). The conversion from international units per milliliter (IU/mL) provided by the WHO International Standard for *P. falciparum* (ISPf) [143] to parasites/ μL can be performed as follow. The ISPf comes in lyophilised form, and once resuspended it has a concentration of 10^9 IU/mL (as per manufacturer’s instructions). Padley *et al.* [143] reported that the lyophilised ISPf was prepared from a blood sample whose average parasitaemia was 9.8% (detected by light microscopy). Estimating a red blood cells (RBC) concentration of 5×10^6 RBC/ μL [144], the initial parasite concentration of the blood sample was 490,000 parasites/ μL (9.8% of red blood cells are infected). Therefore, 490,000 parasites/ μL is equivalent to 10^9 IU/mL. Table 2.3 gives the conversion from IU/mL to parasite/ μL for different concentrations of the initial sample.

Table 2.3: **Conversion table from international units (IU) per milliliter provided by the WHO International Standard for *P. falciparum* [143] to parasites/ μL .**

Concentration in IU/mL	Concentration in parasites/ μL
1.0E+09	4.9E+05
1.0E+08	4.9E+04
1.0E+07	4.9E+03
1.0E+06	4.9E+02
1.0E+05	4.9E+01

2.4.3 Primers

The primer sequences for LAMP detection of *E. coli*, *Plasmodium* species (*P. falciparum*, *P. vivax*, *P. malariae*, or *P. ovale*), and *BRCA1* gene are provided in Table 2.4. All primers were purchased from Eurofins Scientific. The primers were mixed together in a 5X primer mix or a 25X primer mix that required 5 μL to be added to each LAMP reaction. The concentrations associated with the primer mixes for LAMP are given in Table 2.5.

Real-time PCR was also used for the detection of *E. coli*. The two primers used for the PCR assay were based on the outer primer sequences developed for LAMP by Hill *et al.* [33], F3 and B3 (Table 2.4). The primers were mixed together in a 5X primer mix and 5 μL of this was added to each PCR reaction (Table 2.6).

Table 2.4: Primers sequences of LAMP assays.

Assay	Gene Target & Amplicon size	Primer Name	Sequence (5' to 3')	Reference
<i>E. coli</i>	malB, 204 bp	F3	GCC ATC TCC TGA TGA CGC	Hill <i>et al.</i> [33]
		B3	ATT TAC CGC AGC CAG ACG	
		LF	CTT TGT AAC AAC CTG TCA TCG ACA	
		LB	ATC AAT CTC GAT ATC CAT GAA GGT G	
		FIP	CAT TTT GCA GCT GTA CGC TCG CAG CCC ATC ATG AAT GTT GCT	
		BIP	CTG GGG CGA GGT CGT GGT AT TCC GAC AAA CAC CAC GAA TT	
<i>Plasmodium</i>	PgMt19, 220 bp	F3	TCG CTT CTA ACG GTG AAC	Polley <i>et al.</i> [144]
		B3	AAT TGA TAG TAT CAG CTA TCC ATA G	
		LF	CAC TAT ACC TTA CCA ATC TAT TTG AAC TTG	
		LB	TGG ACG TAA CCT CCA GGC	
		FIP	GGT GGA ACA CAT TGT TTC ATT TGA TCT CAT TCC AAT GGA ACC TTG	
		BIP	GTT TGC TTC TAA CAT TCC ACT TGC CCG TTT TGA CCG GTC ATT	
<i>BRCA1</i>	Homo sapiens DNA, chromosome 17 GenBank Accession #AP023477.1, 210 bp	F3	TCC TTG AAC TTT GGT CTC C	Tanner <i>et al.</i> [145]
		B3	CAG TTC ATA AAG GAA TTG ATA GC	
		LF	GCA GAT AGG CTT AGA CTC AA	
		LB	AGA ACC AGA GGC CAG GCG	
		FIP	ATC CCC AGT CTG TGA AAT TGG GCA AAA TGC TGG GAT TAT AGA TGT	
		BIP	GCA GCA GAA AGA TTA TTA ACT TGG GCA GTT GGT AAG TAA ATG GAA GA	

Table 2.5: **LAMP primer mixes for the detection of *E. coli malB* gene, *Plasmodium* species, and *BRCA1* gene.** The column ‘Conc. in final reaction’ provides the expected primers concentration in the final 25 μL LAMP reaction. Column ‘Conc. in primer mix’ gives the primers concentrations in the primer mix. Given that 5 μL of primer mix will be added into the final LAMP mix of 25 μL (see Section 2.5), the primer mix will undergo a 5-fold dilution in the final reaction. The volumes needed from the stock solutions allow to prepare 5 μL of primer mix. To avoid difficulties in pipetting small volumes, the primer mix solutions are usually created in larger batches.

Assay	Primer Name	Conc. in final reaction (μM)	5X primer mix		Conc. in final reaction (μM)	25X primer mix	
			Conc. in primer mix (μM)	Volume needed from 30 μM stock (μL)		Conc. in primer mix (μM)	Volume needed from 100 μM stock (μL)
<i>E. coli</i>	F3	0.2	1	0.167	1	5	0.25
	B3	0.2	1	0.167	1	5	0.25
	LF	1	5	0.833	5	25	1.25
	LB	1	5	0.833	5	25	1.25
	FIP	0.8	4	0.667	4	20	1.00
	BIP	0.8	4	0.667	4	20	1.00
	Nuclease-free water			1.667			0.00
<i>Plasmodium</i>	F3	0.1	0.5	0.083	0.5	2.5	0.125
	B3	0.1	0.5	0.083	0.5	2.5	0.125
	LF	0.6	3	0.500	3	15	0.750
	LB	0.6	3	0.500	3	15	0.750
	FIP	0.8	4	0.667	4	20	1.000
	BIP	0.8	4	0.667	4	20	1.000
	Nuclease-free water			2.500			1.250
<i>BRCA1</i>	F3	0.16	0.8	0.133	0.8	4	0.2
	B3	0.16	0.8	0.133	0.8	4	0.2
	LF	0.8	4	0.667	4	20	1.0
	LB	0.8	4	0.667	4	20	1.0
	FIP	0.64	3.2	0.533	3.2	16	0.8
	BIP	0.64	3.2	0.533	3.2	16	0.8
	Nuclease-free water			2.333			1.0

Table 2.6: **PCR primer mix (5X) for the detection of *E. coli malB* gene:** primer concentrations and volumes per reaction.

Primer name	Concentration of final PCR reaction (μM)	5X primer mix	
		Concentration of primer mix (μM)	30 μM stock Volume required (μL)
F3	0.2	1	0.17
B3	0.2	1	0.17
Nuclease-free water			4.66
Final volume			5

2.5 Real-Time LAMP Conditions

The real-time LAMP was performed in QuantStudioTM 3 Real-Time PCR System instrument (Applied Biosystems; Thermo Fisher Scientific Inc.). The thermal profile for the detection of *E. coli malB* gene was 66 °C for 60 cycles (equivalent to 60 minutes), whilst for the detection of *P. falciparum* and *BRCA1* gene it was 63 °C for 30 minutes. For all DNA targets, a melt curve stage at 95 °C for 15 s and 60 °C for 1 min was carried out. To ensure the target DNA was the one amplified, the melting temperature (T_m) indicated by the melt curve was observed. In all the experiments the melting curves for each assay were visualised in QuantStudioTM Design & Analysis Software (Applied Biosystems). Each amplicon was found only in single peak in the melt curves at a similar temperature as the positive control, unless otherwise specified.

The final LAMP reaction mix (25 μL total) contained 5 μL of primer mix (Table 2.5), 15 μL of isothermal master mix and 5 μL of sample.

All assays were run either in duplicate ($n = 2$) or triplicate ($n = 3$), as specified in the following chapters. In the no template controls (NTCs), 5 μL of NFW was added as the sample. NTCs and positive controls (PCs) with already purified DNA were always run. NTCs serve to make sure false positive results are not obtained in the absence of the target DNA, whereas PCs can serve to make sure the reagents have not deteriorated and are performing well. In the PCR tubes where paper discs were added (see Section 2.14), the final LAMP amplification mix was made of 5 μL of 5X primer mix, 15 μL of master mix from Optigene Ltd. (ISO-004), an additional 1 μL of green fluorescent dye (Green Fluorescent Dye, Cat No.: 30078-1; Cambridge Bioscience, Cambridge, England). The paper disc was added directly to this LAMP amplification mix, making a final volume of 21 μL . The PC was created by adding 4 μL of sample to the LAMP amplification mix.

2.6 Real-Time PCR Conditions

The real-time PCR (qPCR) was performed in QuantStudio™ 3 Real-Time PCR System instrument (Applied Biosystems; Thermo Fisher Scientific Inc.). The thermal profile used was the one suggested in the manufacturer’s instructions for Brilliant II SYBR® Green QPCR Master Mix (Agilent technologies): 95 °C for 10 minutes, 40 cycles at 95 °C for 30 seconds and 95 °C for 1 minute, and a melt curve stage at 95 °C for 15 s and 60 °C for 1 min. The melting curves were recorded to confirm the amplification of the target DNA, as already explained in Section 2.5.

The final qPCR reaction mix (25 µL total) contained 5 µL of 5X primer mix (Table 2.6), 12.5 µL of master mix, 6.5 µL of NFW and 1 µL of sample.

Each assay was run either in duplicate ($n = 2$) or triplicate ($n = 3$). NTCs used 1 µL of NFW instead of the sample, whereas, 1 µL of already purified DNA was added into the PCs.

2.7 Computation of Time-to-Positive Values in Real-Time LAMP and Cycle Threshold Values in qPCR

Raw fluorescence data was collected using the QuantStudio™ 3 Real-Time PCR System instrument, exported into Microsoft Excel 365 files and analysed in MATLAB®. The data was used to compute the time-to-positive (TTP) value during LAMP or the cycle threshold (Ct) value during qPCR. The second derivative of the fluorescence signal was calculated for each assay. The TTP and Ct values correspond to the time, or cycle, at which the maximum value of the second derivative is detected, as illustrated in Fig. 2.1. The sample was considered positive (amplified) if the maximum of its second derivative was greater than the maximum of the second derivative of the NTC. The inflection point derived from the second derivative of the amplification curve highlights the first increase in the reporter dye emission, *i.e.*, the largest change in fluorescence (green dashed-lines, Fig. 2.1A). If the fluorescent signal did not increase within 60 minutes in LAMP (or 40 cycles in qPCR), the sample was considered negative.

The MATLAB® script used is given in Appendix B.1. When the signal was particularly noisy, for example in the presence of additives such as pullulan, the implemented

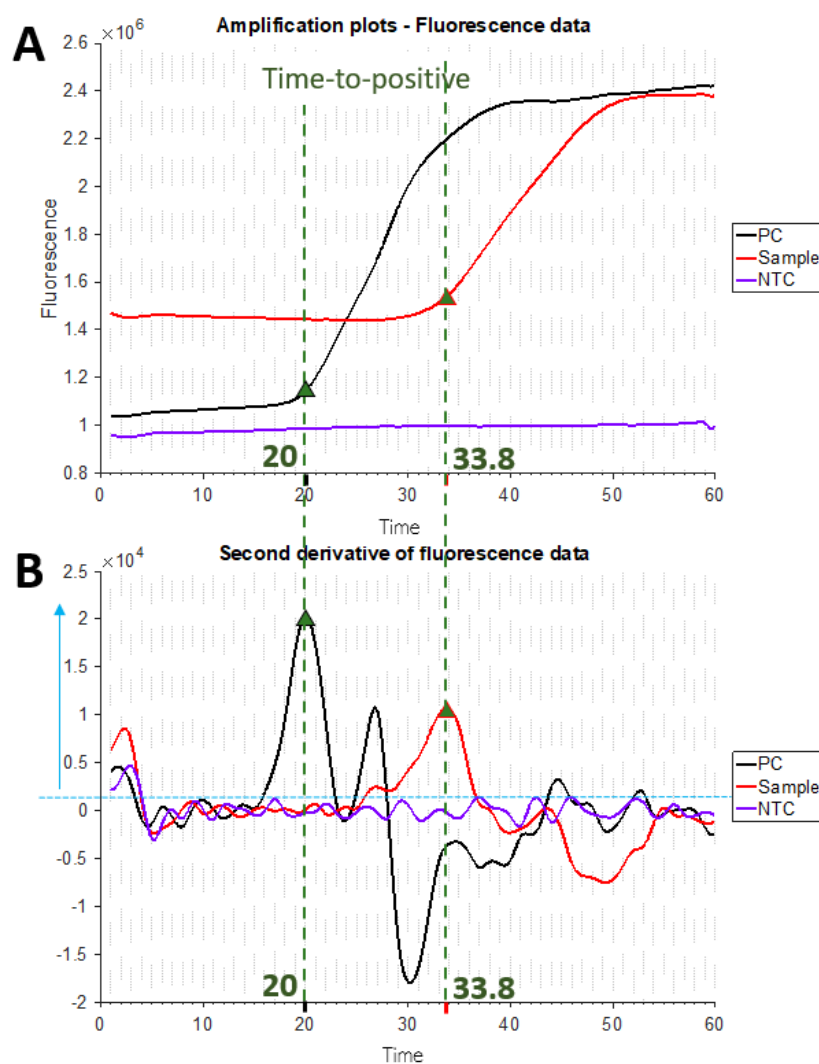


Figure 2.1: **Time-to-positive (TTP) value computation.** Example to show how the TTP values have been determined for each amplification curve. **A.** Amplification plot. The raw fluorescence data are plotted as a function of time. Three amplification plots are given: one for the NTC (purple line), PC (black) and one where the paper disc is added to the amplification mix (Sample, red line). **B.** Second derivative of the raw fluorescent data. The second derivative of the fluorescence was computed for each assay and its maximum value (max) was found (green triangles). The TTP was determined as the time at which the max of the second derivative of the fluorescence was found for each assay. The max of the second derivative was evaluated for each assay only if it had a greater value than the NTC second derivative max (area above the light blue dotted-line in B). The second derivative allows to find the inflection point of the amplification curve that highlights a first raise in the reporter dye emission, *i.e.*, the biggest change in fluorescence.

algorithm did not work well. The first peak of the second derivative of the fluorescent data corresponding to the inflection point could not be identified, but signal peaks corresponding to high signal variations were obtained instead. In these cases, the TTP (or CT) value was manually selected by analysing the second derivative peaks and selecting the time (or cycle) at which the first peak of the second derivative appeared.

2.8 Analytical Sensitivity of the Real-Time LAMP and qPCR Assays

Analytical sensitivity was examined for *E. coli malB* gene detection and *Plasmodium* species.

Analytical sensitivity was first evaluated using 10-fold dilutions of *E. coli malB* gene synthetic DNA ranging from 1×10^5 to 1 copies per LAMP reaction in LAMP and from 1×10^9 to 1 copies in qPCR. The sensitivity was also tested using extracted DNA from an original 10^8 CFU/mL *E. coli* K12 sample with subsequent 10-fold dilutions of the initially extracted DNA both in LAMP and qPCR reactions.

Analytical sensitivity of the *Plasmodium* LAMP assay was analysed using 10-fold dilutions of the WHO International Standard for *P. falciparum* DNA [143] from 10^4 IU/mL to 10^7 IU/mL.

Each condition was run in triplicate using the in QuantStudio™ 3 Real-Time PCR System instrument (Applied Biosystems; Thermo Fisher Scientific Inc.). The limit of detection (LOD) was determined as the lowest concentration of NA that consistently produced positive results (amplification) in all the replicates tested [146].

2.9 Statistical Analysis for Real Time LAMP and qPCR results

One-way ANOVA with Tukey-Kramer's post-hoc test was performed to compare the time-to-positive (TTP) in LAMP or cycle threshold (Ct) values in qPCR amongst the samples (for $n \geq 2$) and the positive control. The analysis of variance was performed using MATLAB® and its built-in functions *anova1* and *multcompare* (Appendix B.2). *Anova1* performs one-way ANOVA and tests the hypothesis that the different samples are drawn from populations with the same mean against the alternative hypothesis that the population means are not the same. *Multcompare* was used to perform a Tukey-Kramer's multiple comparison test and to understand which pair of samples were significantly different. A statistically significant difference between samples was chosen to be for p-value < 0.05 . The symbols associated with p-values in graphical representation are given in Table 2.7. TTP and Ct data is presented as mean TTP \pm standard deviation and mean Ct \pm standard deviation, respectively.

Table 2.7: Graphical symbols for p-values.

P-value	Symbol
$p \geq 0.05$	ns
$0.01 \leq p < 0.05$	*
$0.001 \leq p < 0.01$	**
$0.0001 \leq p < 0.001$	***
$p < 0.0001$	****

2.10 Conversion of DNA Concentration from ng/ μ L to copies/reaction

To convert the measured concentration of DNA (using NanoDropTM Lite Spectrophotometer, Thermo Fisher Scientific Inc.) from ng/ μ L to copy number in the final volume reaction, the ‘Calculator for determining the number of copies’ [147] was used. In this calculator, the users input the amount of the DNA template present, in ng, and the length of the template, in bp. The equation used assumes that the average weight of a base pair (bp) is 650 Daltons and it computes the number of copies of the template as follow:

$$\text{Number of copies} = \frac{\text{Template amount [ng]} \times \text{Avogadro's number [number/mole]}}{\text{Template length [bp]} \times (1 \times 10^9) \text{ [ng/g]} \times 650 \text{ [g/mole of bp]}} \quad (2.1)$$

with *Avogadro's number* = 6.022×10^{23} molecules/mole. The template amount was determined by multiplying the volume of the template DNA added to the final reaction mixture, *e.g.*, 5 μ L or 1 μ L, to the measured concentration of DNA in ng/ μ L. The synthetic *E. coli malB* gene DNA is 204 bp long. When using the extracted DNA from *E. coli* K12 bacterial culture, a length of 4,639,675 bp was considered as reported for *E. coli* K12 MG1655 by Lukjancenko *et al.* [148].

2.11 Lateral Flow DNA Detection Assay and Interpretation of Results

To assess amplification outcomes on lateral flow DNA detection strips (LFSs), fluorescein isothiocyanate (FITC) and biotin moieties were incorporated on the 5'-end of FIP and LF primers for the detection of *E. coli malB* gene detection, and of LB and LF primers for the detection of *Plasmodium* species and BRCA1 gene. The same in-

strument and real-time LAMP protocol described in Section 2.5 were used when the amplification outcomes were assessed on LFSs.

During amplification, the primers labelled with FITC and biotin are integrated into the double stranded DNA amplicons. The LFSs recognise the FITC and biotin complex that forms during amplification [149]. Fig. 2.2 illustrates the structure of LFSs, how to interpret the results and the underlying detection mechanism. The amplified product is deposited on the sample pad, and it moves along the LFS by capillary force [150]. The conjugation pad contains streptavidin coated gold nanoparticles that bind to the biotin in the amplified product. The amplified product keeps flowing towards the absorbent pad, and when it reaches the test line, the anti-FITC embedded in the test line captures the FITC within the amplicons. Therefore, the test becomes red due to the gold nanoparticles attached to the biotin and FITC complex in the modified LAMP DNA amplicons. The excess gold nanoparticles continue to move along the LFS and they are trapped at the control line by immobilised streptavidin, resulting in two red lines. If no amplicons with FITC and biotin complex are present (negative samples), only the control line turns red as the FITC and biotin molecules will bind to their respective targets on the strip.

LFSs from Ustar Biotechnologies Ltd. were used (U-Star Disposable Nucleic Acid Detection Strips, Type 3; Hangzhou, Zhejiang, P.R. China). To test the LAMP products on LFSs, 10 μ L of each sample were deposited on LFSs using pipettes after the incubation time. Then, 30 μ L of either water or the manufacturer's buffer (Ustar Biotechnologies Ltd.) were added onto the strip to let the sample flow through the test and control lines. After 10 to 15 minutes, the LFSs results were imaged.

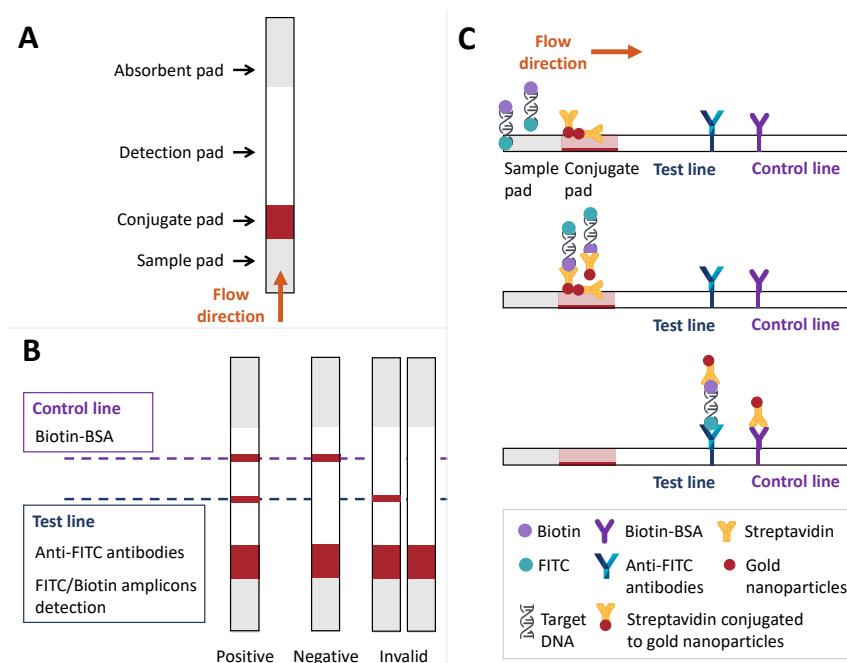


Figure 2.2: **Interpretation of test results on lateral flow strips (LFSs).** **A.** Schematic of the lateral flow detection strip. **B.** Interpretations of test results: *Positive* result indicates the presence of the target DNA in the sample and two lines appear; *Negative* result indicate the absence of the target DNA in the sample and only the control line appears; *Invalid*, the assay is invalid and no lines appear or no control line appears. **C.** Schematic of the binding of molecules and detection mechanism. If the target DNA is present in the sample, during the LAMP reaction amplicons are generated with both biotin- and FITC-labelled primers, as a complex bearing two ligands. The control and test lines contain immobilized Biotin-BSA and anti-FITC antibodies, respectively. The conjugate pad contains golden nanoparticles.

2.12 Colour Intensity of Test Bands on Lateral Flow Strips

Following amplification and deposition of the sample on LFSs, DNA test strips were imaged using the automatic settings of a HONOR (Huawei Technologies Co., Ltd., Shenzhen, China) camera, for digital records, and of a phone app CamScanner (INTSIG Information Co., Ltd., Shanghai, China) for scanning LFSs. Postprocessing and line intensity analysis from the scanned images was carried out using ImageJ (<http://imagej.nih.gov/ij/>). The raw images were converted into greyscale (16 bit, weighted RGB conversion -0.30, 0.59, 0.11). Grey tones were measured at the control and test line in addition to the LFS background to compute the normalised intensity as suggested by Lee *et al.* [151] (Eq. 2.2).

$$\text{Normalised Intensity} = \frac{I_{Test} - I_B}{I_{Control} - I_B} \quad (2.2)$$

Where I_{Test} , $I_{Control}$, and I_B are the grey values measured at the test, control line, and background, respectively. For negative controls and negative results, the normalised

intensity is expected to be as close as possible to 0, whereas positive LFS results are expected to have a very high normalised value.

2.13 Plastic Cassettes for Point-of-care Devices

Plastic cassettes of diagnostic devices were produced in the laboratory by laser cutting (LS3020 Desktop Laser, HPC Laser Ltd., Halifax, United Kingdom) poly(methyl methacrylate) (PMMA) slabs. The layout of the devices was designed using Fusion 360[®] (Autodesk) or CoreIDraw, and it was successively imported into the RetinaEngrave software (Full Spectrum Laser, Las Vegas, NV, United States) for laser cutting. 2, 3 and 4 mm thick PMMA slabs (Stockline Plastic, Glasgow, UK) were used for different purposes and cut at the calibrated speed and power (3.00 and 90.0 respectively for 2 mm, 2.00 and 100.0 for 3 mm, and 1.00 and 100.0 for 4 mm).

2.14 Paper-Based Protocol to Extract Genomic Material from Bacteria Present in Large Volumes

A fast method for the sample pretreatment of large samples that relies on cellulose filter paper and that is equipment-free has been developed. *Escherichia coli* was used as a proof-of-concept pathogen, and *E. coli malB* gene was the DNA target.

This section describes the protocol followed for the extraction of *E. coli* genomic DNA from a large sample (100 μ L) using a filter paper disc. Initial experiments were performed using Whatman[®] Grade 1 filter paper (GE Life Sciences), taking inspiration from the work by Zou *et al.* [21] (Fig. 2.3). The very first efforts focused on understanding if already purified *E. coli* DNA could bind onto a paper disc and if the paper disc could have been introduced directly into the LAMP reaction for real-time readings without affecting the fluorescence measures. After, the extraction procedure using Whatman[®] Grade 1 filter paper has been optimised in terms of lysis buffer and temperature, and DNA-paper contact time (DNA incubation). The optimisation was conducted by evaluating the developed method against a magnetic beads-based purification protocol (MagaZorb[®] DNA Mini-Prep Kit, Promega Corporation), and using time-to-positive (in minutes) or cycle number for comparative analysis. Further ex-

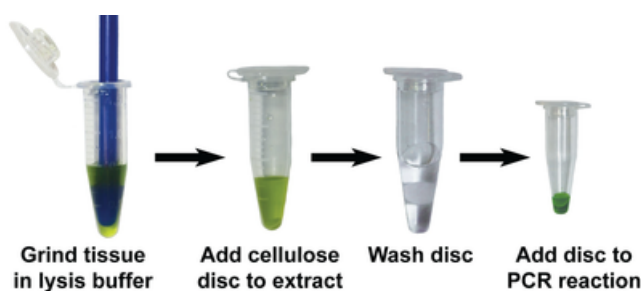


Figure 2.3: **Outline of the nucleic acid purification method performed by Zou *et al.* [21].** A tissue is ground in a 1.5 mL tube with a plastic pestle in the presence of extraction buffer. A 3-mm diameter Whatman[®] Grade 1 disc is transferred in the tube and nucleic acids are captured. The disc is then washed in 200 μ L 10 mM Tris buffer (pH 8) for one minute to remove contaminants present in the crude extract. The disc is transferred to a tube containing the amplification reaction and PCR-based amplification is performed without removing the disc from the tube. This procedure has been tried on a wide range of plant and animal tissues and the nucleic acid amplification was performed by LAMP too. Reproduced with permission from [21]. Copyright 2017 Zou *et al.*

periments to optimise the established procedure and improve its user-friendliness have involved reducing the number of steps and the time-to-positive of the assay by using different types of paper.

2.14.1 DNA Binding Investigation

The ability of a paper disc to bind and release DNA was first investigated. 3-mm diameter cellulose discs were cut from a piece of Whatman[®] Grade 1 filter paper using a hole puncher. 3 μ L of already purified *E. coli* DNA was pipetted onto a paper disc (Fig. 2.4A(i)) and, after 5 min of incubation at room temperature, the disc was transferred into a tube containing 200 μ L nuclease-free water (NFW) using tweezers (Fig. 2.4A(ii)). After one minute in NFW (acting as wash buffer), the cellulose disc was transferred into a LAMP amplification reaction in 0.1 mL PCR tubes (as described in Section 2.5, and in Fig. 2.4A(iii)). The optimization of incubation time for the DNA binding was done at different time intervals: 1, 5 and 10 minutes. DNA binding in cellulose paper is associated with the fluid transport through the paper matrix, which in turn is a function of the square root of time (Lucas-Washburn's equation, Eq. 1.1). The DNA incubation time was thus the first element investigated.

This first procedure was compared to a second one (referred to as “in tube”) that differs only in that the purified *E. coli* DNA was not pipetted onto a paper disc, but the paper disc was immersed in a tube where 10 μ L of DNA sample had been diluted in 90 μ L of NFW (Fig. 2.4B). After 5 min of incubation at room temperature (Fig. 2.4B(i)), the disc was transferred to the washing step as before (Fig. 2.4B(ii)). The “in tube” procedure was investigated to make sure that DNA binding to cellulose paper occurred

even when larger DNA samples were taken into account.

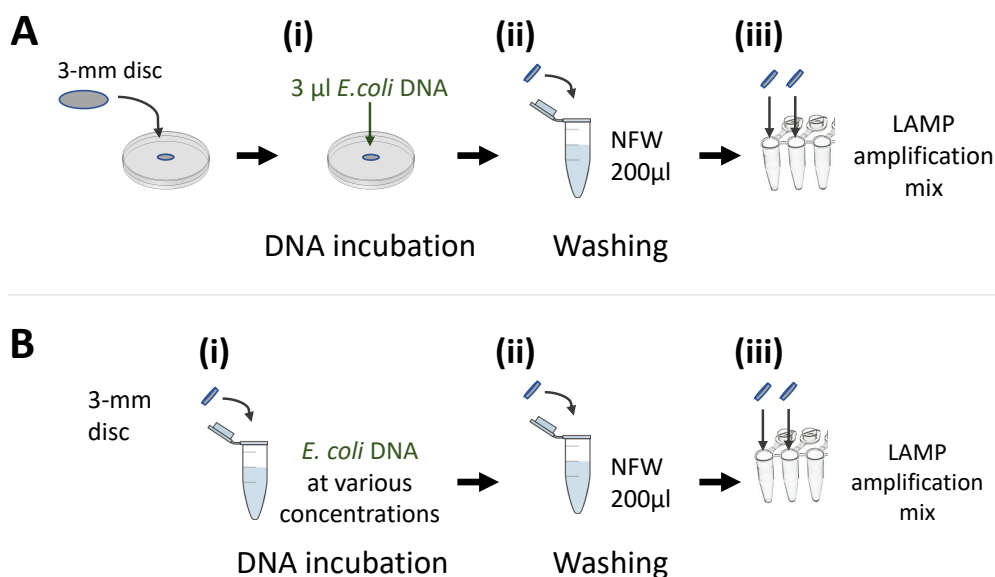


Figure 2.4: **Procedures to investigate DNA-paper binding properties.** Investigation of DNA binding onto Whatman[®] Grade 1 filter paper following two different procedures. **A.** First procedure: three main steps are involved. A paper disc is placed on a flat surface, such as a Petri dish. (i) Already purified DNA is pipetted onto the paper disc and incubated at room temperature for 5 min. (ii) The disc is transferred into a tube containing 200 µL NFW and incubated at room temperature for 1 minute. (iii) The cellulose disc is transferred into a LAMP amplification reaction in PCR tubes. **B.** “In tube” procedure: three main steps are involved. (i) A cellulose disc is transferred in a tube where already purified DNA is diluted in NFW. The disc is incubated at room temperature for 5 min and gently swirled. (ii) The disc is transferred into a tube containing 200 µL NFW and incubated at room temperature for 1 minute. (iii) The cellulose disc is transferred into a LAMP amplification reaction in PCR tubes.

2.14.2 DNA Extraction Procedures and Use of Different Papers

Two different DNA extraction procedures based on paper have been investigated in order to evaluate the feasibility of adding proteinase K to the chemical lysis during sample pretreatment. Proteinase K is used to perform enzymatic lysis and it is often used in combination with other types of lysis, *e.g.*, chemical lysis, to maximise the lysis efficiency of the targeted pathogen. The additional use of proteinase K usually aid the lysis step in case of pathogens that are difficult to lyse, making the procedure universal.

The ability to capture and release purified DNA was investigated using different types of paper for both the DNA extraction methods described in Sections 2.14.2.1, and 2.14.2.2. The filter papers were chosen based on their different characteristics (Section 2.3). 10^8 CFU/mL *E. coli* sample was obtained as described in Section 2.1, and used for

DNA extraction. A LAMP reaction followed each paper-based DNA extraction and the time-to-positive values of each sample were compared. The shorter the time-to-positive, the better performing was considered the procedure used.

2.14.2.1 DNA extraction based on Zou *et al.* (2017)

A schematic of the DNA extraction procedure followed is shown in Fig. 2.5A. 3-mm diameter discs were cut using a hole puncher and the extraction procedure in Fig. 2.5B was performed.

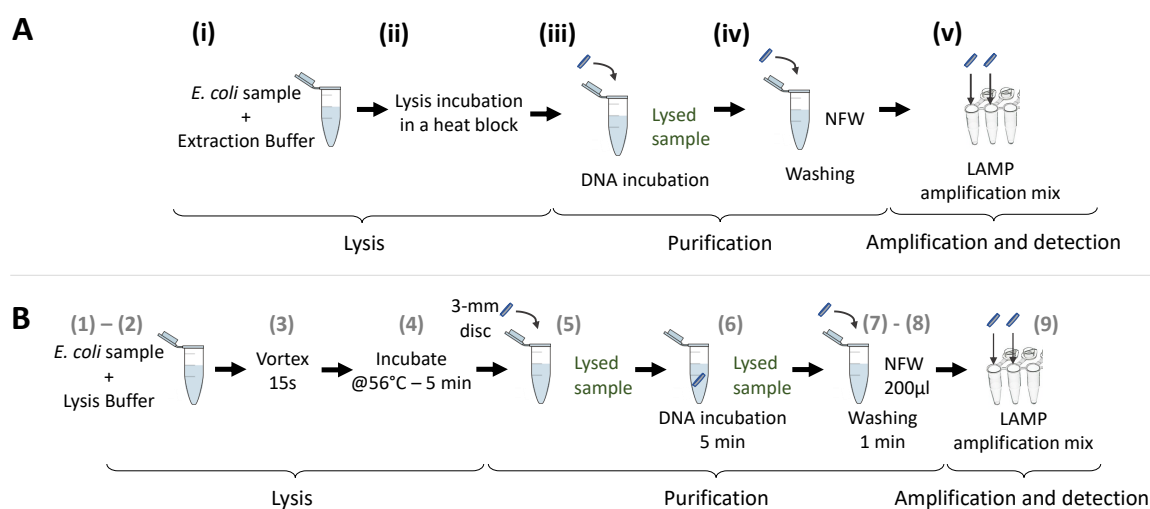


Figure 2.5: **Schematic of paper-based sample pretreatment procedure of *E. coli* bacterial sample.** **A.** General steps involved in the paper-based sample pretreatment: (i) the sample is mixed with the lysis buffer in a tube and vortexed; (ii) the mixture is incubated to allow for bacterial lysis; (iii) a cellulose paper disc is transferred in the tube containing the lysate, and the disc is incubated at room temperature and gently swirled to allow for the DNA to bind to the paper (DNA incubation); (iv) the disc is washed by transferring it in a tube containing nuclease-free water (NFW) and incubated at room temperature; (v) the cellulose disc is transferred into a LAMP amplification reaction in PCR tubes for further amplification and detection. **B.** Paper-based DNA extraction from *E. coli* bacterial culture. 9 steps involved in the paper-based extraction procedure: (1)–(2) 100 µL of sample is mixed with 400 µL of lysis buffer (at 1:5 ratio) in a tube, and (3) vortexed for 15 s. (4) The mixture is incubated in a heat block at 56 °C for 5 min. (5) A 3-mm paper disc is transferred in a tube that contains the lysate. (6) The disc is incubated at room temperature for 5 min and gently swirled. (7) The disc is transferred into a tube containing 200 µL NFW, and (8) incubated at room temperature for 1 minute. (9) The paper disc is transferred into a LAMP amplification reaction in PCR tubes for the amplification and detection steps. The procedure counts 6 less steps compared to the 15-steps gold-standard magnetic beads-based method (Promega Corporation), and 4 less steps than an “origami” magnetic beads-based method previously developed in my group (Reboud *et al.* [17]).

To increase the user-friendliness of the initially developed procedure, the feasibility of reducing the number of handling steps performed was investigated. First of all, the possibility of eliminating the washing step of the paper disc from the procedure shown in Fig. 2.5B was examined. Thus, after the 5 minutes incubation of the paper disc in the lysate, the disc was directly transferred into the LAMP amplification reaction

(going directly from step 6 to step 9 in Fig. 2.5B).

Secondly, the possibility of eliminating the heating lysis step was evaluated in order to avoid the need for a heat block or water-bath in the sample pretreatment phase (Fig. 2.6A). After combining the lysis and DNA incubation period together, the final procedure consisted of mixing a 100 μ L of resuspended bacterial cells pellet with 400 μ L of lysis buffer at 1:5 ratio (Fig. 2.6B). A 3-mm paper disc was immersed in the tube containing the sample and the lysis buffer, and it was incubated at room temperature for 6 min. After, the supernatant was discarded and the paper disc was washed with 600 μ L of NFW. After the washing step, the paper disc was transferred into a LAMP amplification reaction in PCR tubes for the amplification and detection steps. This paper-based DNA extraction procedure requires 7 total steps, 8 less compared to the gold-standard magnetic beads-based method (Promega Corporation), and 6 less than the “origami” beads-based procedure previously developed by Reboud *et al.* [17].

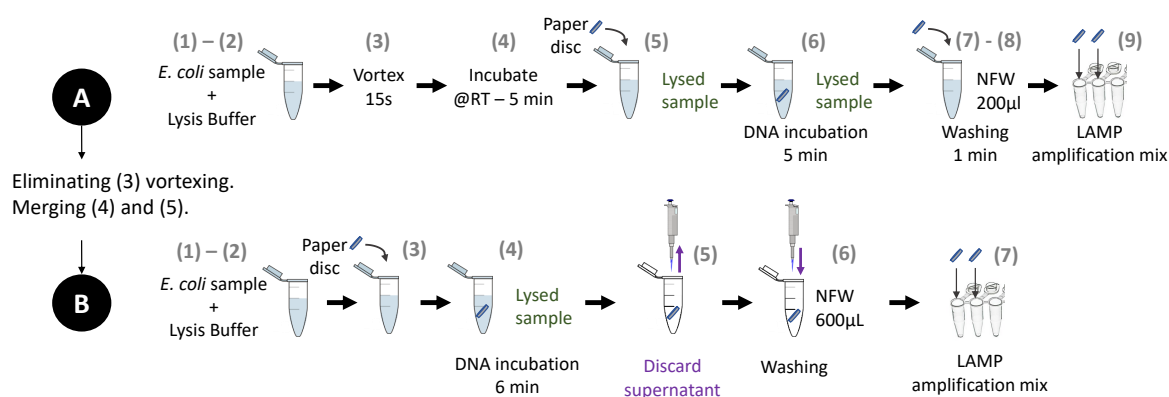


Figure 2.6: **Schematic of the reduction of steps for the paper-based DNA extraction from *E. coli* bacterial sample.** **A. 9-steps method:** shows the 9 steps involved in the paper-based extraction procedure when heating is not required. (1)-(2) 100 μ L of sample is mixed with 400 μ L of lysis buffer (at 1:5 ratio) in a tube and (3) vortexed for 15 s. (4) The mixture is incubated at room temperature for 5 min. (5) A 3-mm paper disc is transferred in a tube that contains the lysate using tweezers. (6) The disc is incubated at room temperature for 5 min and gently swirled. (7) The disc is transferred into a tube containing 200 μ L nuclease-free water (NFW) and (8) incubated at room temperature for 1 minute. (9) The paper disc is transferred into a LAMP amplification reaction in PCR tubes for the amplification and detection steps. The number of steps was further reduced to 7 as shown in **B. 7-steps method:** (1)-(2) 100 μ L of sample is mixed with 400 μ L of lysis buffer (at 1:5 ratio) in a tube. (3) A 3-mm paper disc is transferred in the tube containing the sample and the lysis buffer. (4) The disc is incubated at room temperature for 6 min and gently swirled. (5) The supernatant is discarded. (6) The paper disc is washed with 600 μ L of NFW. (7) The paper disc is transferred into a LAMP amplification reaction in PCR tubes for the amplification and detection steps.

After the optimisation of the procedure followed by LAMP, further optimizations were performed using qPCR. In order to do this the possibility of introducing an elution step before LAMP amplification was evaluated (as shown in Fig. 2.7). This elution step was merely used for quantification purposes when using qPCR (the details of qPCR

are given in Section 2.6). qPCR was used to investigate the performance of the DNA extraction procedure when using paper discs of different sizes, such as 3-mm, 5-mm and 6-mm diameter discs, and a different number of discs, *i.e.*, one, two or three discs per sample. Different types of papers were investigated too. The lower the Ct value, the better the ability to bind and release purified DNA was considered for the specific paper disc used. In the end, the possibility of adding 10 μ L of proteinase K to the

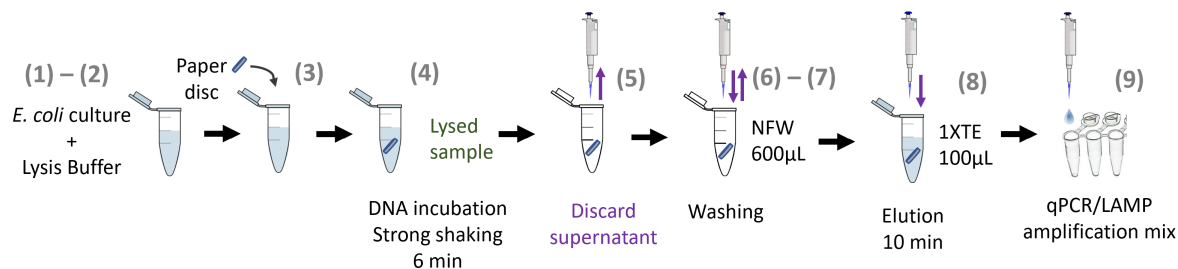


Figure 2.7: **Addition of an elution step in the DNA extraction procedure.** Steps followed for the paper-based DNA extraction procedure when an additional elution step is introduced: (1)-(2) 100 μ L of sample is mixed with 200 μ L of lysis buffer (at 1:3 ratio) in a tube. (3) A paper disc is transferred in the tube containing the sample and the lysis buffer. (4) The disc is incubated at room temperature for 6 min and gently swirled. (5) The supernatant is discarded. (6) The paper disc is washed with 600 μ L of NFW. (7) The NFW is discarded. (8) 100 μ L of 1X TE buffer (pH 8) are added in the tube containing the washed paper disc. The paper and the elution buffer are incubated at room temperature for 10 minutes. (9) 5 μ L and 1 μ L of eluant are added to a LAMP and qPCR amplification reactions respectively, in PCR tubes for the amplification and detection steps.

bacterial sample, in step (1)-(2) (Fig. 2.6B), was evaluated.

An analytical sensitivity test was carried out in order to understand the lowest detectable concentration of bacteria in the initial sample using the paper-based extraction described in Fig. 2.6B (7-steps method). The stored bacterial cells were resuspended as described in Section 2.1 to obtain a 10^8 CFU/mL sample. 10-fold serial dilutions in 1X PBS were conducted from the initial sample concentration ranging from 10^7 CFU/mL to 10^2 CFU/mL. DNA was extracted from each sample using the 7-steps method (Fig. 2.6B). Each condition was run in duplicate using the in QuantStudio™ 3 Real-Time PCR System instrument (Applied Biosystems; Thermo Fisher Scientific Inc.).

2.14.2.2 DNA extraction based on MagaZorb® Kit

When using the paper-based DNA extraction procedure described in Fig. 2.6B, the addition of 10 μ L of proteinase K to the sample inhibited further amplification. A second paper-based DNA extraction method was introduced in order to evaluate the possibility of introducing proteinase K during the lysis step. This method uses the reagents provided in the MagaZorb® DNA Mini-Prep Kit and follows the manual

instructions (with the right volume ratios), but rather than introducing magnetic beads during the binding step, a paper disc is used. No magnet is used during the washing step and this method is described in detail in Fig. 2.8.

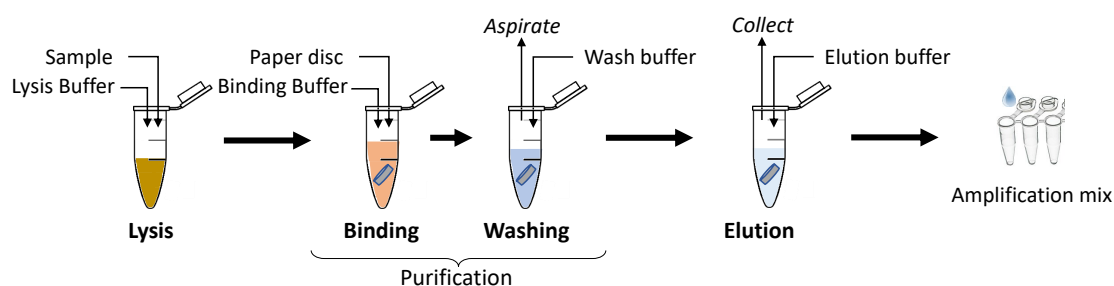


Figure 2.8: **Schematic of paper-based DNA extraction using MagaZorb[®] reagents.** Steps followed for the paper-based DNA extraction procedure that follows the manual instructions. **Lysis** (4 steps): (1) Add 100 μL of sample. (2) Add 100 μL of lysis buffer and (3) vortex 15 s. (4) Incubate at 56 $^{\circ}\text{C}$ for 10 min. **Binding** (6 steps): (5) Add 250 μL of binding buffer to the lysate and (6) vortex 15 s. (7) Add a paper disc to the mixture and (8) vortex for 15 s. (9) Incubate at room temperature for 10 min and (10) remove supernatant **Washing** (2 steps): (11) Wash the paper disc using 500 μL of washing buffer. (12) Remove supernatant. **Elution** (3 steps): (13) Add 100 μL of elution buffer and mix by swirling. (14) Incubate at room temperature for 10 min. (15) Remove disc from supernatant (eluate) and use the eluate for further amplification in the elution mix.

2.14.3 DNA Extraction Using Lysis Buffer Air-Dried on Paper Discs

To further reduce the handling steps during the paper-based DNA extraction described in Fig. 2.6B, the two lysis buffers were air-dried directly onto paper discs. Whatman[®] Grade 1, Grade 3, CF5, and GF/DVA were punched in 5-mm diameter discs. Two paper discs of each type were placed in the same well of a flat-bottom 96-well plate. 100 μL of lysis buffer were deposited onto the the paper discs and let them air-dry for one week before using the discs in the paper-based extraction procedure. The paper-based DNA extraction used in this scenario is described in Fig. 2.9. When using extraction buffer # 2 from Zou *et al.* [21], a 2X concentration was used (see Section 2.2). Therefore, 100 μL of 2X lysis buffer was deposited onto the discs. Experiments were carried out both by adding 100 μL NFW to dilute the 2X concentrated lysis buffer (in step (2), Fig. 2.9) and without the further addition of NFW.

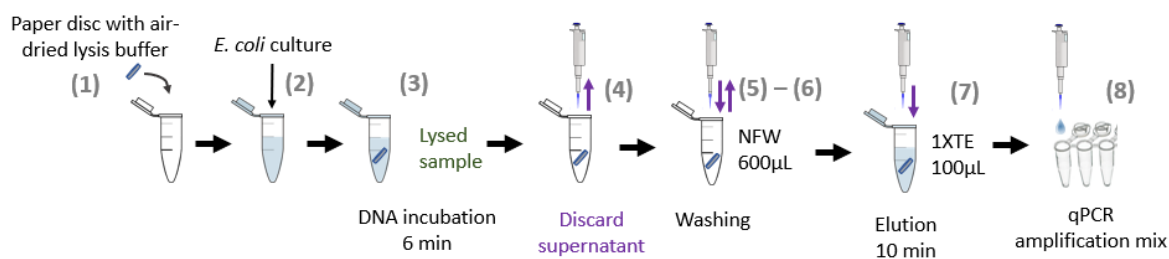


Figure 2.9: **Schematic of the paper-based DNA extraction with lysis buffer air-dried on the paper disc.** Steps followed: (1) The paper disc with lysis buffer dried on is transferred in an empty tube. (2) 100 μL of sample are added. (3) The disc is incubated at room temperature for 6 min and gently swirled. (4) The supernatant is discarded. (5) The paper disc is washed with 600 μL of NFW. (6) The NFW is discarded. (7) 100 μL of 1X TE buffer (pH 8) are added in the tube containing the washed paper disc. The paper and the elution buffer are incubated at room temperature for 10 minutes. (9) 1 μL of eluant is added to the qPCR amplification mix, inside PCR tubes for the amplification and detection steps.

2.14.4 Chitosan-Functionalised Paper

Chitosan-functionalisation has been suggested to improve the sensitivity of paper-based extraction procedures by increasing DNA capture and release action [82]. Therefore, the role of chitosan-functionalised paper was investigated in the developed 7-steps paper-based DNA extraction method.

Low and medium molecular weight chitosan were used. Solutions of 1% (w/v) chitosan were freshly prepared in 0.5 M acetic acid which was continuously stirred on a hot plate at 50 $^{\circ}\text{C}$. Stirring lasted about two hours, until solutions were completely clear, indicating the complete dissolution of the chitosan.

The first experiment focussed on understanding if amplification was possible when Whatman[®] Grade 1 paper was functionalised with chitosan. For this first experiment, Whatman[®] Grade 1 paper was cut into $1 \times 1 \text{ cm}^2$ squares and pretreated with a 1% (w/v) low molecular weight chitosan acidic solution following two slightly different protocols described below.

A. Chitosan-functionalisation of Whatman[®] Grade 1 with washing: $1 \times 1 \text{ cm}^2$ paper squares were incubated for 1 hour in a chitosan solution at room temperature. Thereafter, chitosan-functionalised paper was dried at room temperature for 1 hour. Each paper square was washed three times with 200 μL with nuclease-free water, and dried at room temperature.

B. Chitosan-functionalisation of Whatman[®] Grade 1 without washing: this protocol differs from A for the fact that the paper squares are not washed three times but are directly allowed to dry at room temperature.

Regardless of the protocol used for treating paper, 3-mm diameter discs were cut from

the chitosan-functionalised $1 \times 1 \text{ cm}^2$ squares and the procedures in Fig. 2.6B was followed. Three 3-mm discs were immersed in the same biological sample ($n = 1$) and placed in three separate PCR tubes (three technical replicates) to perform LAMP. When using chitosan-functionalised paper, the bacterial lysis was performed using an acidic buffer with 50 mM MES (pH 5.5) instead of 50 mM Tris-HCl (pH 8), to make sure that the chitosan had positive charges when in contact with DNA.

Successively, the ability to enhance the capture and release of DNA on chitosan-functionalised Fusion 5 paper that had been previously plasma-treated was investigated, as suggested by Gan *et al.* [82] and Bengtson *et al.* [86]. Fusion 5 paper was cut into $5 \times 2 \text{ cm}^2$ squares and plasma cleaned for 2-3 minutes on each side. The Fusion 5 paper was then incubated overnight in a 1% (w/v) chitosan (medium molecular weight) acidic solution at room temperature. Thereafter, chitosan-functionalised paper was washed with nuclease-free water, and stored at room temperature. The 7-step paper-based DNA extraction procedure with the elution step was carried out as shown in Fig. 2.7. 5-mm diameter discs were hole-punched from the chitosan-functionalised $5 \times 3 \text{ cm}^2$ squares of Fusion 5 and a procedures similar to the one in Fig. 2.7 was followed. Instead of 100 μL of bacterial sample, 100 μL of already purified DNA ($\sim 1 \text{ ng}/\mu\text{L}$) in 1X TE buffer was used. The acidic lysis buffer (pH 5.5) containing 50 mM MES ensured that the chitosan had positive charges when in contact with DNA. Therefore, 100 μL of already purified DNA were mixed with 200 μL of the acidic lysis buffer, and a 5-mm disc of the pretreated Fusion 5 paper was immersed in the solution for 6 min at room temperature. The supernatant was then removed and the disc was washed with 600 μL of MES buffer (pH 5.5). 100 μL of 1X TE elution buffer (pH 8) was used for eluting the DNA from the paper disc, for 10 min at room temperature, before performing LAMP. The same procedure, with the same acidic buffers, was followed using Whatman[®] Grade 3 paper for comparison. Time-to-positive values were used for comparative analysis and the method was assessed against a magnetic beads-based DNA extraction procedure (MagaZorb[®] DNA Mini-Prep Kit, Promega Corporation), following the manufacturer's instructions with the adjusted volume ratio.

2.15 Techniques for easy on-board-storage of molecular reagents at room temperature

This section describes the strategies investigated to ease the shipping and storage of molecular reagents through the elimination of cold chain and retention of activity in extreme environmental conditions. For this purpose, pullulan ($M_n = \sim 200$ kDa, Polysciences Inc., Warrington, PA) and trehalose (D-(+)-trehalose dihydrate, Sigma-Aldrich) were used as preservatives for different LAMP reagents.

Pullulan and trehalose were dissolved at different concentrations in various liquid components of the LAMP reagents, and solid tablets were created as described in Fig. 2.10. Tablets were then stored either at room temperature or at 35 °C. Upon use, they were transferred into an Eppendorf tube and resuspended with the corresponding volumes to obtain a final LAMP reaction mix of 25 μ L.

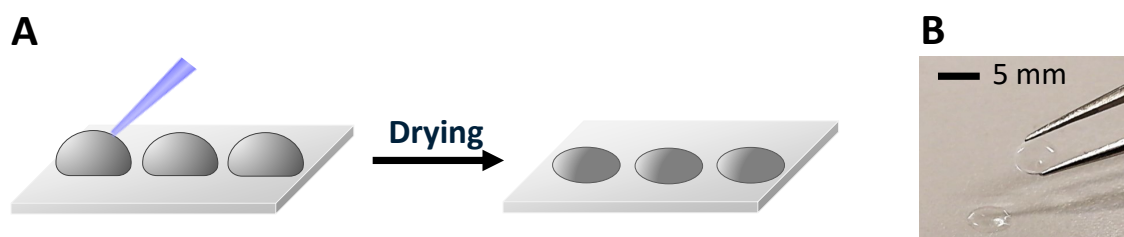


Figure 2.10: **Disc-shaped pullulan films.** **A.** Schematic of the pullulan solution drying process. Pullulan was dissolved into aqueous reagents. Once fully dissolved, the solution containing pullulan was pipetted in droplets on the non-sticky side of an adhesive film (MicroAmpTM Optical Adhesive Films, Applied BiosystemsTM, Thermo Fisher Scientific Inc.) attached to a Petri dish. After drying, the droplets formed a rigid disc-shaped tablet that could be peeled off the drying substrate with the help of tweezers. The procedure was first reported by Jahanshahi-Anbuhi *et al.* [123]. **B.** Example of a dried pullulan tablet that can be manipulated with tweezers.

To evaluate the stability of pullulan as a matrix for storing LAMP reagents, pullulan tablets were first prepared with various amplification components, such as primer mix, DNA polymerase, and isothermal amplification buffer. The performance of these tablets stored for varying amounts of time was tested and compared to the liquid LAMP assay stored under optimal conditions (at -20 °C). Then, the addition of trehalose was evaluated, and the effect of shipping the pullulan-trehalose tablets to a field site under uncontrolled conditions and returning them to the UK laboratory for analysis was also assessed. Finally, the solid-formed tablets were stored inside a POC device that was shipped for a field-trip in Kocoge (Tororo), Uganda.

2.15.1 Molecular Reagents Stored in Pullulan and Trehalose Tablets

Pullulan was chosen as a preservative because it is a non-hygroscopic, thermally stable, and biodegradable polysaccharide able to form tablets upon drying [73]. Therefore, pullulan can store reagents in a solid and ready-to-use format that could be easily integrated inside a POC device.

LAMP was performed using the master mixes indicated in Section 2.4.1, and the final LAMP reaction mix (25 μL) contained 15 μL of an isothermal master mix, 5 μL of primer mix, and 5 μL of DNA template. Pullulan tablets were resuspended in nuclease-free water (NFW) for their corresponding volume in the reaction, *i.e.*, pullulan tablets containing only primer mix were resuspended with 5 μL of NFW in each LAMP assay. The real-time LAMP was performed with the thermal profiles described in Section 2.5, but when pullulan tablets were used, the reaction time was increased to 120 minutes for all the targeted DNA sequences.

The concentrations of synthetic *E. coli malB* gene DNA template tested were 10^{-4} , 10^{-5} , 10^{-6} , and 10^{-7} ng/ μL . The concentrations of WHO International Standard for *P. falciparum* DNA used were 10^6 , and 10^5 IU/mL. 10^{-7} ng/ μL of *E. coli malB* gene DNA and 10^5 IU/mL of *P. falciparum* DNA are the limit of detection of the liquid assays when reagents are stored in optimal conditions at -20 °C (as shown in Chapter 4).

2.15.1.1 Molecular Reagents Stored in 10% (w/v) Pullulan Solutions

Pullulan tablets with a 10% (w/v) concentration were created for the detection of *E. coli malB* gene. The primers sequences used for this are given in Table 2.4. Tablets containing primers for LAMP were made by preparing a 5X primer mix (as described in Table 2.5) and by adding 0.7 mg of pullulan to 7 μL of the 5X primer mix. Pullulan tablets were created also for detection on LFSs. The same volumes were used with labelled primers, FIP-FITC and LF-biotin. To avoid difficulties in measuring small amounts of pullulan, the pullulan-primer mix solution was created in larger batches. The final concentration of primers in the solution was 5 times the concentration of primers in the final 25 μL reaction. 7 μL droplets of the mixture were deposited on a Petri dish as explained in Fig. 2.10. The Petri dish was covered with aluminium foil to minimise exposure to light and placed in an oven at 35 °C for drying and storage. Tablets containing the master mix were made by mixing 20 μL of ISO-004-LYO with

2 mg of pullulan. Here again 20 μL was deposited onto a Petri dish, covered with aluminium foil and stored at 35 $^{\circ}\text{C}$. The droplets dried and they formed tablets that were transferred into 0.1 mL qPCR tubes using tweezers at the time of use. 7 μL of the pullulan-primer mix solution, rather than the usual 5 μL , and 20 μL of the pullulan-master mix solution, rather than 15 μL , were prepared to account for possible liquid losses during pipetting caused by the high viscosity of the pullulan solution [119]. Each pullulan-primer mix tablet was resuspended in 5 μL of NFW, 5 μL template, and 15 μL of ISO-004 master mix, whilst each tablet containing ISO-004-LYO was resuspended with 15 μL of the proprietary resuspension buffer supplied by OptiGene Ltd., 5 μL of primer mix (5X) and 5 μL of DNA template. The real-time LAMP reaction was performed as explained previously, and the reactions containing pullulan tablets were compared with the LAMP reagents stored in optimal conditions at -20 $^{\circ}\text{C}$ until use. With regards to the pullulan tablets containing ISO-004-LYO, their performance over time was compared also with ISO-004-LYO freeze-dried and stored in the same conditions. A non-disclosure agreement was signed with OptiGene Ltd., and the advised freeze-drying procedure was carried out in a Labconco FreeZone Triad Benchtop Freeze Dryer (VWR International Ltd., Avantor Inc., Radnor Township, Pennsylvania, United States) [17]. Aliquots of 15 μL of ISO-004-LYO in 0.1 mL qPCR tubes were created, and the freeze-drying process was completed in 24 hours. Upon use, the freeze-dried LAMP pellets were resuspended with 15 μL of resuspension buffer (proprietary composition supplied by OptiGene Ltd.), 5 μL of primer mix and 5 μL of *E. coli malB* gene DNA template.

The tablets were stored for up to 54 days and the TTP values were compared across different storage conditions to evaluate the stability of reagents over time. TTPs were used to assess the differences in amplification times and the reduction in limit of detection due to storing reagents in pullulan tablets.

2.15.1.2 Molecular Reagents Stored in 10% (w/v) Pullulan and 0.5 M Trehalose

The addition of trehalose to pullulan in the creation of tablets was investigated to guarantee long-term stability of LAMP reagents. LAMP reagents for the detection of the *E. coli malB* gene were stabilised in tablets containing 10% (w/v) pullulan and 0.5 M trehalose. The potential degradation of FITC and biotin labels over time,

that could limit colorimetric detection on LFSs, was investigated by creating pullulan tablets containing only the labelled primer mix. Two concentrations of primers were used in this experiment: the same concentration used when reagents are stored at $-20\text{ }^{\circ}\text{C}$ (5X primer mix, Table 2.5), and 5 times that concentration (25X primer mix, Table 2.5). Pullulan tablets containing 5X labelled primer mix were prepared as explained in Section 2.15.1.1. A single pullulan-trehalose tablet containing 25X labelled primer mix was made by adding $6.429\text{ }\mu\text{L}$ of the primer mix to $2.250\text{ }\mu\text{L}$ of trehalose (2 M), $0.321\text{ }\mu\text{L}$ of NFW and by adding 0.9 mg of pullulan in a total volume of $9\text{ }\mu\text{L}$. The 25X labelled primer mix for each tablet was made by mixing $0.321\text{ }\mu\text{L}$ F3 primer (100 μM), $0.321\text{ }\mu\text{L}$ B3 primer (100 μM), $1.286\text{ }\mu\text{L}$ FIP-FITC primer (100 μM), $1.286\text{ }\mu\text{L}$ BIP primer (100 μM), $1.607\text{ }\mu\text{L}$ LF-biotin primer (100 μM), $1.607\text{ }\mu\text{L}$ LB primer (100 μM). Larger batches were made to avoid pipetting small volumes and measuring small amounts of pullulan. $9\text{ }\mu\text{L}$ were placed on an adhesive film on a Petri dish and exposed to air-flow in a fume cabinet to accelerate the drying process (about 1 hour). The Petri dish was then wrapped with aluminium foil to protect the tablets from light and kept at $35\text{ }^{\circ}\text{C}$ for later use. When needed, each tablet was moved to a 0.1 mL qPCR tube with forceps and mixed with $5\text{ }\mu\text{L}$ of NFW, $15\text{ }\mu\text{L}$ of ISO-004 master mix, and $5\text{ }\mu\text{L}$ *E. coli malB* gene DNA template. The tablets were tested on LFSs after 10 and 30 days of storage.

A mixture of pullulan and trehalose was used to preserve LAMP reagents following the ‘two-pill method’ introduced by Leung *et al.* [26]. NEB master mix (Section 2.4.1) was deployed to have full control on the reagents components and to separate the salts and amplification buffer from the other elements of the LAMP amplification mix (Fig. 2.11). Two separate tablets of 10% (w/v) pullulan and 0.5 M trehalose were created, one containing WarmStart[®] Bst 2.0, dNTPs and labelled primer mix, and the second containing MgSO_4 , and Isothermal Amplification Buffer. Each tablet containing the DNA polymerase (Bst 2.0) and primers (Tablet 1) was made by mixing $1.15\text{ }\mu\text{L}$ of WarmStart[®] Bst 2.0 (8000 U/mL), $4.04\text{ }\mu\text{L}$ dNTPs (10 mM), $5.77\text{ }\mu\text{L}$ of labelled primer mix (25X), $0.29\text{ }\mu\text{L}$ of NFW, $3.75\text{ }\mu\text{L}$ of trehalose (2 M), and 1.5 mg of pullulan, to make a 10% (w/v) pullulan solution. The $5.77\text{ }\mu\text{L}$ of 25X labelled primer mix was made as described in Table 2.5, with $0.29\text{ }\mu\text{L}$ F3 primer (100 μM), $0.29\text{ }\mu\text{L}$ B3 primer (100 μM), $1.15\text{ }\mu\text{L}$ FIP-FITC primer (100 μM), $1.15\text{ }\mu\text{L}$ BIP primer (100 μM), $1.44\text{ }\mu\text{L}$ LF-Biotin primer (100 μM), $1.44\text{ }\mu\text{L}$ LB primer (100 μM). $15\text{ }\mu\text{L}$ of the resultant mixture were used to create tablets as described in Fig. 2.10. The air-flow of a fume

cabinet was used for 1 hour to dry the droplets. The tablets were then stored at 35 °C inside the Petri dish covered with aluminium foil. Tablets containing the Isothermal Amplification Buffer and MgSO₄ (Tablet 2) were made by mixing 1.4 μL of MgSO₄ (100 mM), 3.5 μL of Isothermal Amplification Buffer (10X), 0.35 μL of NFW, 1.75 μL of trehalose (2 M) and 0.7 mg of pullulan. Once pullulan was dissolved, 7 μL droplets were pipetted onto a Petri dish that was transferred into a vacuum chamber for 1 hour. The disc-shaped tablets that formed were sealed inside the Petri dish using parafilm, covered with aluminium foil, and stored at 35 °C until use. Both types of tablets were tested in a LAMP assay after 10 and 30 days of storage.

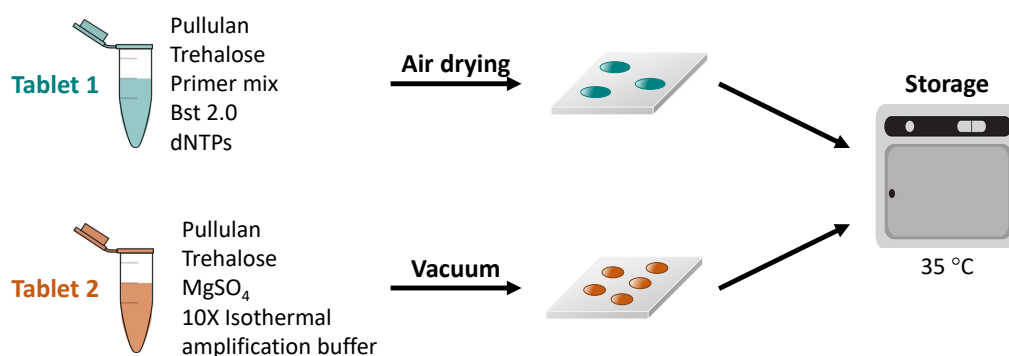


Figure 2.11: **Schematic of the ‘two-pill method’ [26] to store LAMP reagents in pullulan-trehalose tablets.** Tablet 1 is initially prepared as a solution of WarmStart[®] Bst 2.0, dNTPs, labelled primer mix, trehalose, and pullulan is dissolved in this solution. The solution is then air-dried for a day (or the air-flow of a fume-hood is used to fasten drying) to form disc-shaped tablets. Tablet 2 is initially created as a solution of MgSO₄, Isothermal amplification buffer, trehalose, and pullulan is dissolved in it. The solution is then vacuum-dried for about 1 hour to form disc-shaped tablets. Both Tablet 1 and 2 are stored within aluminium foil and at 35 °C inside an incubator. Upon use the two tablets were resuspended with nuclease-free water and other LAMP reagents.

Tablet 1 and Tablet 2 (Fig. 2.11) were used separately to carry out the LAMP reaction or together in a single LAMP assay (Tablet 1+Tablet 2). Tablet 1 was tested at various time points up to 30 days of storage, and upon use it was resuspended in a qPCR tube with 2.5 μL of Isothermal Amplification Buffer (10X), 1 μL of MgSO₄ (100 mM), 0.25 μL of LAMP Fluorescent dye (25X), 16.25 μL of water, and 5 μL of *E. coli malB* gene DNA template. Tablet 2 was resuspended with 1 μL of WarmStart[®] Bst 2.0 (8000 U/mL), 3.5 μL dNTPs (10 mM), 5 μL of labelled primer mix (5X), and 0.25 μL of LAMP Fluorescent dye (25X), 10.25 μL of water, and 5 μL of *E. coli malB* gene DNA template. To test the two tablets together, Tablet 1 and Tablet 2 were added into the same 0.1 mL qPCR tube and resuspended with 0.25 μL of LAMP Fluorescent dye (25X), 19.25 μL of NFW, and 5 μL of *E. coli malB* gene DNA template in each tube.

The amplification results were evaluated on LFSs, and the LAMP Fluorescent dye was added to each reaction to enable real-time fluorescent detection for confirmatory purposes.

2.15.1.3 Reagents Stored in 5% (w/v) Pullulan and 0.5 M Trehalose or 10% (w/v) Pullulan and 0.5 M Trehalose

To investigate the effects of different pullulan concentrations on the LAMP limit of detection, tablets were prepared using the two-pill method (described in Figure 2.11) to a final pullulan concentration of either 5% (w/v) or 10% (w/v). The volumes to create Tablets 1 and 2 are given in Table 2.8. The dried disc-shaped tablets were stored at 35 °C until use, and tested after 10 days of storage. Tablet 1 and Tablet 2 were placed in the same reaction tube with the following combinations: (1) Tablet 1-10% and Tablet 2-5%, (2) Tablet 1-5% and Tablet 2-10%, (3) Tablet 1-5% and Tablet 2-5%. Each pair of tablets was resuspended with 0.5 µL of LAMP Fluorescent Dye (25X), 19.5 µL of NFW, and 5 µL of *E. coli malB* gene DNA template to each pair of tablets, resulting in a final volume of 25 µL of LAMP mixture. The stability of Tablet 1-5% and Tablet 2-5% was tested again after storing them at 35 °C for 14 days.

The analytical sensitivity of the different tablet combinations was assessed on LFSs, and real-time fluorescent readings were carried out for confirmatory purposes.

Table 2.8: **Optimised formulation of the stored dry Tablet 1 and 2 for LAMP test.** The amount of pullulan used to obtain 5% and 10% (w/v) pullulan in Tablet 1 is 0.8 mg and 1.6 mg, respectively; whereas for Tablet 2 is 0.35 mg and 0.7 mg, respectively.

Tablet 1	
Component	Volume used per reaction (µL)
Bst 2.0 (8000 U/mL)	1.71
dNTPs (10 mM)	4.00
Trehalose (2M)	4.00
Primer mix (25X)	5.71
dH ₂ O	0.57
Total volume	16.00
Tablet 2	
Component	Volume used per reaction (µL)
MgSO ₄ (100 mM)	1.40
Isothermal Amplification Buffer (10X)	3.50
Trehalose (2M)	1.75
dH ₂ O	0.35
Total volume	7.00

2.15.1.4 Storage of Molecular Reagents Returned from the Field

LAMP tablets for the detection of *Plasmodium* species (*P. falciparum*, *P. vivax*, *P. malariae*, *P. ovale*) and *BRCA1* gene were prepared using the two-pill method. Tablet 1 includes the primer mix specific for *Plasmodium*, DNA polymerase and dNTPs, and it was created with 5% (w/v) pullulan and 0.5 M trehalose. Tablet 2 contains MgSO₄ and the Isothermal Amplification Buffer and it was prepared with 10% (w/v) pullulan and 0.5 M trehalose. NEB master mix components were used. The 25X labelled primer mixes (one for *Plasmodium* species and one for *BRCA1*) were prepared by pre-mixing the 6 primers so that the final concentration of primers in the reaction would correspond to 5 times the concentration needed when using reagents stored at -20 °C, as indicated in Table 2.5. Tablet 1 was prepared as described in Table 2.8, with 5% (w/v) pullulan solution. 16 µL of the mixture was used to create disc-shaped tablets. The air-flow of a fume cabinet was used for 1 hour for drying. Tablet 2 was prepared as described in Table 2.8 with 10% (w/v) pullulan concentration. 7 µL of the solution were used to create the tablet and 1 hour vacuum was performed for drying. Once dried, Tablet 1 and Tablet 2 were moved inside 1.5 mL tubes using tweezers. The tubes were sealed with parafilm (PARAFILM[®] M), transported to Uganda (during a field-trip), and brought back to the UK for lab testing. A transparent zip bag containing the tubes was put in a crate along with other materials required for the field trip. The crate was shipped as a hold luggage by plane and during the 10-days field-trip, it was carried out for field testing every day and kept in air-conditioned rooms at night. Once back in the laboratory, the tubes were kept inside a cabinet at room temperature. The performance of rehydrated reagents was evaluated after they have undergone uncontrolled temperature changes during the shipment to Uganda and back to the UK. The reagents in each tube were resuspended with 20 µL of water, and 5 µL of target DNA (either WHO standard for *P. falciparum* DNA, or genomic DNA for *BRCA1* gene), before running the LAMP reaction (Fig. 2.12). The analytical sensitivity of the reagents that were sent to Uganda was evaluated on LFSs. Melting curves and gel electrophoresis were used to verify that the test line on LFSs was specific for the target DNA. The results were compared with reagents that were kept in optimal conditions at -20 °C.

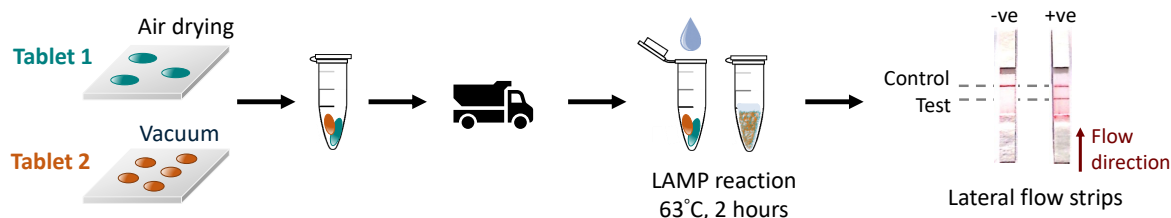


Figure 2.12: **Two-pill method used to ship LAMP reagents to Uganda under uncontrolled temperature conditions.** Tablet 1 and Tablet 2 for the detection of *Plasmodium falciparum* and *BRCA1* are prepared using the two-pill method [26]. One Tablet 1 and one Tablet 2 per reaction were stored inside a sealed 1.5 mL Eppendorf tube and shipped to Uganda and back to the UK. The reagents were resuspended with nuclease-free water upon use, LAMP was performed the performance of the LAMP reagents stored in pullulan-trehalose tablets was assessed on LFSs.

2.15.2 Storage of Molecular Reagents In-the-field and in a Paper-Based Device.

Pullulan-trehalose tablets storing LAMP reagents for the detection of *Plasmodium* species and *BRCA1* gene have been prepared as described in Section 2.15.1.4. They were then shipped and used outside laboratory settings, in a primary school in Kocoge (Tororo, Uganda). Before shipment, LAMP reagents were either stored inside 1.5 mL microcentrifuge tubes as explained in Section 2.15.1.4 or incorporated inside a device specifically designed for the diagnosis of malaria at the point-of-need.

2.15.2.1 Modified DNA Extraction from Blood for Use on the Point-Of-Care Device

In previous works led by Garrett [152] and Reboud *et al.* [17], the magnetic beads-based protocol provided by MagaZorb[®] DNA Mini-Prep Kit was scaled-down to accommodate DNA extraction from a finger prick of whole blood (5 μ L). The protocol developed by Garret [152] (Fig. 2.13A) used the reagents provided by MagaZorb[®] DNA Mini-Prep Kit and is described in Fig. 2.13A. The method consisted of 19 manual steps. Efforts were made to simplify this protocol to avoid the lysis heating step at 65 $^{\circ}$ C and the addition of binding buffer. Eliminating the heating step was crucial to avoid extra equipment that might result in difficulties when being integrated into a POC device. Nucleic acid extraction was performed from whole blood preserved in sodium citrate and purchased by Cambridge Bioscience (Cat # BLD1DC4CIT09-FS, Cambridge Bioscience Ltd., Cambridge, UK) and, during laboratory testing, *BRCA1* gene was targeted. The blood donors had given their consent for their blood to be used for research purposes, and no additional ethical approval was needed. The LAMP mas-

ter mix from NEB was used (Section 2.4.1), and the primers and 5X primer mix for *BRCA1* are given in Tables 2.4, 2.5. The optimised DNA extraction protocol has 11 steps (Fig. 2.13B), and it combines the lysis and binding step. It consisted of adding 5 μ L of Lysis Buffer, 2 μ L of magnetic beads reagent, and 5 μ L of whole blood to the bottom of a 1.5 mL microcentrifuge tube. The reagents were mixed by gently flicking the bottom of the tube and incubated for 20 minutes at room temperature. The tube was flicked at three minutes intervals. Then, the tube was inserted in the magnetic rack until the beads settled. The supernatant was removed and 40 μ L of Wash Buffer was added to the tube. The solution was mixed by tapping the bottom of the tube. After the solution formed a homogenous mix, the tube was placed on the magnetic rack again, and the supernatant was discarded after the beads coagulated. The beads were then coagulated at the bottom of the tube with the help of the magnetic rack and 5 μ L of NFW were added. 5 μ L of the magnetic beads mixture was mixed with the help of a pipette and transferred into the final 25 μ L LAMP mixture. Magnetic beads were therefore included in the final amplification reaction. The results were assessed on LFSs.

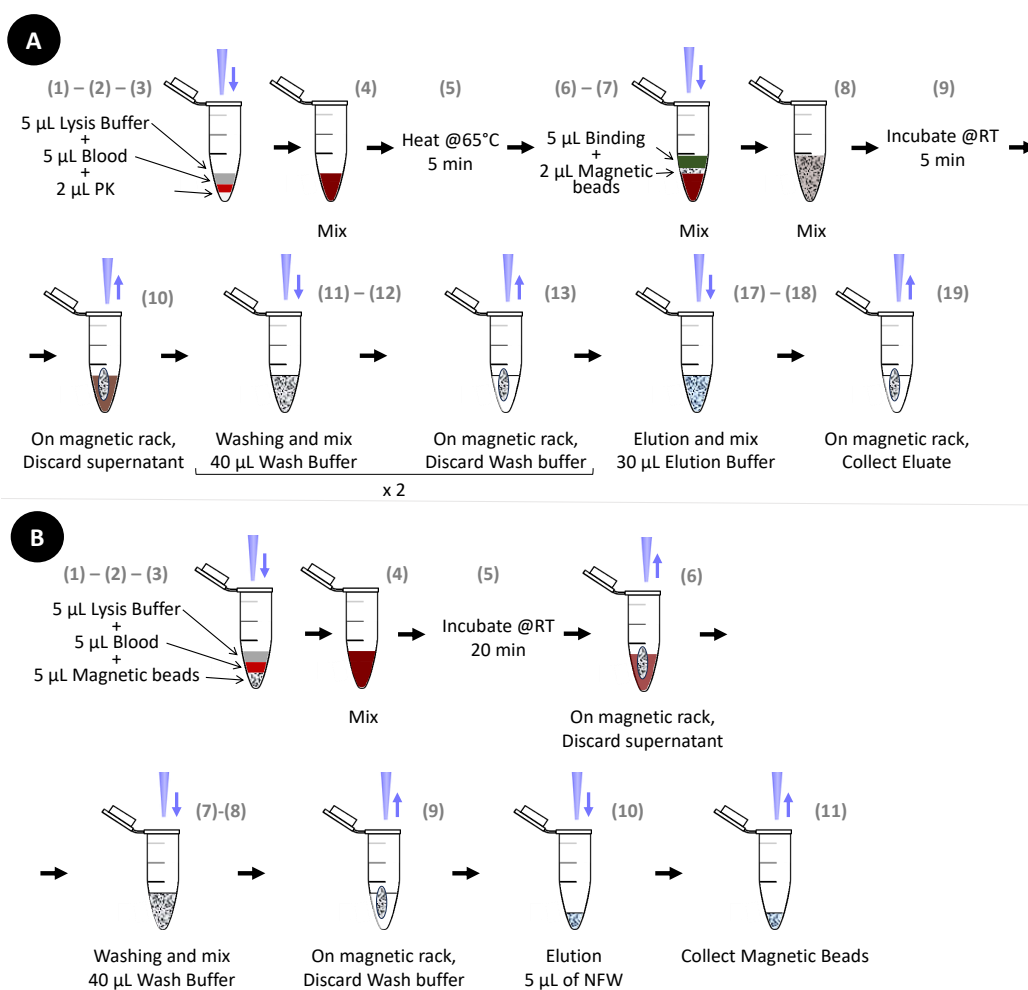


Figure 2.13: **Modified DNA extraction from blood finger prick.** **A.** DNA extraction method from blood developed by Garrett [152]. The method consisted of adding 2 μ L of proteinase K (PK) to a 1.5 mL microcentrifuge tube, then 5 μ L of whole blood and 5 μ L of Lysis Buffer (1-3). The bottom of the tube was flicked gently to properly mix the reagents (4). The mixture was incubated at 65 $^{\circ}$ C for 10 minutes (5), and after, 10 μ L of Binding Buffer was added (6). The bottom of the tube was flicked again for mixing purposes. 2 μ L of Magnetic beads reagent (containing magnetic beads) was added to the tube (7), and the solution was mixed (8) before incubation at room temperature (RT) for 5 minutes (9). The tube was flicked at two minutes intervals. The tube was inserted in the magnetic rack and the beads were given one minute to settle, then the supernatant was removed (10). 40 μ L of Wash Buffer was added to the tube (11), and the beads were mixed by tapping the bottom of the tube (12). The tube was placed on the magnetic rack again, and after the beads coagulated, the supernatant was discarded (13). This wash step was done two more times until a clear solution was obtained (14)-(16). Then, 30 μ L of Elution Buffer was added to the tube (17) and the beads were gently dispersed by tapping the bottom of the tube to release the DNA into the eluate (18). The magnet was used to separate the beads and the eluate was moved to a new tube for further analysis (19). 5 μ L of the eluate was added to the final 25 μ L LAMP mix. **B.** The improved DNA extraction method has 11 steps. The procedure involves adding 5 μ L of Lysis Buffer, 2 μ L of Magnetic beads reagent, and 5 μ L of whole blood to the bottom of a 1.5 mL microcentrifuge tube (1)-(3). The reagents were mixed by gently flicking the bottom of the tube (4) and incubated for 20 minutes at room temperature (5). The tube was flicked every three minutes intervals. Next, the tube was inserted in the magnetic rack until the beads settled. The supernatant was removed (6) and 40 μ L of Wash Buffer was added to the tube (7). The solution was mixed by tapping the bottom of the tube (8). After, the tube was placed on the magnetic rack again, and the supernatant was discarded after the beads coagulated (9). The beads were then coagulated at the bottom of the tube with the help of the magnetic rack and 5 μ L of nuclease-free water (NFW) were added (10). 5 μ L of the magnetic beads mixture was mixed with the help of a pipette and transferred into the final 25 μ L LAMP mixture (11).

2.15.2.2 Overview of Diagnostic Method

The process illustrated in Fig. 2.13B in tubes was translated into a POC device for the detection of *Plasmodium* species and *BRCA1* gene. Both the sample processing, and LAMP can be performed within the plastic cassette; this eliminates the need for costly devices, such as thermocyclers, and complex handling steps. A schematic of the plastic device is provided in Fig. 2.14A, B. The working principle of the device is similar to the one previously introduced by Ngamsom *et al.* [103], where magnetic beads are deployed to bind nucleic acids and move them through the NAATs steps.

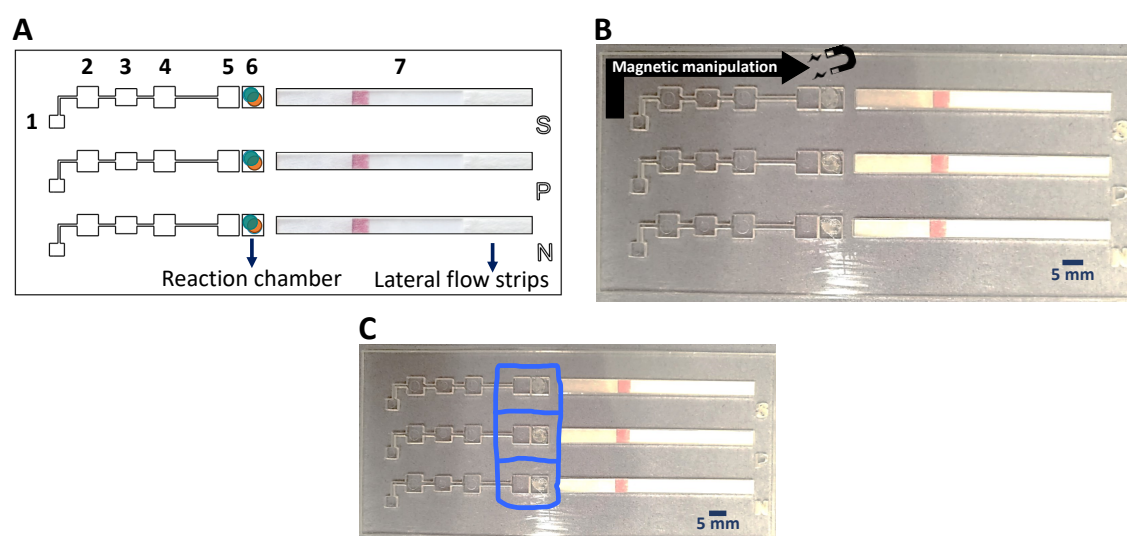


Figure 2.14: **Schematic of the point-of-care (POC) device for the detection of malaria from blood.** **A.** Chamber 1 (Sample) content: 5 μL of Lysis Buffer, 2 μL of magnetic beads reagent and 5 μL of whole blood. Chambers 2, and 4 were filled with 50 μL of castor oil. Chambers 3 (Washing) and 5 (Resuspension): 40 μL and 50 μL of nuclease-free water (NFW), respectively. Chamber 6 (Reaction/Smplification): LAMP reagents stored dry in pullulan-trehalose tablets. Chamber 7: lateral flow strips. **B.** Direction of magnetic beads manipulation. This was followed for all the three reactions tested (sample, positive control and negative control). **C.** The blue lines indicate where to apply the super glue before the second adhesive film sealing.

Empty chambers were filled with castor oil (50 μL in chambers (2), (4)), and NFW (40 μL in chamber (3), and 50 μL in chamber (5)). Next, 5 μL of Lysis Buffer and 2 μL of magnetic beads reagent (from MagaZorb[®] DNA Mini-Prep Kit, Promega) were added into the sample chamber (1) one at a time. 5 μL of whole blood sample was added to the sample chamber. This was performed for all the three reactions incorporated into the diagnostic cassette (sample, positive control, and negative control); 5 μL of NFW was added to the negative control instead of whole blood. The device was then incubated for 20 min at room temperature. In the meantime, 20 μL of superglue was applied around the resuspension and reaction chambers ((5)-(6)) of the device (Fig. 2.14C). The top part of the device was sealed with adhesive film (Nunc[™] Seals,

Tapes, and Foils, Polypropylene, Cat. No 232701, Thermo Fisher Scientific Inc.) and pressed firmly with the tweezer handle. This second seal was performed from the left side of the device (where chamber (1) is) to the right side of the device (where lateral flow strips are, chamber (7)). To ensure the reagents and samples do not leak during the heating process, an extra layer of MicroAmpTM Optical Adhesive Film was applied over the device, wrapping it and covering the left side where chamber (1) is located. This was done to avoid any possible leakage of biological material from the device during the heating step. After the device was fully sealed, it was gently shaken horizontally every 5 minutes for the total incubation time (20 minutes). An external magnet (20 mm diameter \times 5 mm thick \times 5.2 mm c/s, N42 neodymium magnet; pull force = 8.3 kg, Magnet Expert Ltd, UK) was used to pull the DNA-bound magnetic beads from the sample chamber (1), through the oil and washing chambers ((2)-(4)), to the resuspension chamber (6) (Sample preparation, Fig. 2.15A). Once all the beads were in the resuspension chamber (5), the walls between chamber (5) and (6) were broken with the help of a 15 mL centrifuge tube. The device was then tapped to let all the liquid to flow from chamber (5) to (6) so that pullulan-trehalose tablet got dissolved. A 5 minute incubation period ensured that all the dried reagents were dissolved. Finally, the device was placed either on a heat block or inside the heater designed by a colleague, Xin Guo, [153] so that the aluminium covered both the resuspension and reaction chambers (Amplification, Fig. 2.15B). The amplification reaction was performed for 120 minutes at 63 °C. After, the 3-mm thick wall between the reaction chamber (6) and the lateral flow strips (7) was broken to let the liquid flow through the LFSs (Detection, Fig. 2.15C). As an alternative, a puncher was used to open the reaction chamber (6) and the LFSs chamber (7), and a pipette was used to transfer 10 μ L of the reaction mixture onto the LFSs and additional 30 μ L of NFW to let the sample flow through.

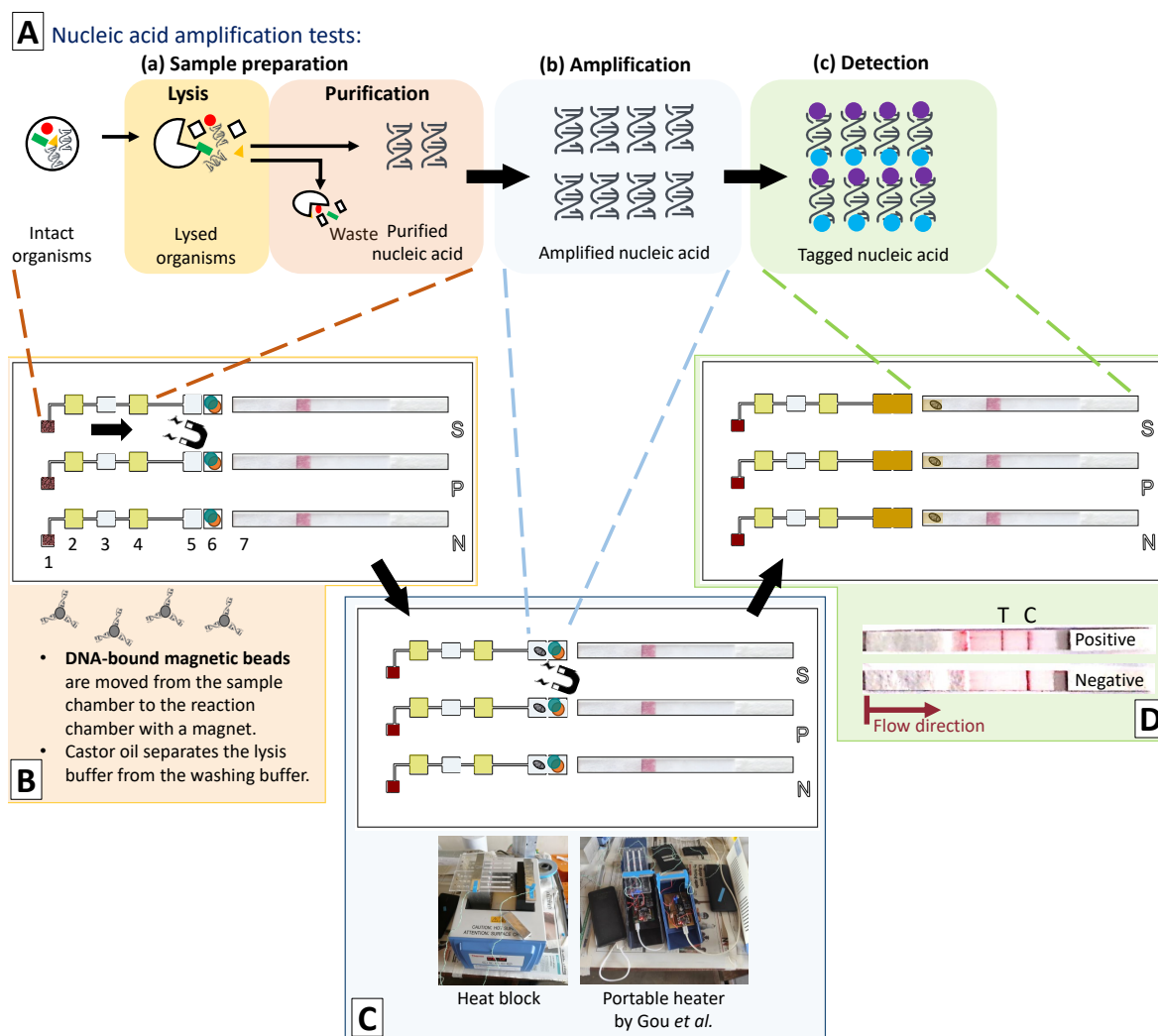


Figure 2.15: **Functioning of the point-of-care (POC) device for the detection of malaria from blood.** **A.** Steps of nucleic acid amplification tests (NAATs): sample preparation/pretreatment, amplification, and detection. **B.** Sample preparation in the POC device. The lysis of the blood sample is performed in chamber (1). The extracted DNA binds to magnetic beads that are then moved through chambers (2)-(4) for purification using a magnet. **C.** Amplification of DNA in the POC device. Once all the beads were moved in the resuspension chamber (5), the walls between chamber (5) and (6) were broken. All the liquid was then moved from the resuspension chamber (5) to the amplification chamber (6) by gently tapping the device. After pullulan-trehalose tablets dissolved (approx. 5 minutes), the device was placed either on a heat block or in a portable heater [153]. Amplification was carried out at 63 °C for 2 hours. **D.** Detection of amplified material inside the POC device. After amplification, the 3-mm thick wall between the reaction chamber (6) and the lateral flow strips (7) was broken. The liquid flowed through the LFSs and, after 5 minutes, the results were visualised. As an alternative, after amplification, a puncher was used to open both the reaction (6) and the LFSs (7) chambers. In this scenario, a pipette was used to transfer 10 μ L of the reaction mixture on the LFSs. Additional 30 μ L of nuclease-free water was added to carry out the lateral flow assay.

2.15.2.3 Interpreting Results in the Diagnostic Cassette

The diagnostic cassette had both negative and positive control reactions, and the results visualised on LFSs of these controls helped to determine the outcome of the diagnostic test. Fig. 2.16 shows examples of positive, negative and invalid results from the diagnostic cassettes used in the final field trials. A test result was considered valid

if NTC (N) = negative, PC (P) = positive and there was a positive or negative result for the tested sample (S).

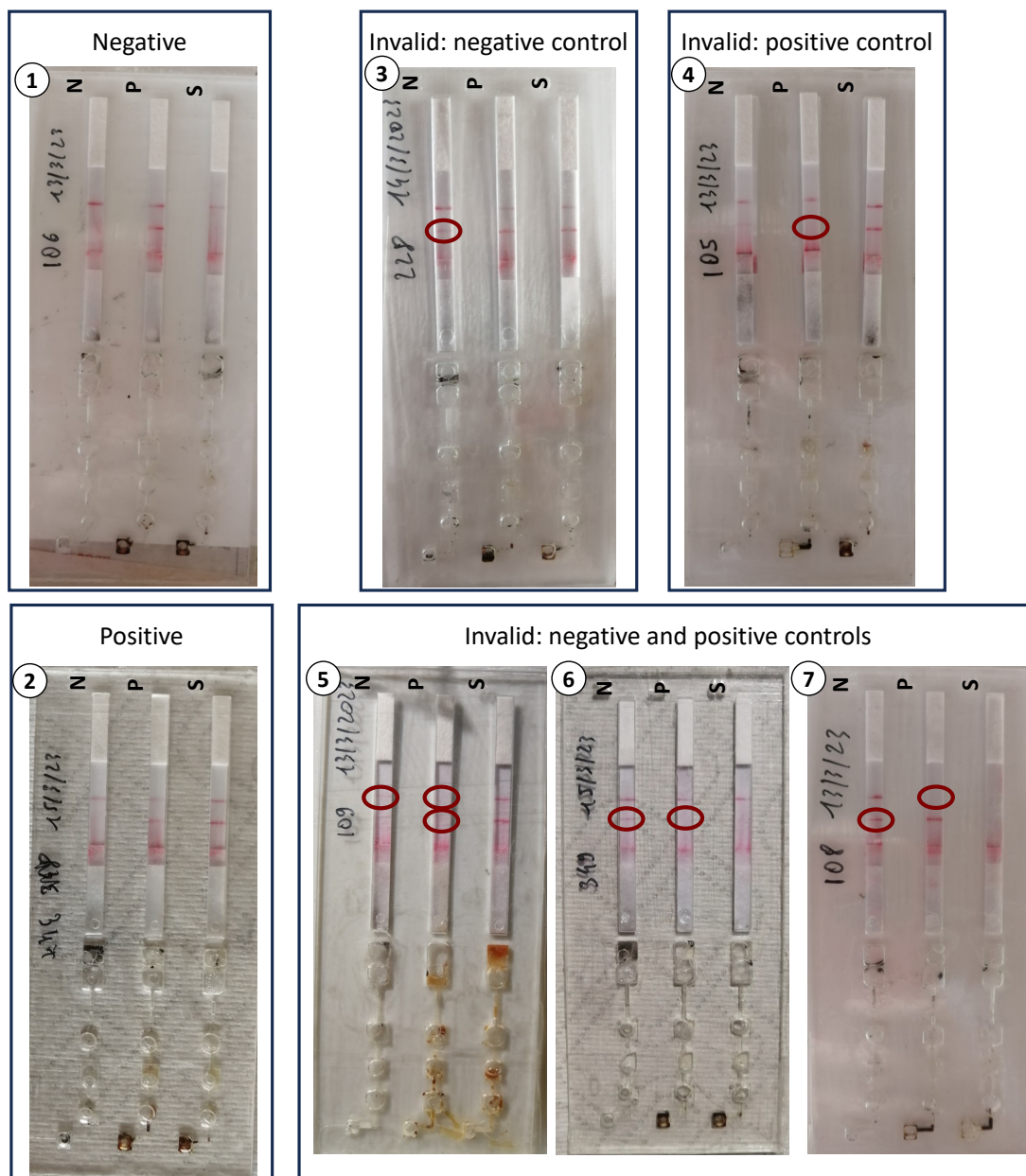


Figure 2.16: **Results interpretation on diagnostic cassette for detection of malaria.** The Diagnostic Cassette can give valid results only if the positive control (P) and negative control (N) tests strips give expected results, along with the test result (S). A valid negative result is shown in (1). A valid positive result is given in (2). The pictures (3)-(7) show examples of invalid tests, where either the negative or positive test do not have a line, or have extra lines. The errors are marked with red circles.

2.15.2.4 Plastic Diagnostic Cassette Design and Fabrication

The device was made using a 2-mm thick PMMA slab, as explained in Section 2.13. The diagnostic cassette external dimensions were 12.8 cm \times 57.3 cm. The cassette consists of 7 chambers whose dimensions were carefully made to accommodate the

liquids necessary to perform all the NA amplification steps described in Fig. 2.13B. Dimensions were derived as indicated in Table 2.9. Larger chambers and an additional running buffer chamber have been trialed. The results and observations for all designs tested are given in Chapter 4.

Table 2.9: **Volumes of chambers incorporated in the plastic cassette to perform the nucleic acid amplification test.** The reaction chamber (6) containing the dried LAMP reagents is 5 mm × 5 mm. The lateral flow strip chamber (7) needed to accommodate the LFSs, and its dimensions are 60 mm × 4 mm.

	Volume of liquid (mm ³)	Area needed (mm ²)	Dim. for squared chambers (mm)	Final dimensions of chambers		Final Area (mm ²)	Final Volume (mm ³)
				Width (mm)	Length (mm)		
Chamber 1 (Sample)	12	6.3	2.5	3	2.5	7.5	14.25
Chambers 2, 4 (Oil)	50	26.3	5.1	5	5.5	27.5	52.25
Chamber 3 (Washing Buffer)	40	21.1	4.6	4	5.5	22	41.8
Chamber 5 (Resuspension Buffer)	50	26.3	5.1	5	5.5	27.5	52.25

2.15.2.5 Device Assembly for Field Trials

Before assembly, all materials (excluding the LFSs) were exposed to UV for 30 minutes for disinfection. The plastic cassettes were then cleaned with disinfectant (ChemgeneLab Disinfectant, Medimark InternationalTM) using lens tissues (Fig. 2.17A). The top part of the device was sealed with MicroAmpTM Optical Adhesive Film (Applied BiosystemsTM, Thermo Fisher Scientific Inc.). The film was initially pressed gently against the plastic to ensure proper adhesion, and then strongly adhered to the PMMA layer using the back side of tweezers (Fig. 2.17B). The ‘top side’ of the device was defined as the side where the three letters defining the three tests N (for NTC), P (for PC) and S (for sample) were correctly readable. The cassette was arranged so that the ‘top side’ was facing down, and punchers were used to make holes in chambers (1)-(5) (Fig. 2.17C). A 2 mm punch was used for the sample (1), washing (3) and resuspension (5) chambers, and a 3 mm punch for the oil chambers (2), (4). The holes enable sample pretreatment reagents to be loaded in the field. Next, the devices were exposed to UV light for 30 minutes. Always with the device facing down, the LFSs were loaded into the corresponding chambers (7). Tablet 2 (containing the Isothermal Amplification Buffer and MgSO₄, Section 2.15.1.4) was transferred inside each reaction chamber (6)

with tweezers (Fig. 2.17C). Tablet 1 specific for the detection of *Plasmodium* species (containing labelled primer mix, DNA polymerase and dNTPs, Section 2.15.1.4) was added to chamber (6) in the sample (S) and NTC control (N) reactions, and Tablet 1 specific for the detection of *BRCA1* was added to chamber (6) in the positive control (P) reaction (Fig. 2.17D). Finally, two pieces of MicroAmp™ Optical Adhesive Films were stuck on the bottom side of the device, to seal the LFSs and tablets inside (Fig. 2.17D). Tweezers were pushed along the bottom part of the cassette to ensure full adhesion of the adhesive film on the PMMA cassette.

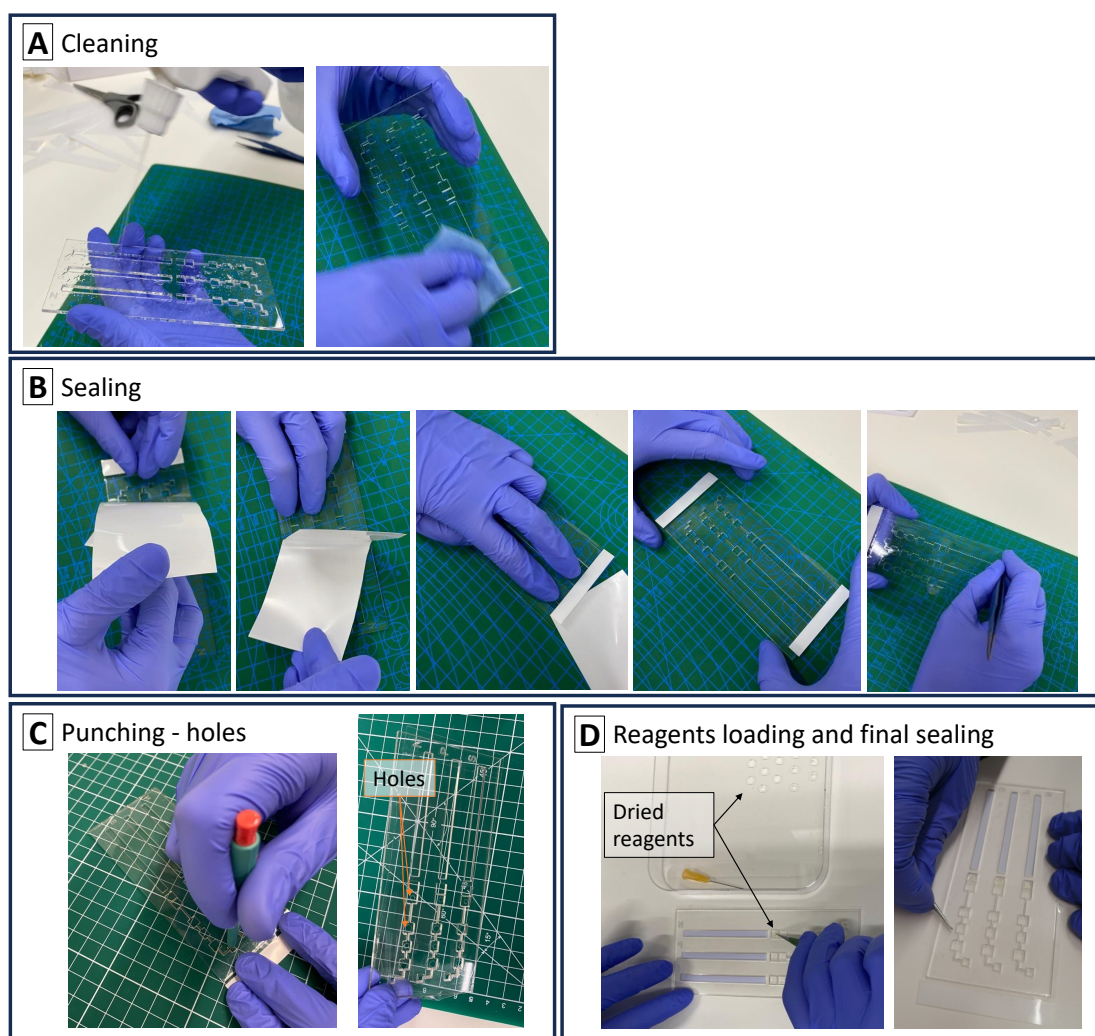


Figure 2.17: **Assembly of the point-of-care malaria cassette.** The ‘top side’ of the device is defined as the side where the letters N, P and S are properly readable. **A.** Disinfectant and lens tissue were used to clean the plastic cassettes before assembly. **B.** The top part of the device was sealed with MicroAmp™ Optical Adhesive Film and pressed firmly with tweezers. **C.** The plastic cassette was arranged with the top part facing down, and holes were punched in chambers (1)-(5). The holes enable to load the sample pretreatment reagents. The devices were then exposed to UV light for 30 minutes. **D.** With the device still facing down, the LFSs were inserted into chambers (7). Next, one Tablet 2 (Isothermal Amplification Buffer and MgSO_4) was placed in each reaction chamber (6) with tweezers. Tablet 1 (labelled primer mix, DNA polymerase, dNTPs) for *Plasmodium* pan detection was added to chamber (6) in sample (S) and NTC control (N) reactions, and Tablet 1 for *BRCA1* gene detection was added to chamber (6) in positive control (P) reactions. Lastly, two pieces of MicroAmp™ Optical Adhesive Films were used to seal the bottom part of the device.

2.15.2.6 Field Work

The preparations for field work are described in this section, including storage and transport of reagents and consumables; field-work details are also given.

Sample Size A sample size analysis was performed to determine the number of devices necessary to test the sensitivity of the microfluidic diagnostic device. The sample size calculator used was developed as a side-project during the covid-19 pandemic when access to the lab was disrupted [154,155]. To meet a specific accuracy of the diagnostic device, the following parameters were chosen: ‘Estimate accuracy of a single test’ and ‘Based on sensitivity/specificity’. The prevalence was set at 50% based on the previous field-trips performed in the same Tororo District by colleagues [152]. Sensitivity was set at 97% given the WHO and Foundation for Innovative Diagnostics (FIND) minimal requirements [17], and specificity at 99%. The margin of error was set at 10%, the confidence level at 98%, and the failure rate in sampling (due to possible device failure, withdraw of participants or contamination) at 30% (high number based on previous field-trip experiences). The sample calculator suggested a sample size of 45 to estimate the required sensitivity, and 16 to estimate the specificity; therefore, a total of 60 devices were produced in the laboratory and shipped to the field.

An in-depth description of the sample size calculator and personal contribution is given in Appendix A.1.

Diagnostic Devices, Equipment and Reagents Organisation The paper-based diagnostic devices were prepared in the laboratory before the field trials, as described in Section 2.15.2.5. A batch of 5 devices were packed in a sealed transparent bag, along with two desiccant packets (MiniPax[®] absorbent packets, Merck, Sigma-Aldrich) to limit the exposure to moisture. LAMP reagents stored dry inside tubes (as described in Section 2.15.1.4) were transported inside transparent bags with the same desiccant packets. The technicians from the Vector Control Division of the Ministry of Health Uganda procured the tools for RDTs and microscopic inspections.

Most of the field work equipment was brought from Glasgow to Uganda as flight hold luggage, in travel crates that were suitable for air and road travel. The equipment had to be durable and well-protected because of the poor road conditions while travelling across Uganda. Moreover, the group learned from previous field trips that buffers and reagents needed to be packed in small aliquots and stored separately during travel to

prevent cross-contamination, in case leakages occurred.

Enrolment and Workflow The study was led in conjunction with the Vector Control Division of the Ministry of Health of Uganda, and it was approved by the Institutional Review Boards (IRBs), Vector Control Division Research and Ethics Committee (VCD-REC) , VCDREC/078, and Uganda National Council for Science & Technology (UNCST), HS 2193. 20 school children between the ages of 6 and 14 years were recruited from a randomly chosen year group every day under the supervision of the teachers. The teacher, and the staff from the Vector Control Division of the Ministry of Health of Uganda obtained consent from both parents and children, collected students' personal data (for treatment purposes), and collected samples. A unique identifier (ID) was assigned to every child and the samples were used for the different types of diagnostic tests. No personal data were shown to the investigators.

The Ministry of Health of Uganda provided CareStart Malaria RDTs that were used as a qualitative field reference technique. Technicians from the Vector Control Division of the Ministry of Health carried out optical microscopy and Giemsa staining at the same time as microfluidic and RDT testing in the school classroom (Fig. 2.18A, B, C), as described by Reboud *et al.* [17]. Blood samples were obtained by fingerstick. A sterile lancet was used to prick a single finger and produce four blood spots. The first droplet was collected with a capillary tube and added to the malaria RDT cassette; the second droplet was put into an microcentrifuge tube; the third was spotted onto a FTA[®] card; and the last was smeared onto a clean microscopy slide. The finger was disinfected again and covered with a plaster. Each diagnostic cassette was labelled with the patients' ID number. The blood in the microcentrifuge tube was used in the plastic cassette, as described in Section 2.15.2.2. The workflow was very similar to the one described by Garrett (Sections 4.5.3 in [152]), with the sample pretreatment and amplification steps performed in different areas of the classroom to avoid contamination (Fig. 2.18C, D).



Figure 2.18: **Field testing.** **A.** Optical microscopy and Giemsa staining performed by technical staff of the Vector Control Division of the Ministry of Health, Uganda. **B.** Rapid Diagnostic Tests. **C.** Sample pretreatment performed inside the point-of-care (POC) device in the sample preparation area. **D.** Amplification carried out inside the POC device, in the amplification area.

2.16 Modular Paper- and Plastic-Based Device Design, Assembly, and Fabrication

This section describes the methodologies used to develop a proof-of-concept POC molecular device that consists of a layered structure of dried reagents and pullulan tablets where each layer contains one or more reagents. Pullulan tablets are used both to spatio-temporally control events and stabilise reagents, thus enabling to merge the sample-pretreatment and amplification in one chamber. The methods described in earlier sections were modified to integrate the paper-based DNA extraction from *E. coli* samples, dried LAMP reagents, LAMP and amplicon detection into a simple POC device.

First, a simple method for creating prototypes by layering PMMA sheets is described. Next, the dissolution rate of pullulan tablets with different dimensions and concentrations was observed to identify the optimal tablet for achieving the desired fluid control in the POC device. Finally, the full device operation was tested by integrating and adapting previous studies about sample preparation and reagents storage.

2.16.1 Overview of Point-Of-Care Molecular Device

The plastic device for the detection of *E. coli* enables sample processing and LAMP without the need for expensive equipment, such as thermocyclers, and complicated handling steps. A schematic of the plastic device is provided in Figures 2.19 and 2.20.

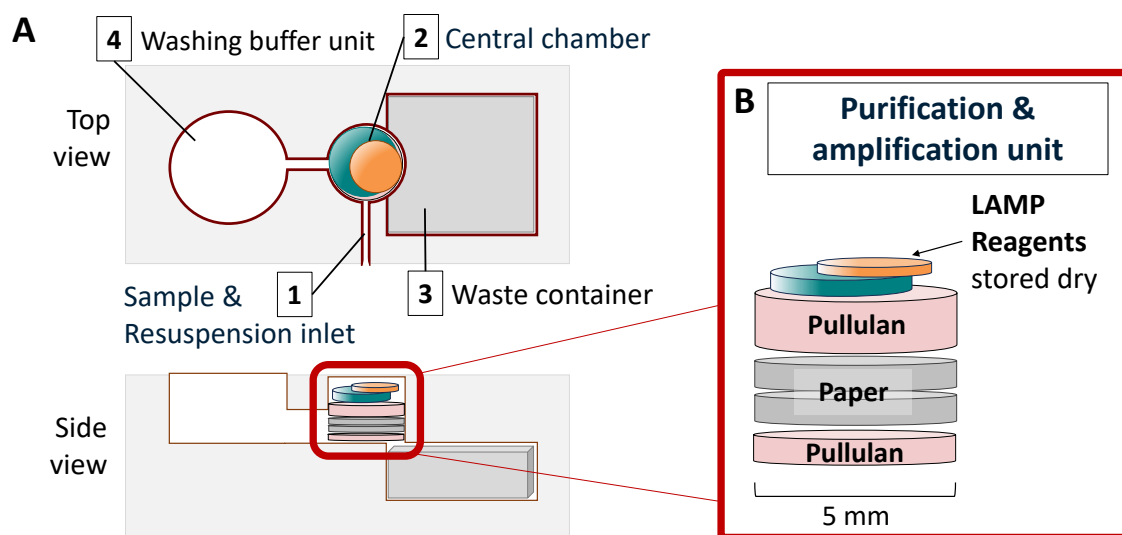


Figure 2.19: **Schematic of the diagnostic device for *E. coli* detection.** **A.** Top and side view. **B.** Detailed schematic of central chamber (2) content, where sample pretreatment and amplification occur. The chamber is filled with two paper discs sandwiched between two pullulan discs, and LAMP dried reagents above the top pullulan disc. The two paper discs have lysis buffer dried on them and are used for sample lysis, and DNA capture/release (following extraction principles described in Fig. 2.9). The bottom pullulan disc serves to guarantee incubation of the sample with the paper discs (as in step (3) in Fig. 2.9). The top pullulan disc separates the paper discs from the dried LAMP reagents, allowing for a physical separation between sample pretreatment and amplification.

100 μL of sample specimen is inserted inside the device, via the sample & resuspension inlet (1), using a pipette tip. The sample reaches the central well (2) where it is incubated onto the two paper discs thanks to the delay action of the bottom pullulan layer. After the bottom pullulan layer has dissolved, the lysed sample flows into the waste container, where there is an absorbent pad (3). Once all the lysed sample has flowed into the absorbent pad, 500 μL of NFW (acting as washing buffer) is added from the washing chamber (4) very slowly, so that the fluid has time to flow through the paper discs and get to the absorbent pad without overflowing above the top pullulan layer. At this point, the sample preparation is complete, and the extracted DNA is trapped onto the paper discs. The device is then moved upside down and tapped to let the paper discs reach the bottom, where the dried LAMP reagents are stored. 50 μL of resuspension buffer (NFW) are introduced through the sample & resuspension inlet (1) to dissolve the dried LAMP reagents, before the inlet is sealed with parafilm to prevent leakages. The device is placed onto a heater for two hours to perform LAMP. After, the central chamber (1) is opened, and the LAMP product are let flow onto the LFSs. The purification & amplification unit (Fig. 2.19B), from bottom to top, consists of a bottom pullulan disc, two 5-mm diameter paper discs with lysis buffer dried on, a top

pullulan disc that separates the sample preparation from the amplification reagents (dried LAMP reagents stored in pullulan and trehalose).

The techniques involved in this process will be explored in more detail in subsequent sections.

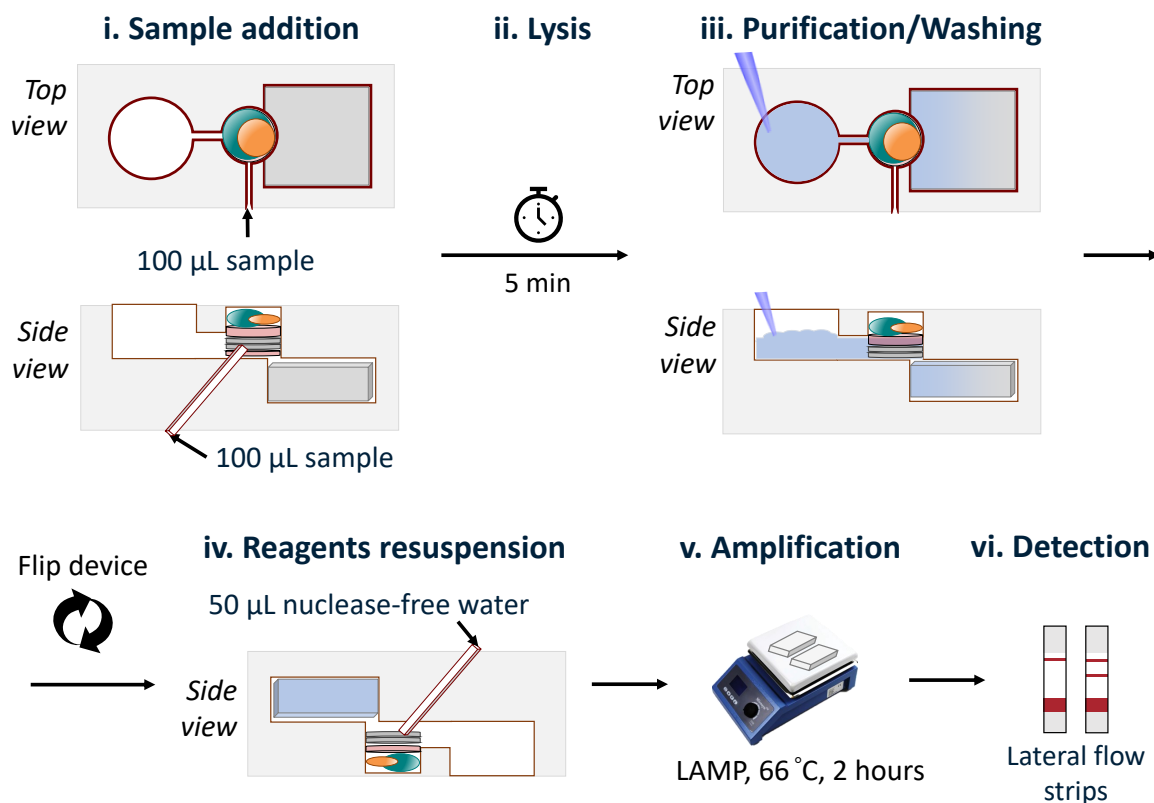


Figure 2.20: **Schematic of the working mechanism of the device and handling steps involved.** The sample specimen is introduced into the device using a pipette tip (i). The sample reaches the central well where it is incubated onto two paper discs sandwiched between two pullulan layers. The pullulan layer at the bottom delays the sample flow until it dissolves (ii). Then, the lysed sample moves to the waste container (absorbent pad) and 500 μL of nuclelease-free water (acting as washing buffer) is slowly added from the washing chamber to wash the paper discs (iii). The device is flipped and tapped to drop the paper discs to the bottom. 50 μL of nuclelease-free water (acting as resuspension buffer) is added to dissolve the stored dry LAMP reagents (iv), and then the device is heated for two hours (v). After LAMP incubation, the central chamber (1) is opened, and the LAMP product flows to the lateral flow strips (vi).

2.16.2 Device Design and Fabrication

As shown in Fig. 2.19, the device consists of a sample & resuspension inlet (1), a purification & amplification unit (2), waste container (3), and a washing buffer unit (4). The device was produced using PMMA slabs that were cut through using a laser cutter to create the microfluidic features (Section 2.13). Three different PMMA layers were stuck together using acetone, as explained in the following sections.

2.16.2.1 Plastic Cassette

The PMMA layers for the plastic cassette were designed as explained in Section 2.13. Three different PMMA layers were bonded together using pure acetone, to create a 3-dimensional (3D) plastic cassette (Fig. 2.21). A simple and quick liquid phase solvent bonding process was used to stack PMMA layers, as shown in Fig. 2.22A.

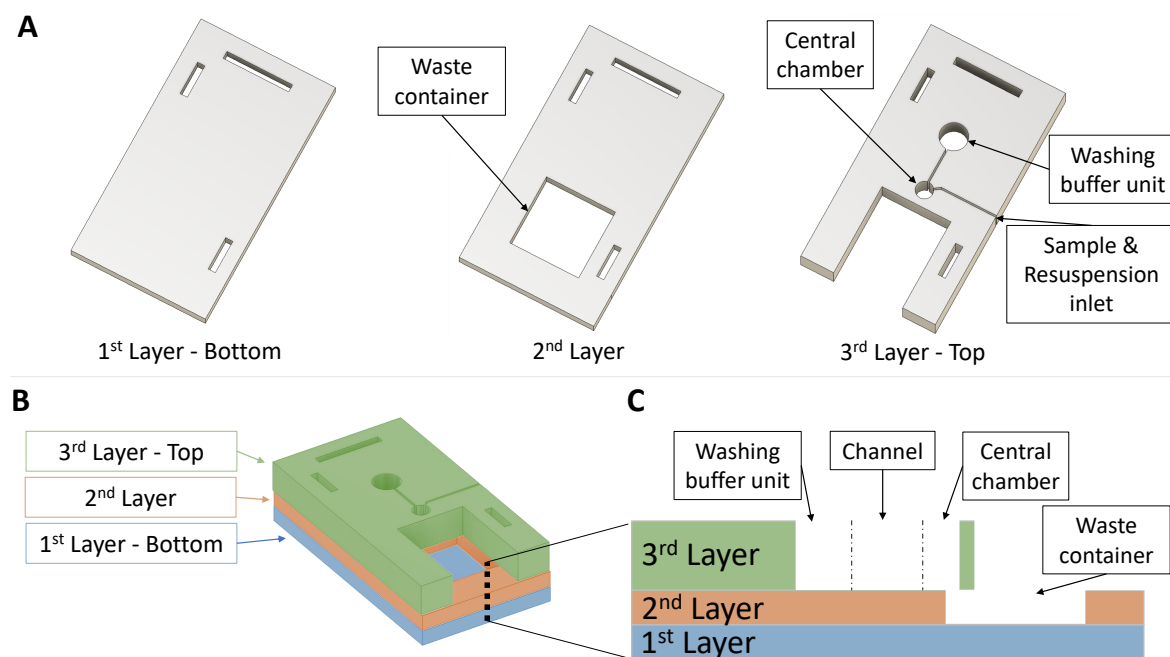


Figure 2.21: **Example of three poly(methyl methacrylate) (PMMA) layers that constitutes the 3D structure of the point-of-care device.** PMMA layers are numbered from bottom to top, *e.g.*, first, second and third layer. The second layer accommodates the waste container, whilst the third layer contains the central chamber, the washing buffer unit, the sample&resuspension inlet and the connecting channels. Each PMMA layer has 2 to 3 rectangular holes used to align the three layers during the stacking process. In **A** the three separate PMMA layers are given. **B** shows how the three PMMA layers are stacked on top of each other, and **C** shows a cross section of the PMMA plastic cassette.

The first and second layers were 2 mm thick, whereas the third (top) layer was 4 mm thick. The first PMMA layer that forms the base of the device was cut into a rectangular shape of 4.1 cm \times 7.4 cm from a 2-mm-thick PMMA sheet. All the device layers were subsequently laser-cut with an outer perimeter of 4.1 cm \times 7.4 cm. The waste container was shaped into a 2.1 cm \times 2.1 cm square from a second 2-mm-thick PMMA sheet (Fig. 2.21), to accommodate 2 cm \times 2 cm square of Whatman[®] CF7. The cotton linter CF7 was cut with a blade into shape, then it was inserted in the allocated space into the device. The third layer includes the sample & resuspension inlet, the central chamber for the purification & amplification unit, the washing buffer unit, and the channel connecting the washing buffer unit with the central chamber. The central chamber was shaped into a 5-mm diameter well to accommodate the 5-mm diameter

paper discs. The washing unit was shaped into a well of either 8, 5, or 3 mm in diameter. The channel width was of 0.5 mm or 0.2 mm. Additional small wells of 2-mm diameter have been added in the channels of some designs, at different distances from the central chamber, to prevent liquid to flow from the sample chamber to the channels. The second and third layers were aligned on top of each other so that there was an overlap between the waste container and the sample chamber of 1.5 mm or 0.75 mm, to leave space for the liquid to flow into the absorbent pad. Each PMMA layer has 2 to 3 rectangular holes that are 2.1 mm wide and 10 or 20 mm long. These rectangles were cut so that when stacking the PMMA sheets, it was possible to align the three layers by inserting small PMMA cut-outs (2 mm × 10 mm × 6 mm or 2 mm × 20 mm × 6 mm) into the holes.

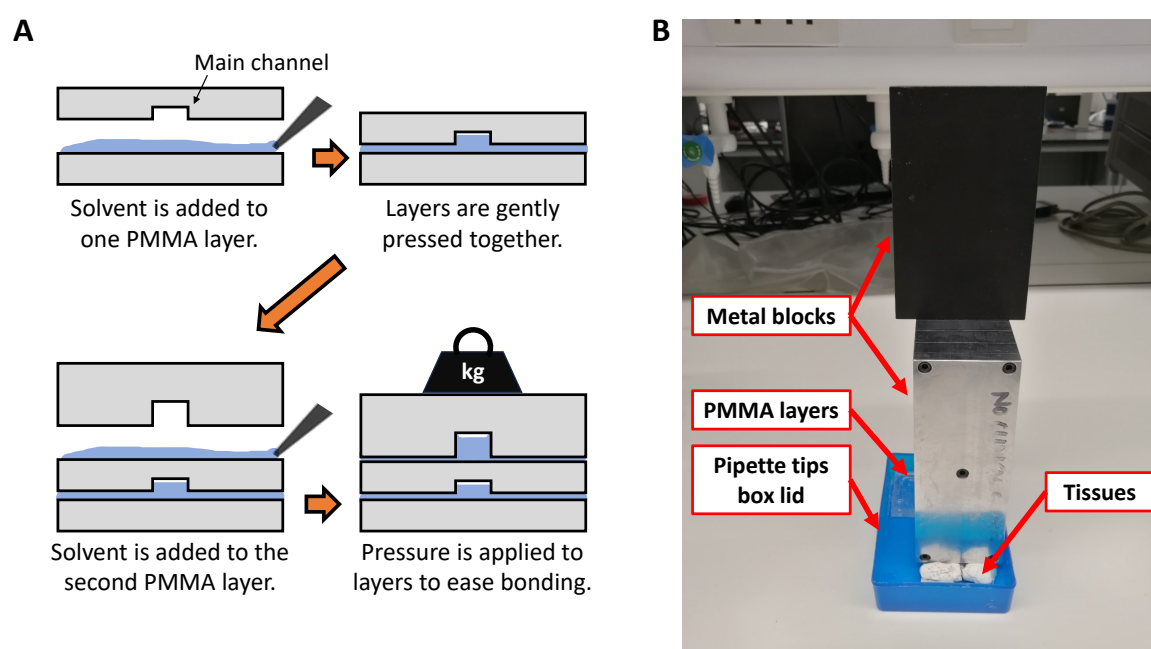


Figure 2.22: **Bonding process of three poly(methyl methacrylate) (PMMA) layers.** **A.** Schematic of the liquid phase solvent bonding process. A general liquid phase solvent bonding process with pure acetone was used. **B.** Weights applied on PMMA layers to create the plastic cassette for *E. coli* detection. Pressure between the PMMA layers was applied using two metal blocks of 1.72 kg and 0.84 kg on top of each other. The lid of a pipette tips box was used to prevent pure acetone to touch the bench surface. To ensure that the PMMA layers received the weight and that the metal blocks were stable, tissues were folded and placed accordingly.

Prior to stacking, plastic layers were cleaned with 70% ethanol and dried with lens cleaning paper. 800 μ L of acetone was added to the bottom layer of the stack using a pipette, and the two PMMA layers were brought together to create a uniform film of solvent while avoiding air bubbles at the bonding interface. Additional 800 μ L of acetone was added to the second layer of the stack, and the top PMMA layer was placed on top. Pressure was applied on the bonding stack for one hour and a half at

room temperature by adding weights on top of the stack (Fig. 2.22B). After bonding, a air blow gun was used to remove any remaining liquid in open channels.

2.16.2.2 Purification and Amplification Unit

The content of the purification & amplification unit (Fig. 2.19B), from bottom to top, consists of a bottom air-dried pullulan disc ($\varnothing 6$ mm, 2.8% w/v pullulan), two $\varnothing 5$ mm Whatman[®] Grade 3 paper discs with lysis buffer dried on, a top air-dried pullulan disc ($\varnothing 6$ mm, 3% w/v pullulan), and LAMP reagents stored in 5%/10% (w/v) pullulan and 0.5M trehalose (see Section 2.15.1.3). A 2X concentration of lysis buffer # 2 from Zou *et al.* [21] was dried on the paper discs as described in Sections 2.2, 2.14.3. Pullulan discs with different concentrations, 2.2%, 2.4%, 2.6%, 2.8%, were tested as bottom delay layer (see Section 2.16.3.2 for detailed volumes). Each component was added inside the chamber using tweezers from bottom to top, before the device was sealed.

2.16.2.3 Final Assembly

After the three PMMA layers were put together (Section 2.16.2.1), super glue (Cyanoacrylate 20 g, RS components Ltd., Northants, United Kingdom) was used to attach a silicone tube (2-mm inner diameter and 4-mm outer diameter) where the sample & re-suspension inlet is. The silicone tube was added to facilitate sample's introduction inside the device using a pipette.

Once the absorbent pad was inserted in the waste container and all the components of the purification & amplification unit were transferred into the sample chamber (Section 2.16.2.2), the device was sealed using an adhesive film (MicroAmp[™] Optical Adhesive Films). The back side of tweezers was used to make the adhesive film adhere with PMMA, and the adhesive film was wrapped around the device so that also the sides of the device were closed (Fig. 2.23). In some of the devices an extra piece of PMMA was added on the top layer to fill in the open space above the waste container that served to insert the absorbent pad. In this case, the device was sealed after having added the extra piece. A $\varnothing 2$ mm hole puncher or a blade were used to create a hole in the washing buffer unit to allow introduction of washing buffer.

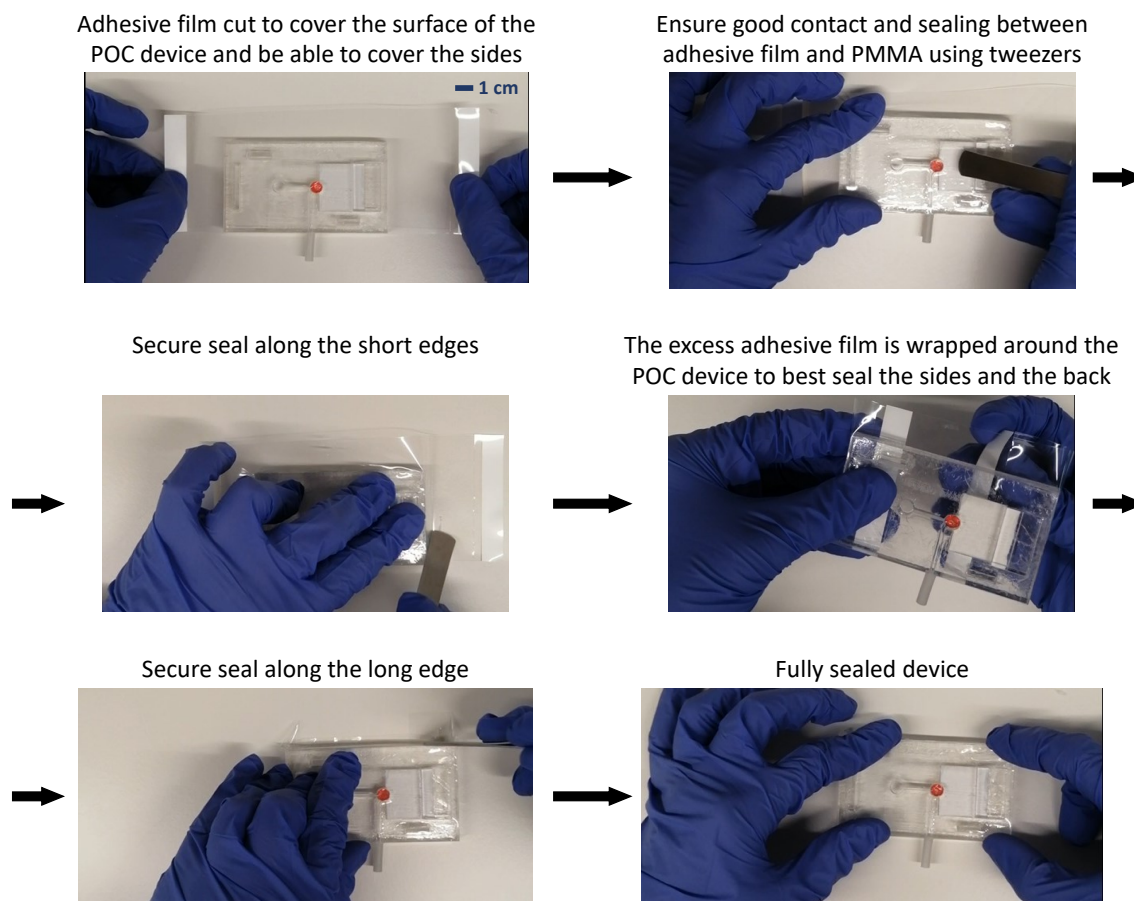


Figure 2.23: Device sealing process using an adhesive film.

2.16.3 Pullulan Tablets as Delay Layers for Fluids Control

Pullulan can be used as a timing element that can spatio-temporally control reagents release and fluid motion [123]. This section describes the method used to measure the dissolution time of pullulan in a 100 μL solution; 100 μL was used to simulate the expected volume of the sample specimen introduced in the POC device (Section 2.16.1).

2.16.3.1 Creation of Pullulan tablets with a defined dimension

To create pullulan tablets of 5-mm and 6-mm diameter that fit the central chamber of the POC device, glass slides with hydrophilic circles of the desired diameters were used. To form circles with the required sizes, a method similar to pattern transfer by photolithography with a negative photoresist was applied to deposit SU-8. The glass areas that needed to remain hydrophilic were covered with SU-8. Hydrophobic barriers were created around the SU-8 circles via salinization.

First, the photoresist was deposited on the glass substrate ($5.2 \times 7.1 \times 1.2 \text{ cm}^3$) through spin coating. Then, a photomask with the desired pattern was aligned over the glass

and UV-light was shone on it. The unexposed resist could then be removed by a developer, leaving the desired pattern on the photoresist. The photomask and the patterned glass slides were kindly provided by Yunus Aslan.

The pattern created consisted of 15 circles of either 5-mm or 6-mm diameter aligned in 3 rows and 5 columns. To create hydrophobic barriers around the circles, Trichloro(1H,1H,2H,2H-perfluorooctyl) silane (silane) (Sigma-Aldrich) was used. To prepare the glass for silanization, the glass slides were placed in a vacuum chamber along with a weighting boat with a drop of silane. Then the vacuum was turned on to let the silane evaporate. After 15 minutes, the vacuum was turned off and the chamber was kept closed for 15 more minutes. Next, everything was removed from vacuum and the glass slides were covered with acetone, inside a glass Petri dish. Acetone was used to remove SU-8 from glass slides (red spots) to free the hydrophilic circles. Finally, the glass was cleaned with NFW, and air-dried. Pullulan solutions of different concentrations were prepared, and 50 μL or 25 μL of them were deposited on the hydrophilic circles using a pipette (Fig. 2.24A). After 3 to 5 days of air-drying (Fig. 2.24B), each tablet was peeled off the glass slide using tweezers, and placed directly inside the POC device or collected in a small Petri dish for later use. When all the pullulan tablets were peeled off the glass slide, the glass slide was clean with NFW to remove any residual pullulan remained and 70% ethanol, and it was reused.

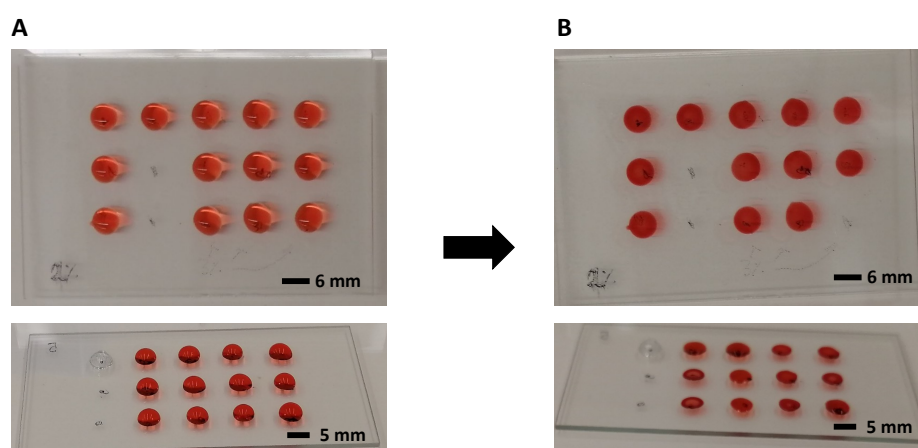


Figure 2.24: Pullulan tablets drying on glass slides to control pullulan discs dimensions.

2.16.3.2 Pullulan Tablets Containing Allura Red

Red pullulan tablets were created with the addition of Allura Red AC (Sigma-Aldrich, Merck KGaA) to monitor dissolution properties. The concentration of allura red re-

quired to perform the best colour change analysis was determined as explained in Section 2.16.3.3, and it was 0.1 g/L. Equations 2.3 describe how to calculate the concentration of allura red ($Concentration_I$) in the initial pullulan solution ($Volume_{Tab}$) to obtain 0.1 g/L allura red ($Concentration_F$) when the tablet is dissolved in 100 μ L ($Volume_F$).

$$Mass_I = Concentration_I \times Volume_{Tab} \quad (2.3a)$$

$$Concentration_F = \frac{Mass_I}{Volume_F} = \frac{Concentration_I \times Volume_{Tab}}{Volume_F} \quad (2.3b)$$

$$Concentration_I = \frac{Volume_F}{Volume_{Tab}} \times Concentration_F \quad (2.3c)$$

Where $Mass_I$ is the mass of allura red in the initial pullulan solution. For example, to make pullulan tablets from 50 μ L of pullulan solution that, once dissolved in 100 μ L, will yield a final concentration of 0.1 g/L allura red, the concentration of allura red needed in the initial pullulan solution would be derived as indicated below (Eq. 2.4).

$$Volume_{Tab} = 50 \mu L, Volume_F = 100 \mu L, Concentration_F = 0.1 g/L, \quad (2.4a)$$

$$Concentration_I = \frac{100 \mu L}{50 \mu L} \times 0.1 g/L = 0.2 g/L \quad (2.4b)$$

Before creating pullulan tablets, a stock solution of 10.5% (w/v) pullulan was prepared and filtered with a 0.2 μ m syringe filter. The stocks solution was preserved in a fridge until use.

All the tested pullulan solutions with allura red were prepared as indicated in Tables 2.10, and 2.11. The pullulan solutions to create the tablets that were later tested on the POC device are the ones in Table 2.11.

Table 2.10: **Pullulan tablets of different (w/v) concentrations that formed \varnothing 5-mm discs.** Tablets with 1%, 2%, 5% (w/v) pullulan were prepared to evaluate the dissolution rate. The final volume of each pullulan solution used to form one tablet was 25 μ L, but preparing solutions in larger volumes is recommended. The concentration of allura red in each pullulan solution is 0.4 g/L (derived as indicated by Eq. 2.3).

Final pullulan concentration	1%	2%	5%
Stock solution	Volume (μ L)		
Pullulan (10.5%)	2.38	4.76	11.90
Allura Red (25 g/L)	0.40	0.40	0.40
Nuclease-free water	22.22	19.84	12.70

Table 2.11: **Pullulan tablets of different (w/v) concentrations tested inside the point-of-care device; \varnothing 6-mm discs.** Tablets with 2-3% (w/v) pullulan were prepared to evaluate which tablet would allow for the best incubation time as bottom pullulan layer when the sample specimen was introduced inside the device. The final volume of each pullulan solution used to form one tablet was 50 μ L, but preparing solutions in larger volumes is recommended. The concentration of allura red in each pullulan solution is 0.2 g/L (derived from Eq. 2.3).

Final pullulan concentration	2%	2.2%	2.4%	2.6%	2.8%	3%
Stock solution	Volume (μ L)					
Pullulan (10.5%)	9.52	10.48	11.43	12.38	13.33	14.29
Allura Red (25 g/L)	0.40	0.40	0.40	0.40	0.40	0.40
Nuclease-free water	40.08	39.12	38.17	37.22	36.27	35.31

2.16.3.3 Dissolution Rate of Pullulan Tablets

To study the dissolution rate of pullulan tablets at different concentrations in a 100 μ L of liquid, colour change over time was used. The idea was to detect a colour difference between a pullulan tablet dissolving over time and either the non-dissolved pullulan tablet, the solvent, or pullulan tablet already dissolved in the solvent. Pullulan tablets of different concentrations were created by mixing pullulan, NFW and allura red, as described in detail in Sections 2.16.3.1, and 2.16.3.2. The solvent was a Xylene Cyanol FF (Thermo Fisher Scientific Inc.) solution.

The colour difference between RGB values (ΔE) of two areas of interest was computed using the MATLAB[®] built-in function *deltaE*; ΔE was computed for each pixel within two areas of interest in each image taken.

Colour Change (ΔE) Analysis - The highest difference in colour that the camera could detect when using a combination of allura red and xylene cyanol solutions was compared to unmixed allura red and xylene cyanol solutions. A flat-bottom 96-well plate was used to mix allura red and xylene cyanol solutions. The initial concentrations of allura red and xylene cyanol solutions used were 1, 0.5, 0.2, 0.1, 0.01 g/L and 4, 2, 1, 0.04, 0.004 g/L respectively. Each well contained a total of 100 μ L, 50 μ L of allura red solution and 50 μ L of xylene cyanol, meaning that each initial solution was further diluted two times. In the first row, A (Fig. 2.25A), 50 μ L of allura red and 50 μ L of NFW were added, obtaining a final row of concentrations of 0.5, 0.25, 0.1, 0.05, 0.005 g/L. In the first column, 1 (Fig. 2.25A), 50 μ L of xylene cyanol and 50 μ L of NFW were added, obtaining a final column with 2, 1, 0.5, 0.02, 0.002 g/L xylene cyanol solutions. The matrix of concentrations is shown in Fig. 2.25B. A picture of the 96-well plate for image analysis was taken using a camera (Nikon D5300 with Nikon

18-55 mm VR, Nikon Corp., Japan), and the settings were ISO4000, F6.3, 1/640.

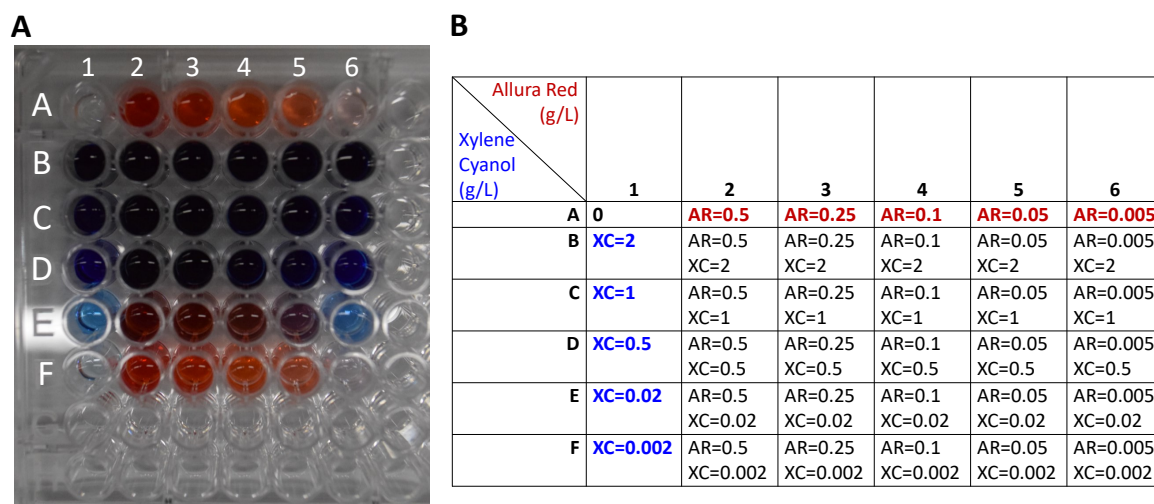


Figure 2.25: **Different combinations of Allura Red and Xylene Cyanol for pullulan tablets dissolution analysis.** **A.** 96-well plate containing different concentrations of allura red (AR) and xylene cyanol (XC). Control wells for XC are in column 1, whereas control wells containing only AR are in row A. **B.** Concentrations of AR and XC in the used wells of the 96-well plates.

For each well containing a combination of allura red and xylene cyanol solutions ('mixed' wells), the colour change (ΔE) was computed both with the respective allura red concentration in row A (red control), and with the respective xylene cyanol concentration in column 1 (blue control). For example, ΔE for 'mixed' well D2 was computed both with A2 (red control) and D1 (blue control). A larger ΔE value indicates a greater discrepancy in colour perception. ΔE computed for each 'mixed' well with each control was plotted onto a graph to best visualise the results. To understand how pullulan tablets dissolve, the combination of allura red and xylene cyanol that showed the highest ΔE when compared to the blue control was selected. It was also ensured that this mixture had a significant ΔE when compared to the red control. The MATLAB[®] code for this study was kindly provided by a colleague, Olivia McGleish (Appendix B.3.1).

Dissolution Measurements Set-Up and Image Acquisition - A PMMA mould was designed and cut from a 3-mm thick PMMA slab (Section 2.13), to create wells and allow for pullulan tablets dissolution measurements (Fig. 2.26A). A PMMA mould was used to obtain shallow wells ($\varnothing 8$ mm) that enabled the algorithm to detect the wells automatically. The wells were formed by sealing one side of the PMMA mould with an adhesive film (MicroAmp[™] Optical Adhesive Films). To facilitate the automatic identification of the wells, the edges of the wells used for image acquisition were coloured

with a black permanent marker (Fig. 2.26B). Six 8 mm diameter discs were punched from a second adhesive film, and they were placed inside each well using tweezers. The adhesive film used for creating the wells had their ‘sticky’ part exposed inside the well, which interfered with the even distribution of the liquid within the well. Therefore the 8-mm discs were used to cover the ‘sticky’ part of the adhesive film and expose again the smooth side of the film. The tip of tweezers was used to attach the discs to the other adhesive film inside the well. The camera was set up as shown in

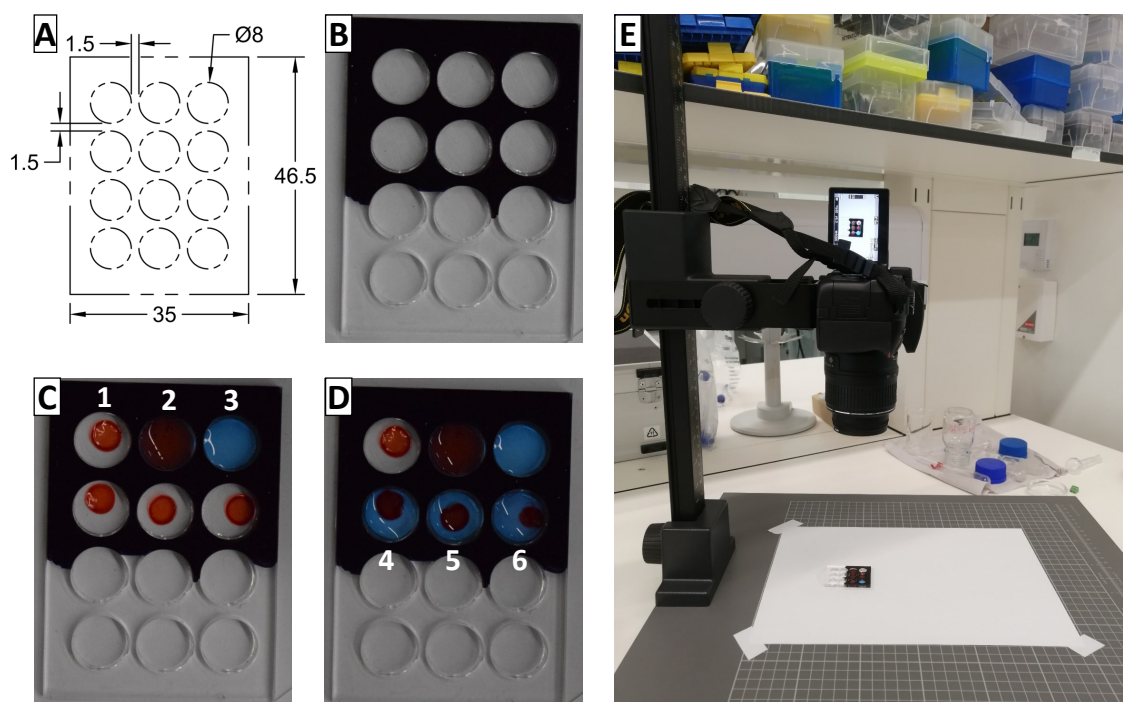


Figure 2.26: **PMMA mould for pullulan tablets dissolution measurements.** **A.** Dimensions of the PMMA in mm. **B.** Control 1. 3-mm thick PMMA mould sealed at the bottom. 6 wells have been marked with permanent black marker to facilitate automatic identification of the wells by the algorithm. **C.** Control 2 containing ‘well controls’. Three controls were added into the first three wells: (1) pullulan tablet only, (2) pullulan tablet dissolved in 100 μL of 0.02 g/L of xylene cyanol solution, and (3) 100 μL of 0.02 g/L of xylene cyanol solution. **D.** First picture taken after 100 μL of xylene cyanol solution were added to all the three wells. The replicates were numbered as 4, 5, 6, to simplify analysis. Images were after taken every 30 seconds. **E.** Camera set up for image acquisition.

Fig. 2.26E to facilitate the image capture every 30 seconds. A white A4 paper was secured on the board where the mould was placed, to create a white background. Two controls pictures were taken: with empty wells (Control 1), Fig. 2.26B, and with the three controls (Control 2: pullulan tablet only, 100 μL of 0.02 g/L of xylene cyanol solution, and pullulan tablet dissolved in 100 μL of 0.02 g/L of xylene cyanol solution), Fig. 2.26C. After, three tablets were added in the remaining wells ($n = 3$). When 100 μL of xylene cyanol solution was added to the first well containing the dried tablet, a stopwatch was started. The first picture was taken after all three wells were filled

with xylene cyanol solution (Fig. 2.26D) and pictures were taken every 30 seconds for 10 or 15 minutes. The camera settings were ISO4000, F6.3, 1/640. These settings allowed to capture a sharp and well-exposed image. A high ISO value was used to increase the sensitivity of the sensor to light, allowing us to capture a well-exposed image despite the low-light conditions. A moderate aperture (F) was used to achieve a good depth of field and focus on the wells. Images were captured every 30 seconds manually, because the built-in camera function was not optimal in the 10-15 minutes time-span.

Image Analysis and Statistical Analysis of ΔE - Images were used to compute the colour difference between the wells containing the pullulan tablets dissolving and each ‘well control’ (pullulan tablet only, 0.02 g/L of xylene cyanol solution, and pullulan tablet dissolved in xylene cyanol solution). The colour change was observed over time, and it was expected to reduce when the wells containing dissolving tablets were compared to the already dissolved tablet, until reaching a plateau. On the contrary, the colour change was expected to increase when the wells were compared to the xylene cyanol solution.

Images were acquired every 30 seconds. The mean value of the ΔE between two areas of interest was computed for each image ($\mu_{\Delta E}$) and plotted over time, resulting in a signal (Mean ΔE).

The MATLAB[®] code for wells identification was kindly provided by Olivia McGleish (Appendix B.3.2). The first control image served to automatically identify all the wells position (Control 1, Fig. 2.26B). The second control, Control 2, Fig. 2.26C, was used to compute the colour change between each well with pullulan tablets dissolving, wells 4, 5, 6 (Fig. 2.26D), and each ‘well control’ 1, 2 or 3 (Fig. 2.26C). The colour difference (ΔE) was computed for each pixel in each pair of wells, *e.g.*, Well 4 vs Well control 1, Well 4 vs Well control 2, Well 4 vs Well control 3. The mean of the ΔE for each pair of wells was computed ($\mu_{\Delta E}$), and this was done for all the loaded images, to understand how ΔE changed over time. For the first pullulan tablets studied, the information provided by comparing the wells with each ‘well control’ were observed to understand which comparison/ ΔE was providing the most meaningful information. It was then decided to compute the ΔE between each well containing the dissolving pullulan tablet and the already dissolved tablet in xylene cyanol solution. The mean of the ΔE for wells 4, 5, 6 compared to ‘well control 2’ was plotted for each image over time, and this

resulting signal (mean ΔE signal) was used to derive the time at which the pullulan tablet was considered completely dissolved in the solution. The pullulan tablets were considered completely dissolved when the mean ΔE signal reached plateau (time-to-plateau). The plateau was identified using a standard deviation filter and detecting the first point at which the filtered signal had a value lower than 0.15 (Appendix B.3.2). For each pullulan concentration, the experiment was run in triplicate ($n = 3$), in wells 4, 5, and 6. Mean and standard deviation of the three time-to-plateau identified for each replicate were computed and compared for tablets of different pullulan concentrations.

2.16.4 Microfluidic Device Testing and Development

To ensure the proper functioning of the device and the fluid dynamics, several tests were performed on the microfluidics of the device. The first test assessed the possibility of air-drying the pullulan layer at the bottom of the purification & amplification unit directly into the central chamber, to simplify assembly and reduce possible liquid leakages. The second test examined the dissolution behaviour of the pullulan tablets in the device. The tablets whose dissolution properties were studied as described in Sections 2.16.3.2 and 2.16.3.3 were used, and their dissolution behaviour on the device was compared with their dissolution properties from the previous characterisation. The third test evaluated the washing process of the paper discs inside the purification & amplification unit, by observing a colour change on the paper discs (step (iii) in Fig. 2.20). The last test consisted in running the whole workflow in the device, from PMMA stacking and assembly, to sample addition, heating, and detection, as described in Fig. 2.20 (Section 2.16.1).

The design of the POC device was adjusted according to the results of these tests, as explained in detail in Section 5.1.2. All the experiments in this section were performed using red or blue died water with allura red and xylene cyanol, respectively.

2.16.4.1 Pullulan Drying Inside The Device

To create the bottom pullulan tablet directly in the central chamber (Fig. 2.19B), 2% (w/v) pullulan solution (Table 2.11) was applied at 50 μL volume. However, the central chamber and the waste container share an opening, which allows the liquid to flow from the 2nd layer to the lower 1st PMMA layer. To prevent the pullulan solution from flowing from the 2nd to the 1st layer, polydimethylsiloxane (PDMS) was used

to seal the opening between the two layer temporarily, as shown in Fig. 2.27. The pullulan was let dry for 3-4 days and pictures were taken to understand if the drying was successful. Different channels geometries were tested to observe the behaviour of the liquids and if they were overflowing in adjacent channels.

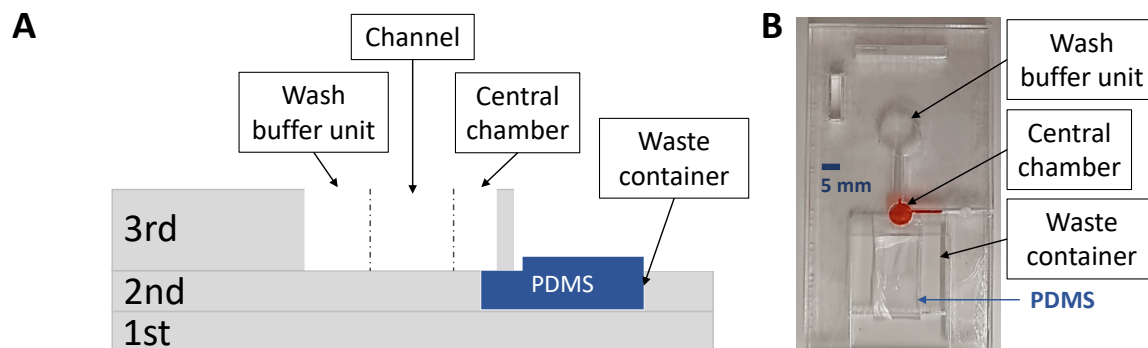


Figure 2.27: **Schematic of polydimethylsiloxane (PDMS) position to seal central chamber in point-of-care device.** **A.** Schematic of the cross-section of the point-of-care device. The three PMMA layers are shown and the PDMS is inserted in the 2nd layer. **B.** Image that shows the device from the top with PDMS inserted in the 2nd layer.

A very thick PDMS layer was made using a PDMS premix (one part curing agent and 10 parts base) available in the laboratory. 75 mL of premix was poured into a large square Petri dish covered in aluminium, and bubbles were removed by vacuuming the mixture. The mix was then cured overnight at 75 °C. From the thick PDMS layer, rectangles of about 1 cm×2 cm were cut out using a blade. About 4 mm on the long edge were cut to a thickness of about 2 mm to allow the PDMS to fit in the 2-mm-thick waste container.

2.16.4.2 Pullulan Incubation Studies and Washing of Paper Discs

Tablets containing a variety of pullulan w/v concentrations, from 2.2% to 2.8%, were prepared as described in Sections 2.16.3.2, and 2.16.3.1. One tablet at a time was added to the central chamber and two paper discs were placed on top of them (Section 2.16.2.2). In this set of experiments, paper discs did not have lysis buffer dried on them. A pipette tip was used to introduce 100 µL of a xylene cyanol solution into the device through the sample & resuspension inlet. The liquid reached the central well and the time elapsed before the liquid began to flow into the absorbent pad (incubation time) was measured using a camera that filmed the whole process (Fig. 2.28). The camera set-up was the same as the one described in Section 2.16.3.3.

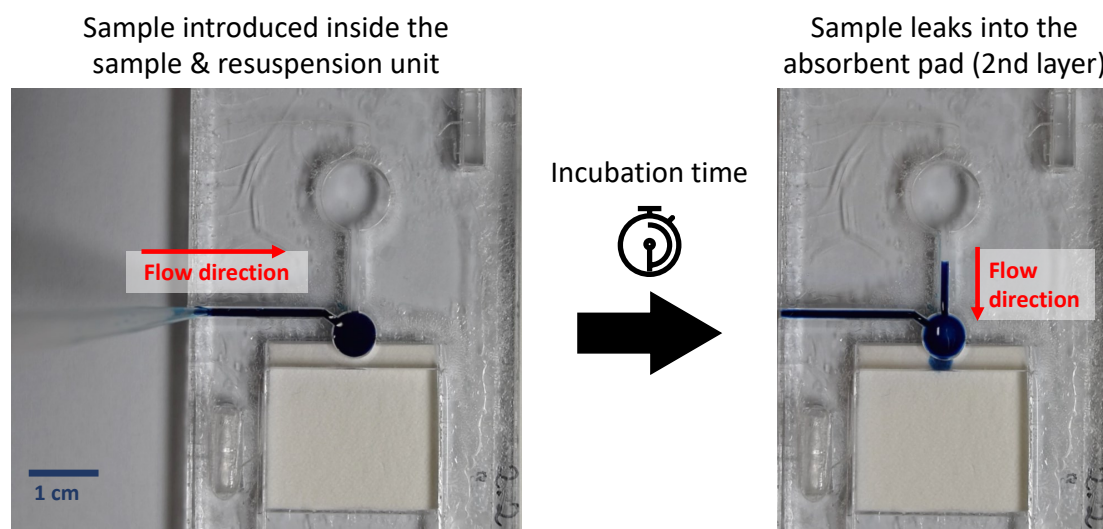


Figure 2.28: **Incubation time on the device determined by pullulan discs.** 100 μL of a xylene cyanol solution is introduced through the sample & resuspension inlet using a pipette. The time recorded between when all the liquid is pipetted into the sample & resuspension channel and when the liquid begins to flow into the absorbent pad is considered the incubation time that the pullulan tablet allows for.

To investigate the feasibility of washing both paper discs, after 6 minutes from the introduction of the xylene cyanol solution, 500 μL of NFW was added into the washing buffer unit very slowly until all the 500 μL flowed into the absorbent pad. The two paper discs were then taken out the central chamber and a picture was taken to observe the washing. The washing process was also tried after adding all the other components of the purification & amplification unit, such as the top pullulan tablet and two pullulan tablets mimicking the dried LAMP reagents. The two tablets mimicking dried LAMP reagents were created as described in Section 2.15.1.3 but without the use of molecular reagents; one tablet was created with 16 μL of 5% (w/v) pullulan and 0.5 M trehalose solution, the second tablet was created with 7 μL of 10% (w/v) pullulan and 0.5 M trehalose solution. When all the components of the purification & amplification unit were included, and after the 500 μL flowed into the absorbent pad, tweezers were used to take out the LAMP reagents tablets and paper discs. Also in this case, a picture was taken to observe the extent of dissolution of the upper pullulan layer and LAMP tablets, and the washing performance.

2.16.4.3 Full device operation

Devices were assembled as described in Section 2.16.2 and the full device operation was tested as illustrated in Fig. 2.20 (Section 2.16.1), starting from sample addition, to

reagents resuspension, heating for amplification and detection. After sample loading and washing, the washing unit was sealed with an extra piece of adhesive film and the sample & resuspension inlet was sealed carefully with parafilm. Observations about liquids flowing properly, heating for amplifications and general functioning of the device were drawn. The materials needed to test the full operation of the devices are given in Fig. 2.29.

No real sample or molecular reagents were used in these experiments. 100 μL sample specimen was substituted with 100 μL of xylene cyanol solution. The two tablets mimicking dried LAMP reagents were created as described above.

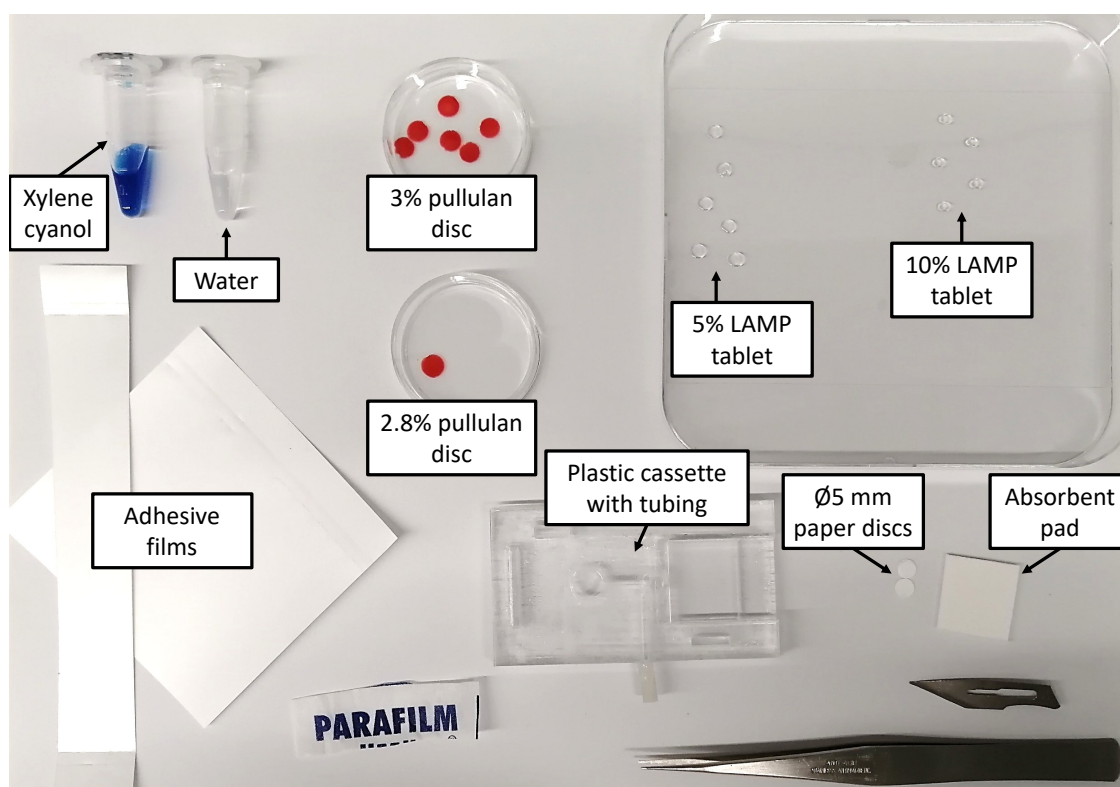


Figure 2.29: Materials needed to assemble and test the full operation of the *E. coli* point-of-care device.

2.16.5 Sample Processing and DNA Extraction On The Device Cassette

The paper-based DNA extraction with lysis buffer air-dried on paper discs (Section 2.14.3) was further evaluated to integrate the paper-based DNA extraction into the POC device described in Section 2.16.1.

The first step was to test the feasibility of drying extraction buffer # 2 [21] onto paper discs at two different temperatures. Next, the paper-based DNA extraction was

performed inside the POC device. The performance of extracting DNA from 100 μL of the same sample of *E. coli* bacterial cells (10^8 CFU/mL) resuspended as shown in Section 2.1 using the POC device, was compared to the *E. coli* DNA extracted using the magnetic-bead based method MagaZorb[®] DNA Mini-Prep Kit (Promega) (gold standard), and to the paper-based DNA extraction with lysis buffer air-dried on paper discs described in Section 2.14.3. Lastly, the paper-based DNA extraction with lysis buffer dried on two 5 mm diameter Whatman[®] Grade 3 discs was performed without the elution step, and the discs were directly inserted into 50 μL of LAMP reaction mix. The LAMP master mix used for these experiments is the one from NEB and it had the following final concentration in the 25 μL LAMP reaction: 1X Isothermal Amplification Buffer, additional 4 mM MgSO_4 , 0.48 U/ μL Bst 2.0 WarmStart[®] DNA Polymerase, 1.4 mM dNTPs and 0.5X LAMP Fluorescent dye (Table 2.2). 5 μL of 5X primer mix (for the detection of *E. coli*, Table 2.5) was added to obtain 20 μL LAMP mix. For a 50 μL LAMP reaction volume, the volumes for NEB master mix shown in Table 2.2 were doubled, and 10 μL of 5X primer mix was added to each reaction. For all the experiments described in this section, TTP values were extrapolated as shown in Section 2.7 and compared.

The DNA extraction performance of lysis buffer dried at 70 °C was compared with the lysis buffer air-dried on two paper discs. The drying step was carried out at 70 °C to ensure a rapid and complete evaporation of the lysis buffer and avoid premature or unwanted dissolution of the pullulan tablet in the purification & amplification unit during device assembly (Fig. 2.19B). 100 μL of 2X lysis buffer (extraction buffer # 2 [21], Section 2.2) was deposited on two 5-mm diameter Whatman[®] Grade 3 discs (as illustrated in Section 2.14.3). The discs were either air-dried for two weeks at room temperature or dried at 70 °C for 2 hours. After drying, the performance in extracting DNA of the lysis buffer dried in these two different ways was compared by carrying out the paper-based DNA extraction described in Fig. 2.9 and adding 1 μL of the eluant to the qPCR amplification mix (Section 2.6). Three biological replicates ($n = 3$) were run for each type of drying from the same *E. coli* sample. Additionally, three negative controls were prepared by adding 100 μL of 1X PBS instead of the sample, to rule out any false positives arising from the drying procedure. To ensure the validity and investigate the reproducibility of the results of the paper-based DNA extraction when the lysis buffer was dried at 70 °C, the DNA extraction was repeated with six biological

samples and three negative controls.

Next, the paper-based DNA extraction was performed on the POC device. The lysis buffer was dried on two paper discs as described above. The PMMA layers of the POC device were assembled as described in Section 2.16.2.1, and the design of the third PMMA layer is provided in Fig. 2.30A. The purification unit consisted of a 2.8% (w/v) pullulan disc, and two 5-mm Whatman[®] Grade 3 discs with lysis buffer dried on. The pullulan disc was prepared as described in Table 2.11 (Section 2.16.3.2), but adding 0.4 μL of NFW instead of allura red. A schematic of the DNA extraction is provided in Fig. 2.30B. 100 μL of *E. coli* sample was introduced inside the device, via the sam-

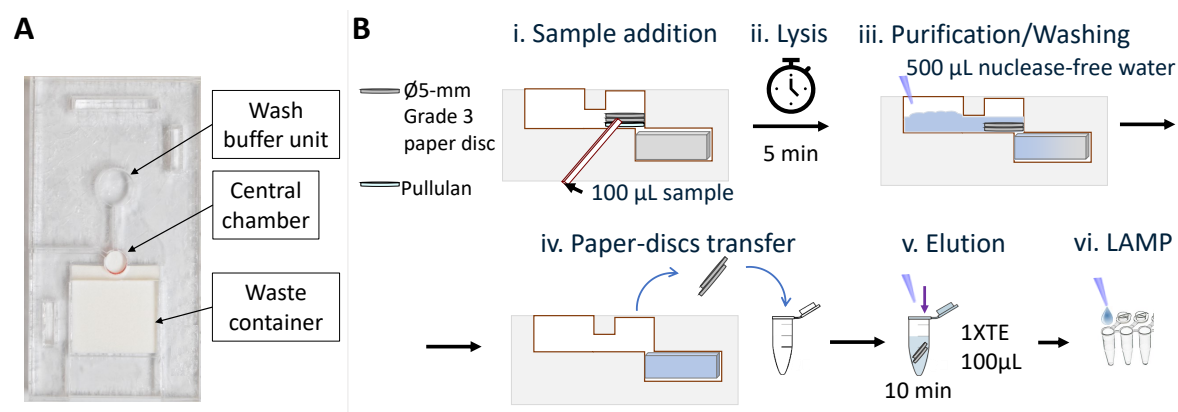


Figure 2.30: **Schematic of sample pretreatment on the point-of-care device.** **A.** Plastic cassette used for testing DNA extraction. **B.** Schematic of sample pretreatment on the device. The sample specimen is introduced into the device using a pipette tip (i). The sample reaches the central well where it is incubated onto two paper discs. The pullulan layer at the bottom delays the sample flow until it dissolves (ii). Then, the lysed sample moves to the waste container (absorbent pad) and 500 μL of washing buffer (NFW) are slowly added from the washing chamber to wash the paper discs (iii). The paper discs are transferred inside a tube (iv). Elution is performed by adding 1X TE buffer and incubating for 10 minutes at room temperature. 5 μL of eluant is added to the LAMP mix and real time LAMP is performed (vi).

ple & resuspension inlet, using a pipette tip. The sample reached the central well where it was incubated onto the two paper discs; this was facilitated by the delay action of the bottom pullulan layer. After 6 minutes, 500 μL of washing buffer (NFW) were added from the washing chamber. After all the washing buffer had flowed into the absorbent pad (2 cm \times 2 cm square of CF7), the two discs were transferred into a tube containing 100 μL of 1X TE buffer for elution. The paper discs were incubated for 10 min. 5 μL of eluant were transferred into the LAMP amplification mix for amplification. The experiment was performed in triplicate. Negative controls were also carried out by adding 100 μL of 1X PBS buffer instead of sample to exclude the possibility that the device handling led to false positive results. The performance of this extraction was compared to the gold standard and the paper-based DNA extraction performed in

tubes (as described above).

The paper-based DNA extraction with lysis buffer dried on 5-mm Whatman[®] Grade 3 discs was performed as described in Fig. 2.9 (Section 2.14.3). After washing, the two discs were transferred directly into the LAMP amplification mix and 10 μ L of NFW were added to the reaction to achieve a final volume of 50 μ L and guarantee that both two discs were immersed into the amplification mixture. The results were also visualised on LFSs.

Chapter 3

Paper-based Protocol to Extract Genomic Material from Bacteria in Large Volumes

This chapter describes the development of a new equipment-free protocol for nucleic acid extraction from a larger sample (100 μ L) than the usual finger prick volume using filter paper, and that can be performed at room temperature. A paper-based DNA extraction protocol has the potential to reduce the number of handling steps in sample pretreatment compared to the magnetic beads-based DNA extraction method previously implemented in a point-of-care (POC) device developed in my group (Reboud *et al.* [17]). Using paper in the extraction procedure can also reduce the number of buffers needed and it holds promise for an easy integration in a fully enclosed paper-based POC device, which can be used by unskilled healthcare personnel.

E. coli has been chosen as a proof-of-concept pathogen and *E. coli malB* gene was the conservative region that was targeted using LAMP [33]. The concentration of primers for an optimal LAMP assay has been optimised in Section 3.1.1 and the analytical sensitivity of the LAMP and qPCR assays is provided in Section 3.1.2.

Preliminary experiments focussed on investigating the paper ability to capture and release DNA for sample pretreatment application (Section 3.1.3). Whatman[®] Grade 1 filter paper was used and inspiration was taken from the work conducted by Zou *et al.* [21]. The results that led to an instrument-free and paper-based DNA extraction method consisting of seven handling steps are presented in Section 3.1.4. The established paper-based extraction method was optimised in terms of performance by inves-

tigating strategies to reduce the time-to-positive (TTP) or cycle threshold (Ct) values in LAMP and qPCR of the extracted DNA, respectively. The optimisation ranged from changing the components of the lysis buffer (Section 3.1.6) to the use of different paper sizes and types (Sections 3.1.7, 3.1.10). A second paper-based DNA extraction method similar to the one used by Reboud *et al.* [17] and the protocol by MagaZorb[®] DNA Mini-Prep Kit (Promega corporation) was investigated in order to introduce proteinase K during the lysis step (Section 3.1.8). Finally, Section 3.1.9 demonstrates how the lysis buffer can be stored dry onto paper-discs to facilitate the transport of reagents and their ‘on-board’ storage. The results are furthermore discussed in Section 3.2.

3.1 Results

As reported in Section 2.5, experiments involving a paper disc transferred directly into 21 μL of LAMP amplification mix, used a final mix of 5 μL of 5X primer mix (Table 2.5), 15 μL of master mix (ISO-004, Optigene Ltd.), and an additional 1 μL of green fluorescent dye (Green Fluorescent Dye, Cambridge Bioscience). The positive control (PC) was created by adding 4 μL of sample to make a final volume of 25 μL . The composition of the final qPCR reaction is the one indicated in Section 2.6. The statistical analysis performed to compare the TTP in LAMP and Ct values in qPCR amongst samples is described in Section 2.9.

3.1.1 Optimization of the Concentration of Primers for the Detection of *E. coli malB* Gene with LAMP

Three different concentrations of primers were tested for the LAMP reaction, as indicated in Table 3.1.

Table 3.1: Concentrations of primers used in the final LAMP reaction for the detection of *E. coli malB* gene.

	Concentration of primers [μM]		
	Concentration 1	Concentration 2 [33]	Concentration 3
F3 and B3	0.067	0.2	0.2
FIP and BIP	0.534	1.6	0.8
LF and LB	0.266	0.8	1

The final LAMP reaction mix (total, 25 μL) contained 15 μL of isothermal master mix, 1 μL of additional fluorescent die and 4 μL of *E. coli malB* gene synthetic DNA sequence

(this is the same LAMP reaction mix used when paper discs are deployed but no paper is used in this section). Concentration 1 was first considered because it was an established concentration used within the AB group in the Biomedical Research Division at The University of Glasgow. However, amplification of a sample with DNA concentration of 20.0 ± 1.79 ng/ μ L (extracted from a bacterial culture of 9.13×10^8 CFU/mL) occurred very late, after 20 minutes (results not shown). For this reason Concentrations 2 and 3 were investigated. The limit of detection (LOD) for all the 3 concentrations was 1,820 copies/reaction (Fig. 3.1).

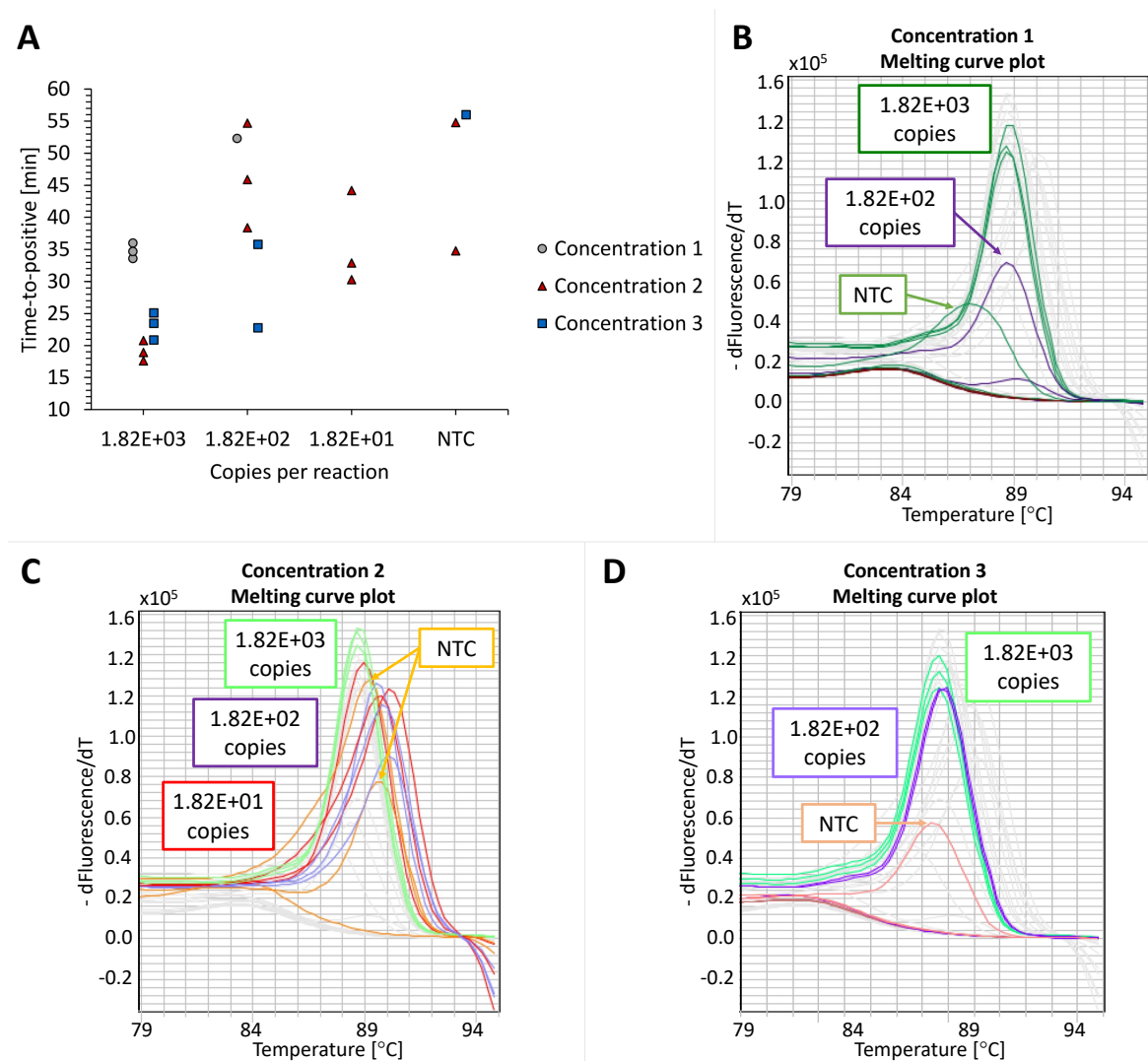


Figure 3.1: **Time-to-positive values (TTPs) and melting curve plots of LAMP reaction for the detection of *E. coli malB* gene using three different concentrations of primers.** The three primer concentrations used are given in Table 3.1. **A.** TTPs of LAMP reaction performed with Concentration 1, 2 and 3. Data points denote the TTPs for each LAMP assay. Data points with the same color and shape are replicates run in the same conditions ($n = 3$). **B.** Melt curve plots for Concentration 1. **C.** Melt curve plots for Concentration 2 by Hill *et al.* [33]. **D.** Melt curve plots for Concentration 3.

Using Concentration 1, it was possible to detect 1,820 copies within 40 minutes, while 1,820 copies/reaction were detected within 25 minutes and 30 minutes when using

Concentration 2 and 3, respectively (Fig. 3.1A). Most of the repeated experiments detected 182 copies/reaction when using Concentrations 2 and 3, but amplification did not occur consistently for all the replicates. When using very low concentrations of template DNA (lower than 182 copies) and Concentration 2, the melting curves started shifting from the reference value of 88.66 °C to 89.90-90.20 °C (Fig. 3.1C). This shift of approximately 2 °C led to think that Concentration 2 appeared to be prone to false positives after 30 minutes of LAMP incubation. In the end, Concentration 3 was chosen for further experiments because it appeared to be less prone to false positives after long running times (>30 min) compared to Concentration 2 and offered the same LOD (1,820 copies of *E. coli malB* gene synthetic DNA). Moreover, Concentration 3 gave shorter TTP values than Concentration 1. Therefore, the final LAMP reaction mix contained 0.2 μM of each outer primer (F3, B3), 0.8 μM of each inner primer (FIP, BIP), and 1 μM of each loop primer (LF, LB).

3.1.2 LAMP and qPCR Assays for the Detection of *E. coli malB* Gene

The analytical sensitivity of LAMP using Concentration 3 (Table 3.1) was tested a second time using 10-fold dilutions of *E. coli malB* gene synthetic DNA ranging from 1.82×10^5 to 1.82 copies/reaction. The associated standard curve is shown in Fig. 3.2A, with a correlation R^2 of 97%.

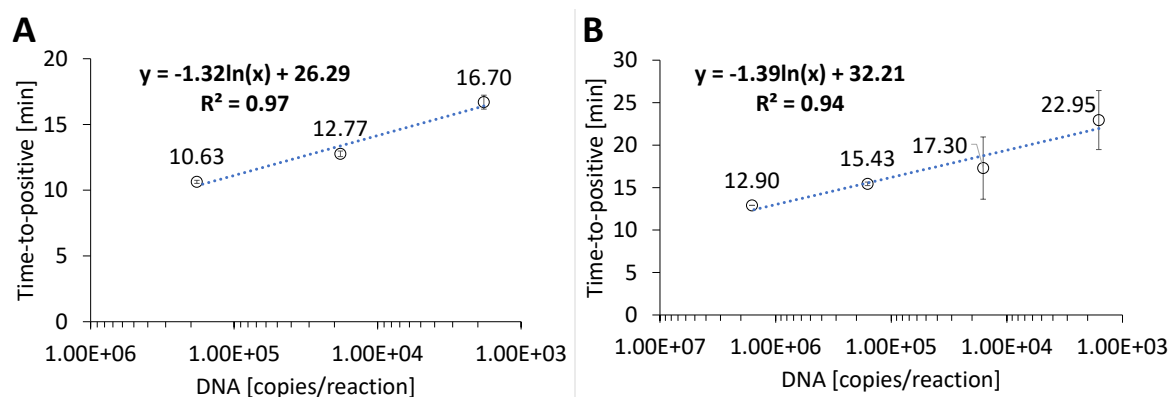


Figure 3.2: **Analytical sensitivity and standard curves of the LAMP assay for the detection of *E. coli malB* gene.** 4 μL of sample was introduced in the final 25 μL of LAMP reaction. **A.** Standard curves obtained using *E. coli malB* gene synthetic DNA (204 bp). **B.** Standard curves obtained using *E. coli* genomic DNA extracted using a magnetic beads-based method. The length of the genome sequence of *E. coli* strain K12 is 4,639,675 bp [148]. The circles indicate the mean of the TTP values of 3 replicates ($n = 3$), and the vertical bars denote the standard deviation of the replicates.

The LOD using synthetic DNA in LAMP is 1,820 copies (10^{-7} ng/μL sample concen-

tration, Table 3.2). It was possible to detect 182 copies, but only two, out of three replicates amplified. The analytical sensitivity of this assay is lower than the one presented in Hill *et al.* [33], where a sensitivity of 10 copies was claimed. The sensitivity was also tested using extracted DNA from an original 10^8 CFU/mL *E. coli* K12 sample with subsequent 10-fold dilutions of the initially extracted DNA. The standard curve using extracted DNA is provided in Fig. 3.2B. The LOD using *E. coli* DNA extracted through the magnetic beads-based extraction method (MagaZorb[®] DNA Mini-Prep Kit) is 16,000 copies (2.01×10^{-2} ng/ μ L sample concentration, Table 3.3). The assay was able to detect 1,600 copies, but only two replicates out of three amplified. The LAMP assay appeared to not be sensitive enough for in-field applications. However, the focus of this chapter and the primary goal of my PhD project is not to create a sensitive and specific LAMP assay for *E. coli* detection, but to provide further advances in integrating the nucleic acid amplifications tests onto a sample-in-answer-out device where *E. coli* only serves as a proof-of-concept pathogen.

Table 3.2: **Conversion table for 204 bp long *E. coli malB* gene synthetic DNA from ng/ μ L to copy number per LAMP reaction.** 4 μ L of sample whose concentration was measured in ng/ μ L was added to the final 25 μ L LAMP reaction. The conversion was obtained as explained in Section 2.10.

Concentration in ng/ μ L	Concentration in copies/reaction
1.00E-05	1.82E+05
1.00E-06	1.82E+04
1.00E-07	1.82E+03
1.00E-08	1.82E+02

Table 3.3: **Conversion table for 4,639,675 bp long *E. coli* genomic DNA from ng/ μ L to copy number per LAMP reaction.** DNA was extracted using the magnetic beads-based method. The concentration of DNA in the extracted sample was measured in ng/ μ L and 4 μ L of this was added to the final 25 μ L LAMP reaction. The conversion was carried out as explained in Section 2.10.

Concentration in ng/ μ L	Concentration in copies/reaction
2.01E+01	1.60E+07
2.01E+00	1.60E+06
2.01E-01	1.60E+05
2.01E-02	1.60E+04
2.01E-03	1.60E+03

The analytical sensitivity of qPCR was also tested using 10-fold dilutions of *E. coli malB* gene synthetic DNA ranging from 4.5×10^8 to 4.5 copies/reaction. The associated amplification curves and standard curve are shown in Fig. 3.3A, and B, with a correlation R^2 of 100%. The LOD in qPCR using synthetic DNA is 45 copies (10^{-7} ng/ μ L sample concentration, Table 3.4).

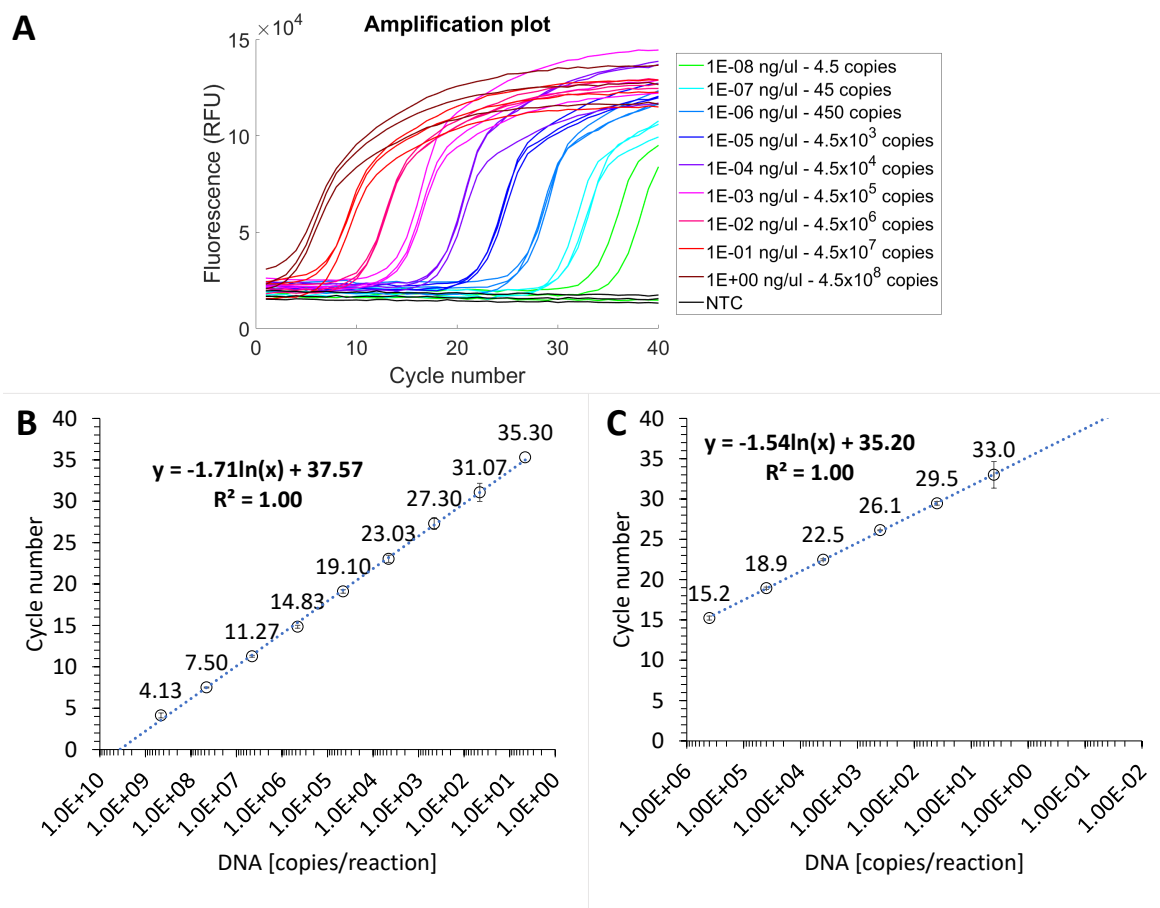


Figure 3.3: **Analytical sensitivity and standard curves of the qPCR assay for the detection of *E. coli malB* gene.** **A** Amplification curves obtained using 10-fold dilutions of *E. coli malB* gene synthetic DNA ranging from 4.54×10^8 to 4.54 copies/reaction. **B.** Standard curves obtained using *E. coli malB* gene synthetic DNA (204 bp). **C.** Standard curves obtained using *E. coli* genomic DNA extracted using a magnetic beads-based method: 4,639,675 bp. The circles indicate the mean of the cycle threshold (Ct) values of 3 replicates ($n = 3$), and the vertical bars are the standard deviation of the replicates.

The sensitivity was also tested using extracted DNA from an original 10^8 CFU/mL *E. coli* K12 sample with subsequent 10-fold dilutions of the initially extracted DNA. The standard curve using extracted DNA is provided in Fig. 3.3C. The LOD in qPCR using *E. coli* DNA extracted using the magnetic beads-based method is 4 copies (2.01×10^{-4} ng/ μ L sample concentration, Table 3.5).

Table 3.4: **Conversion table for 204 bp long *E. coli malB* gene synthetic DNA from ng/ μ L to copy number per reaction in qPCR.** 1 μ L of template whose concentration was measured in ng/ μ L was added to the final 25 μ L qPCR reaction. The conversion was obtained as explained in Section 2.10.

Concentration in ng/ μ L	Concentration in copies/reaction
1.00E+00	4.54E+08
1.00E-01	4.54E+07
1.00E-02	4.54E+06
1.00E-03	4.54E+05
1.00E-04	4.54E+04
1.00E-05	4.54E+03
1.00E-06	4.54E+02
1.00E-07	4.54E+01
1.00E-08	4.54E+00

Table 3.5: **Conversion table for 4,639,675 bp long *E. coli* genomic DNA from ng/ μ L to copy number per reaction in qPCR.** *E. coli* DNA was extracted using the magnetic beads-based method and its concentration was measured in ng/ μ L. 1 μ L of sample was used in the final 25 μ L qPCR reaction, and the conversion was carried out as explained in Section 2.10.

Concentration in ng/ μ L	Concentration in copies/reaction
2.01E+01	4.00E+05
2.01E+00	4.00E+04
2.01E-01	4.00E+03
2.01E-02	4.00E+02
2.01E-03	4.00E+01
2.01E-04	4.00E+00

3.1.3 Ability of Filter Paper to Capture DNA

As described in Chapter 2.14.1, the first step was to evaluate the ability of *E. coli* DNA to bind to (or being captured by) Whatman[®] Grade 1 filter paper. The very first experiment was performed with an already purified DNA sample and aimed at observing the ability of DNA to bind to untreated filter paper. Attention was paid to DNA amplification rather than the reaction efficiency. The concentration of primers used for this set of experiments is Concentration 1, given in Table 3.1. The DNA concentration of the given stock was ~ 5 ng/ μ L. Following the procedure illustrated in Fig. 2.4A, with 1 min contact time, the time-to-positive of the sample was found to be 27.9 ± 7 min against the positive control (PC), with no paper disc, at 20 min. This result showed the possibility of using Whatman[®] Grade 1 to trap DNA onto it and release it in a second moment into the LAMP reaction mix to perform nucleic acid (NA) amplification.

DNA incubation time was addressed as the first element that could have affected the

efficiency of the procedure (as explained in Chapter 2.14.1). The DNA concentration of the already extracted DNA was 5 ng/ μ L and a 10-fold dilution of DNA was performed to obtain a concentration of 0.5 ng/ μ L that was used for investigating different DNA-paper incubation times. DNA was incubated onto paper for 1, 5 and 10 min, and the results are presented in Fig. 3.4. Amplification was obtained only for the two replicates of the reference sample with 5 ng/ μ L DNA incubated for 1 min, and the 0.5 ng/ μ L DNA incubated for 5 min. In the other samples, amplification did not occur. After one minute of incubation either no amplification or very late amplification was obtained, showing that probably 1 min is not enough to allow DNA binding. On the other hand, no amplification after 10 minutes was linked to the idea that DNA has the time to diffuse to the innermost part of the paper disc having difficulties in being released in the successive LAMP step. Therefore, the DNA incubation time onto the paper has been optimized as 5 minutes.

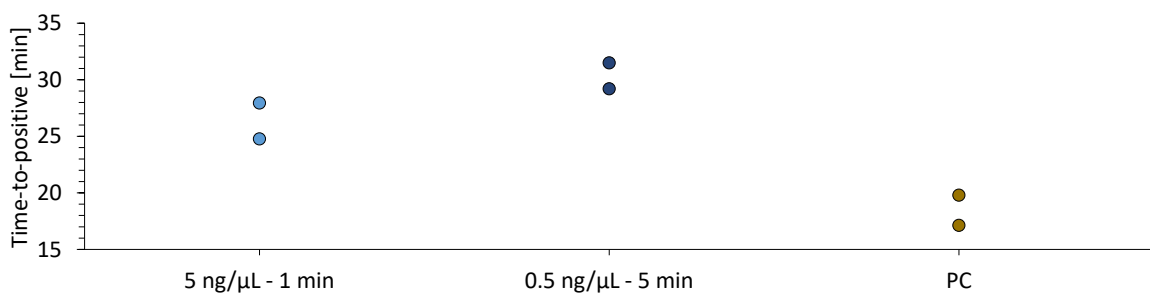


Figure 3.4: **DNA-paper incubation time comparison when using the first procedure:** Time-to-positive values are given for different samples taken into account. The data points represent the time, in minutes, at which each assay was amplified (time-to-positive). The experiment was run in duplicate ($n = 2$). *PC* is the positive control whose DNA concentration is ~ 5 ng/ μ L. Two negative controls were analysed: no template control with paper disc, *i.e.*, 3 mm paper disc was washed 1 min before being put in the LAMP mix, and no template control. All negative controls did not show amplification (data not shown). In the first sample, 3 μ L of 5 ng/ μ L DNA sample was pipetted onto a paper disc and incubated for 1 min (5 ng/ μ L - 1 min). In the other three samples, 3 μ L of 0.5 ng/ μ L DNA was pipetted onto the paper disc and incubated for 1 min (0.5 ng/ μ L - 1 min), 5 min (0.5 ng/ μ L - 5 min) and 10 min (0.5 ng/ μ L - 10 min). Amplification did not occur for those samples with 0.5 ng/ μ L DNA incubated for 1 min and 10 min.

A new stock of already purified DNA was used for the next experiments. Its concentration was measured and it was 54.8 ± 1.2 ng/ μ L. A second procedure was carried out and compared with the previous one. The difference between the two procedures lies in the way that the paper discs and the DNA comes into contact, *i.e.*, in the second procedure (“in tube”) the paper disc is immersed in the sample, see Fig. 2.4B. When using the “in tube” procedure, the stock solution was diluted by 10-fold, to make a sample volume of 100 μ L. The “in tube” results were compared to the initial procedure

in Fig. 3.5, using the non-diluted DNA stock sample.

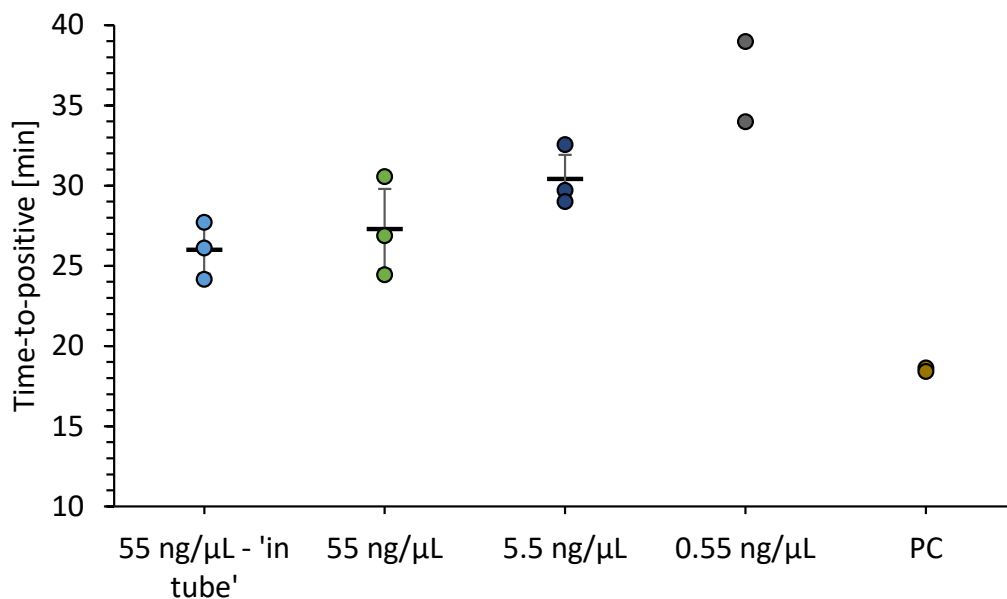


Figure 3.5: **Comparison between the first and “in tube” procedures.** Time-to-positive values (TTPs) are shown for different DNA concentrations. The data points represent the TTPs for each biological replicate. The horizontal bars represent the mean value of the TTPs of the three biological replicates run for the same sample ($n = 3$). In case of less than three positive replicates, the horizontal bar is not given. *PC* is the positive control whose DNA concentration is 54.8 ± 1.2 ng/μL. Two negative controls were investigated, one with a washed paper disc, and one with the no template control. All negative controls did not show amplification (data not shown). “In tube” stands for the second procedure where the paper disc is immersed in the sample rather than the sample being pipetted onto the disc. The other concentrations relates to the procedure where the DNA is pipetted onto the discs.

The “in tube” procedure shows a time-to-positive mean value of 26.7 ± 2.1 min, which is slightly lower than the one of the first procedure (27.2 ± 3.1 min) and it has a lower standard deviation ($n = 3$), *i.e.*, the variation of time-to-positive values in the triplicate is smaller (Fig. 3.5). Therefore, the “in tube” procedure was investigated more in-depth and a sensitivity experiment was performed using a series of 10-fold dilutions from 5 to 0.005 ng/μL (results in Fig. 3.6).

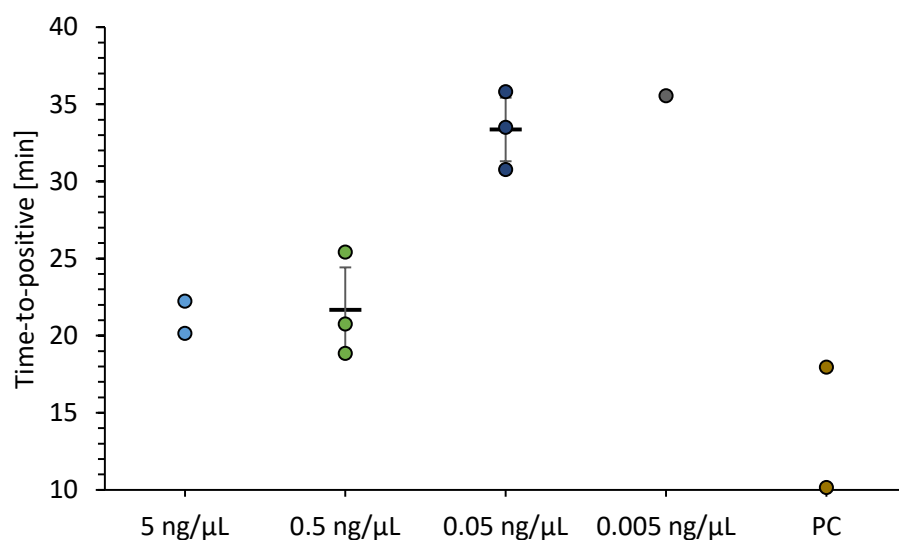


Figure 3.6: **Sensitivity of “in tube” procedure.** Time-to-positive values (TTPs) for each concentration of already purified DNA. The data points represent the TTPs of each assay. The horizontal bars represent the mean value of the TTPs of assays belonging to the triplicate run for the same sample ($n = 3$). *PC* is the positive control whose DNA concentration is 54.8 ± 1.2 ng/μL. The negative control (no template control with paper disc) did not show any amplification (data not shown). The paper disc is immersed in the sample.

Fig. 3.6 shows that the sample with 0.05 ng/μL DNA becomes positive at 33.4 ± 2.5 min. Even if the time-to-positive is high and the variation among the three replicates is high, a relatively low concentration was detected. In general, amplification happens faster when the “in tube” procedure is followed than when using the first procedure. However, the fact that the TTP values for the sample with 5 ng/μl in Fig. 3.6 are lower than the TTP values for a concentration of 55 ng/μl in Fig. 3.5 shows that some handling issues have probably been encountered. Please, note that these experiments have been performed in the very first months of my PhD programme, where I was still becoming familiar with molecular biology procedures and the equipment. In any case, when comparing the above mentioned experiments, “in tube” procedure was quite well-performing and therefore have been employed for further experiments.

In conclusion, Whatman[®] Grade 1 can capture DNA and release it into the final LAMP amplification mix generating clear amplification curves both when a solution of DNA is directly deposited onto the paper disc, or when the paper discs are immersed in a solution containing DNA. The paper discs inserted into the LAMP amplification mix interfered with the detection of the emitted fluorescence in the real-time LAMP instrument by generating curves that are not completely flat in the first minutes, making it difficult to identify the baseline for noise reduction of the signals. Nevertheless, it was still possible to determine the TTP values using the second derivative of the fluorescence signal (as explained in Section 2.7).

3.1.4 Reduction of Initial Number of Steps and Procedure Optimization of the Paper-Based DNA Extraction Method Based on Zou *et al.* (2017)

In this section, all paper-based extractions were carried out from a 10^8 CFU/mL *E. coli* K12 sample, and the concentration of primers used was Concentration 3 (Table 3.1), unless otherwise stated.

3.1.4.1 Optimization of Lysis Temperature, Buffer and Incubation Times

As a first step, the feasibility of removing the paper washing step (step 8 in Fig. 2.5B) from the DNA extraction procedure was evaluated to decrease the number of handling steps. No amplification was observed in the absence of the washing step highlighting its importance in removing possible LAMP inhibitors from the paper disc (results not shown).

Successively, the DNA extraction procedure illustrated in Fig. 2.5B was performed using two different lysis buffers. The two lysis buffers tested were the extraction buffer # 2 from Zou *et al.* [21] ('LB by Zou et al.' in Fig. 3.7A) and the lysis buffer provided in the MagaZorb[®] DNA Mini-Prep Kit ('LB by Magazorb kit' in Fig. 3.7A). When using 'LB by Zou et al.', 100 μ L of sample was mixed with 400 μ L of lysis buffer at 1:5 ratio, following the protocol in [21]. When using 'LB by Magazorb kit', 100 μ L of sample was mixed with 200 μ L of lysis buffer at 1:3 ratio, following the manufacturer protocol. The experiment was performed for three biological replicates ($n = 3$) for each sample (Fig. 3.7A). One-way ANOVA with Tukey-Kramer's post-hoc test was performed to compare the TTPs amongst the positive control and the samples extracted using the two different lysis buffers (as explained in Section 2.9). The mean TTP values when using 'LB by Zou et al.' and 'LB by Magazorb kit' were 13.47 ± 0.57 min and 13.87 ± 0.15 min, respectively. No statistically significant differences were observed for p -value < 0.05. Therefore, the successive experiments were performed using the extraction buffer # 2 from Zou *et al.* [21] since the concentration of each component was known, unless otherwise specified.

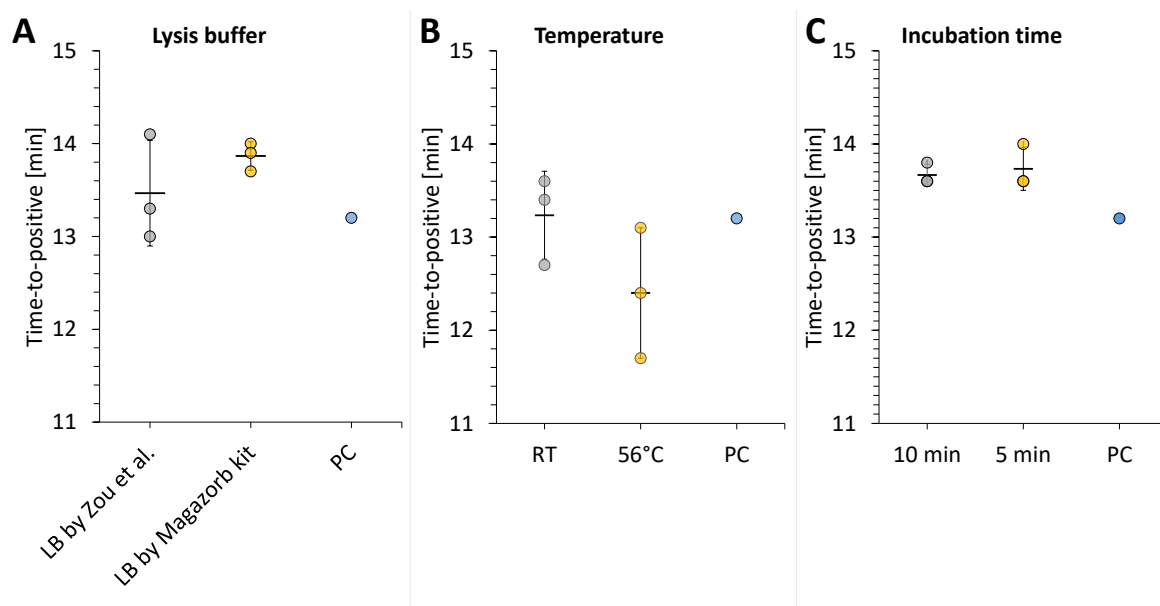


Figure 3.7: **Time-to-positive values (TTPs) of paper-based extraction when changing lysis step conditions, *i.e.*, lysis buffer, temperature and incubation time.** In all graphs, the x-axis includes the different DNA extraction conditions. PC is the positive control whose DNA concentration is 19 ng/ μ L. The experiments were performed for three biological replicates ($n = 3$) for each DNA extraction condition. The data points represent the time (in minutes) at which each biological replicate was amplified. The horizontal bars represent the mean value of the TTPs of the three biological replicates. Error bars are the standard deviation for $n = 3$. The PC was extracted following the manual instructions from MagaZorb[®] DNA Mini-Prep Kit and in this experiments served only to make sure that the reagents were working properly. NTCs are not shown but they represent the no template controls containing a paper disc. **A.** TTPs of paper-based extraction using two different lysis buffers: extraction buffer # 2 from Zou *et al.* [21] (LB by Zou et al.) or the lysis buffer provided in the MagaZorb[®] DNA Mini-Prep Kit (LB by Magazorb kit). **B.** TTPs of paper-based extraction using two different lysis temperatures: room temperature (RT) and 56 °C. **C.** TTPs of paper-based extraction for 5 and 10-min lysate-paper incubation time. The paper disc is incubated with the lysate for 10 or 5 minutes. No statistically significant differences were observed for p -value < 0.05 when using one lysis buffer rather than the other, or room temperature rather than 56 °C, or 5 minutes incubation than 10 minutes.

As explained in Chapter 2.14, the performance of the lysis step at room temperature (Step 4 in Fig. 2.6A) was assessed to avoid the use of an external heating during the sample pretreatment. The two temperatures investigated for the lysis were 56 °C (as used in the instructions provided in MagaZorb[®] DNA Mini-Prep Kit) and room temperature. Three biological replicates ($n = 3$) were carried out for each temperature condition and the results are given in Fig. 3.7B. To compare the time-to-positive amongst the samples extracted using the two different lysis temperatures the statistical analysis described in Section 2.9 was used. The mean TTP values when the lysis happened at room temperature was 13.23 ± 0.47 min, while at 56 °C amplification happened at 12.40 ± 0.70 min. Lysing the sample at room temperature did not show a statistically significant difference (p -value > 0.05) than lysing the sample at 56 °C. This result allowed to eliminate the heating step during the sample pretreatment.

Taking into account the DNA incubation time investigated in Section 3.1.3, the best performing time of contact between the lysate (DNA) and the paper-disc (Step 6 in Fig. 2.6A) was investigated again. This time, 5 and 10 min were considered to understand which incubation time gave the shortest TTP. The experiment was performed in biological triplicate ($n = 3$) for 5 and 10 min incubation time. One-way ANOVA with Tukey-Kramer's post-hoc test was carried out to compare the time-to-positive amongst the different incubation times. When the lysate and paper-disc were incubated for 5 min the mean time-to-positive value was 13.73 ± 0.23 min. This TTP value was not significantly different ($p\text{-value} > 0.05$) from the TTP value of a 10-minutes incubation time (13.67 ± 0.12 min). This is in contrast with what it was found previously in Section 3.1.3, where a 10 minute contact time between the DNA and paper did not lead to amplification. It is important noting that the two experiments have different types of samples that come in contact with the paper disc: in Section 3.1.3, 3 μL of an already purified DNA were pipetted onto the paper disc, while in this experiment the paper disc is immersed in 500 μL of sample and lysis buffer. The lysed sample is very diluted when in contact with paper. Moreover, the lysis buffer contains several reagents and chemicals that might interfere with the binding of DNA to the paper. Therefore, the results presented in Fig. 3.7C are not in contrast with the results shown in Fig. 3.4 (Section 3.1.3), as it might appear at first sight.

3.1.4.2 Reduction of Handling Steps

The number of steps were reduced from 9 to 7 as explained in Section 2.14, Fig. 2.6. The method involving 9 steps and a 1 min washing (Fig. 2.6A) was compared with the method requiring 7 steps (Fig. 2.6B). The results in Fig. 3.8 show that the 7-steps method leads to a significantly faster (13.83 ± 0.06 min) amplification of the extracted DNA compared to the 9-steps method (14.07 ± 0.06 min), with $p\text{-value} < 0.02$. This results confirm that the 7-steps method can be successfully used in the sample pretreatment of large samples.

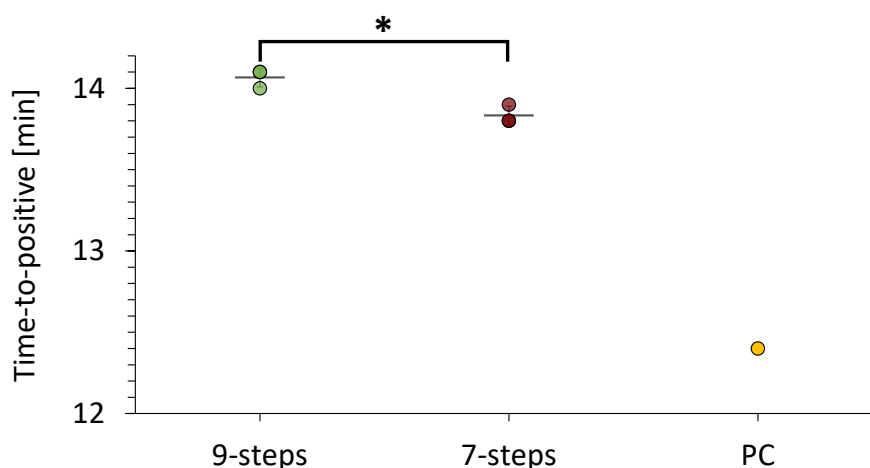


Figure 3.8: **Time-to-positive values (TTPs) of paper-based extraction performed using the 9-steps or 7-steps methods.** TTPs are given for DNA extracted using the method illustrated in Fig. 2.6A (9-steps) and the method in Fig. 2.6B (7-steps). The experiment was performed in biological replicates ($n = 3$). The data points represent the time (in minutes) at which each biological replicate amplified. The x-axis shows the different samples. PC is the positive control whose DNA concentration is 19 ng/ μ L. The horizontal bars represent the mean value of the TTPs of the biological replicates whose DNA extraction was performed with the same conditions. Error bars represent the standard deviation for $n = 3$. The PC was extracted following the manual instructions from MagaZorb[®] DNA Mini-Prep Kit and in this experiment served only to make sure that the reagents were working properly. NTCs are not shown but they represent the no template controls containing a paper disc. The TTPs amongst the two different methods were compared by carrying out a one-way ANOVA with Tukey-Kramer's post-hoc test. A statistically significant difference was observed when using the 9-steps or 7-steps methods (p -value <0.02), showing a faster DNA amplification for the 7-steps method.

3.1.4.3 Analytical Sensitivity of the 7-steps Paper-Based DNA Extraction Method

An analytical sensitivity experiment was carried out in order to understand the lowest detectable concentration of bacteria in the initial sample (described in Section 2.14.2). The sensitivity experiment was performed in duplicate and the results are shown in Fig. 3.9. The lowest concentration of bacteria that is possible to detect from a 100 μ L sample is 10^5 CFU/mL. Only one of the two replicates where the DNA was extracted from a sample containing 10^4 CFU/mL amplifies and the amplification happens extremely late (after 40 minutes), meaning that the developed paper-based DNA extraction method is not able to consistently detect a sample containing 10^4 CFU/mL. This result is in line with the analytical sensitivity of the LAMP assay developed in tubes. Moreover, looking at the amplification plot in Fig. 3.9A, it is possible to observe that when the disc is inserted into the LAMP amplification mix, the curves are not completely flat when compared to the first 5 minutes of the PC (where no paper disc was inserted into the amplification reaction). This behaviour has been connected to the

fact that Whatman[®] Grade 1 has some auto-fluorescence (as previously reported by Ali *et al.* [156]) and it interferes with the fluorescence measurements.

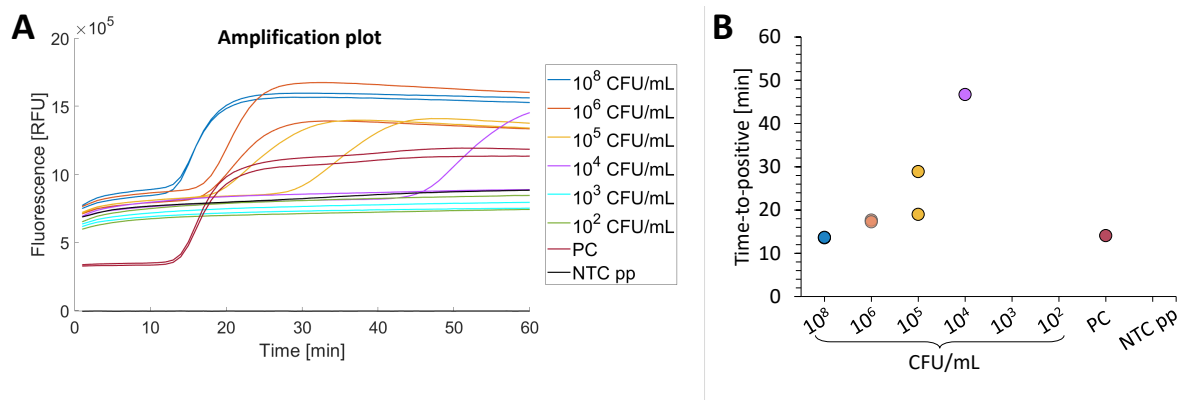


Figure 3.9: **Analytical sensitivity experiment of the paper-based sample pretreatment for the detection of *E. coli malB* gene from a bacterial sample, using LAMP.** The amplification plot and the time-to-positive values for each dilution from the initial sample concentration of 10⁸ CFU/mL are shown in **A** and **B**, respectively. 10-fold serial dilutions of the initial samples were carried out, and the experiments were done in duplicate ($n = 2$). The DNA was extracted using the 7-steps method (described in Section 2.14, Fig. 2.6B). The data points in **B** represent the time (in minutes) at which each biological replicate amplified ($n = 2$). The positive control (PC) ($n = 2$) was extracted following the manual instructions from MagaZorb[®] DNA Mini-Prep Kit and in this experiment served only to make sure that the reagents were working properly. NTC pp = no template control containing a paper disc.

All in all, the reduction of the number of handling steps in the sample pretreatment opens the route towards a pipetting-free sample-in-result-out diagnostic device.

3.1.4.4 Brief Evaluation of Using Different Papers in the 7-steps Paper-Based DNA Extraction Method

Once the procedure for the extraction of DNA from *E. coli* bacterial culture was established, the effects that using different filter papers have on the performance of the extraction became of interest. However, before proceeding in a detailed assessment of the different performances (as done in Section 3.1.7), it was observed very briefly the effect of using 3-mm discs of either Whatman[®] Grade 1, Grade 3 or GF/DVA (glass fibers). This experiment consisting in immersing three 3-mm discs in each *E. coli* sample, meaning that the TTP values shown in Fig. 3.10 belong to three technical replicates from one biological sample ($n = 1$). While this experiment cannot be used to draw conclusions on the performance of different papers considering $n = 1$, it can be exploited to discuss the different physicochemical properties of filter paper and glass fibers.

The established sample pretreatment procedure has assumed the LAMP reaction mix

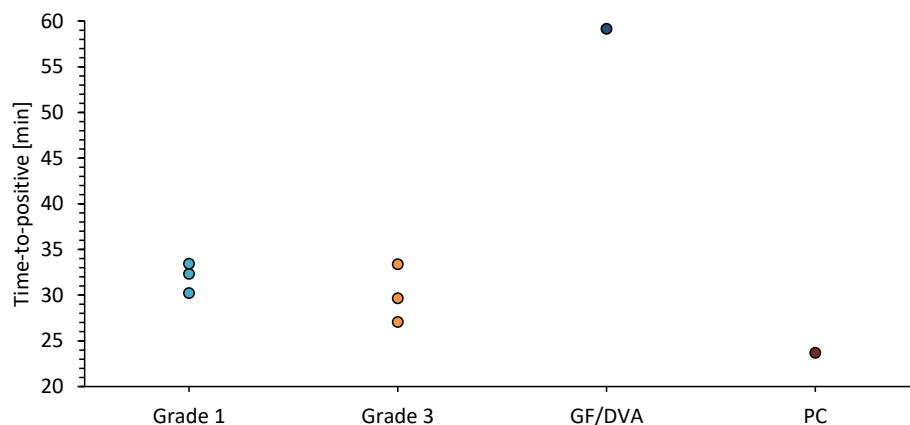


Figure 3.10: **Time-to-positive values (TTPs) of the 7-steps paper-based DNA extraction procedure performed using different paper substrates.** TTPs are given for different papers used in the 7-steps paper-based DNA extraction. Three types of paper were investigated: Whatman[®] Grade 1, Grade 3 or GF/DVA (glass fibers). One biological sample ($n = 1$) and three technical replicates were performed for each type of paper. The dots represent the time (in minutes) at which each assay amplified. PC is the positive control whose DNA concentration is approx. 20 ng/ μ L; Grade 1, Grade 3 and GF/DVA represent the samples for which the DNA extraction was performed using Grade 1, Grade 3 and GF/DVA paper discs (x-axis), respectively. The NTCs are not provided in the plot as no amplification was detected. Two types of NTCs were performed either containing a paper disc of Grade 3 or GF/DVA. This experiment used Concentration 1 of primers (Table 3.1).

as the elution fluid. When the glass fibers paper was used, only one of the three replicates amplified at 59 minutes. This outcome was expected, as it had been previously shown that glass fibers have positive surface charges that prevent an easy release of DNA that is known to be negatively charged [21, 157]. The electrostatic interaction of opposite charges between the filter itself and the DNA causes the DNA to be effectively trapped by the filter but released with difficulty. From these observations, an additional elution step appear necessary to allow the captured DNA to be released and further detected when using glass fibers.

3.1.4.5 Use of Proteinase K

The possibility of adding 10 μ L of proteinase K to the sample containing bacteria, before step (1), was evaluated using the 7-steps method (Fig. 2.6B). The introduction of proteinase K has the potential of making the DNA extraction procedure more universal in the presence of difficult-to-lyse samples (see Section 2.14.2). The proteinase K added was the one supplied in the MagaZorb[®] DNA Mini-Prep Kit (Promega Corporation), and the volume used was the one suggested in the manufacturer's instructions. Two lysis buffers have been tested when adding proteinase K: the sample was mixed with

either four volumes of the extraction buffer # 2 from Zou *et al.* [21] ('LB by Zou et al.' in Fig. 3.11) or one volume of the lysis buffer provided in the MagaZorb[®] DNA Mini-Prep Kit ('LB by Magazorb kit' in Fig. 3.11). The experiment was carried out in biological triplicate ($n = 3$) (Fig. 3.11).

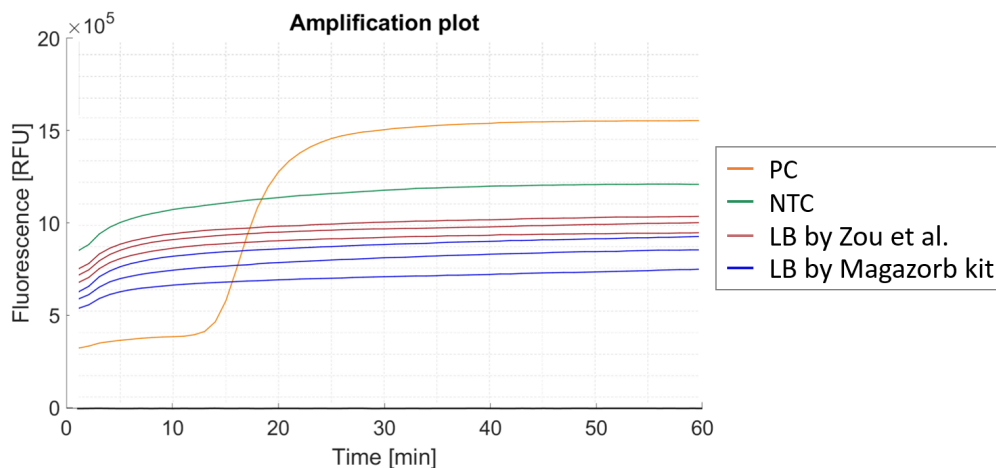


Figure 3.11: **Amplification plot of the 7-steps method when proteinase K is added to the sample.** 10 μL of proteinase K were added to the 100 μL bacterial sample, before step (1), using the 7-steps method (Fig. 2.6B). The experiment was performed in biological triplicate ($n = 3$). The x-axis shows the time (minutes) and the y-axis shows the fluorescence value (RFU). PC is the positive control whose DNA concentration is 19 $\text{ng}/\mu\text{L}$.

No amplification was observed regardless the lysis buffer used, implying that the washing step is not sufficient to wash out from the paper the proteinase K that inhibits further reaction. Probably, extra washing steps should be performed in order to be able to introduce proteinase K into the sample pretreatment.

3.1.5 Introduction of an Additional Elution Step for Quantitative Comparative Analysis Using qPCR of the Paper-Based DNA Extraction Method

To assess and optimise the performance of the paper-based DNA extraction method established in Section 3.1.4 when using different types of paper, qPCR was used instead of LAMP. qPCR offers better comparative quantitative measures than the time-to-positive values detected in LAMP, and it guarantees more stable and reproducible measurements of the cycle threshold values across experiments. This section describes the steps followed to evaluate the performance of the established paper-based DNA extraction method using qPCR. Section 3.1.7 gives the results obtained when using different types of papers in the 7-steps paper-based DNA extraction method.

The results in Section 3.1.3 demonstrated the possibility of immersing a paper disc directly into the LAMP reaction mix to investigate the ability of paper to capture DNA. Therefore, as a first step, the effect that a paper disc could have in the amplification mix and the subsequent real-time fluorescence reading using qPCR were investigated. The final qPCR amplification mix was made of 24 μL as described in Section 2.6 to which 1 μL of *E. coli malB* gene synthetic DNA was added (total final volume of qPCR reaction was 25 μL). The qPCR amplification mix was prepared either as indicated in Section 2.6 or by adding 1 μL of extra fluorescent dye to the mix. When the additional fluorescent green dye was added, the final qPCR mix (total 25 μL) contained 5 μL of 5X primer mix (Table 2.6), 12.5 μL of master mix (Brilliant II SYBR[®] Green QPCR Master Mix), 5.5 μL of NFW, 1 μL of green fluorescent dye (Cambridge Bioscience) and 1 μL of sample. The results are shown in Fig. 3.12. Four different positive controls were prepared: (1) 1 μL of synthetic DNA ('PC w/o dye'), (2) the reaction mix was prepared with 1 μL of extra fluorescent dye and 1 μL of synthetic DNA ('PC w/ dye'), (3) a 3-mm paper disc was added into the reaction before the addition of 1 μL of synthetic DNA ('PC pp w/o dye'), (4) the reaction mix was prepared with 1 μL of extra fluorescent and a 3-mm paper disc was added into the reaction before the addition of 1 μL of synthetic DNA ('PC pp w/ dye'). In the same way, the experiment had four different no template controls: (1) 1 μL of NFW was added as sample, instead of synthetic DNA ('NTC w/o dye'), (2) the reaction mix was prepared with 1 μL of extra fluorescent dye and 1 μL of NFW ('NTC w/ dye'), (3) a 3-mm paper disc was added into the reaction before the addition of 1 μL of NFW ('NTC pp w/o dye'), (4) the reaction mix was prepared with 1 μL of extra fluorescent dye and a 3-mm paper disc was added into the reaction before the addition of 1 μL of NFW ('NTC pp w/ dye'). The paper disc affected the real-time fluorescence readings by preventing the signal to have a clear increase in fluorescence when the target DNA is in the sample. For example, the amplification curves of the sample not containing the paper disc, 'PC w/o dye', and of the one containing the disc, 'PC pp w/o dye', appear very different with a very clear increase in fluorescence in the absence of the paper disc and a flat amplification curve when the paper is present. The addition of one extra microliter of green fluorescent dye to the qPCR reaction mix did not allow for any amplification to be visualised. This result led to the necessity of introducing an elution step in order to use qPCR to assess the performance of the paper-based DNA extraction method when using different types of papers.

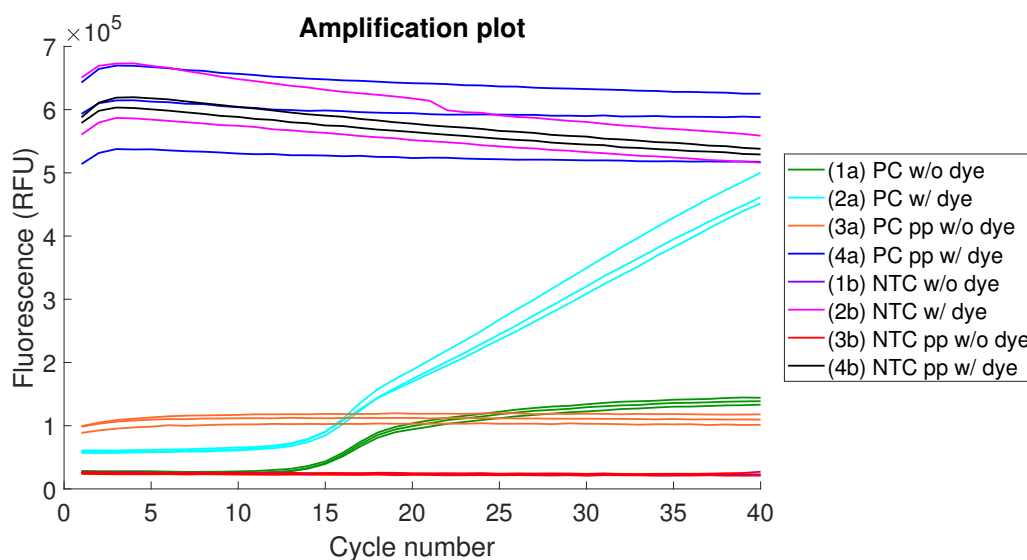


Figure 3.12: **Interaction of paper disc with fluorescence reading in qPCR.** A 3-mm Whatman Grade 1 paper disc was added to qPCR reactions to understand if it interfered with the real-time fluorescence reading. PCs were run in triplicate ($n = 3$) and they are composed of: (1a) 1 μL of synthetic DNA ('PC w/o dye'), (2a) the reaction mix was prepared with 1 μL of extra fluorescent dye and 1 μL of synthetic DNA ('PC w/ dye'), (3a) a 3-mm paper disc was added into the reaction before the addition of 1 μL of synthetic DNA ('PC pp w/o dye'), (4a) the reaction mix was prepared with 1 μL of extra fluorescent and a 3-mm paper disc was added into the reaction before the addition of 1 μL of synthetic DNA ('PC pp w/ dye'). NTCs were run in duplicate ($n = 2$) and were made as: (1b) 1 μL of NFW was added as sample, instead of synthetic DNA ('NTC w/o dye'), (2b) the reaction mix was prepared with 1 μL of extra fluorescent dye and 1 μL of NFW ('NTC w/ dye'), (3b) a 3-mm paper disc was added into the reaction before the addition of 1 μL of NFW ('NTC pp w/o dye'), (4b) the reaction mix was prepared with 1 μL of extra fluorescent dye and a 3-mm paper disc was added into the reaction before the addition of 1 μL of NFW ('NTC pp w/ dye').

An elution step was added to the paper-based sample pretreatment method, as shown in Section 2.14.2 (Fig. 2.7). A LAMP reaction was used to assess if the extracted DNA (entangled into the paper disc fibers) was eluted from the paper disc and released into 1X TE buffer. 4 μL of the eluant were added to the final LAMP amplification mix for a total volume of 25 μL . Fig. 3.13 shows that the extracted DNA is eluted into 100 μL of 1X TE buffer after 10 min incubation at room temperature. However, the mean time-to-positive value of the eluted DNA (15.50 min \pm 0.26 min) is higher than the one without elution (12.80 min \pm 0.25 min), and significantly different (p -value < 0.001). The additional elution step leads to a significant loss in performance of the extraction method, when compared to the PC value (11.4 min). In fact, in this experiment, the PC can be directly compared to the extracted DNA. The PC contains DNA that was extracted with the beads-based protocol (MagaZorb[®] DNA Mini-Prep Kit, Promega Corporation), from the same *E. coli* K12 bacterial culture and using the same initial volume and elution volume.

Increasing the elution temperature from room temperature to 66 $^{\circ}\text{C}$ did not improve

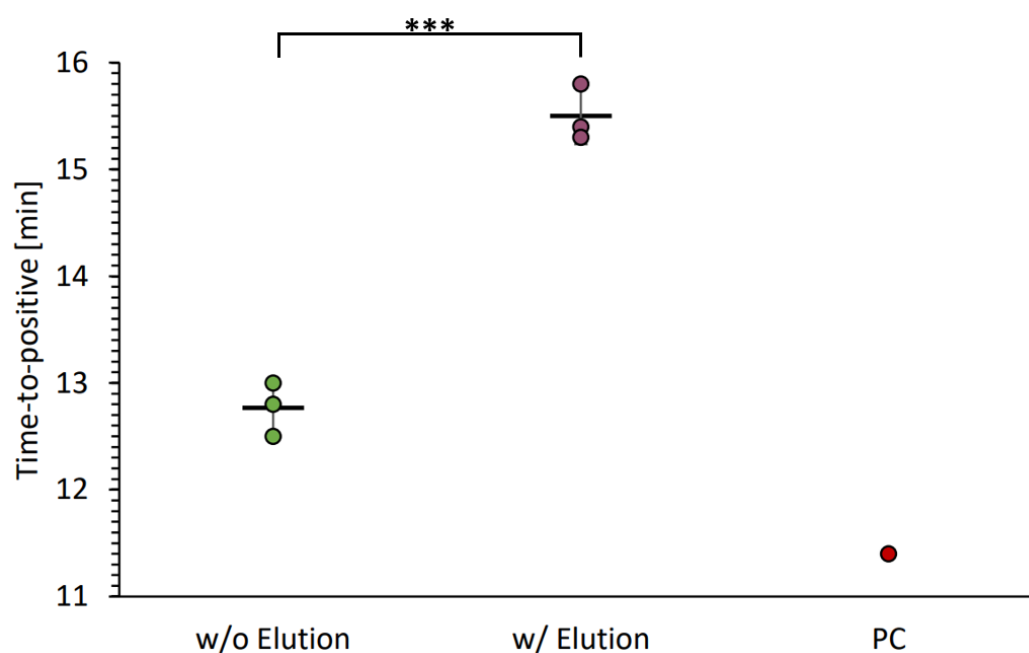


Figure 3.13: **Time-to-positive values of paper-based extraction performed using the 7-steps methods with and without an additional elution step.** Time-to-positive values are given for DNA extracted using the method illustrated in Fig. 2.6B and Fig. 2.7. The data points represent the time-to-positives (in minutes) at which each biological replicate amplified ($n = 3$). The x-axis shows the different samples. The horizontal bars represent the mean value of the time-to-positive values of all the biological replicate whose DNA extraction was performed with the same conditions. Error bars represent the standard deviation for $n = 3$. PC is the positive control whose DNA concentration is 19 ng/ μ L. The PC was extracted following the manual instructions from MagaZorb[®] DNA Mini-Prep Kit. NTCs are not shown but they represent the no template controls containing either a paper disc (final volume of 21 μ L) or 4 μ L of NFW (final volume of 25 μ L). No amplification was detected in all NTCs. A statistically significant difference was observed among the two samples (p -value <0.001).

the release of DNA from the paper disc by decreasing the time-to-positive ($n = 1$, 1 minute difference). Higher temperatures make DNA more motile and, thus, this might have increased the amount of DNA released into the elution buffer.

3.1.6 Lysis Buffer Optimization in the Paper-Based DNA Extraction Procedure

Optimisation of the lysis buffer from Zou *et al.* [21] used in the paper-based DNA extraction was performed using qPCR and the additional elution step, as described in Fig. 2.6B. The optimisation consisted in investigating the volume of the lysis buffer to be used, and the role of EDTA and Guanidine HCl (GuHCl). Moreover, the performance of the paper-based extraction was assessed when using an acidic lysis buffer (pH 5) to be used in applications where paper is pretreated with chitosan.

In this section, all paper-based extractions were carried out from a 10^8 CFU/mL *E. coli* K12 sample, and the concentration of primers used was Concentration 3 (see Table 3.1).

3-mm or 6-mm Whatman[®] Grade 1 paper discs were used (Section 3.1.7 investigates the effects of different sizes of paper discs.). One-way ANOVA with Tukey-Kramer's post-hoc test was performed to compare the time-to-positive amongst the positive control and the samples, as explained in Section 2.9, unless otherwise specified.

3.1.6.1 Volume Optimization of Extraction Buffer # 2 by Zou *et al.* (2017)

The initially established paper-based extraction procedure (described in Fig. 2.6B), involved mixing 100 μL of sample with 400 μL of lysis buffer at 1:5 ratio, as suggested in Zou *et al.* [21]. By reducing the volume of the lysis buffer to 200 μL (Fig. 3.14), and thus the amount of liquids involved into the paper-based DNA extraction procedure in general, a simplified integration of this method onto a sample-in-answer-out device can be achieved. The experiment was performed in biological duplicate ($n = 2$) and following the procedure described in Fig. 2.7. The 100 μL sample was lysed either by adding 200 μL ('200 μL LB' in Fig. 3.14) or 400 μL ('400 μL LB' in Fig. 3.14) of lysis buffer. Since the addition of 200 μL of lysis buffer provides lower Ct values than using 400 μL , the final procedure consisted in mixing a 100 μL of re-suspended bacterial cells pellet with 200 μL of lysis buffer at 1:3 ratio.

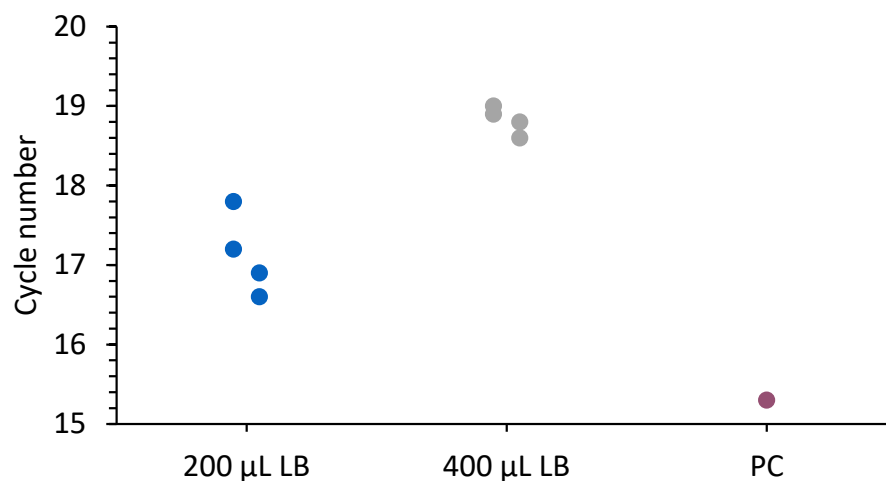


Figure 3.14: **Cycle threshold (Ct) values of paper-based extraction performed using 200 μL or 400 μL of lysis buffer.** Ct values are given for DNA extracted when 100 μL of sample are lysed by adding 200 μL or 400 μL of lysis buffer, at 1:3 and 1:5 ratio, respectively. Three 3-mm discs were used for each extraction. Each extraction was run under the same conditions twice (biological duplicate, $n = 2$). The data points represent the Ct values, in cycle number, at which each assay amplified (two technical replicates for each biological sample). The x-axis shows the different samples. PC is the positive control whose DNA concentration is 19 $\text{ng}/\mu\text{L}$. The elution volume used for this experiment was 40 μL . The PC was extracted following the manual instructions from MagaZorb[®] DNA Mini-Prep Kit and in this experiment served only to make sure that the reagents were working properly. NTCs are not shown but they represent the no template controls containing NFW.

3.1.6.2 EDTA Concentration in the Lysis Buffer

The extraction buffer # 2 introduced in [21] did not contain any EDTA in its formulation (Section 2.2). Therefore, the performance with 50 mM EDTA on top of the initial formulation was checked. EDTA is a chelating agent that sequesters metal ions, such as magnesium and calcium, to destabilise cells membranes (Fig. 3.15). In

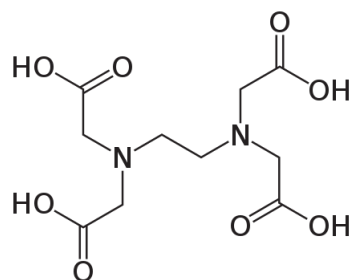


Figure 3.15: **Structural formula of ethylenediaminetetraacetic acid (EDTA).** The EDTA molecule consists of two ethylenediamine groups (CH_2N) linked to four carboxymethyl groups ($\text{CH}_2\text{CO}_2\text{H}$), and its full chemical formula is $\text{C}_{10}\text{H}_{16}\text{N}_2\text{O}_8$. Reproduced under public domain.

combination with Tris-HCl, EDTA is a common component of lysis buffers. The performance of using these different lysis buffers was assessed against the DNA extraction using MagaZorb[®] DNA Mini-Prep Kit ('PC'), using the Ct values (cycle number) for comparative analysis. Fig. 3.16 shows that there is no statistically significant difference ($p\text{-value} > 0.05$) when EDTA is added to the initial composition of the extraction buffer # 2 [21] ('LB by Zou et al. + 50mM EDTA') compared to the original composition of the buffer ('LB by Zou et al.'). However, using the lysis buffer provided in the MagaZorb[®] Kit ('LB by Magazorb kit') leads to better performance ($p\text{-value} < 0.01$) than using extraction buffer # 2 [21] with and without 50 mM EDTA. Given the results in Fig. 3.7A (Section 3.1.4) where extraction buffer # 2 [21] and the lysis buffer from the MagaZorb[®] Kit led to similar performances in LAMP, and the fact that 50 mM EDTA do not bring significant performance benefits over the original extraction buffer # 2 composition, it was decided to use the composition of buffer # 2 suggested in [21].

3.1.6.3 Guanidine HCl Concentration in the Lysis Buffer

Using the lysis buffer from Magazorb kit leads to a statistically significant better performance ($p\text{-value} < 0.01$) than using extraction buffer # 2 [21], as shown in Fig. 3.16. Therefore, the role of Guanidine HCl (GuHCl) (Fig. 3.17) was investigated in the performance of the paper-based DNA extraction. According to the patent associated with the MagaZorb[®] DNA Mini-Prep Kit [141], their proprietary lysis buffer contains 6 M

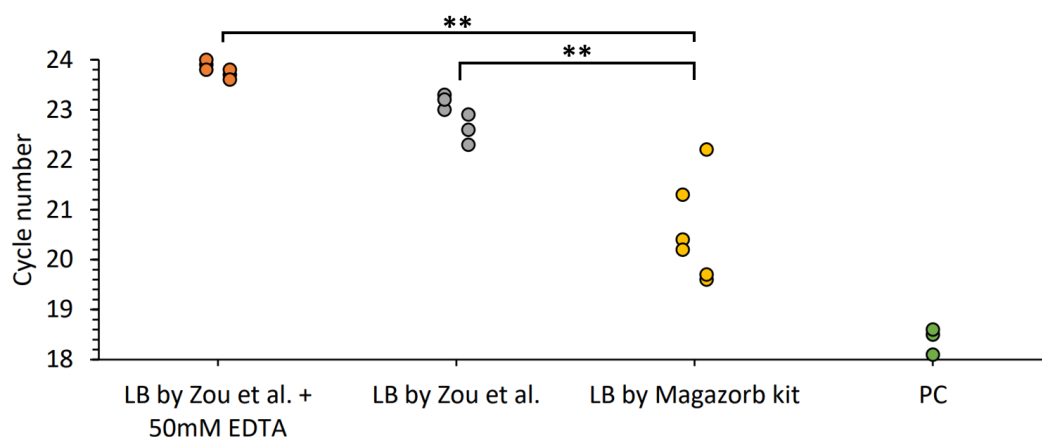


Figure 3.16: **Cycle threshold (Ct) values of paper-based extraction performed using different concentration of EDTA in the lysis buffer.** Ct values are given for DNA extracted using 200 μ L of extraction buffer # 2 [21] (LB by Zou et al.), 200 μ L of extraction buffer # 2 [21] containing an additional 50 mM EDTA (LB by Zou et al. + 50mM EDTA) and 100 μ L of the lysis buffer provided in MagaZorb[®] DNA Mini-Prep Kit (LB by Magazorb kit). The data points represent the Ct values at which each assay amplified. Two biological replicates with the same extraction conditions were carried out ($n = 2$) (data points given on two different columns), and three technical replicates for each biological sample are given on the same column. One 6-mm disc was used for each extraction. NTCs are not shown but they represent the no template controls containing NFW. Using the lysis buffer from Magazorb kit brings a statistically significant improvement in performance (p -value <0.01) than using extraction buffer # 2 with or without EDTA.

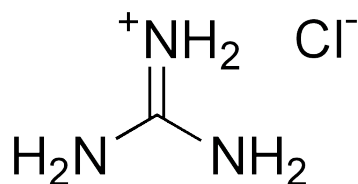


Figure 3.17: **Structural formula of Guanidine hydrochloride (GuHCl).** Guanidinium hydrochloride, also known as guanidine chloride, is the hydrochloride salt of guanidine, and its chemical formula is CH_6ClN_3 . GuHCl comprises a network of guanidinium cations and chloride anions connected by $\text{N-H} \cdots \text{Cl}$ hydrogen bonds.

GuHCl, and the concentration of GuHCl was increased from 0.8 M to 2 M GuHCl in extraction buffer # 2 [21]. Higher concentrations of GuHCl were not considered because GuHCl is a toxic compound [158] and it forms toxic and corrosive fumes, *e.g.*, hydrogen chloride and nitrogen oxides, upon combustion [159,160]. The need to avoid high concentrations of GuHCl came from the fact that we envision a sample-in-answer-out device that can be easily handled and disposed of, without causing any harm to its users and the environment. The performance of each lysis buffer used was evaluated against the DNA extraction using the beads-based method from the MagaZorb[®] Kit ('PC'), and Ct values (cycle number) for comparative analysis. The results in Fig. 3.18 show that there is no statistically significant difference (p -value >0.05) when using the extraction buffer # 2 [21] containing 0.8 M GuHCl ('LB by Zou et al.') or 2 M GuHCl ('LB by Zou et al. + 2M GuHCl'). However, the lysis buffer provided in the

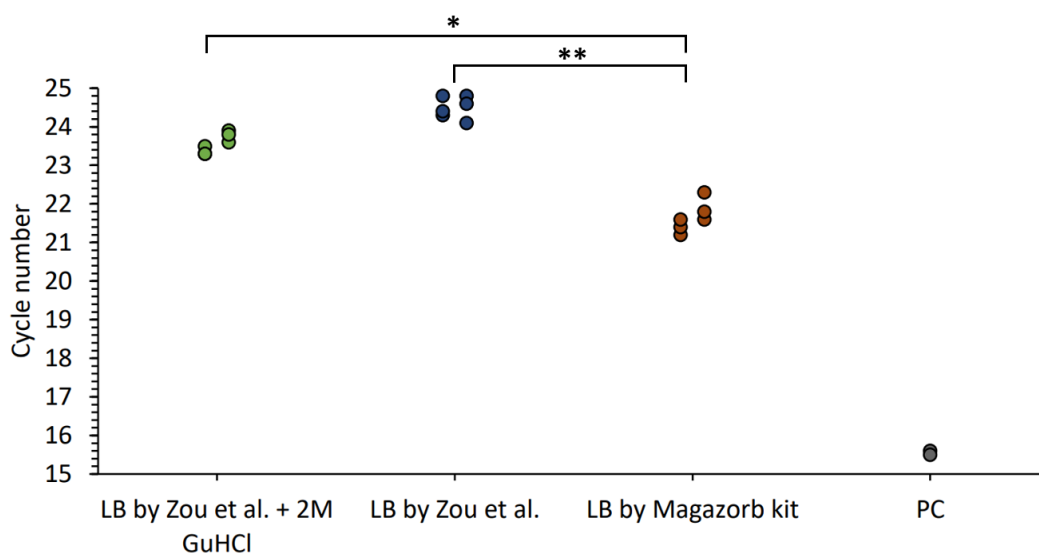


Figure 3.18: **Cycle threshold (Ct) values of paper-based extraction performed using different concentration of GuHCl in the lysis buffer.** Ct values are given for DNA extracted using 200 μL of extraction buffer # 2 [21] ('LB by Zou et al. '), 200 μL of extraction buffer # 2 [21] containing 2 M GuHCl ('LB by Zou et al. + 2M GuHCl') and 100 μL of the lysis buffer provided in MagaZorb[®] DNA Mini-Prep Kit ('LB by Magazorb kit'). One 6-mm disc was used for each extraction ($n = 2$). NTCs are not shown but they represent the no template controls containing NFW. Using the lysis buffer from Magazorb kit improves significantly the performance of the extraction method than using extraction buffer # 2 with 0.8 mM or 2 mM GuHCl (p-value<0.01 and p-value<0.05, respectively).

MagaZorb[®] Kit ('LB by Magazorb kit') leads to better performance than using extraction buffer # 2 [21] with 0.8 M GuHCl (p-value<0.01) or 2 M GuHCl (p-value<0.05). GuHCl is a common component of lysis buffers as it is a chaotropic agent able to induce cell permeabilisation and protein denaturation. Even if high concentrations of GuHCl are usually used to improve cell lysis, this was not investigated further for the reasons explained above. The concentration of components in the lysis buffer is the one provided in Section 2.2.

3.1.6.4 Acidic and Alkaline Lysis Buffers

For applications where paper is functionalised with chitosan, the lysis buffer needs to be acidic, with a pH lower than 6.3. An acidic pH during the DNA-paper incubation guarantees that chitosan is positively charged and, thus, more prone to capture negatively charged DNA molecules [85]. Therefore, the possibility of using an acidic lysis buffer to not decrease the performance of the paper-based DNA extraction was examined. The acidic lysis buffer with pH 5.5 was prepared as described in Section 2.2, and its use was compared with extraction buffer # 2 [21] ('LB by Zou et al. ') and the lysis buffer provided in MagaZorb[®] DNA Mini-Prep Kit ('LB by Magazorb kit'). The acidic pH of 5.5 was chosen based on previously published works by Gan *et al.* [82] and

Bengston [86].

The results for this experiment are shown in Fig. 3.19, and the performance of each lysis buffer used was evaluated against the DNA extraction using the beads-based method from the MagaZorb[®] Kit ('PC'), using Ct values (cycle number) for comparative analysis. There is no statistically significant difference ($p\text{-value} > 0.05$) when using the acidic version of extraction buffer # 2 ('Acidic LB with MES (pH 5.5)') or extraction buffer # 2 [21] ('LB by Zou et al.'). However, the lysis buffer provided in the MagaZorb[®] Kit ('LB by Magazorb kit') leads to better performance than using extraction buffer # 2 [21] with pH 8 or pH 5.5 ($p\text{-value} \leq 0.05$). The acidic version of extraction buffer # 2 with pH 5.5 can be used without it interfering significantly with the paper-based extraction.

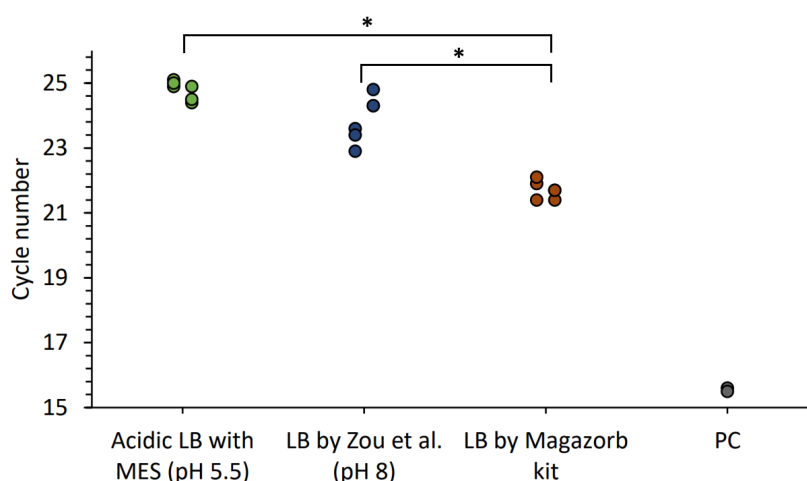


Figure 3.19: **Cycle threshold (Ct) values of the paper-based DNA extraction performed with lysis buffers having different pH (pH 5.5, pH 8, pH 6.3).** Ct values are given for DNA extracted using 200 μL of an acidic version of extraction buffer # 2 ('Acidic LB with MES (pH 5.5)'), 200 μL of extraction buffer # 2 [21] ('LB by Zou et al.') and 100 μL of the lysis buffer provided in MagaZorb[®] DNA Mini-Prep Kit ('LB by Magazorb kit'). One 6-mm disc was used for each extraction ($n = 2$). NTCs are not shown but they represent the no template controls containing NFW. Using the lysis buffer from Magazorb kit improves significantly the performance of the extraction method than using extraction buffer # 2 with 0.8 mM or 2 mM GuHCl ($p\text{-value} < 0.01$ and $p\text{-value} < 0.05$, respectively).

In the very first experiments, following the paper-based method illustrated in Fig. 2.5B where the heating step was still present, no significant difference was observed in time-to-positive values when using the lysis buffer from Zou *et al.* [21] or the one provided in the MagaZorb[®] DNA Mini-Prep Kit (Fig. 3.7A, Section 3.1.4.1). However, when the lysis buffer optimization was performed using the 7-steps method with elution and qPCR, the lysis buffer provided in the Magazorb kit led to better performances (lower Ct value) in all the experiments in this (Section 3.1.6), when compared to the lysis buffer from Zou *et al.* [21]. The difference in behaviour when using LAMP or qPCR

might be associated with inhibitory effects of some components of the Magazorb kit onto the LAMP reaction, that cannot be completely washed out from the paper discs during the washing steps. Moreover, the exact composition of the lysis buffer provided with the Magazorb kit is not known, therefore, extraction buffer # 2 from Zou *et al.* [21] was considered as the lysis buffer to be used in the final 7-steps sample pretreatment procedure.

3.1.7 Use of Different Papers in DNA Extraction Based on Zou *et al.* (2017)

Further optimisation of the paper-based DNA extraction from large sample of bacterial cultures, using the elution step, was carried out using Whatman[®] Grade 1 and Grade 3 filter papers to evaluate the effect of the size of the paper discs and the number of discs. The performance of the method when using Whatman[®] Grade 470, CF4, CF5 was also investigated. The paper-based DNA extraction method developed when using different sizes of paper discs or different types of paper was always evaluated against a beads-based purification method (MagaZorb[®] DNA Mini-Prep Kit), using qPCR and the Ct values (cycle number) for comparative analysis.

Figures 3.20-3.23 provides the results for this section. The paper-based DNA extractions were carried out in duplicate ($n = 2$). The data points represent the Ct values at which each assay amplified (three technical replicates for each biological sample). The x-axis shows the different samples. PC is the positive control whose DNA concentration is 19 ng/ μ L and it was obtained through a beads-based purification method. NTCs are not shown but they represent the no template controls containing NFW. A statistical analysis was conducted as described in Section 2.9.

The introduction of an additional elution step to the DNA extraction method made it possible to evaluate the effects that the size of the paper disc could have on the performance of the extraction itself. When performing a LAMP reaction the paper disc cannot be larger than 3 mm in diameter, because otherwise it would not fit the 0.1 mL strip PCR tubes and it would not be completely immersed inside the LAMP amplification mix. By using 100 μ L of elution buffer, paper discs up to 6 mm in diameter could be completely immersed in the elution buffer during the incubation time. Therefore, the performance of different sizes of paper discs was investigated. Fig. 3.20 shows the results of the DNA extraction method when using either three 3-mm paper

discs, one 5-mm paper disc or 6-mm paper disc of Whatman[®] Grade 1. The exper-

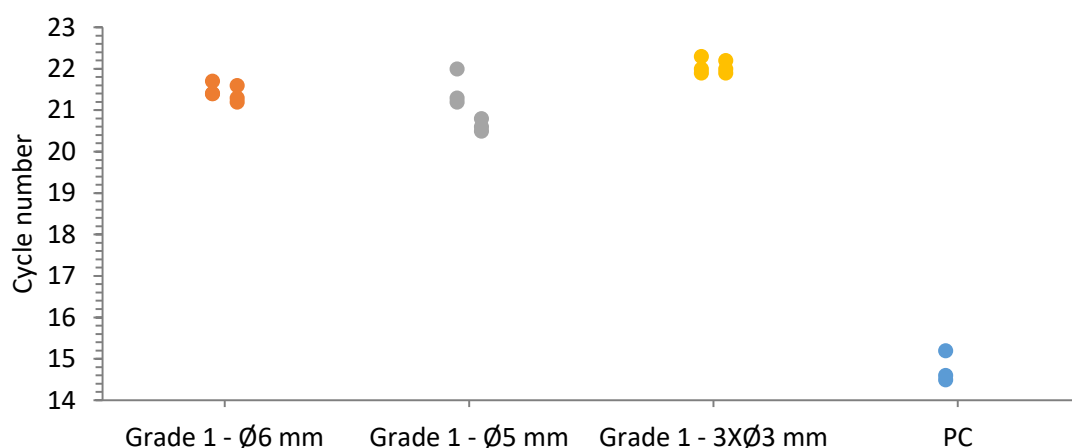


Figure 3.20: **Cycle threshold (Ct) values of the paper-based DNA extraction performed with different sizes of Whatman[®] Grade 1 paper discs.** Ct values are given for DNA extracted using either three 3-mm paper discs, one 5-mm paper disc or 6-mm paper disc. Ct values of each qPCR assay are represented as data points in the graph. Two biological replicates were performed ($n = 2$) (data points with same colour but on different columns) and three technical replicates are given for each biological replicate (data points on the same column). Using three different sizes of Whatman[®] Grade 1 paper did not bring to a statistically significant difference in performance ($p\text{-value} > 0.05$).

iment was carried out in biological duplicate ($n = 2$), with three technical replicates for each biological sample. No statistically significant difference was observed when using three different sizes of Whatman[®] Grade 1 paper ($p\text{-value} > 0.05$). The surface areas of the three different paper discs were 84.82 mm^2 , 78.54 mm^2 and 113.10 mm^2 for three 3-mm discs, one 5-mm disc and one 6-mm disc, respectively. Based on the results shown in Fig. 3.20, the surface areas tried in this experiment did not cause a significant change in performance of the method, meaning that any of the dimensions tried could be used for the paper-based extraction. For further experiments it was decided to use either 5-mm or 6-mm paper discs because they are easier to handle. On the contrary, five cycles of difference can be observed when using the paper-based DNA extraction method compared to the beads-based extraction, this highlights a loss in sensitivity of the assay of more than 10-fold when using the paper-based method.

After investigating the paper-based method's performance with different disc sizes, the effect of using one or two 5-mm discs of Whatman[®] Grade 1 was examined. The impact of thicker paper was also studied using Whatman[®] Grade 3 that has a particle retention size half that of Grade 1. The results (Fig. 3.21) show no statistically significant difference when using one or two 5-mm paper discs of Grade 1 ($p\text{-value} > 0.05$), or when using one 5-mm paper disc of Grade 3 ($p\text{-value} > 0.05$). As already observed in the previous experiment, there is a significant loss in sensitivity (about 5 cycles difference)

when using the developed paper-based extraction method instead of the beads-based method (PC).

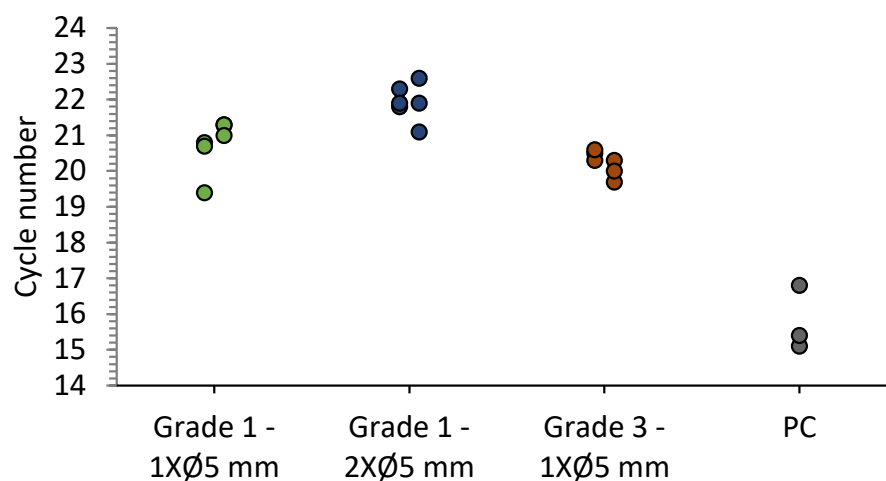


Figure 3.21: Cycle threshold (Ct) values of the paper-based DNA extraction performed with one or two 5-mm paper discs of Whatman[®] Grade 1, compared to using one disc of Whatman[®] Grade 3 paper. The data points represent the Ct values of each qPCR assay. Two biological replicates were performed ($n = 2$) (data points with same colour but on different columns) and three technical replicates are given for each biological replicate (data points in the same column). No statistically significant difference was observed for $p < 0.05$ in Ct values when DNA extraction is performed with one or two 5-mm paper discs of Grade 1, or one 5-mm paper disc of Grade 3.

Using two 5-mm discs of Whatman[®] Grade 1 did not bring a significant difference in the Ct values (Fig. 3.21). Therefore, the impact of an increased number of Whatman[®] Grade 3 paper discs was studied. One, two or three 5-mm Whatman[®] Grade 3 paper discs were used in each DNA extraction and the Ct values thus obtained were compared to using one 5-mm Whatman[®] Grade 1 paper disc. The results in Fig. 3.22 shows that using three 5-mm paper discs of Grade 3 reduces the Ct values significantly compared to when only one 5-mm paper discs of Grade 1 is used ($p\text{-value} < 0.5$). However, even though no difference in Ct values is detected when using a different number of 5-mm Grade 3 paper discs, there seems to be a trend of Ct values reducing as the number of discs is increased. As shown already in Fig. 3.21, no statistically significant different Ct values are observed when using one 5-mm paper discs of Grade 1 or Grade 3. These results show how the different properties of Grade 1 and Grade 3 filter paper start affecting the performance of the DNA extraction only when the number of discs of Grade 3 is increased. This is probably due to the fact that a higher surface area present in the sample allows for a better capture of those DNA fragments that would otherwise remain unbound. Therefore, in our experiments the link between the average particle retention size of the filter paper and the DNA capture efficiency is not as clear

as illustrated by Gan *et al.* [91].

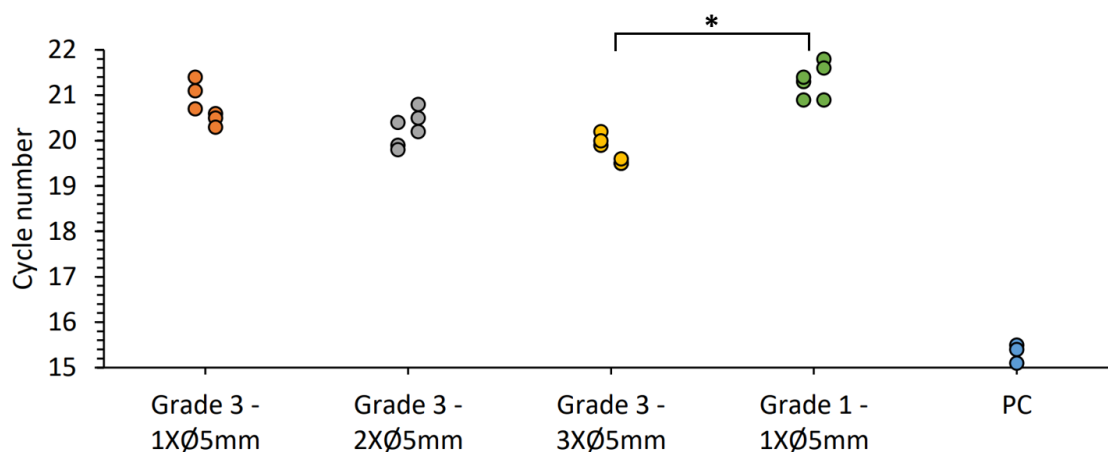


Figure 3.22: Cycle threshold (Ct) values of the paper-based DNA extraction performed with one, two or three 5-mm paper discs of Whatman[®] Grade 3, compared to one 5-mm disc of Whatman[®] Grade 1 paper. The data points represent the Ct values of each qPCR assay. Two biological replicates were performed ($n = 2$) (data points with same colour but on different columns) and three technical replicates are given for each biological replicate (data points in the same column). A statistically significant difference in Ct values was observed for $p < 0.05$ only when three 5-mm paper discs of Grade 3 were used compared to one 5-mm paper disc of Grade 1.

The performance of the paper-based extraction method using four types of paper with different physicochemical properties has been tested and no significant difference was observed (Fig. 3.23). In Fig. 3.23A there have been some problem during the pipetting of one of the biological samples using Grade 3, therefore, it is not possible to statistically compare the samples using Grade 3 with the ones using CF4 and Grade 470 to extract DNA. Between CF4 and Grade 470 there is no significant difference. Both CF4 and Grade 470 are usually used as sample pads in lateral-flow applications, but Grade 470 is thicker than CF4 and has a higher wicking rate and water absorption. The characteristics of Grade 470 appear to not affect significantly the capturing and release of DNA during the DNA extraction process, but it appears to slightly reduce the variance as compared to using CF4 both among technical and biological replicates. Fig. 3.23B shows that the performances of CF4, CF5 and Grade 3 are not statistically different. However, CF5 appears to decrease the variation in Ct values within the same biological sample. Given the lower cost of Grade 3 and the not clear advantage of using CF4, CF5 or Grade 470 over Grade 3, this type of paper was preferred for further optimizations.

The use of glass fibers paper was not investigated further because they are not able to release the captured DNA into the final amplification when there is no elution step, as previously shown in Fig. 3.10.

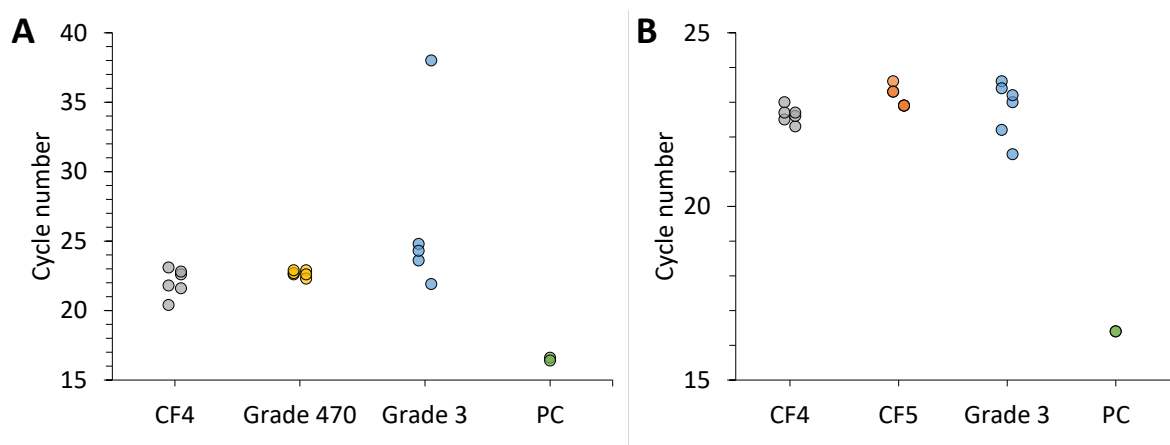


Figure 3.23: **Cycle threshold (Ct) values of the paper-based DNA extraction performed using 5-mm paper discs of Whatman[®] Grade 3, Grade 470, CF4, CF5.** The dots in the graphs represent the Ct values of each qPCR assay. Two biological samples were run using each type paper ($n = 2$, extraction was performed in two separate tubes using the same type of paper), and three biological replicates were carried out for each biological samples (dots located on the same column). **A.** Comparison in performance of CF4, Grade 470, Grade 3 5-mm paper discs. No statistically significant difference was observed when extracting DNA using CF4 or Grade 470 paper discs. **B.** Comparison in performance of CF4, CF5, Grade 3 5-mm paper discs. No statistically significant difference was observed when extracting DNA using the different types of paper for p -value < 0.05 . PC = DNA from the same bacterial culture extracted using MagaZorb[®] DNA Mini-Prep Kit.

In summary, Grade 3 filter paper had the most consistent Ct value results and using three 5-mm diameter discs led to a significant reduction in Ct value (better performance) than using one 5-mm disc of Grade 1. On the one hand, CF5 and Grade 470 decreased the variation in Ct values within the same biological sample. On the other hand, the advantage of using CF4, CF5 or Grade 470 over Grade 3 paper was not clear and given the lower cost of Grade 3 compared to the others, Grade 3 was considered the best paper to trap and release DNA and it was used for further optimizations of the paper-based DNA extraction based on Zou *et al.* [21].

3.1.8 Paper-based DNA Extraction Based on Magazorb[®] Kit

As introduced in Section 3.1.4, a second paper-based DNA extraction procedure was introduced based on the manufacturer's instructions provided in MagaZorb[®] DNA Mini-Prep Kit, as described in Fig. 2.8. This method was investigated in order to understand if it was possible to introduce proteinase K during the lysis step, and maximise the lysis efficiency of the targeted pathogen. Optimisation of the paper-based DNA extraction based on the MagaZorb[®] Kit was performed by using different types of papers, *i.e.*, Whatman[®] Grade 3, GF/DVA (glass fibers) and a silica membrane. This method was always assessed against the original beads-based purification method

(MagaZorb[®] DNA Mini-Prep Kit), using the Ct values (cycle number) for comparative analysis (as described in Section 2.9).

The paper-based DNA extractions were carried out in duplicate ($n = 2$). The data points in Figures 3.24 and 3.25 represent the Ct values at which each assay amplified (three technical replicates for each biological sample). The x-axis shows the different samples. PC is the positive control whose DNA concentration is 19 ng/ μ L and it was obtained through the gold-standard beads-based purification method. NTCs are not shown but they represent the no template controls containing NFW.

Fig. 3.24A-3.24C show that when using the paper-based DNA extraction method, that uses all the reagents provided in the MagaZorb[®] Kit (Fig. 2.8), it is possible to use proteinase K in the lysis step (sample name: 'PK + Magazorb kit method'). On the contrary, when using the 7-steps method with the elution step (Fig. 2.7) amplification does not occur in all the assays, or it occurs very late, after 35 cycles, as already shown in Fig. 3.11. This is probably due to specific chemical interactions and pH conditions created by the sequential use of the proprietary buffers of the Magazorb[®] Kit. Such buffers might be able to properly inactivate proteinase K and wash it out from the paper discs efficiently. Using Magazorb[®] Kit paper-based method to extract DNA leads to a later amplification with respect to the PCs that amplify at 15.5 minutes. Therefore, the Magazorb Kit paper-based method does not perform as well as the beads-based method. Moreover, the fluorescent signals of the amplification curves when the paper-based methods are used, in Fig. 3.24A, are noisy. Therefore, the algorithm implemented in MATLAB[®] was not able to properly identify all the second derivatives peaks. Only four out of six peaks were recognised automatically for the two biological samples 'PK + Magazorb kit method' in the second derivative of the fluorescent signal (Fig. 3.24B). The two peaks that the algorithm was not able to identify have been manually selected from Fig. 3.24B (see details in Section 2.7).

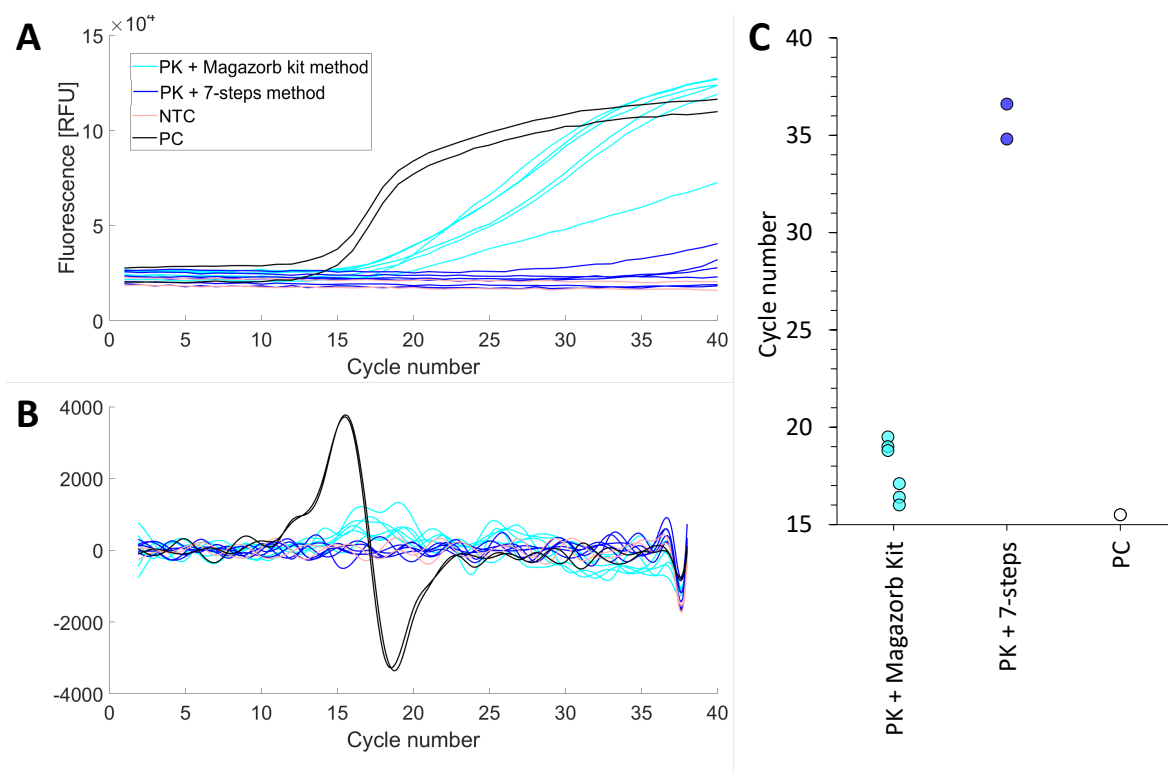


Figure 3.24: **qPCR results when proteinase K is added to the paper-based DNA extraction methods.** **A.** Amplification plot. **B.** Second derivatives of the amplification signal. **C.** Ct values. The data points represent the Ct values of each qPCR replicate. Two biological replicates were performed ($n = 2$), *i.e.*, the DNA extraction performed with the same type of paper disc (5-mm diameter) was performed twice. Three technical replicates are given for each biological replicate (data points in the same column). There was no statistically significant difference in performance for DNA extraction carried out using different types of paper for p -value < 0.05 .

Different types of paper were investigated in order to improve the performance of the MagaZorb[®] Kit paper-based method. The results of using a 5-mm disc of Whatman[®] Grade 3, GF/DVA and a silica membrane are provided in Fig. 3.25. No statistically significant difference in Ct values is observed when using GF/DVA or silica membrane rather than the most common Grade 3. This result was not expected as GF/DVA and silica membrane have very different physico-chemical properties than Grade 3 [157]. Given the different surface charges of the three types of paper [157] and the higher surface area per unit volume of silica membrane than glass fibers [85], different performances were expected in sample pretreatment. In particular, the higher surface area per unit volume of the silica membrane than glass fibers led to expect a higher amount of nucleic acids to be captured by the former. This would explain the slightly lower Ct values using silica membranes than using GF/DVA, however, the difference in performance does remain not significant. Moreover, silica membranes have been previously demonstrated to capture approx. 80% of nucleic acid samples (100-50000 bp long) in the presence of high salt concentrations and low pH [161]. Even though

the exact composition of the Magazorb[®] Kit reagents are not known, a patent associated with their kit [141] indicates that the lysis buffer has a low pH of 6.3 and a high concentration of GuHCl of 6 M. This composition seems to confirm what was previously demonstrated and that the Magazorb[®] Kit reagents facilitate the capture of DNA onto silica membranes.

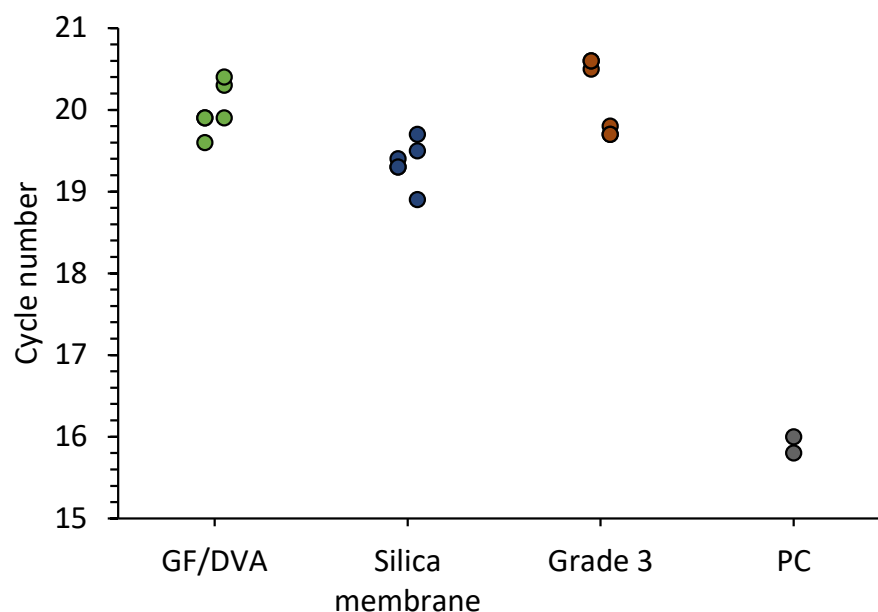


Figure 3.25: **Cycle threshold (Ct) values of the Magazorb Kit paper-based DNA extraction performed with different types of paper.** The types of papers used are Whatman[®] Grade 3, GF/DVA and a silica membrane. Two biological replicates were performed ($n = 2$) and three technical replicates are given for each biological replicate (data points in the same column).

To understand the behaviour of GF/DVA a brief experiment for $n = 1$ was performed and its results are provided in Fig. 3.26. The Magazorb Kit paper-based DNA extraction was performed using either 100 μL of lysis buffer provided in the kit or 200 μL of extraction buffer # 2 by Zou *et al.* [21], with and without the use of proteinase K. The lysis buffer provided in the kit has pH 6.3 and 6 M GuHCl, whereas the lysis buffer by Zou *et al.* has pH 8 and a very lower concentration of GuHCl (0.8 M). From a first look, the results in Fig. 3.26 show that these chemical differences do not affect the performance of the method as amplification is possible using both lysis buffers. This confirms what was speculated in Section 3.1.4, Fig. 3.10, that the elution step is an essential step to allow the release of DNA from the glass fibers. Moreover, GF/DVA discs can be used with the lysis buffer from the Magazorb Kit when proteinase K is present, as it allows for amplification, but they do not lead to amplification of those samples when the lysis buffer from Zou *et al.* is used with proteinase K. This last observation suggests that the lysis buffer plays a key role in the final inactivation of

proteinase K, thus preventing the final inhibition of the amplification reaction. More in detail, this experiment consisted in immersing two 6-mm discs in each *E. coli* sample. Therefore, the Ct values shown in Fig. 3.26 belongs to technical replicate from one biological sample ($n = 1$).

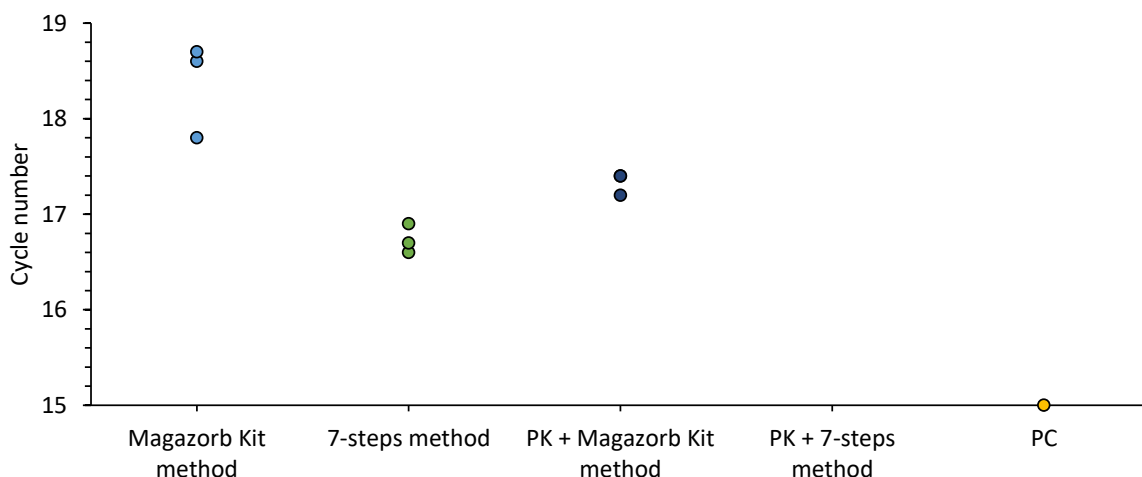


Figure 3.26: **Cycle threshold (Ct) values of the Magazorb Kit paper-based DNA extraction performed with two different lysis buffers.** The Magazorb Kit paper-based DNA extraction was performed using either 100 μ L of lysis buffer provided in the kit or 200 μ L of extraction buffer # 2 by Zou *et al.* [21], with and without the use of proteinase K ($n = 1$). The data points are the Ct values for each technical replicate. Two 6-mm discs in each sample were used.

The paper-based DNA extraction based on Magazorb kit was not validated in LAMP due to the high amount of handling steps that it requires. Therefore, this method could be hard to integrate into a fully enclosed device that requires minimal human input. However, it could be a viable option to replace the extraction method based on magnetic beads.

3.1.9 Paper-based DNA Extraction Using Lysis Buffer Air-Dried on Paper Discs

In an effort to further reduce the handling steps of the paper-based DNA extraction, the lysis buffer was air-dried onto the paper disc. Whatman[®] Grade 1, Grade 3 and CF5 filter papers were used to evaluate the different effects on the performance of the 7-steps DNA extraction method when 100 μ L of 2X extraction buffer # 2 was air-dried onto the paper discs for one week (described in Fig. 2.9). Whatman[®] Grade 3, CF5 and GF/DVA papers were used to evaluate the different effects on the performance of the paper-based DNA extraction based on the Magazorb Kit (Fig. 2.8) when 100 μ L of lysis buffers were air-dried onto the paper discs for one week. The paper-based DNA

extraction methods when using lysis buffers air-dried onto paper discs were evaluated against a beads-based purification method (MagaZorb[®] DNA Mini-Prep Kit). Ct values (cycle number) were used for comparative analysis and the statistical analysis was carried out as shown in Section 2.9.

The paper-based DNA extractions were carried out in duplicate and Figures 3.27-3.29 provide the results. Three technical replicates are given for each biological sample ($n = 2$), and the Ct values at which each assay amplified are represented as data points. Different samples are provided on the x-axis. PC was obtained through a beads-based purification method and its DNA concentration was 19 ng/ μ L. NTCs are not shown but they represent the no template controls containing NFW.

It was observed that after one week, extraction buffer # 2 from Zou *et al.* was completely dried onto two 5-mm paper discs, whereas the lysis buffer taken from the MagaZorb[®] Kit did not dry completely. The paper discs were taken with tweezers out of the wells even when the lysis buffer was not completely dried, and they were used in the DNA extraction as described in Section 2.14.3. The variation in drying time between the two lysis buffers likely results from differences in the composition and hygroscopic properties of their reagents. Additionally, altering the environmental temperature and humidity conditions significantly impacts reagent drying times.

Fig. 3.27 shows that using the air-dried lysis buffer onto paper discs gives comparable performance results than using liquid lysis buffers (when using the same type of paper). This demonstrates that air-dried lysis buffer on paper can be effectively used in the developed paper-based DNA extraction method to further reduce handling steps. No paper pretreatment is required. A significant difference in Ct values, for p -value < 0.05, was found when the normal procedure that uses all liquid reagents and Grade 1 paper is compared to using the dried lysis buffer onto Grade 3 paper, with the latter having better performance. The PC amplifies at 16.5 cycles, about 7 cycles before the paper-based DNA extraction methods. This delay in amplification highlights a loss in sensitivity when using the developed paper-based DNA extraction method with respect to the magnetic beads-based method. This result is consistent with the results shown in previous sections.

In order to reduce the amount of liquids handled during the paper-based DNA extraction, the possibility of eliminating the addition of 100 μ L of NFW to obtain 1X lysis buffer was investigated. For this experiment, 100 μ L of 2X extraction buffer # 2 by Zou *et al.* were air-dried onto two 5-mm discs of Whatman[®] Grade 3 for one week.

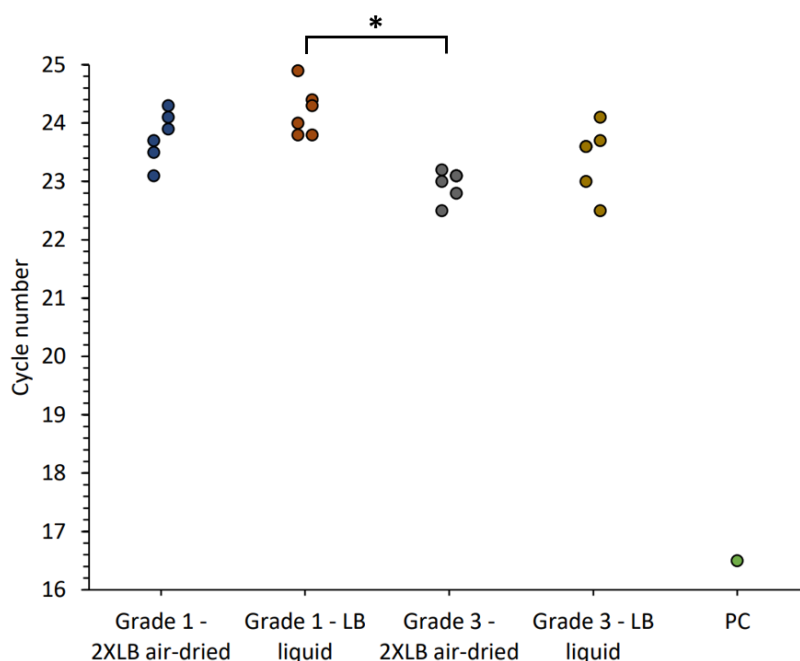


Figure 3.27: **Cycle threshold (Ct) values of the 7-steps method with elution performed with air-dried lysis buffer.** The 7-steps paper-based DNA extraction method with elution was performed using either two 5-mm discs of Whatman[®] Grade 1 or Grade 3 as described in Fig. 2.7 (LB liquid). The data points represent the Ct value of each assay (technical replicate) for $n = 2$. The Ct values of these extractions were compared with the paper-based DNA extraction method described in Fig. 2.9, where 100 μL of extraction buffer # 2 by Zou *et al.* [21] were air-dried onto two 5-mm Grade 1 or Grade 3 discs before being used for extraction and 100 μL of NFW were added to obtain 1X the lysis buffer concentration (2XLB air-dried).

Fig. 3.28 shows that it is possible to avoid the dilution of the 2X lysis buffer, and thus perform the extraction as described in Fig. 2.9. In fact, Ct values obtained when the air-dried 2X lysis buffer is not further diluted in 100 μL ('2XLB air-dried- non resuspended') are not significantly different ($p\text{-value} > 0.05$) from the Ct values obtained by using all liquid reagents ('LB liquid').

The 7-steps DNA extraction method when 100 μL of 2X extraction buffer # 2 were air-dried onto two 5-mm paper discs (Fig. 2.9) was performed using Whatman[®] Grade 3 and CF5 filter papers ($n = 2$) and the differences in performance are provided in Fig. 3.29A. CF5 was chosen as second paper to test because its thickness is about three times the thickness of Grade 3 and its performance are similar to the ones of Grade 3 (see Section 3.1.7). The greater thickness allows two 5-mm paper discs of CF5 to imbibe almost completely the 100 μL of lysis buffer, leaving less liquid not absorbed compared to Grade 3. Moreover, the possibility of using the lysis buffer provided in the Magazorb kit air-dried for one week was evaluated onto two 5-mm discs Whatman[®] Grade 3, CF5 and GF/DVA papers, without further dilution and following the Magazorb extraction method. The results for the latter are given in Fig. 3.29B. On the one

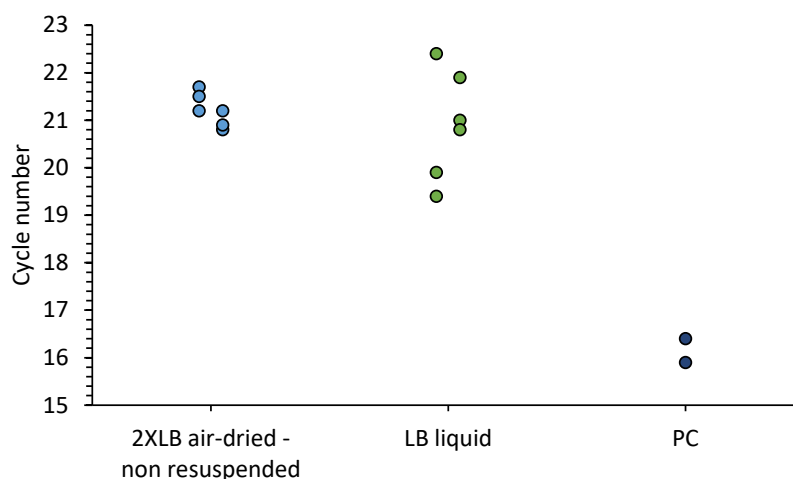


Figure 3.28: **Cycle threshold (Ct) values of the 7-steps method with elution performed with air-dried lysis buffer when the dilution step is not performed.** Experiments were carried out as described in Fig. 2.9, without the addition of NFW in step (2) for $n = 2$ ('2XLB air-dried- non resuspended'). This was compared with the 7-steps paper-based method described in Fig. 2.7 ('LB liquid'). No statistically significant difference was observed for $p < 0.05$.

hand, Grade 3 paper performs better than CF5 ($p\text{-value} < 0.05$), as seen in Fig. 3.29A. This behaviour might be due to the fact that more components of the lysis buffer are deeply absorbed into the paper discs of CF5 during the drying and not properly released when the sample is deposited onto the discs. On the other hand, Fig. 3.29B shows that it is feasible to use the air-dried lysis buffer provided in the Magazorb kit when performing the paper-based DNA extraction method based on the kit, but no significant differences can be observed when using different types of paper to carry out the extraction ($p\text{-value} > 0.05$).

Whatman[®] Grade 3 paper is the best performing paper to be used in the paper-based DNA extraction methods when the lysis buffer is air-dried onto the paper-discs. This is in line with what was discussed in Section 3.1.7.

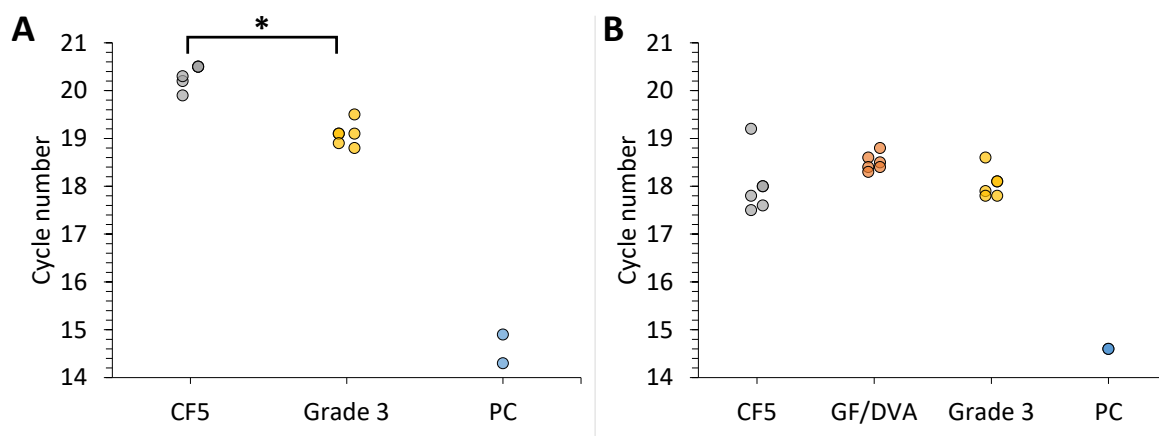


Figure 3.29: **Cycle threshold (Ct) values of the two paper-based DNA extraction methods developed performed with lysis buffer air-dried on the paper substrates.** The two paper-based DNA extraction methods used are the one based on the 7-steps method (A), described in Fig. 2.9, and the one based on the Magazorb Kit (B), described in Fig. 2.8. Different types of papers have been tested for each method. Lysis buffers were air-dried on two 5-mm discs of each type of paper. The paper-based DNA extractions were carried out in duplicate ($n = 2$). The data points represent the Ct values at which each assay amplified (three technical replicates for each biological sample are given on the same column). **A.** Ct values of the 7-steps method using CF5 and Grade 3 paper. DNA extraction using Grade 3 paper performs significantly better than using CF5 (p -value <0.05). **B.** Magazorb Kit-based method using CF5, Grade 3 and GF/DVA paper. No statistically significant difference is observed for $p < 0.05$ when DNA extraction is performed with the different types of paper.

3.1.10 Chitosan-Functionalised Paper

Whatman[®] Grade 1 and Fusion 5 were treated with chitosan (see Section 2.14.4) and 3-mm or 5-mm discs were used in the extraction of DNA from *E. coli* bacterial culture. The first goal was to understand if chitosan-functionalised Grade 1 paper led to amplification as with untreated paper discs. The second step was to evaluate the use of chitosan-functionalised Fusion 5 discs and assess if it was enhancing the extraction performances compared to untreated Grade 3 paper, as previously demonstrated in the literature [82,86]. When using chitosan-functionalised paper, an acidic lysis buffer ($\text{pH} < 6.3$) was needed to make sure that chitosan was positively charged when in contact with DNA. The acidic lysis buffer described in Section 2.2 was used as it was also demonstrated in Section 3.1.6.4 that there is no significant difference than using its alkaline counterpart containing Tris-HCl ($\text{pH} 8$).

The first results obtained from the extraction procedure using low molecular weight chitosan-functionalised Grade 1 paper that had been washed or not washed are shown in Fig. 3.30. Chitosan-functionalised paper can be used to detect target DNA ('Chitosan Washed' and 'Chitosan Non-washed'). A delay in amplification of ~ 8 min compared to non-treated Grade 1 paper ('Untreated' in Fig. 3.30) was observed.

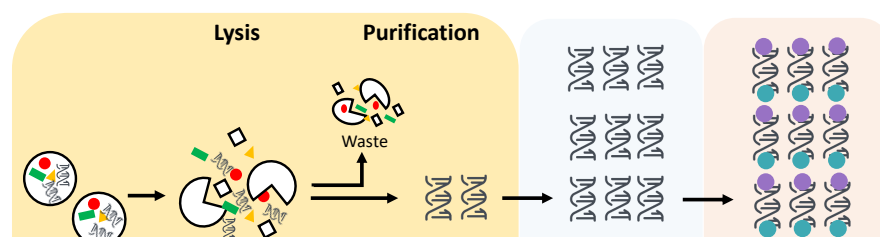


Figure 3.30: **Amplification plot and time-to-positive values (TTPs) of paper-based extraction procedure performed using chitosan-functionalised Whatman[®] Grade 1 paper discs.** Three 3-mm discs were used for each biological sample ($n = 1$). Results are shown for the extraction performed using untreated paper discs (Untreated), chitosan-functionalised paper discs with washing (Chit Washed), and chitosan-functionalised paper discs without washing (Chit Non-washed). LAMP was performed with primers Concentration 1 (Table 3.1). **A.** Amplification plot. The curves belong to each LAMP assay. NTCs = no template controls containing different chitosan-functionalised paper discs. **B.** TTPs. The dots represent the time (in minutes) at which each assay (technical replicate) amplified. The x-axis includes the different samples, *i.e.*, Untreated, Chit Washed, Chit Non-washed. PC = positive control whose DNA concentration is approx. 20 ng/ μ L.

Given $n = 1$, it is not possible to draw any valuable conclusion from Fig. 3.30. However, it can be observed that chitosan-functionalised Grade 1 paper without washing ('Chit Non-washed') leads to a very delayed and not clear amplification of the DNA target (see Amplification plot in Fig. 3.30A). For instance, in a successive experiment it was observed that a concentration as low as 0.04% (w/v) chitosan inhibits the final LAMP reaction. This result allowed to speculate about the necessity of the washing step during the chitosan-functionalisation process of paper. In fact, the washing allows to remove the excess chitosan that the paper does not adsorb after incubation and that could be successively dispersed in the reaction mixture thus inhibiting it.

To better understand the nature of DNA binding to chitosan-functionalised paper, already purified DNA (~ 1 ng/ μ L) was employed. Fusion 5 paper was pretreated with medium molecular weight chitosan as indicated in Section 2.14.4 and its performance was compared with untreated Grade 3 paper. High molecular weight chitosan has proven to form more stable complexes with DNA than lower molecular chitosan [88], so a lower Ct value was expected when performing the DNA procedure using functionalised paper with medium molecular weight chitosan. Chitosan-functionalised paper does not bring a clear improvement in performance of the 7-steps paper-based DNA extraction method (Fig. 3.31), in contrast with what was assessed in [82, 86]. It is clear that two technical replicates of the 'Fusion 5' sample amplify very late, distorting the

one-way ANOVA analysis.

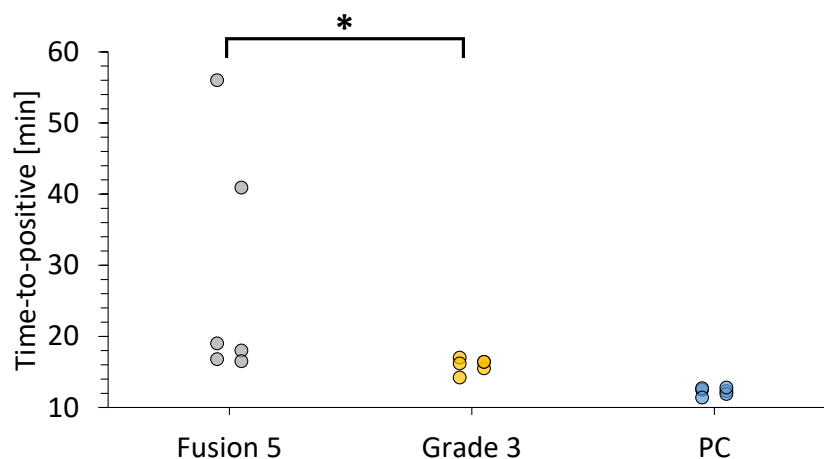


Figure 3.31: **Time-to-positive values (TTPs) of paper-based extraction procedure performed using chitosan-functionalised Fusion 5 paper disc compared to untreated Whatman® Grade 1.** Time-to-positive values are given for paper-based DNA extraction performed using a 5-mm disc of chitosan-functionalised Fusion 5 paper or a 5-mm disc of untreated Grade 1 paper. The experiment was carried out in biological duplicate ($n = 2$). The data points represent the time (in minutes) at which each assay (technical replicate) amplified. The x-axis includes the different samples, *i.e.*, DNA extraction performed under the same conditions. PC is the positive control and it consisted of already purified DNA, extracted a second time using the magnetic beads-based method (gold-standard). NTCs are not shown but they represents the no template controls containing 1 μ L of NFW.

To improve DNA extraction using chitosan-functionalised Fusion 5 paper discs, the concentration of chitosan in the paper pretreatment could be reduced from 1% to 0.05% (w/v) following what was done by Gan *et al.* [82] and Bengston [86]. A lower concentration of chitosan during the paper pretreatment phase might help to avoid the release of excess chitosan from the paper, thus avoiding possible LAMP reaction inhibition. The choice of making 1% (w/v) chitosan solutions derived from a careful consultation of different papers and beads functionalization methods for DNA capturing [82, 86, 87, 89, 162].

Pretreating paper with chitosan adds an extra level of difficulty in preparing the components that would be integrated in a potentially enclosed device. Additionally, given the difficulties in proving that Fusion 5 pretreated with chitosan brings a real performance enhancement of the paper-based extraction procedure, the use of chitosan-functionalised paper was not investigated further.

3.2 Discussions

A fast method for nucleic acid extraction from large samples at room temperature that relies on cellulose filter paper and that is instrument-free has been developed. This

method creates the basis for a portable and equipment-free LAMP POC diagnostic device that integrates sample pretreatment with limited user intervention and that it is suitable for applications in resource-limited settings.

Nucleic acid sample pretreatment is the first essential step to perform isothermal nucleic acid amplification tests (NAATs) that have the potential to bring accurate lab-based methodologies to in-field setting. The reduction of the number of handling steps in the sample pretreatment opens the route towards a pipetting-free sample-in-result-out diagnostic device that integrates all the NAATs steps. The method developed in this study reduces (1) the number of handling steps from 15 of the gold-standard beads-based method (Promega) to 7 steps, and (2) the number of liquids involved, and (3) it eliminates the need for external heating. The lowest concentration of *E. coli* bacteria that the method can detect from a 100 μ L sample using Whatman[®] Grade 1 paper is 10^5 CFU/mL. This result is in line with the analytical sensitivity of the LAMP assay developed in tubes.

The performance of our simplified DNA extraction method was investigated using papers with different pore sizes, capillary flow time and surface characteristics. Among the filter papers, cotton linters and glass fibers used, Whatman[®] Grade 3 was considered the best to trap and successively release DNA. To further improve the potential integration of our paper-based method into a LAMP POC device, efforts have focused in store-drying the lysis buffer directly on the paper discs. Extraction buffer # 2 from Zou *et al.* was successfully air-dried onto Whatman[®] Grade 3 paper and effectively used for paper-based extraction, thus opening the route for our method to be implemented in remote areas and outside laboratory settings.

A second paper-based DNA extraction procedure was briefly studied to introduce proteinase K (PK) during the lysis step, and maximise the lysis efficiency of the targeted pathogen. This method is based on the manufacturer's instructions provided in MagaZorb[®] DNA Mini-Prep Kit (Promega), and the magnetic beads were simply substituted with paper discs. The high amount of handling steps of this method is not suitable for an easy integration into an enclosed device where all reagents can be stored 'on-board' and with no user-intervention. However, it can be considered as an alternative to magnetic beads-based extraction methods.

A nucleic acid (NA) extraction from blood and human cell lines using untreated cellulose-based paper was introduced by Zou *et al.* [21]. The authors used a ratio

of four volumes of extraction buffer to one volume of sample and rinsed the paper disc with a wash buffer for 1 minute. The lysis step was done in a tube before adding the paper to the solution, and the paper disc captured DNA in a few seconds. We demonstrated that our cellulose-based paper performed comparably to the commercially available paramagnetic beads-based NA extraction method (MagaZorb[®] DNA Mini-Prep Kit, Promega) using a lower lysis volume than in Zou *et al.* [21], and a 1-minute washing with nuclease-free water. Unlike what was discussed in Section 3.1.8, Zou *et al.* were able to include PK in the lysis of cell lines, without affecting the PCR reaction [21]. Their results indicate that rinsing paper for 1 minute is sufficient to remove any potential PCR inhibitors. It was not clear how they achieved these results without thermally deactivating PK, which was a necessary step when using their extraction buffer # 2. Zou *et al.* [21] extended their work to use different kinds of papers [157]. Interestingly, the authors chemically modified Whatman[®] Grade 1 with spermine, polyvinylpyrrolidone (PVP 40) and cationic polymers to investigate possible improvements in trapping and releasing abilities of paper. They pretreated paper with 1.25% (w/v) chitosan solutions as an effective cation polymer for trapping and releasing DNA, however, treated paper did not lead to any amplification in PCR. The use of chitosan-functionalised paper was explored in our study to understand whether it enhanced the sensitivity of the paper-based extraction procedure (Section 3.1.10) by capturing more DNA than normal paper and accelerating the reaction. However, the results did not match our expectations, *i.e.*, untreated paper showed an earlier amplification of the DNA target than chitosan-functionalised paper. Moreover, chitosan pretreatment of Fusion 5 did not improve the NA extraction method performance, on the contrary of what Gan *et al.* [82] and Bengston *et al.* [83,86] reported. For future work, we suggest using a lower concentration of chitosan solution such as 0.05% (w/v) instead of 1% (w/v), as recommended by [82]. A lower concentration of chitosan might reduce the amount of chitosan that is not properly adsorbed by the paper, thus facilitating washing it away during the sample pretreatment. It could also enable faster time-to-positive since chitosan concentration is inversely correlated with amplification efficiency due to the adsorption of enzymes [82]. Furthermore, we advise paying more attention to the pH of the washing buffer. Lastly, the addition of an elution step before amplification with a pH higher than 8.5 might be implemented to guarantee the total release of DNA from the chitosan-functionalised paper. Since chitosan pretreatment of paper adds complexity to the preparation of the components for a potential POC

device, this approach was not pursued further.

A more recent work that performs NA extraction on Whatman[®] Grade 3 was conducted by Malpartida-Cardenas *et al.* [163]. Their NA extraction consists in pretreating paper with a surfactant as lysis buffer, spotting the sample, incubating the sample and paper overnight, washing the paper for one minute in PBS buffer and eluting the paper discs for 5 minutes at room temperature (or transferring the discs in LAMP reagents). The method was proven for blood samples and only preliminary work is presented for bacterial pathogens. In comparison, the paper-based method with lysis buffer dried on paper, which was developed in this work, is very similar, but does not require sample incubation overnight. Both methods are successful in extracting DNA rapidly, easily and without equipment.

Zou *et al.* [21], Malpartida-Cardenas *et al.* [163] and our study highlight the increased interest in developing cheap and fast paper-based NA extraction methods that could be easily integrated into POC diagnostic devices. A pilot study to evaluate a novel POC device for the detection of SARS-CoV-2 that incorporates a simple paper-based purification method similar to Zou *et al.* [21], called SnapDx and developed by Prakash lab at Stanford University Bioengineering, further illustrates this trend [164]. Further work assessing the feasibility of our paper-based DNA extraction method is described in this thesis in Section 5.1.3.

It is hypothesized that the proposed method for DNA extraction from *E. coli* using Grade 3 paper could be applicable to other types of bacteria, both gram negative and gram positive. Moreover, based on the findings of Malpartida-Cardenas *et al.* [163], we anticipate that our methods could also work with blood spot samples.

The paper-based DNA extraction method introduced in this chapter has several advantages over the conventional paramagnetic beads-based kits, such as lower reagent volumes, fewer reagent types and simpler handling steps. However, to make our method suitable for a disposable POC diagnostic device that can be used in rural areas, we need to improve not only the limit of detection, but also the safety of the reagents involved. For instance, many commercial lysis buffers, including the one from Promega, contain guanidine HCl (GuHCl) and surfactants, such as sodium dodecyl sulfate (SDS). These chemicals are harmful to aquatic life and humans, and can release toxic and corrosive gases, such as hydrogen chloride and nitrogen oxides, when incinerated [165,166]. Since incineration is the main way of disposing hospital waste in developing countries [167],

alternative chemicals must be investigated.

In this chapter, a paper-based sample extraction method was introduced to address challenges faced by current paper-based POC devices, such as the number of manual steps required and the ability to function in in-field settings without external equipment. The developed method consists of six steps and can be completed in less than ten minutes. Notably, the method reduces the number of reagents compared to standard magnetic beads-based methods, and it allows for the storage of lysis buffer in a dried form on paper discs, simplifying the handling of liquid reagents. This sample pretreatment approach lays the groundwork for seamless integration into a fully enclosed sample-in-answer-out POC diagnostic device, which will be discussed further in Chapter 5. However, before implementing the sample pretreatment in an enclosed device, the challenge of pre-loading and storing LAMP reagents within the device was addressed (as explored in Chapter 4). The study aimed at extending the shelf-life of LAMP reagents in the absence of a cold chain and enhance access to paper-based POC NAATs in low-resource settings.

3.3 Contribution to Knowledge

In this chapter we discussed how to decrease the number of handling steps in the sample pretreatment for molecular testing by avoiding the use of external equipment, such as heating, and by using low-cost paper discs. A paper-based DNA extraction method was investigated with the vision of easily incorporating it in a fully enclosed sample-in-answer-out point-of-care diagnostic device.

We demonstrated that sample pretreatment of a relatively large volume (100 μ L) of *E. coli* K12 sample can be easily performed in 6 steps and less than 10 minutes. The paper pretreatment requires sterilisation via UV light on both sides and drying of lysis buffer onto the paper at room temperature. The DNA extraction steps consist of adding the sample and incubating it for 6 minutes, washing the paper with nuclease-free water and transferring the discs directly into the LAMP reaction or eluting them for 10 minutes at room temperature. Compared to traditional paramagnetic beads-based kits, our paper-based DNA extraction method offers the benefit of reduced reagent volumes, fewer reagents, easier handling steps and rapidity.

Given the success in extracting DNA from *E. coli* K12 our method might be generalised to other bacterial species, both gram negative and gram positive. Based on the results by Zou *et al.* [21] and Malpartida-Cardenas *et al.* [163], we expect our method to be also compatible with blood spot samples.

Therefore, our DNA extraction method represents a valuable option to be integrated in POC devices.

Chapter 4

Easy-on-board-storage of Molecular Reagents for the Long-Term and at Room Temperature Using Pullulan

The goal of this study is to investigate the effects of reagents stored in a mixture of pullulan and trehalose on the limit of detection of a LAMP assay targeting either *E. coli* (*malB* gene) or *Plasmodium* species. Pullulan and trehalose have been used as long-term preservatives for isothermal nucleic acid amplification reactions [26] and they can enable deployment of point-of-care (POC) diagnostic tests in low-resource settings. In fact, the limited shelf-life of molecular reagents at ambient temperature still represents one of the major barriers for the effective use of POC diagnostic devices when refrigeration is not available, as is the case in most low-resource settings. LAMP reagents stored dry in pullulan-trehalose tablets have also been shipped to underserved communities and used on-site to study their stability.

In the following sections the results of experiments conducted to optimize the dry-storage of molecular reagents in pullulan and trehalose tablets are provided. The effects of 10% (w/v) pullulan tablets on the storage of primer mix and master mix was separately evaluated over about 60 days (Section 4.1.1) for the detection of *E. coli malB* gene. After, the use of the isothermal master mix from New England Biolabs (NEB) was studied and the concentrations of its components optimised to obtain a sensitive LAMP assay with short amplification times (Section 4.1.2). The master mix from NEB was used to study molecular reagents storage in a combination of pullulan and trehalose mixtures (Sections 4.1.3, 4.1.4). The optimised concentration of pullulan-

trehalose tablets was then used to detect *Plasmodium* species and ship the stored dry reagents to the field, test them at the point-of-need, and analyse them back in the UK laboratory (Sections 4.1.5, 4.1.8).

4.1 Results

Different LAMP reagents were formulated into tablets and combined with the other liquid components of the LAMP reaction. The preservation of reagents over time was evaluated and the impact on the limit-of-detection (LOD) of the assay at low target DNA concentrations was assessed.

The final LAMP reaction mix (25 μL total) contained 5 μL of primer mix, 15 μL of isothermal master mix and 5 μL of sample (as described in Section 2.15.1). As samples, synthetic *E. coli malB* gene DNA template, the WHO International Standard for *P. falciparum* DNA and Jurkat Genomic DNA were used (details in Section 2.4). DNA was also extracted from *E. coli* bacterial culture using the gold standard magnetic-beads based method. The primer concentrations used in the liquid LAMP reactions are given in Table 2.5.

4.1.1 Molecular Reagents Stored in 10% (w/v) Pullulan Solutions

The stability of LAMP primer mix and the master mix ISO004-LYO (Optigene Ltd.) for the detection of *E. coli malB* gene was investigated using 10% (w/v) pullulan tablets. The two reagent mixes were stored and tested separately, and their activity was investigated after storage for up to six weeks. The performance of the tablets was assessed by determining the time-to-positive values (TTPs) of the real-time LAMP, as explained in Section 2.15.1.1.

The master mix ISO-004-LYO stored in 10% (w/t) pullulan tablets fails to amplify the lowest DNA concentrations (10^{-6} and 10^{-7} ng/ μL) after two weeks of storage, while the freeze-dried master mix can detect 10^{-7} ng/ μL for up to five weeks of storage (Fig. 4.1).

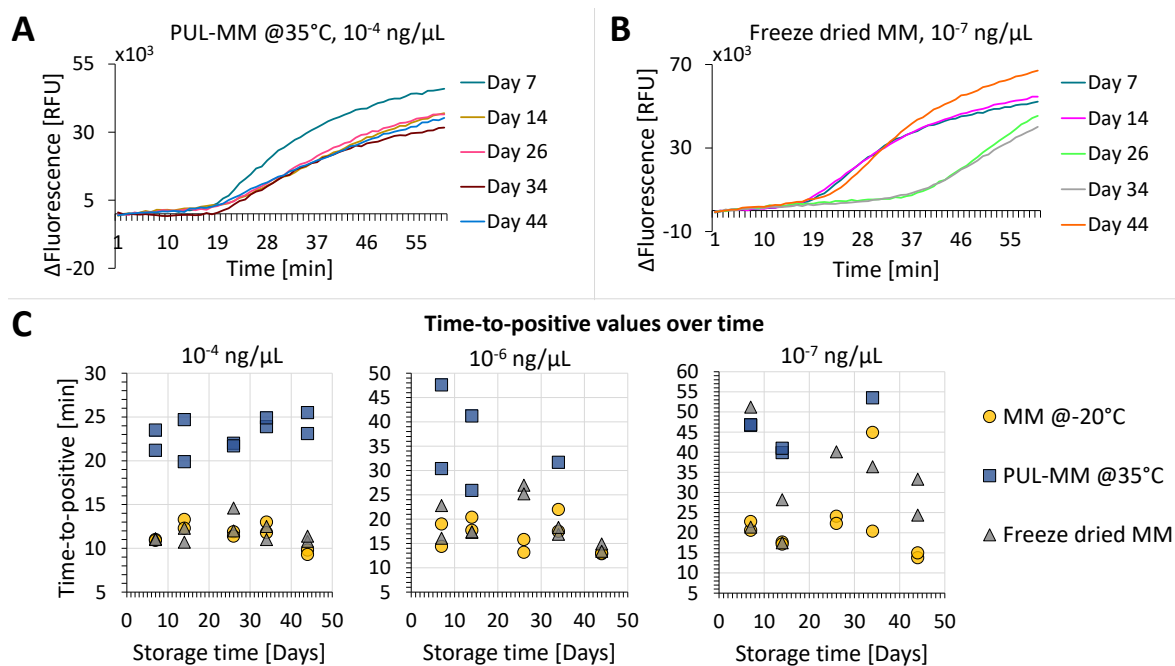


Figure 4.1: **Master mix ISO004-LYO stored in 10% (w/t) pullulan tablets at 35 °C over time.** Each assay was run in duplicate ($n = 2$) and tested over 44 days of storage. **A.** LAMP amplification plot of tablet-based assays containing master mix ISO004-LYO, stored dry at 35 °C (PUL-MM @35 °C). The synthetic DNA has a concentration of 10^{-4} ng/μL (2.3×10^6 copies/reaction). Curves for only one repeat are shown. **B.** LAMP amplification plot of assays using freeze dried master mix ISO004-LYO at 35 °C (Freeze dried MM) until use. The synthetic DNA concentration of the assay is 10^{-7} ng/μL (2.3×10^3 copies/reaction). Curves for only one replicate are given. **C.** Comparison of time-to-positive values (TTPs) over time (days) between LAMP master mix ISO004-LYO stored in pullulan tablets at 35 °C (PUL-MM @35 °C); master mix ISO004-LYO freeze dried following manufacturer instructions and stored at 35 °C (Freeze dried MM); and master mix ISO004 stored at -20 °C (MM @-20 °C) until use. Three different concentrations of *E. coli malB* gene synthetic DNA were tested: 10^{-4} , 10^{-6} , 10^{-7} ng/μL. ΔFluorescence is the fluorescence value at each minute subtracted by the mean value of the first five fluorescent values of each assay.

The pullulan-stored master mix has a reduced stability and limit of detection (LOD) compared to the freeze-dried master mix. Moreover, the reagents stored in pullulan exhibit higher and more variable TTP values in the first two weeks, indicating slower reactions that may affect the feasibility of in-field applications. The decreased reactivity of the pullulan-stored master mix could be due to loss of reagent during tablet preparation. In fact, the increased viscosity of the initial solution could have led to reagent loss during the pipetting process for making the tablets [119]. Another possible explanation could be the degradation of the fluorophore (reporter dye) during long-term pullulan storage. Even if pullulan tablets have a significant decrease in LOD, they still represent a useful option for dry and solid storage of master mix. In fact, high sensitivity may not be a crucial factor in some contexts, where the convenience of shipping devices and preventing unwanted mixing of reagents during transport through store dry is more important.

The primer mix, on the other hand, shows no loss of activity after six weeks of stor-

age at 35 °C in 10% (w/t) pullulan tablets (Fig. 4.2). The lowest concentration of 10^{-7} ng/ μ L is detected, as shown by the TTP values in Fig. 4.2B. LAMP primers can be safely stored in pullulan tablets for at least six weeks.

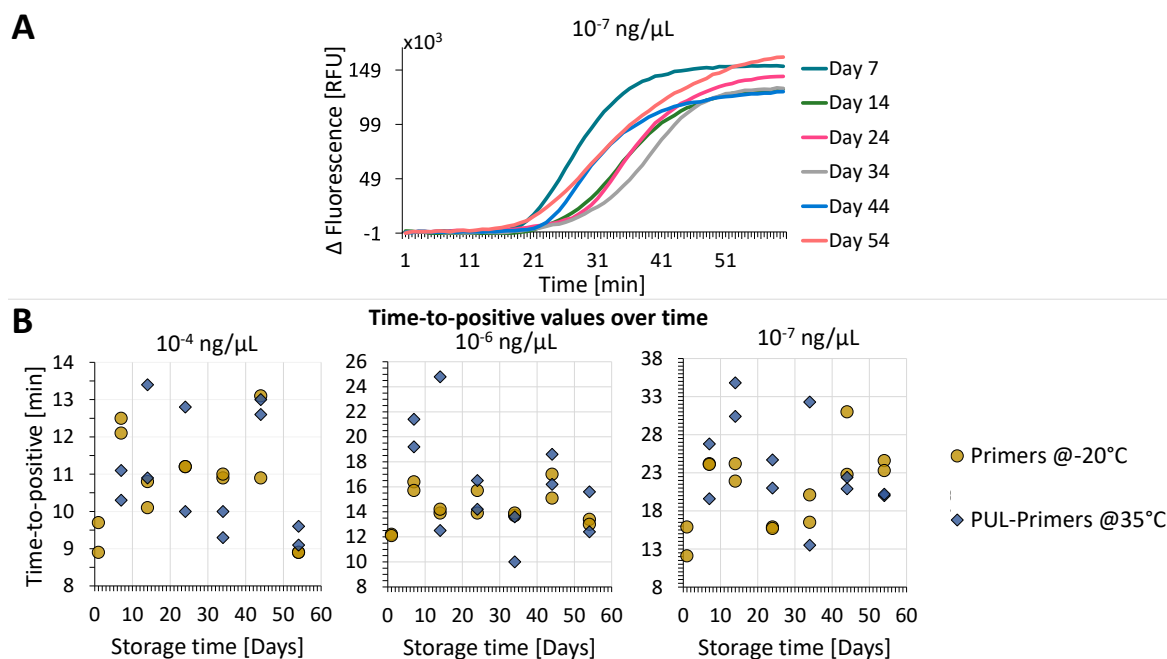


Figure 4.2: **Primer mix stored in 10% (w/t) pullulan tablets at 35 °C over time (days).** Each assay was run in duplicate ($n = 2$) and tested over 54 days. **A.** LAMP amplification plot of tablet-based assays containing primer mix stored at 35 °C (PUL-Primers @35 °C). The synthetic DNA has a concentration of 10^{-7} ng/ μ L (2.3×10^3 copies/reaction). Curves are shown for only one repeat. Δ Fluorescence is the fluorescence value at each minute subtracted by the mean value of the first five fluorescent values of each assay. **B.** Comparison of time-to-positive values (TTPs) over time between LAMP primer mix stored in tablets at 35 °C (PUL-Primers @ °C) and stored at -20 °C (Primers @-20 °C) until use. Three different concentrations of *E. coli malB* gene synthetic DNA were tested: 10^{-4} , 10^{-6} , 10^{-7} ng/ μ L.

4.1.2 Optimization of LAMP Master Mix Concentrations (New England Biolabs)

As discussed in Section 4.1.1, the long-term storage of reagents requires full control on the LAMP assay components. This is essential to optimise the performance and stability of the assay. Many commercially available LAMP reagents are pre-mixed and their contents and concentrations are proprietary information. The LAMP reagents provided by NEB (WarmStart[®] Bst 2.0 DNA polymerase, Deoxynucleotides, LAMP Fluorescent Dye) are available as separate reagents to allow for individual reagent optimisation.

In this section, the effect of different reagent concentrations on the performance of the LAMP assays was investigated. The LAMP assay conditions that resulted in a lower

time-to-positive was considered as optimal.

Firstly, the performance of the NEB LAMP assay was compared with pre-mixed ISO-004 master mix (Optigene Ltd.). The initial composition of NEB master mix used (15 μL) was as suggested by the manufacturer: 1X Isothermal Amplification Buffer, additional 2 mM MgSO_4 , 0.32 U/ μL Bst 2.0 WarmStart[®] DNA Polymerase, 1.4 mM Deoxynucleotide (dNTPs) Solution Mix and 1X LAMP Fluorescent Dye. Each reaction contained 5 μL of primer mix, and 15 μL of isothermal master mix. 5 μL of *E. coli* synthetic DNA sample was added to each assay and amplification was carried out at 66 $^\circ\text{C}$ for 60 minutes. The TTPs were calculated as explained in Section 2.7 and compared. The LAMP amplification plot and the TTPs (Fig. 4.3) show that the amplification of the NEB master mix using the manufacturer's recommended conditions is slower than the one of Optigene.

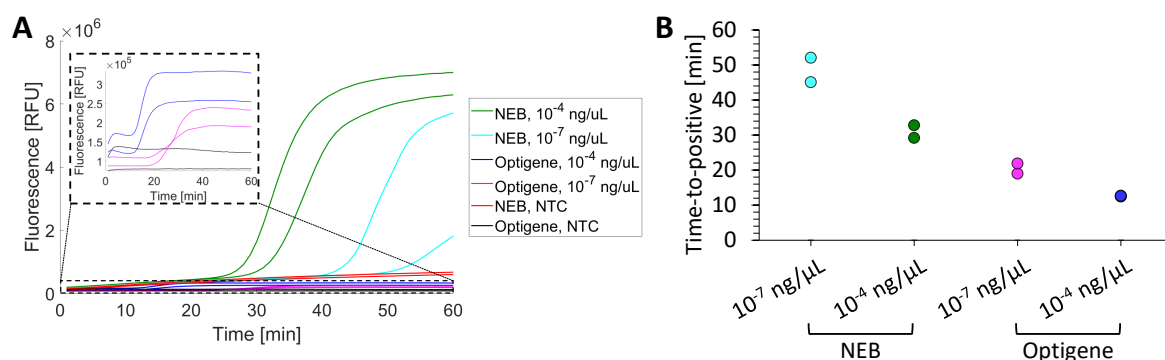


Figure 4.3: **Performance of LAMP assay carried out using the master mix provided by New England Biolabs (NEB) or by Optigene Ltd. (ISO-004).** The assays were run in duplicate ($n = 2$) and the *E. coli* synthetic DNA concentrations used were 10^{-4} ng/ μL and 10^{-7} ng/ μL . In the no template controls (NTCs), 5 μL of NFW was added as the template. The lowest concentration tried is 10^{-7} ng/ μL , because it is the limit-of-detection of the LAMP assay when using ISO-004 (Section 3.1.2). The LAMP assay performed using NEB master mix and ISO-004 are indicated as ‘NEB’, and ‘Optigene’, respectively. **A.** Amplification plot. **B.** Time-to-positive (TTP) values derived from the amplification curves.

Therefore, increasing concentrations of MgSO_4 (final reaction concentrations of 4 mM, 6 mM and 8 mM) were tried and the TTP values compared in Fig. 4.4A. 6 mM MgSO_4 resulted in the fastest amplification times (12.50 ± 0.20 min). Moreover, half the concentration of dye recommended by the NEB protocol (0.5X) led to similar amplification to 1X LAMP Fluorescent Dye in the final LAMP assay, suggesting that 1X dye is unnecessary. Therefore, subsequent experiments were performed with a final concentration of 6 mM MgSO_4 (2 mM MgSO_4 are already included in the 1X Isothermal Amplification Buffer) and 0.5X LAMP Fluorescent Dye in the 25 μL LAMP reaction. Betaine is often added to isothermal NA amplification tests as it can lower the melting temperature of

GC-rich DNA sequences [25, 168]. However, Ma *et al.* [169] demonstrated that betaine can be detrimental for LAMP reaction efficiency, and our results are in line with their findings: the addition of 800 mM betaine (N,N,N-trimethylglycine) (Thermo Fisher Scientific Inc.) [95] to the LAMP mixture does not bring any advantage in terms of amplification performance (Fig. 4.4B). Moreover, NEB LAMP master mix (‘NEB w/o Betaine’) has shorter TTP values than the master mix from Optigene Ltd. (about 6 minutes), indicating that 6 mM MgSO₄ has a great effect on the performance of the NEB LAMP master mix compared to Optigene Ltd.. When betaine was added to the LAMP assay, 5 μ L of already purified DNA (20 ng/ μ L, Section 2.1) was added to the LAMP mix.

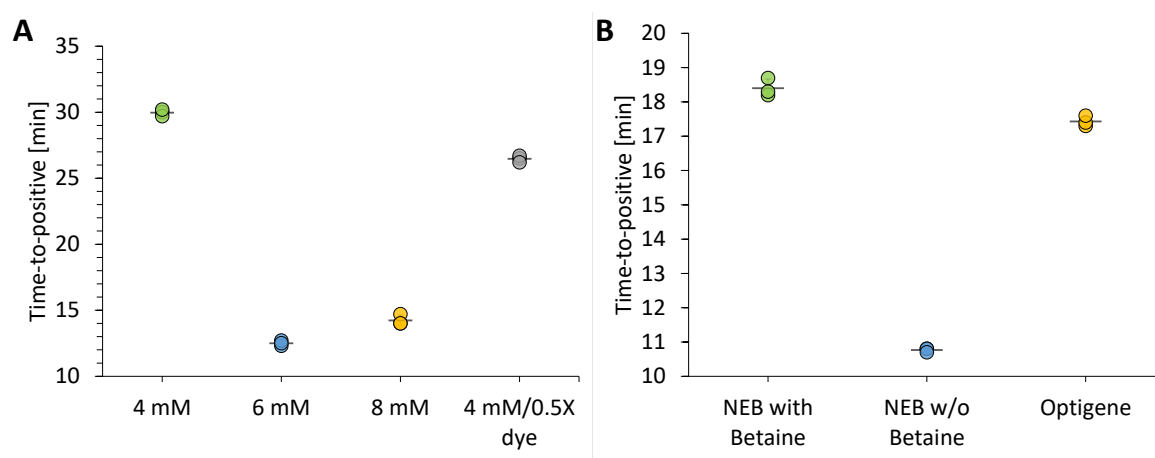


Figure 4.4: **Optimisation of MgSO₄ and betaine concentration in LAMP master mix (New England Biolabs).** Time-to-positive values (TTPs) were used for comparative analysis. TTPs were derived from the amplification curves as described in Section 2.7. The dots represent the TTPs for each LAMP reaction. The horizontal bars represent the mean value of TTPs of LAMP reactions run under the same conditions. The optimisation factor was tested in technical triplicate ($n = 3$). **A.** TTP values of LAMP assays performed with NEB master mixes containing different MgSO₄ final concentrations, *i.e.*, 4 mM, 6 mM, or 8 mM. The MgSO₄ concentrations are given in the x-axis. The assay ‘4 mM/0.5X dye’ has a 4 mM MgSO₄ and 0.5X LAMP Fluorescent Dye concentration in the final 25 μ L LAMP reaction. The *E. coli* synthetic DNA concentration used was 10^{-4} ng/ μ L. **B.** TTP values of LAMP assays performed with NEB master mix with the addition of betaine (NEB with Betaine) or without the addition of betaine (NEB w/o Betaine), and with the master mix purchase from Optigene Ltd. (Optigene). ‘NEB with Betaine’ LAMP reaction has 800 mM betaine, in addition to the components listed in Table 2.2. The *E. coli* genomic (‘already purified’) DNA concentration used was 20 ng/ μ L.

The analytical sensitivity of the optimised NEB LAMP assay was carried out using 10-fold dilutions of *E. coli malB* synthetic DNA ranging from 2.27×10^7 to 227 copies (Figures 4.5). The conversion from ng/ μ L to copy number for these experiments is given in Table 4.1. The associated standard curve is shown in Fig. 4.5. The limit of detection (LOD) using synthetic DNA in LAMP is 2,270 copies, that corresponds to about 1,820 copies previously shown when using the master mix from Optigene Ltd. (Section 3.1.2). However, the detection of 2,270 copies present a late amplification and

high variability. This causes the linear correlation to be extremely poor $R^2 = 0.70$ (Fig. 4.5A). If the lowest concentration that the assay can detect is not included in generating the standard curve, then the correlation goes up to 99% (Fig. 4.5B). The same LOD was observed when running the assay with labelled primers and on lateral flow strips (LFSs).

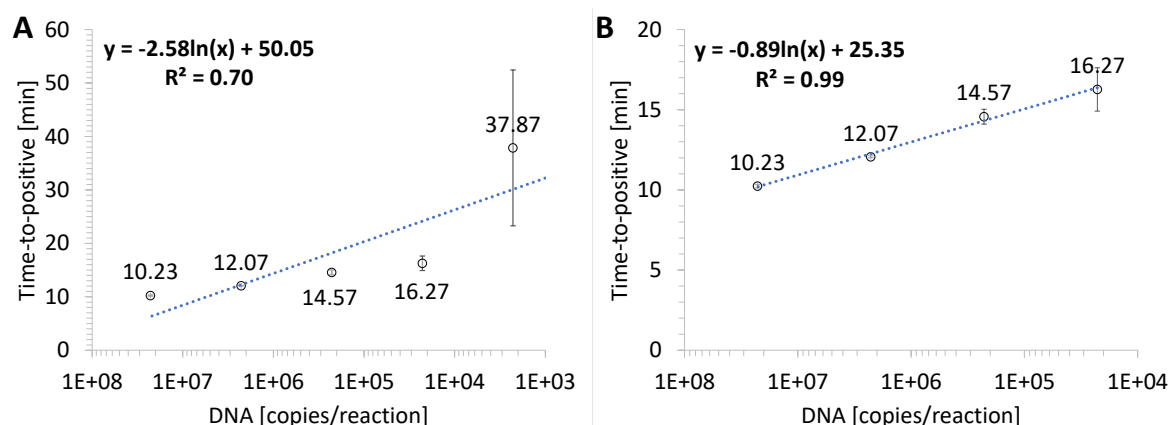


Figure 4.5: **Analytical sensitivity and standard curves of the optimised LAMP assay with New England Biolabs reagents (NEB).** Time-to-positive (TTP) were derived from the amplification curves as described in Section 2.7. The dots represent the mean value of TTPs for each *E. coli malB* gene synthetic DNA concentration. 5 μL of DNA template whose concentration was measured in $\text{ng}/\mu\text{L}$ was added to the final 25 μL LAMP reaction. The template concentration was then converted in copies/reaction as described in Table 4.1. Each DNA concentration was run in triplicate ($n = 3$). TTP data is presented as mean TTP \pm standard deviation. **A.** Standard curve. **B.** Standard curve excluding the sample whose concentration is 10^{-7} $\text{ng}/\mu\text{L}$ (limit-of-detection).

Table 4.1: **Conversion table for 204 bp long *E. coli malB* gene synthetic DNA from $\text{ng}/\mu\text{L}$ to copy number per reaction in LAMP.** 5 μL of template whose concentration was measured in $\text{ng}/\mu\text{L}$ was added to the final 25 μL LAMP reaction. The conversion was obtained as explained in Section 2.10.

Concentration in $\text{ng}/\mu\text{L}$	Concentration in copies/reaction
1E-03	2.27E+07
1E-04	2.27E+06
1E-05	2.27E+05
1E-06	2.27E+04
1E-07	2.27E+03
1E-08	2.27E+02

4.1.3 Molecular Reagents Stored in 10% (w/v) Pullulan and 0.5 M Trehalose

The ‘two-pill method’ proposed by Leung *et al.* [26] was used to stabilize LAMP reagents with pullulan and trehalose. This method was based on the idea that dried-reagents could be affected by the salts present in them [25, 26]. Trehalose was an

essential ingredient for the tablet formulation when the master mix components from NEB were used. This was because a combination of trehalose (a small disaccharide) and pullulan (a large polysaccharide) provide better long-term stability by having both a dense molecular arrangement of the disaccharide and a high physical resilience of the polysaccharide [170]. Two separate tablets were created: one (Tablet 1) containing primer mix, WarmStart[®] Bst 2.0 and dNTPs, and the second (Tablet 2) containing the Isothermal Amplification Buffer and MgSO₄, as explained in Section 2.15.1.2. Upon use the tablets were resuspended as described in the Section 2.15.1.2 and then the LAMP products were either visualised in real-time or added onto LFSs as explained below.

Whenever Tablet 1 and 2 were created as described in Section 2.11 but without the addition of trehalose, and stored at 35 °C overnight, LAMP amplification was not observed. This suggests that the presence of an additional additive to pullulan is essential for the storage of such reagents. The only LAMP component that can be successfully stored in pullulan tablets without additional trehalose is the primers (as discussed in Section 4.1.1). Trehalose was chosen as an additive because of its stabilising properties of biomolecules during lyophilisation [116, 170]. *E. coli malB* gene was used as DNA target sequence.

4.1.3.1 Optimal Concentration of Labelled Primers for Long-Term Storage

Until this point unlabelled primers were stored dry in pullulan tablets and amplification was measured by fluorescence of a double-stranded DNA intercalating dye using a gold-standard bench-top thermocycler. This method is unsuitable for use in resource limited settings, so the use of primers labelled with molecules that allow for visualisation of amplification results on LFSs was investigated. To do this it was necessary to understand which primers to label on their 5'-end with fluorescein isothiocyanate (FITC) and biotin for LFS detection (Section 2.11). The FITC and biotin moieties were incorporated on the 5'-end of all primers, and three different labeled combinations were considered: LF-biotin and LB-FITC, LF-biotin and FIP-FITC, and LB-FITC and BIP-biotin. The reasoning behind choosing these combinations is as follows. In general, the outer primers (F3/B3) are not suitable for labelling as their role in the LAMP reaction is to enable DNA strands displacement and, theoretically, they will not be abundant in the final amplified products. Therefore, loop primers (LF/LB) and in-

ternal primers (FIP/BIP) represent a better choice for labelling with fluorescent or biotinylated tags. The far ends of the amplicons should correspond to the ends of the FIP and BIP primers. However, for labelling, the loop primers are preferable over the internal primers for two reasons. First, the synthesis yield of labelled FIP/BIP primers would be lower than that of labelled loop primers, due to their length and the direction of synthesis. This would increase synthesis costs. Second, labelled FIP/BIP primers would have a higher chance of forming primer dimers due to their length, ~ 40 -bp, compared to LF/LB primers that are shorter (~ 20 -bp). Therefore, it is usually recommended to label the loop primers first, then exploring combinations of a labelled loop primer and a labelled internal primer, and finally labelling both internal primers as a last option. In the second scenario, as shown in Fig. 4.6 (bottom step), the loop primers bind to the single-stranded products that originate from the internal primers. For example, in the early stages of amplification, Loop B binds to the product that

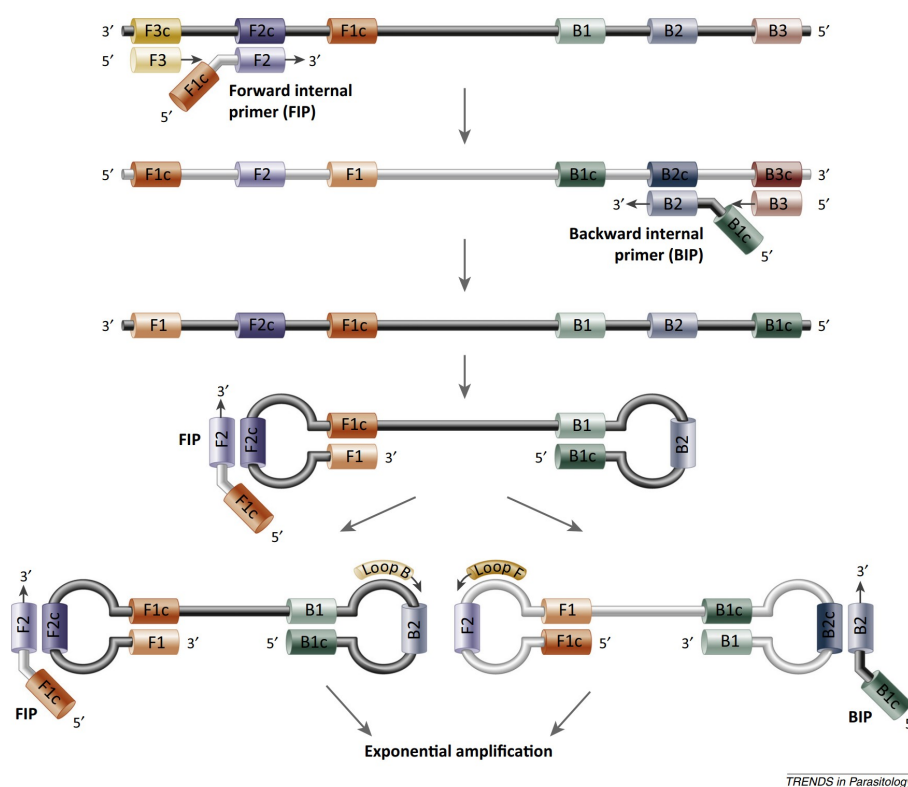


Figure 4.6: **Simplified schematic of loop-mediated isothermal amplification (LAMP).** Six primers are used to detect six to eight different regions of DNA target. A DNA polymerase that can displace the original double-stranded DNA begins synthesis. Two of the primers form loop structures that enable more rounds of amplification to occur. Image reproduced from Alhassan *et al.* [171] and with permission of the rights holder, Elsevier (Appendix A.5).

comes from BIP primer. Similarly, Loop F binds to the product that comes from FIP primer. This means that if FIP primer and LB were to be labelled, three fragments need to join to form a double-labelled product, whereas if BIP primer and LB were

labelled, only two fragments are needed.

The OligoAnalyzerTM Tool [172,173] was used to study the possibility of primer dimers among the pairs of labelled primers. If the pair of labelled primers is prone to primer dimer, there is a higher chance for false positive on the LFSs. The hetero-dimers function was used and the concentration values were selected from Tables 2.4, and 2.2. The Gibbs free energy change (ΔG) indicates how likely a dimer is to form spontaneously, and primers should have a ΔG higher than -9 kcal/mole, which means they are less prone to hybridize to each other instead of the DNA template [172]. Fig. 4.7A shows that the highest ΔG of dimer structures (-5.24 kcal/mole) occurs when LF-biotin and FIP-FITC are tagged. Therefore LF-biotin and FIP-FITC are least likely to form primer dimers and cause false positives. $\Delta G = -8.24$ kcal/mole of LF-biotin and LB-FITC implies a higher risk of false positive which was verified on LFSs (Fig. 4.7B). The

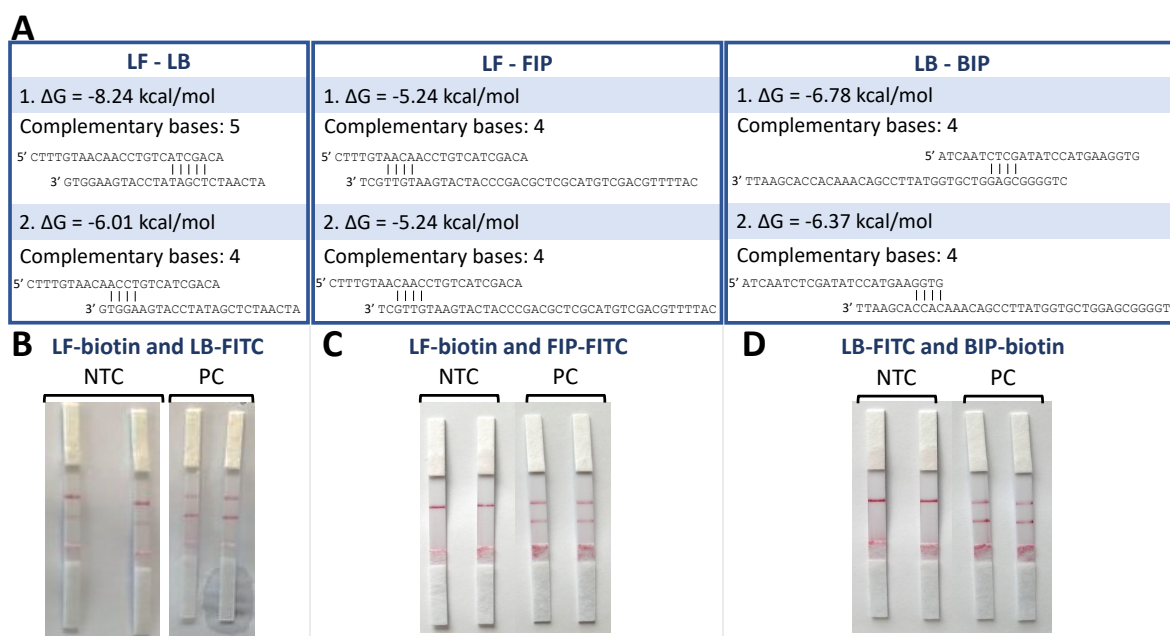


Figure 4.7: Gibbs free energy change (ΔG) of labelled primers for the detection of *E. coli malB* gene. **A.** ΔG for each pair of labelled primers considered, LF-LB, LF-FIP, and LB-BIP. Values were obtained using the hetero-dimers function of OligoAnalyzerTM Tool [172,173]. For each pair of primers possible dimerization is given with the associated ΔG and number of base pairs interacting. **B.** LAMP amplification results visualised on lateral flow strip (LFSs), when the labelled primers in the mix are the loop primers (LF-biotin and LB-FITC). **C.** LAMP results visualised on LFSs, when the labelled primers in the mix are LF-biotin and FIP-FITC. **D.** LAMP results visualised on LFSs, when the labelled primers in the mix are LB-FITC and BIP-biotin. In **A**, **B** and **C**, the concentration of the sample used to run the LAMP reaction is 10^{-4} ng/ μ L (PC: positive control). Nuclease-free water (NFW) was added instead of sample in the negative controls (NTC). LFSs were run with 10 μ L of the amplification product and 30 μ L of NFW ($n = 2$).

$\Delta G = -6.78$ kcal/mole of LB-FITC and BIP-biotin is lower than the one of LF-biotin and FIP-FITC, therefore the latter labelled primers combination was chosen for further experiments. Fig. 4.7C, and D, show the absence of primer dimer on the lateral flow

assays for the combinations LF-biotin and FIP-FITC, and LB-FITC and BIP-biotin respectively. The lateral flow assays were performed with a final LAMP reaction mix of 25 μL : 5 μL of primer mix, 15 μL of ISO-004 master mix and 5 μL of sample.

The unsuitability of using labelled loop primers was further demonstrated by the presence of faint test lines on LFSs when only loop primers were included in the primer mix (Fig. 4.8). In this experiment, the final LAMP reaction mix (25 μL) had 5 μL of loop primer mix, 15 μL of ISO-004 master mix and 5 μL of NFW. The mix was run on lateral flow strips after 2 hours incubation at room temperature and after incubation at 66 $^{\circ}\text{C}$ for 60 minutes (mimicking amplification conditions). Decreasing concentrations of primers were included in the primer mix to understand when test lines would not show as positive anymore (as described in Table 4.2). Fig. 4.8 clearly show the high interaction of loop primers that affect the readings on LFSs.

Table 4.2: Volumes to prepare 5 μL primer mix containing only labelled loop primers (LF/LB) for detecting *E. coli malB* gene.

Final concentration of loop primers	0.8 μM	0.4 μM	0.2 μM
	Volumes (μL)		
LF-Biotin (30 μM)	0.667	0.333	0.167
LB-FITC (30 μM)	0.667	0.333	0.167
Nuclease-free water	3.667	4.333	4.667
Final volume	5	5	5

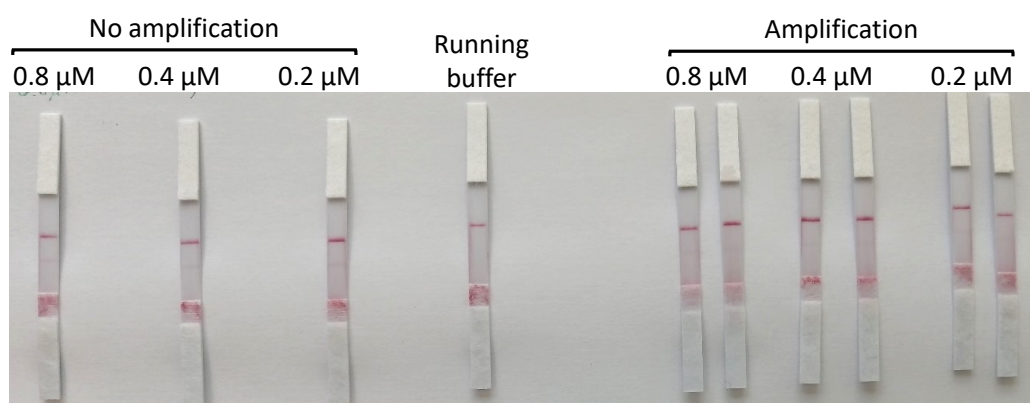


Figure 4.8: Lateral flow assay results obtained with a primer mix made of only loop primers for the detection of *E. coli malB* gene. Only LF-biotin and LB-FITC were included in the primer mix with different final LAMP reaction concentration (0.8 μM , 0.4 μM , 0.2 μM). All LAMP assays did not contain any target DNA, and nuclease-free water was used instead. Some samples were run on LFSs before amplification (No Amplification, $n = 1$), while other were incubated for 1 hour at 66 $^{\circ}\text{C}$ (Amplification, $n = 2$). LFSs were run with 10 μL of the amplification product and 30 μL of nuclease-free water as running buffer.

The effects of biotin and FITC degradation on the detection of target DNA on LFSs when labelled primers are stored dry in pullulan tablets were then studied. 10% (w/v)

pullulan tablets including only the labelled primer mix were made. 5X primer mix for the detection of *E. coli malB* gene was made as indicated in Table 2.5, and 10% (w/v) pullulan was added to the solution. 7 μL of the solution was used to make air-dried tablets. 5X labelled primer mix stored in pullulan-trehalose tablets showed a 10X loss in LOD after 10 days of storage at 35 °C with the assay being able to detect 10⁻⁶ ng/ μL . (Fig. 4.9A, upper panels). The LOD remained the same up to 60 days storage at 35 °C (Fig. 4.9). Very faint test lines can be visualised in the NTCs of labelled primers stored

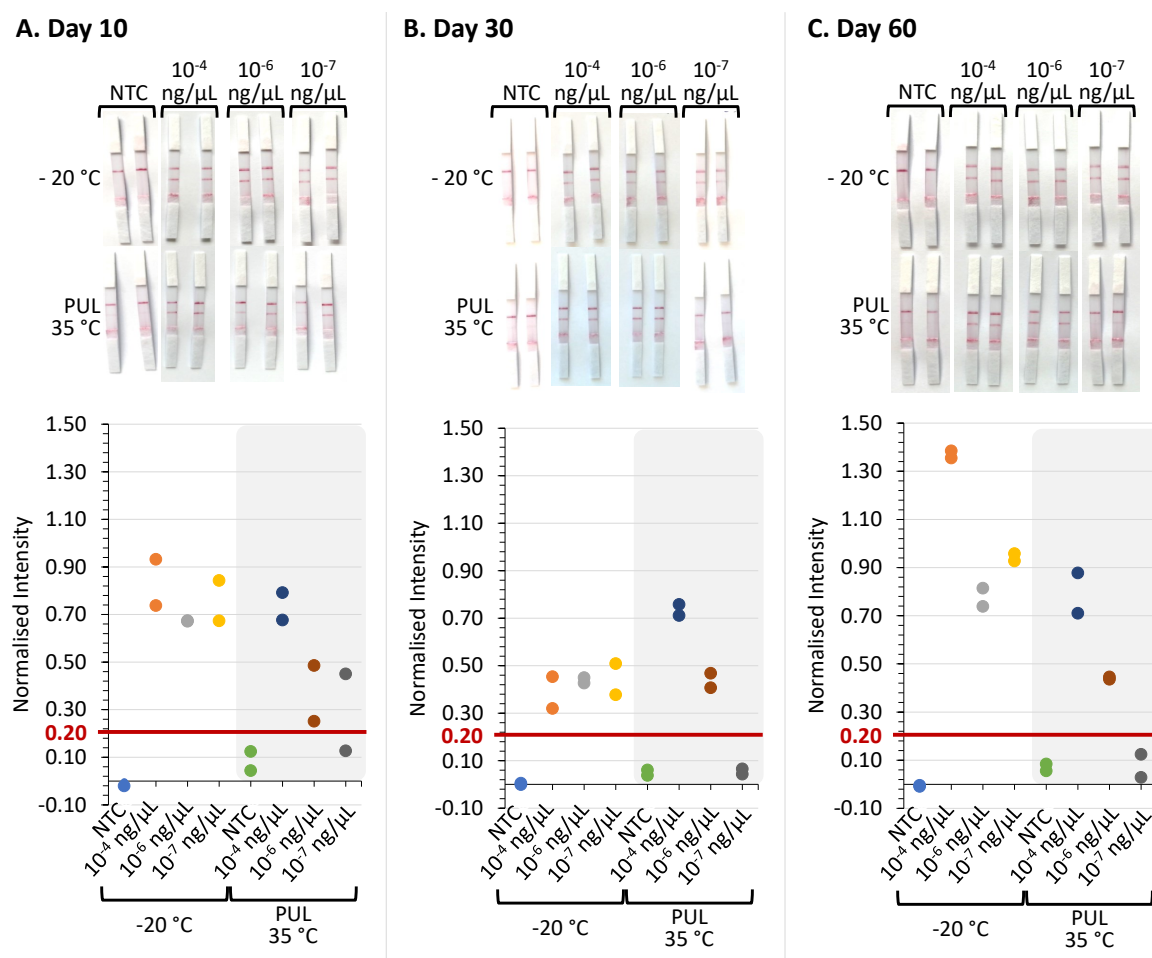


Figure 4.9: 5X labelled primer mix stored in 10% (w/v) pullulan tablets at 35 °C and tested after 10, 30, and 60 days. The tablet-based assay with labelled primer mix for the detection of *E. coli malB* gene is compared to reagents stored at -20 °C over time, after 10 days **A**, 30 days **B**, 60 days **C**. Assays were run in duplicate ($n = 2$) and different concentrations of *E. coli malB* gene synthetic DNA were used to assess the sensitivity on lateral flow strips (LFSs) (upper panels). Nuclease-free water (NFW) was added instead of sample in the negative controls (NTC). LFSs were run with 10 μL of the amplification product and 30 μL of NFW. Normalised intensity (Section 2.12) was computed for each LFS (lower panel).

dry in pullulan-trehalose tablets. In this case, the normalised intensity (NI) (calculated as described in Section 2.12) allows to clearly distinguish between positive and negative LFS results by setting a NI threshold at 0.2 (Fig. 4.9, lower panels). The presence of test lines in the NTCs was hypothesised to be associated with an unknown interaction

of trehalose and ISO-004 master mix, whose specifics are unknown. The results in Section 4.1.1 showed that primers stored in 10% pullulan tablets were stable up to 54 days. Therefore, the loss in LOD of the assay when including labelled primers we hypothesised to be associated with the degradation of biotin and FITC during storage, rather than degradation of primers.

To compensate for the LOD reduction seen in Fig. 4.9, the primer concentration in the final pullulan-trehalose tablets was increased. Tablets with 25X the original primer concentration were made, based on Fig. 4.10 that shows how different primer concentrations in the final LAMP reaction affect the LFSs DNA detection. The liquid LAMP reaction mix (25 μL) had 5 μL of primer mix, 15 μL of ISO-004 master mix and 5 μL of NFW. Decreasing concentration of the 5X primer mix prepared as shown in Table 2.5 were used: 4.5X, 4X, 2.5X, 1X, 0.5X (Table 4.3). 5 μL of these primer mixes were added to each reaction, and 5 μL of 10^{-7} ng/ μL synthetic *E. coli* DNA (LOD of the LAMP assay). The goal was to find the lowest primer concentration that could detect the same small amount of target DNA as our optimised assay using fresh reagents (10^{-7} ng/ μL) on LFSs. This helped us estimate how much degradation labelled primers undergo in pullulan after 10 days of storage at 35 °C.

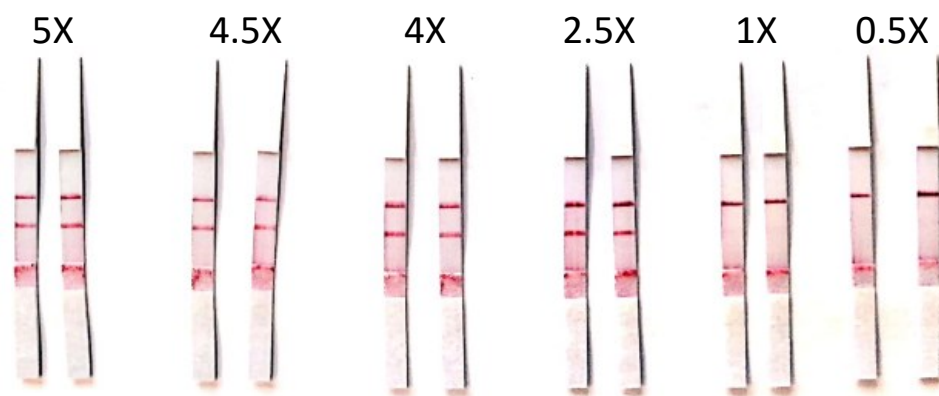


Figure 4.10: **LAMP assay for the detection of *E. coli malB* gene run with different primer mixes concentrations.** Decreasing concentrations of primer mix were trialled on lateral flow strips: 5X (Table 2.5), 4.5X, 4X, 2.5X, 1X, 0.5X (Table 4.3). The final LAMP reaction mix (25 μL) was made of 5 μL of primer mix, 15 μL of ISO-004 master mix and 5 μL of nuclease-free water. 10^{-7} ng/ μL was used as synthetic *E. coli* DNA sample, which corresponds to the limit-of-detection of the optimised LAMP assay. Each assay was run in duplicate ($n = 2$).

1X primer mix does not allow for DNA target detection (Fig. 4.10), therefore, it was hypothesised that the tags on primers degrade with a 5X factor in less than 10 days when stored dry at 35 °C. Therefore, a 5X higher concentration of primers was used in the final reactions when reagents were stored in pullulan-trehalose tablets.

Table 4.3: Primer mix concentrations used to understand the lowest concentrations that allowed to detect the target DNA on the lateral flow assay.

Primer name	4.5X		4X		2.5X		1X		0.5X	
	Conc. in final LAMP reaction (μM)	Conc. in primer mix (μM)	Conc. in final LAMP reaction (μM)	Conc. in primer mix (μM)	Conc. in final LAMP reaction (μM)	Conc. in primer mix (μM)	Conc. in final LAMP reaction (μM)	Conc. in primer mix (μM)	Conc. in final LAMP reaction (μM)	Conc. in primer mix (μM)
F3	0.18	0.9	0.16	0.8	0.1	0.5	0.04	0.2	0.02	0.1
B3	0.18	0.9	0.16	0.8	0.1	0.5	0.04	0.2	0.02	0.1
FIP-FITC	0.72	3.6	0.64	3.2	0.4	2	0.16	0.8	0.08	0.4
BIP	0.72	3.6	0.64	3.2	0.4	2	0.16	0.8	0.08	0.4
LF-Biotin	0.9	4.5	0.8	4	0.5	2.5	0.2	1	0.1	0.5
LB	0.9	4.5	0.8	4	0.5	2.5	0.2	1	0.1	0.5

25X primer mix (Table 2.5) were used to create 10% (w/v) pullulan and 0.5 M tablets. These tablets resulted stable for 30 days, without loss in LOD (Fig. 4.11).

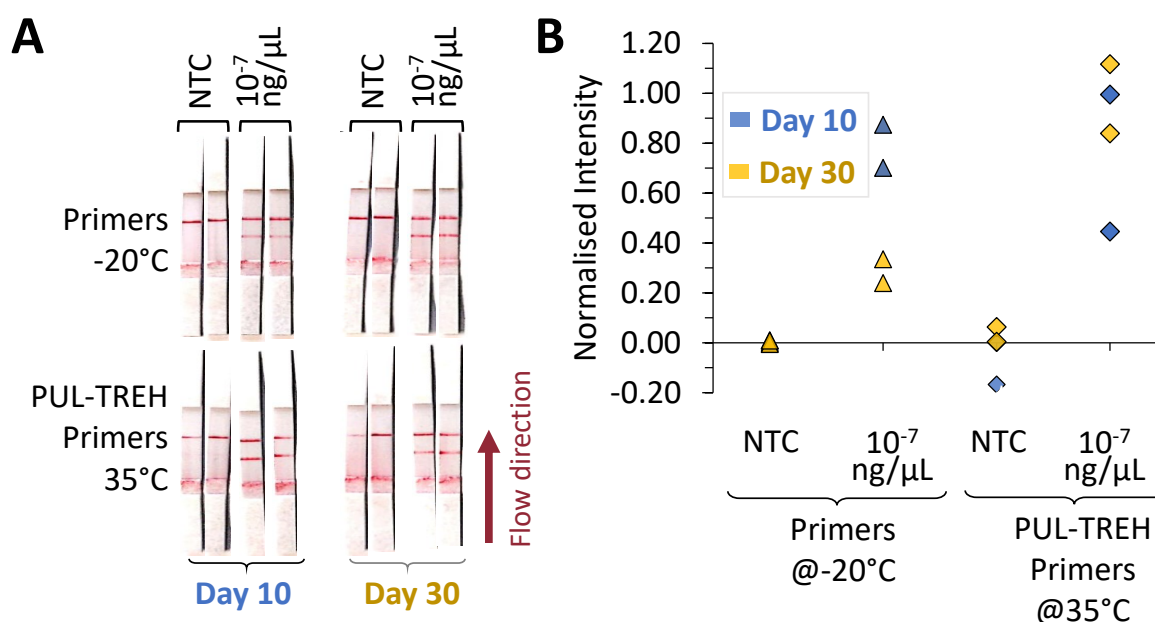


Figure 4.11: 25X labelled primer mix stored in 10% (w/v) pullulan and 0.5 M trehalose tablets at 35 °C and tested after 10 , 30 days, for the detection of *E.coli malB* gene. **A**. The tablet-based assay limit-of-detection (LOD) was assessed on lateral flow strips (LFSs) after 10 and 30 days (n = 2). **B**. Normalised intensity (Section 2.12) was computed for each LFS. Nuclease-free water (NFW) was added instead of sample in the negative controls (NTC). LFSs were run with 10 μL of the amplification product and 30 μL of NFW.

4.1.3.2 Two-pills method

The ‘two-pill method’ [26] was used to create two separate 10% (w/v) pullulan and 0.5 M trehalose tablets. Tablet 1 contains primer mix, WarmStart[®] Bst 2.0 and dNTPs; Tablet 2 includes Isothermal Amplification Buffer and MgSO₄. It was observed that Tablet 2 led to amplification of the DNA target only if it was dried in vacuum. Air-drying Tablet 2 did not lead to any amplification upon tablet resuspension, contrary

to what was demonstrated by Leung *et al.* [26]. To determine the optimal duration of the LAMP reaction for the tablet-based assays, Tablets 1 and 2 were separately resuspended as described in Section 2.15.1.2, and the real-time LAMP fluorescence changes of each tablet were measured. This was done because previous studies [25] reported that dried LAMP mixtures had longer reaction times than liquid ones. Our results confirm this finding (Fig.4.12) and also shows that the tablet-based assays is less prone to unspecific amplification, as reported by Gao *et al.* [174] (Fig.4.12). Based on these observations, the reaction time was set to 120 minutes (2 hours), which was consistent with Diego *et al.*'s findings [25].

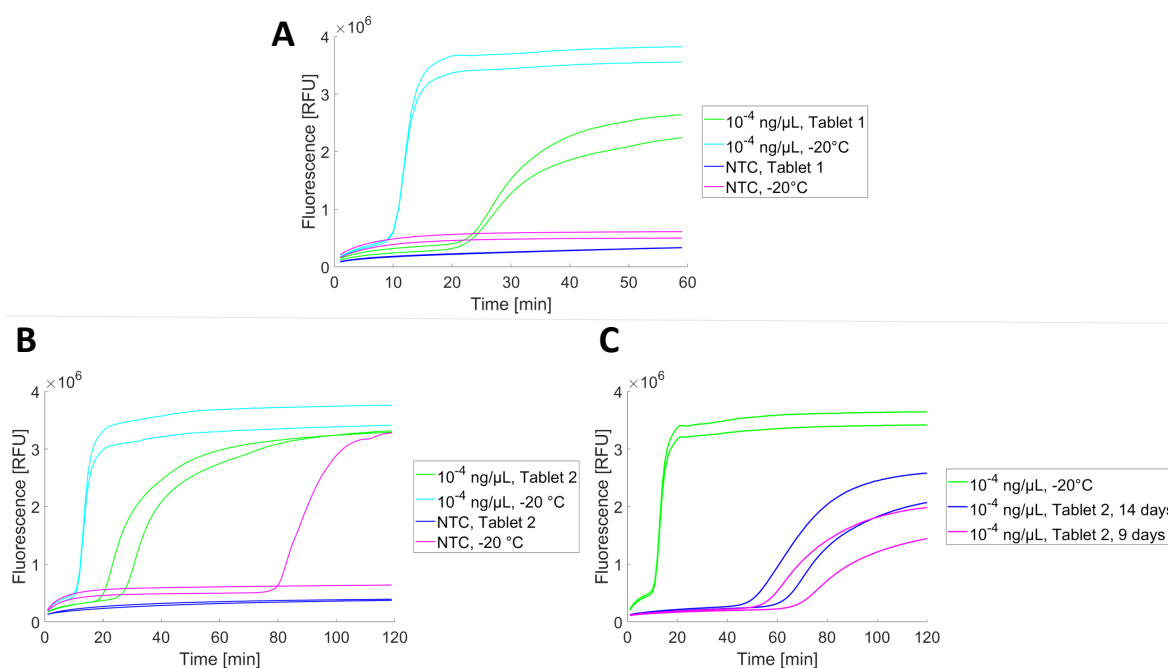


Figure 4.12: **LAMP amplification plots of reagents stored in separate 10% (w/v) pullulan and 0.5 M trehalose tablets, compared to reagents stored at -20 °C.** **A.** Amplification plot of Tablet 1 (25X primer mix, WarmStart Bst 2.0 and dNTPs) tested after one day of storage at room temperature ($n = 2$). Slower amplification of reagents stored in Tablet 1 than reagents stored at -20 °C. **B.** Amplification plot of Tablet 2 (Isothermal Amplification Buffer and $MgSO_4$) tested after 2 days of storage at room temperature ($n = 2$). Reagents stored in Tablet 2 amplifies after the reagents stored in optimal conditions. After about 80 minutes one of the no template controls (NTC) whose reagents were stored at -20 °C shows amplification associated with unspecific amplification. None of the NTCs of the tablet-based assay amplifies in 120 min. **C.** Positive amplification plots of Tablet 2 tested after 9 days and 14 days of storage at room temperature, compared to reagents stored in optimal conditions ($n = 2$). Amplification of tablet-based assays have a delayed amplification that increases with the time of storage (amplification around 60 minutes, compared to approx. 20 min after 2 days of storage in B).

After setting the amplification time to two hours, a new set of experiments was conducted. Tablet 1 now was prepared with 25X labelled primer mix, WarmStart[®] Bst 2.0 and dNTPs. Each Tablet 1 and 2 was dried and stored at 35 °C. The tablets were used in three ways: only Tablet 1 ('Tab 1'), only Tablet 2 ('Tab 2'), or both Tablets 1

and 2 ('Tab 1 + 2'). They were resuspended as described in Section 2.15.1.2, heated at 66 °C for the LAMP reaction, and tested on LFSs. Having all the reagents for the isothermal amplification reaction in a solid form would make it easier to transport and use them in POC devices. Tablet 1 cannot detect 10^{-7} ng/ μ L (2.3×10^3 copies/reaction) reliably after 10 days at 35 °C when resuspended with the Isothermal Amplification Buffer and MgSO₄ stored at -20 °C (Fig. 4.13A). However, the LOD did not decrease further on day 30 (Fig. 4.13D). This suggests that the DNA polymerase degrades quickly in the first 10 days of storage. Tablet 2 remains stable for 30 days at 35 °C when resuspended with labelled primer mix, WarmStart[®] Bst 2.0 and dNTPs stored at -20 °C (Fig. 4.13D). When Tablets 1 and 2 are combined and resuspended with fluorescent dye and water after 10 days of storage, LFSs detects the highest concentration (10^{-4} ng/ μ L) with strong test lines for both repeats (Fig. 4.13A). The melting curves show two peaks around 86 °C. (Fig. 4.13B). One of the two samples with 10^{-6} ng/ μ L was also detected on LFSs, but the melting curve did not show any peak around 86 °C. The gel results in Fig. 4.13C confirm the melting curve peaks in Fig. 4.13B for the highest DNA concentration (10^{-4} ng/ μ L), showing a ladder-like banding pattern in lanes 8-9. Lane 7 has a very faint ladder-like banding pattern, suggesting that the LFSs detected LAMP amplicon products for 10^{-6} ng/ μ L that the melting curve did not recognise. After 30 days, Fig. 4.13D shows that only the highest DNA concentration (10^{-4} ng/ μ L) produced visible test lines for both repeats in LAMP reactions with Tablets 1 + 2. However, the melting curves did not show the expected peak at 86 °C for any concentration (data not shown). To investigate the reason for this discrepancy, the samples were run on agarose gel electrophoresis (Fig. 4.13E). The gel confirmed that there was no target DNA amplification in lanes 2-6, as indicated by the absence of a ladder-like pattern. Lanes 5 and 6 showed a 'smear' that indicated unspecific amplification at the highest concentration. Moreover, Tablets 1 + 2 were resuspended in 50 μ L instead of the recommended 25 μ L to check if the resuspension volume affected the LOD. After 30 days of storage and 50 μ L of final LAMP reaction, the LOD did not improve.

The assay's detection ability deteriorates significantly (over 100-fold higher LOD) after 10 days of storing the LAMP reagents in 10% pullulan-trehalose tablets. This could be due to the increased viscosity of the LAMP solution, which hinders the mixing of the reagents and affects their reactivity. After 30 days, the viscosity problem is compounded by potential degradation of reagents.

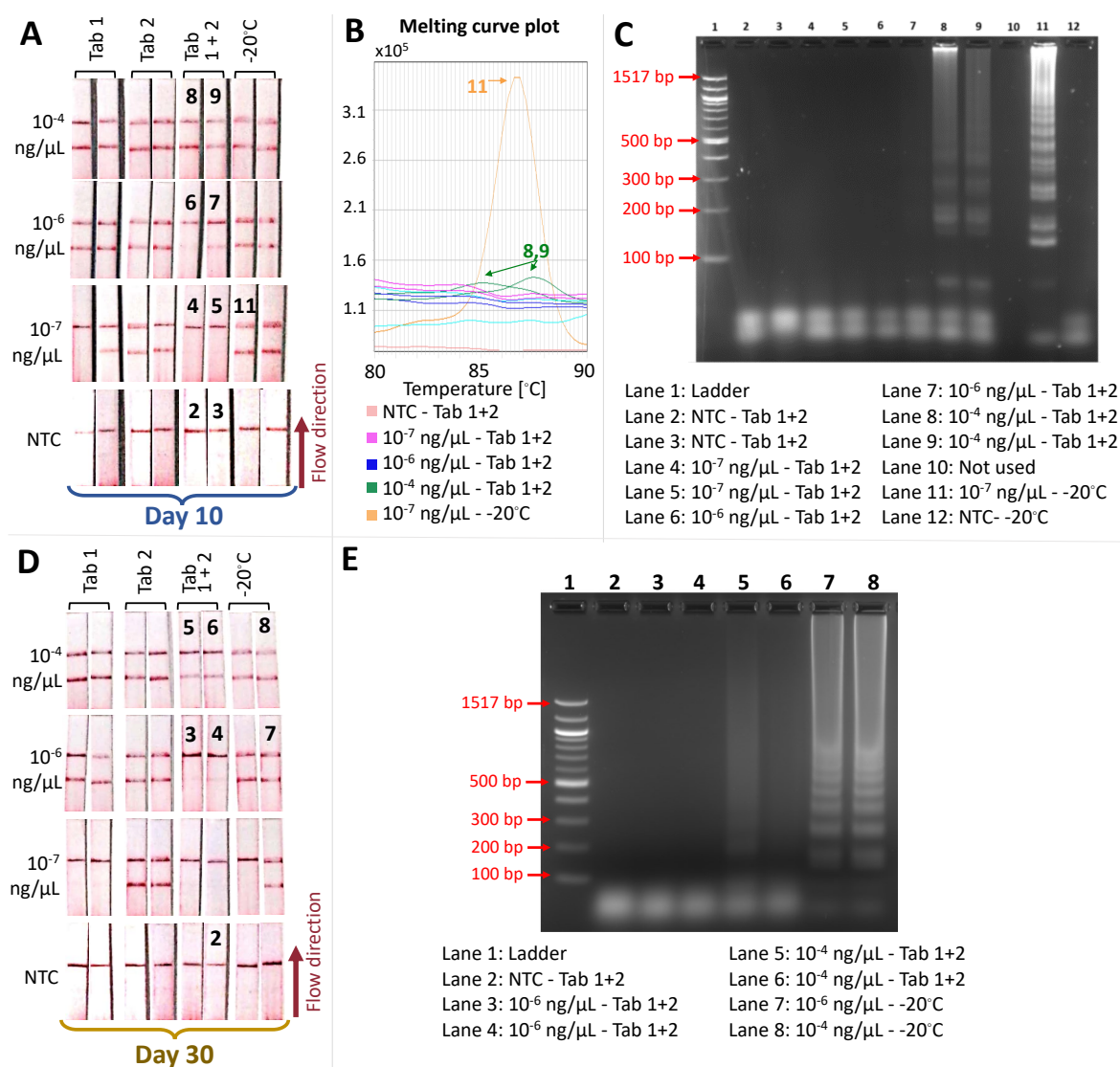


Figure 4.13: LAMP reagents stored in two 10% (w/v) pullulan and 0.5 M trehalose tablets for 10 and 30 days at 35 °C. The reagents were divided into two tablets: Tablet 1 with labelled primers, WarmStart Bst 2.0 and dNTPs, and Tablet 2 with Isothermal Amplification Buffer and MgSO_4 . The tablets were tested individually (Tab 1 or Tab 2) or in combination (Tab 1 + 2). Each sample was run in duplicate ($n = 2$). **A**. Stability and limit-of-detection (LOD) of LAMP reagents in pullulan-trehalose tablets evaluated by lateral flow detection after 10 days. Melt curve plot **B** and gel electrophoresis **C** of Tab 1 + 2 assays after 10 days of storage. The numbers on the lateral flow strips (LFSs) in **A** correspond to the associated curves in **B** and the lanes in **C**. **D**. Stability and limit-of-detection (LOD) of LAMP reagents in pullulan-trehalose tablets evaluated on LFSs after 30 days. The LOD visualised on gel electrophoresis of Tab 1 + 2 (**E**) is compared to lateral flow assays in **D**. The numbers on the LFS in **D** correspond to the lanes in **E**. In **C** and **E**, LAMP reactions showed the typical ladder-like pattern. Starting from the initial stem loop formation of the reaction between the outer primers (F3/B3), the LAMP reaction produces progressively larger sub-products with random termination, resulting in a smear with multiple bands that resemble a ladder [4, 175, 176].

4.1.3.3 Optimisation of WarmStart[®] Bst 2.0 DNA polymerase concentration

Given the results in Section 4.1.3.2, different concentrations of WarmStart[®] Bst 2.0 DNA polymerase in Tablet 1 were tested to understand if after 10 days of storage at 35 °C, the DNA polymerase underwent significant degradation. The tablets were

created with the reagents and volumes indicated in Table 4.4.

Table 4.4: **Volumes of reagents to create 10% (w/v) pullulan and 0.5M trehalose tablets containing different concentrations of DNA polymerase and dNTPs.** To the tablet whose Bst 2.0 concentration was 0.32, 0.48 and 0.64 U/mL, 0.8, 1 and 1 mg of pullulan were added to the solution respectively. After pullulan was dissolved, 8, 10 and 10 μ L were used to create tablets and dried in a fume cabinet.

Bst 2.0 concentration (U/mL)	0.32	0.48	0.64
	Volumes of reagents (μ L)		
Bst 2.0 (8000 U/mL)	1.333	1.667	2.500
dNTPs (10 mM)	4.667	5.833	4.375
Trehalose (2 M)	2.000	2.500	2.500
Water	-	-	0.625
Total volume	8	10	10

It was expected that higher concentrations of DNA polymerase would have led to faster amplification, however this was not the case (Fig. 4.14). Concentrations of 0.32 U/mL or 0.48 U/mL WarmStart[®] Bst 2.0 led to better amplification performances after 10 days stored dry than the highest concentration 0.64 U/mL. WarmStart[®] Bst 2.0 is not glycerol-free, therefore, higher concentrations of DNA polymerase in the LAMP reaction corresponds to higher concentrations of glycerol that can cause amplification delays. A final reaction concentration of 0.48 U/mL was chosen to create tablets in subsequent experiments.

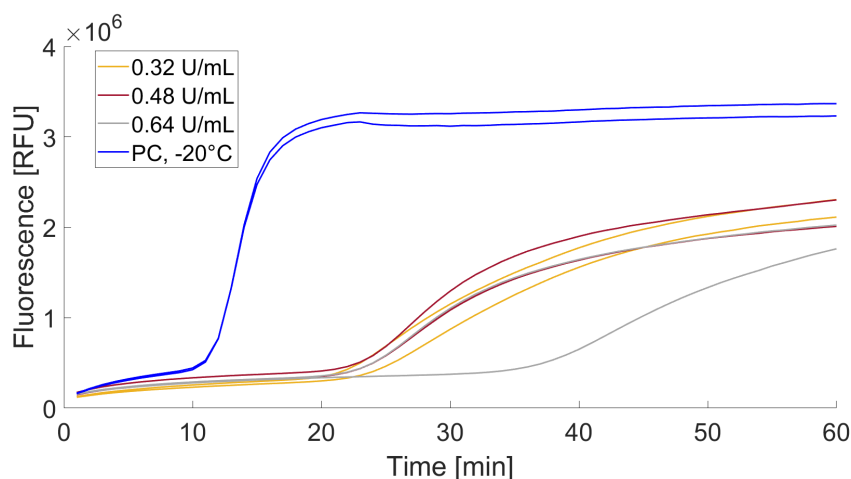


Figure 4.14: **Amplification plot of tablet-based LAMP assays with different concentrations of WarmStart[®] Bst 2.0 from New England Biolabs (NEB).** Tablets were created as explained in Table 4.4, with three different concentrations of Bst DNA polymerase: 0.32, 0.48, 0.64 U/mL. Each tablet containing DNA polymerase and dNTPs was used after 10 days of storage at 35 °C. They were resuspended with 3.6 μ L of nuclease-free water and the rest of the reagents necessary for LAMP reaction. 5 μ L of *E. coli malB* gene synthetic DNA was added to each assay in a concentration of 10^{-4} ng/ μ L. Each LAMP assay was run in duplicate ($n = 2$). PC is the positive control whose reagents have been stored in optimal conditions, at -20 °C.

4.1.4 Reagents Stored in 5% (w/v) Pullulan and 0.5 M Trehalose or 10% (w/v) Pullulan and 0.5 M Trehalose

Both Tablet 1 and Tablet 2 were prepared with pullulan at 5% or 10% (w/v) and trehalose at 0.5 M. Tablet 1 ('Tablet 1-5%', 'Tablet 1-10%') has 25X labelled primer mix, WarmStart[®] Bst 2.0 and dNTPs; and Tablet 2 ('Tablet 2-5%', 'Tablet 2-10%') has Isothermal Amplification Buffer and MgSO₄. In this set of experiments, the WarmStart[®] Bst 2.0 concentration in Tablet 1 was increased from 0.32 U/ μ L to 0.48 U/ μ L to avoid LOD reduction due to DNA polymerase instability when pullulan concentration was lowered from 10% to 5%, as reported by Jahanshahi-Anbuhi *et al.* [119] and recommended by Kumar *et al.* [22]. Tablet 1 and Tablet 2 with different pullulan concentrations were combined and resuspended in the same solution, as described in Section 2.15.1.3. Fig. 4.15 shows that pullulan-based tablets with LAMP reagents could detect 10⁻⁶ ng/ μ L of target DNA, using either 5% or 10% (w/v) pullulan tablets after 10 days of storage at 35 °C. The melting curves all have peaks that are consistent with specific amplification, including those with weak test lines on LFSs (Fig. 4.15B, C). When a mix of Tablet 1 and 2 with 5% and 10% (w/v) pullulan are used, the LOD improves compared to using two tablets with 10% (w/v) pullulan, which could only detect consistently 10⁻⁴ ng/ μ L (2.3x10⁶ copies/reaction) (Figures 4.13, and 4.15). Therefore, these results suggest that when tablets are used together, they should not have 10% (w/v) pullulan each to achieve a LOD similar to the liquid LAMP assays, and that high pullulan concentrations in the final LAMP reaction affect the performance of the assay. Our findings contradict previous studies that reported no effect of pullulan on bio-assays [122], and they indicate that the pullulan concentration in the bio-assay should be below a certain threshold to preserve the assay LOD. However, this also implies a trade-off between the LOD and the stability of reagents over time, as lower pullulan concentrations reduce the shelf-life of reagents [119]. Furthermore, Fig. 4.15A demonstrates a decrease in LOD, with only 10⁻⁶ ng/ μ L (2.3 × 10⁴ copies/reaction) detected, when both Tablets 1 and 2 contain 5% (w/v) pullulan. This could be related to the reduced reactivity of reagents stored in lower pullulan concentrations, especially the WarmStart[®] Bst 2.0 DNA polymerase, as suggested by Jahanshahi-Anbuhi *et al.* [119]. The combination of tablets with the lowest LOD in Fig. 4.15A is Tablet 1-10% and Tablet 2-5%, but this combination showed inconsistent detection ability for 10⁻⁷ ng/ μ L (2300 copies/reaction) in a second experiment (Fig. 4.15D). For

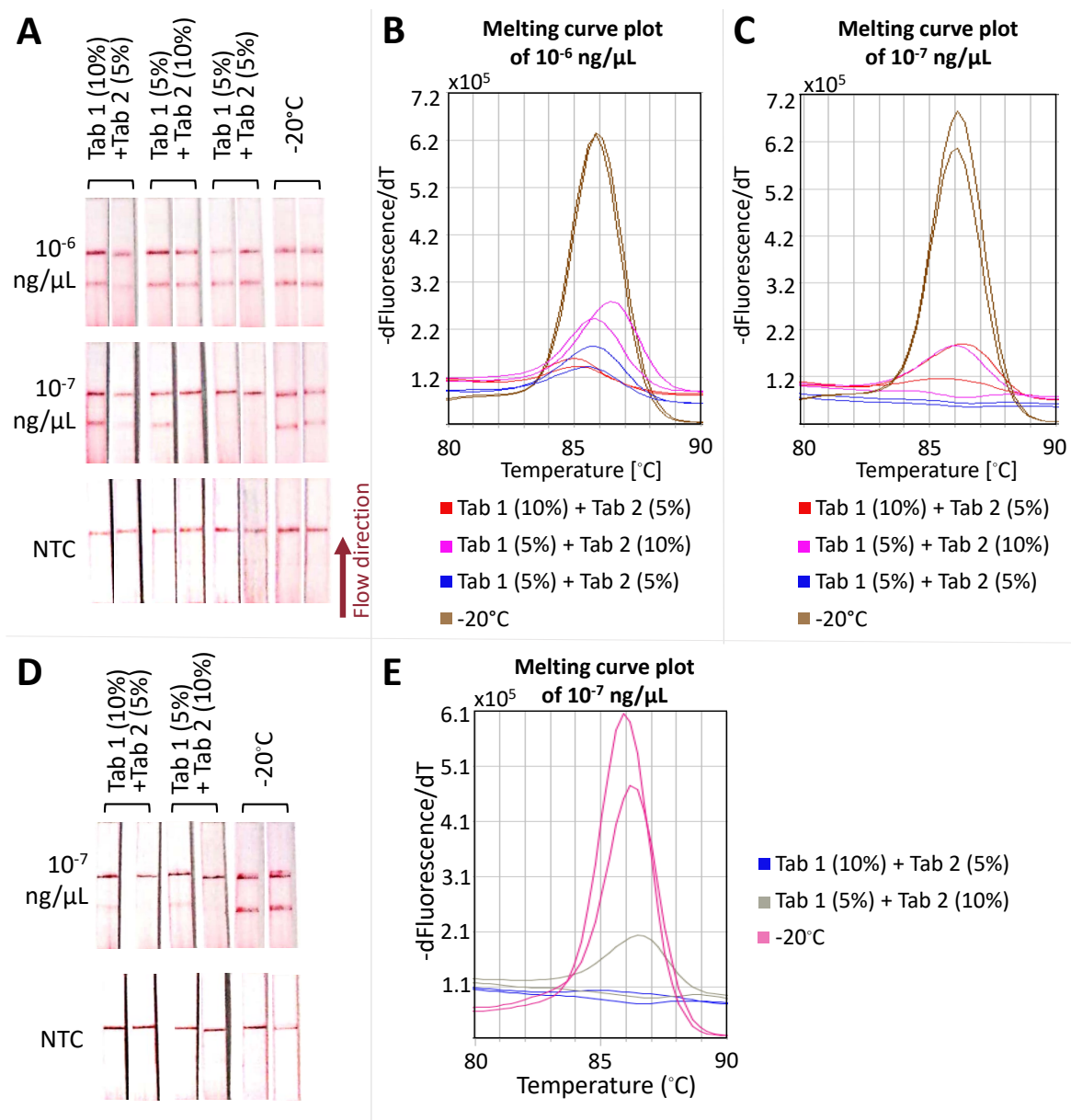


Figure 4.15: **Stability of LAMP reagents stored in two separate 5% or 10% (w/v) pullulan and 0.5 M trehalose tablets for 10 days at 35 °C.** Tablet 1 (Tab 1) stores labelled primers, WarmStart Bst 2.0 and dNTPs. Tablet 2 (Tab 2) contains Isothermal Amplification Buffer and MgSO_4 . The tablets were tested dissolving them together in the final LAMP assay in different pullulan combinations, and 5 μL of sample containing different concentrations of *E. coli malB* gene synthetic DNA was added. Each sample was run in duplicate ($n = 2$). Tablets combinations used were: Tab 1-10% + Tab 2-5%; Tab 1-5% + Tab 2-10%, Tab 1-5% + Tab 2-5%. **A.** Stability and limit-of-detection (LOD) of LAMP reagents in pullulan-trehalose tablets evaluated on LFSs. **B.** Melting curves of 10^{-6} ng/ μL samples (2.3×10^4 copies/reaction) compared to assays run on LFSs in **A**. All melting curves show one peak. **C.** Melting curves of 10^{-7} ng/ μL samples (2300 copies/reaction) compared to assays run on LFSs in **A**. The combination Tab 1-5% + Tab 2-5% show no peaks. **D.** LOD of LAMP reagents in pullulan-trehalose tablets analysed on LFSs a second time. **E.** Melting curves of 10^{-7} ng/ μL samples (2.3×10^4 copies/reaction) compared to assays run on LFSs in **D**.

this second run of the experiment, the reagents stored at -20 °C have two peaks at 85.9 °C and 86.1 °C in their melting curves (Fig. 4.15E), while the reagents stored in pullulan-trehalose tablets have only one peak at 86.4 °C, using Tablet 1-5% and Tablet 2-10%. Additionally, the drying process resulted in different outcomes for the

tablets depending on their composition: Tablet 1–5% formed sticky discs upon drying that could be detached from the drying surface more easily than Tablet 1–10%; and Tablet 2–10% was more resistant and easier to handle with tweezers than Tablet 2–5%. Therefore, based on the ease of handling and robustness of the tablets, the combination of Tablet 1–5% and Tablet 2–10% was selected to prepare reagents for in-field studies (Sections 4.1.5, 4.1.8).

4.1.5 Storage of Molecular Reagents Returned from the Field

In Section 4.1.4, the pullulan concentrations in each tablet were optimised to preserve LAMP reagents and ensure the accuracy of the assay. In this section, the behaviour of dried LAMP reagents exposed to uncontrolled and harsh temperature conditions was examined, as described in Section 2.15.1.4. Tablet 1 contains WarmStart[®] Bst 2.0, dNTPs, 25X labelled primer mix, 0.5 M trehalose and 5% (w/v) pullulan, while Tablet 2 contains Isothermal Amplification Buffer, MgSO₄, 0.5M trehalose and 10% (w/v) pullulan. For this purpose, two types of Tablet 1 were prepared, one containing primers to detect *Plasmodium* species and one to detect *BRCA1* gene (as explained in detail in Section 2.15.1.4).

Before proceeding to test the dried reagents, the analytical sensitivity of the liquid LAMP assay for the detection of *Plasmodium* species was investigated (as described in Section 2.8). For LAMP assay reagents stored in optimal conditions (at -20 °C), in both real-time LAMP and on LFSs, a limit-of-detection of 10⁵ IU/mL was observed (Fig. 4.16A, C); this confirms what reported by Reboud *et al.* [17]. Additionally, the assay is sensitive to unspecific amplification after 30 minutes (Fig. 4.16). In the melting curve, the negative controls and 10⁴ IU/mL sample have clear shifted melting temperatures peaks (T_m) compared to the other positive samples (Fig. 4.16A).

Using the two-pills method for storing dried reagents, *P. falciparum* at 10⁶ IU/mL can be detected after 60 days of storage (Fig. 4.17), which is a 10-fold decrease in LOD compared to reagents stored at -20 °C under optimal conditions (Fig. 4.16C). The results from the melting curve peaks and the gel electrophoresis support this (Fig. 4.17B, C): the melting temperatures of the 10⁶ IU/mL samples tested with reagents stored dry are 80.3 °C, 80.81 °C and 80.75 °C, which are similar to the ones of the same sample tested with reagents stored at -20 °C, 81.27 °C (Fig. 4.17C). This indicates that the test line on the LFSs exposed to those samples (7-9) are detecting the target DNA. On the

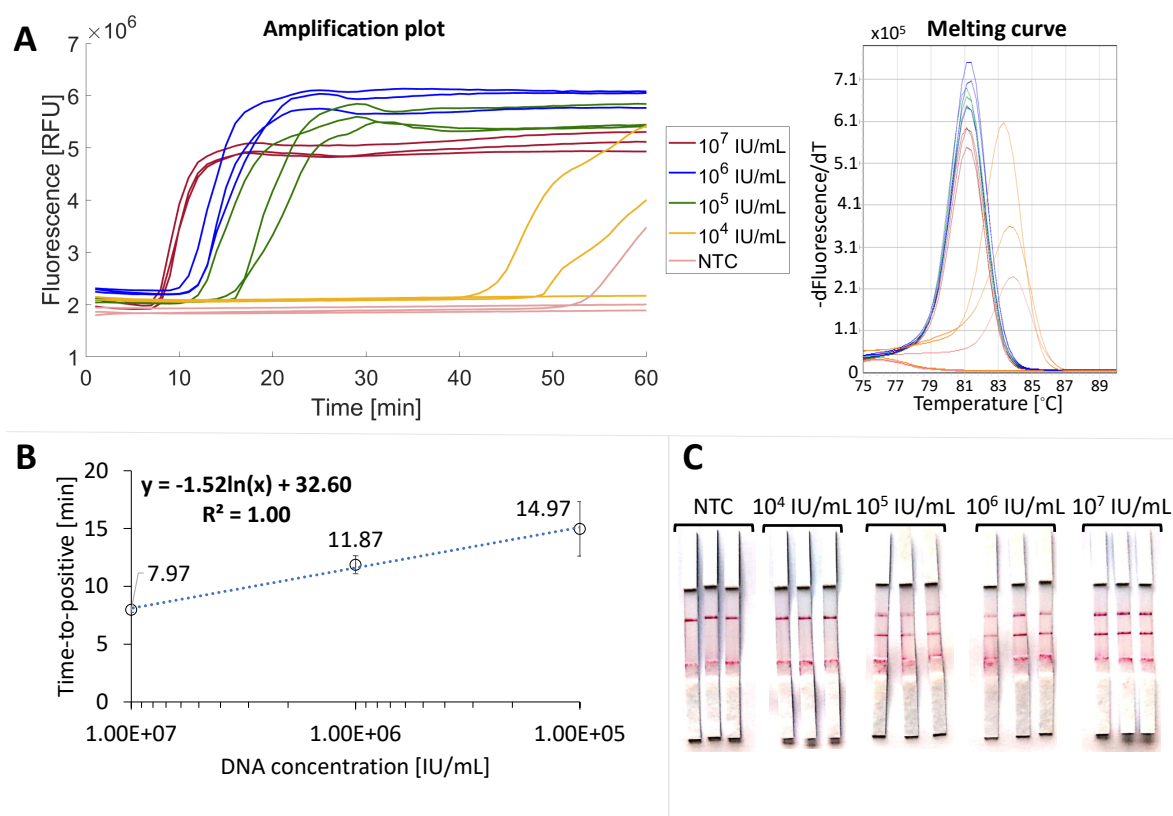


Figure 4.16: **Limit-of-detection (LOD) of LAMP assays for *Plasmodium falciparum* detection.** The *P. falciparum* concentrations investigated are 10^7 , 10^6 , 10^5 , 10^4 IU/mL. For each concentration, LAMP assays were run in triplicate ($n = 3$). **A.** Amplification and melting curve. **B.** Analytical sensitivity and standard curves of *P. species* LAMP assay. The dots represent the mean time-to-positive values (TTPs) of the LAMP assay run with the same DNA concentration. The vertical bars represent the standard deviation of the three repeats of the same LAMP assay. Therefore, TTP data is presented as mean TTP \pm standard deviation. **C.** Lateral flow assay results.

gel, lanes 7-9 (corresponding to the sample tested on strips 7-9) show a characteristic ladder-like pattern of bands, indicating successful amplification of the target DNA. No amplification pattern is observed for NTCs or 10^5 IU/mL samples (Fig. 4.17C).

After 6 months of tablet-based storage, the LAMP assay can detect *BRCA1* gene (Fig. 4.18). The LAMP assay was able to detect 10 ng/ μL of human genomic DNA (Jurkat Genomic DNA), Fig. 4.18A; both the melting curve peaks (Fig. 4.18B), and the gel electrophoresis (Fig. 4.18C) support this result. Samples in lanes 4, 6, 7 and 9 of the gel electrophoresis show a ladder-like bands pattern; this suggests that amplification has occurred, corresponding to the positive results for the same samples ran on LFSs 4, 6, 7 and 9. Whilst samples in lanes 5 and 8 do not show a ladder-like pattern on the gel electrophoresis, they do peak at the expected temperature in the melting curve and show positive results on the LFSs 5 and 8; it can therefore be assumed that amplification did take place for samples 5 and 8 too. Thus, amplification occurred in all positive samples. Other lanes, including NTCs, do not show any ladder-like band

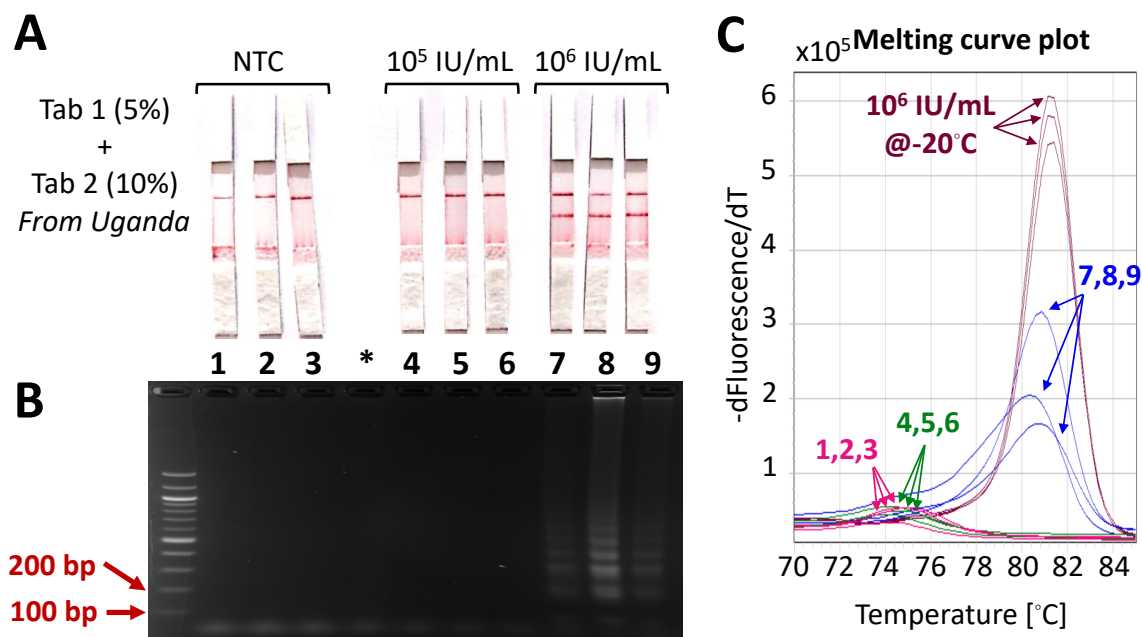


Figure 4.17: Validation of LAMP assays using tablet-based, dried reagents brought back from the field, for the detection of *Plasmodium* species. The *P. falciparum* concentrations investigated are 10^6 , and 10^5 IU/mL. The dried reagents were tested after 2 months of storage ($n = 3$). **A**. Limit-of-detection assessed on lateral flow strips (LFSs). Gel electrophoresis (**B**) and melting curves (**C**) of samples run on LFSs in **A**. NTCs are the no template control, where LAMP assays were run with water instead of sample. * Well not used.

pattern, suggesting no amplification occurred (Fig. 4.18C).

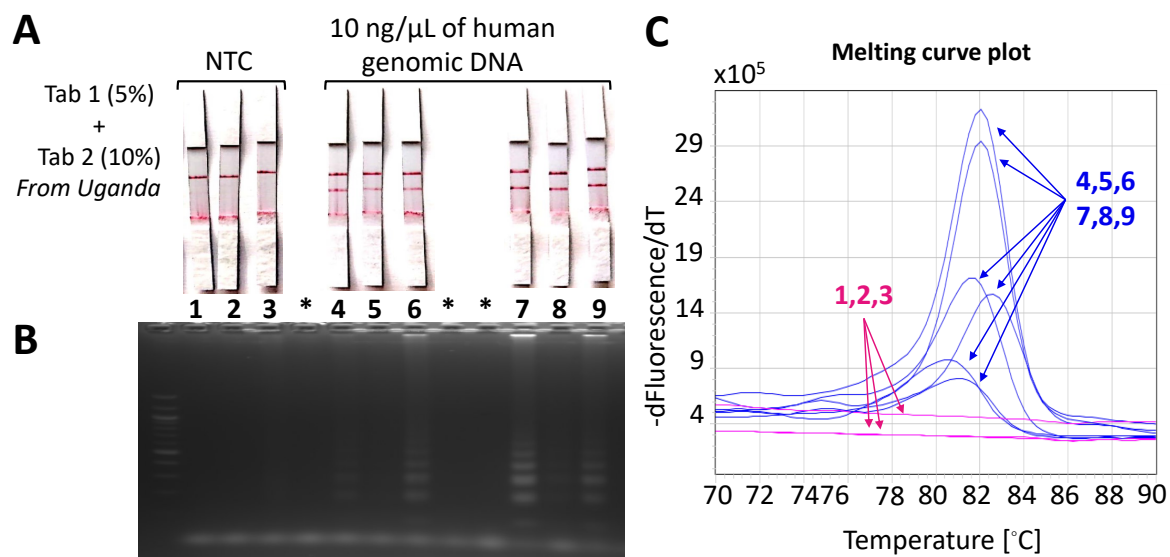


Figure 4.18: Validation of LAMP assays of dried reagents brought back from the field for the detection of *BRCA1* gene. The human genomic DNA used had a concentration of 10 ng/μL. The tablet-based assays were tested after 6 months of storage ($n = 3$). **A**. Limit-of-detection assessed on lateral flow strips. Gel electrophoresis (**B**) and melting curves (**C**) of samples run on LFSs in **A**. NTCs are the no template control, where LAMP assays were run with water instead of sample. * Wells not used for this analysis.

Some tablet-based LAMP reagents were also stored in a point-of-care device inside a sealed bag with desiccants (Fig 4.19A). These dried reagents were exposed to the same

field conditions explained in Section 2.15.1.4 and then used after six months to detect *P. falciparum* and *BRCA1* gene in the laboratory. No amplification was observed using either LAMP assay. Moreover, a visual difference between the reagents stored inside Eppendorf tubes sealed with parafilm or inside the device was observed (Fig. 4.19B). The reagents in the device became less rigid than the ones in tubes, indicating that

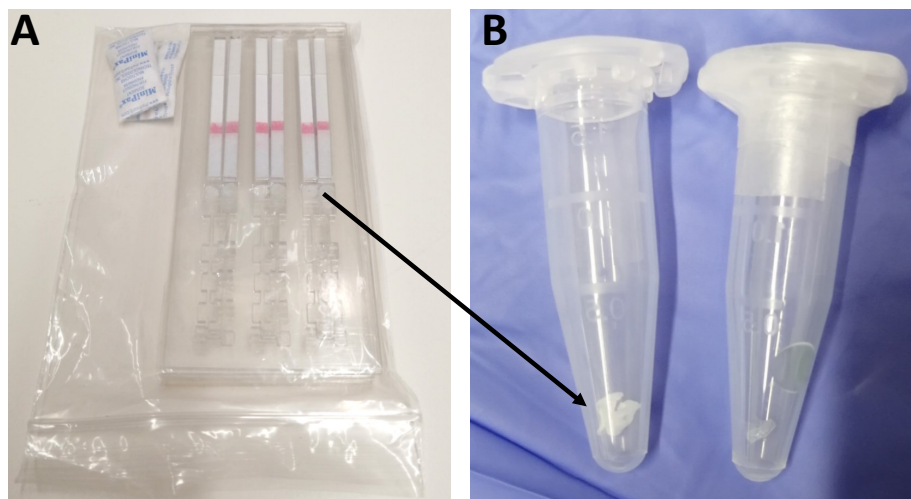


Figure 4.19: **Tablet-based LAMP reagents brought back from the field.** **A.** Point-of-care devices inside a closed plastic bag with desiccants (5 devices per bag). **B.** Tablet-based LAMP reagents brought back from the field. Tablets stored inside the device and transferred into Eppendorf tubes when tested after six months of storage (left). Tablets shipped to the field and back inside a 1.5 mL Eppendorf tube sealed with parafilm (right).

the storage method affects the long-term stability of the tablet-based reagents. It was hypothesised that humidity was a major factor.

We have demonstrated that the two-pills method, when tablets are properly sealed, can enable complex transport logistics without decreasing the assay performance significantly. This opens the route for easy diagnostic access in remote areas.

4.1.6 Summary of Results about Molecular Reagents Stored in Pullulan

A summary of the results obtained for the storage of LAMP reagents in different pullulan and trehalose solution is provided in Table 4.5.

Table 4.5: **Summary of the results obtained for the storage of loop-mediated amplification (LAMP) reagents in different pullulan and trehalose solutions.** The reagents dried and stored in pullulan tablets are given in the first column. All tablets were stored at 35 °C until use, except for the tablets returned from the field whose temperature conditions were uncontrolled. Each tablet was resuspended with the LAMP reagents necessary for a successful assay to a final volume of 25 µL.

10 % Pullulan (<i>E. coli</i> LAMP assay)			
Reagents	Limit of detection (LOD)	Days of stability tested (days)	Comparison to LOD of LAMP reagents stored at -20 °C
1X Primer mix	10 ⁻⁷ ng/µL	54	Equal
Master Mix (Optigene)	10 ⁻⁷ ng/µL	14	Equal
10 % pullulan and 0.5 M trehalose (<i>E. coli</i> LAMP assay)			
Tablet 1: 5X Labelled primers (from 25X primer mix), 0.48 U/µL WarmStart Bst 2.0, 1.4 M dNTPs. Tablet 2: 1X Isothermal Amplification Buffer, 6 mM MgSO ₄ .			
Reagents	LOD	Days of stability tested (days)	Comparison to LOD of LAMP reagents stored at -20 °C
25X Labelled primer mix	10 ⁻⁷ ng/µL	30	Equal
Tablet 1	10 ⁻⁶ ng/µL Inconsistent 10 ⁻⁷ ng/µL	30	10 times lower
Tablet 2	10 ⁻⁷ ng/µL	30	Equal
Tablet 1 + 2	10 ⁻⁴ ng/µL	10	10 ³ times lower
0.5 M trehalose and 10% or 5% pullulan (<i>E. coli</i> LAMP assay)			
Tablet 1: 5X Labelled primers (from 25X primer mix), 0.48 U/µL WarmStart Bst 2.0, 1.4 M dNTPs. Tablet 2: 1X Isothermal Amplification Buffer, 4 mM MgSO ₄ .			
Reagents	LOD	Days of stability tested (days)	Comparison to LOD of LAMP reagents stored at -20 °C
Tablet 1 (10% pullulan) + Tablet 2 (5% pullulan)	10 ⁻⁶ ng/µL Inconsistent 10 ⁻⁷ ng/µL	10	10 times lower
Tablet 1 (5% pullulan) + Tablet 2 (10% pullulan)	10 ⁻⁶ ng/µL Inconsistent 10 ⁻⁷ ng/µL	10	10 times lower
Tablet 1 (5% pullulan) + Tablet 2 (5% pullulan)	10 ⁻⁶ ng/µL	10	10 times lower
0.5 M trehalose and 10% or 5% pullulan			
Tablet 1 (5% pullulan): 5X Labelled primers (from 25X primer mix), 0.48 U/µL WarmStart Bst 2.0, 1.4 M dNTPs. Tablet 2 (10% pullulan): 1X Isothermal Amplification Buffer, 4 mM MgSO ₄ .			
LAMP assay and reagents	LOD	Days of stability tested (days)	Comparison to LOD of LAMP reagents stored at -20 °C
<i>Plasmodium Falciparum</i> Tablet 1 + 2	10 ⁶ IU/mL	60	10 times lower
<i>BRCA 1</i> Tablet 1 + 2	10 ng/µL	180	

4.1.7 Modified DNA Extraction from Blood for Use on the Point-of-Care Device

As explained in Section 2.15.2.1, the 19-steps protocol developed by Garret [152] to extract DNA from 5 μ L of whole blood was further simplified. First of all, the use of the binding buffer was investigated (Fig. 4.20A), followed by the elimination of the heating step and proteinase K (PK) (Fig. 4.20B, C).

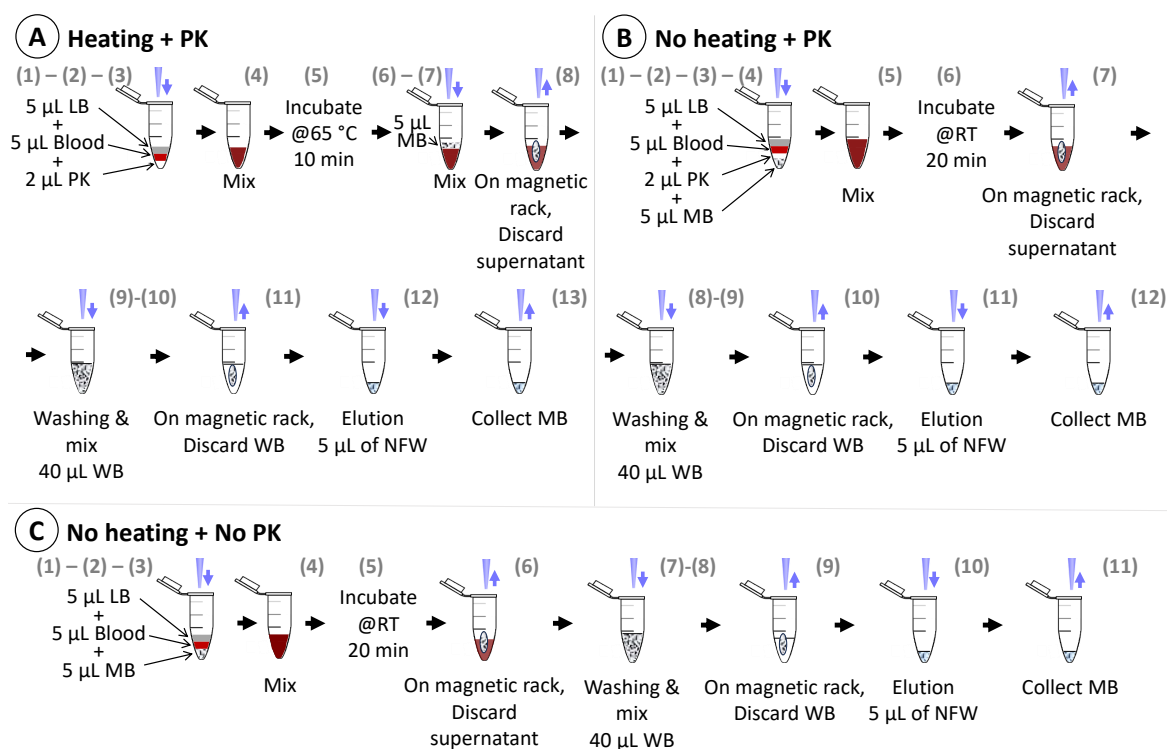


Figure 4.20: **Schematic of simplified DNA extraction methods from whole blood.** Three extraction methods were tested. **A.** Heating + proteinase K (PK); this method eliminates the need of using binding buffer, previously used by Garrett [152]. **B.** No heating + Proteinase K (PK); compared to A, this method eliminates the heating step at 65 °C. **C.** No heating + No PK; this eliminates the need for both proteinase K and heating at 65 °C. In A, B and C, LAMP targeting *BRCA1* was performed, and 5 μ L of the resuspended magnetic beads were used. LB: lysis buffer; PK: Proteinase K; MB: Magnetic beads reagent; WB: Washing buffer. All reagents used are from MagaZorb[®] DNA Mini-Prep Kit, Promega.

Results from the three DNA extractions targeting *BRCA1* gene (Fig. 4.21) indicated that deactivating PK, using heat, is required; otherwise, PK inhibits the final LAMP reaction [177].

During extraction, and washing, the magnetic beads did not homogeneously disperse in the washing buffer, and the washing buffer (after the first wash) contained blood residues. This did not interfere with the final LAMP reaction, because LAMP is less sensitive to blood inhibitors than PCR [178]. The results in Fig. 4.22 confirm the results presented above (Figure 4.21) that heating is a key step for the deactivation

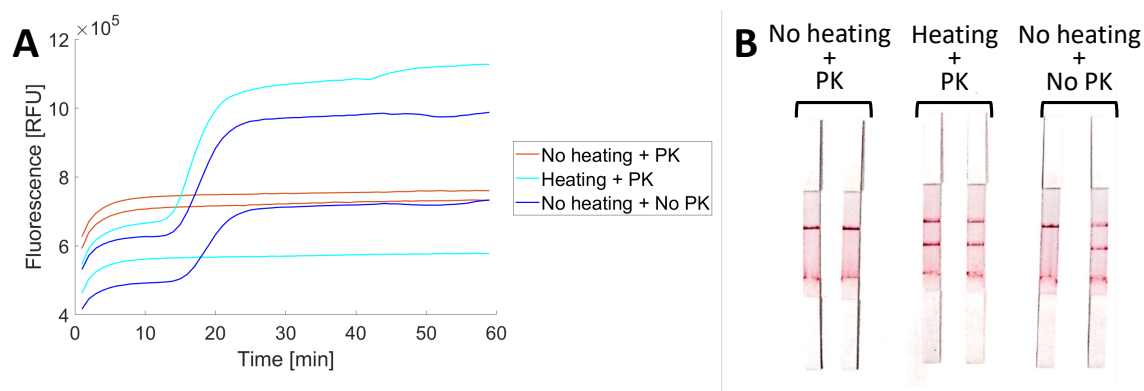


Figure 4.21: **Results of simplified DNA extraction methods from whole blood.** The three extraction methods described in Fig. 4.20 were performed: No heating + Proteinase K (PK), Heating + PK, No heating + No PK. LAMP targeting *BRCA1* gene was performed and 5 μL of the resuspended magnetic beads were used. Each extraction method was performed in duplicate ($n = 2$). **A.** Amplification curves of the LAMP results for each method. **B.** Lateral flow results of each method. Nuclease-free water was used as running buffer.

of PK and consecutive success of LAMP reaction. In addition, the 11-step DNA extraction performed as explained in Fig. 4.20C has no time-to-positive values that are significantly different from the ones obtained when performing the 13 steps outlined in Fig. 4.20A.

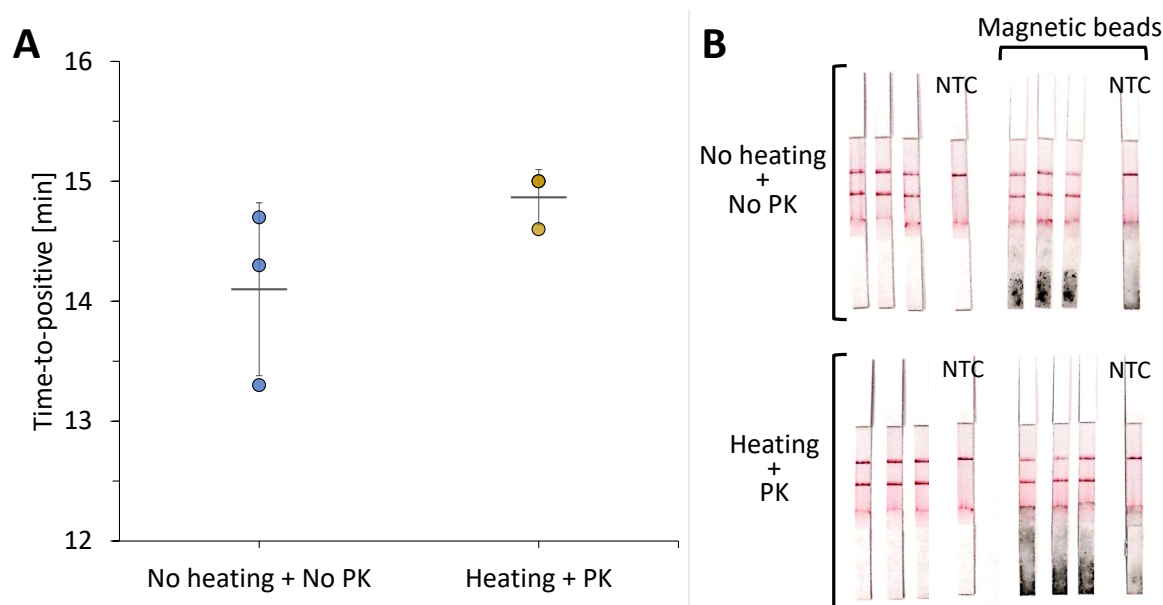


Figure 4.22: **Comparison of simplified DNA extraction methods from whole blood.** Two extraction methods (Fig. 4.20B, C) were performed; one including both heating and Proteinase K (Heating + PK), and one that excluded the use of both components (No heating + No PK). LAMP targeting *BRCA1* gene was performed and 5 μL of the resuspended magnetic beads were used. Each extraction method was performed in triplicate ($n = 3$). **A.** Time-to-positive values of the LAMP results for each method. **B.** Lateral flow strips (LFSs) results of each method. Nuclease-free water was used as running buffer. 10 μL of the final amplified sample added to the LFSs avoiding pipetting magnetic beads (left) or with magnetic beads (right).

Moreover, it was observed that the presence of magnetic beads in the sample does not affect neither amplification nor result visualisation on LFSs.

As a result, the protocol that was integrated inside a point-of-care diagnostic device for in-field testing was the one in Fig. 4.20C.

4.1.8 Paper Device and Storage of Molecular Reagents In-The-Field

4.1.8.1 Microfluidic Device Development

The plastic cassette was created from a 2-mm thick PMMA layer, as explained in Section 2.15.2.4. The process was sped up by combining capabilities that had already been proven. Our device was based on a similar working principle as the ones introduced by Trick *et al.* [179] and Rodriguez-Mateos *et al.* [102], that use magnetic beads to capture DNA during lysis and to move it through different chambers for successive purification and amplification. Rodriguez-Mateos *et al.* [102] and Ngamsom *et al.* [103] used mineral oil to separate the lysis, purification, and amplification steps, exploiting the immiscible filtration assisted by surface tension fluids [180]; castor oil was used instead, which was used for a similar function by other members of our research group. Several experiments were conducted to test the performance of the liquid handling system. Effectiveness of the chambers and the microfluidic systems at separating fluids was evaluated using red and blue dyed water.

The first designs tested consisted of 8 chambers (design **a**, Fig. 4.23): sample chamber (1), washing chamber (3), separations chambers (2), (4), resuspension chamber (5), amplification chamber (6), LFS chamber (7), and running buffer chamber (8). The dimensions of chambers (1)-(7) were derived as described in Section 2.15.2.4 (Fig. 4.23C, D). The additional running buffer chamber (8) served to add extra liquid to let the sample flow on the LFSs, after heating the device to perform LAMP. Once the thin wall between chamber (8) and (6) is broken, the running buffer flows through. Chamber (8) contained 60 μL of running buffer (either NFW or the running buffer included with U-Star Disposable Nucleic Acid Detection Strips, Type 3). The main difference between designs **a - 1** and **a - 2** were the channels (Fig. 4.23). The channels in **a - 1** are straight, 0.5 mm wide, and 4 mm long. In **a - 2**, the gate widths tapers from 1.5 mm to 0.5 mm wide, and are 3 mm long. Design **a** was used to observe the movement of magnetic beads across the chambers. Each design was first sealed on one side with acetate film (MicroAmpTM Optical Adhesive Films), loaded with the required liquid volumes (Fig. 4.23C), then sealed on the other side with an acetate film. The liquids

were added in the following order: castor oil in chambers (2) and (4), washing buffer (MagaZorb[®] DNA Mini-Prep Kit, Promega) in chamber (3), and nuclease-free water in chamber (5). Next, lysis buffer, PK, the magnetic beads reagent (MagaZorb[®] DNA Mini-Prep Kit, Promega), and NFW (in lieu of a sample), were added into chamber (1), one at a time. Magnetic beads were dragged from chamber (1) to chamber (5) as indicated in Figures 4.23A, B.

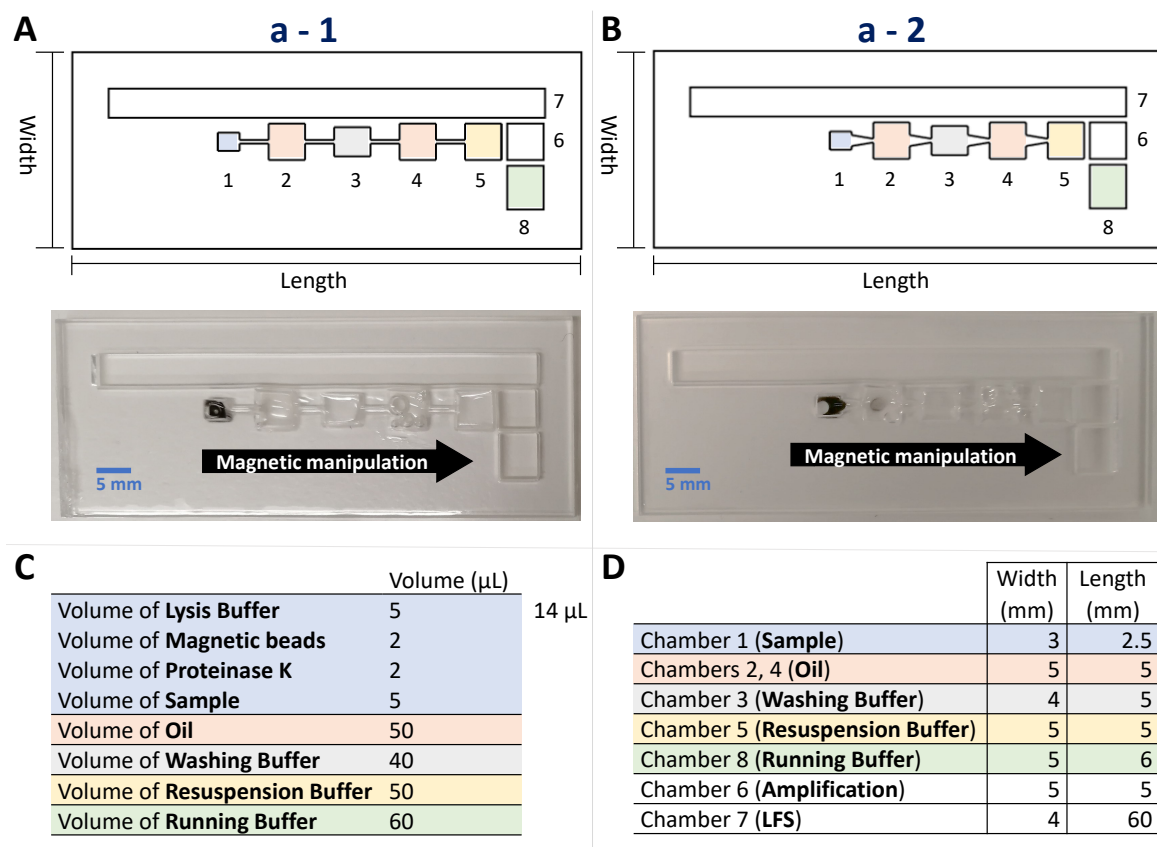


Figure 4.23: **Dimensions of the point-of-care device for the detection of malaria: designs a.** Each design consists of 8 chambers. **A.** Design a - 1. External width: 27 mm; External length: 70 mm. **B.** Design a - 2. External width: 27 mm; External length: 70 mm. In A and B, the wall thickness between chambers (5)-(6), (6)-(7), (8)-(6) is 0.8 mm. **C.** Volumes of liquid that each chamber should accommodate. **D.** Dimensions of chambers that approximately accommodate the volumes in C. The chambers number in D are color-coded and numerated in A, B.

Proper magnetic bead manipulation was achieved in both designs **a** (Fig. 4.23A, B); however, the presence of air-bubbles formed during the sealing process meant that magnetic beads remained stuck at the liquid-air interface. The 0.8-mm-thick walls between chambers (5)-(6), (6)-(7), (8)-(6) were very hard to break using the tip of a 15 mL falcon tube. The chambers dimensions used in design **a** are smaller than the ones calculated in Section 2.15.2.4, Table 2.9, but they were large enough to accommodate the necessary liquids; this was probably due to the presence of the channels and laser cutting inaccuracies that increased the volume available for the liquids compared to

the initial 2D design.

A new set of designs (designs **b**) was created (Fig. 4.24). Different channel dimensions and shapes were tested to find those optimal for moving magnetic beads; the designs characteristics are described in Fig. 4.24. The chambers volumes and dimensions are the same as in Figures 4.23C, D.

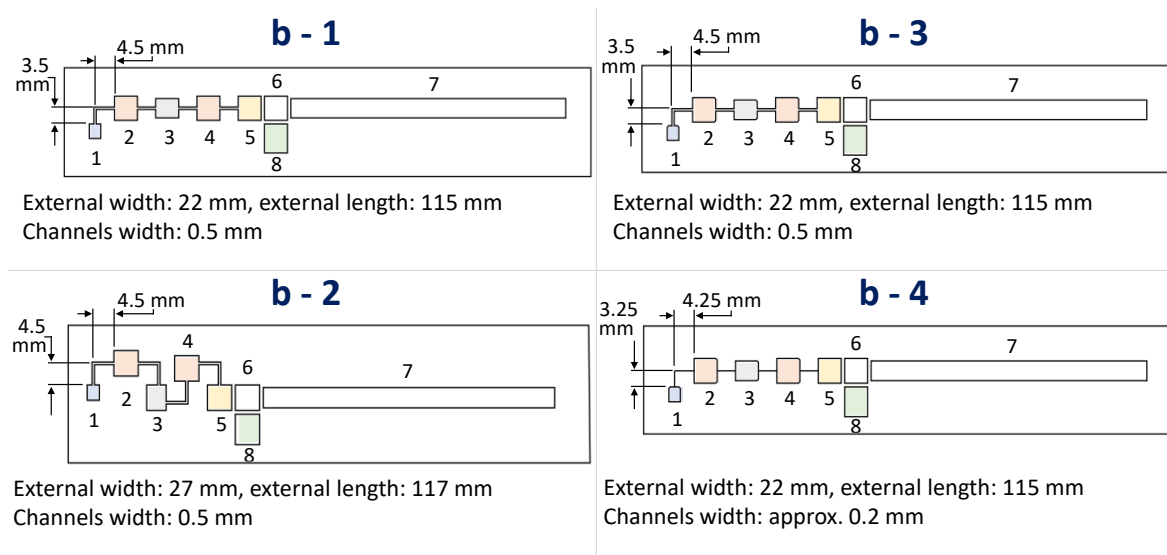


Figure 4.24: **Dimensions of the point-of-care device for the detection of malaria: designs b.** Each design has 8 chambers (dimensions in Fig. 4.23D), numbered in each design. **b - 3** has the same dimensions as **b - 1**. The distance between chambers (2)-(5) is 4 mm in **b - 1**, **b - 3** and **b - 4**. In **b - 2**, each connecting channel has the dimensions indicated for the channels between chambers (1) and (2). Wall thickness (length) between chambers (5)-(6), (6)-(7), (8)-(6) is 0.75 mm.

The channel connecting chambers 1 and 2 include an angle in all designs **b**; this was designed to prevent potential unwanted leakages of magnetic beads from channel 1 into channel 2, that were observed in designs **a**. The corners of the right side of the chambers in designs **b - 3**, **b - 4**, were slightly rounded to prevent magnetic beads from being trapped in the chamber corners during movement. Again, each design was first sealed on one side with acetate film (MicroAmpTM Optical Adhesive Films), loaded with the required liquid volumes (Fig. 4.23C), and sealed at the top with an acetate film. Washing buffer was dyed using Allura Red AC (Sigma-Aldrich, Merck KGaA), with a concentration of 0.25 g/L allura red, to facilitate fluid monitoring within the device. Water was dyed blue using a Xylene Cyanol FF (Thermo Scientific), with a concentration of 0.25 g/L, and used as resuspension buffer. It was observed that the angle in the channel connecting chambers (1) and (2) prevented most of the magnetic beads from flowing into chamber (2) (before using the magnet), compared to design **a - 1**. No differences in terms of liquid leakage from one chamber to the adjacent one were observed between **b - 1** and **b - 2**; since **b - 2** required more complicated

magnet manipulation, it was discarded for future tests. The rounded corners on the right edge of the channels of **b - 3** appear to not bring any significant advantage in preventing magnetic beads to get trapped in the corners. The small channels in **b - 4** made magnetic manipulation extremely difficult, so the design was discarded. All designs **b** were strongly agitated to understand if any liquid mixing would occur among chambers; all designs appeared to be very stable and liquids did not mix, which was a good indicator that loading the reagents in the device, prior to shipping them to the field, would not lead to reagent leakage during the journey. Due to presence of very thin walls between chambers (5)-(6), (6)-(7), (8)-(6), the sealing needed to be performed very slowly and carefully to prevent overflowing of liquids among chambers. The results showed that **b - 1** was the most user-friendly and effective design for transferring magnetic beads from chamber (1) to chamber (5). Based on this, **b - 1** was also used to break the walls between chamber (5) and (6) and simulate the heating conditions for the LAMP reaction as in real scenarios. The device was heated for 1 hour at 66 °C on a heat block, and leakage of the oil and other liquids was monitored. After heating, some liquid went also into the LFSs chamber (Fig. 4.25).

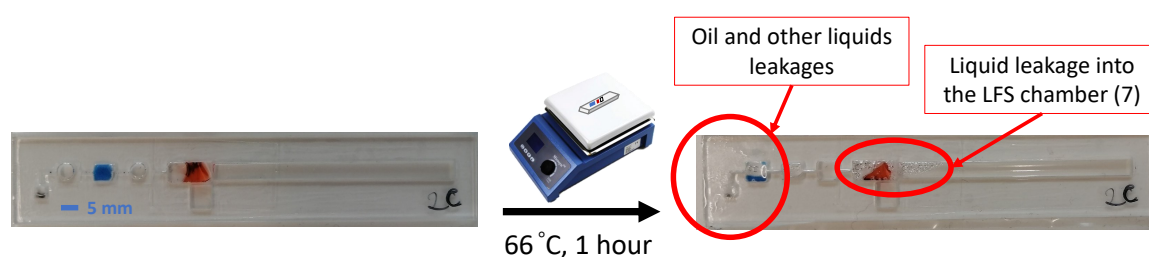


Figure 4.25: **Heating process of the malaria diagnostic cassette; design b - 1.** After the magnetic beads were moved to the reaction chamber (6) using the magnet, the device was placed on a heat block for 2 hours. After heating, castor oil leakages and liquid overflowing from chamber (6) to (7) were observed.

There are a few possible factors that could cause the liquid to leak out of the device. The PMMA plastic cassette of the POC device was sealed with the same acetate film as in previous studies [17,152], since it was proven to be effective. However, the amplification time had to be extended from 30 minutes [17, 152] to 90 minutes, which might have compromised the seal. Another potential factor is the thermal dilatation of castor oil and air inside the device. Castor oil has a coefficient of cubical expansion of $0.0007\text{ }^{\circ}\text{C}^{-1}$ [181], which means that 50 μL of castor oil would increase by 1.57 μL when heated from 21 °C to 66 °C, according to the equation *Coefficient of cubical expansion = Increase in volume / (Original volume \times Rise in temperature)*. Similarly, using the ideal gas law and assuming constant pressure and number of moles of air, the volume

change of air can be calculated with the equation $V_2 = V_1 \times (T_2/T_1)$, where V_1 and V_2 are the initial and final volumes, and T_1 and T_2 are the initial and final temperatures in kelvins. For instance, if there are 10 μL of air in one chamber, the volume increase ($V_2 - V_1$) would be about 0.82 μL . It was difficult to control the amount and formation of air bubbles in the device after loading the reagents and during sealing. Therefore, the combined effect of castor oil and air expansion might have led to the leakage. We did not find any simple solutions for this problem that did not require a more complex device design or additional external equipment.

Different types of walls were then investigated to understand which thickness and shape eased the breaking of the walls between chambers (5)-(6), (6)-(7) and (8)-(6). Fig. 4.26 gives examples of the walls tried, without providing detailed information about the dimensions. All the walls' designs were hard to break, therefore the simplest straight wall as in previous designs was maintained.

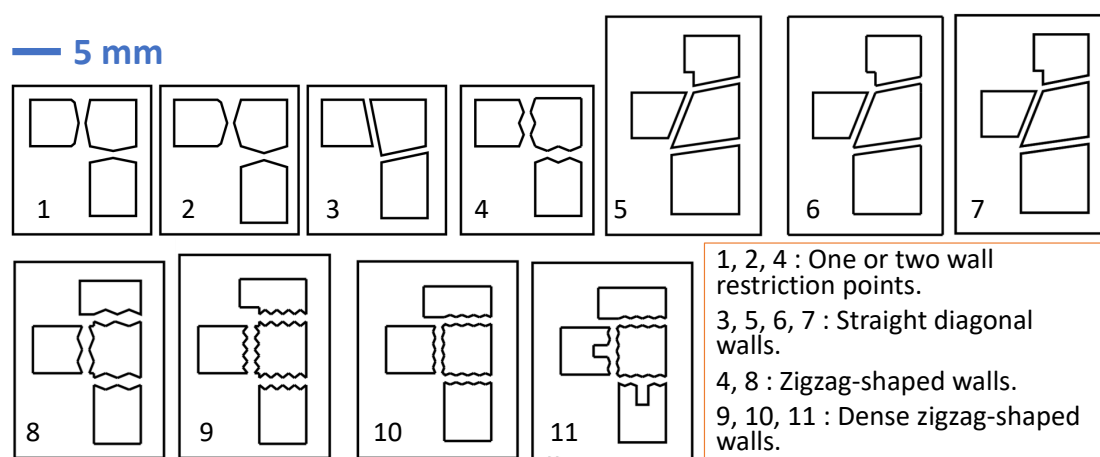


Figure 4.26: Different types of walls and thicknesses between chambers (5)-(6), (6)-(7) and (8)-(6).

The feasibility of using a single sample chamber (1) for both the sample and positive control testing was explored, to reduce reagent consumption and use only 5 μL of whole blood. The proposed method involved separating the magnetic beads at the final resuspension (5) and reaction (6) chamber stages. Three designs (c) were examined for separating the magnetic beads (Fig. 4.27A) and the best one was selected to test the whole magnetic manipulation process (Fig. 4.27B). The resuspension buffer was removed from design c to simplify device handling. The 50 μL of final LAMP reaction should be sufficient to allow the amplicons flow through LFSs, since the typical volume used on LFSs for result visualisation is 40 μL .

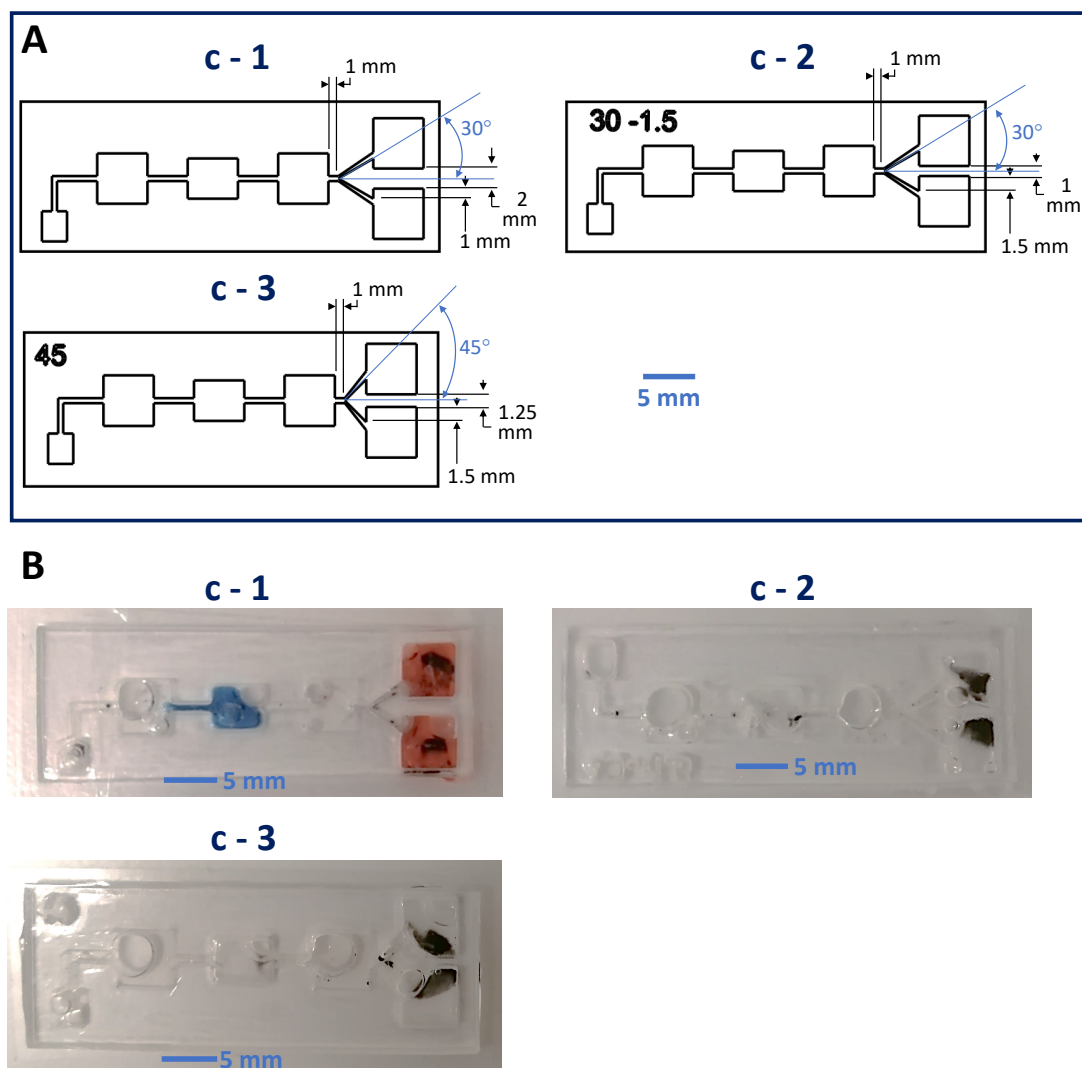


Figure 4.27: **Dimensions of the point-of-care device for the detection of malaria and magnetic beads handling: designs c.** The cassettes include 5 chambers, from the sample (1) to the resuspension (5) chambers. The dimensions of the chambers are given in Fig. 4.23. **A.** Dimensions of the plastic cassette. **B.** Results of magnetic beads handling inside the different cassette designs.

The idea was to label *Plasmodium* PAN Loop B primer with 2, 4-dinitrophenyl (DNP TEG) rather than with FITC, and to create an additional test line on the LFSs to detect DNP (with anti-DNP antibodies). This would have avoided cross-contamination between chambers due to possible liquid leakage during heating. The full device exploiting design **c - 1**, was sealed as described in Section 2.15.2.5; MicroAmp™ Optical Adhesive Film was used to seal the top part of the device. After turning the plastic cassette upside down, holes in chambers (1)-(5) were made with a biopsy punch to allow successive loading of liquids. LFSs were placed in chambers (7). Tablets storing reagents were not required for this set of tests, so chamber (6) was left empty. Finally, the bottom part of the device was sealed with two pieces of MicroAmp™ Optical Adhesive Films (Fig. 2.17D). The liquids were loaded in the corresponding chambers

using pipettes and through the holes in the film. A second adhesive film was then applied (Nunc™) as described in Section 2.15.2.2. Magnetic beads were manipulated as explained in Section 2.15.2.2 and heating was performed at 66 °C for 2 hours. Liquid in the full device **c - 1** overflowed from the amplification chamber (6) to the LFS chamber (7) both before being heated in one of the devices (device at the bottom), and after being heated in a second device (device in the middle, Fig. 4.28). In addition, some of the liquid from the reactions in chambers (5)-(6) flowed back to chamber (4) during the heating process (Fig. 4.28). This highlighted that the fluid control during heating is suboptimal when a ‘separator’ is used in the fluidic system (design **c**); ‘separators’ were therefore dismissed. Leakage of oil and other liquids was also observed.

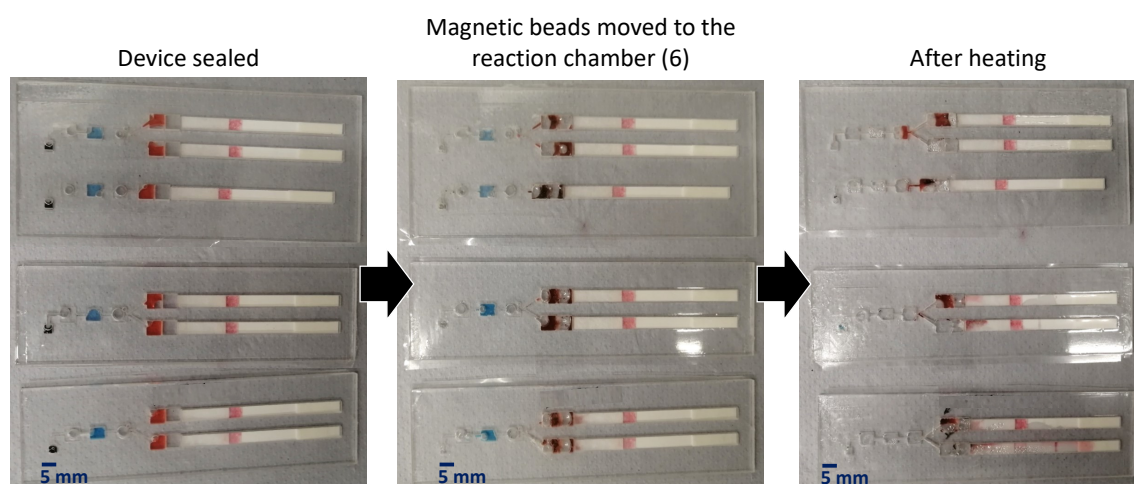


Figure 4.28: **Results of liquid and magnetic beads handling in the device: design c - 1.**

Another option that could have reduced the amount of reagents used was to multiplex the positive control and the sample. This could have involved labelling the *Plasmodium* PAN LB primers with DNP instead of FITC and adding an extra test line on the LFSs. However, this would have required LAMP optimization for the primer concentrations (now 12 primers in a single reaction), which could have caused the formation of primer dimers and affected the accuracy of the results. The changes in the primer volumes would have also altered the composition of Tablet 1. Due to the time constraints and the risk of false negatives, this option was not explored further.

Since liquid overflow from the amplification (6) to the LFS (7) chambers was still an issue in the design, different thicknesses of wall between the two chambers were trialled (1, 1.5, 2, 3 and 5 mm) to make sure the acetate film sealing was proper. The heating of these devices was not performed as shown in Fig. 4.25, on a heat block, but using an aluminium band (Fig. 4.29), like the one used by Guo *et al.* [153]. This reduced

leakages of castor oil, probably due to the fact that the heat was focussed only on a localised region of the device during the LAMP reaction.

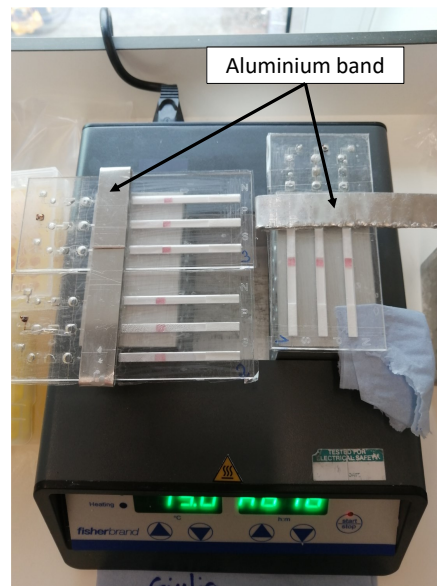


Figure 4.29: **Heat block and aluminium bands used to perform LAMP on the point-of-care device for malaria.** Aluminium bands were cut so that they covered the resuspension and amplification chambers of the plastic diagnostic cassette.

Liquid overflowing from chamber (6) to (7) was not observed for all the thicknesses (Fig. 4.30).

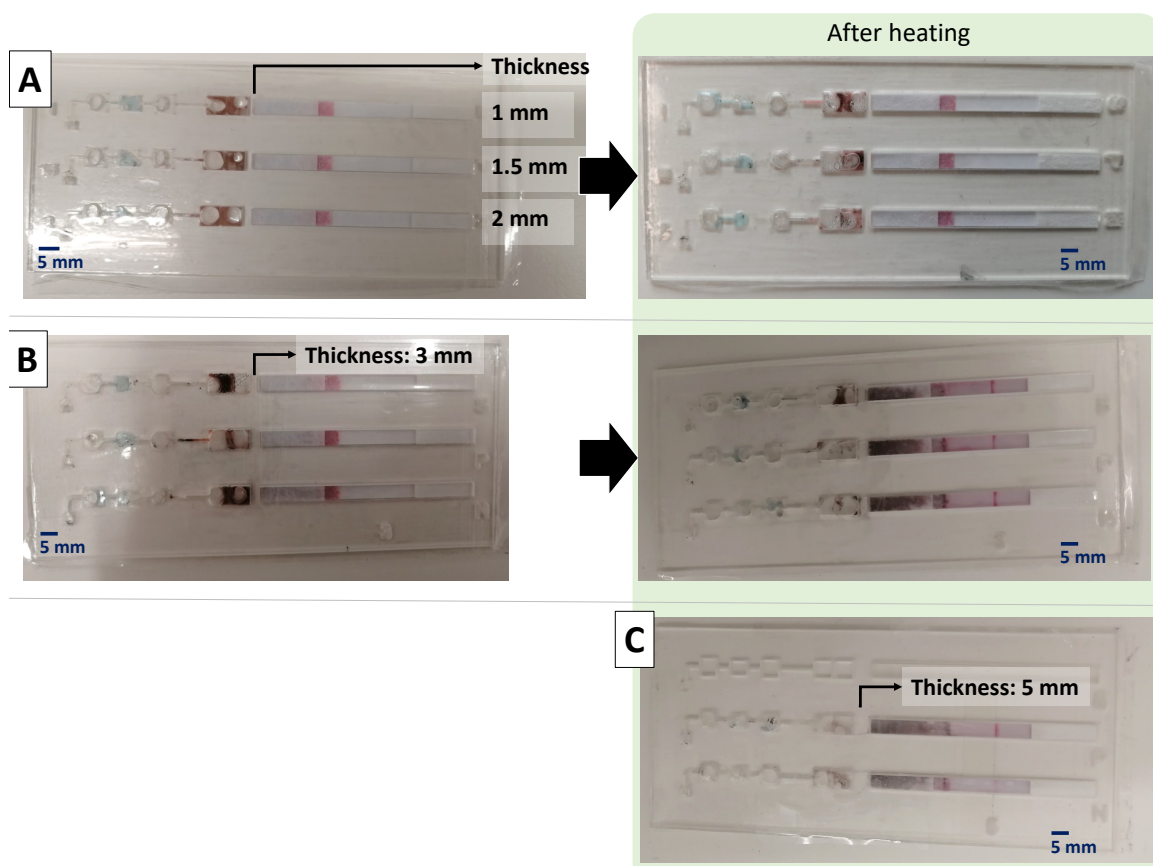


Figure 4.30: **Liquid manipulation and heating of the point-of-care device for the detection of malaria with different wall thicknesses between the reaction (6) and LFS (7) chambers.** The design used is **b – 1** (Fig. 4.24) with the exclusion of the running buffer chamber (8), and different wall thicknesses between chambers (6) and (7). Results before (left) and after heating (right) are shown. **A.** Wall thicknesses of 1 mm, 1.5 mm, and 2 mm. **B.** Wall thickness: 3 mm. **C.** Wall thickness: 5 mm.

A 3-mm thickness between chambers was chosen for further testing because the successive flow of liquid from chamber (6) to (7) by breaking the walls was faster than with a 5-mm thickness. Even if lower wall thicknesses than 3 mm did not show leakage, they increase the risk of leakage, so device **b - 1** was used to perform a full assay on the POC device. The device was assembled as described in Section 2.15.2.5, and used with whole blood as described in Section 2.15.2.2, with the only difference being that washing buffer was used in chamber (3). The sealing process was optimised from previous experiments by adding super glue, and a further film to prevent biological material from leaking out during heating (as described in Section 2.16.1). After 2 hours of heating, sufficient liquid was available to flow through the LFSs; however no control line appeared for any test, and the results were invalid (Fig. 4.31A).

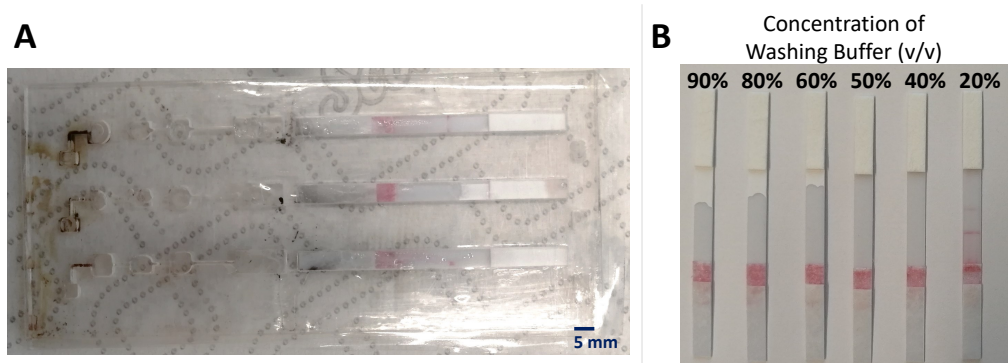


Figure 4.31: **Results of full DNA extraction and LAMP assay carried out on the point-of-care device.** Dried reagents for the detection of *BRCA1* gene from whole blood were used. The design used is **b - 1** (Fig. 4.24) with the exclusion of the running buffer chamber (8), and 3-mm thick walls between chambers (6) and (7). **A.** Device after heating and after breaking walls to let amplicons flow to the lateral flow strips (LFSs). **B.** Different concentrations (v/v) of washing buffer (Promega) in nuclease-free water were run on LFSs. 40 μ L of each solution was run on one LFS.

A possible cause of the failure to see the results on the LFSs was the improper handling of the device, which allowed the washing buffer to mix with the amplicons and interfere with the movement of gold nanoparticles from the conjugate pad to the test and control lines. This hypothesis was confirmed by running different dilutions of washing buffer in NFW (Fig. 4.31B). A concentration as low as 40% washing buffers in a 50 μ L water sample applied to the LFSs could prevent the visualization of the results. Therefore, nuclease-free water was used as washing buffer to prevent inhibition of results visualisation on LFSs. For field-testing, design **b - 1** was chosen and it was assembled as described in Section 2.15.2.5, and operated as explained in Section 2.15.2.2. Results using red dyed water as a running buffer, in Fig. 4.32, show that the control line appears in the absence of washing buffer. It is also clear that the washing buffer (red) flows towards the LFSs, which support our hypothesis that the washing buffer was interfering with proper result visualisation in Fig. 4.31A. Design **b - 1** was modified with a larger sample chamber (1) ($3 \times 3.5 \text{ cm}^2$), because whole blood easily overflowed from the sample chamber with its initial dimensions.



Figure 4.32: **Results of full DNA extraction and LAMP assay carried out on the point-of-care device.** Dried reagents for the detection of *BRCA1* gene from whole blood were used. The design used is **b – 1** (Fig. 4.24) with the exclusion of the running buffer chamber (8), a 3-mm thick wall between chambers (6) and (7), and a sample chamber (1) with dimensions $3 \times 3.5 \text{ cm}^2$. Picture is taken after 2 hours heating at $66 \text{ }^\circ\text{C}$ and after breaking the walls to allow amplicons through the lateral flow strips.

4.1.8.2 Results from the field

The point-of-care malaria cassette was deployed in the Tororo District (Uganda) which is a malaria endemic region. The microscopy results from our study suggests 72% prevalence of malaria in the study cohort ($N = 90$). 48 cassettes were processed in total and only 9 could be used for analysis (18%), Table 4.6.

Table 4.6: **Summary of the number (No.) of point-of-care (POC) malaria cassettes used during in-field testing.** The No. of tests performed every day and the number of valid cassettes for analysis is given.

	Day 1	Day 2	Day 3	Day 4
No. of POC tests performed	10	14	16	8
No. of valid POC tests	1	3	2	3
% of validity	10.0 %	21.4 %	12.50 %	37.5 %
	Total tested			48
	Total valid			9

37 cassettes could not be included in the analysis due to either leaks ($N = 12$), failure of controls ($N = 20$) (as described in Section 2.15.2.3), or contamination events (NTC(N)= positive) ($N = 7$). Compared to microscopy, the following results were recorded: 4 true-positive test results, 1 true-negative, 3 false-negative, and 1 false-

positive test results. A possible reason for the false-negative outcomes is the variation in temperature during the LAMP process on the heating devices (Fig. 4.33). The amplification station, where heating occurred, was situated between two large, unprotected windows. Therefore, it was very hard to monitor the temperature and ensure its stability given the sudden changes in temperatures occurring throughout the day. The malaria RDT outcomes for the 9 samples that were analysed were in accordance with the microscopy outcomes.

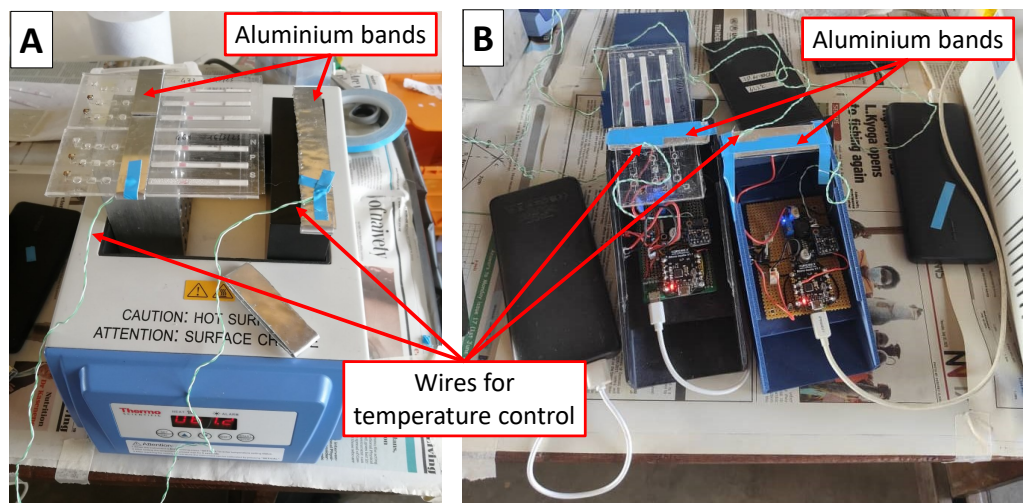


Figure 4.33: **LAMP reaction set-up in the field.** **A.** Heat block and aluminium bands used to perform LAMP on the point-of-care device for malaria. Aluminium bands were designed to cover only the resuspension and amplification chambers of the plastic diagnostic cassette. A generator powered the heat block, which was used to cover for the portable heating devices during malfunctions and to increase testing capacity by accommodating multiple devices. **B.** Portable heating devices [153]. When possible, the temperature of the aluminium bands was monitored using a thermocouple data logger.

On the final day of testing, the scaled-down DNA extraction from blood was performed in tubes (as described in Sections 2.15.2.1, 4.1.7) but using NFW as washing buffer. The reagents were stored dry and sealed in 1.5 mL Eppendorf tubes wrapped in parafilm. After the supernatant was removed from the tube and only magnetic beads remained at the bottom, 25 μ L of NFW was added to the tube. This volume was then moved inside another tube where the dried LAMP reagents were stored. Amplification was performed on a heat block and 10 μ L of the LAMP product was run on LFSs. The LAMP reaction time was reduced from 120 minutes to 90 minutes due to the time restrictions on the final day of testing. For each test, three types of stored dry reagents were used: one to detect malaria in the whole blood sample (Tablet 1 which contained *Plasmodium* PAN primers), two to detect *BRCA1* gene as positive and negative controls of the DNA extraction (Tablet 1 which included *BRCA1* primers). In total, 10 tests were

processed, of which only 4 were used for analysis (40%). 6 tests were discarded due to failure of positive controls ($N = 5$) and contamination ($N = 1$). Compared to microscopy, 4 true-positive test results were recorded. Positive control failures could have been associated with the reduction of reaction time (which may not have allowed timely amplification of the target DNA), and with temperature fluctuations during the LAMP process on the heating block [152].

4.1.8.3 Factors affecting the paper device in-the-field and trouble-shooting

The field trial resulted in a considerable number of cassettes being unusable due to leakage issues from one chamber to the other, as well as malfunctioning of the lateral flow assay controls. Some cassettes presented multiple controls issues, leading to 81.25% of samples being excluded from analysis. When the DNA extraction was performed in tubes, 60% of the samples were not included due to failure of the positive controls. Failures were often associated with unreliable heating systems and frequent failure of portable heaters. The heating system had a variable temperature that could not be easily adjusted and monitored when using the diagnostic device. Moreover, some aluminium bands were uneven (Fig. 4.33), which may have compromised the uniformity of heating across reaction chambers in a single device. 31% of the cassettes was excluded from the analysis because of failed positive controls (no test lines), which probably resulted from uncontrolled temperature variations [152].

For the final 7 samples out of the 10 run in tubes, the temperature was closely monitored using a thermocouple data logger (USB TC-08 Thermocouple Data Logger, Pico technology, United Kingdom), in order to measure the temperature of the actual reaction. A thermocouple was placed inside a 1.5 mL tube, and closed. The tube contained 50 μL of NFW to simulate the expected reaction volume and the thermocouple was immersed in the water at the bottom of the tube (25 μL of NFW was a too low volume to submerge the thermocouple). Of these 7 tests, 3 positive controls failed probably due the short amplification time.

A second possible explanation for the failure of positive controls in the diagnostic cassettes could be the reduction of the LAMP reagents' concentration by using 50 μL of resuspension volume of the dried reagents instead of 25 μL , as previously tested in tubes. The dilution certainly affects the sensitivity of the assays negatively. Finally, evaporation during amplification might have been a detrimental parameter for the suc-

cess of LAMP reaction as it alters the temperature of the reaction and the effective concentration of primers and enzymes [182]. In certain devices, it was extremely hard to collect 10 μL of amplified products to run on the LFSs, suggesting significant evaporation occurred. Previous studies have shown that a layer of mineral oil on top of the LAMP reaction can prevent evaporation whilst heating occurs [102, 182]. In the case of our device, the castor oil in chamber (4) was insufficient to prevent evaporation during amplification because the final reaction chamber (5)+(6) was half-empty due to the increase chamber volume created by breaking the wall between chambers (5) and (6). Different resuspension strategies of dried reagents are probably needed to ensure no evaporation during amplification.

Trouble Shooting In-The-Field On the first day of testing, the 3-mm thick wall was broken, allowing the LAMP products to flow into chamber (7) on the LFSs. All test results were invalid; the control line did not appear because the gold nanoparticles did not move beyond the conjugate pad (Fig. 4.34).

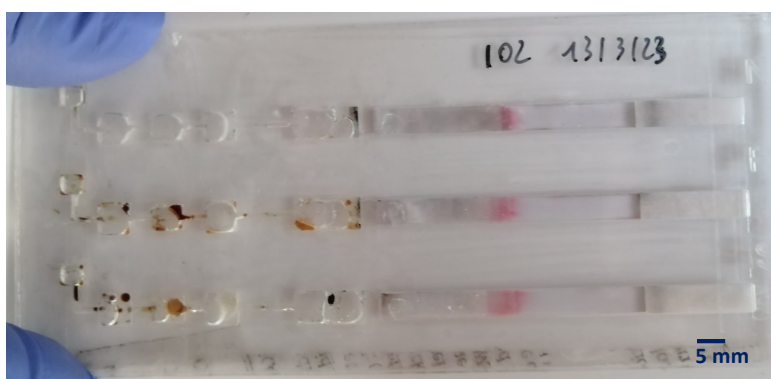


Figure 4.34: **Example of issues encountered during the field-trial:** gold nanoparticles would remain in the conjugate pad of the lateral flow strips (not flowing beyond).

In subsequent tests, therefore, 10 μL of the LAMP amplification product was transferred from chamber (6) to the LFSs using a pipette. To do so, both chambers (6) and (7) were punched-open with a biopsy punch, and 30 μL of NFW was added to each LFS to let the amplicons flow. This was a tedious and error-prone process that increased the risk of contamination and variability. On day 1, faint test lines were observed on the negative samples (N), which invalidated the results. A test line present in the negative control (N), however, did not always correspond to a test line being present in the positive control (P), contrary to what would be expected in case of contamination events where both the negative and positive controls result positive. On days 3 and 4,

there were still high numbers of test lines present in negative controls; therefore, we tried to investigate the possible source of contamination by running two cassettes (so, 6 LFSs) with negative samples only. One LFS resulted positive out of 6 LFSs, which ruled out contamination as the cause of these issues. Some additional experiments were conducted to investigate the causes of test lines appearing in the negative control of the diagnostic device.

Four hypotheses were tested: (H1) positive test lines are linked to strips heating too much and for too long, (H2) the glue used in the sealing enters the resuspension chamber and interferes with the reaction, (H3) castor oil interferes with the reaction, and (H4) something uncontrollable happens during the amplification reaction that generates false positives. To test H1, the reaction time was reduced to 90 min and the heating set-up changed to minimise strip heating (the devices in aluminium bands were moved on the heat block so that the LFSs were not in direct contact with the heat-block); positive test lines were still observed. To test H2, NFW (instead of whole blood) was added to the sample chamber in two devices. One device was sealed with super glue as per protocol, and the second without. In both cases, some very faint test lines showed up in all the LFSs, Fig. 4.35. When glue was used, one of the LFSs did exhibit a very faint line on the control line too. These results indicated that the glue was probably not the primary cause of the issues, but could still interfere with result visualisation.

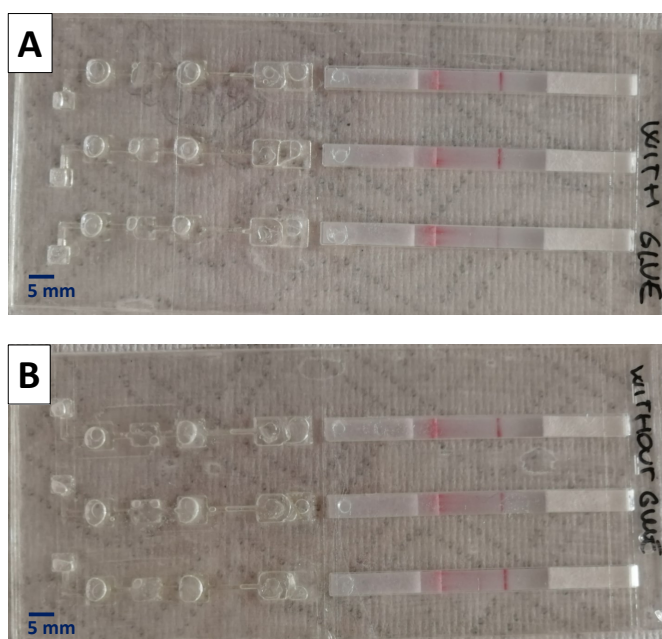


Figure 4.35: **Results of devices sealed with or without the use of super glue.** Trouble shooting of hypothesis H2: glue used in the sealing enters the resuspension chamber and interferes with the reaction. **A.** Second sealing performed using super glue as per protocol. **B.** Second sealing performed without super glue.

To test H3, four sets of dried LAMP reagents, stored in 1.5 mL Eppendorf tubes, were resuspended either with 50 μ L of NFW (two tubes), or with 25 μ L of NFW and 25 μ L of castor oil (two tubes). 50 μ L from each tube was run on separate LFSs. Liquid from two tubes from each condition was run on LFSs before amplification and neither of them showed positive test lines. The second set of tubes from each condition was heated at 66 $^{\circ}$ C for 90 minutes before being added to LFSs. Results from the two reactions were negative, suggesting that oil did not interfere with the LAMP reaction. The last hypothesis tested was H4. The resuspension chamber was sealed from the adjacent oil chamber (4) with parafilm. Then, 50 μ L of NFW was added in chamber (5), and the wall was broken to resuspend reagents held in chamber (6). After 2 hours of heating, the liquid in chamber (6) was transferred to the LFSs using a pipette. Results from one control was positive, and the other two were negative; this implies that something might have happened during the reaction that caused false positives (Fig. 4.36).

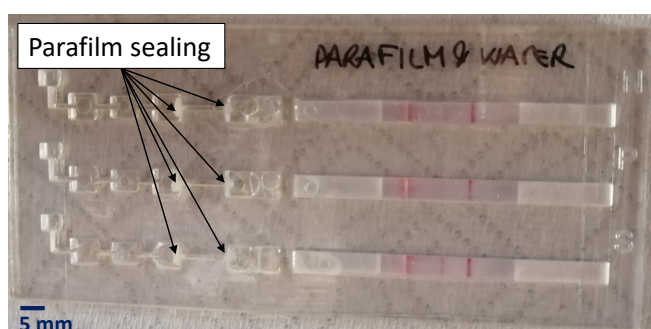


Figure 4.36: **Results of a device whose resuspension chambers are sealed from the adjacent oil chambers (4) with parafilm.** Trouble shooting of hypothesis H4: something uncontrollable happens during the reaction that generates false positives.

Unfortunately, none of the experiments performed led to a clear conclusion. Further troubleshooting was then performed back in the laboratory, in the UK.

Trouble Shooting Back in the Lab (UK) Upon our return to the UK laboratory, we observed that LFSs batches from the same supplier (U-star) had inconsistent performance with different running buffers (Fig. 4.37). Indeed, the new batch of LFSs used for the field work and inside the diagnostic devices was more prone to false positives than the old batch (previously used for lab testing and in Sections 4.1.1-4.1.4, 4.1.7) when water was used as running buffer. Therefore, during the field trial the NFW as running buffer might have caused faint test lines in the negative controls (N) LFSs (Fig. 4.37).

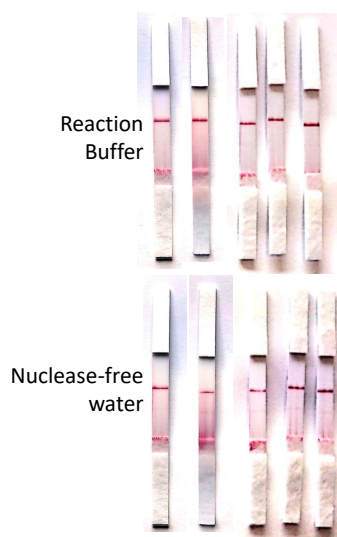


Figure 4.37: New batch of lateral flow strips (LFSs) run with 40 μL of provided running buffer (upper panel) and 40 μL of nuclease-free water (lower panel).

To evaluate the possibility of false positive results due to unspecific binding on the test line, 40 μL of NFW or the running buffer supplied with the LFSs were ran on LFSs as negative controls before running the samples. Therefore, either water or the specific running buffer was chosen to run the samples on the LFSs. The results on LFSs of the trouble-shooting described in this section were performed using resuspension buffer to help amplicons flow through the strips.

The first thing investigated was the functionality of the reagents used in the field for sample preparation. Lysis buffer, magnetic beads, and NFW brought back from the field, along with reagents stored in the lab (at constant room temperature) were used to extract DNA from whole blood (purchased by Cambridge Bioscience Ltd., Cat # BLD1DC4CIT09-FS), following the protocol described in Section 2.15.2.1 (Fig. 2.13B). The LAMP reaction contained primers that targeted the *BRCA1* gene. The reagents brought back from the field are still functional because they led to DNA amplification (Fig. 4.38). No significant difference in time-to-positive values was observed when using the reagents brought back from the field compared to the ones regularly stored in the lab.

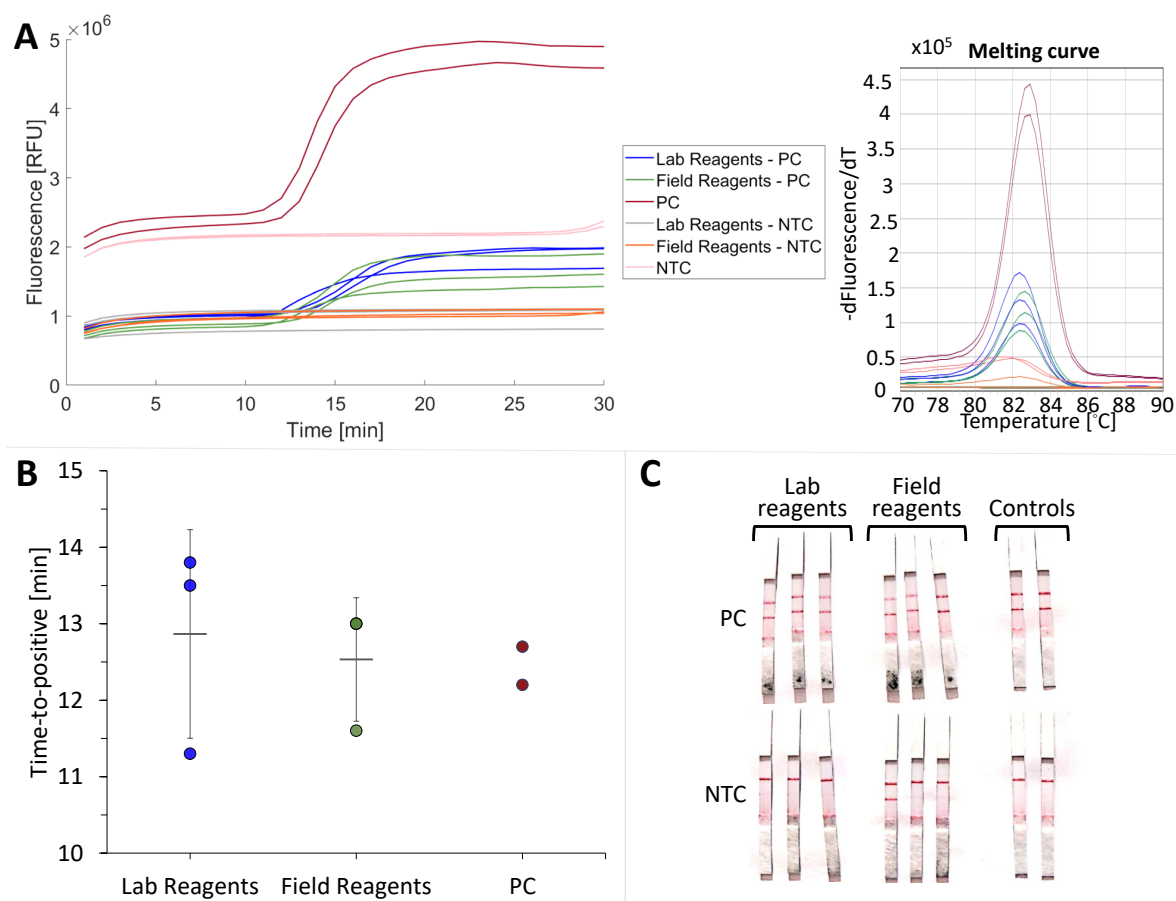


Figure 4.38: **DNA extraction from whole blood performed with reagents brought back from the field.** DNA extraction was carried out following the protocol in Fig. 2.13B using sample pretreatment reagents stored at controlled room temperature in the laboratory (Lab reagents) or brought back from the field (Field reagents). LAMP assays containing primers specific for *BRCA1* were run to test the performance of the Field reagents in comparison to the Lab reagents. Whole blood was used for extraction and sample were extracted in triplicate ($n = 3$). **A.** Amplification and melting curve. **B.** Time-to-positive values (TTPs) derived from A. Data points are the TTPs for each biological repeat. The horizontal bars represent the mean value of the TTPs of the biological replicates whose DNA extraction was performed with the same conditions. Error bars represent the standard deviation for $n = 3$. No statistically significant difference was observed for p -value < 0.05 . **C.** Lateral flow assay results. PC: positive control (10 ng/ μ L of Jurkat human genomic DNA). NTC: no template control.

From the results in Fig. 4.38, we ruled out the possibility that the sample pretreatment reagents were malfunctioning.

After showing that LAMP reagents stored dry inside the diagnostic cassette for 6 months lost re-activity (Section 4.1.5), the whole diagnostic device was tested using the protocol given in Sections 2.15.2.2. The devices brought back from the field were used to understand if internal handling of reagents might have affected results visualisation. Whole blood was used in the positive control (P), NFW in the negative control (N) and the WHO standard for *P. falciparum* DNA was used in the sample test (S). Three cassettes were tested (Fig. 4.39).

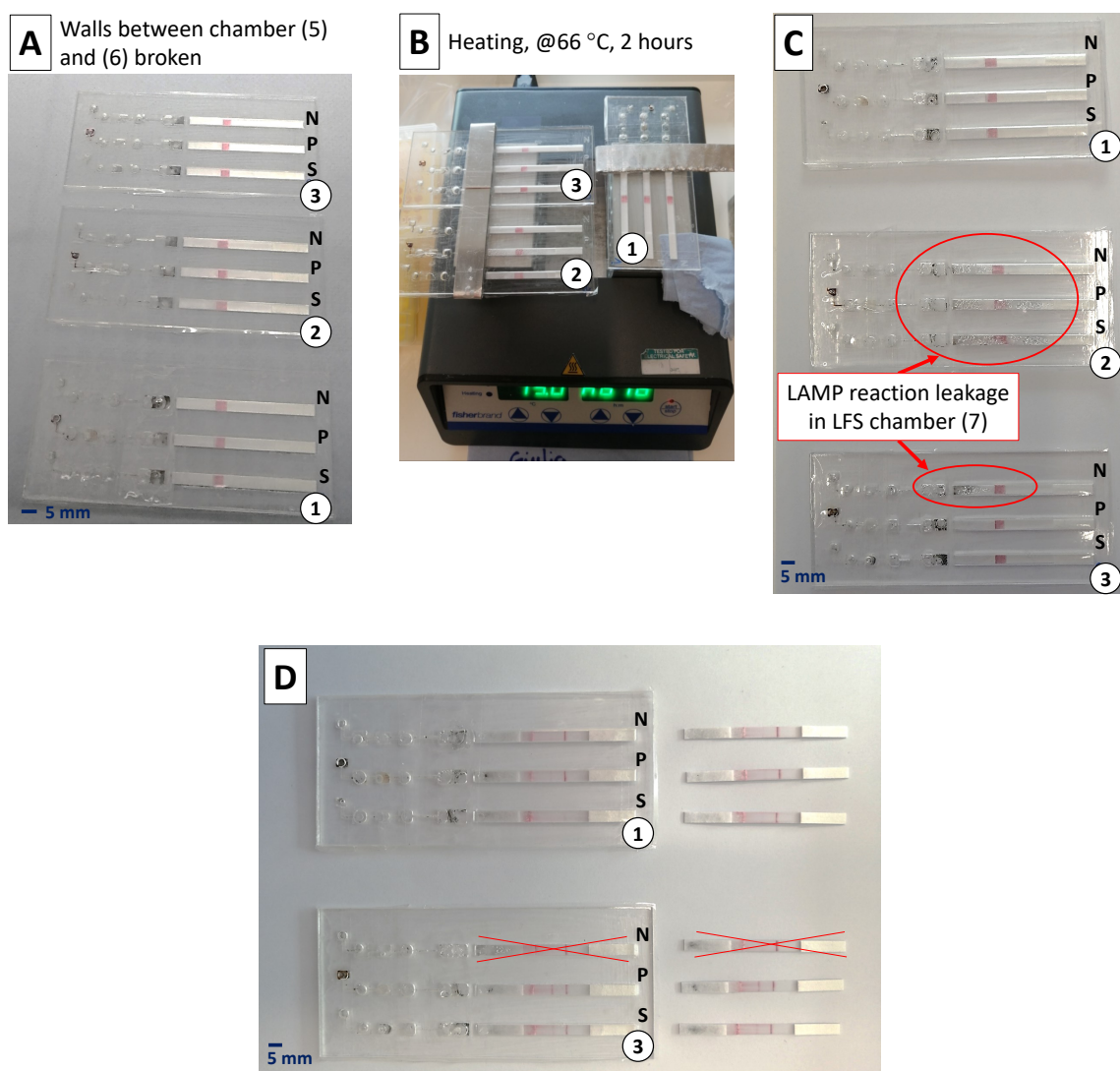


Figure 4.39: **Testing of plastic cassettes for malaria diagnostics in the laboratory in UK, after they were shipped to Uganda.** Three diagnostic cassettes are used (no. 1, 2, 3). Whole blood was used in the positive control (P), nuclease-free water in the negative control (N) and the WHO standard for *P. falciparum* DNA in the sample test (S). **A.** Liquids and samples were loaded into the corresponding chambers; the cassette was closed and magnetic beads were dragged to the resuspension chamber. The picture shows the merged resuspension (5) and amplification (6) chambers. **B.** Heating of plastic cassettes on a heat block using aluminium bands. **C.** Devices after they underwent heating. **D.** Results of LAMP amplicons run on lateral flow strips (LFSs). LFSs from a fresh set but same batch are shown (right) and amplified LAMP assays were run on these too.

Cassette no. 2 was excluded from the analysis because leakage occurred during heating (Fig. 4.39B, C). The amplicons were run on the LFSs by punching open the reaction (6) and LFS chambers (7), and adding 10 μ L of the amplified product and 30 μ L of the running buffer on LFSs. The negative control of cassette no. 3 was excluded for the same reason. All tests in cassette no. 1 are negative (Fig. 4.39D), as expected given the inactivity of LAMP reagents. For unclear reasons, the sample test (S) of cassette no. 1 does not show the control line and the result was invalid inside the device. On the contrary, both the sample test (S) and the positive control (P) of cassette no. 3

were positive. This would have been the results expected if the LAMP reagents were functional. The positive results of cassette no. 3 suggested that sample handling inside the device is unstable and generates results that cannot be successfully interpreted and understood. LFSs from a new aluminium pouch (fresh set but same batch) were also used to run the amplified LAMP assays outside the device, to rule out the possibility that the LFSs inside the device were not functional. Only one LFS result did not reflect the same result as its corresponding strip inside the device (Cassette no. 1, sample test). We therefore assumed that the LFSs were properly stored inside the device and that they did not undergo degradation during shipping and storage.

A further limitation of our study is that we did not verify the functionality of the LAMP reagents inside the devices after coming back from the field trip. We waited for 6 months before testing them, and we could not guarantee that the LAMP reagents were still functional inside the device soon after our return. Therefore, our assumption that the reagents inside the devices were functional during field-testing, and after 10 days storage under uncontrolled conditions, might have been incorrect.

4.2 Discussions

4.2.1 Tablet-Based Storage of Reagents

We demonstrated that LAMP reagents stored dry in pullulan-trehalose tablets can be successfully integrated with lateral flow assays, shipped to underserved communities, and used on-site at the point-of-care. Tablet-based assays are a simple and affordable way to stabilise labile bioreagents over the long term and in extreme environmental conditions. This can significantly improve diagnostic support in resource-limited settings by offering lower device costs, easier shipping, and enhanced ease of use.

Paper-based devices based on nucleic acid tests, such as loop-mediated amplification (LAMP), have demonstrated their potential for use outside laboratory settings for the accurate and rapid detection of diseases [32, 96, 183]. However, the limited shelf-life of reagents at ambient temperature represents one of the major barriers for their deployment, when refrigeration is not available, as is the case in most low-resource settings, where infectious diseases have their highest burden. One of the main challenges in reagent stability is the susceptibility of enzymes to degradation by water [104, 105, 184].

To preserve the activity of such protein-based reagents for long-term use, dry storage is preferable over liquid conditions, especially for point-of-care devices that require simple design and manufacturing. Existing methods used to dry pre-mixed LAMP reagents for storage, such as freeze-drying [22–24] and drying by concentration/desiccation [25], are experimentally laborious and requires sophisticated equipment. In the past decade, pullulan and trehalose have been used to encapsulate biomolecules and retain reagent reactivity [26]. These additives offer simple and inexpensive methods for long-term stabilization of enzymes [119]. However, they have only been demonstrated in laboratory settings where temperatures and humidity conditions are optimally controlled. Their use in uncontrolled transport and storage conditions is yet to be investigated.

In this chapter we studied the effects of reagents stored in a mixture of pullulan and trehalose on the limit of detection of a LAMP assay targeting two important pathogens in sub-Saharan Africa: *E. coli* (*malB* gene) and *Plasmodium* species. Our results showed that pullulan-trehalose tablets are a viable option for storing LAMP reagents at high (35 °C) and variable temperatures with minimal impact on assay performance, but further optimization is needed to enhance storage and reaction outcomes.

We demonstrated the ability of well-sealed stored dry LAMP reagents to detect 10^5 IU/mL of *P. falciparum* after two months of uncontrolled temperature conditions, that corresponds to 490 parasites per μL of blood (see conversion Table 2.3). The limit-of-detection (LOD) of the tablet-based assay, however, is higher than the one of the liquid assay, which can detect about 49 parasites/ μL . These LOD is comparable to or lower than those of the WHO-prequalified malaria rapid diagnostic tests (RDTs) for *P. species* [185,186]. Tan *et al.* [186] reported that the LOD of the RDTs tested with cultured *P. falciparum* parasites varies from 49 to 1556 parasites/ μL , depending on the test and the antigen detected. Only two RDTs achieved LODs of 49 parasites/ μL , whilst the others had an LOD equal to or above 100 parasites/ μL . Considering the WHO recommendation that RDTs should consistently detect 2000 parasites/ μL [185], our results are promising. Nevertheless, further improvement to lower the LOD of the tablet-based assay is required.

To make Tablet 1, we used WarmStart[®] Bst 2.0 DNA polymerase from New England Biolabs, which has glycerol in its composition. Glycerol is a common additive in commercially available enzymes, as it helps to preserve the protein structure in aqueous solutions [187]. Glycerol can also slow down LAMP amplification [174], therefore, de-

ploying a glycerol-free polymerase would be advisable to shorten the amplification times and potentially improve the assay LOD. However, purchasing a polymerase without glycerol was challenging, as they are usually custom-made, thus requiring long shipping times and high costs. Moreover, the high viscosity of glycerol limited the amount of enzyme we were able to add with precision to the final pullulan-trehalose tablet. A higher enzyme concentration in the tablet could improve the long-term use of the reagents (and its LOD over time) by accounting for enzyme degradation. However, higher DNA polymerase concentrations would also increase the cost of the reagents. Another way to enhance the long-term stability of reagents stored in pullulan-trehalose is to prepare them under nitrogen and dry them under vacuum [122]. This method, however, reduces the simplicity and cost efficiency of the process, making it less attractive. By creating dry and stable reagents in a simple way, we can achieve two important goals. First, we can lower the energy consumption during the production process. Second, we can enable the manufacturing of these reagents in low- and middle-income countries or even in ‘DIY settings’ near the end-use locations. This way, we can increase access at a community level of long lasting nucleic acid amplification reagents.

Air-drying reagents is a simpler, lower-cost and more accessible method than lyophilisation, which is commonly used to store LAMP reagents in a dry format. We estimated that freeze-drying the ISO-004-LYO from Optigene Ltd. that takes about 24 hours and consumes about 66.24 kWh (238.464 MJ) when performed in the Labconco FreeZone Triad Benchtop Freeze Dryer (VWR International Ltd). On the contrary, air-drying does not consume any energy, while vacuuming reagents (Laboport[®], © KNF Group Ltd., Edinburgh, UK) or drying them in a traditional biosafety cabinet for one hour uses about 0.25 kWh (0.882 MJ) and 1.8 kWh (6.48 MJ) [188], respectively. Therefore, freeze-drying consumes more than 250 times the electrical energy used for vacuuming the samples for 1 hour. This has implications for both the environmental impact and the affordability of large scale production.

Humidity, as well as temperature, plays a crucial role in the long-term storage of dried LAMP reagents. We observed how the storage method of dried reagents affected the final assay performance, and we found that moisture-resistant sealing such as parafilm was necessary. Pullulan has been reported to have low moisture permeability [189] and to form films that are stable under high humidity conditions (99% RH) [73], but it may require high concentrations to provide an effective moisture barrier. This is not

suitable for our application, where we have shown that high concentrations of pullulan complicate the production phase and the release of reagents in the final solution.

4.2.2 Paper Device and Storage of Molecular Reagents In-The-Field

We evaluated a molecular device that integrates all the nucleic acid (NA) amplification steps (from sample pretreatment to amplification and result visualisation) in a single diagnostic cassette, for use at the point-of-need. The device incorporates a simplified DNA extraction method for DNA extraction from blood samples. It also utilizes immiscible phases constrained in the microscale and magnetic beads to draw DNA across the purification and amplification steps, in a similar way to Rodriguez-Mateos *et al.* [102], and Ngamsom *et al.* [103]. Platforms that use microscale immiscible phases and magnetic particles have the advantage of removing the need for valves, movable parts, and pumps [190]. However, there are still some challenges for their implementation in resource-limited settings. Examples include: the need for a heat source to perform NA amplification; storage of reagents inside the device; and a trade-off between automation and deployability [190]. In fact, automated devices may offer better reproducibility and throughput, but also require more instruments and complexity, which may limit their accessibility and usability in remote settings. Manual devices may be more suitable for low-resource settings, but may have lower capacity and reliability.

With our study, we aimed at understand if our diagnostic platform was compatible with the portable heater developed by the colleague Guo *et al.* [153], and to address the challenge of reagent storage without the need for cold chain. Furthermore, we wanted to validate our POC device using clinical samples in a point-of-need scenario.

Our diagnostic cassette requires a total operational time of 2 hours and 45 minutes, divided into 25 minutes for reagents loading and sample lysis, 2 hours for amplification reaction and 15 minutes for result visualisation. Our collaborators from the Vector Control Division (Ministry of Health Uganda) confirmed that the processing time, although long, is tolerable in the deployed context because the targeted end-user (children in school or family members in rural areas) are willing to wait for that time to receive a result and possible medication. Nevertheless, the wider research group is working on optimizing the method to reduce the processing time.

The long amplification time required by the dried LAMP reagents limits the diagnostic device performance and reliability. Not only is the testing capacity reduced compared to a device that can be operated within one hour, but also the amplification reaction becomes more vulnerable to temperature fluctuations. The latter was the case in our testing scenario, where the diagnostic process took place in a classroom, where external weather conditions, such as rain or wind, affected the indoor temperature and, consequently, the heaters. Moreover, limiting amplification times would also reduce evaporation during heating that, as explained in Section 4.1.8.3, affects the accuracy and stability of the results. Methods to decrease dried reagents amplification times have been briefly discussed in Section 4.2.1.

One of the factors that could have affected the reliability of our device was the final volume of the LAMP reaction; we resuspended the tablet-based reagents with 50 μL , instead of 25 μL , that would provide the correct final concentration of reagents. Using 25 μL to resuspend the dried reagents was not possible because the low liquid volume was not compatible with the device design. To use 50 μL with the correct reagent concentrations, the volumes for preparing the tablets would need to be changed, which would result in longer drying times under vacuum and higher reagents costs. Trade-offs between accuracy and costs would need to be considered, especially when the deployability of these devices is more likely in poorer and remote areas.

Another issue encountered in the field was blood clotting when the lysis was performed for longer than 20 minutes inside the device, leading to the formation of magnet aggregates, which hindered the movement of the magnetic beads across the chambers. Due to this, some of the diagnostic cassettes were excluded from analysis. This phenomenon was not observed during testing in the lab, probably because the blood used for lab analysis contained anticoagulants. To ensure a high throughput in the field, we performed the lysis in tubes and then added the lysed samples to the device for further processing. The throughput challenges were related to the way that blood samples were collected. Each day, all 20 children's blood samples were collected within the first hour of the morning, to minimize the disruption of school activities. It was difficult to process samples quickly because the reagents needed to be loaded onto the devices, there were only two people doing the tests, and there was a limited space for heating (about four devices at one time).

A major and final challenge we faced during field testing was the on-site reagent loading process. It was difficult, time-consuming, and required skilled staff. This increased the number of manual steps and the risk of contamination. Therefore, loading the reagents is recommended in laboratory-controlled environments. The reagents loaded in the device, during lab testing, did not seem to mix after vigorous shaking. However, the device could be exposed to uncontrolled pressure and temperature changes during transportation that could affect its performance [190]. Transporting the device in a controlled environment is very expensive, and our device is not yet reliable enough to be transported with all the reagents already loaded.

We also learned that the effectiveness of our POC device in the lab does not necessarily translate to effectiveness in the field, and that the testing conditions are a key factor to consider during device design. This is an aspect that is often neglected in the current literature, where POC devices are evaluated in laboratory settings, with clinical samples, but rarely in the actual point-of-need scenarios.

We took inspiration from the platform developed by Rodriguez-Mateos *et al.* [102] and Ngamsom *et al.* [103] to test the viability of storing tablet-based reagents on the device, and showing the results on lateral flow strips, without needing extra manual steps to move the amplified products to the strips. We showed that LAMP reagents can be stored ‘on board’, but we could not integrate LFSs because of unclear invalid results (as explained in Section 4.1.8.3).

Although we were able to store the LAMP reagents on our POC device, it was not possible (at least at this stage of development) to store all the sample preparation reagents inside the device. As discussed in detail in Section 4.1.8.3, the on-site use of the POC device was hindered by various factors that were difficult to overcome. We recognize this as a limitation and plan to address it in future work.

Furthermore, since the reagents have to be loaded on-site, the current POC device does not offer any advantage over the scaled-down DNA extraction from blood in tubes that was described in Section 4.1.7. During the field trip, we gained valuable insights into the real-world use context. Initially, the device design prioritized usability for untrained personnel, aiming to minimize steps and ensure practicality even for individuals lacking specialized skills. The imagined scenario saw the end-user as a school teacher carrying

out diagnostic tests in a classroom with no electricity or temperature control. To overcome the absence of electricity, portable heating devices were employed. Additionally, a heat block powered by a generator was available at the use-site in case the portable heaters malfunctioned. Surprisingly, the heat block served a dual purpose: not only did it compensate for portable heater malfunctions, but it also increased testing capacity, as discussed earlier. However, loading reagents into the device proved complex; trial and error were necessary to avoid oil leakage, which could compromise the device's sealing. As an alternative, we observed that the scaled-down DNA extraction from blood was a viable method for the technical personnel accompanying the group to the testing site. In the actual scenario, in fact, the technicians would likely be the ones conducting tests at the community level - not teachers - making technicians the end-users. In hindsight, proactive discussions with technical staff before the validation trip and on-site device deployment would have been beneficial; by considering acceptability within the community and the Ugandan healthcare structure, involving technicians early on could have optimized diagnostic testing procedures (as further discussed about co-design in Section 7.2).

We are confident that the work outlined in this chapter, with its successes and limitations, can serve as a foundation for guiding the design of more robust and user-appropriate devices.

4.3 Contribution to Knowledge

In this chapter, we have presented novel approaches to preserve the reagents for isothermal nucleic acid amplification reactions, such as LAMP, to facilitate the implementation of point-of-care diagnostic tests in low-resource settings. Pullulan-trehalose tablets are low-cost and easy to manufacture, and they enable complex transport logistics of LAMP reagents without significant decrease in performance. This opens up the possibility for easy access to accurate diagnostics globally.

Compared to currently available LAMP reagents storage techniques based on lyophilisation [22–24] and concentration/desiccation [25], pullulan-trehalose tablets offer a simple, cost-effective and energy efficient production method.

To the best of our knowledge, this is the first time that pullulan-trehalose tablets have been used for:

- Testing the limit-of-detection of LAMP reagents. Leung *et al.* [26] limited their investigation to prove that the tablet-based assay work in preserving amplification reagents. However, the concentrations of the target DNA used were very high as their amplification was very fast.
- Lateral flow strips detection.
- Shipping and in-field testing. We have successfully demonstrated that LAMP reagents stored dry in pullulan-trehalose tablets can be successfully transported and used in field conditions without compromising the assay performance.

We also introduce a simplified blood extraction procedure that yields comparable results to more complex methods.

Chapter 5

Modular Paper- and Plastic-Based Device Design, Assembly, And Fabrication

The goal of this study is to develop a modular device that can perform point-of-care (POC) testing by combining sample preparation and DNA amplification in one chamber. This would be very beneficial for low-resource settings, as it would reduce the manual steps and the time needed for the testing. One of the main difficulties of having sample preparation and amplification in the same tube is to eliminate the inhibitors [191]. These are substances from the sample or the pretreatment chemicals, such as detergents, chaotropic agents, and enzymes, that can affect the amplification process and lower its efficiency or specificity. Therefore, it is important to optimize the reaction conditions and timing to achieve a successful integration of sample preparation and amplification in one chamber. We address this problem by creating a layered structure of dried reagents and pullulan tablets that can control the fluid flows and the reagent mixing in space and time. Each layer has one or more reagents that are stabilised and regulated by the pullulan tablets.

The fast and instrument-free paper-based nucleic acid extraction from *E. coli* samples presented in Chapter 3 and the techniques to store dry LAMP reagents explored in Chapter 4 are modified to suit a simple POC (Fig. 5.1).

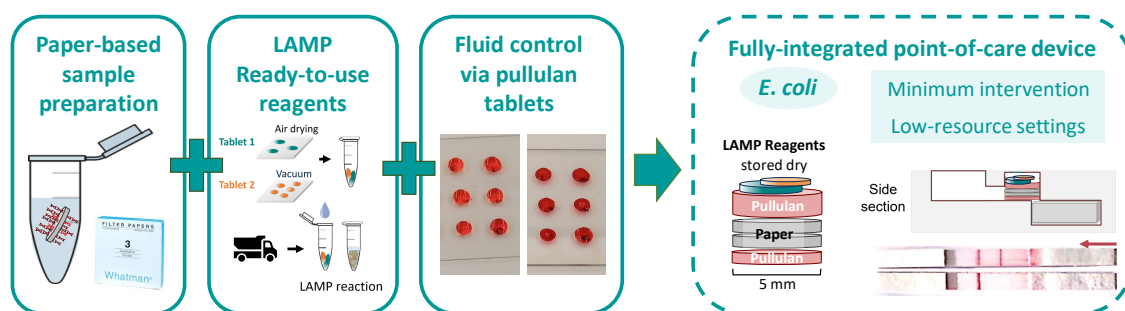


Figure 5.1: **Table of content figure of Chapter 5.** The paper-based sample preparation from *E. coli* samples presented in Chapter 3 is combined with the techniques to store LAMP reagents in a dry-format explored in Chapter 4 and pullulan tablets to control fluids. The aim is to develop a user-friendly and robust paper-based point-of-care device that can be used outside laboratory settings and at the point of need.

The following sections present the results of the experiments conducted to optimize the pullulan tablet parameters and the POC device design. The effects of tablet size and concentration on the dissolution time are shown in Section 5.1.1, which helps to select the best tablet for fluid control. The development and testing of different POC device prototypes are described in Section 5.1.2, where the fluid flows and performance are briefly evaluated. Next, the paper-based sample preparation method from Chapter 3 is adapted to fit the POC device and the results are reported in Section 5.1.3. A discussion of the main findings and implications is provided in Sections 5.2, 5.3.

5.1 Results

5.1.1 Dissolution rate of pullulan tablets at different concentrations

Pullulan tablets were used to regulate the timing of sample pretreatment and amplification steps inside the purification & amplification unit in the POC device (Fig. 2.19B). As outlined in Section 2.16.1, the bottom tablet facilitates sample and paper incubation for approximately 6 minutes. The top pullulan tablet is engineered to dissolve more slowly than the bottom tablet, after the introduction of the sample into the chamber via the sample inlet (Fig. 2.20i). This difference in dissolution time between the bottom and top tablets ensures that the sample pretreatment step remains separate from the LAMP reagents stored above during sample incubation and washing (Fig. 2.20i-iii). Therefore, the dissolution properties of pullulan tablets were studied to determine the optimal size and pullulan concentration to allow effective separation between the

sample pretreatment and the subsequent amplification step.

The initial objective was to determine the optimal colour change that the camera could capture when using a mixture of allura red and xylene cyanol solutions, as opposed to using the individual solutions of allura red and xylene cyanol. The experiment set-up and the concentration investigated are given in Section 2.16.3.3. Each well in Fig. 5.2A contains a different concentration of allura red and xylene cyanol ('mixed' wells, numbered from 1 to 24). The colour change (ΔE) was computed for each 'mixed' wells with the respective allura red concentration in row A (red control), and xylene cyanol concentration in column 1 (blue control). ΔE is computed for each pixel in the two wells of interest, for example C4 versus A4, therefore, the mean of the ΔE ($\mu_{\Delta E}$) was computed and plotted as shown in Fig. 5.2. For each mixed well there is a mean ΔE value that compares it to the red control and the blue control. The colour perception discrepancy is higher when the ΔE value is larger.

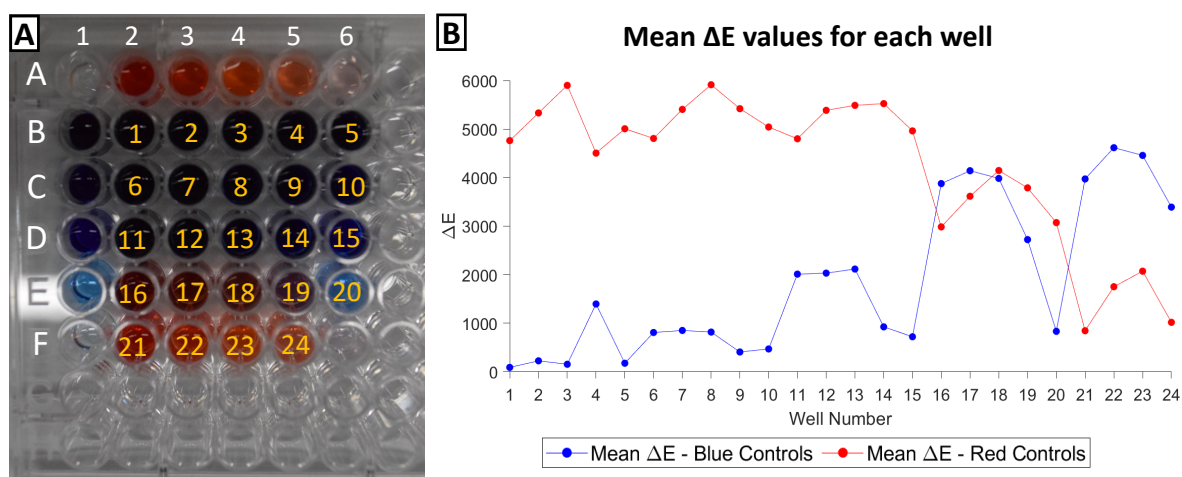


Figure 5.2: **Colour change detected by the camera.** **A.** 96-well plate containing different concentrations of allura red and xylene cyanol. The 'mixed wells' are numbered from 1 to 24. Blue control wells are in column 1, whereas red control wells are in row A. **B.** Mean ΔE values computed for each mixed well compared to the respective red and blue controls.

The highest values of ΔE when the mixed wells are compared to the blue controls are found in wells 16, 17, 18, 21, 22, 23 and 24, whilst the highest values of ΔE when the wells are compared to the red controls can be found from well 1 to well 15, before a drop in ΔE is observed. We wanted to ensure a high ΔE when the wells were compared to both controls, therefore the choice was restricted to wells number 16, 17 and 18. These wells had a high ΔE when compared to the blue controls, and the ΔE compared to the red control was still not as low as observed for wells 21, 22, or 23, where the $\mu_{\Delta E}$

values dropped below 2,500. The final choice ended on well 18, with a concentration of 0.1 g/L allura red and 0.02 g/L of xylene cyanol, because its ΔE value compared to the red control ($\mu_{\Delta E} = 4,146$) was higher than those of well 16 ($\mu_{\Delta E} = 2,984$) and 17 ($\mu_{\Delta E} = 3,615$).

The dissolution behaviour of nine different pullulan tablets was tested. The pullulan tablet dissolving over time was studied against the non-dissolved pullulan tablet, the pullulan tablet already dissolved in the xylene cyanol solvent, or the solvent. Fig. 5.3 provides the ‘Mean ΔE signal’ for each well compared to the well controls for one of the tablets tested. The colour change decreases when the wells containing dissolving tablets are compared to the already dissolved tablet, Well control 2, Fig. 5.3B. This is in line with the fact that the two wells should have similar colours after the tablets are fully dissolved. On the contrary, the colour change increases when the wells are compared to the xylene cyanol solution (Well control 3), Fig. 5.3C, as the red colour becomes more evident in the dissolving wells. The colour difference between the wells with tablets dissolving in them and the single tablet remained high throughout the experiment (Fig. 5.3A). It was decided to compute the ΔE between each well containing the dissolving pullulan tablet and the already dissolved tablet in xylene cyanol solution as Well control 2 represents the outcome of the pullulan tablet dissolving.

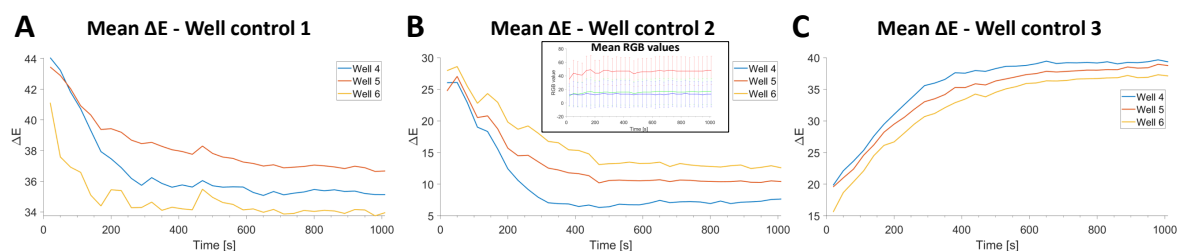


Figure 5.3: **Mean ΔE of each well compared to the well controls.** Mean- ΔE signal between each well containing the pullulan tablets dissolving (wells 4, 5, 6) and each ‘well control’. **A.** Wells 4, 5, 6, are compared with Well control 1m (pullulan tablet only). **B.** Wells 4, 5, 6, are compared with Well control 2 (100 μL of 0.02 g/L of xylene cyanol solution). The mean and standard deviation of the RGB values (red, green and blue) of Well control 2 are provided over time, to show that they remain constant. **C.** Wells 4, 5, 6, are compared with Well control 3 (pullulan tablet fully dissolved in xylene cyanol solution).

The first three pullulan tablets were created using 25 μL of solution to form 5-mm diameter discs, and had a pullulan concentration of 1%, 2%, 5% (w/v) pullulan (Table 2.10). Six more pullulan tablets were created using 50 μL of solution, and 6-mm diameter discs were formed. The pullulan concentrations investigated were between 2%, and 3% (w/v) pullulan (Table 2.11). The time-to-plateau at which the tablets

were considered completely dissolved were derived comparing the dissolving tablets with Well control 2 as described in Section 2.16.3.3, and they are given in Fig. 5.4.

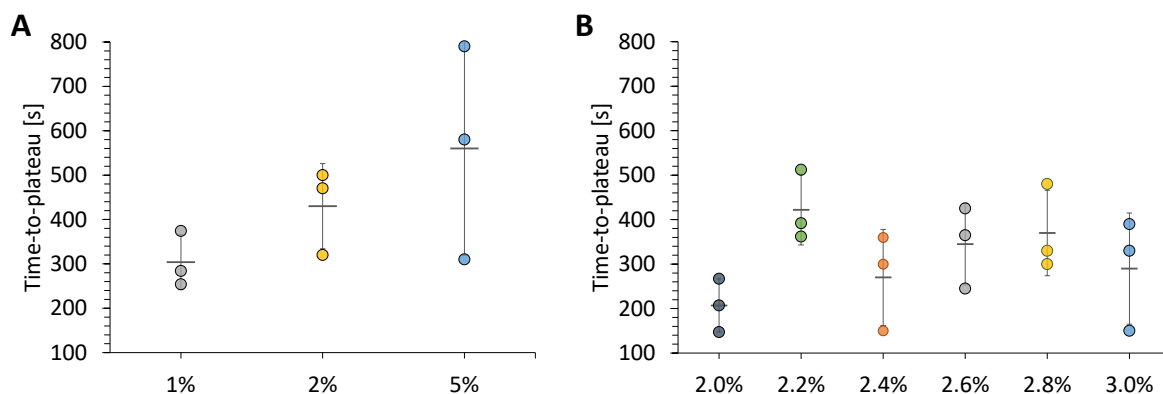


Figure 5.4: **Time-to-plateau values of pullulan tablets with different dimensions and concentrations.** Pullulan tablets of specific dimensions were created as described in Section 2.16.3. Experiments were run in triplicate ($n = 3$). The data points are the time-to-plateau value at which each pullulan tablet was considered dissolved. The horizontal bars represent the mean time-to-plateau value of pullulan tablets with the same concentration. Error bars represent the standard deviation for $n = 3$. **A.** Time-to-plateau values of 5-mm pullulan discs. 25 μL of pullulan solution was used to create of 1%, 2%, 5% (w/v) pullulan discs. **B.** Time-to-plateau values of 6-mm pullulan discs. 50 μL of pullulan solution was used to create of 2%, 2.2%, 2.4%, 2.6%, 2.8%, 3% (w/v) pullulan discs.

The 5-mm discs with 1%, 2%, 5% (w/v) pullulan were completely dissolved after 5.1 ± 1.0 min, 7.2 ± 1.6 min and 9.3 ± 4.0 min respectively (Fig. 5.4A). To ensure that the sample and the paper discs have enough contact time in the purification & amplification unit, which needs at least 6 minutes of incubation, the pullulan discs with 2% and 5% concentrations and 5-mm diameters are suitable options, since they dissolve completely after 7 minutes. However, the 5% concentration has a high intra-replicate variability that could be caused by excessive pullulan concentration (as discussed in Chapter 4). Hence, the use of 5% pullulan discs was avoided for further experiment. Moreover, 1% and 2% pullulan tablets were very difficult to peel off the glass slides once dried. Therefore, the possibility of making pullulan tablets using 50 μL of pullulan solution was investigated. This time, 6-mm discs were formed. The discs whose concentration was of 2%, 2.2%, 2.4%, 2.6%, 2.8%, 3% (w/v) pullulan were fully dissolved after 3.5 ± 1.0 min, 7.0 ± 1.3 min and 4.5 ± 1.8 min, 5.8 ± 1.5 min, 6.2 ± 1.6 min and 4.8 ± 2.1 min, respectively (Fig. 5.4B). For pullulan discs of 2.4%, 2.6%, 2.8% an increasing trend of time-to-plateau can be observed. 2.8% concentration is a suitable option to guarantee 6 minutes incubation time of the sample and the paper discs in the purification & amplification unit as it fully dissolves after about 6 minutes. The mean ΔE signal of 2.2% pullulan tablet in Fig. 5.5B and the results in Fig. 5.4B show that the tablet fully dissolves after approximately 7 min. This figure is out of line with

the increasing time needed for full dissolution of the tablets that is observed for 2% and from 2.4% to 2.8%, and it is probably due to the presence of bubbles within the dissolving wells. Mean ΔE curves are provided for each concentration of 6-mm pullulan discs in Fig. 5.5. In addition, the volume of pullulan solution used and the concentration affected the ease of removing the tablets from the glass slides. The tablets made with 50 μL pullulan solution were easier to peel off than the ones made with 25 μL . The higher the pullulan concentration, the less likely the discs were to break during the peeling process.

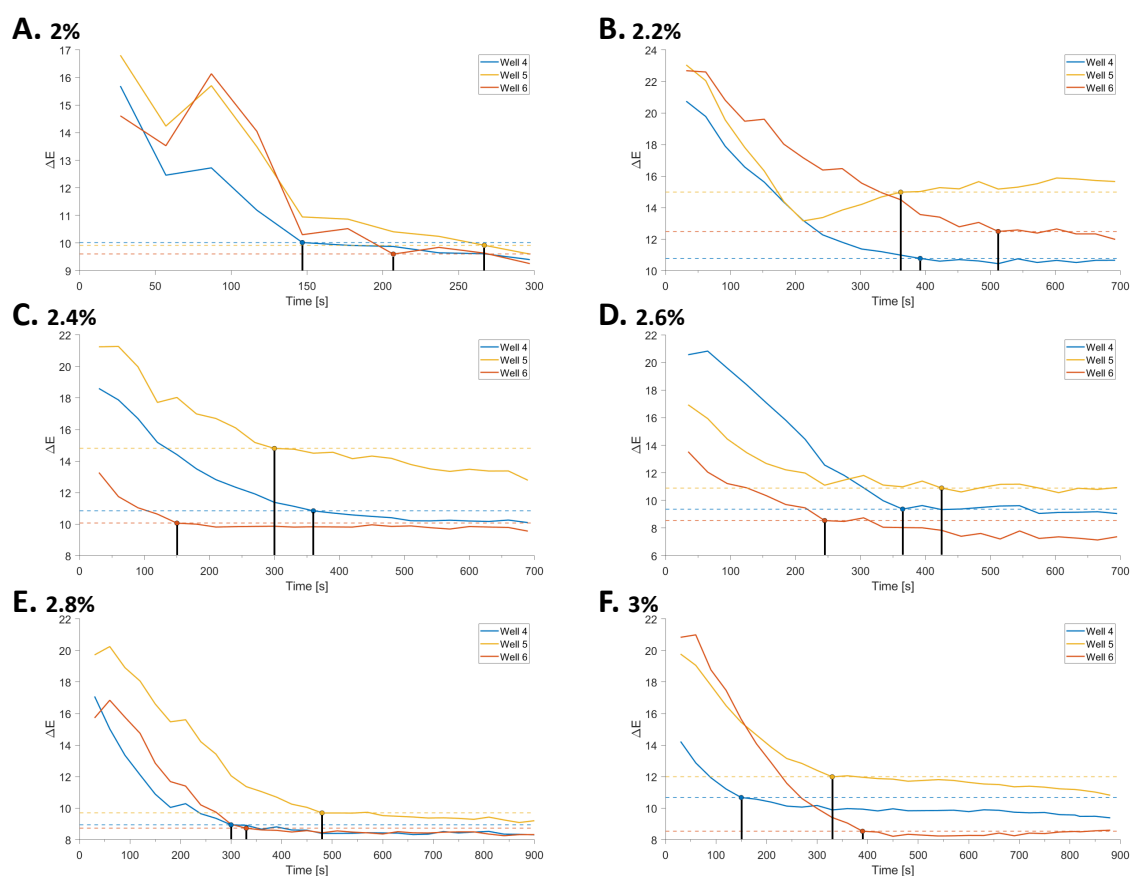


Figure 5.5: Mean ΔE curves against Well control 2 of 6-mm pullulan discs with concentrations between 2% and 3%. Pullulan tablets were created using the volumes indicated in Table 2.11. Experiments were run in triplicate ($n = 3$), well 4, 5 and 6. The dots indicate the point of the curve where the plateau of the signals commence. The black vertical lines indicate the time at which the plateau started on the y-axis (time-to-plateau).

5.1.2 Microfluidic Device Development

The 3D plastic cassette was assembled as explained in Section 2.16.2.1, and three poly(methyl methacrylate) (PMMA) layers were stacked on each other using a simple liquid phase solvent bonding process with acetone (Fig. 2.21). Acetone was pipetted onto the first PMMA layer and a second layer contacted it. The process was repeated

for the third layer on top of the second. Pressure was applied to enhance the solvent-induced softening of the interface and to facilitate the interdiffusion of polymer chains across the interface, which resulted in bonding each pair of layers [192]. Acetone and PMMA have a very similar Hildebrand solubility parameters (δ 20.4 MPa^{1/2} for acetone and δ 20.1 MPa^{1/2} for PMMA) [193], which suggests that pure acetone aggressively dissolves PMMA causing poor bonding uniformity and microchannel deformation [192]. However, in our application these do not represent a limitation as there is no need for good control of channels' geometry and edges. This also allowed us to apply low pressures to ensure the PMMA bonding, about 26 kPa (derived as described in Appendix A.2), which is very low compared to the pressure used in [192]. The simplicity and rapidity of this method was prioritised over the cited limitations.

As explained in Section 2.16.2.1, the first and second layers (from the bottom) were created from a 2-mm thick PMMA sheet. The second layer of the device accommodates the waste container, and the first layer was used to seal the bottom of the waste container. Figure 5.6 provides the dimensions of the first and second PMMA layers used for the POC device.

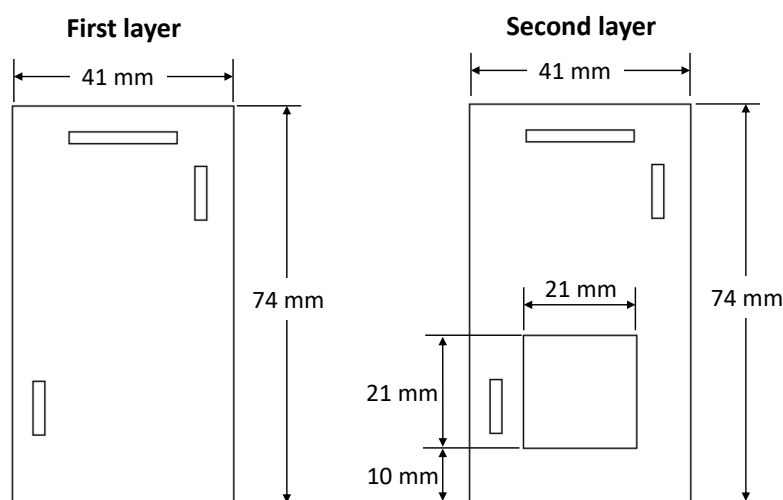


Figure 5.6: **Dimensions of the first and second layer of the point-of-care device.** The dimensions of the two layers shown were used to laser cut two 2-mm thick PMMA sheets.

The waste container is a square with dimensions 2.1×2.1 cm² and it holds a 2×2 cm² square of Whatman[®] CF7. The absorbent pad was made of cotton linter CF7, which had a thickness of about 1,870 μ m, close to the desired 2 mm. The pad needed to absorb around 600 μ L of waste (100 μ L from the sample and 500 μ L from the washing buffer) without leaking. To find the optimal size of CF7, three squares of 1×1 cm², 1×2 cm², and 2×2 cm² were tested with 650 μ L of dyed water. The 2×2 cm² square

was the only one that did not leak any liquid, so it was selected as the absorbent pad. The third layer was created from a 4-mm thick PMMA sheet. The central chamber in the third layer was shaped into a 5-mm diameter well to accommodate the two 5-mm Whatman[®] Grade 3 discs for the sample preparation, as a result of the best performing paper-based DNA extraction (Section 3.1.7). The 4-mm thickness of the third layer (*Height*) was derived by the simple volume formula $Volume = Height \times \pi \times Radius^2$ where the volume was 100 μL (sample volume) and the radius was 2.75 mm. A diameter of 5.5 mm was considered in this calculation for the central chamber to account for laser cutting inaccuracies.

The initial design tested was **a** (Fig. 5.7), followed by three variations of **b** (Fig. 5.7) to explore the feasibility of drying pullulan on the device (as explained in Section 2.16.4.1). To stop liquid from overflowing into adjacent channels, an abrupt geometry change in the microchannels was generated by incorporating 2-mm-diameter wells in the channels [194]. Moreover, the diameter of the washing chamber was set to 8 mm to accommodate the addition of a blister pouch containing 500 μL water (Microfluidic ChipShop, Jena, Germany) to easily introduce the washing buffer in the device. This pouch would be mounted on the plastic cassette with a ring of double sided adhesive tape above the washing buffer unit, and it would allow to avoid the use of pipettes. During prototyping development, however, the blister pouch was not used.

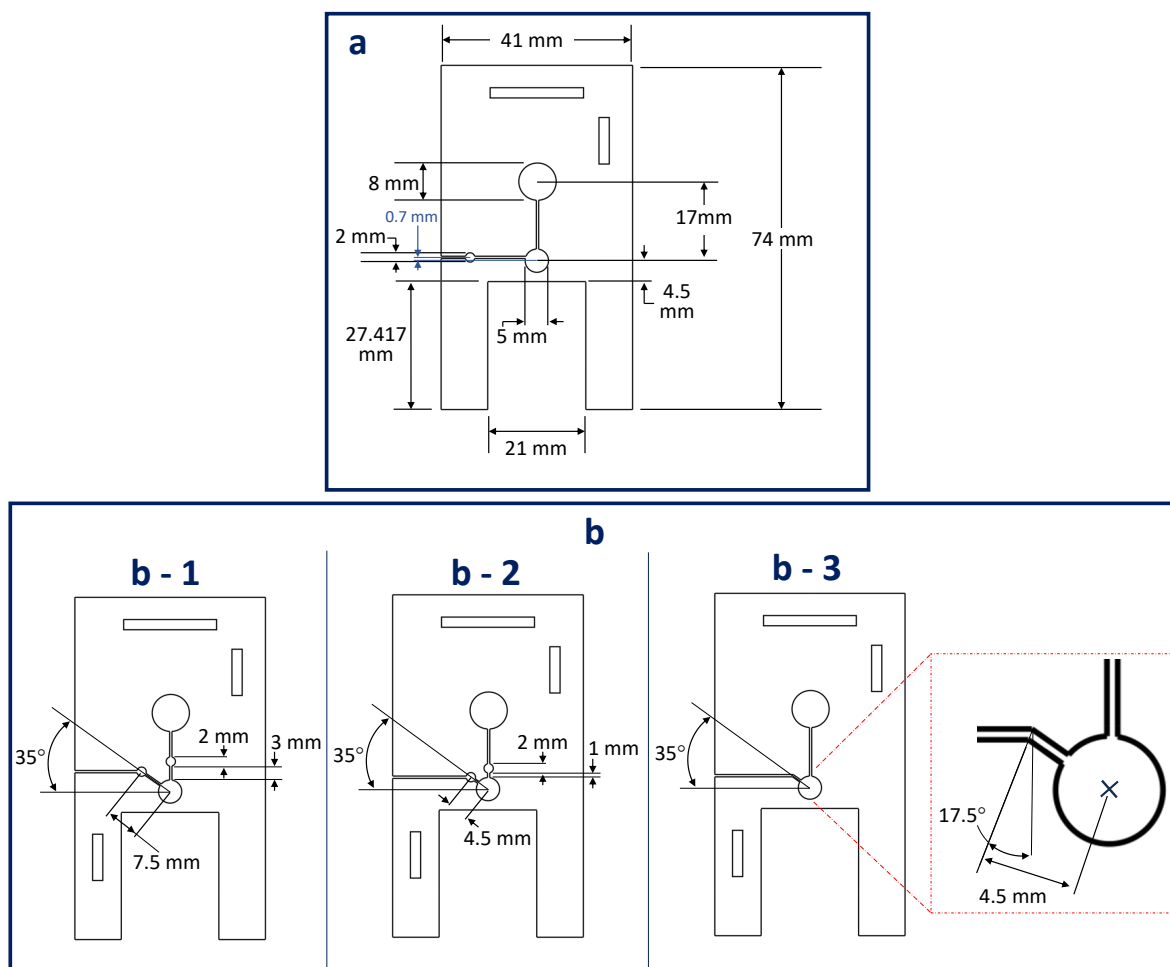


Figure 5.7: **Dimensions of the third layer of the POC device: designs a and b.** The dimensions of the third layer for design **a** and **b** are provided. All channels have a width of 0.5 mm. All the wells added to the channels have a diameter of 2 mm. When dimensions are not indicated, it means that they are the same as the previous version.

Polydimethylsiloxane (PDMS) was used to seal the central chamber (as shown in Fig. 2.27) to create the bottom pullulan tablet directly into the chamber. The results in Fig. 5.8 shows that the addition of small wells is not always necessary to stop the fluid flow before drying and that none of the presented variations allowed the drying of pullulan inside the device. Therefore, design **b - 3** with simple straight channels was chosen for studying pullulan incubation as described in Section 2.16.4.2. Moreover, it was not possible to dry pullulan directly inside the device because pullulan did not form uniform tablets, but it accumulated at the edges of the wells/channels. The different drying pattern of pullulan tablets inside the device and on glass slides is associated with a combination of phenomena, such as the Marangoni and capillary flow, convection and evaporation [195], and it depends on the substrate wettability [196]. To avoid PMMA surface treatment and additional device assembly complexity, drying pullulan tablets on glass slides was carried on.

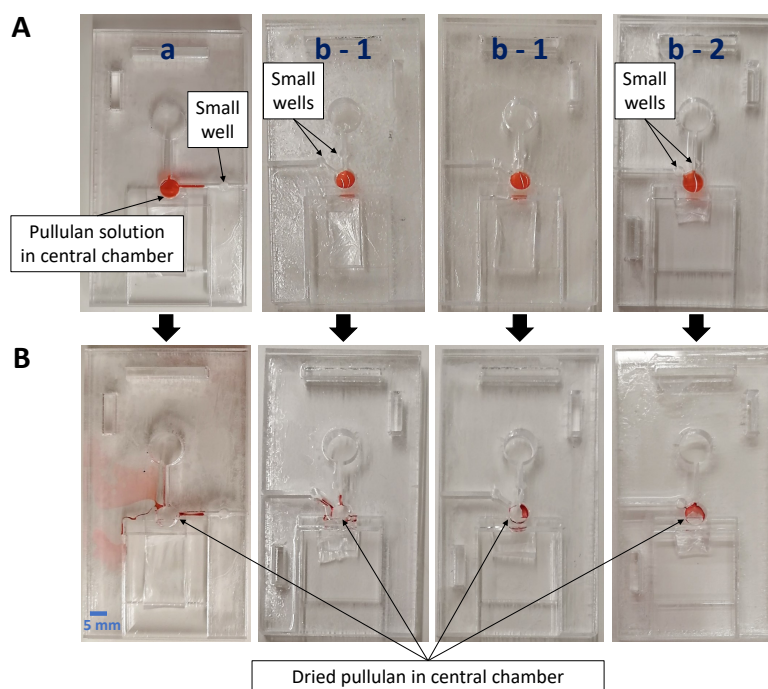


Figure 5.8: **Results of drying pullulan inside the point-of-care device.** Designs **a**, **b - 1** and **b - 2** were used to dry pullulan directly inside the central chamber, with the help of PDMS. Pictures taken as soon as the pullulan solution was inserted in the central chamber are given in **A**. Pictures were taken after about 4 days of drying, bottom panel (**B**).

The incubation times provided by 6-mm pullulan discs containing 2%, 2.2%, 2.6%, and 2.8% (w/v) pullulan are shown Fig. 5.9. 100 μ L of 1 g/L xylene cyanol solution was introduced as sample to best visualise when the sample started flowing in the absorbent pad (as explained in Section 2.16.4.2). 6-mm diameter pullulan discs were chosen over 5-mm discs because they were able to cover the whole bottom surface of the central chamber. In fact, the central chamber had a diameter larger than 5 mm due to laser cutting inaccuracies, and the pullulan discs shrank slightly when they dried on glass slides. As a result, the discs with a diameter of 5 mm did not fit the central chamber well.

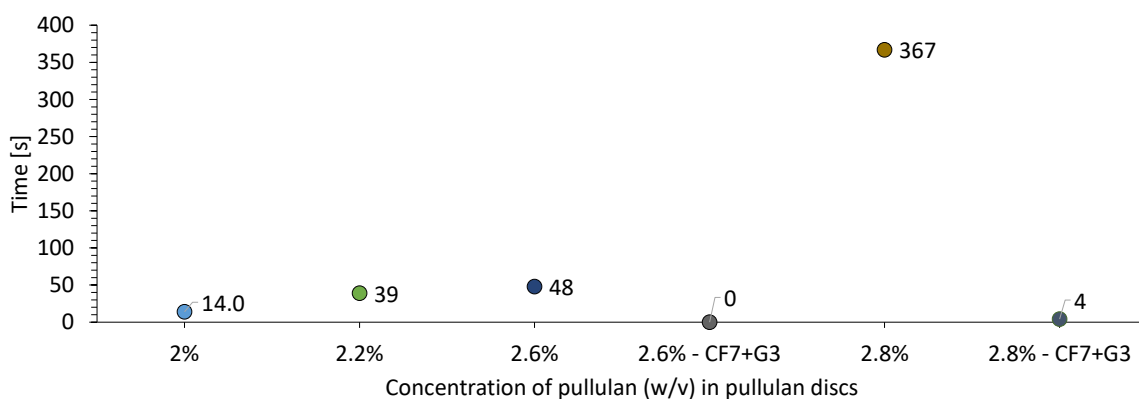


Figure 5.9: **Results of incubation time provided by pullulan discs on POC device.** 6-mm pullulan discs with 2%, 2.2%, 2.6%, and 2.8% (w/v) pullulan were created (Section 2.16.3.2) and inserted into the central chamber. Above the pullulan disc two 5-mm paper-discs were added. The time between when the sample reached the central well and when it starts flowing into the absorbent pad (incubation time) was recorded in seconds, as explained in Fig. 2.28. When using discs with 2.6% and 2.8% the addition of Whatman[®] Grade 3 in the waste container was also tested (2.6%-CF7+Grade 3 and 2.8%-CF7+Grade 3).

The incubation time results show that 2.8% pullulan disc allows for the longest incubation time (367 s = 6 min and 7 s) when the absorbent pad is only composed of CF7 paper. This incubation time corresponds to the 6 minutes of incubation between the *E. coli* sample and the paper-discs needed to perform the paper-based DNA extraction described in Sections 2.14.3, and 3.1.9, and to what it was observed in Section 5.1.1. All the other pullulan discs allow for an incubation time shorter than a minute. This is partially connected to their faster dissolution, but mostly to a bad displacement of the discs inside the central chamber of the device. In fact, all the discs showed a dissolution time higher than 1 min in Section 5.1.1.

Pictures after incubation and after washing the paper discs in the central chamber were taken for different pullulan discs concentrations, and they are given in Fig. 5.10. These pictures were captured to observe the behaviour of pullulan tablets and if the washing was bringing to a change in the colour of the discs after washing. 100 μ L of 1 g/L xylene cyanol solution was introduced as sample and the washing was performed using 500 μ L of nuclease-free water (NFW). After washing the two paper discs are expected to have a lighter blue colour than before washing.

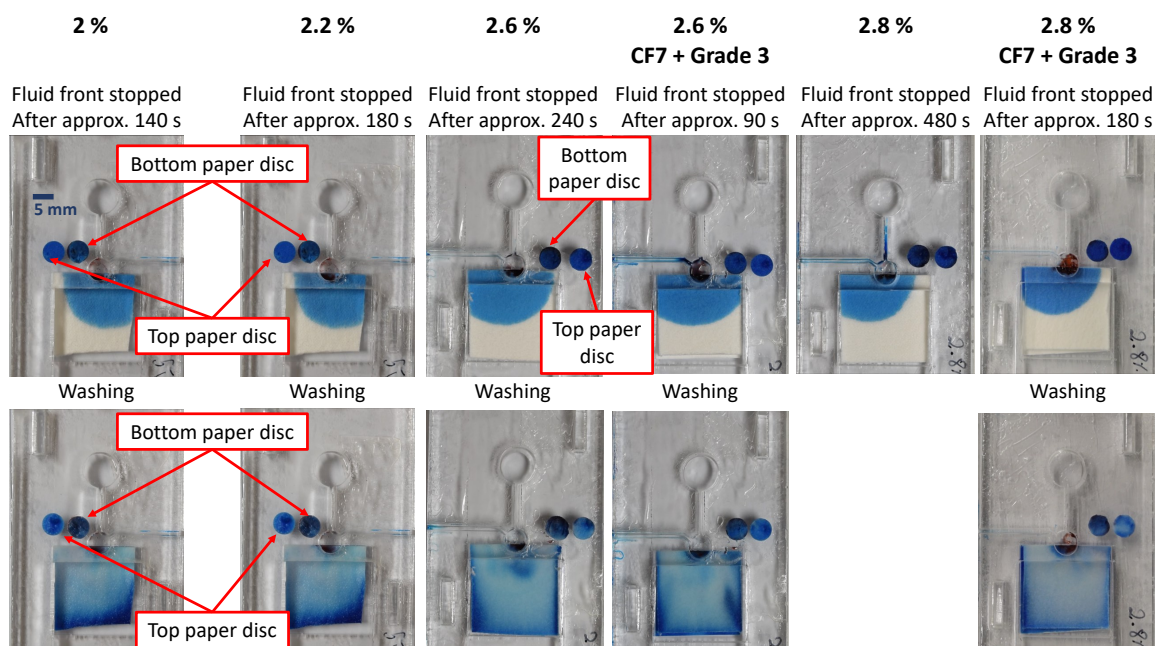


Figure 5.10: **Pictures of paper-discs soon after the fluid front in the absorbent pad stops and after washing.** 6-mm pullulan discs with 2%, 2.2%, 2.6%, and 2.8% (w/v) pullulan were used and inserted into the central chamber. Above the pullulan disc two 5-mm paper-discs were added. For each pullulan disc two pictures were taken: soon after the fluid front stopped flowing into the absorbent pad (upper panel) and after washing the paper discs with 500 μL of nuclease-free water (bottom panel). When using discs with 2.6% and 2.8% the addition of Whatman[®] Grade 3 in the waste container was also tested (2.6%-CF7+Grade 3 and 2.8%-CF7+Grade 3). In all the pictures the bottom disc is the one located closest to the central chamber.

Fig. 5.10 (upper panel) shows that after the fluid front of the sample has stopped flowing in the absorbent pad, the bottom pullulan tablet is fully dissolved (upper panel). However, this is not true when an additional layer of Whatman[®] Grade 3 is added into the waste container below the usual CF7 absorbent pad (‘2.6%-CF7+Grade 3’ and ‘2.8%-CF7+Grade 3’ pullulan tablets in Fig. 5.10). The extra paper layer increases the chance that the absorbent pad comes in direct contact with the paper discs in the central well (especially if the pullulan tablet is not well placed), which leads to a shorter incubation time and the liquid reaching the absorbent pad before the tablet dissolves completely. Fig. 5.10 (bottom panel) show the two discs taken out of the central chamber after washing them, for each concentration of pullulan discs. From the pictures the top paper disc appears slightly lighter than before washing (upper panel) in all the pictures, while the bottom paper discs do not appear to undergo a significant change in colour. A possible explanation for the small difference in colour of the bottom disc might be that the disc has absorbed some pullulan solution from the pullulan disc underneath it, which affects its colour change or rinsing. All in all, the washing appears to be working on the device as most of the blue dye (sample) is

pushed towards the edge of the absorbent pad by the NFW. No images are presented for the 2.4% pullulan discs because the sample failed to reach the absorbent pad even after 12 minutes of waiting, possibly due to a faulty placement of the pad in the waste container.

Therefore, given the results shown in Figures 5.9, 5.10, that match the dissolution results from Section 5.1.1, pullulan discs of 2.8% were chosen as bottom pullulan layer inside the purification & amplification unit. The results in Figures 5.9, 5.10 were obtained using pullulan tablets the day after they were fully dried (4 days). The incubation time was computed for a 6-mm pullulan disc containing 2.8% pullulan about 10 days after it was fully dried. The incubation time was of 0 seconds as the sample flowed into the absorbent pad while it was still being pipetted into the sample inlet. This behaviour suggests that the pullulan disc was not well placed inside the device, and that the properties of the pullulan tablet can change if not stored properly in a well-sealed container. This is in contrast from what shown previously in the literature where pullulan is shown to have low moisture permeability [73, 119], but it is in line with what observed when reagents were stored in pullulan tablets in improperly sealed devices in Section 4.1.5.

During incubation, it was observed that some sample flows into the channel connecting the washing buffer unit with the central chamber (Fig. 5.11A). The abrupt change in geometry prevented the sample to get into the washing unit, and once the pullulan was dissolved, the capillary force led the liquid into the absorbent pad. This implies that some of the sample (in the sample & resuspension channel and in the channel connecting the washing unit with the central chamber) is not properly incubated with the paper discs. However, from a fluidic perspective the overflowing inside other channels does not represent a major concern. To avoid overflowing, the washing buffer (NFW) should be added gradually to the washing buffer unit, so that it can soak into the absorbent pad. If the washing buffer is not introduced slowly, Fig. 5.11B, it will fill up the central chamber and overflow in the adjacent sample & resuspension inlet. Even though this is not desirable, the overflowing in the inlet can help cleaning some remaining sample in the inlet after the absorbent pad has absorbed it.

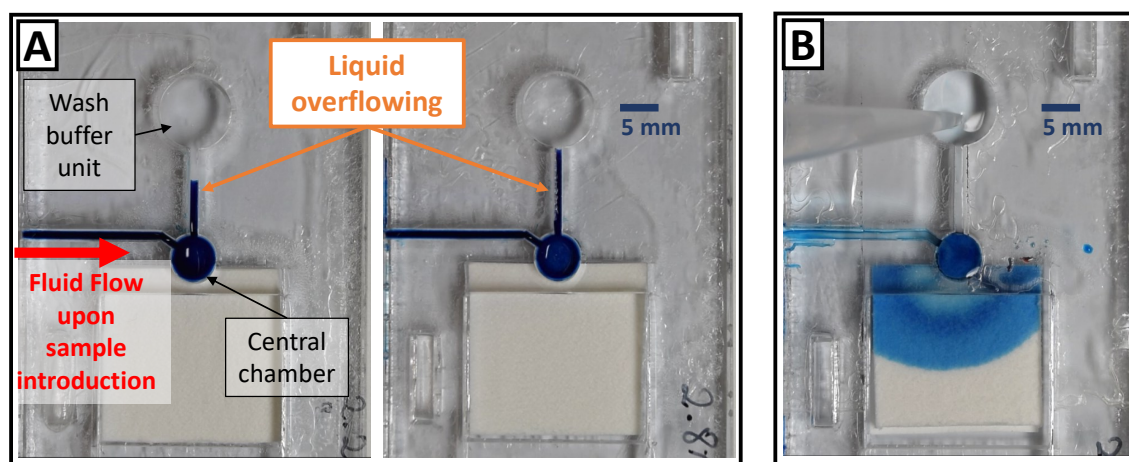


Figure 5.11: **Examples of liquids overflowing in adjacent channels inside the POC device, during sample incubation and washing.** **A.** Sample overflowing in the channel connecting the washing buffer unit and the central chamber during incubation. **B.** Washing buffer overflowing in the sample & resuspension inlet during washing.

Designs **b - 1** and **b - 3** were also used to experiment some extra features, such as wetting the bottom part of the central chamber to facilitate adherence of the bottom pullulan disc and applying a thin glue layer in the sample inlet channel. To wet the bottom part of the central chamber a paper disc was fully imbibed with NFW and pressed against the bottom of the central chamber using tweezers. 20 μL of super glue (Cyanoacrylate 20 g, RS PRO, RS Components Ltd., Northants, UK) were added to the sample channel to understand if lifting up the channel would allow to reach the paper discs without interfering with the pullulan tablet at the bottom. A pipette was used, and the glue was inserted from the side, in the same way the sample specimen is added at the sample inlet. The super glue was let dry for 1 hour before the device was ready to be tested. For these experiments a 6-mm pullulan disc containing 2% pullulan was used. The incubation times when using the normal device and the two variations, with additional glue and central chamber wetted are given in Fig. 5.12.

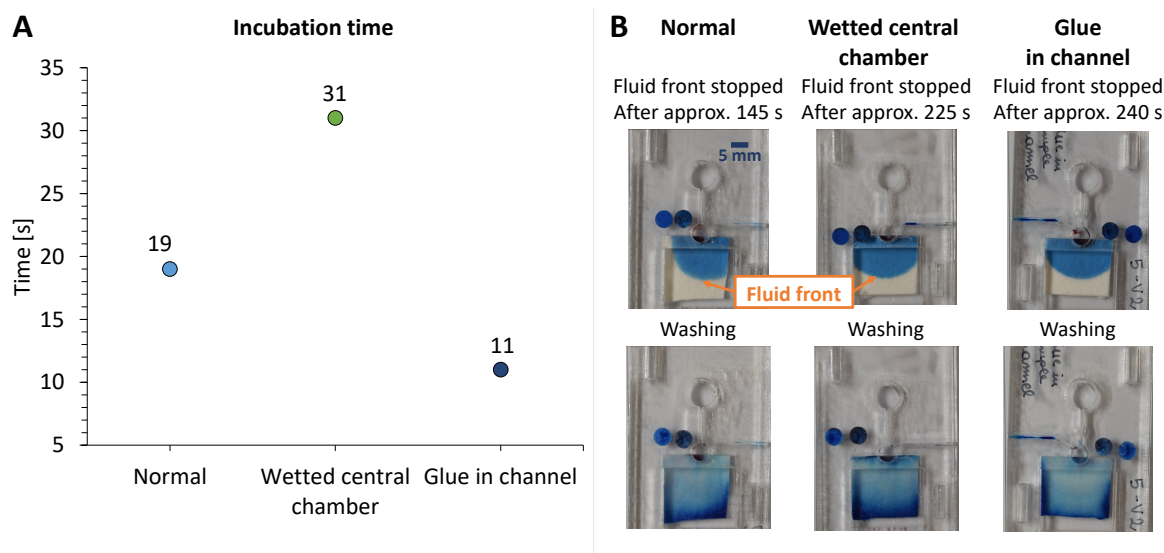


Figure 5.12: **Results of incubation time provided by a 2% pullulan disc on POC device with either pre-wetted central chamber or addition of glue in the sample inlet.** A 6-mm pullulan disc with 2% (w/v) pullulan was created (Section 2.16.3.2) and inserted in the central chamber using tweezers. Two 5-mm paper discs were added on top of the pullulan disc. The incubation time was computed as the time between when all the sample is pipetted into the device and when it starts flowing into the absorbent pad, as explained in Fig. 2.28. Incubation times are compared among a device in which the pullulan disc was added as usual (Normal) or after pre-wetting the central chamber (Wetted central chamber), and with a device in which the sample inlet contains a thin layer of glue (Glue in channel). **A.** Incubation time results for the different devices ($n = 1$). **B.** Pictures of paper-discs soon after the fluid front in the absorbent pad stops (which would correspond to the end of step (ii) in Fig. 2.20) and after washing (after step (iii) in Fig. 2.20). In all the pictures the bottom disc is the one located closest to the central chamber.

The results show a higher incubation time when the central chamber is pre-wetted (31 s) than when the pullulan disc is inserted in the chamber as usual (14 s). This suggests that wetting the lower part of the chamber might increase the adherence of the pullulan tablet to the walls and bottom part of the central chamber, thus preventing any liquid leakage into the absorbent pad before the pullulan disc is fully dissolved. The methodology used by Jahanshahi-Anbuihi *et al.* [123] for preparing multiple layers of pullulan films by applying 0.5 μL of a 20% (w/v) pullulan solution between them was not used for two reasons: (1) the aperture between the second and third layer of the device would have caused the 20% pullulan to be absorbed by the absorbent pad underneath, and (2) we wanted to avoid the addition of high pullulan concentrations in the purification & amplification unit because it was previously observed that high concentrations of pullulan can lower the limit-of-detection of the assay (Section 4.1.3.2). Additionally, as seen in Fig. 5.12B, the third layer design, which was used when the sample inlet had a glue layer, prevented some of the sample from flowing into the absorbent pad. This is mainly due to the presence the small $\varnothing 2$ mm well in the sample inlet. After washing, the same amount of sample remained in the initial part of the

channel, because the $\varnothing 2$ mm well blocked the washing buffer from overflowing in the sample channel beyond the small well. This does not happen when using the design used for the ‘Normal’ and ‘Wetted’ central chamber (Fig. 5.12). In these devices the sample is washed away from the sample inlet after washing (bottom panel) compared to after the pullulan disc has fully dissolved (upper panel). We believe that this is more related to the geometry of the device, rather than the presence of the thin glue layer.

To enhance further pullulan incubation duration, the second PMMA layer was modified to reduce the opening between the third and second layer as shown in Fig. 5.13. However, the reduction of the opening prevents the liquid from flowing from the third to the second layer. After more than one hour the sample from the central chamber was not able to flow into the absorbent pad, even if the bottom pullulan disc was clearly dissolved. This showed how the fluids flow is very sensitive to even minor changes inside the device.

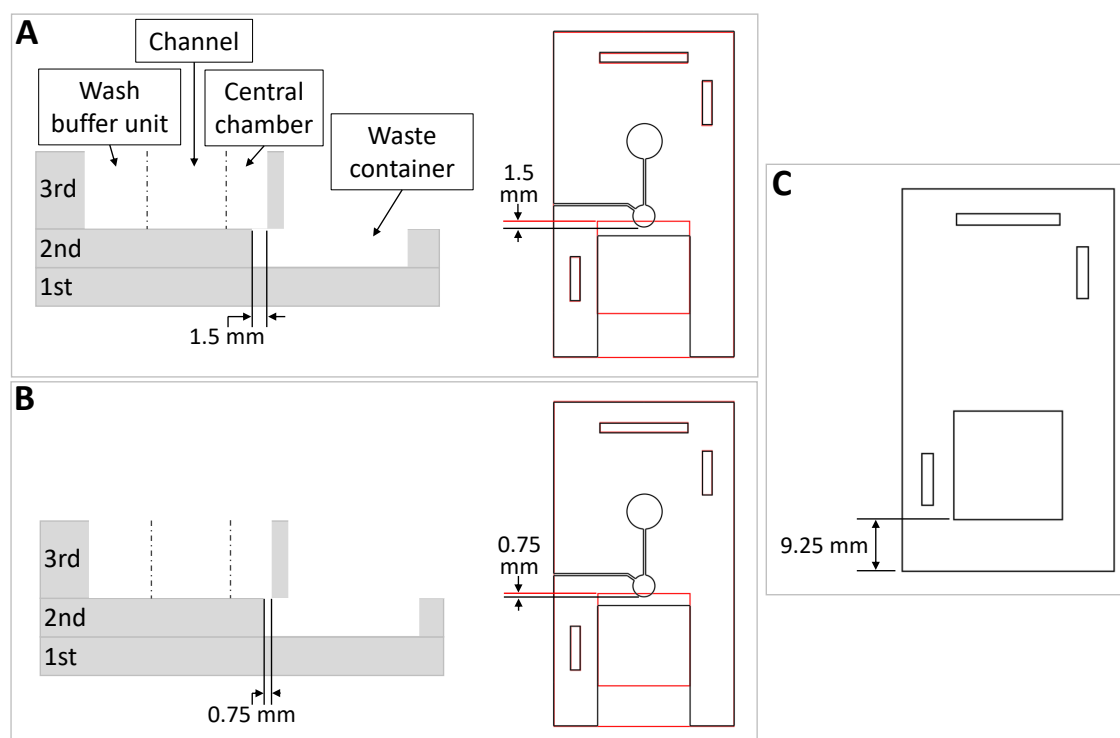


Figure 5.13: **Dimensions of the second layer of the point-of-care device that reduces overlap between central chamber and waste container. A.** Cross section of three PMMA layer (left) and top side (right). The overlap between the central chamber and the waste container is 1.5 mm. **B.** Cross section of three PMMA layer (left) and top side (right). The overlap between the central chamber and the waste container is 0.75 mm. **C.** Dimensions of the second layer that reduces overlap between central chamber and waste container.

Design **b - 3** was also used for testing the full device operation as described in Section 2.16.4.3. 0.02 g/L of xylene cyanol solution were introduced in the device through

the lateral tubing. Once all the sample was pipetted into the device, incubation was allowed for 6 minutes, during which time the sample flowed into the absorbent pad. 500 μL of NFW were added into the washing buffer unit, very slowly and the paper discs were washed. After about 2 minutes, the device was flipped and tapped to move the paper discs to the bottom of the central unit. 50 μL of NFW was added to dissolve the mimicking LAMP reagents, and then the device was placed on a heat block at 66 $^{\circ}\text{C}$. After two hours, the central chamber was opened to check if any liquid was available to run on LFSs. This was done in duplicate (two devices) and some pictures taken during the device operation are given in Fig. 5.14. One of the challenges we faced was the paper movement at the bottom of the central chamber, sometimes it got stuck (Fig. 5.14E, F) and prevented the full contact and immersion in the resuspended LAMP reagents. In the device using real reagents, this would lead to lower LAMP performance due to improper DNA elution from the paper discs into the LAMP mix. 25 μL were too little to resuspend the mimicking LAMP reagents as they would hardly reach the central chamber and remain in the sample & resuspension inlet. To overcome this, 50 μL of NFW water were used for resuspension, and air was pushed through the pipette so that no liquid remained in the channel. The use of 50 μL implies that the amount of LAMP reagents in the final device need to be adjusted to have a final reaction containing 50 μL , that would lead to increasing costs of the device. A second issue was evaporation, as can be observed in Fig. 5.14C, D, where condensation can be observed on the adhesive film covering the absorbent pad. The resuspended LAMP mix tends to evaporate quickly in the device, leaving not enough liquid to run on the lateral flow strips. This would compromise the accuracy and reliability of the results. Therefore, other designs of the third PMMA layer were introduced to reduce evaporation as much as possible by reducing the ‘free’ space available in the device.

Reduction of the internal spaces that remained available for reagent evaporation after reagent resuspension and heating was investigated. For this purpose the device designs **c**, **d**, **e** were developed (Figures 5.15, 5.18). When these designs were tested, the purification & amplification unit consisted of a 2.8% pullulan bottom disc, two 5-mm Grade 3 paper discs, 3% pullulan top disc, one 5% pullulan tablet and one 10% pullulan tablets (as described in Section 2.16.4.2). The latter pullulan tablets were used to mimic the presence of LAMP reagents in the central chamber. Pictures were taken to understand if they underwent undesired dissolution during the sample preparation

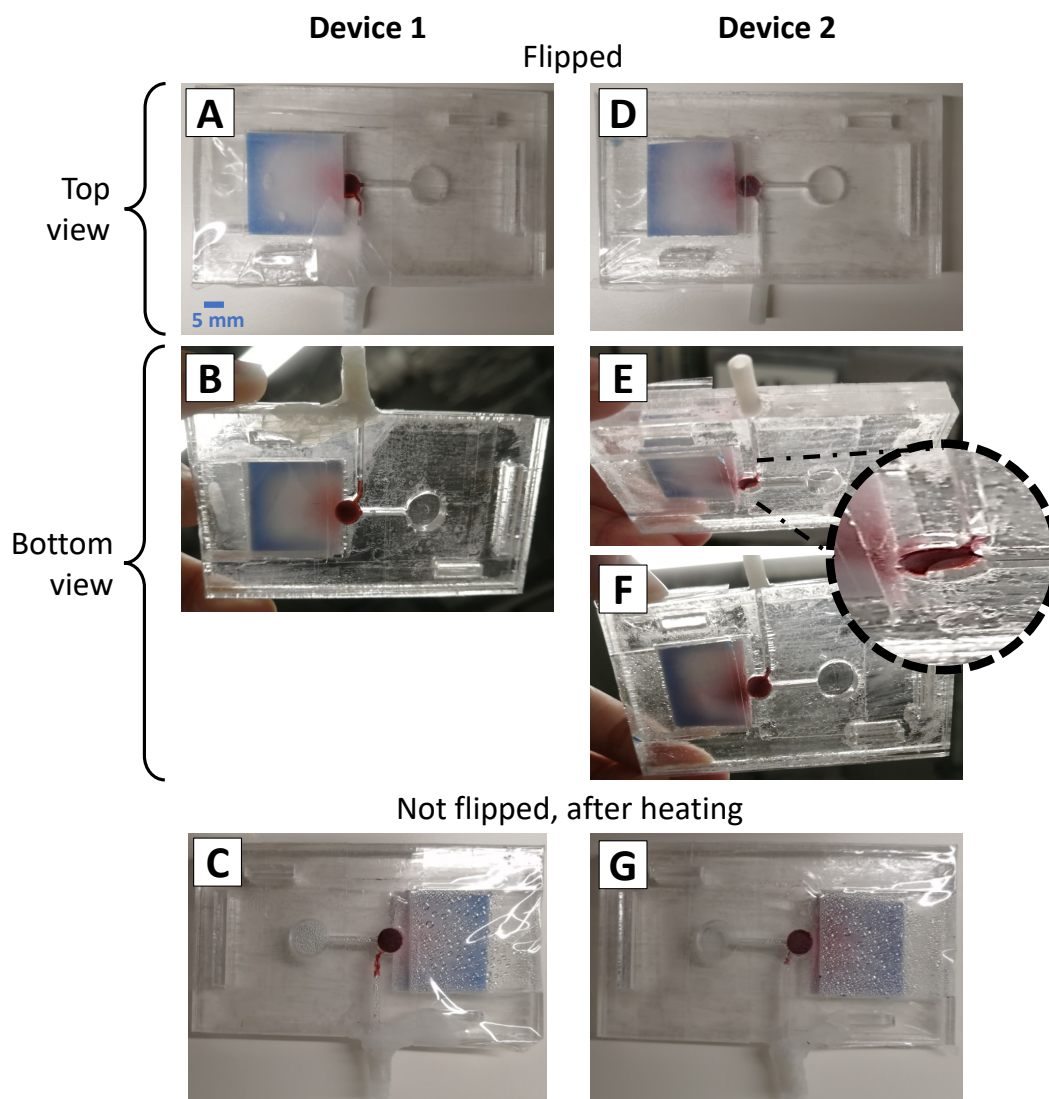


Figure 5.14: **Results of full device operation (design b - 3)**. Design b - 3 was used for testing the full device operation, from sample loading to heating. The experiment was run in duplicate and pictures were taken for device 1 (A-C), and device 2 (D-G). After loading the resuspension buffer, both devices were flipped and tapped to let the paper discs reach the (now) bottom of the central chamber. For each device, pictures were taken of the top-view (A, D) and of the bottom view (B, E, F). A zoom in of the central chamber of E is provided to clearly visualise that the paper discs were not properly placed at the bottom of the chamber after tapping. After two hours of heating at 66 °C, the two devices were flipped back in the initial position (not flipped) and picture C and G were taken for device 1 and 2, respectively.

and washing procedure.

The first efforts were moved towards reducing the channel width and washing buffer unit diameter as shown in the designs c - 1, - 2, - 3, - 4, - 5 (Fig. 5.15). The width of the channels was reduced from 0.5 mm to a thin line of approximately 0.2 mm. Three different scenarios were tested: one where both the sample and the washing channels were reduced c - 1, one where only the washing channel was reduced c - 2, and one where only the sample inlet was reduced c - 3. The washing buffer unit diameter was

reduced from $\varnothing 8$ mm in **b** to $\varnothing 5$ mm in **c - 1, - 2, - 3, - 5** and to $\varnothing 3$ mm in **c - 4**.

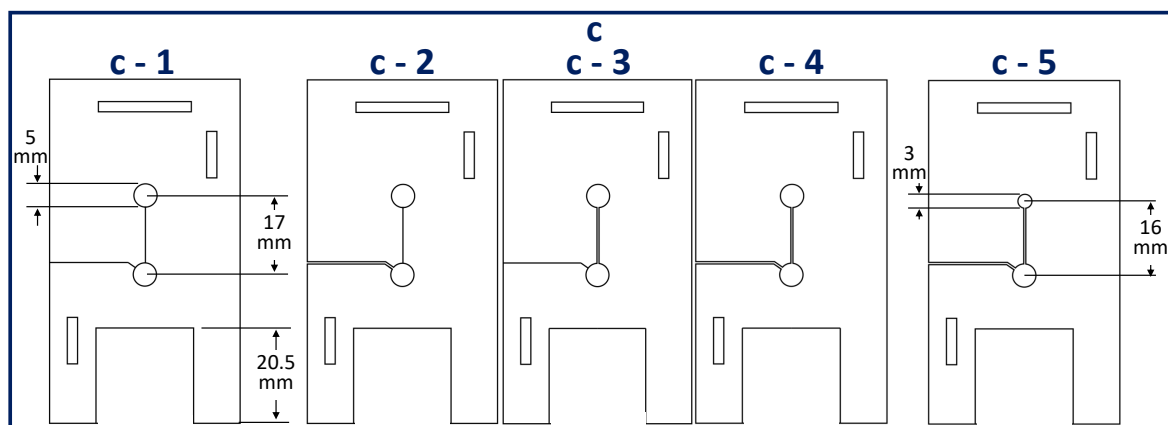


Figure 5.15: **Dimensions of the third layer of the POC device: designs c.** The dimensions of the third layer for design **c** are given. All the channels in **c - 1** have a width of 0.2 mm. In **c - 2**, the sample & resuspension channel is 0.5 mm wide, whilst the channel connecting the washing unit to the central chamber has a width of 0.2 mm. In **c - 3**, the sample & resuspension channel is 0.2 mm wide, and the washing channel has a width of 0.5 mm. All the channels in **c - 4** and **- 5** have a width of 0.5 mm. The washing unit in **c - 1, - 2, - 3, - 4** has a diameter of 5 mm. The washing unit in **c - 5** has a diameter of 3 mm. The central chamber and sample & resuspension channel of **c** have the same dimensions as **b - 3**, indicated in Fig. 5.7. The outer dimensions and the distance of the central chamber from the bottom edge are the same as **a** (Fig. 5.7).

The results in Figures 5.16, 5.17 show that when the channels width is reduced to 0.2 mm, the liquid is not often able to flow through the channels (designs **c - 1, c - 3** Fig. 5.16). This is probably due to the liquid phase solvent bonding process chosen to stack PMMA layers. As explained above, the strong solvent effect of acetone on PMMA causes microchannel deformation [192]. When microchannels have a width of 0.5 mm, the potential deformation of the PMMA can be neglected as the fluid flows through them. However, this assumption may not hold for microchannels that are 0.2 mm wide. The dissolution of the PMMA in these narrower channels could cause them to become blocked.

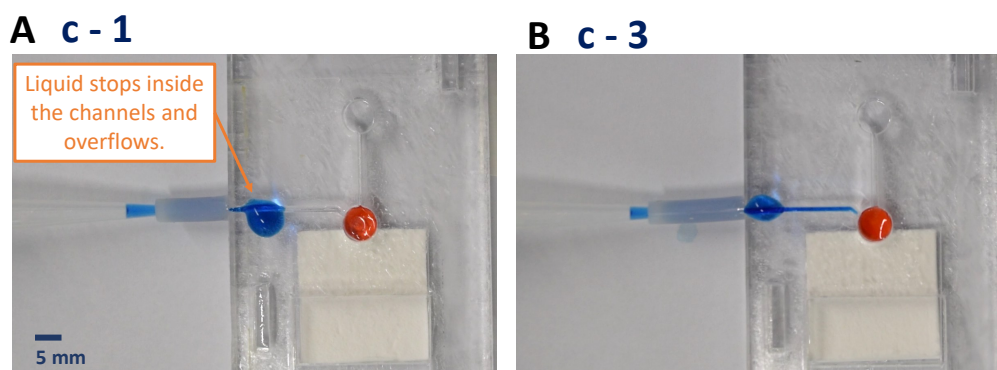


Figure 5.16: **Results of designs c - 1 and c - 3 testing.** **A.** Sample is introduced in the sample inlet of **c - 1**. **B.** Sample is pipetted in the sample inlet of **c - 3**.

However, when the flow in the 0.2 mm wide channels is possible, like in design **c - 2** (Fig. 5.17A), it is harder to control that the washing buffer does not go above the top 3% pullulan disc, causing unwanted dissolution of LAMP mimicking reagents. For example, Fig. 5.17A shows pictures taken (1) before the sample was introduced, (2) as soon as all the sample was pipetted inside the device from the sample inlet, (3) 3 and (4) 5 minutes after sample introduction, and (5,6,7) during the washing. The small movement of one LAMP tablet that can be observed in Fig. 5.17A1-4 demonstrates the initial dissolution of the 3% top pullulan disc and potential unwanted dissolution of the second LAMP tablet. Washing buffer (NFW) overflowing above the upper pullulan disc can be observed in Fig. 5.17A5-7. Fig. 5.17A8, shows that one LAMP tablet is not dissolved yet (10% pullulan tablet held with tweezers), while the second LAMP tablet (5% pullulan) is dissolved. The top pullulan disc, however, is not fully dissolved. This is evident from the difference in colour of the two discs in picture 8, with the top disc being intense red. The poor control of liquid flow and higher risks of blockages in 0.2 mm-wide channels, 0.5 mm-wide channels were used for further studies. This channel width also allowed us to keep the simple and quick liquid phase solvent bonding process to bond PMMA layers.

Controlling that the washing buffer did not exceed the upper limit of the 3% pullulan disc was very challenging also with design **c - 4** (Fig. 5.17B3). The 3 mm-diameter of the washing buffer unit requires very small amounts of washing buffer to be introduced in the washing unit. For example, adding 50 μL of NFW for 10 times is effective in not overflowing above the top pullulan disc. However, this manual operation is very cumbersome. Fig. 5.17B4 shows that only one LAMP tablet is not fully dissolved after washing. The second LAMP tablet (5% pullulan) is fully dissolved, whilst the top pullulan disc is not. In Fig. 5.17B5 the tweezers are holding the bottom edge of the upper paper disc, which reveals that the top 3% pullulan disc has not dissolved. This suggests that the second LAMP tablet may be trapped in the upper paper disc and did not reach the absorbent pad through the lower paper disc. The washing of paper discs was also tried on **c - 5** (5 mm-diameter of the washing buffer unit, Fig. 5.17C), but this time the waste container had three paper layers: Whatman[®] CF7, Grade 3, and Grade 1. The 5 mm-diameter of the washing buffer unit, allowed for a better control of washing unit flow to avoid it overflowing above the top pullulan disc. This led to both the LAMP tablets to not dissolve prematurely during the sample preparations step (Fig. 5.17C4). In fact, the top pullulan disc has not melted away on the upper

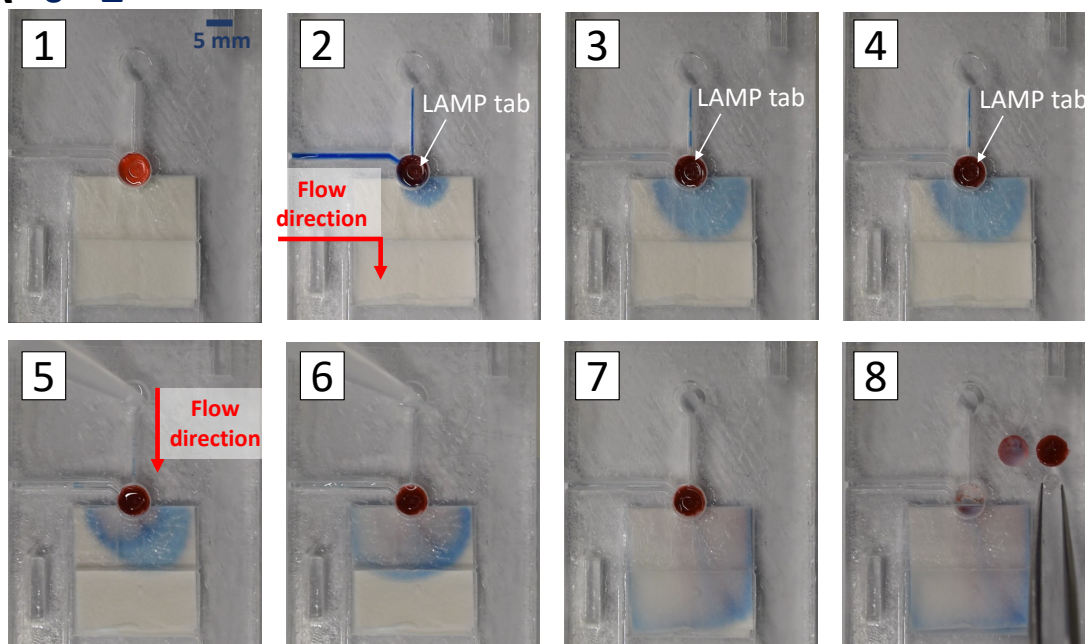
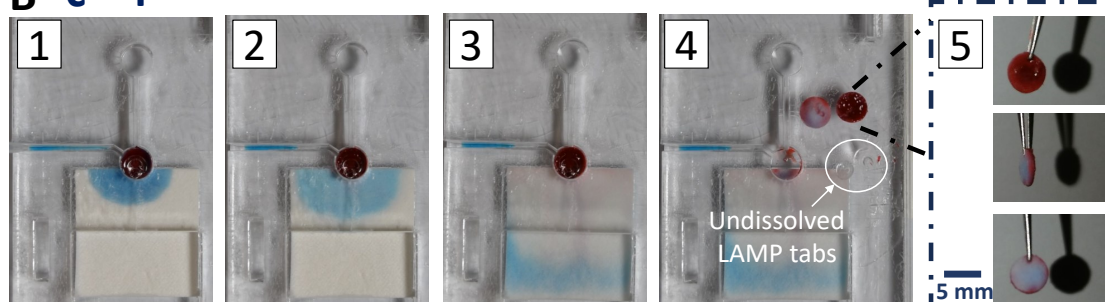
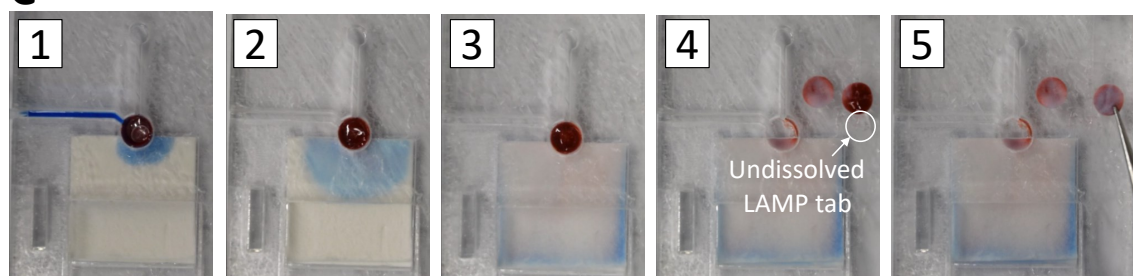
A c - 2**B c - 4****C c - 5**

Figure 5.17: **Results of designs c - 2 and c - 4 testing.** **A.** Pictures of **c - 2** were taken (1) before the sample was pipetted into the inlet, (2) as soon as all the sample was introduced in the device, (3) 3 and (4) 5 minutes after sample introduction, and (5,6,7) during the washing. Picture 8 shows the components of the purification & amplification unit left in the central well after washing. The components were taken out the central chamber using tweezers. The paper disc closer to the central chamber is the bottom disc. **B.** Pictures of **c - 5** were taken (1) as soon as all the sample was introduced in the device through the inlet, (2) 5 minutes after sample introduction, (3) when all the washing buffer was introduced in the device. Pictures 4 and 5 show the components of the purification & amplification unit left in the central chamber after washing. The components were taken out the central chamber using tweezers. The paper disc closer to the central chamber is the bottom disc. The tweezers in picture 5 holds the upper paper disc flipped upside down (top-red). **C.** Pictures 1-4 of **c - 4** were taken as for **c - 5**. Picture 5 shows the upper paper disc flipped upside down (top-red).

paper disc (Fig. 5.17C5). Therefore, a larger washing buffer unit is recommended for easier manual handling. However, a smaller washing unit of 3 mm diameter can reduce the space available for evaporation after heating. Moreover, there was no incubation of the sample by the 2.8% pullulan bottom tablet in the experiments with designs **c - 4** and **c - 5**.

A way to further reduce the space above the waste container was to add an extra piece of PMMA to fill the empty space on the third layer of designs **c - 4** and **c - 5**. PMMA cut outs of $21.5 \times 21 \text{ cm}^2$ were used and super glue was added at the edges to seal the cutout to the third layer. The feasibility of closing completely or almost completely the third layer was then investigated by creating designs **d** (Fig. 5.18).

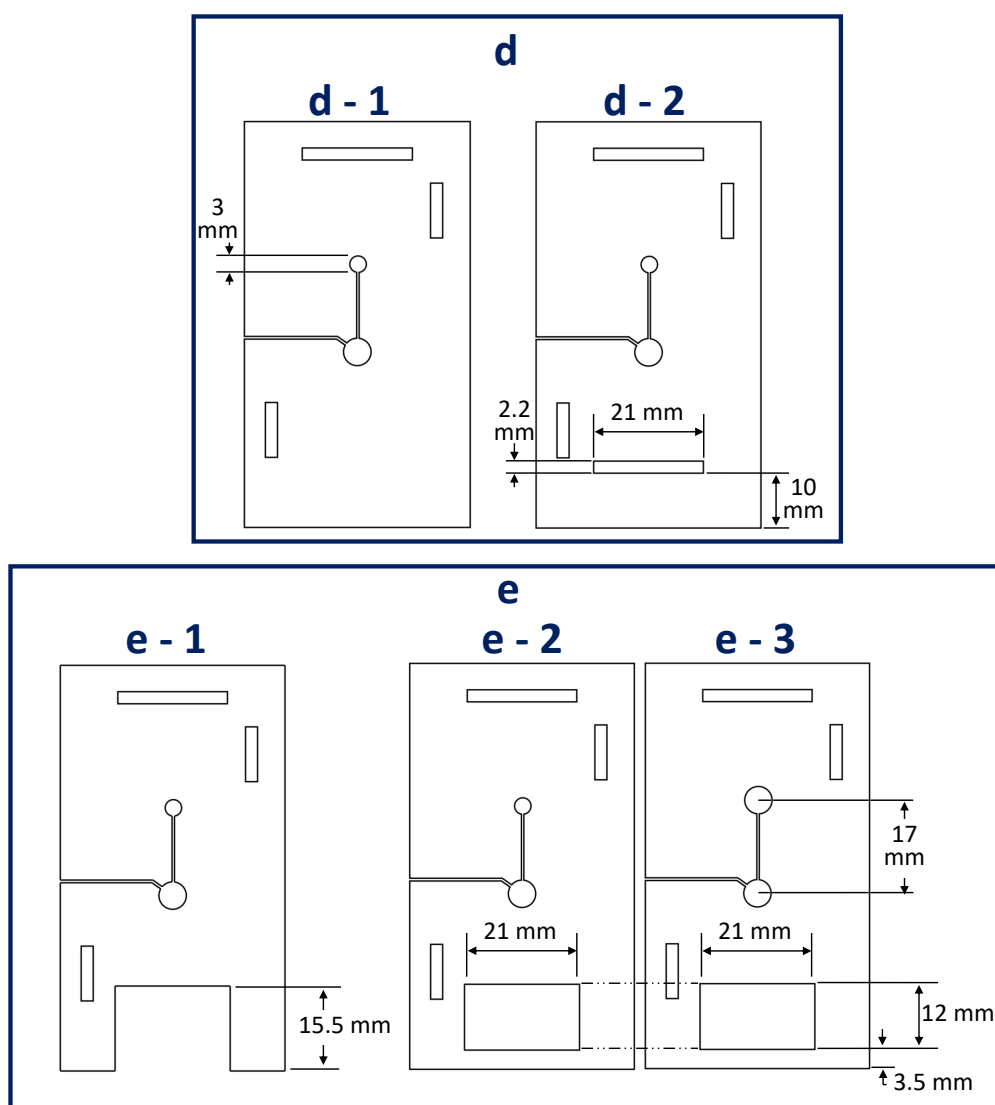


Figure 5.18: **Dimensions of the third layer of the POC device: designs d and e.** All the channels in have a width of 0.5 mm. In **c - 2**. The washing unit in **d**, and **e - 1**, - **2** has a diameter of 5 mm. The washing unit in **e - 3** has a diameter of 5 mm. The central chamber and sample & resuspension channel of **d** and **e** have the same dimensions as **b - 3** (Fig. 5.7). The outer dimensions and the distance of the central chamber from the bottom edge are the same as **a** (Fig. 5.7).

Since the third layer is closed and the absorbent pad cannot be inserted after assembling the PMMA layers, the assembly procedure described in Section 2.16.2.1 was adjusted. The absorbent pad was inserted after the first PMMA layer and second PMMA layer were brought together and before the addition of the third layer. When the third layer was sealed with the PMMA cutout and glue, the sample was not able to flow in the absorbent pad and incubation occurred for more than an hour. It was observed that some glue reached the absorbent pad below the cut-out ('c - 5 + glue' in Fig. 5.19), and this might have prevented proper flow conditions. When the device was fully closed (designs d), no fluid movement was observed. The absorbent pad showed signs of PMMA uptake, which might have blocked the flow (darker colour of the absorbent pad in 'd - 1' and 'd - 2' than in 'c - 5', Fig. 5.19). We also attempted to inject fluid directly into the central chamber without the bottom pullulan disc, but no fluid reached the waste container. Results in Fig. 5.19 exemplifies that sealing the device either using glue or a fully close device is not a viable strategy to reduce the available space for evaporation, unless the assembly method is profoundly modified.

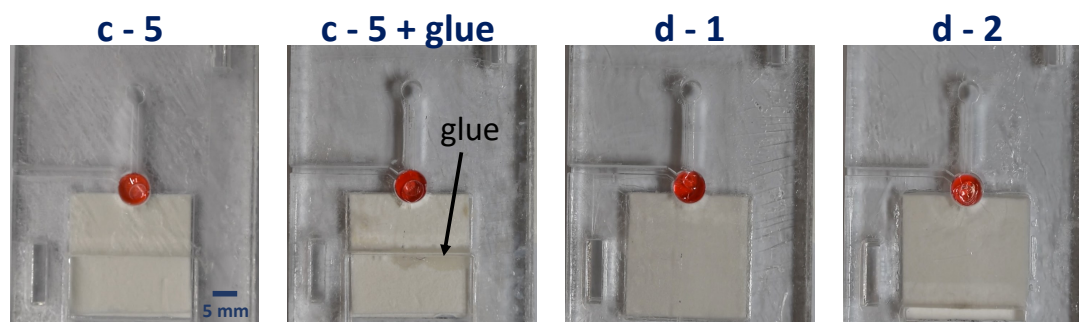


Figure 5.19: **Pictures of the waste container of the point-of-care device sealed.** Device designs **c - 5**, **d - 1** and **d - 2** were used to test possible sealing strategies of the waste container to reduce the available space for evaporation of liquids within the device. **c - 5** was sealed using a PMMA cutout and super glue ('c - 5 + glue'). The sealing strategies are compared with unsealed **c - 5**, on the left.

The last designs tried for the third PMMA layer are **e**, shown in Fig. 5.18. These layers cover the waste container of the second layer for a larger portion than previous designs. Moreover, **e - 2** allows to seal the third and second PMMA layer at the edge too, leaving less space for potential evaporation between the layers. The third layer of design **e - 1** was sealed in three different ways: gluing the edges of the PMMA cutout to the third layer (like we did for **c - 4**), gluing only the lower part of the PMMA cutout that was in contact with the second layer (making sure that no glue would leak into the absorbent pad), and by simply adding the cutout in the available space. The

cutout dimensions were 12 cm \times 21.5 cm. All sides of the cutout were laser cut 0.5 mm larger than the actual space above the waste container to account for laser cutting inaccuracies, and to be able to wedge in the cutout piece in the available space. Again, as experience before, when gluing the edges of the PMMA cutout to the third layer some glue leaked into the absorbent pad and flow was observed from the third to the second layer. Surprisingly, when gluing only the part of the cutout piece that was in contact with the second layer no flow was observed of the sample into the absorbent pad. By simply wedging in the cutout in the available space, without the use of glue, the sample flowed from the central chamber to the absorbent pad. A PMMA cutout was wedged in the third layer with design **e - 2** too, and no glue was used. Also in this configuration, the sample flowed into the absorbent pad. As expected, no incubation was observed since the absorbent contained three layers of paper (as explained in the results of Fig. 5.9). The results of this study and those shown in Fig. 5.19 indicate that glue is not a suitable material for closing the device and that some anomalous phenomena occur in the channels when the waste container is well sealed. One possible explanation for this observation is that the paper and the capillary forces are not the main factors affecting the phenomenon, but rather the internal pressure of the device. This contradicts the expected capillary-based fluid transport in paper [47, 52].

Designs **e - 2** and **e - 3** were used for testing the full device operation as described in Section 2.16.4.3. We noticed that the adhesive film sealing interferes with the liquid containment above the 3% pullulan top disc, when the sample and washing buffer are loaded in the channels. This happens because the liquid reaches the full height of the channels with the adhesive film sealant in place. This time, after the washing was performed as usual using 500 μ L of NFW, the washing unit was filled with parafilm to prevent evaporation. After 2 hours at 66 $^{\circ}$ C, the central chamber was opened to check if any liquid was available to run on LFSs. With these device designs major evaporation happened and no liquid was available to run on lateral flow strips, as already observed before. Most of the evaporated liquid accumulated in the space available in the waste container and in the gaps between the cutout and the third layer. Evaporation might occur between each PMMA layer too. To avoid evaporation between the PMMA layers, a uniform bonding method is recommended.

The device design should undergo major changes to perform sample preprocessing and amplification in one pot. For example, valves and other elements are needed to

isolate the amplification chambers from the rest of the channels and cavities in the device.

5.1.3 Sample Processing and DNA Extraction On The Device Cassette

To evaluate the feasibility of integrating the paper-based DNA extraction with dried lysis buffer investigated in Section 3.1.9 with the POC device studied in Section 5.1.2, a series of experiments were conducted as described in Section 2.16.5. First, the lysis buffer was dried on paper discs at two different temperatures (room temperature and 37 °C). Then, DNA was extracted from *E. coli* cells (10^8 CFU/mL) using three methods: the POC device (Section 2.16.5), the 7-steps paper-based method in tubes (Section 2.14.2), and the MagaZorb[®] DNA Mini-Prep Kit (Promega) as the gold standard. Additionally, DNA was extracted from *E. coli* culture using paper discs without elution and added directly to the LAMP reaction mix. Time-to-positive (TTP) or cycle threshold (Ct) values were used for comparative analysis, and one-way ANOVA with Tukey-Kramer's post-hoc test was performed.

In section Section 2.14.3, the lysis buffer air-dried on two 5-mm Whatman[®] Grade 3 discs was successfully used for DNA extraction. The extraction buffer # 2 [21] was left to dry at room temperature for a week before use. However, to ensure the complete evaporation of the buffer and the full dryness of the paper discs, the buffer was also dried onto paper discs at 70 °C. Humid paper discs could interfere with the dissolution of the pullulan tablet in the purification & amplification unit. The 7-steps paper-based DNA extraction method adjusted to perform qPCR was carried out as described in Section 2.14.3. 1 μ L of the eluant was added to the qPCR mix, which was made of 5 μ L 5X *E. coli* primer mix (Table 2.6), 12.5 μ L of master mix, and 6.5 μ L of NFW (Section 2.6). The performance of the lysis buffer dried at 70 °C was compared with the lysis buffer dried at room temperature using Ct values, and the results are provided in Fig. 5.20.

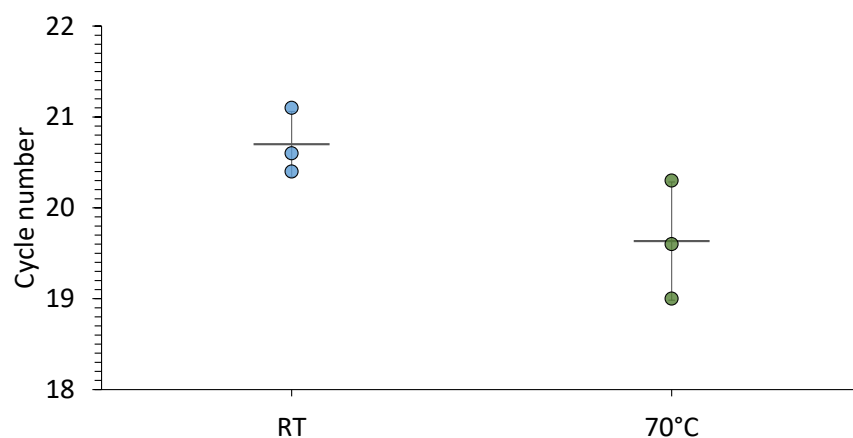


Figure 5.20: **Cycle threshold (Ct) values of the 7-steps paper-based DNA extraction procedure performed with lysis buffer dried on the paper discs at room temperature or at 70 °C.** The paper-based DNA extraction performed is the one described in Fig. 2.9. 100 μ L of extraction buffer # 2 was dried on two 5-mm Whatman[®] Grade 3 discs either at room temperature ('RT') or in an oven at 70 °C ('70 °C'). Experiments were run in triplicate ($n = 3$). Negative controls were performed ($n = 3$) too, and no amplification occurred. The horizontal bars represent the mean value of the Cts of the biological replicates whose DNA extraction was performed with the same conditions. Error bars represent the standard deviation for $n = 3$. No statistically significant difference was observed for $p\text{-value} < 0.05$.

The mean Ct values when using lysis buffer dried at 70 °C ('70 °C') or at room temperature ('RT') were 19.63 ± 0.65 min and 20.70 ± 0.36 min, respectively. No statistically significant differences were observed for $p\text{-value} < 0.05$. To test the replicability of the paper-based DNA extraction method with the lysis buffer dried at 70 °C, the DNA extraction was repeated with six biological samples and three negative controls, and 5 μ L of eluant was added in a LAMP mix (total reaction volume 25 μ L). As expected, all the negative controls did not show amplification and the mean TTP value was 8.57 ± 0.21 min. The small standard deviation indicates a small variation in TTP values among biological samples and thus good reliability of the extraction method. Therefore, the successive experiments were performed using the extraction buffer # 2 dried at 70 °C.

The paper-based DNA extraction was performed on the POC device as described in Fig. 2.30 (Section 2.16.5). The first and second layers of the plastic cassette used are the ones shown in Fig. 5.6, and design **b - 3** was used for the third layer (Fig. 5.7, Section 5.1.2). The results in Fig. 5.21 demonstrates that sample pretreatment can be successfully performed on the POC device. Amplification occurred for the *E. coli* positive samples run on the device ('Extracted DNA - PC'), with mean TTP value of 11.90 ± 3.04 min. During the DNA extraction, only one of the three devices provided

sample incubation on the paper-discs of about 6 minutes. This indicates that DNA extraction on the POC device is successful even without prolonged incubation. Even though the LAMP amplification curves show amplification for two negative samples (at 38.3 and 56 min), and the melting curves are not able to provide clear results (Fig. 5.21A), they are due to unspecific amplification. This can be observed from the additional control performed via gel electrophoresis (Fig. 5.21B). The negative controls in lanes 3, and 4, that showed amplification, do not have a ladder-like pattern. The negative control in lane 3 that amplified at 38.3 min has a ‘smear’ that is indicative of non-specific amplification, and it is nothing similar to the ladder-like patterns observed for the positive samples (lanes 5-7) and the positive control from synthetic DNA in lane 10.

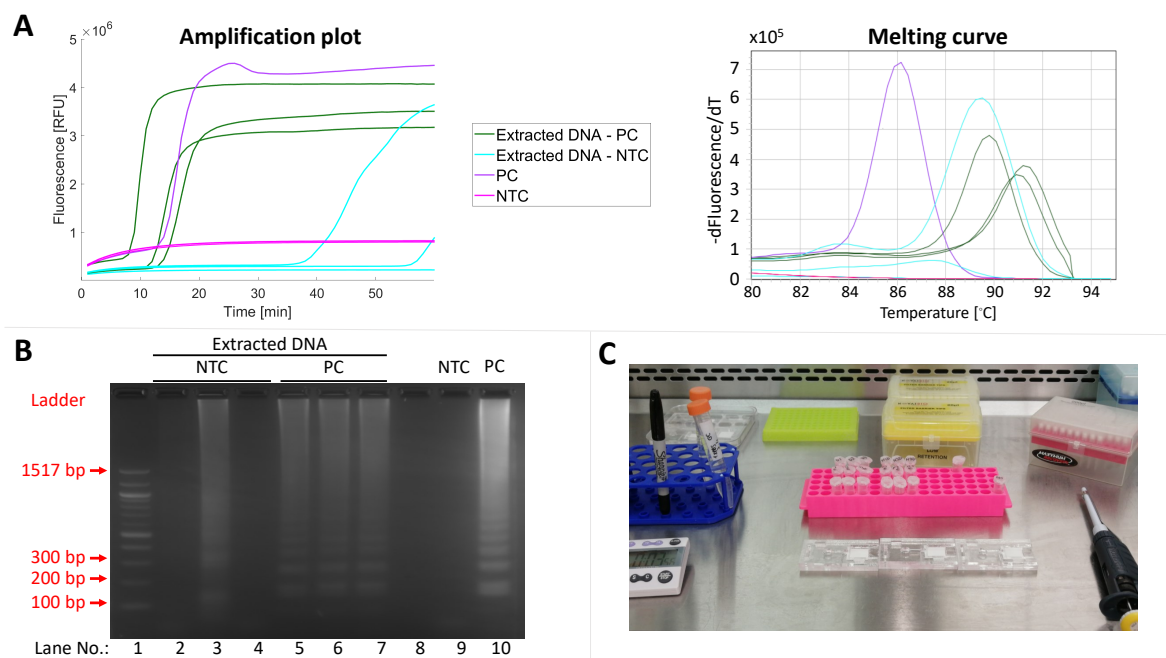


Figure 5.21: Results of the paper-based DNA extraction procedure performed on the point-of-care device. The paper-based DNA extraction performed is the one described in Fig. 2.30. The experiment was run in triplicate ($n = 3$), and negative controls were performed ($n = 3$) too. **A.** Amplification plot and melting curve. *E. coli* samples were run on the device ‘Extracted DNA - PC’ and amplification occurred at 11.90 ± 3.04 min. The melting temperatures (T_m s) of the three positive samples are 89.79, 91.05, 91.33 °C. DNA extraction was performed on the device also using 100 μ L of 1X PBS instead of using *E. coli* (‘Extracted DNA - NTC’), to ensure the absence of contamination on the device. One ‘Extracted DNA - NTC’ amplified after 38.3 min and showed a T_m of 89.37 °C. The positive control (‘PC’) has a concentration of 10^{-6} ng/ μ L *E. coli malB* gene synthetic DNA. Non-target controls (‘NTC’) were run adding 5 μ L of NFW to the LAMP mix. ‘PC’ and ‘NTC’ were run to make sure the reaction was working properly. **B.** Gel electrophoresis control was used to confirmed the results in A. The ladder is in lane 1. **C.** Laboratory set-up to perform sample pretreatment on the POC device. DNA extraction was performed inside a biosafety cabinet Class I.

The results from the paper-based extraction performed in the POC device were compared to those from the paper-based DNA extraction performed in tubes (as described above) and the MagaZorb[®] DNA Mini-Prep Kit extraction (as the gold standard),

using TTP values. Fig. 5.22 shows that performing the sample pretreatment using the 7-steps method in tubes ('7-steps method') gives comparable performance results than using the beads-based gold standard ('Magazorb kit'), with mean TTP values of 8.83 ± 0.12 min and 9.03 ± 0.15 min, respectively. This confirms what already demonstrated in Sections 3.1.4.4, 3.1.9, that the 7-steps paper-based method with lysis buffer already dried onto the paper discs can be effectively used in the developed paper-based DNA extraction method to further reduce handling steps. No significant difference in TTP values, for $p\text{-value} < 0.05$, was observed when carrying out the DNA extraction on the POC device ('Device-based'). The higher mean TTP value and standard deviation (11.80 ± 3.18) min observed, illustrates a reduced replicability of the results and the possibility of a decreased performance in DNA extraction when using the POC device. This potential loss in performance in laboratory settings, where the assay can perform optimally, is not ideal. In fact, in real-world scenarios, there may be several external factors that can interfere with the assay's performance, as discussed briefly in Sections 4.1.8.3, and 4.2.2. Therefore, this limitation should be considered when evaluating the POC device. To better assess the performance of paper-based extraction carried out on the POC device, an analytical sensitivity analysis should be performed. However, due to lack of time this was not carried out.

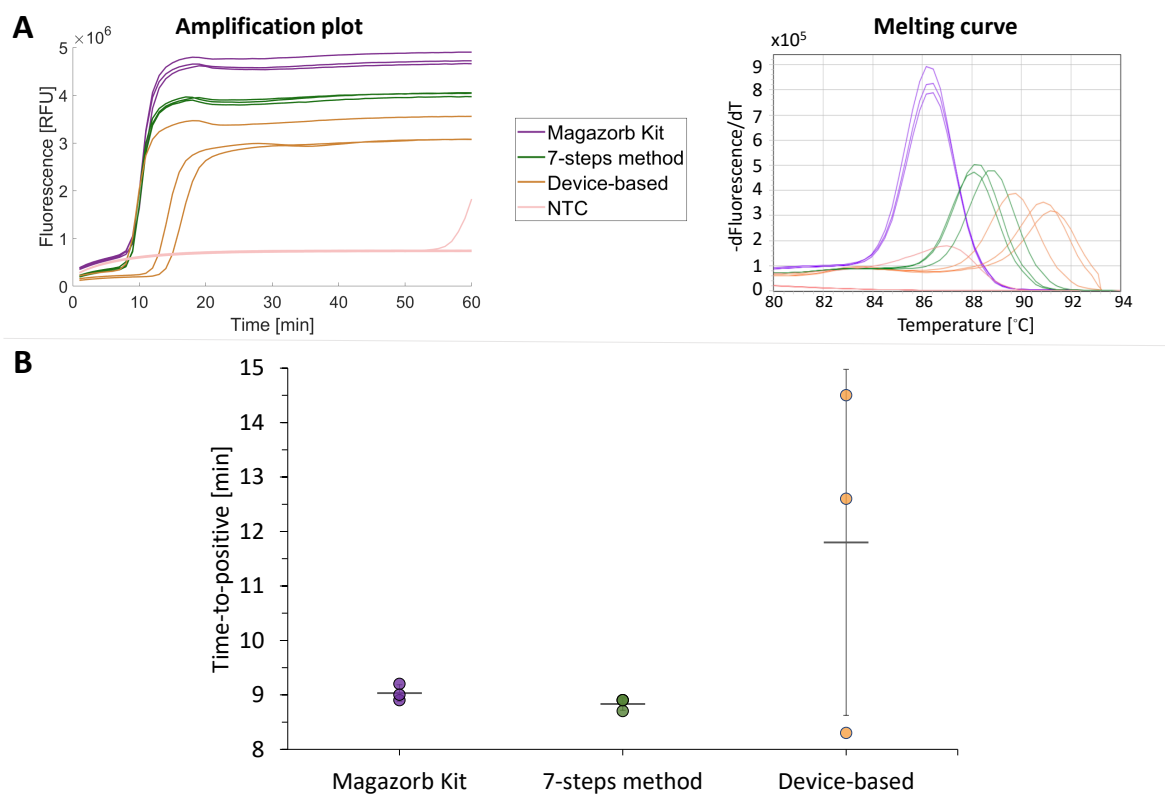


Figure 5.22: **Results of the paper-based DNA extraction procedure performed on the point-of-care (POC) device compared with the paper-based 7-steps method performed in tube and the gold standard.** The paper-based DNA extraction performed in the POC device (‘Device-based’) is the one described in Fig. 2.30). The paper-based 7 steps-method is the one described in Fig. 2.9 (‘7-steps method’). The gold standard extraction is indicated as ‘Magazorb kit’. The experiment was run in triplicate ($n = 3$). **A.** Amplification plot and melting curve. Three non-targeting controls (‘NTC’) were run adding 5 μL of NFW to the LAMP mix to ensure that the reaction was carried out properly. **B.** Time-to-positive (TTP) values of the three DNA extraction methods tested. The horizontal bars represent the mean of the TTP values of the biological replicates whose DNA extraction was carried out under the same conditions. Error bars represent the standard deviation for $n = 3$. No statistically significant difference was observed for $p\text{-value} < 0.05$.

In Chapter 3, the 7-steps paper-based DNA extraction was tested using one 3-mm diameter Whatman[®] Grade 1 disc, and the 7-steps method with the lysis buffer already dried on two 5-mm Whatman[®] Grade 3 discs was assessed only with qPCR. Therefore, the feasibility of performing the 7-steps paper-based DNA extraction using two 5-mm Whatman[®] Grade 3 discs was explored since the discs were able to properly capture DNA fragment and release them into the elution buffer using qPCR, as shown in Section 3.1.7. The 25 μL of LAMP reaction used for the paper-based DNA extraction experiments performed in Chapter 3 was not enough to cover two 5-mm discs. Therefore, the volume of the LAMP reaction was increased to 50 μL as explained in Section 2.16.5, and as in line with the volume calculated by Manzanas *et al.* [197]. The increased volume also aligns well with the need to resuspend LAMP reagents inside the central chambers of the POC device with 50 μL , because 25 μL was not enough liquid

to reach the central chamber. The results of the 7-steps paper-based DNA extraction using two 5-mm Whatman[®] Grade 3 discs with lysis buffer already dried on them are given in Fig. 5.23. Negative sample underwent DNA extraction to ensure that possible carry overs from the sample preparation (such as the lysis buffer) did not affect the LAMP amplification.

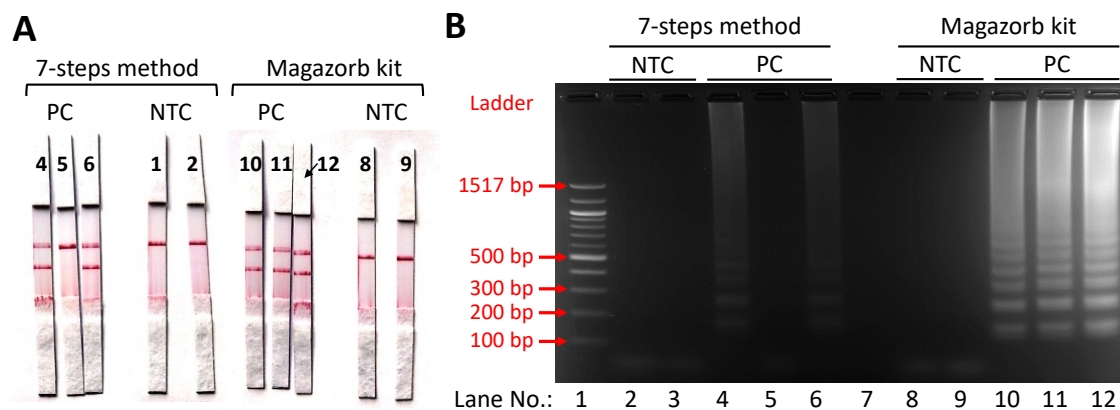


Figure 5.23: Lateral flow strips result of the 7-steps paper-based DNA extraction procedure with lysis buffer already dried on paper discs and directly inserted in LAMP mix. The lysis buffer was dried on to two 5-mm diameter Whatman[®] Grade 3 discs, DNA was extracted using the 7-steps method and the paper discs were immersed in 50 μ L LAMP reaction mix ('7-steps method'). This extraction method was compared with the beads-based gold standard extraction method ('Magazorb kit'). The sample was extracted in triplicate ($n = 3$) for each method. **A.** Lateral flow strips (LFSs) results. **B.** Gel electrophoresis control was used to confirmed the results in A. Lane 1 contains the ladder and lane 7 was not used. The number on the LFSs in A corresponds the corresponding lane in B.

It is not possible to visualise and analyse results using real-time LAMP because the paper discs interfere with fluorescent reading. The LFSs in Fig. 5.23A show that only two out of three positive samples extracted with the 7-steps method came positive. The negative result associated with one of the positive sample might have been caused by excess washing, as by mistake 800 μ L washing were used instead of the correct 600 μ L. However, the negative outcome could be due to a lower replicability of the method as more unforeseen LAMP inhibitors from the lysis buffer could have been carried over into the LAMP amplification mix by the paper discs. In Chapter 3, the paper-based DNA extraction LAMP amplification was performed with a single small 3-mm diameter paper disc. This small disc size reduced the surface area available for DNA and other molecules adsorption compared to the larger 5-mm discs. Therefore, the risk of chemical carryover that could have either inhibitory or amplifying effects on the final LAMP reaction was minimal and of little concern. The LFSs results were confirmed by gel electrophoresis (Fig. 5.23B). The gel displays faint but clear ladder-like patterns for the paper-based extracted positive samples (lanes 4, 6), that are similar to the ones

extracted with the beads-based gold standard method (lanes 10-12).

These results show the feasibility of performing a paper-based DNA extraction method that includes the drying of lysis buffer on paper substrates to simplify pretreatment reagents storage that can be combined with LAMP reaction. This opens the route to integrate the paper-based DNA extraction methodology into an enclosed device.

5.2 Discussions

A proof-of-concept POC molecular device that combines the sample pretreatment and amplification in one chamber was investigated. Fluid flows and timed reagent release are controlled thanks to a layered structure of dried reagents and pullulan tablets. We successfully performed an easy and rapid sample pretreatment, and we have established the foundations for a simple LAMP POC diagnostic device that can be used in low-resource settings with limited equipment or portability issues.

Nucleic acid (NA) sample preparation, amplification, and detection are essential steps for point-of-care tests that can diagnose diseases quickly, and accurately. Many POC NA amplification tests (NAATs) exist as closed automated devices that use single-use integrated cartridges with pre-measured dried reagents ready for hydration. However, these cartridges are very costly. Some recent cartridges-based POC diagnostics for covid are AcculaTM SARS-CoV-2 Test (Thermo Fisher Scientific Inc.) and AscencioDx COVID-19 Test (Anavasi Diagnostics, WA, United States). Their prices, US\$ 30 dollars per test plus the detection unit US\$ 99, and US\$ 34 with US\$ 250, respectively are unaffordable for many low-resource settings where the disease burden is high [86]. Therefore, many researchers have tried to combine NAATs steps into paper-based portable devices that can be used at home, in small clinics, and in doctor's offices. However, most of these devices are not able to perform all NAATs steps [32,96]. Phillips *et al.* [12] designed a molecular diagnostic device that incorporates all the NAATs, with dried reagents, wax valves, and disposable microheaters. However, the device still needs auxiliary benchtop equipment, trained personnel, and has limited sensitivity [96]. The device by Tang *et al.* [11] is a sample-in-answer-out device that only requires sample deposition to run, and it is fully disposable. The first paper-based sample-in-answer-out microfluidic device that also included sample collection was invented by Lafleur *et al.* [13].

This chapter described a device that aimed to automate all the steps of NAATs with minimal human involvement. The device we developed did not show any significant improvement over the existing devices in the literature, but it has a great potential to achieve high accuracy based on the results from Chapters 3, and 4. With further optimisation, the device would require six handling steps: (1) depositing the sample, (2) washing the sample pretreatment unit, (3) flipping and tapping the device to ensure contact between paper discs and amplification reagents, (4) resuspending the amplification reagents, (5) heater activation, and (6) LFS detection. This device is not fully functional yet, and some of the challenges that need to be addressed are listed below.

1. **Washing sample pretreatment unit.** In Chapter 3, we demonstrated that the washing step is one of the corner stones of the paper-based sample pretreatment that cannot be eliminated. The washing buffer is currently pipetted inside the washing unit and extra sealing is then applied on the device. This is not a practical option in in-field settings, as it is cumbersome and a possible contamination source. A blister water pouch like the one available from Microfluidic ChipShop could represent a reasonable alternative (Fluidic 1175). The water pouch would deliver the washing buffer to the central chamber, but it would not allow us to control the flow rate and volume; this may cause overflowing in the central chamber and untimely dissolution of reagents. Another alternative to avoid adding the washing buffer separately to the device is to use a sampling vessel with a self-healing septum, such as the one from Microfluidic ChipShop (Fluidic 276). However, the complexity of the device would increase as to open the valve, a cannula for piercing the septum and a valve for the cannula are need. This method would also result in slower fluid release inside the device and a better sealing after the removal of the vessel.

To reduce the costs of the device the blister pouch represents the best alternative, but the central chamber should be modified to prevent the LAMP reagents from dissolving prematurely.

2. **Valves.** The tests performed on the POC device to understand the fluid flows in Section 5.1.2 made clear the advantage of introducing valves. For example, valves would be beneficial to properly seal the central amplification chamber during LAMP to avoid excess evaporation, and to automate the amplified material flow to LFSs without relying on intercalating mechanisms. Several

valves have been presented in the literature, stretching from soluble polymer bridges [72, 198, 199] and laser direct-writing delays [200], to wax such as heat controlled wax [12, 13, 70]. Probably, the most applicable valve to control the flow from the amplification chamber to the detection zone would be heat controlled wax whose melting temperature is above the LAMP amplification temperature of 66 °C. For example, candelilla wax (Sigma-Aldrich) could be a suitable wax as its melting point is at 68 - 72 °C and it does not inhibit LAMP or LFSs redout (colleague's results, not available). However, this would require a heating system able to switch temperature from the one of LAMP reaction to the melting temperature of the wax, and a more complicated device assembly to deposit the wax in the right position inside the device, without interfering with the other components of the central chamber. An intercalating system might still represent the simplest option to integrate on the device.

To prevent excessive evaporation from the central chamber during amplification, mechanical/geometrical valves may be required to seal it off. These valves could also replace the upper pullulan disc by creating a barrier between the amplification reagents and the paper discs used for sample preparation. This would simplify the choice of washing container and make the blister pouch a feasible option (as described above). The valve could consist of a movable strip similar to the one introduced by Connelly et al. [10], which would be shifted after the sample pretreatment and device inversion, to bring the paper discs in contact with the LAMP reagents. After adding the resuspension buffer, the strip could be moved back to its original position to isolate the amplification zone from the channels used during sample preparation. This would introduce some extra manual steps, but they are relatively easy. The strip movement could also be integrated with a mechanical design that triggers the release of the resuspension buffer in the amplification zones.

To achieve a device that can produce an output from an input sample without any intermediate steps, the design of the device must necessarily become more complex.

3. **Heating unit.** Our laboratory's heat block is not suitable for low-resource settings. Smaller and portable heaters could be used instead [96]. For instance, Buser *et al.* [201] proposed a strategy for designing electricity-free precision

heaters compatible with nucleic acid amplification, and Lee *et al.* [151] used a similar heater in their POC device for covid detection. Alternatively, we could use heaters powered by batteries, that can be directly incorporated into the device [12, 202], that are reusable, and that have batteries or cell phone connections [13, 153].

As we mentioned in Section 5.1.2, we focused on the simplicity of the liquid phase solvent bonding method to make the PMMA cassette, but we also noticed that the unevenness of the bonding could cause some liquid to evaporate and leak during the heating amplification step. To ensure consistent bonding, we could use the liquid phase solvent techniques proposed by Wan *et al.* [192] and Liga *et al.* [203], which use lower solvent concentrations and a heat press. For mass production, PMMA bonding could be avoided by using injection moulding to reduce manufacturing time and costs.

The total cost of the current device unit is given in Table 5.1, this does not include the price of the portable heater. The addition of blister pouches, valves and other

Table 5.1: Cost analysis per point-of-care device and assay.

Material	Cost (bulk quantity)*	Quantity/device	Cost/device
PMMA sheet – 2 mm	41.21 USD/1 m ²	60.68 cm ²	0.25 USD
PMMA sheet – 4 mm	72.39 USD/1 m ²	30.34 cm ²	0.22 USD
Whatman CF7 paper	0.03 USD/1 cm ²	4 cm ²	0.11 USD
Adhesive films	3.21 USD/sheet	1	3.21 USD
Tubing	87.03 USD/50 m	2 cm	0.03 USD
Acetone	65.91 USD/1 L	1.6 mL	0.11 USD
		Total/device	3.93 USD
Material	Cost (bulk quantity)*	Quantity/reaction	Cost/reaction
Triton X100	130.81 USD/ 1 L	1mL	0.13 USD
Tween-20	59.94 USD/100 mL	2 mL	0.95 USD
Guanidine HCl	103.25 USD/100 g	152.8 mg	0.16 USD
Tris-HCl solution (1M, pH 8)	93.03 USD/1 L	10 mL	0.93 USD
Primers	410 USD/~3.7 mL	10 µL	3.79 USD
Isothermal buffer	43.18 USD/6 mL	5 µL	0.04 USD
dNTPs	93.98 USD/0.8 mL	7 µL	0.82 USD
MgSO4	33.02 USD/6mL	2 µL	0.01 USD
Bst 2.0 WarmStart DNA polymerase	383.54 usd/1 mL	2 µL	0.77 USD
Nuclease free water	106.93 usd /1 L	651 µL	0.07 USD
Lateral flow strip	2.54 USD/strip	1	2.54 USD
Whatman Grade 3 paper	0.002 USD/1 cm ²	0.39 cm ²	0.00078 USD
		Total/device	10.45 USD
		Total sum	14.38 USD

* Based on GBP prices on 1 June 2024, converted to USD.

components, as discussed before, would increase the unit cost of the device. The highest cost associated with the assay is primarily linked to the price of the primers and the lateral flow strips. The elevated cost of the primers results from the FITC and

Biotin labeling, which enables visualization of lateral flow strip results. However, if lateral flow strips are ordered in bulk directly from the manufacturer and reagents are purchased for large-scale production, the cost of both components can be reduced. Regarding the plastic cassette discussed in this chapter, it will likely be manufactured using either injection moulding or hot embossing, which would significantly reduce the total cost and which would be chosen depending on the final production volumes. In fact, injection moulding is usually the preferred choice for large-scale production despite higher initial costs. Hot embossing is instead efficient for medium volumes and intricate microstructures.

The cost of a device on the market extends beyond the prices of raw materials and it also encompasses the manufacturing, technicians needed to make the devices, and the entire ecosystem required to bring it successfully to market and ensure its functionality. Factors contributing to the price of a device include manufacturing costs which cover expenses related to production facilities, labour, machinery, and quality control during the manufacturing; labour costs such as skilled technicians and engineers; quality assurance and testing for compliance with safety standards; market entry costs, *i.e.*, personnel and resources in marketing, distribution, sales, and administration; regulatory compliance such as certifications; ongoing support and maintenance.

With the extensive use of diagnostic tests in both rural and urban areas, future efforts for the development of new POC diagnostic devices should take into account the environmental impact of these tests [3,204]. A possible way to enhance the sustainability of our device would be to explore alternative solutions for the fabrication process and the materials [204,205]. The fabrication method currently uses solvents but does not require additional equipment such as hot press that consume more energy. However, the device is made of PMMA and designed for single use, which creates a lot of plastic waste and environmental impact. Using recycled PMMA would represent a first step, but further research is needed to explore the possibility of using other bio-based and bio-degradable plastics.

The POC that combines the sample pretreatment and amplification in one chamber is still under development, but it lays the foundation for future research on single pot reactions.

5.3 Contribution to Knowledge

In this chapter we discussed how to increase the user-friendliness of molecular point-of-care devices by integrating sample preparation and nucleic acid amplification in a single chamber, and by easing the storage of reaction reagents ‘on-board’. Combining all the nucleic acid amplification steps in one single chamber and storing all the reagents into the device would bring great advantages for point-of-care devices deployability in in-field settings, as it would eliminate the need for auxiliary equipment, and reduce manual steps. To achieve this, we used a layered design of dried reagents and pullulan tablets to regulate the fluid movement and the reagent mixing in a spatial and temporal manner, following the approach proposed by Jahanshahi-Anbuhi *et al.* [123] Leung *et al.* [26].

We demonstrated that sample pretreatment of a relatively large volume (100 μ L) of *E. coli* K12 sample can be easily performed in our paper-based POC device, in a quicker and simpler way than in the paper-based sample pretreatment devices developed by Cordray *et al.* [94] that uses about 9 steps. Our sample pretreatment takes about 20 minutes, and it requires 5 steps.

To make the device compatible with all NAATs steps, significant modifications are required. Valves would play a crucial role in ensuring proper isolation of the amplification chamber, as shown by Tang *et al.* [11] and Lafleur *et al.* [13]. However, our device represents a step forward in the direction of a fully enclosed nucleic acid test for infectious diseases diagnosis that is easy to operate, and suitable for low-resource settings.

Chapter 6

Enzyme-free Amplification Strategies

Chapters 3, 4 and 5 explored strategies to address the most critical challenges in the design of high-performance molecular diagnostic devices for the detection of infectious diseases that can be deployed anywhere there is a pressing need, *i.e.*, the reagents long-term stability, their easy on-board storage, and simplicity of the device. However, Chapter 4 has highlighted how the present reliance of NAATs-based diagnostic devices on enzymatic reactions decreases their performance over time and in in-field scenarios. Enzyme-free biosensor systems offer a powerful alternative to NAATs and they can also overcome the limitation of heating required, for example, by LAMP in low-resource settings. These strategies have the important advantage of not requiring complex and energy-intensive instrumentation, with all reagents being stored under ambient conditions, without refrigeration. This chapter describes the work carried out during a 12-week placement at McMaster University (Hamilton, Ontario, Canada) in the LiLab, where the combination of an enzyme-free amplification method, catalytic hairpin assembly (CHA), with lateral flow assays was investigated to facilitate the applicability of CHA at the point-of-use.

The following sections are based on an enzyme-free biosensor recently introduced by McMasters researchers [128] that uses a 4-way junction (4WJ) as a control element and a split G-quadruplex (SGq) for fluorescent readouts [128]. The 4WJ was used to either increase or decrease the fluorescence signal depending on the CHA-mediated formation of full G-quadruplexes from the SGq components. The biosensing strategy incorporated a (1) DNAzyme-mediated RNA cleavage for the recognition of *E. coli* bacteria (DRC),

an (2) assembly-mediated strand release reaction (ASR) with the potential formation of 4WJ, a (3) CHA and the (4) SGq assembly (SGR) (Fig. 6.1A). The fluorescence signal was generated by the binding of protoporphyrin IX to the full G-quadruplex [128]. To simplify the assay and make it suitable for point-of-care applications, the original design with a fluorescence output was modified to a lateral-flow assay output based on the immobilization of FITC/Biotin (FAM/Biotin) labeled amplified products with anti-FITC(FAM) antibodies (Fig. 6.1B). LFSs are the most straightforward method for untrained personnel to visualise diagnostic results, as they do not leave room for free interpretations. The amplification products of CHA are represented by the hybridised hairpins 1 and 2, that were functionalised with fluorescein amidites (FAM) and biotin (Fig. 6.1C).

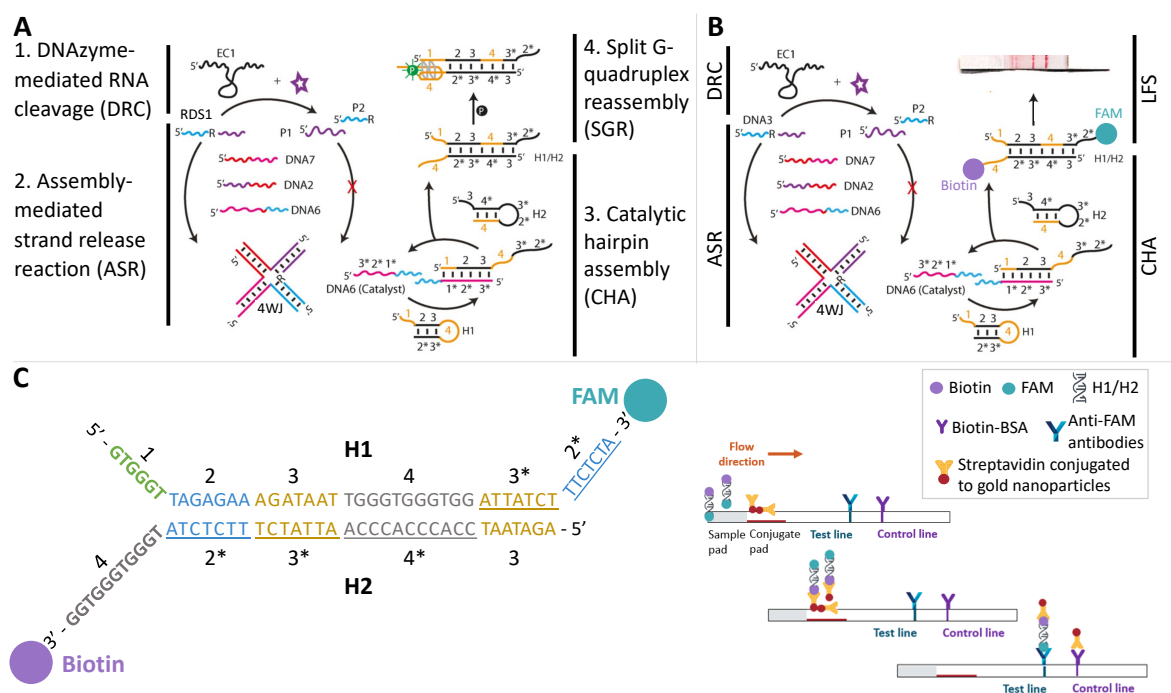


Figure 6.1: **Enzyme-free DNA biosensing system.** **A.** DNA biosensing system introduced by Zhou *et al.* [128]. The RNA cleaving DNAzyme (EC1) is activated by a target that serves as its main input (DRC). This DNAzyme cuts an RNA-containing DNA substrate, RDS1, which is part of a 4-way junction (4WJ). The 4WJ formation (ASR) regulates the release of a DNA output that triggers the catalytic hairpin assembly (CHA), whose product (hybridised hairpins H1/H2) controls the assembly of a split G-quadruplex as a fluorescence signal generator (SGR). **B.** Modified biosensing system for results readouts on lateral flow strips (LFSs). DRC, ASR and CHA steps are the same as in A. **C.** Products of CHA used for results visualisation lateral flow strips (LFSs). The two hairpins H1 and H2 hybridise because of the CHA initialisation. To assess amplification outcomes on LFSs, FAM and biotin moieties were incorporated on the 3'-end of H1 and H2, respectively. The bold sequences in H1 and H2 are split G-quadruplex sequences. Images in A and B are reproduced and modified from Zhou *et al.* [128], with permission of the rights holder John Wiley & Sons - Books (Appendix A.5).

The initial research efforts focused on optimizing the CHA reaction to assess its hybridization efficiency (Section 6.1.1). The concentration ratios of hairpins were ex-

amined, along with those between hairpins and triggering DNA. Additionally, various parameters, such as CHA reaction incubation time and different hairpin designs were investigated. Moreover, strategies for stabilizing hairpins and minimizing reaction leakage, which could lead to false positive results on LFSs, were explored. Subsequently, the concentrations of the DNA sequences involved in the 4WJ structure were studied (Section 6.1.2). The goal was to ensure that no excess of the DNA sequence responsible for initiating the CHA process would remain free in the solution if the target pathogen was absent. In Section 6.1.3, the DRC reaction was explored across different pathogen target concentrations. At last, a second enzyme-free biosensor that utilised the same DRC, ASR, CHA, and LFS architecture was preliminarily investigated for detecting *Clostridioides difficile*, as discussed in Section 6.1.4. Ultimately, the goal was to integrate a DNAzyme-based amplification method into a paper-based diagnostic system, as detailed in Section 6.2.

6.1 Results

The oligonucleotides sequences used, the materials and a brief description of the methods are provided in Appendix A.3. The results provided in this section are qualitative as no quantitative fluorescence measurements were carried out.

6.1.1 Optimisation of catalytic hairpin assembly (CHA) reaction for result visualisation on lateral flow strips

The design of the CHA system was based on the one previously published by Zhou *et al.* [128]. The CHA solution (total 80 μ L) contained 0.5 μ M of each hairpins H1 and H2, and 15 nM of triggering DNA6 in a reaction buffer (pH 8, 5 mM Tris-HCl, 0.5 mM EDTA, 100 mM NaCl, 20 mM KCl and 50 mM MgCl₂), and it was incubated for 1 hour. Native polyacrylamide gel electrophoresis (nPAGE) was used to assess the performance of the CHA and fine-tune the CHA reaction. All the CHA reaction mixtures tried had a total volume of 80 μ L and contained H1 probe, H2 probe and either the catalyst DNA (DNA6) or not in the reaction buffer (unless otherwise specified).

The first step was to optimise the concentration ratio between the hairpins (H1, H2) and the triggering DNA (DNA 6). The concentration of DNA6 was held constant (15 nM) across the reactions while H1 and H2 concentrations changed: 15 nM, 30 nM,

45 nM, 60 nM. The reaction was incubated for 1 h at room temperature. The results in Fig.6.2B shows that most of the DNA6 is involved in the CHA reaction after 1 hour when the [DNA6]:[Hairpins] ratio is 1:4. The band corresponding to DNA6 in lane 7 is less intense than in lane 6, indicating a greater hybridisation efficiency of H1 and H2 in the CHA product. Therefore, the concentrations of hairpins used for the following reactions was set to 60 nM, instead of 500 nM as in the initial CHA (Fig. 6.2A).

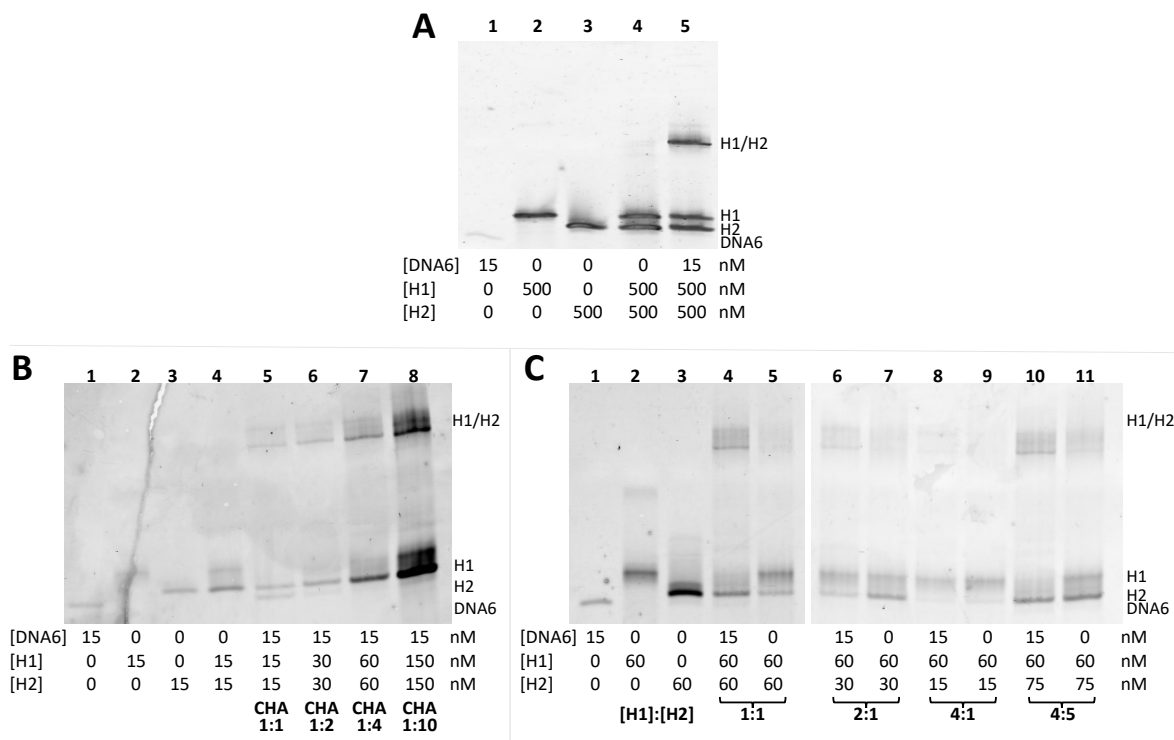


Figure 6.2: **Performance assessment of catalytic hairpin assembly (CHA) on nPAGE.** CHA reactions were incubated for 1 hour and 20 μ L of the mixture were run on a large 15% nPAGE gel at 600 V for 3.5 h, at 4 $^{\circ}$ C. **A.** Concentrations of DNA6, H1 and H2 probes given in [128]. Lanes 1, 2 and 3 shows the position of DNA6 (CHA catalyst), H1 probe, and H2 probe, respectively. The original positions of H1 and H2 is maintained when they are loaded together (lane 4), and no new band for the H1/H2 complex is observed, implying that H1 and H2 do not hybridize without the triggering DNA. On the other hand, a new band appears in the upper position for the H1/H2 complex when DNA6 was present (lane 5), demonstrating that DNA6 can initiate the CHA reaction and facilitate the hybridization of H1 and H2. **B.** Different concentrations of DNA6 investigated in relation to the hairpins concentration. [DNA6]:[H1] ([H1]=[H2]). **C.** Different concentrations of H2 investigated in relation to H1 concentration. [H1]:[H2]. The different samples were run on two separate gels given the limited space.

One of the factors that affect the hybridisation efficiency of the CHA system is the concentration ratio between hairpin H1 and hairpin H2, which determines the balance between the formation of H1-H2 duplex and H1-triggering DNA complex. The concentration of DNA6 and H1 was held constant at 15 nM and 60 nM in the reactions, respectively, while the concentration of the H2 probe was varied from 15 nM, 30 nM, 60 nM to 75 nM. According to the results in Fig. 6.2C, the optimal ratio of hairpins concentration ([H1]:[H2]) for the CHA reaction is 1:1 (lanes 4 and 5). This ensures that

all H1 molecules participate in the catalytic process, even though some H2 molecules remain unused. In fact, the band corresponding to H1 in lane 4 is less intense than in lanes 6 and 8, indicating its greater involvement into the final H1/H2 hybridisation. The CHA incubation time also influences the hybridisation efficiency, as longer incubation time allows more time for the hairpins to interact with the triggering DNA and form stable complexes. However, the greatest hybridization efficiency of the CHA products was 30 minutes and 1 hour (Fig. 6.3). In fact, the bands intensity corresponding to the H1/H2 hybrid in lanes 9 and 11 (CHA incubated for 1.5 hour and 2 hours respectively) are less intense than in lane 7 (CHA incubated for 1 hour), suggesting a less efficient CHA reaction for incubation times about 1 hour.

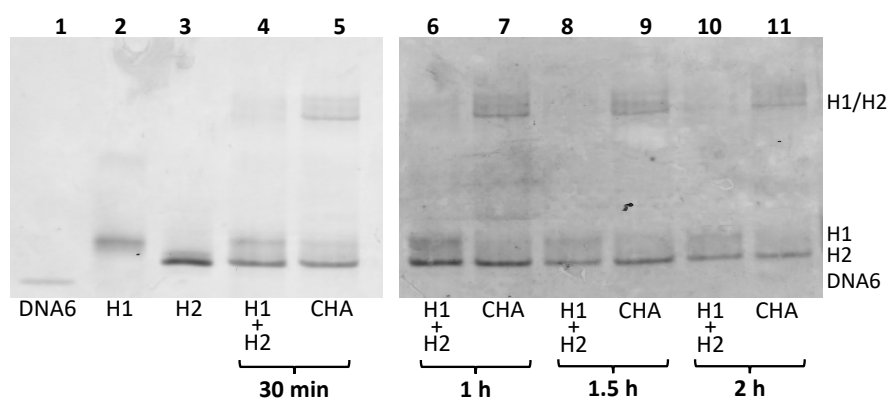


Figure 6.3: **Performance assessment of catalytic hairpin assembly (CHA) for different incubation times.** CHA reactions were incubated for 30 minutes, 1 hour, 1 and a half hour or 2 hours and 20 μ L of the mixture were run on a large 15% nPAGE gel at 600 V for 3 h, at 4 $^{\circ}$ C. [DNA6]=15 nM, [H1]=[H2]=60nM. The different samples were run on two separate gels given the limited space.

Finally, different hairpins sequences were tested to avoid the formation of the G-quadruplex given that for the LFSs readout it was not necessary. Each hairpin sequence has different hybridisation properties, such as melting temperature, stability, and folding structure. The sequences were designed and tested for optimal performance of the CHA system. 7 different hairpins structures were investigated that reduced the number of Guanosine-5'-triphosphate (GTP) in the G-quadruplex forming sequences of H1 and H2. It was decided to modify sequence number 4 in H1 and H2 and its complementary (Fig. 6.1) so that the catalysts sequence DNA6 could have remained unaltered, since it binds to the sequence elements 123 of H1. Briefly, H1 and H2 have a special structure that allows them to interact with DNA6, a trigger sequence that contains 1*, 2* and 3* elements. DNA6 can hybridise with the matching parts 123 of H1 and form a tail with 43*2*. This tail can then bind to the sequence element 3 of H2 and extend the pairing

with parts 4*3*2* of H2. This makes DNA6 detach from H1 and start another round of the CHA reaction (Fig. 6.1A). The OligoAnalyzer™ Tool [172, 173] was used to study the melting temperatures, hairpins formations via the Gibbs free energy change (ΔG), and hybridisation stability of hairpins. The hairpin sequences investigated and the results of the analysis on the OligoAnalyzer™ Tool are given in Appendix A.4. Among the 7 hairpins pairs investigated, 3 were assessed for CHA efficacy on nPAGE (these options were numbered as 2, 4, 7 and their ΔG is given in Table 6.1). A clear

Table 6.1: **Gibbs free energy (ΔG) of hairpins in kcal/mol.** The salts condition entered in the analysis were $[\text{Na}^+]=100$ mM, and $[\text{Mg}^{2+}]=50$ mM. Temperature was set at 25 °C. ΔG between H1 and DNA6 is -32.95 kcal/mol.

	ΔG (kcal/mol)		
	H1	H2	H1/H2
Original	-13.73	-15.86	-56.66
Option 2	-13.73	-14.33	-52.70
Option 4	-13.73	-14.24	-54.41
Option 7	-13.73	-13.43	-53.29

conclusion about the CHA efficiency of different hairpin pairs cannot be drawn from the results shown in Fig. 6.4. Without the catalyst DNA (DNA6), the H1/H2 complex forms new bands in the upper position for all the tested hairpin sequences (lanes 4, 8, 12, 16). This indicates that H1 and H2 hybridise undesirably when DNA6 is missing. This phenomenon is also called ‘leakage’. Moreover, the loading dye that was used to run the samples interfered with the visualization of the results in Fig. 6.4B, as it absorbed the same wavelength as the one used for detection.

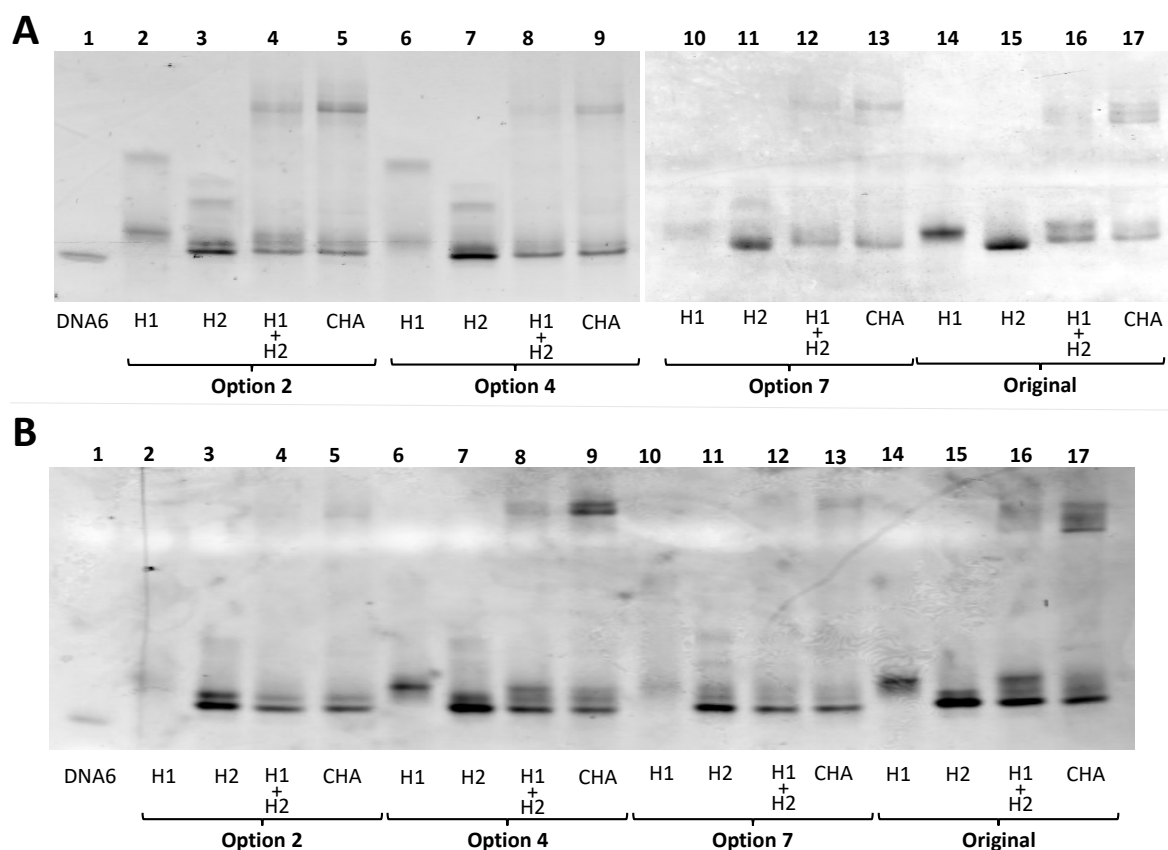


Figure 6.4: **Performance assessment of different catalytic hairpin assembly (CHA) on nPAGE.** In all CHA reactions DNA6 has a concentration of 15 nM and H1 and H2 a concentration of 60 nM each. The different sequences used for H1 and H2 are given in Appendix A.4. Reactions were incubated for 1 hour before they were run on 15% nPAGE. **A.** Experiment 1. A large 15% nPAGE was run at 600 V for 3.5 h, at 4 °C. The different samples were run on two separate gels given the limited space. **B.** Repetition of experiment in A. A small 15% nPAGE was run for 1 hour and 20 minutes on ice.

As shown in the gel image in Fig. 6.4A, some of the hairpins H1 and H2 exhibit multiple bands, such as lanes 2, 3, 6, and 7. This may indicate the presence of alternative secondary structures in the nucleic acid molecules. Unlike denaturing PAGE, native PAGE can separate nucleic acids based on both their molecular weight and their conformation.

The hairpins proposed by Zhou *et al.* [128] were further investigated for LFSs readouts as there was not enough time to optimise the other hairpins combinations. FAM and biotin labels on the 3'-end of H1 and H2, respectively, were used to evaluate the effects of amplification on LFSs (as indicated in Fig. 6.1C). To label H1 and H2, there were four different options (Fig. 6.5). Options **b** and **d** were discarded because the FAM label was where the G-quadruplex formed when H1 and H2 hybridised, which might have interfered with the detection of the FAM label on the test line of LFSs. Option **c** was chosen over option **a** because the FAM label is ideally on H1, which only opens in the presence of DNA6 that initiates the CHA reaction.

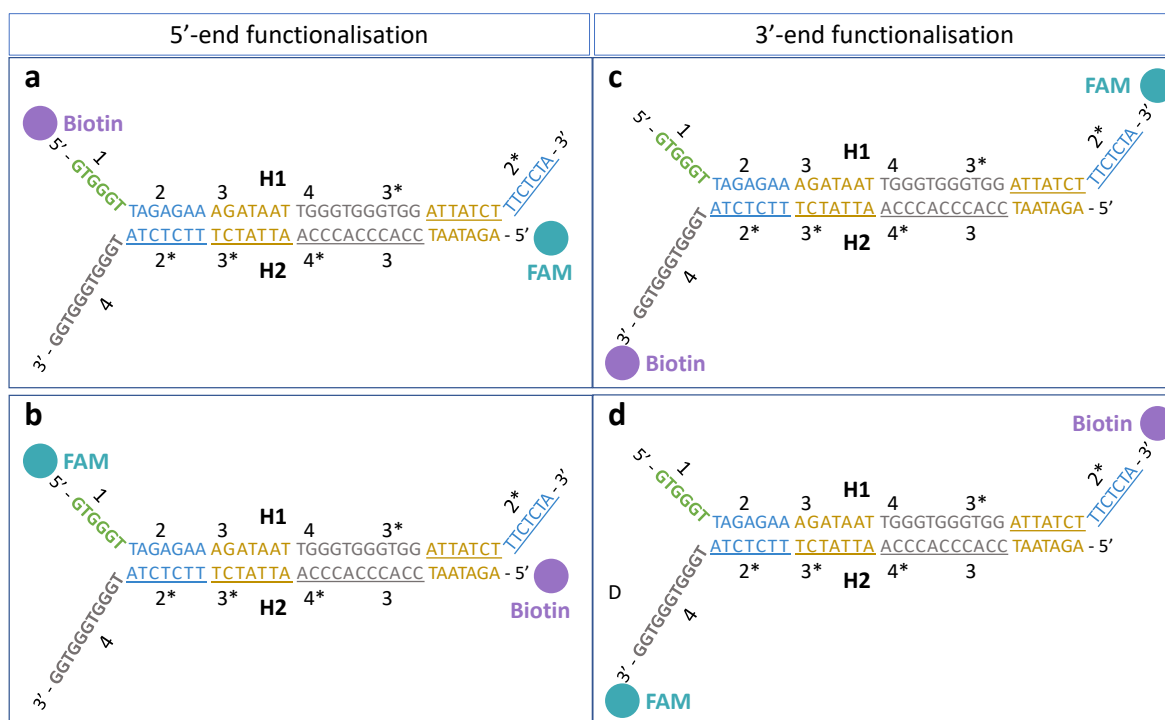


Figure 6.5: **Labelling options of hairpins for CHA and lateral flow assay integration.** The CHA ‘amplification products’ are represented by hybridised DNA sequences H1 and H2. Lateral flow assay readout on U-Star Disposable Nucleic Acid Detection Strips (Type 3) is possible if one hairpin is labelled with a fluorophore molecule, FITC or FAM, and the second hairpin with Biotin, as briefly described in Fig. 6.1C. Four possible combinations are possible based on the position of the labels on H1 and H2.

When running the CHA products on the LFSs test lines appeared even in the absence of DNA6, confirming unwanted hybridisation of H1 and H2 visualised on the gels. To avoid unwanted hairpins formation, we first explore ways to increase the hairpins stability by increasing the concentration of Mg^{++} in the reaction buffer and incubating the hairpins overnight at 4 °C (Fig. 6.6).

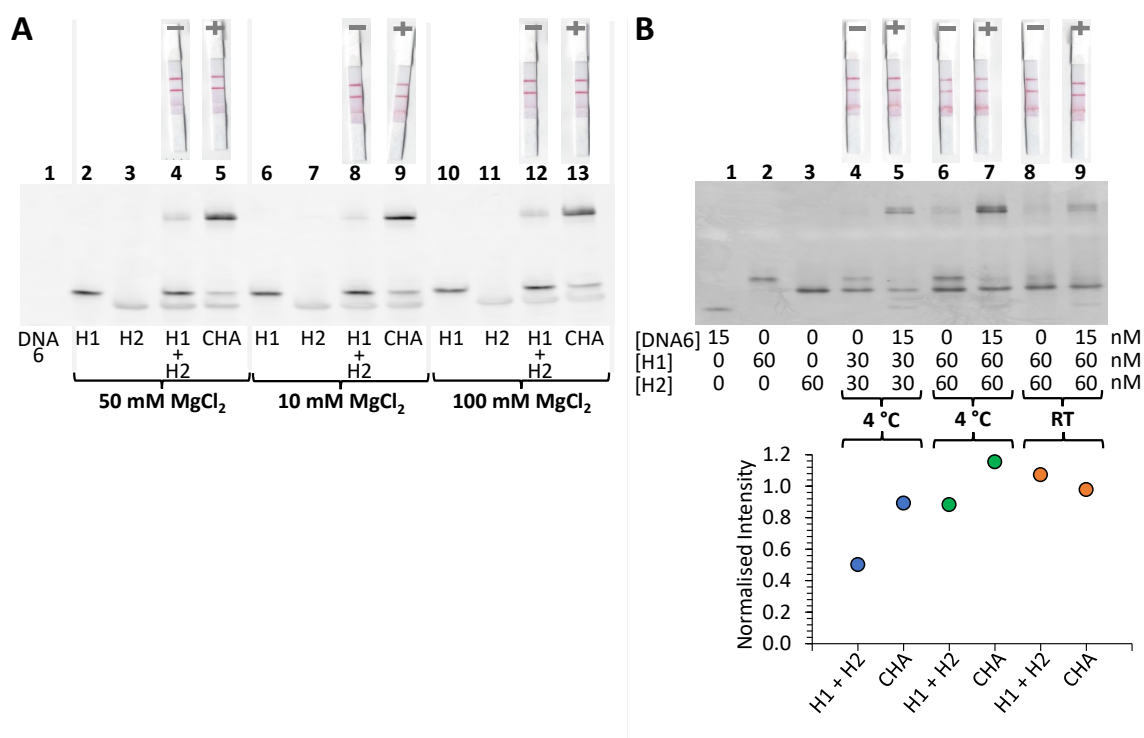


Figure 6.6: **Assessment of hairpins stability on nPAGE and lateral flow strips.** CHA reactions were incubated for 1 hour before they were run on 15% nPAGE. Small nPAGE was run for 1 hour and 20 minutes on ice. The stability of hairpins was tested in different buffers or temperature conditions. **A.** The hairpins were folded in three different reaction buffers (pH 8) whose MgCl₂ concentrations changed. Reactions buffer contains 5 mM Tris-HCl, 0.5 mM EDTA, 100 mM NaCl, 20 mM KCl and either 100, 50, or 10 mM MgCl₂. [DNA₆] = 15 nM, [H1] = [H2] = 500 nM. **B.** The hairpins were folded either at 4 °C overnight or at room temperature (RT) for 15 minutes. Hairpins concentrations of 30 nM and 60 nM were also tried to understand if a difference in test lines when DNA₆ is absent could be visualised by naked eye. Normalised intensities of the lateral flow strips were computed as indicated in Section 2.12.

Before starting the CHA reaction, the hairpin solutions were separately heated at 90 °C for 10 min and cooled down on ice for 15 min, then incubated at room temperature (RT, ~22 °C) for another 15 min in reaction buffer. This would allow the hairpin structures to form. Folded structures of nucleic acids are stabilized by the metal ions in the solution, such as Na⁺ and Mg²⁺ ions, through electrostatic screening [206]. To examine the influence of Mg²⁺ ions on H1 and H2 stability, their concentrations in the reaction buffer were varied. It was hypothesised that higher levels of Mg²⁺ ions would reduce the leakage of H1 and H2 by stabilizing their structures. However, the results in Fig. 6.6A show leakage for all MgCl₂ concentrations that was also detected on LFSs. A second way to increase hairpins stability was to incubated hairpins in reaction buffer over night at 4 °C, rather than at room temperature for 15 minutes. This would have let them have enough time to form the secondary structures. Neither this modification led to significant reduction in leakage (Fig. 6.6B). The LFSs do not show consistent results based on the normalised intensity (NI) when the hairpins are formed at 4 °C

or room temperature ('RT') (lanes 6-9), except that the presence or absence of the catalyst CHA DNA (DNA6) in the solution is not distinguishable by naked eye (LFSs of lanes 6, 7 and 8, 9). The NI decreases when the hairpin concentrations in the solution drops from 60 nM to 30 nM (from lanes 6, 7 to lanes 4, 5), but the LFS in lane 4 has a strong test line that would be interpreted as positive by any untrained personnel without using NI. Another factor that may affect the folding behaviour of hairpins is the concentration of the hairpin molecules in the initial solution. However, this aspect was not systematically investigated in this study.

Since none of the methods investigated made the harpins more stable and stopped the LFSs from detecting the leakage, we examined the minimum H1 and H2 concentrations that the LFSs could sense (Fig. 6.7). For further experiments, it was decided to use the original reaction buffer (with 50 nM MgCl_2) to avoid any potential change in the whole reaction that included the DRC and ASR.

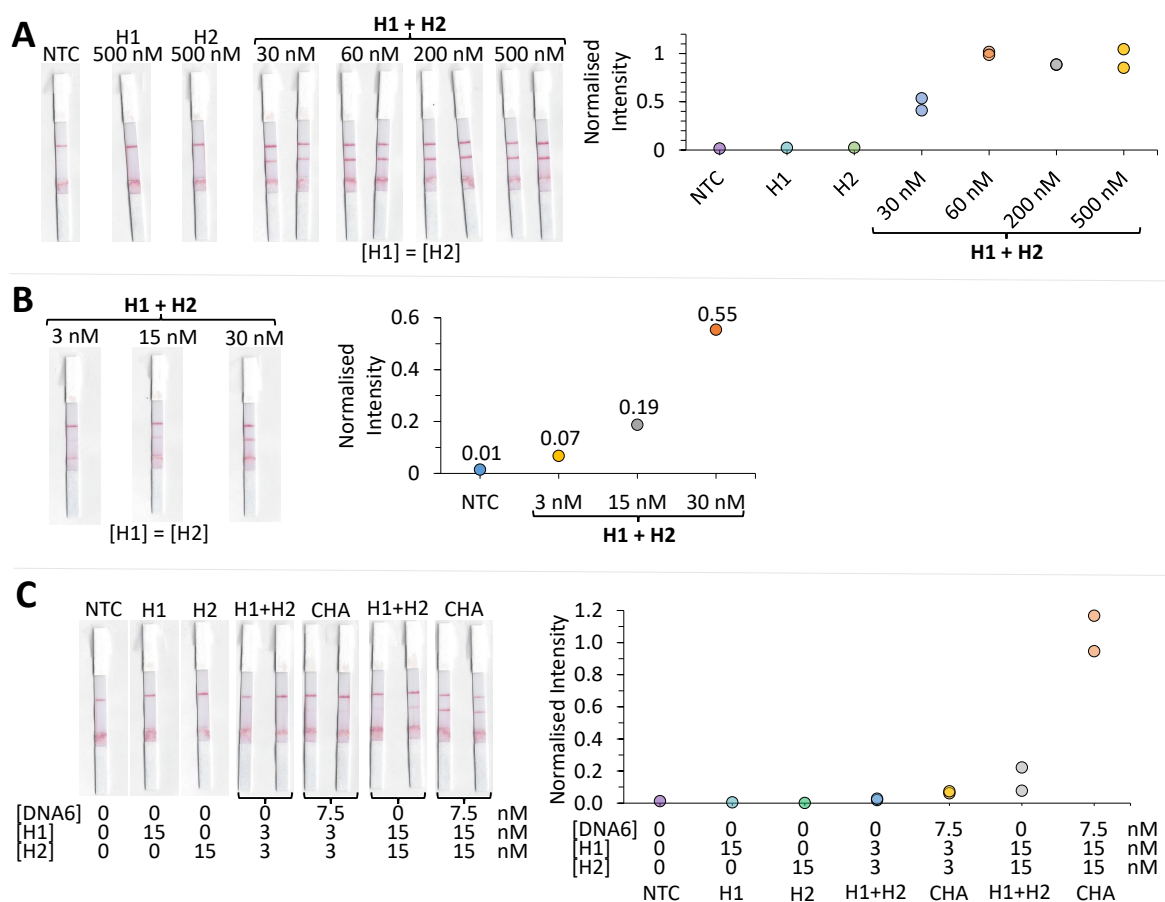


Figure 6.7: **Assessment of CHA leakage on lateral flow strips (LFSs).** CHA reactions and H1/H2 solutions were incubated for 1 hour before 10 μ L of each solution was run on lateral flow strips (LFSs). 30 μ L of proprietary running buffer (U-Star) was added. NTC represents LFSs run with 40 μ L of proprietary running buffer. In all CHA reactions [DNA6] = 7.5 nM. In all H1/H2 solutions (H1+H2), [H1] = [H2]. In each figure, LFSs belong to the same picture, but because of limited space, cutouts are shown. The normalised intensity of the LFSs test lines are computed as described in Section 2.12. **A.** H1/H2 solutions run on LFS ($n = 2$). The concentration of each hairpin was 30 nM, 60 nM, 200 nM and 500 nM. **B.** H1/H2 solutions run on LFS, and each hairpin was 3 nM, 15 nM, or 60 nM. **C.** H1/H2 solutions and CHA reactions run on LFS ($n = 2$). Hairpin concentrations used are 3 nM, or 15 nM.

Solutions of only H1 and H2 were created with different concentrations of each hairpin (500 nM, 200 nM, 60 nM, 30 nM, 15 nM or 3 nM) and no catalyst DNA was introduced. The hairpins were incubated overnight at 4 $^{\circ}$ C in separate solutions before being combined. Leakage was detected on LFSs for all hairpins concentration (Fig. 6.7A), but the extent of leakage increased with increasing hairpins concentrations from 3 nM to 30 nM, as indicated by the test line intensity increasing (Fig. 6.7B). The test line intensity was the lowest for 3 nM of H1/H2 solution without the trigger DNA (Fig. 6.7B), but this concentration of hairpins did not produce clear test lines in the presence of DNA6 (Fig. 6.7C). However, using 15 nM of each H1 and H2 for CHA resulted in a noticeable difference in test line normal intensities between H1/H2 solution with and without DNA6 ('CHA' and 'H1 + H2', respectively) (Fig. 6.7C). Therefore using 3 nM

of each hairpin to perform CHA is not a valuable solution.

The experiment was repeated a second time (Fig. 6.8) and using 7.5 nM as final concentration of hairpins represented a good concentration that allowed to visually see a difference between H1/H2 solutions without and with DNA6 (LFSs 7, 8).

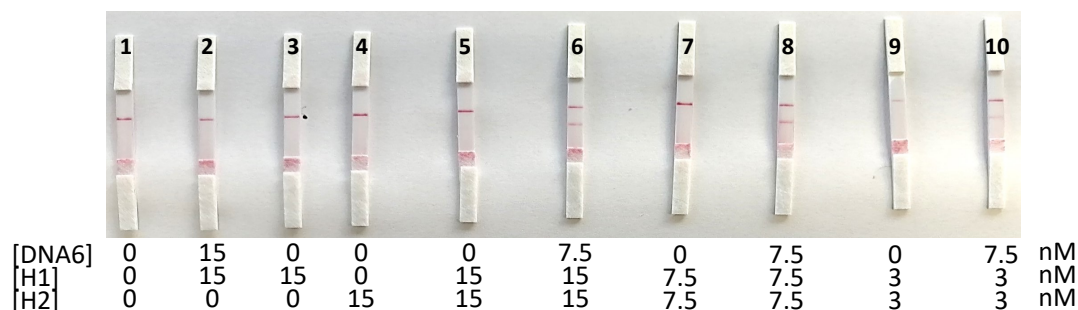


Figure 6.8: **Assessment of hairpins stability on lateral flow strips.** CHA reactions and H1/H2 solutions were incubated for 1 hour before they were run on lateral flow strips (LFSs). 10 μ L of solution was added to the sample pad and 30 μ L of proprietary running buffer (U-Star) was added. LFS 1 has 40 μ L of proprietary running buffer. In CHA reactions the concentration of DNA6 was kept constant at 7.5 nM. The concentration of each hairpin was changed from 15 nM (LFSs 5, 6), to 7.5 nM (LFSs 7, 8) and 3 nM (LFSs 9, 10).

To determine the optimal ratio of H1 and H2 that minimizes false positives in the LFSs readout, further research is needed. For example, changing labels on the hairpins could also be a factor influencing result visualisation. Another possible approach is to modify the LFSs or use specific LFSs that have lower sensitivity and find a balance between leakage and detection.

6.1.2 Optimisation of the assembly-mediated strand release reaction (ASR) and 4-way junction (4WJ)

While studying the CHA reaction, the concentrations of the DNA sequences forming the 4WJ were optimised so that no excess DNA6 would be ‘free’ in the solution if there was no target pathogen. This would prevent CHA from starting non-catalytically.

DNA6 concentration in the solution was decreased from 40 nM (same concentration as the other DNA sequences in the solution) (1:1), to 30 nM (1:0.75), 20 nM (1:0.5), and 10 nM (1:0.25) (Fig. 6.9).

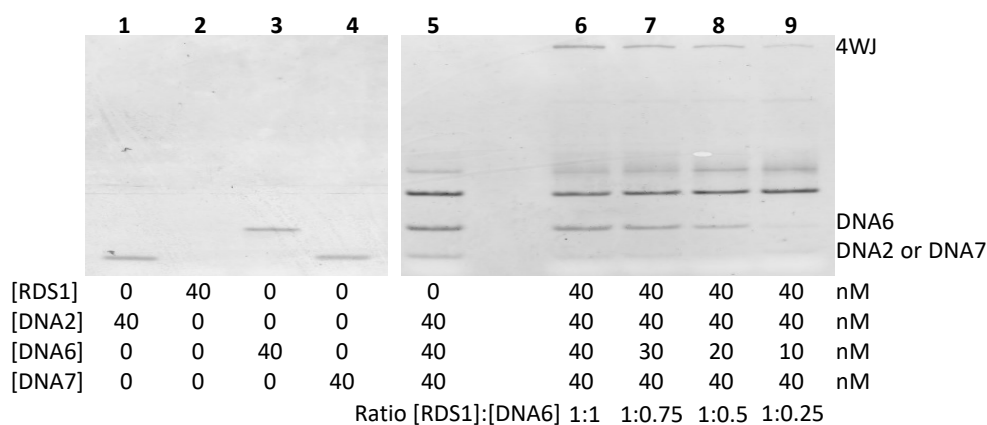


Figure 6.9: **Assessment of four-way junction (4WJ) formation on nPAGE.** The 4WJ was assembled in a 30 μ L solution of reaction buffer, and the concentration of DNA6 was varied. The concentrations of DNA6 investigated are 40, 30, 20, 10 nM. [DNA2] = [DNA7] = [RDS1] = 40 nM. The samples are identified as ratios of [RDS1]:[DNA6].

As DNA6 concentration in the 4WJ solution was reduced, the band intensities for both DNA6 and the upper band of the 4WJ decreased (lanes 7, 8, 9, Fig. 6.9). The assembly of the 4WJ (when DRC and ASR reactions are combined) indicates the absence of the target pathogen in the solution. When the 4WJ solution contains RDS1, DNA2, DNA7 and DNA6 in a proportion of 1:1:1:0.25, most of DNA6 is involved in the 4WJ (lane 9). This means that for 40 nM of RDS1, DNA2 and DNA7 in the 4WJ solution, DNA6 should be 10 nM, and consequently 5 nM in the CHA solution. Assuming that the CHA solution contains 5 nM DNA6, we can infer from Fig. 6.2B that the final solution should have four times more hairpins than DNA6. Therefore, the concentrations of H1 and H2 should be 20 nM each in the final solution. The LFSs experiments used 7.5 nM of DNA6 and 15 nM of each H1 and H2 (Fig. 6.7), so the LFSs signal at 5 nM of DNA6 might not be strong enough on the test line for accurate CHA measurements.

6.1.3 DNA-zyme mediated RNA cleavage

The RNA-cleaving DNAzyme (reaction DRC in Fig. 6.1) activity was briefly explored. The cleavage (clv) activity of the DNAzyme was studied for different concentration of pathogen target, using both crude extracellular matrix (CEM) and crude intracellular mixture (CIM) of an *E. coli* culture. CEM obtained from 10^9 , 10^8 , and 10^7 CFU/mL and CIM 10^8 CFU/mL were tested. The incubation time was varied from 15, 30, 60, to 120 min and the clv activity measured. The results were analysed on 10% denaturing polyacrylamide gel electrophoresis (dPAGE) as described in Appendix A.3. As expected, the clv activity increases with higher concentration of CEM cells and longer incubation

time (Fig. 6.10).

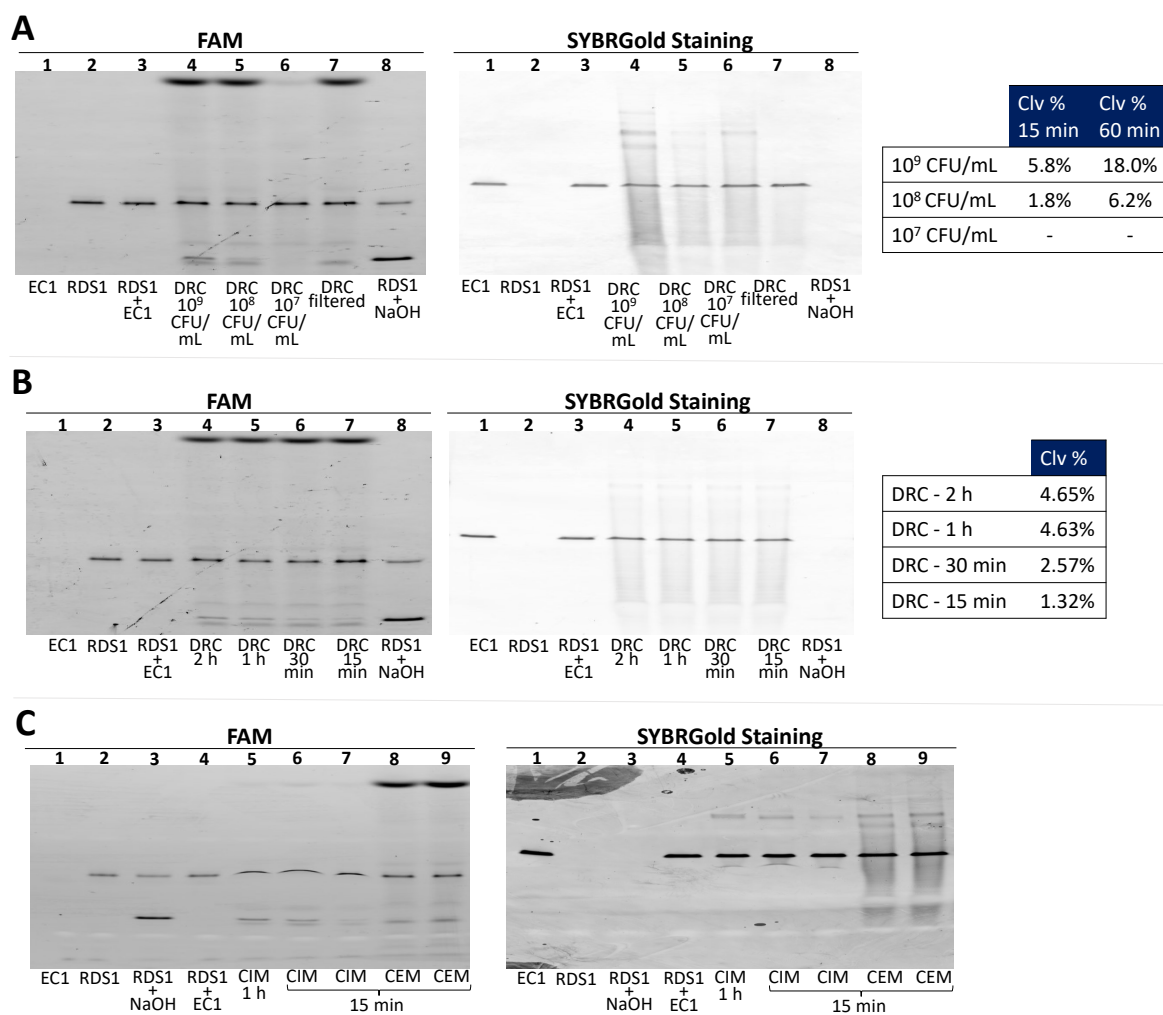


Figure 6.10: **Assessment of DNAzyme-mediated RNA cleavage for the recognition of *E. coli* bacteria (DRC) on 10% denaturing PAGE.** The DNAzyme (EC1) and substrate containing the single RNA linkage (RDS1) are mixed (EC1+RDS1). A total volume of 30 μ L is used, and 500 nM EC1, and 40 nM RDS1 (Section A.3). The cleavage activity (Clv %) of the DNAzyme is studied when crude extracellular matrix (CEM) and crude intracellular mixture (CIM) are added to EC1+RDS1 (DRC). Clv % is computed as described in Appendix A.3. RDS1+NaOH is the control marker; NaOH was used to cleave the substrate in the absence of the target pathogen. **A.** Different concentration of pathogen target, using CEM, 10⁹-10⁷ CFU/mL are assessed on dPAGE and the Clv % is given. Clv % is given for DRC reaction incubated for 15 or 60 min. Only the dPAGE for DRC reaction time of 15 min is shown. **B.** Clv % computed for different incubation periods of DRC reaction, from 2 h to 15 min. CEM with concentration 10⁸ CFU/mL is used. **C.** Cleavage activity of the DNAzyme for CIM and CEM at 10⁸ CFU/mL is visualised. The DRC reaction was performed in the same conditions for CIM and CEM, with 15 min incubation. The DRC reaction was also performed for 1 hour when using CIM.

6.1.4 Enzyme-free biosensor for *Clostridioides Difficile* detection

The project in collaboration with the LiLab (McMaster University) and colleague Menghan Zhang (University of Glasgow) continued to design a DNA-based biosens-

ing system for the detection of *Clostridioides difficile* (*C. Difficile*). *C. Difficile* is a bacterium that can cause diarrhea and inflammation of the colon, and affects about half a million people in the US every year [207]. One of the modes of transmission of the infection is through contact with contaminated stool, and it is more common in healthcare settings. *C. diff* infection can be life-threatening, especially for older adults: one in 11 patients over 65 who get infected in a healthcare setting die within a month [207]. Therefore, a rapid and simple diagnostic test that can be done near the patient's bed would be very useful for enhancing the quality of care and avoiding fatal outcomes in hospital settings. The sensing system was built on the work carried out by Zou *et al.* [139], thus including 4 steps: DNAzyme-mediated RNA cleavage (DRC), assembly-mediated strand release reaction (ASR) via a 4WJ, catalytic hairpin assembly (CHA), and result visualisation on lateral-flow assays. The DRC was developed at McMaster university by the PhD student So Yeon Lee, and consisted of a *trans*-acting DNAzyme (substrate sequence separated from the DNAzyme [208]) with a single adenine ribonucleotide linkage. In this project, we followed the designs of Li *et al.* [209] and Zhou *et al.* [128] to construct two sets of sequences that could form 4WJ compatible with the CHA systems introduced by the two groups. Knowing the DNAzyme substrate sequence and the catalyst DNA sequence for CHA, two more DNA sequences needed to be designed to form a functional 4WJ. Two possible 4WJ conformations for each set of sequences were considered: (1) the DNA sequences form a junction with a square planar geometry, and four duplex arms extending from it, (2) the DNA sequences form a junction with a stacked-X structure, and two pairs of arms form coaxial double helices that have 2-fold symmetry [210]. 4WJ with conformation (2) was chosen because the base pairs length of the designed DNA sequences allowed to easily distinguish them on a 15% nPAGE gel. The melting temperatures of each DNA sequence involved in the 4WJ was quickly investigated using the OligoAnalyzerTM Tool [172,173] to make sure that they were above room temperature (>25 °C). The formation of 4WJ and CHA were initially tested separately using 15% nPAGE, and the same reaction buffer described in Section 6.1 was used for all sets as this buffered represented the optimal conditions for the cleavage activity of the DNAzyme developed by the student at McMaster. The concentrations of hairpins in each CHA system was optimised to achieve the best catalytic efficiency following the optimisation process of Section 6.1. Next, the 4WJ and CHA systems were combined and performed in a sequential order. The results provided by the CHA by Zhou *et al.* work [128] combined with the 4WJ

we designed, gave clearer results than the other set of sequences in terms of clarity of DNA sequences interactions. A fluorescent quantification method for the biosensor output was also used. The method used a dsDNA-specific dye, *i.e.*, SYTOXTM Green Nucleic Acid Stain (Thermo Fisher Scientific Inc.), following the protocol provided by the manufacturer [211]. The hairpin sequence H2 (Appendix A.3) was labelled with Biotin as described before, and the fluorescent readout consisted in conjugating biotinylated H2 onto a streptavidin-coated plate to immobilise H2. The CHA reaction (incubation of H1, H2 and DNA6) was performed for 30 minutes at room temperature, and then the plate was washed with Tris buffered saline (TBS, pH 7.4, Thermo Fisher Scientific Inc.) to remove any excess folded hairpins and H1/DNA6 complex. In this way only H1/H2 complexes remained conjugated to the plate and fluorescent staining with SYTOX was performed as per protocol [211]. The fluorescence of the mixture was measured using a microplate reader (SynergyTM HT Multi-Mode Microplate Reader, BioTek[®] Instruments, Inc.) at 528 nm. As described in Section 6.1, Biotin and FAM were used to label hairpins H1 and H2 for LFS reading. However, the combination of 4WJ and CHA did not produce clear and optimal results, and we observed leakage of H1/H2 and ambiguous interactions of DNA sequences. Due to time constraints, we could not continue the project. Nevertheless, we believe that the new biosensor can be developed with further optimisation.

6.2 Discussions and Conclusions

This work demonstrated that CHA results on LFSs can be easily read by using commercially available nucleic acid lateral flow assay (U-Star Disposable Nucleic Acid Detection Strips, Type 3), which potentially enables its deployability at the point-of-care. The use of LFSs to read CHA results is a novel approach that was recently reported by Wang *et al.* [138], Zou *et al.* [139] and Su *et al.* [140] for the detection of SARS-CoV-2 infection and hepatitis C virus, respectively.

A more comprehensive approach to move to a full point-of-care use of CHA would be to incorporate the CHA biosensor developed by Zhou *et al.* [128] into a fully paper-based device, as shown briefly in Fig. 6.11.

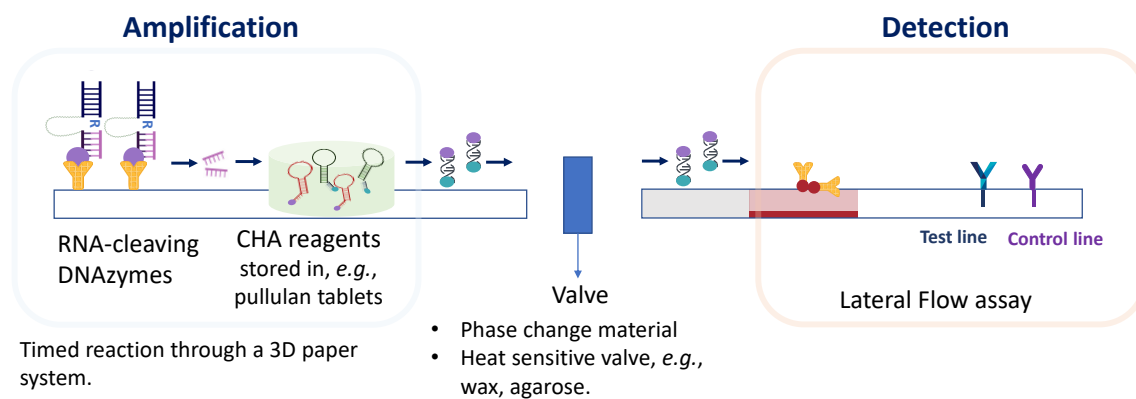


Figure 6.11: **Schematic of a fully paper-based device that integrates a DNzyme biosensor with lateral flow assay.** CHA amplification and detection are performed on a perp strip and are separated by a valve. The reagents necessary to performed CHA (DNA sequences H1 and H2) can be stored in pullulan tablets that dissolve when the sample has reached them. Detection and results visualisation is performed on nucleic acid lateral flow assays.

Enzyme-free amplification techniques, such as CHA, have the great advantage over isothermal amplification techniques, like LAMP, of being stable at room temperature and not requiring a heating step. However, the efficacy of the biosensing reaction depends on specific temperatures. CHA relies on the folding and unfolding of oligonucleotides (hairpins), and hairpins stability is sensitive to temperature changes. This can increase the risk of CHA leakage and false positive results on LFSs. Therefore, CHA may not be suitable for universal and easy application in different parts of the world, where the environmental conditions may vary.

Unfortunately, due to time constraints, it was not possible to evaluate the effectiveness of each optimised technique in combination (DRC, ASR and CHA tested in Section 6.1), and to proceed further with the project.

6.3 Contribution to knowledge

The preliminary results in this chapter demonstrate that CHA results can be effectively read using commercially available nucleic acid lateral flow assay. This enables an easier interpretation of CHA results compared to the most common fluorescent readings.

Recently, Zou *et al.* [139] and Su *et al.* [140] reported CHA-LFS-based methods for detecting SARS-CoV-2 infection and hepatitis C virus, respectively. However, the integration of the enzyme-free biosensor introduced by McMasters researchers [128] with LFS readings has the potential to expand the application of CHA and LFSs beyond viral detection.

Our study sheds light on the challenges associated with reading CHA results on LFSs, and implementing enzyme-free biosensors in in-field settings. To achieve reliable results using CHA, intensive optimization efforts are essential to minimize reaction leakages which can lead to false positive results in the LFSs readouts. Additionally, these types of biosensors require precise optimization for specific temperature and pH conditions, which can be difficult to control outside laboratory environments. Therefore, the implementation of enzyme-free biosensors is still limited to settings where environmental conditions control is feasible.

Chapter 7

Conclusions and Future Works

7.1 Summary of Findings and Conclusions

Nucleic acid amplification based diagnostic tests (NAATs) are the gold standard for pathogen detection, as they offer higher sensitivity compared to immunological tests [32]. After researchers have expanded detection capabilities of NAATs, such as polymerase chain reaction (PCR), to several pathogens, they have more recently focused on boosting isothermal NAATs as rapid and single-temperature alternatives to PCR. However, these methods have the limitation of being carried out in well-equipped laboratories by trained personnel, involving many manual steps, and of deploying materials that need to be stored in cold conditions. Given the ability of NAATs to detect low density infections, that are common in both low and high transmission settings, it is important to increase their accessibility at a point-of-care (POC) level by reducing the number of handling steps, eliminating the need for cold storage, and simplifying the overall operations.

The presented studies targeted possible improvements to the user-friendliness and reagent robustness of nucleic acid-based diagnostic devices in challenging environmental conditions, such as high temperatures, and high levels of humidity. The main findings and conclusions will be divided per chapter.

The introduction discussed how sample preparation represents one of the main drawbacks of NAATs, because of more than 10 manual steps required, and the need for benchtop equipment that uses electricity, i.e., heaters and centrifuges. Chapter 3 describes a 6-steps paper-based sample preparation method that can lyse and extract

DNA in 10 minutes without external heating or complex steps. The method uses paper discs with dried lysis buffer to capture and release DNA from 100 μL of *E. coli* K12 samples. Compared to conventional magnetic beads-based kits (which are often regarded as the best option due to their scalability and versatility for different sample types [212]), the introduced paper-based DNA extraction method brings advantages in terms of reagent consumption, handling simplicity and speed. The method could possibly be generalised to other bacterial species, and fully integrated in POC devices. Paper-based sample pretreatments methods are a relevant research topic, as shown by the recent literature [10–13, 21, 91, 92, 163] and the potential market entry of SnapDx [164] which is the first product that uses paper-based sample pretreatment for the detection of SARS-Cov-2.

The stability of molecular POC devices depends on the cold chain to maintain NAATs reagents functional. As discussed in Chapter 4, pullulan and trehalose can preserve and store LAMP reagents in a solid format at high temperatures. Pullulan-trehalose tablets offer a simple, cost-effective and energy efficient manufacturing method compared to other LAMP reagents storage techniques based on lyophilisation and concentration [22–25]. Therefore, LAMP reagents stabilised in these tablets could be produced nearer the end-use and increase access to reagents with long shelf-life at a community level. Pullulan-trehalose tablets in high temperatures and under uncontrolled conditions have shown a general 10-fold loss in limit-of-detection (LOD) compared to reagents stored at $-20\text{ }^{\circ}\text{C}$ (both for *E. coli malB* gene and *P. falciparum*). Even though there is a decrease in performance of reagents stored dry in pullulan-tablets compared to fresh reagents, they can be combined with lateral flow assays and greatly simplify transport logistics of low-cost POC devices in remote areas. If appropriate reagents sealing is applied, pullulan tablets represent an advantageous LAMP reagents storage method.

Moreover, in Chapter 4, pullulan-trehalose tablets have been stored and shipped inside a POC device for the detection of malaria in the field, in Uganda. To simplify the sample preparation from blood and reduce the manual steps and complexity in the POC device, a method that uses magnetic-beads and gives comparable results to more sophisticated methods was developed. The method requires 11 steps (instead of 19 steps as in Garret [152]), and only a magnet as external equipment. Following the platforms of Rodriguez-Mateos *et al.* [102] and Ngamsom *et al.* [103], stored dry reagents and

lateral flow strips results visualisation were introduced to avoid unnecessary manual handling steps. Even though the device was able to provide a result in 2 hours and 45 minutes, it presented several limitations in terms of reagents loading and unreliable results. Our field testing showed the challenges of translating lab-based methods to field conditions, which may pose additional problems that are not evident in controlled laboratory environments and are often overlooked. A functional prototype device that uses immiscible fluids and can operate in remote locations requires further development.

Chapter 5 showed how to combine sample preparation and nucleic acid amplification in one chamber to simplify POC NAATs devices. The device had all the reagents stored inside and used a layered structure of dried reagents and pullulan tablets to automate fluid movement, so it could work in in-field settings without extra equipment or manual steps. The main challenge in making a fully sample-in-answer-out device was reagents evaporation during LAMP, therefore the prototyped platform was used to carry out lysis and DNA purification only. The sample pretreatment (based on the methods from Chapter 3) was tested for 100 μL of *E. coli* K12 sample with a high bacterial concentration, took about 20 minutes, 5 steps and it needed two pipette tips. The LOD of the paper-based DNA extraction tested in tubes with 3-mm diameter discs (Section 3.1.4.3) was similar to the beads-based gold standard and the performance of sample pretreatment was the same when the lysis buffer was dried on paper or fresh (Section 3.1.9), so we envision that performing the sample pretreatment on the device would not negatively affect the LOD of the assay. To enclose all NAAT steps in ‘one chamber’, however, considerable changes on the initial proof-of-concept paper-based POC device are needed.

The paper-based molecular POC device presented is not fully functional yet, but it shows how NAATs for infectious diseases diagnosis can be simplified and their reagents can be enclosed in a single device that can work in environmentally challenging settings. We have introduced a proof-of-concept ‘one pot’ paper-based POC device that invites further research and development.

Chapter 6 delved into the enzyme-free amplification method known as catalytic hairpin assembly (CHA) and its integration with lateral flow assays. Zhou *et al.* [128] developed an enzyme-free biosensor for the detection of *E. coli* that, when combined with lateral flow strip readouts, could offer an alternative to the commonly used LAMP

method. This approach enhances the stability of reaction reagents and eliminates the need for a heating step during DNA amplification, making it suitable for reagent storage in environments without refrigeration. Our preliminary results demonstrate that CHA results can be interpreted using commercially available nucleic acid lateral flow assays, thus simplifying result interpretation compared to the more common fluorescent readings. However, further investigations are necessary to fully incorporate the CHA-based biosensor from Zhou *et al.* [128] into a fully paper-based device. There are still challenges associated with implementing enzyme-free biosensors in real-world settings. Understanding the potential use of enzyme-free biosensors within different levels of healthcare settings requires careful consideration of the optimized reaction working temperature and pH conditions.

7.2 Future Works

With this research, I have shown how translating a lab-based proof-of-concept diagnostic platform into a test that can be used in the field is a challenging and time-consuming process. However, the recent outbreaks of global health threats such as Ebola, Zika, SARS, MERS CoV, and COVID-19 have highlighted the urgency of accelerating the development, validation and production of diagnostic tools and reagents for infectious diseases to strengthen epidemic preparedness [213]. There are many different formats that POC diagnostic devices can have, such as paper-based systems, microfluidic platforms (lab-on-a-chip technologies), electrical biosensors, smartphone-based methods, and hybrid solutions [214]. Among these, POC paper-based molecular devices that use NAATs, such as loop-mediated isothermal amplification (LAMP), have gained interest as accurate, low-cost and rapid platforms. However, as already highlighted in the previous section, the challenges posed by the high number of manual steps and the reagent storage at cold temperatures need to be addressed to guarantee accurate and sensitive results in resource limited settings.

A potential solution to simplify sample pretreatment would be optimising LAMP reactions to eliminate the need for NA extraction steps, which requires a deep understanding of biological processing and that has compromised the tests' sensitivity so far [215–217]. Integrating microfluidic devices with paper-based methods could streamline the sample preparation procedure, avoiding complex manual steps and bulky equipment. In fact, microfluidic devices from thermoplastic polymers offer a promising low-

cost solution as they can integrate multiple functions such as mixing, separation, and detection [218, 219]. Moreover, injection moulding and hot embossing methods enable mass production at a low cost per unit of polymer-based microfluidic devices, making this type of devices suitable for single-use POC applications [219, 220]. Lastly, 3D printing technology could revolutionise microfluidics by making it more accessible and affordable for both end-users and researchers across different domains [221, 222]. In fact, even though 3D printing may present some limitations at larger scales compared to other fabrication methods, it can allow for local and timely production of diagnostics in remote areas or when supply chains are disrupted [223].

Future works could focus on improving the microfluidic systems to also isolate the LAMP reaction chambers from adjacent channels and wells during the reaction thus avoiding evaporation of reagents. This might require the study of low cost valves that can be easily integrated in microfluidic systems without the need for external bulky equipment. 3D printed examples have been recently put forward by Chan *et al.* [224], but other types of valves, such as polymer micro valves with pneumatic chambers [225], and self-healing membranes could be investigated. To further reduce user's handling steps and make the POC NAATs devices fully automated, portable heating units powered by batteries or cell phones, as suggested by Tang *et al.* [11] and Phillips *et al.* [12], could be integrated directly with the microfluidic platforms.

Another way to overcome the limitation of heating required by LAMP in low-resource settings is to use enzyme-free biosensor systems. As explained in Chapter 6, these strategies have the important advantage of not requiring complex and energy-intensive instrumentation, with all reagents being stored under ambient conditions, without refrigeration. Moreover, they do not rely on enzymes that may degrade over time and affect the performance of POC NAATs in the field. Efforts could focus on investigating further these techniques to make them stable in a wider range of temperatures and integrate this types of biosensors in paper-based devices, thus opening the route for their applications outside laboratory settings.

Co-designing POC diagnostic technologies with the end-users, is essential to ensure their effectiveness [226]. By engaging the end-users in the early stages of the design process through methods such as site visits, surveys, and pilot studies, the researchers can gain a deeper understanding of the needs and preferences of the target audience. This can lead to more successful POC devices that are tailored to the needs of end-users

and integrate well with the local healthcare system, not only from a technical perspective but also by allowing the simultaneous detection of multiple relevant diseases. For instance, the target product profiles (TPPs) developed by the joint effort of the World Health Organisation (WHO), the Foundation for Innovative New Diagnostics (FIND) and other organisations, are not enough to capture the specifics of the local health care context and the end-users' needs. To fill this gap, Bengtson *et al.* [227] have proposed an intermediate guideline called the concept target product profile (CTTP) that integrates elements of design thinking and use case scenarios. For example, a major difficulty in the application of POC technologies is to interpret data in a way that is meaningful for medical purposes, and to help non-specialist users (such as health workers and volunteers) to refer patients appropriately. However, if the end-user is a qualified lab technician who knows how to conduct diagnostic tests, full automation is not required, and may even be undesirable for the them.

One of the objectives of conducting field trials is to evaluate the performance of the novel POC device under real-world conditions but also to assess the needs and preferences of the end-users. Site visits also allow the understanding of how the POC devices would be stored and disposed of after use. This is particularly relevant for rural areas, where appropriate disposal facilities might not be available [167, 228]. The extensive use of disposable diagnostic devices has led to concerns about the environmental and health risks posed by the amounts of plastic and biohazard waste produced [3]. By way of example of the global environmental impact of diagnostic tests, a WHO report on healthcare waste, associated with its own initiatives in COVID-19, estimated many tens of thousands of extra waste (mainly plastic) generated over the 18 month period between March 2020 and November 2021 [228]. It was highlighted how 97% of plastic waste from tests is generally incinerated, producing well known carcinogens, such as dioxins and polycyclic aromatic hydrocarbons [167, 229]. Such figures highlight the importance of undertaking environmental impact analyses, implemented as early as the design phase of diagnostic devices to inform manufacturing decisions - which do not directly affect the patient, but ultimately contribute to potential deleterious outcomes, downstream, on both human health and the environment [230]. Therefore, the identification of environmental hotspots among the reagents and materials used in already developed devices would serve as a guideline for the future development of POC NAATs with a reduced environmental impact.

The work presented in this study introduced new techniques to stabilise and store-dry reagents to develop new diagnostics for areas of the world where refrigeration is not available (whilst reducing the overall carbon footprint of the test using low-power techniques). Such diagnostics will free diagnostic infrastructure from the “cold-chain” that often constrains treatment campaigns in remote areas. However, more work is needed to improve assays sensitivity and accuracy over the long term, by for example introducing glycerol-free DNA polymerase (as discussed in Section 4.2.1).

Moreover, this study demonstrates the importance of multidisciplinary to succeed in developing fully integrated sample-in-answer-out POC NAATs. Scientists, local stakeholders, industrial designers are all key experts in making effective POC diagnostic devices that could be potentially commercialised. Paper-based POC molecular detection platforms have the great potential to enable surveillance and epidemiological monitoring in endemic settings, where sensitivity, cost and convenience are essential factors.

Bibliography

- [1] Theo Vos, Stephen S Lim, Cristiana Abbafati, Kaja M Abbas, Mohammad Abbasi, Mitra Abbasifard, Mohsen Abbasi-Kangevari, Hedayat Abbastabar, Foad Abd-Allah, Ahmed Abdelalim, et al. Global burden of 369 diseases and injuries in 204 countries and territories, 1990–2019: a systematic analysis for the global burden of disease study 2019. *The Lancet*, 396(10258):1204–1222, 2020.
- [2] Mickey Urdea, Laura A Penny, Stuart S Olmsted, Maria Y Giovanni, Peter Kaspar, Andrew Shepherd, Penny Wilson, Carol A Dahl, Steven Buchsbaum, Gerry Moeller, et al. Requirements for high impact diagnostics in the developing world. *Nature*, 444(1):73–79, 2006.
- [3] Kevin J Land, Debrah I Boeras, Xiang-Sheng Chen, Andrew R Ramsay, and Rosanna W Peeling. Reassured diagnostics to inform disease control strategies, strengthen health systems and improve patient outcomes. *Nature microbiology*, 4(1):46–54, 2019.
- [4] Tsugunori Notomi, Hiroto Okayama, Harumi Masubuchi, Toshihiro Yonekawa, Keiko Watanabe, Nobuyuki Amino, and Tetsu Hase. Loop-mediated isothermal amplification of dna. *Nucleic acids research*, 28(12):e63–e63, 2000.
- [5] Myriam Vincent, Yan Xu, and Huimin Kong. Helicase-dependent isothermal dna amplification. *EMBO reports*, 5(8):795–800, 2004.
- [6] Olaf Piepenburg, Colin H Williams, Derek L Stemple, and Niall A Armes. Dna detection using recombination proteins. *PLoS biology*, 4(7), 2006.
- [7] Mats Nilsson, Mats Gullberg, Fredrik Dahl, Karoly Szuhai, and Anton K Raap. Real-time monitoring of rolling-circle amplification using a modified molecular beacon design. *Nucleic Acids Research*, 30(14):e66–e66, 2002.
- [8] WHO Global Health Estimates. The top 10 causes of death. <https://www.who.int/news-room/fact-sheets/detail/the-top-10-causes-of-death>, 2020 (accessed April 8, 2021).
- [9] Luc Bissonnette and Michel G. Bergeron. Portable devices and mobile instruments for infectious diseases point-of-care testing. *Expert Review of Molecular Diagnostics*, 17(5):471–494, 2017. PMID: 28343420.
- [10] John T Connelly, Jason P Rolland, and George M Whitesides. “paper machine” for molecular diagnostics. *Analytical chemistry*, 87(15):7595–7601, 2015.
- [11] Ruihua Tang, Hui Yang, Yan Gong, MinLi You, Zhi Liu, Jane Ru Choi, Ting Wen, Zhiguo Qu, Qibing Mei, and Feng Xu. A fully disposable and integrated paper-based device for nucleic acid extraction, amplification and detection. *Lab on a Chip*, 17(7):1270–1279, 2017.
- [12] Elizabeth A Phillips, Taylor J Moehling, Karin FK Ejendal, Orlando S Hoilett, Kristin M Byers, Laud Anthony Basing, Lauren A Jankowski, Jackson B Bennett, Li-Kai Lin, Lia A Stanciu, et al. Microfluidic rapid and autonomous analytical device (microraad) to detect hiv from whole blood samples. *Lab on a Chip*, 19(20):3375–3386, 2019.
- [13] Lisa K Lafleur, Joshua D Bishop, Erin K Heiniger, Ryan P Gallagher, Maxwell D Wheeler, Peter Kauffman, Xiaohong Zhang, Enos C Kline, Joshua R Buser, Sujatha Kumar, et al. A rapid, instrument-free, sample-to-result nucleic acid amplification test. *Lab on a Chip*, 16(19):3777–3787, 2016.

- [14] Nikunja Kolluri, Shwetha Kamath, Patrick Lally, Mina Zanna, James Galagan, Jesse Gitaka, Moses Kamita, Mario Cabodi, Srinivasa Raju Lolabattu, and Catherine M Klapperich. Development and clinical validation of iso-imrs: A novel diagnostic assay for p. falciparum malaria. *Analytical Chemistry*, 93(4):2097–2105, 2021.
- [15] Carlos Manzananas, Md Mahbulul Alam, Julia C Loeb, John A Lednicky, Chang-Yu Wu, and Z Hugh Fan. A valve-enabled sample preparation device with isothermal amplification for multiplexed virus detection at the point-of-care. *ACS sensors*, 6(11):4176–4184, 2021.
- [16] Xin Ye, Jin Xu, Lijuan Lu, Xinxin Li, Xueen Fang, and Jilie Kong. Equipment-free nucleic acid extraction and amplification on a simple paper disc for point-of-care diagnosis of rotavirus a. *Analytica chimica acta*, 1018:78–85, 2018.
- [17] Julien Reboud, Gaolian Xu, Alice Garrett, Moses Adriko, Zhugen Yang, Edridah M Tukahebwa, Candia Rowell, and Jonathan M Cooper. Paper-based microfluidics for dna diagnostics of malaria in low resource underserved rural communities. *Proceedings of the National Academy of Sciences*, 116(11):4834–4842, 2019.
- [18] Natalia M Rodriguez, Winnie S Wong, Lena Liu, Rajan Dewar, and Catherine M Klapperich. A fully integrated paperfluidic molecular diagnostic chip for the extraction, amplification, and detection of nucleic acids from clinical samples. *Lab on a Chip*, 16(4):753–763, 2016.
- [19] Navjot Kaur, Joy S Michael, and Bhushan J Toley. A modular paper-and-plastic device for tuberculosis nucleic acid amplification testing in limited-resource settings. *Scientific Reports*, 9(1):15367, 2019.
- [20] Kentaro Yamada, Hiroyuki Shibata, Koji Suzuki, and Daniel Citterio. Toward practical application of paper-based microfluidics for medical diagnostics: state-of-the-art and challenges. *Lab on a Chip*, 17(7):1206–1249, 2017.
- [21] Yiping Zou, Michael Glenn Mason, Yuling Wang, Eugene Wee, Conny Turni, Patrick J Blackall, Matt Trau, and Jose Ramon Botella. Nucleic acid purification from plants, animals and microbes in under 30 seconds. *PLoS biology*, 15(11), 2017.
- [22] Sujatha Kumar, Ryan Gallagher, Josh Bishop, Enos Kline, Joshua Buser, Lisa Lafleur, Kamal Shah, Barry Lutz, and Paul Yager. Long-term dry storage of enzyme-based reagents for isothermal nucleic acid amplification in a porous matrix for use in point-of-care diagnostic devices. *Analyst*, 145(21):6875–6886, 2020.
- [23] Esra Agel and Hasan Sagcan. Optimization of lyophilized lamp and rt-pcr reaction mixes for detection of tuberculosis. *The EuroBiotech Journal*, 4(4):230–236, 2020.
- [24] Xin Song, Felicity J Coulter, Ming Yang, Jessica L Smith, Fikadu G Tafesse, William B Messer, and John H Reif. A lyophilized colorimetric rt-lamp test kit for rapid, low-cost, at-home molecular testing of sars-cov-2 and other pathogens. *Scientific Reports*, 12(1):7043, 2022.
- [25] J García-Bernalt Diego, P Fernández-Soto, B Crego-Vicente, S Alonso-Castrillejo, B Febrer-Sendra, A Gómez-Sánchez, B Vicente, J López-Abán, and A Muro. Progress in loop-mediated isothermal amplification assay for detection of schistosoma mansoni dna: towards a ready-to-use test. *Scientific reports*, 9(1):1–11, 2019.
- [26] Vincent Leung, Meredith Brooks, Sophia Emerson, Monsur Ali, and Carlos DM Filipe. Ready-to-use thermally stable mastermix pills for molecular biology applications. *Biotechnology progress*, 35(2):e2764, 2019.
- [27] United Nations. Transforming our world: the 2030 agenda for sustainable development, general assembly resolution a/res/70/1. <https://documents-dds-ny.un.org/doc/UNDOC/GEN/N15/291/89/PDF/N1529189.pdf?OpenElement>, 2015 (accessed November 22, 2023).
- [28] Michael C Larkins and Aparna Thombare. Point-of-care testing. In *StatPearls [Internet]*. StatPearls Publishing, 2023.

- [29] Paul K Drain, Emily P Hyle, Farzad Noubary, Kenneth A Freedberg, Douglas Wilson, William R Bishai, William Rodriguez, and Ingrid V Bassett. Diagnostic point-of-care tests in resource-limited settings. *The Lancet infectious diseases*, 14(3):239–249, 2014.
- [30] Mitasha Bharadwaj, Michel Bengtson, Mirte Golverdingen, Loulotte Waling, and Cees Dekker. Diagnosing point-of-care diagnostics for neglected tropical diseases. *PLoS neglected tropical diseases*, 15(6):e0009405, 2021.
- [31] WHO Global Malaria Programme. Nucleic acid amplification-based diagnostics. <https://www.who.int/teams/global-malaria-programme/case-management/diagnosis/nucleic-acid-amplification-based-diagnostics>, 2021 (accessed December 12, 2023).
- [32] Navjot Kaur and Bhushan J Toley. Paper-based nucleic acid amplification tests for point-of-care diagnostics. *Analyst*, 143(10):2213–2234, 2018.
- [33] Joshua Hill, Shilpa Beriwal, Ishwad Chandra, Vinod K Paul, Aarti Kapil, Tripti Singh, Robert M Wadowsky, Vinita Singh, Ankur Goyal, Timo Jahnukainen, et al. Loop-mediated isothermal amplification assay for rapid detection of common strains of escherichia coli. *Journal of Clinical Microbiology*, 46(8):2800–2804, 2008.
- [34] Peter Lippa and Ralf Junker. *Point-of-care testing: Principles and clinical applications*. Springer, 2018.
- [35] Eniyu C Oriero, Jan Jacobs, Jean-Pierre Van Geertruyden, Davis Nwakanma, and Umberto D’Alessandro. Molecular-based isothermal tests for field diagnosis of malaria and their potential contribution to malaria elimination. *Journal of Antimicrobial Chemotherapy*, 70(1):2–13, 2015.
- [36] Enno Stürenburg, Norbert Gässler, Aline Schröder, and Udo Reischl. Molecular biological tests. *Point-of-Care Testing: Principles and Clinical Applications*, pages 81–89, 2018.
- [37] Laura Magro, Camille Escadafal, Pierre Garneret, Béatrice Jacquelin, Aurélia Kwasiborski, Jean-Claude Manuguerra, Fabrice Monti, Anavaj Sakuntabhai, Jessica Vanhomwegen, Pierre Lafaye, et al. Paper microfluidics for nucleic acid amplification testing (naat) of infectious diseases. *Lab on a Chip*, 17(14):2347–2371, 2017.
- [38] Anjum Qureshi and Javed H Niazi. Biosensors for detecting viral and bacterial infections using host biomarkers: a review. *Analyst*, 145(24):7825–7848, 2020.
- [39] Abul Kalam Azad, Al Hakim, Md Mehadi Hasan Sohag, and Mahbuba Rahman. Metabolomics in clinical diagnosis, prognosis, and treatment of infectious diseases. In *Metabolomics*, pages 71–119. Elsevier, 2023.
- [40] Sharma T Sanjay, Guanglei Fu, Maowei Dou, Feng Xu, Rutao Liu, Hao Qi, and XiuJun Li. Biomarker detection for disease diagnosis using cost-effective microfluidic platforms. *Analyst*, 140(21):7062–7081, 2015.
- [41] Bambang Kuswandi, M Amrun Hidayat, and Eka Noviana. Paper-based sensors for rapid important biomarkers detection. *Biosensors and Bioelectronics: X*, page 100246, 2022.
- [42] Jiayi Chen, Jiahuan Zhou, Yunchi Peng, Yafeng Xie, and Yongjian Xiao. Aptamers: A prospective tool for infectious diseases diagnosis. *Journal of Clinical Laboratory Analysis*, 36(11):e24725, 2022.
- [43] Quanyuan Wan, Xiaohui Liu, and Youli Zu. Oligonucleotide aptamers for pathogen detection and infectious disease control. *Theranostics*, 11(18):9133, 2021.
- [44] Ali Bodaghi, Nadia Fattahi, and Ali Ramazani. Biomarkers: Promising and valuable tools towards diagnosis, prognosis and treatment of covid-19 and other diseases. *Heliyon*, 2023.
- [45] Whui Lyn Then and Gil Garnier. Paper diagnostics in biomedicine. *Reviews in Analytical Chemistry*, 32(4):269–294, 2013.
- [46] Zhuoqi Yao, Philip Coatsworth, Xuewen Shi, Jiakai Zhi, Lixuan Hu, Ren Yan, Firat Güder, and Hai-Dong Yu. Paper-based sensors for diagnostics, human activity monitoring, food safety and environmental detection. *Sensors & Diagnostics*, 1(3):312–342, 2022.

- [47] Max M Gong and David Sinton. Turning the page: advancing paper-based microfluidics for broad diagnostic application. *Chemical reviews*, 117(12):8447–8480, 2017.
- [48] Seokbin Hong and Wonjung Kim. Dynamics of water imbibition through paper channels with wax boundaries. *Microfluidics and Nanofluidics*, 19:845–853, 2015.
- [49] Emanuel Elizalde, Raúl Urteaga, and Claudio LA Berli. Rational design of capillary-driven flows for paper-based microfluidics. *Lab on a Chip*, 15(10):2173–2180, 2015.
- [50] Conor K Camplisson, Kevin M Schilling, William L Pedrotti, Howard A Stone, and Andres W Martinez. Two-ply channels for faster wicking in paper-based microfluidic devices. *Lab on a Chip*, 15(23):4461–4466, 2015.
- [51] Noosheen Walji and Brendan D MacDonald. Influence of geometry and surrounding conditions on fluid flow in paper-based devices. *Micromachines*, 7(5):73, 2016.
- [52] Sooyoung Chang and Wonjung Kim. Dynamics of water imbibition through paper with swelling. *Journal of Fluid Mechanics*, 892:A39, 2020.
- [53] Kevin J Land. *Paper-based Diagnostics: Current Status and Future Applications*. Springer, 2018.
- [54] Jeong Hoon Lee. Paper-based medical diagnostic devices. 2021.
- [55] Andres W Martinez, Scott T Phillips, Manish J Butte, and George M Whitesides. Patterned paper as a platform for inexpensive, low-volume, portable bioassays. *Angewandte Chemie*, 119(8):1340–1342, 2007.
- [56] Xiao Wang, Joshua A Hagen, and Ian Papautsky. Paper pump for passive and programmable transport. *Biomicrofluidics*, 7(1):014107, 2013.
- [57] Yao Lu, Weiwei Shi, Lei Jiang, Jianhua Qin, and Bingcheng Lin. Rapid prototyping of paper-based microfluidics with wax for low-cost, portable bioassay. *Electrophoresis*, 30(9):1497–1500, 2009.
- [58] Derek A Bruzewicz, Meital Rechtes, and George M Whitesides. Low-cost printing of poly (dimethylsiloxane) barriers to define microchannels in paper. *Analytical chemistry*, 80(9):3387–3392, 2008.
- [59] Koji Abe, Kaori Kotera, Koji Suzuki, and Daniel Citterio. Inkjet-printed paperfluidic immunochemical sensing device. *Analytical and bioanalytical chemistry*, 398:885–893, 2010.
- [60] Xu Li, Junfei Tian, Thanh Nguyen, and Wei Shen. based microfluidic devices by plasma treatment. *Analytical chemistry*, 80(23):9131–9134, 2008.
- [61] Girish Chitnis, Zhenwen Ding, Chun-Li Chang, Cagri A Savran, and Babak Ziaie. Laser-treated hydrophobic paper: an inexpensive microfluidic platform. *Lab on a Chip*, 11(6):1161–1165, 2011.
- [62] Seong-Geun Jeong, Jongmin Kim, Si Hyung Jin, Ki-Su Park, and Chang-Soo Lee. Flow control in paper-based microfluidic device for automatic multistep assays: A focused minireview. *Korean Journal of Chemical Engineering*, 33(10):2761–2770, 2016.
- [63] Elain Fu, Barry Lutz, Peter Kauffman, and Paul Yager. Controlled reagent transport in disposable 2d paper networks. *Lab on a Chip*, 10(7):918–920, 2010.
- [64] Elain Fu, Stephen A Ramsey, Peter Kauffman, Barry Lutz, and Paul Yager. Transport in two-dimensional paper networks. *Microfluidics and nanofluidics*, 10(1):29–35, 2011.
- [65] Bhushan J Toley, Brittney McKenzie, Tinny Liang, Joshua R Buser, Paul Yager, and Elain Fu. Tunable-delay shunts for paper microfluidic devices. *Analytical chemistry*, 85(23):11545–11552, 2013.
- [66] Hong Liu and Richard M Crooks. Three-dimensional paper microfluidic devices assembled using the principles of origami. *Journal of the American Chemical Society*, 133(44):17564–17566, 2011.
- [67] Joong Ho Shin, Juhwan Park, Seung Hoon Kim, and Je-Kyun Park. Programmed sample delivery on a pressurized paper. *Biomicrofluidics*, 8(5):054121, 2014.

- [68] Juhwan Park, Joong Ho Shin, and Je-Kyun Park. Pressed paper-based dipstick for detection of foodborne pathogens with multistep reactions. *Analytical chemistry*, 88(7):3781–3788, 2016.
- [69] Barry Lutz, Tinny Liang, Elain Fu, Sujatha Ramachandran, Peter Kauffman, and Paul Yager. Dissolvable fluidic time delays for programming multi-step assays in instrument-free paper diagnostics. *Lab on a Chip*, 13(14):2840–2847, 2013.
- [70] Bao Thai Tran, Patsamon Rijiravanich, Nitipon Puttaraksa, and Werasak Surareungchai. Wax gates in laminated microfluidic paper-based immunosensors. *Microchemical Journal*, 178:107343, 2022.
- [71] Dohwan Lee, Tevhide Ozkaya-Ahmadov, Chia-Heng Chu, Mert Boya, Ruxiu Liu, and A Fatih Sarioglu. Capillary flow control in lateral flow assays via delaminating timers. *Science Advances*, 7(40):eabf9833, 2021.
- [72] Jared Houghtaling, Tinny Liang, Gregory Thiessen, and Elain Fu. Dissolvable bridges for manipulating fluid volumes in paper networks. *Analytical chemistry*, 85(23):11201–11204, 2013.
- [73] Sana Jahanshahi-Anbuhi, Aleah Henry, Vincent Leung, Clémence Sicard, Kevin Pennings, Robert Pelton, John D Brennan, and Carlos DM Filipe. Paper-based microfluidics with an erodible polymeric bridge giving controlled release and timed flow shutoff. *Lab on a Chip*, 14(1):229–236, 2014.
- [74] Bhushan J Toley, Jessica A Wang, Mayuri Gupta, Joshua R Buser, Lisa K Lafleur, Barry R Lutz, Elain Fu, and Paul Yager. A versatile valving toolkit for automating fluidic operations in paper microfluidic devices. *Lab on a Chip*, 15(6):1432–1444, 2015.
- [75] Andres W Martinez, Scott T Phillips, Zhihong Nie, Chao-Min Cheng, Emanuel Carrilho, Benjamin J Wiley, and George M Whitesides. Programmable diagnostic devices made from paper and tape. *Lab on a Chip*, 10(19):2499–2504, 2010.
- [76] Yuanhua Li, Lisa Tran, Carlos DM Filipe, John D Brennan, and Robert H Pelton. Printed thin films with controlled porosity as lateral flow media. *Industrial & Engineering Chemistry Research*, 58(46):21014–21021, 2019.
- [77] Jonas Hansson, Hiroki Yasuga, Tommy Haraldsson, and Wouter Van der Wijngaart. Synthetic microfluidic paper: high surface area and high porosity polymer micropillar arrays. *Lab on a Chip*, 16(2):298–304, 2016.
- [78] Sana Jahanshahi-Anbuhi, Puneet Chavan, Clémence Sicard, Vincent Leung, SM Zakir Hossain, Robert Pelton, John D Brennan, and Carlos DM Filipe. Creating fast flow channels in paper fluidic devices to control timing of sequential reactions. *Lab on a Chip*, 12(23):5079–5085, 2012.
- [79] Rui Hua Tang, Li Na Liu, Su Feng Zhang, Xiao Cong He, Xiu Jun Li, Feng Xu, Yong Hao Ni, and Fei Li. A review on advances in methods for modification of paper supports for use in point-of-care testing. *Microchimica Acta*, 186(8):521, 2019.
- [80] Robert Pelton. Bioactive paper provides a low-cost platform for diagnostics. *TrAC Trends in Analytical Chemistry*, 28(8):925–942, 2009.
- [81] Sally M McFall, Robin L Wagner, Sujit R Jangam, Douglas H Yamada, Diana Hardie, and David M Kelso. A simple and rapid dna extraction method from whole blood for highly sensitive detection and quantitation of hiv-1 proviral dna by real-time pcr. *Journal of virological methods*, 214:37–42, 2015.
- [82] Wupeng Gan, Yin Gu, Junping Han, Cai-xia Li, Jing Sun, and Peng Liu. Chitosan-modified filter paper for nucleic acid extraction and “in situ pcr” on a thermoplastic microchip. *Analytical chemistry*, 89(6):3568–3575, 2017.
- [83] Michel Bengtson, Mitasha Bharadwaj, Oskar Franch, Jaco van der Torre, Veronique Meerdink, Henk Schallig, and Cees Dekker. Crispr-dcas9 based dna detection scheme for diagnostics in resource-limited settings. *Nanoscale*, 14(5):1885–1895, 2022.
- [84] Garnpimol C Ritthidej. Nasal delivery of peptides and proteins with chitosan and related mucoadhesive polymers. In *Peptide and protein delivery*, pages 47–68. Elsevier, 2011.

- [85] SA Byrnes, JD Bishop, L Lafleur, JR Buser, B Lutz, and P Yager. One-step purification and concentration of dna in porous membranes for point-of-care applications. *Lab on a Chip*, 15(12):2647–2659, 2015.
- [86] Michel L Bengtson. Development of dna diagnostics of neglected tropical diseases in resource-limited settings. 2021.
- [87] Weidong Cao, Christopher J Easley, Jerome P Ferrance, and James P Landers. Chitosan as a polymer for ph-induced dna capture in a totally aqueous system. *Analytical chemistry*, 78(20):7222–7228, 2006.
- [88] Jigar Lalani and Ambikanandan Misra. Gene delivery using chemical methods. In *Challenges in delivery of therapeutic genomics and proteomics*, pages 127–206. Elsevier, 2011.
- [89] Liyun Guan, Junfei Tian, Rong Cao, Miaosi Li, Zhangxiong Wu, Azadeh Nilghaz, and Wei Shen. Surface modification of cellulose paper for quantum dot-based sensing applications. *BioResources*, 10(1):1587–1598, 2015.
- [90] Phuoc Tung Trieu and Nae Yoon Lee. based all-in-one origami microdevice for nucleic acid amplification testing for rapid colorimetric identification of live cells for point-of-care testing. *Analytical chemistry*, 91(17):11013–11022, 2019.
- [91] Wupeng Gan, Bin Zhuang, Pengfei Zhang, Junping Han, Cai-Xia Li, and Peng Liu. A filter paper-based microdevice for low-cost, rapid, and automated dna extraction and amplification from diverse sample types. *Lab on a Chip*, 14(19):3719–3728, 2014.
- [92] Ruihua Tang, Hui Yang, Jane Ru Choi, Yan Gong, Jie Hu, Ting Wen, XiuJun Li, Bo Xu, Qibing Mei, and Feng Xu. Paper-based device with on-chip reagent storage for rapid extraction of dna from biological samples. *Microchimica Acta*, 184(7):2141–2150, 2017.
- [93] Nikunja Kolluri, Nikolas Albarran, Andy Fan, Alex Olson, Manish Sagar, Anna Young, José Gomez-Marquez, and Catherine M Klapperich. Snapflex: a paper-and-plastic device for instrument-free rna and dna extraction from whole blood. *Lab on a Chip*, 20(18):3386–3398, 2020.
- [94] Michael S Cordray and Rebecca R Richards-Kortum. A paper and plastic device for the combined isothermal amplification and lateral flow detection of plasmodium dna. *Malaria journal*, 14(1):472, 2015.
- [95] Youngung Seok, Hyou-Arm Joung, Ju-Young Byun, Hyo-Sung Jeon, Su Jeong Shin, Sanghyo Kim, Young-Beom Shin, Hyung Soo Han, and Min-Gon Kim. A paper-based device for performing loop-mediated isothermal amplification with real-time simultaneous detection of multiple dna targets. *Theranostics*, 7(8):2220, 2017.
- [96] Navaporn Sritong, Marina Sala de Medeiros, Laud Anthony Basing, and Jacqueline C Linnes. Promise and perils of paper-based point-of-care nucleic acid detection for endemic and pandemic pathogens. *Lab on a Chip*, 2023.
- [97] Carlos Matellan and Armando E del Río Hernández. Cost-effective rapid prototyping and assembly of poly (methyl methacrylate) microfluidic devices. *Scientific reports*, 8(1):6971, 2018.
- [98] Shicheng Liu, Yiqiang Fan, Kexin Gao, and Yajun Zhang. Fabrication of cyclo-olefin polymer-based microfluidic devices using co2 laser ablation. *Materials Research Express*, 5(9):095305, 2018.
- [99] Alfredo E Ongaro, Ieva Keraite, Antonio Liga, Gioacchino Conoscenti, Stuart Coles, Holger Schulze, Till T Bachmann, Khaled Parvez, Cinzia Casiraghi, Nicola Howarth, et al. Laser ablation of poly (lactic acid) sheets for the rapid prototyping of sustainable, single-use, disposable medical microcomponents. *ACS Sustainable Chemistry & Engineering*, 6(4):4899–4908, 2018.
- [100] Hsiang-Wei Lu, Rama Sakamuri, Pranav Kumar, Tanya M Ferguson, Robert W Doebler, Keith D Herrington, Ryan P Talbot, Kris M Weigel, Felicia K Nguyen, Gerard A Cangelosi, et al. Integrated nucleic acid testing system to enable tb diagnosis in peripheral settings. *Lab on a Chip*, 20(21):4071–4081, 2020.

- [101] Kathryn A Kundrod, Maria Barra, Alexis Wilkinson, Chelsey A Smith, Mary E Natoli, Megan M Chang, Jackson B Coole, Akshaya Santhanaraj, Cesaltina Lorenzoni, Celda Mavume, et al. An integrated isothermal nucleic acid amplification test to detect hpv16 and hpv18 dna in resource-limited settings. *Science Translational Medicine*, 15(701):eabn4768, 2023.
- [102] Pablo Rodriguez-Mateos, Bongkot Ngamsom, Cheryl Walter, Charlotte E Dyer, Jesse Gitaka, Alexander Iles, and Nicole Pamme. A lab-on-a-chip platform for integrated extraction and detection of sars-cov-2 rna in resource-limited settings. *Analytica chimica acta*, 1177:338758, 2021.
- [103] Bongkot Ngamsom, Alexander Iles, Moses Kamita, Racheal Kimani, Patrick Wakaba, Pablo Rodriguez-Mateos, Mary Mungai, Charlotte E Dyer, Cheryl Walter, Jesse Gitaka, et al. A sample-to-answer covid-19 diagnostic device based on immiscible filtration and crispr-cas12a-assisted detection. *Talanta Open*, 6:100166, 2022.
- [104] Rajni Kaul and Bo Mattiasson. Improving the shelf life of enzymes by storage under anhydrous apolar solvent. *Biotechnology techniques*, 7(8):585–590, 1993.
- [105] Sanjay V Kamat, Eric J Beckman, and Alan J Russell. Enzyme activity in supercritical fluids. *Critical reviews in biotechnology*, 15(1):41–71, 1995.
- [106] Kunal A Gaidhani, Mallinath Harwalkar, Deepak Bhambere, and Pallavi S Nirgude. Lyophilization/freeze drying—a review. *World journal of pharmaceutical research*, 4(8):516–543, 2015.
- [107] Kyoko Hayashida, Kiichi Kajino, Lottie Hachaambwa, Boniface Namangala, and Chihiro Sugimoto. Direct blood dry lamp: a rapid, stable, and easy diagnostic tool for human african trypanosomiasis. *PLoS Negl Trop Dis*, 9(3):e0003578, 2015.
- [108] Yael Baruch-Shpigler and David Avnir. Enzymes in a golden cage. *Chemical Science*, 11(15):3965–3977, 2020.
- [109] Sonja Kübelbeck, Jules Mikhael, Harald Keller, Rupert Konradi, Annette Andrieu-Brunsen, and Grit Baier. Enzyme-polymer conjugates to enhance enzyme shelf life in a liquid detergent formulation. *Macromolecular bioscience*, 18(7):1800095, 2018.
- [110] Peng Yin, Harry MT Choi, Colby R Calvert, and Niles A Pierce. Programming biomolecular self-assembly pathways. *Nature*, 451(7176):318–322, 2008.
- [111] Robert M Dirks and Niles A Pierce. Triggered amplification by hybridization chain reaction. *Proceedings of the National Academy of Sciences*, 101(43):15275–15278, 2004.
- [112] Itamar Willner, Bella Shlyahovsky, Maya Zayats, and Bilha Willner. Dnazymes for sensing, nanobiotechnology and logic gate applications. *Chemical Society Reviews*, 37(6):1153–1165, 2008.
- [113] Juewen Liu, Zehui Cao, and Yi Lu. Functional nucleic acid sensors. *Chemical reviews*, 109(5):1948–1998, 2009.
- [114] Lael Wentland, Rachel Polaski, and Elain Fu. Dry storage of multiple reagent types within a paper microfluidic device for phenylalanine monitoring. *Analytical Methods*, 13(5):660–671, 2021.
- [115] Maarten A Mensink, Henderik W Frijlink, Kees van der Voort Maarschalk, and Wouter LJ Hinrichs. How sugars protect proteins in the solid state and during drying (review): Mechanisms of stabilization in relation to stress conditions. *European Journal of Pharmaceutics and Biopharmaceutics*, 114:288–295, 2017.
- [116] Buddhisha Udugama, Pranav Kadhiresan, Amila Samarakoon, and Warren CW Chan. Simplifying assays by tableting reagents. *Journal of the American Chemical Society*, 139(48):17341–17349, 2017.
- [117] Hidenori Kawasaki, Toshinori Shimanouchi, and Yukitaka Kimura. Recent development of optimization of lyophilization process. *Journal of Chemistry*, 2019, 2019.

- [118] Siyu Yang and Weijia Wen. Lyophilized ready-to-use mix for the real-time polymerase chain reaction diagnosis. *ACS Applied Bio Materials*, 4(5):4354–4360, 2021.
- [119] Sana Jahanshahi-Anbuhi, Kevin Pennings, Vincent Leung, Meng Liu, Carmen Carrasquilla, Balamurali Kannan, Yingfu Li, Robert Pelton, John D Brennan, and Carlos DM Filipe. Pullulan encapsulation of labile biomolecules to give stable bioassay tablets. *Angewandte Chemie International Edition*, 53(24):6155–6158, 2014.
- [120] S Farris and L Piergiovanni. Emerging coating technologies for food and beverage packaging materials. In *Emerging Food Packaging Technologies*, pages 274–302. Elsevier, 2012.
- [121] April A Krumnow, Iryna B Sorokulova, Eric Olsen, Ludmila Globa, James M Barbaree, and Vitaly J Vodanoy. Preservation of bacteria in natural polymers. *Journal of Microbiological Methods*, 78(2):189–194, 2009.
- [122] Sana Jahanshahi-Anbuhi, H Robert, DM Carlos, et al. Simple and ultrastable all-inclusive pullulan tablets for challenging bioassays. *Chemical science*, 7(3):2342–2346, 2016.
- [123] Sana Jahanshahi-Anbuhi, Balamurali Kannan, Kevin Pennings, M Monsur Ali, Vincent Leung, Karen Giang, Jingyun Wang, Dawn White, Yingfu Li, Robert H Pelton, et al. Automating multi-step paper-based assays using integrated layering of reagents. *Lab on a Chip*, 17(5):943–950, 2017.
- [124] Morgann C Reilly and Tamara L Doering. Chapter 22 - biosynthesis of fungal and yeast glycans. In *Microbial Glycobiology*, pages 393–412. Elsevier, 2010.
- [125] Mahmoud Nasrollahzadeh, Mohaddeseh Sajjadi, S Mohammad Sajadi, and Zahra Issaabadi. Chapter 5 - green nanotechnology. In *Interface science and technology*, volume 28, pages 145–198. Elsevier, 2019.
- [126] Wouter F Tonnis, Maarten A Mensink, Arthur de Jager, Kees van der Voort Maarschalk, Hendrik W Frijlink, and Wouter LJ Hinrichs. Size and molecular flexibility of sugars determine the storage stability of freeze-dried proteins. *Molecular pharmaceutics*, 12(3):684–694, 2015.
- [127] Bingling Li, Andrew D Ellington, and Xi Chen. Rational, modular adaptation of enzyme-free dna circuits to multiple detection methods. *Nucleic acids research*, 39(16):e110–e110, 2011.
- [128] Zhixue Zhou, John D Brennan, and Yingfu Li. A multi-component all-dna biosensing system controlled by a dnazyme. *Angewandte Chemie International Edition*, 59(26):10401–10405, 2020.
- [129] Hong Wang, Huimin Wang, Qiong Wu, Meijuan Liang, Xiaoqing Liu, and Fuan Wang. A dnazyme-amplified dna circuit for highly accurate microrna detection and intracellular imaging. *Chemical science*, 10(41):9597–9604, 2019.
- [130] Meng Liu, Qiang Zhang, Zhongping Li, Jimmy Gu, John D Brennan, and Yingfu Li. Programming a topologically constrained dna nanostructure into a sensor. *Nature communications*, 7(1):1–7, 2016.
- [131] Simcha Shimron, Fuan Wang, Ron Orbach, and Itamar Willner. Amplified detection of dna through the enzyme-free autonomous assembly of hemin/g-quadruplex dnazyme nanowires. *Analytical chemistry*, 84(2):1042–1048, 2012.
- [132] Jumei Liu, Ye Zhang, Huabin Xie, Li Zhao, Lei Zheng, and Huiming Ye. Applications of catalytic hairpin assembly reaction in biosensing. *Small*, 15(42):1902989, 2019.
- [133] Rudi Liu, Erin M McConnell, Jiuxing Li, and Yingfu Li. Advances in functional nucleic acid based paper sensors. *Journal of Materials Chemistry B*, 8(16):3213–3230, 2020.
- [134] Juewen Liu, Zehui Cao, and Yi Lu. Functional nucleic acid sensors. *Chemical reviews*, 109(5):1948–1998, 2009.
- [135] Nasir Ali, Rita de Cássia Pontello Rampazzo, Alexandre Dias Tavares Costa, and Marco Aurelio Krieger. Current nucleic acid extraction methods and their implications to point-of-care diagnostics. *BioMed research international*, 2017(2017):9306564, 2017.

- [136] Yu Jiang, Bingling Li, John N Milligan, Sanchita Bhadra, and Andrew D Ellington. Real-time detection of isothermal amplification reactions with thermostable catalytic hairpin assembly. *Journal of the American Chemical Society*, 135(20):7430–7433, 2013.
- [137] Sai Bi, Shuzhen Yue, and Shusheng Zhang. Hybridization chain reaction: a versatile molecular tool for biosensing, bioimaging, and biomedicine. *Chemical Society Reviews*, 46(14):4281–4298, 2017.
- [138] Wenjing Wang, Axiu Nie, Zhicheng Lu, Jinjie Li, Mingbo Shu, and Heyou Han. Catalytic hairpin assembly-assisted lateral flow assay for visual determination of microrna-21 using gold nanoparticles. *Microchimica Acta*, 186:1–9, 2019.
- [139] Mingyuan Zou, Feiya Su, Rui Zhang, Xinglu Jiang, Han Xiao, Xuejiao Yan, Chuankun Yang, Xiaobo Fan, and Guoqiu Wu. Rapid point-of-care testing for sars-cov-2 virus nucleic acid detection by an isothermal and nonenzymatic signal amplification system coupled with a lateral flow immunoassay strip. *Sensors and Actuators B: Chemical*, 342:129899, 2021.
- [140] Feiya Su, Mingyuan Zou, Huina Wu, Feng Xiao, Yan Sun, Chen Zhang, Wei Gao, Fengfeng Zhao, Xiaobo Fan, Xuejiao Yan, et al. Sensitive detection of hepatitis c virus using a catalytic hairpin assembly coupled with a lateral flow immunoassay test strip. *Talanta*, 239:123122, 2022.
- [141] Ruhangiz D. Nargessi. Magnetic solation and purification of nuclec acids. <https://patentimages.storage.googleapis.com/7e/f9/18/5427fa558ca2a9/US6855499.pdf>, 2001, United States Patent, US 6,855.499 B1.
- [142] Cytiva. Whatman filtration product guide. <https://www.s-und-s.pl/Whatman-filtration-product-guide.pdf>, 2021 (Accessed October 6, 2022).
- [143] David J Padley, Alan B Heath, Colin Sutherland, Peter L Chiodini, Sally A Baylis, and Collaborative Study Group dpadley@ nibsc. ac. uk. Establishment of the 1 st world health organization international standard for plasmodium falciparum dna for nucleic acid amplification technique (nat)-based assays. *Malaria Journal*, 7:1–9, 2008.
- [144] Spencer D Polley, Yasuyoshi Mori, Julie Watson, Mark D Perkins, Iveth J González, Tsugunori Notomi, Peter L Chiodini, and Colin J Sutherland. Mitochondrial dna targets increase sensitivity of malaria detection using loop-mediated isothermal amplification. *Journal of clinical microbiology*, 48(8):2866–2871, 2010.
- [145] Nathan A Tanner and Thomas C Evans Jr. Loop-mediated isothermal amplification for detection of nucleic acids. *Current protocols in molecular biology*, 105(1):15–14, 2014.
- [146] Petr Kralik and Matteo Ricchi. A basic guide to real time pcr in microbial diagnostics: definitions, parameters, and everything. *Frontiers in microbiology*, 8:108, 2017.
- [147] URI Genomics and Sequencing Center. Calculator for determining the number of copies of a template. <http://cels.uri.edu/gsc/cndna.html>, 2004 (last accessed August 11, 2022).
- [148] Oksana Lukjancenکو, Trudy M Wassenaar, and David W Ussery. Comparison of 61 sequenced escherichia coli genomes. *Microbial ecology*, 60(4):708–720, 2010.
- [149] Lunbiao Cui, Yiyue Ge, Xian Qi, Gaolian Xu, Haijing Li, Kangchen Zhao, Bin Wu, Zhiyang Shi, Xiling Guo, Lin Hu, et al. Detection of severe fever with thrombocytopenia syndrome virus by reverse transcription–cross-priming amplification coupled with vertical flow visualization. *Journal of clinical microbiology*, 50(12):3881–3885, 2012.
- [150] Hua Li and Andrew J Steckl. Paper microfluidics for point-of-care blood-based analysis and diagnostics. *Analytical chemistry*, 91(1):352–371, 2018.
- [151] Dohwan Lee, Chia-Heng Chu, and A Fatih Sarioglu. Point-of-care toolkit for multiplex molecular diagnosis of sars-cov-2 and influenza a and b viruses. *Acs Sensors*, 6(9):3204–3213, 2021.
- [152] Alice Catherine Garrett. *Development of a point-of-care molecular diagnostic tool for malaria and schistosomiasis in low-resource settings*. PhD thesis, University of Glasgow, 2021.

- [153] Xin Guo, Muhammad Arslan Khalid, Ivo Domingos, Anna Lito Michala, Moses Adriko, Candia Rowel, Diana Ajambo, Alice Garrett, Shantimoy Kar, Xiaoxiang Yan, et al. Smartphone-based dna diagnostics for malaria detection using deep learning for local decision support and blockchain technology for security. *Nature Electronics*, 4(8):615–624, 2021.
- [154] Elizabeth K Adekanle, Giulia Core, Xin Guo, Elías Kabbas Piñango, Victor J Ochoa Gutierrez, , and Rebecca Thompson. Sample size calculator. <https://power-app2.web.app/>, 2022 (accessed October 25, 2023).
- [155] Xin Guo, Giulia Core, Rebecca Thompson, Elizabeth K Adekanle, Victor J Ochoa Gutierrez, , and Elías Kabbas Piñango. Sample-Size-Calculator, version 1.1.0. <https://github.com/XGuoo/Sample-Size-Calculator>, 2022 (accessed October 25, 2023).
- [156] M Monsur Ali, Christine L Brown, Sana Jahanshahi-Anbuhi, Balamurali Kannan, Yingfu Li, Carlos DM Filipe, and John D Brennan. A printed multicomponent paper sensor for bacterial detection. *Scientific reports*, 7(1):1–10, 2017.
- [157] Michael Glenn Mason and Jose Ramon Botella. Simple nucleic acid extraction. <https://patentimages.storage.googleapis.com/40/a5/6e/0a4ef26d62f23b/WO2018195594A1.pdf>, 2018, International Patent, WO2018195594A1.
- [158] Katherine GB Ertell. A review of toxicity and use and handling considerations for guanidine, guanidine hydrochloride, and urea. 2006.
- [159] NIH: National Library of Medicine. Laboratory chemical safety summary (lcss) of guanidine hydrochloride. <https://pubchem.ncbi.nlm.nih.gov/compound/Guanidine-hydrochloride#datasheet=LCSS>, Accessed October 02, 2022.
- [160] NIH: National Library of Medicine. Laboratory chemical safety summary (lcss) of guanidine. <https://pubchem.ncbi.nlm.nih.gov/compound/Guanidine#datasheet=LCSS>, Accessed October 02, 2022.
- [161] Jinzhao Song, Changchun Liu, Michael G Mauk, Jing Peng, Thomas Schoenfeld, and Haim H Bau. A multifunctional reactor with dry-stored reagents for enzymatic amplification of nucleic acids. *Analytical chemistry*, 90(2):1209–1216, 2018.
- [162] Tahseen Kamal, Sher Bahadar Khan, Sajjad Haider, Yousef Gamaan Alghamdi, and Abdullah M Asiri. Thin layer chitosan-coated cellulose filter paper as substrate for immobilization of catalytic cobalt nanoparticles. *International journal of biological macromolecules*, 104:56–62, 2017.
- [163] Kenny Malpartida-Cardenas, Jake Baum, Aubrey Cunnington, Pantelis Georgiou, and Jesus Rodriguez-Manzano. A dual paper-based nucleic acid extraction method from blood in under ten minutes for point-of-care diagnostics. *Analyst*, 2023.
- [164] Prakash Lab. Snapdx. <https://www.snapdx.org/>, 2021 and ongoing (accessed November 23, 2023).
- [165] International Labour Organization ILO. International chemical safety cards (icscs) of guanidine hydrochloride. http://www.ilo.org/dyn/icsc/showcard.display?p_lang=en&p_card_id=0894&p_version=2, 2000 (accessed November 19, 2023).
- [166] International Labour Organization ILO. International chemical safety cards (icscs) of sodium lauryl sulfate. http://www.ilo.org/dyn/icsc/showcard.display?p_lang=en&p_card_id=0502&p_version=2, 2008 (accessed November 19, 2023).
- [167] Mohsen Ansari, Mohammad Hassan Ehrampoush, Mahdi Farzadkia, and Ehsan Ahmadi. Dynamic assessment of economic and environmental performance index and generation, composition, environmental and human health risks of hospital solid waste in developing countries; a state of the art of review. *Environment international*, 132:105073, 2019.
- [168] Wolfgang Henke, Kerstin Herdel, Klaus Jung, Dietmar Schnorr, and Stefan A Loening. Betaine improves the pcr amplification of gc-rich dna sequences. *Nucleic acids research*, 25(19):3957–3958, 1997.

- [169] Cuiping Ma, Yifan Wang, Pansong Zhang, and Chao Shi. Accelerated isothermal nucleic acid amplification in betaine-free reaction. *Analytical biochemistry*, 530:1–4, 2017.
- [170] Naomi Teekamp, Yu Tian, J Carolina Visser, Peter Olinga, Henderik W Frijlink, Herman J Woerdenbag, and Wouter LJ Hinrichs. Addition of pullulan to trehalose glasses improves the stability of β -galactosidase at high moisture conditions. *Carbohydrate polymers*, 176:374–380, 2017.
- [171] Andy Alhassan, Zhiru Li, Catherine B Poole, and Clotilde KS Carlow. Expanding the mdx toolbox for filarial diagnosis and surveillance. *Trends in parasitology*, 31(8):391–400, 2015.
- [172] IDT Integrated DNA Technologies. How do i use the oligoanalyzer tool to check for possible hairpins and dimers formed by my oligo? <https://www.idtdna.com/pages/support/faqs/how-do-i-use-the-oligoanalyzer-tool-to-analyze-possible-hairpins-and-dimers-formed-by-my-oligo>, (accessed October 27, 2023).
- [173] IDT Integrated DNA Technologies. Oligoanalyzer tool. <https://www.idtdna.com/calc/analyser>, (accessed October 27, 2023).
- [174] Xueqin Gao, Bingqi Sun, and Yifu Guan. Pullulan reduces the non-specific amplification of loop-mediated isothermal amplification (lamp). *Analytical and bioanalytical chemistry*, 411:1211–1218, 2019.
- [175] Giselle Maria Rachid Viana, Luciana Silva-Flannery, Danielle Regina Lima Barbosa, Naomi Lucchi, Suiane Costa Negreiros do Valle, Samela Farias, Nayara Barbalho, Paola Marchesini, Juliana Chedid Nogaredi Rossi, Venkatachalam Udhayakumar, et al. Field evaluation of a real time loop-mediated isothermal amplification assay (realamp) for malaria diagnosis in cruzeiro do sul, acre, brazil. *PloS one*, 13(7):e0200492, 2018.
- [176] Kentaro Nagamine, T Hase, and TJMCP Notomi. Accelerated reaction by loop-mediated isothermal amplification using loop primers. *Molecular and cellular probes*, 16(3):223–229, 2002.
- [177] Dorian Thompson and Yu Lei. Mini review: Recent progress in rt-lamp enabled covid-19 detection. *Sensors and Actuators Reports*, 2(1):100017, 2020.
- [178] Maja Sidstedt, Johannes Hedman, Erica L Romsos, Leticia Waitara, Lars Wadsö, Carolyn R Steffen, Peter M Vallone, and Peter Rådström. Inhibition mechanisms of hemoglobin, immunoglobulin g, and whole blood in digital and real-time pcr. *Analytical and bioanalytical chemistry*, 410:2569–2583, 2018.
- [179] Alexander Y Trick, Hoan Thanh Ngo, Anju H Nambiar, Marisa M Morakis, Fan-En Chen, Liben Chen, Kuangwen Hsieh, and Tza-Huei Wang. Filtration-assisted magnetofluidic cartridge platform for hiv rna detection from blood. *Lab on a Chip*, 22(5):945–953, 2022.
- [180] Scott M Berry, Lindsay N Strotman, Jessica D Kueck, Elaine T Alarid, and David J Beebe. Purification of cell subpopulations via immiscible filtration assisted by surface tension (ifast). *Biomedical microdevices*, 13:1033–1042, 2011.
- [181] Chung-Yee Lee and Qiang Meng. *Handbook of ocean container transport logistics: making global supply chains effective*, volume 220. Springer, 2014.
- [182] Mary E Natoli, Kathryn A Kundrod, Megan M Chang, Chelsey A Smith, Sai Paul, Jackson B Coole, Nathaniel G Butlin, Nathan A Tanner, Ellen Baker, Kathleen M Schmeler, et al. Improving performance of a sars-cov-2 rt-lamp assay for use with a portable isothermal fluorimeter: Towards a point-of-care molecular testing strategy. *Journal of biomolecular techniques: JBT*, 32(3):180, 2021.
- [183] Debayan Das, Manaswini Masetty, and Aashish Priye. Based loop mediated isothermal amplification (lamp) platforms: Integrating the versatility of paper microfluidics with accuracy of nucleic acid amplification tests. *Chemosensors*, 11(3):163, 2023.
- [184] K Rezaei, E Jenab, and F Temelli. Effects of water on enzyme performance with an emphasis on the reactions in supercritical fluids. *Critical reviews in biotechnology*, 27(4):183–195, 2007.

- [185] World Health Organization et al. Malaria rapid diagnostic test performance: results of who product testing of malaria rdts: round 8 (2016-2018). 2018.
- [186] Angelica F Tan, Giri S Rajahram, Timothy William, Mohammad Faruq Abd Rachman Isnadi, Sylvia Daim, Bridget E Barber, Steven Kho, Colin J Sutherland, Nicholas M Anstey, Seda Yerlikaya, et al. Diagnostic accuracy and limit of detection of ten malaria parasite lactate dehydrogenase-based rapid tests for plasmodium knowlesi and p. falciparum. *Frontiers in cellular and infection microbiology*, 12:1023219, 2022.
- [187] Vincent Vagenende, Miranda GS Yap, and Bernhardt L Trout. Mechanisms of protein stabilization and prevention of protein aggregation by glycerol. *Biochemistry*, 48(46):11084–11096, 2009.
- [188] David S. Phillips. Biological safety cabinets, energy efficiency saves resources. http://tools.thermofisher.com/content/sfs/brochures/EnergyEfficiencySavesResources_BioforumEU_0509.pdf, 2009 (accessed November 9, 2023).
- [189] MR Rekha and Chandra P Sharma. Pullulan as a promising biomaterial for biomedical applications: a perspective. *Trends Biomater Artif Organs*, 20(2):116–121, 2007.
- [190] Pablo Rodriguez-Mateos, Bongkot Ngamsom, Alexander Iles, and Nicole Pamme. Microscale immiscible phase magnetic processing for bioanalytical applications. *TrAC Trends in Analytical Chemistry*, page 116867, 2022.
- [191] Amy Creecy, Patricia K Russ, Francesca Solinas, David W Wright, and Frederick R Haselton. Tuberculosis biomarker extraction and isothermal amplification in an integrated diagnostic device. *PLoS one*, 10(7):e0130260, 2015.
- [192] Alwin MD Wan, Amir Sadri, and Edmond WK Young. Liquid phase solvent bonding of plastic microfluidic devices assisted by retention grooves. *Lab on a Chip*, 15(18):3785–3792, 2015.
- [193] Chia-Wen Tsao and Don L DeVoe. Bonding of thermoplastic polymer microfluidics. *Microfluidics and nanofluidics*, 6:1–16, 2009.
- [194] Ayokunle Olanrewaju, Maiwenn Beaugrand, Mohamed Yafia, and David Juncker. Capillary microfluidics in microchannels: from microfluidic networks to capillaric circuits. *Lab on a Chip*, 18(16):2323–2347, 2018.
- [195] Yannis Tsoumpas, Sam Dehaeck, Alexey Rednikov, and Pierre Colinet. Effect of marangoni flows on the shape of thin sessile droplets evaporating into air. *Langmuir*, 31(49):13334–13340, 2015.
- [196] Carmen Morcillo Perez, Marcel Rey, Benjamin D Goddard, and Job HJ Thijssen. Changing the flow profile and resulting drying pattern of dispersion droplets via contact angle modification. *arXiv preprint arXiv:2111.00464*, 2021.
- [197] Carlos Manzananas, Elise Morrison, Young S Kim, Morteza Alipanah, George Adedokun, Shouguang Jin, Todd Z Osborne, and Z Hugh Fan. Molecular testing devices for on-site detection of e. coli in water samples. *Scientific Reports*, 13(1):4245, 2023.
- [198] Gyeo-Re Han, Hee Joon Koo, Hangil Ki, and Min-Gon Kim. Paper/soluble polymer hybrid-based lateral flow biosensing platform for high-performance point-of-care testing. *ACS applied materials & interfaces*, 12(31):34564–34575, 2020.
- [199] Barry Lutz, Tinny Liang, Elain Fu, Sujatha Ramachandran, Peter Kauffman, and Paul Yager. Dissolvable fluidic time delays for programming multi-step assays in instrument-free paper diagnostics. *Lab on a Chip*, 13(14):2840–2847, 2013.
- [200] PJW He, IN Katis, RW Eason, and CL Sones. Engineering fluidic delays in paper-based devices using laser direct-writing. *Lab on a Chip*, 15(20):4054–4061, 2015.
- [201] JR Buser, S Diesburg, J Singleton, D Guelig, JD Bishop, C Zentner, R Burton, P LaBarre, P Yager, and BH Weigl. Precision chemical heating for diagnostic devices. *Lab on a chip*, 15(23):4423–4432, 2015.

- [202] Tamas Pardy, Indrek Tulp, Clemens Kremer, Toomas Rang, and Ray Stewart. Integrated self-regulating resistive heating for isothermal nucleic acid amplification tests (naat) in lab-on-a-chip (loc) devices. *PLoS One*, 12(12):e0189968, 2017.
- [203] Antonio Liga, Jonathan AS Morton, and Maiwenn Kersaudy-Kerhoas. Safe and cost-effective rapid-prototyping of multilayer pmma microfluidic devices. *Microfluidics and Nanofluidics*, 20:1–12, 2016.
- [204] Alfredo Edoardo Ongaro, Zibusiso Ndlovu, Elodie Sollier, Collins Otieno, Pascale Ondo, Alice Street, and Maiwenn Kersaudy-Kerhoas. Engineering a sustainable future for point-of-care diagnostics and single-use microfluidic devices. *Lab on a Chip*, 22(17):3122–3137, 2022.
- [205] Giulia Core. Lab-on-a-chip-fostering a sustainable future. *Frontiers in Lab on a Chip Technologies*, 2:1239134, 2023.
- [206] Zhi-Jie Tan and Shi-Jie Chen. Salt dependence of nucleic acid hairpin stability. *Biophysical journal*, 95(2):738–752, 2008.
- [207] Centers for Disease Control, National Center for Emerging Prevention, and Division of Healthcare Quality Promotion (DHQP) Zoonotic Infectious Diseases (NCEZID). *C. diff (clostridioides difficile)*. <https://www.cdc.gov/cdiff/what-is.html>, 2022 (accessed November, 2023).
- [208] Kha Tram, Pushpinder Kanda, Yingfu Li, et al. Lighting up rna-cleaving dnazymes for biosensing. *Journal of Nucleic Acids*, 2012, 2012.
- [209] Bingling Li, Andrew D Ellington, and Xi Chen. Rational, modular adaptation of enzyme-free dna circuits to multiple detection methods. *Nucleic acids research*, 39(16):e110–e110, 2011.
- [210] Brandt F Eichman, Jeffrey M Vargason, Blaine HM Mooers, and P Shing Ho. The holliday junction in an inverted repeat dna sequence: sequence effects on the structure of four-way junctions. *Proceedings of the National Academy of Sciences*, 97(8):3971–3976, 2000.
- [211] Thermo Fisher Scientific Inc. Sytox green nucleic acid stain protocol. <https://www.thermofisher.com/uk/en/home/references/protocols/cell-and-tissue-analysis/protocols/sytox-green-protocol.html>, (accessed November, 2023).
- [212] Phil Oberacker, Peter Stepper, Donna M Bond, Sven Höhn, Jule Focken, Vivien Meyer, Luca Schelle, Victoria J Sugrue, Gert-Jan Jeunen, Tim Moser, et al. Bio-on-magnetic-beads (bomb): Open platform for high-throughput nucleic acid extraction and manipulation. *PLoS biology*, 17(1):e3000107, 2019.
- [213] Rosanna W Peeling, Debrah I Boeras, and John Nkengasong. Re-imagining the future of diagnosis of neglected tropical diseases. *Computational and structural biotechnology journal*, 15:271–274, 2017.
- [214] Sofia Arshavsky-Graham and Ester Segal. Lab-on-a-chip devices for point-of-care medical diagnostics. *Microfluidics in Biotechnology*, pages 247–265, 2020.
- [215] Veronica L Fowler, Bryony Armson, Jose L Gonzales, Emma L Wise, Emma LA Howson, Zoe Vincent-Mistiaen, Sarah Fouch, Connor J Maltby, Seden Grippon, Simon Munro, et al. A highly effective reverse-transcription loop-mediated isothermal amplification (rt-lamp) assay for the rapid detection of sars-cov-2 infection. *Journal of infection*, 82(1):117–125, 2021.
- [216] Vijay J Gadkar, David M Goldfarb, Soren Gantt, and Peter AG Tilley. Real-time detection and monitoring of loop mediated amplification (lamp) reaction using self-quenching and de-quenching fluorogenic probes. *Scientific reports*, 8(1):5548, 2018.
- [217] Amir Abdulmawjood, Nils Grabowski, Svenja Föhler, Sophie Kittler, Helga Nagengast, and Guenter Klein. Development of loop-mediated isothermal amplification (lamp) assay for rapid and sensitive identification of ostrich meat. *PLoS one*, 9(6):e100717, 2014.
- [218] Md Ehtashamul Haque, Alvaro J Conde, William N MacPherson, Stephen R Knight, Richard M Carter, and Maiwenn Kersaudy-Kerhoas. A microfluidic finger-actuated blood lysate preparation device enabled by rapid acoustofluidic mixing. *Lab on a Chip*, 23(1):62–71, 2023.

- [219] Dan Liu, Ying Wang, Xingrui Li, Mengmeng Li, Qiaoyi Wu, Yanling Song, Zhi Zhu, and Chaoyong Yang. Integrated microfluidic devices for in vitro diagnostics at point of care. *Aggregate*, 3(5):e184, 2022.
- [220] Chandra M Pandey, Shine Augustine, Saurabh Kumar, Suveen Kumar, Sharda Nara, Saurabh Srivastava, and Banshi D Malhotra. Microfluidics based point-of-care diagnostics. *Biotechnology journal*, 13(1):1700047, 2018.
- [221] Jason Collingwood, Karnika De Silva, and Khalid Arif. High-speed 3d printing for microfluidics: Opportunities and challenges. *Materials Today: Proceedings*, 2023.
- [222] Garbis Atam Akceoglu, Yeşeren Saylan, and Fatih Inci. A snapshot of microfluidics in point-of-care diagnostics: multifaceted integrity with materials and sensors. *Advanced Materials Technologies*, 6(7):2100049, 2021.
- [223] Elain Fu and Lael Wentland. A survey of 3d printing technology applied to paper microfluidics. *Lab on a Chip*, 22(1):9–25, 2022.
- [224] Ho Nam Chan, Yiwei Shu, Bin Xiong, Yangfan Chen, Yin Chen, Qian Tian, Sean A Michael, Bo Shen, and Hongkai Wu. Simple, cost-effective 3d printed microfluidic components for disposable, point-of-care colorimetric analysis. *Acs Sensors*, 1(3):227–234, 2016.
- [225] Wonjong Jung, M Jalal Uddin, Kak Namkoong, Wonseok Chung, Joon-Ho Kim, and Joon S Shim. Toward a disposable low-cost loc device: heterogeneous polymer micro valve and pump fabricated by uv/ozone-assisted thermal fusion bonding. *RSC advances*, 10(47):28390–28396, 2020.
- [226] Shikha Sharma, Julia Zapatero-Rodríguez, Pedro Estrela, and Richard O’Kennedy. Point-of-care diagnostics in low resource settings: present status and future role of microfluidics. *Biosensors*, 5(3):577–601, 2015.
- [227] Michel Bengtson, Mitasha Bharadwaj, Astrid Ten Bosch, Hellen Nyakundi, Damaris Matoke-Muhia, Cees Dekker, and Jan-Carel Diehl. Matching development of point-of-care diagnostic tests to the local context: a case study of visceral leishmaniasis in kenya and uganda. *Global Health: Science and Practice*, 8(3):549–565, 2020.
- [228] World Health Organization et al. Global analysis of healthcare waste in the context of covid-19: status, impacts and recommendations. 2022.
- [229] Isiri Inamdar et al. Recycling of plastic wastes generated from covid-19: A comprehensive illustration of type and properties of plastics with remedial options. *Science of The Total Environment*, 838:155895, 2022.
- [230] Alexander Leiden, Felipe Cerdas, David Noriega, Jörg Beyerlein, and Christoph Herrmann. Life cycle assessment of a disposable and a reusable surgery instrument set for spinal fusion surgeries. *Resources, Conservation and Recycling*, 156:104704, 2020.
- [231] Bipasa Biswas. Clinical performance evaluation of molecular diagnostic tests. *The Journal of Molecular Diagnostics*, 18(6):803–812, 2016.
- [232] Peter Fayers. Practical handbook of sample size guidelines for clinical trials. jonathon j. shuster, crc press inc., boca raton, florida, 1993. no. of pages: 212, plus program on diskettes for ibm-pc (msdos) or macintosh. price:£ 51. isbn: 0-8493-4487-5, 1993.
- [233] S Carley, S Dosman, SR Jones, and M Harrison. Simple nomograms to calculate sample size in diagnostic studies. *Emergency Medicine Journal*, 22(3):180–181, 2005.
- [234] Rajeev Kumar Malhotra and A Indrayan. A simple nomogram for sample size for estimating sensitivity and specificity of medical tests. *Indian journal of ophthalmology*, 58(6):519, 2010.
- [235] Thai Thanh Truc. Statistics and sample size pro. https://play.google.com/store/apps/details?id=thaithanhtruc.info.sass&hl=en_GB, 2020 (downloaded on June 28, 2020).
- [236] 2021 StatPages. Power, sample size and experimental design calculations... <https://statpages.info/#Power>, 2020 (accessed April 8, 2021).

- [237] Karimollah Hajian-Tilaki. Sample size estimation in diagnostic test studies of biomedical informatics. *Journal of biomedical informatics*, 48:193–204, 2014.
- [238] Nancy A Obuchowski. Sample size calculations in studies of test accuracy. *Statistical Methods in Medical Research*, 7(4):371–392, 1998.
- [239] Craig A Beam. Strategies for improving power in diagnostic radiology research. *AJR. American journal of roentgenology*, 159(3):631–637, 1992.
- [240] Elise Whitley and Jonathan Ball. Statistics review 4: sample size calculations. *Critical care*, 6(4):1–7, 2002.
- [241] Nathaniel D Mercaldo, Kit F Lau, and Xiao H Zhou. Confidence intervals for predictive values with an emphasis to case–control studies. *Statistics in medicine*, 26(10):2170–2183, 2007.
- [242] Shein-Chung Chow, Jun Shao, Hansheng Wang, and Yuliya Lokhnygina. *Sample size calculations in clinical research*. CRC press, 2017.
- [243] Joseph L Fleiss, Alex Tytun, and Hans K Ury. A simple approximation for calculating sample sizes for comparing independent proportions. *Biometrics*, pages 343–346, 1980.
- [244] Geoffrey T Fosgate. Practical sample size calculations for surveillance and diagnostic investigations. *Journal of veterinary diagnostic investigation*, 21(1):3–14, 2009.
- [245] Nancy M Fenn Buderer. Statistical methodology: I. incorporating the prevalence of disease into the sample size calculation for sensitivity and specificity. *Academic Emergency Medicine*, 3(9):895–900, 1996.
- [246] Meghan Rothenbroker, Erin M McConnell, Jimmy Gu, Malene L Urbanus, Sahar Esmaili Samani, Alex W Ensminger, Carlos DM Filipe, and Yingfu Li. Selection and characterization of an rna-cleaving dnzyme activated by legionella pneumophila. *Angewandte Chemie International Edition*, 60(9):4782–4788, 2021.
- [247] Shirley HJ Mei, Zhongjie Liu, John D Brennan, and Yingfu Li. An efficient rna-cleaving dna enzyme that synchronizes catalysis with fluorescence signaling. *Journal of the American Chemical Society*, 125(2):412–420, 2003.
- [248] Hidetoshi Nishimura. Automatic thresholding. MATLAB Central File Exchange, <https://www.mathworks.com/matlabcentral/fileexchange/8502-automatic-thresholding>, 2023 (accessed September 15, 2023).

Appendix A

Appendices

A.1 Sample Size Calculator

One of the mitigation strategies has been a team-group project whose objective was to create a simple web interface to estimate the sample size needed when designing new diagnostic test studies. The project has been developed in three phases (as described in Section A.1.2) by a team of six PhD students (the Power Team).

I have been the project manager of the team. My duties mainly involved setting a time scale for the project, especially in the first and last phase of the project, actively helping the team leader in organising meetings, ensuring that everyone within the team felt comfortable with the responsibilities given, and overseeing the shared documents/folders. The project started in May 2020 and it is still ongoing.

In this chapter, Section A.1.1 is dedicated to the description of the motivation of the project. A description of the three phases of the project and my personal contribution is given in Section A.1.2. The theory background on sample size estimation specific for diagnostic test studies and the methodology followed to build the web interface are described in Sections A.1.3 and A.1.4. In the last section the results are shown and some conclusions are drawn.

A.1.1 Motivation

When developing new diagnostic tests, the evaluation of their accuracy is a fundamental step to assess the ability of the test to detect the target condition of interest. Diagnostic accuracy indices include sensitivity, specificity, likelihood ratio (LR) and area under the receiver operating characteristic curve (AUC). Moreover, in the process of designing a new diagnostic study, the selection of an optimal sample size is necessary for two important aspects. Firstly, to guarantee that the diagnostic test meets an acceptable accuracy. Secondly, to ensure that the study has high probability (power) to detect the effect [231], *i.e.*, detect that the new test is better than the minimal acceptable performance or than another test, or detect the expected accuracy. Sample size estimation becomes an ethical concern in experiments involving human or animal subjects. For instance, a too high sample size exposes a great number of subjects to the procedure without advancing knowledge and increases the costs of the experiments [232]. On the other hand, an experiment with a very low number of participants might be unable to detect the effect and thus be statistically inconclusive.

As explained more in detail in Section A.1.3, the sample size in diagnostic studies can be determined for either estimating the accuracy of a new diagnostic test, or testing a hypothesis to compare the accuracy of a new diagnostic test with another test or with a specific value. Several tools to compute the sample size when estimating accuracy are available, however,

either they are complex, such as nomograms [233,234], or they require to download a software or an app for a fee [235].

When it comes to estimate the sample size when comparing two diagnostic tests, instead, along with software to be downloaded and apps, there are already many web interfaces available online [236]. However, the theory assumptions behind the calculations used in these web-interfaces are not specified.

Therefore, the goal of the Power Team was to develop a simple web interface for sample size estimation in diagnostic studies that could be used by our research group. The designed web interface facilitates the users in understanding the inputs and outputs necessary for the estimation, and it clearly specifies the assumptions behind the calculations. Moreover, suggestions for the most appropriate values in diagnostic tests are made and supported by references to facilitate the user in choosing the inputs.

A.1.2 Objectives and Contribution

The project has shaped in three phases, and for each phase my contribution is reported.

Phase 1 - From the 5th of May 2020 to the 26th of June 2020.

Objective: Creation of a simple web interface for the computation of the sample size based on the sensitivity and specificity to be obtained by a new developed diagnostic test.

My contribution: Theoretical background study about formulas, inputs and outputs needed for the estimation of the sample size. Development of the story board to determine the final layout of the web interface, paying attention to the buttons to add, and the information to provide to make sure the inputs and outputs were clear. Coordination of team efforts and deadlines. Active definition of the agenda for meetings.

Phase 2 - From 27th of June 2020 to the 23rd of October 2020.

Objective: Expansion of the newly developed sample size calculator with the addition of a hypothesis testing option to compare diagnostic accuracy of two tests. Evaluation of an additional webpage that allows to build a Receiving Operating Curve (ROC) and the characteristics that needed to be included in the web interface to make it a valuable tool.

My contribution: Two sub-teams have been created, the first one in charge of expanding the sample size calculator, the second investigating the possibility of creating a web-based programme to generate ROC curves based on inputs from experimental data. I was coordinating the first team and in charge of adding the possibility to compare the accuracy of new diagnostic studies with previously available ones. I have been designing the story board for the new hypothesis testing part. I have been in charge of creating the Microsoft Excel files that were used for the initial validation step of this new part of the calculator. I have collaborated in validating the web interface values of the old part against literature studies.

Phase 3 - From the 20th of November 2020 to 10th June 2021.

Objective: Addition of final features to the sample size calculator and conclusion of the project through the validation of the finalised web interface with commercially available free software.

My contribution: Looking for free online calculators and software that allow to compute the sample size, based on hypothesis testing. I have been designing the story board for the new hypothesis testing part. I have been in charge of creating the excel files that were used for the initial validation step of the new part of the sample size calculator.

A.1.3 Theory Background

Sample size estimation for studies of the accuracy of diagnostic tests can take two forms [237]:

1. Estimating accuracy. Determining the number of subjects needed to define an expected level of sensitivity and specificity together with the precision of that estimate (confidence interval).
2. Confirming the difference in accuracy between two tests, also known as hypothesis testing. Determining the number of subjects needed to test the hypothesis that a particular parameter will exceed a predetermined level.

Diagnostic accuracy can be evaluated through different indices, such as sensitivity and specificity, or through various indices associated with the receiver operating characteristic (ROC) curve, *e.g.*, area under the curve (AUC). The definitions of these indices are provided in Table A.1.

Table A.1: Accuracy indices for diagnostic tests and their definitions.

Accuracy indices	
Name	Definition
Sensitivity	Percentage of truly infected people who result positive by the diagnostic test.
Specificity	Percentage of truly uninfected people who test negative by the diagnostic test.
Area under the curve (AUC)	The shape of a ROC curve* and the AUC estimate how high is the discriminative power of a diagnostic test. AUC can have values between 0 and 1, the closer to one, the better the test is at discriminating between infected and uninfected individuals.
Positive predictive value (PPV)	Percentage of those testing positive by the test who are truly infected.
Negative predicted value (NPV)	Percentage of those testing negative by the test who are truly uninfected.

* A ROC curve is a plot of a test's sensitivity against its false positive rate (or 1 - specificity) as the parameter for defining a 'positive' result changes, and it depicts the trade-off between sensitivity and specificity [238].

The factors affecting the sample size calculation are reported in Table A.2. Additional inputs to be provided along with the factors in Table A.2, when computing the sample size for estimating accuracy, are a pre-determined value of accuracy that is available from previous published studies or that was determine in laboratory samples, and the prevalence of the disease in the population. If the accuracy index is AUC, instead of the prevalence, the ratio of sample sizes of subjects without to subjects with the condition of interest is required. However, this value could be set equal to 1 if the ratio is not known.

As regards hypothesis testing, the additional inputs required are the different sensitivities (or specificities) that the statistical test have to detect.

The aforementioned notions have been implemented in the following sample size calculations. Formulas are listed in Appendix A.1.5.

Estimating accuracy - Sample size for adequate sensitivity/specificity This sample size calculation is used to establish the number of cases to estimate the sensitivity or specificity of a new diagnostic test. A pre-determined value of sensitivity/specificity is required, and it can be determined from previous published studies. In the case one is interested in estimating both sensitivity and specificity, a separate sample size calculation is performed for each accuracy, and the largest value between the two calculated total sample sizes will be considered as the total study sample size [237]. As outputs, the estimated PPV and NPV calculated as shown in [241] are also given.

Table A.2: **Factors affecting sample size calculation for diagnostic studies.**

Factors affecting sample size calculation in estimating accuracy	
Confidence level, $(1 - \alpha)$	Type I error (false positives), and confidence level for statistical judgment.
Margin of error, M	Precision with which the accuracy of interest is estimated, i.e., difference between the estimated accuracy and the true value that is expected to be detected [237].
Factors affecting sample size calculation in hypothesis testing	
Significance, α	Probability of falsely rejecting the null hypothesis.
Power, $(1 - \beta)$	Probability that the study will find a difference in the two accuracies [239]. β is the probability of failing in rejecting a false null hypothesis.
Factors affecting all sample size calculations	
Failure rate in sampling, q	Factor that considers losses of subjects or samples for example due to contamination, failure to get the test performed in time, subjects' withdrawal and missing data.**

** Most commonly, this failure accounts for 10-20% of recruited subjects, but this information can be derived from similar studies in comparable populations [240].

Estimating accuracy - Sample size for estimating AUC This calculation is used to determine the number of samples/subjects needed in order to estimate the area under the ROC curve of a diagnostic test. Being aware that the AUC can be estimated using parametric (binormal) and nonparametric (Wilcoxon statistic) approaches [237], our calculator uses the binormal approach.

Hypothesis testing - Sample size for testing sensitivity (or specificity) of single diagnostic test This calculation can determine the number of cases needed to ensure that a new diagnostic test has a better accuracy than a pre-specified accuracy value. The null hypothesis states that the accuracy of the new test, Ac , is equal to the pre-specified accuracy, p_0 .

The null and alternative hypothesis are: $H_0 : Ac = p_0$ and $H_a : Ac = p_1$.

Where p_1 is the value of the sensitivity/specificity under the alternative hypothesis.

The calculator implemented in the web interface uses a two-tailed z-score test under the null and alternative hypothesis and normal approximation is the general rule [237]. One-sided tests are often possible but rarely used in clinical research.

Moreover, sample size can be computed using either an unconditional or conditional approach. These approaches refer to the way in which the standard error in the test statistic is estimated [242].

Hypothesis testing - Sample size for comparing the sensitivity (or specificity) of two diagnostic tests This calculation can determine the number of subjects/samples needed to ensure that two diagnostic tests have different accuracies and that the study has high probability to detect the actual difference. The null hypothesis states that

the two tests have equal accuracies, where p_1 and p_2 are the accuracies of each test. The calculator implemented in the web interface uses a two-tailed z-score test under the null and alternative hypothesis for a two-sample test of equality. Normal approximation is the general rule and the two study groups are independent [237], meaning that the two tests are evaluated on different subjects. Moreover, sample size can be computed using either an unconditional or conditional approach. A correction for continuity is also applied (continuity correction factor) to better approximate the exact distribution of the difference between accuracies [243, 244].

A.1.4 Methodology

The methodology followed to build the web interface can be summarised in the following steps:

1. Background and literature study for the identification of the right formulas to use in the sample size calculator.
2. Definition of inputs and outputs for each sample size calculation.
3. Creation of the story board using Microsoft Word. A detailed story board was created to avoid final major changes.
4. Implementation of the formulas for each sample size calculation in Microsoft Excel sheets. This served for a quick validation of the web interface.
5. Development of the web interface. To create the web interface, Angular 9 was used as integrate developer environment (IDE). Angular 9 is a free development platform that combines all the elements necessary to build a web interface: CSS, HTML and TypeScript (an open-source language which builds on JavaScript).
6. Final validation of the web interface with existing software and/or previous literature. This last validation was performed to ensure the correctness of the sample size calculator developed.

The methodology followed for the development of the web-based programme to generate ROC curves was slightly different than the one for the sample size calculator outlined above. The first step was to identify different existing interfaces to understand the inputs required, the outputs generated, the easiness of use and useful features that could be replicated in the web interface. The interfaces investigated were Excel (XLSTAT), Prism, R, Mathematica, Python, and MATLAB. Among those one (Python) was selected based on the feasibility of integrating it into JavaScript, and thus Typescript. A preliminary story board was created using Word. The successive steps would have consisted in implementing the ROC functionality into a web interface also creating dynamic plots. However, due to lack of time and great difficulty in the implementation, this part of the project was suspended, and the sample size calculator was prioritised.

A.1.5 Formulas Used in the Sample Size Calculator

A.1.5.1 Estimate accuracy of a single test

Sensitivity The sample size for estimating a pre-specified sensitivity, Se , can be computed as follow:

$$N' = \frac{Z_{\frac{\alpha}{2}}^2 Se(1 - Se)}{M^2 \times Prev} \quad (A.1)$$

Where $Prev$ is the prevalence of the disease, M the margin of error and $Z_{\frac{\alpha}{2}}$ represents the upper percentiles of standard normal distribution for the α -level.

The final total sample size introducing the failure rate in sampling, q , is:

$$N = \frac{N'}{(1 - q)} \quad (A.2)$$

Specificity The sample size for estimating a pre-specified specificity, Sp , can be computed as follow:

$$N' = \frac{Z_{\frac{\alpha}{2}}^2 Sp(1 - Sp)}{M^2 \times (1 - Prev)} \quad (A.3)$$

Where $Prev$ is the prevalence of the disease, M the margin of error and $Z_{\frac{\alpha}{2}}$ represents the upper percentiles of standard normal distribution for the α -level.

The final total sample size introducing the failure rate in sampling, q , is:

$$N = \frac{N'}{(1 - q)} \quad (A.4)$$

Sensitivity and specificity When both sensitivity, Se , and specificity, Sp , need to be estimated, the sample size is computed as in Equations A.1 and A.3 for sensitivity and specificity, respectively. The largest sample size between the two, is the one the user should consider for their study.

Positive and negative predicted value The estimated positive predicted value, PPV , is computed as in [241]:

$$PPV = \frac{Se \times Prev}{Se \times Prev + (1 - Sp) \times (1 - Prev)} \quad (A.5)$$

Estimated negative predicted value, NPV , is computed as in [241]:

$$NPV = \frac{Sp \times (1 - Prev)}{(1 - Se) \times Prev + Sp \times (1 - Prev)} \quad (A.6)$$

Where $Prev$ is the prevalence of the disease, Se the sensitivity and Sp the specificity.

Area under the ROC curve (AUC) The inputs required are: the AUC that needs to be estimated, the margin of error (M), the confidence level ($1 - \alpha$), the allocation ratio ($R = N_D/N_{ND}$) between the number of subjects with the condition of interest (N_D) over the ones without (N_{ND}). The sample size for estimating a pre-specified AUC can be computed as follow:

$$N = N_D + N_{ND} \quad (A.7)$$

where $N'_D = \frac{Z_{\frac{\alpha}{2}}^2 \times V(AUC)}{M^2}$ and $N_D = \frac{N'_D}{(1 - q)}$,
and where $N_{ND'} = R \times N'_D$ and $N_{ND} = \frac{N_{ND'}}{(1 - q)}$.

Moreover:

$$V(AUC) = N_D Var(\widehat{AUC}) = (0.0099 \times e^{\frac{a^2}{2}}) \times [(5a^2 + 8) + \frac{a^2 + 8}{R}] \quad (A.8)$$

and $a = \varphi^{-1}(AUC) \times 1.414$ and φ^{-1} is the inverse of the standard cumulative normal distribution.

A.1.5.2 Compare two values of accuracy

Test accuracy of a single test In this test, the null hypothesis states that the accuracy of the new test, Ac , is equal to the pre-specified accuracy, p_0 .

The null and alternative hypothesis are: $H_0 : Ac = p_0$ and $H_a : Ac = p_1$. Where p_1 is the value of the sensitivity/specificity under the alternative hypothesis.

Sample size computed using conditional approach [237]:

$$N' = \frac{[Z_{\frac{\alpha}{2}} \sqrt{p_0(1-p_0)} + Z_{\beta} \sqrt{p_1(1-p_1)}]^2}{(p_1 - p_0)^2} \quad (A.9)$$

Sample size computed using unconditional approach [242]:

$$N' = \frac{(Z_{\frac{\alpha}{2}} + Z_{\beta})^2 p_1(1-p_1)}{(p_1 - p_0)^2} \quad (A.10)$$

where $Z_{\frac{\alpha}{2}}$ and Z_{β} represent the upper percentiles of standard normal distribution for the α - and β -levels. The final total sample size introducing the failure rate in sampling q is:

$$N = \frac{N'}{(1-q)} \quad (A.11)$$

Compare accuracy of two tests In this test, the null hypothesis states that the accuracy of the diagnostic test 1, p_1 , is equal to the accuracy of the diagnostic test 2, p_2 . The null and alternative hypothesis are: $H_0 : p_1 = p_2$ and $H_a : p_1 \neq p_2$.

The allocation ratio is the ratio between the number of subjects recruited to perform the diagnostic test number 1, n_1 , and the diagnostic test number 2, n_2 :

$$k = \frac{n_1}{n_2} = \frac{N_1}{N_2}$$

Sample size computed using conditional approach [237]:

$$N_2 = \frac{[Z_{\frac{\alpha}{2}} \sqrt{(1 + \frac{1}{k})p(1-p)} + Z_{\beta} \sqrt{\frac{p_1(1-p_1)}{k} + p_2(1-p_2)}]^2}{(p_1 - p_2)^2} \quad (A.12)$$

where $Z_{\frac{\alpha}{2}}$ and Z_{β} represent the upper percentiles of standard normal distribution for the α - and β -levels, and p is

$$p = \frac{kp_1 + p_2}{1+k} \quad (A.13)$$

Sample size computed using unconditional approach [242]:

$$N_2 = \frac{(Z_{\frac{\alpha}{2}} + Z_{\beta})^2}{(p_1 - p_2)^2} \left[\frac{p_1(1-p_1)}{k} + p_2(1-p_2) \right] \quad (A.14)$$

The final number of subjects to recruit to perform the diagnostic test number 2, n_2 , is:

$$n_2 = \frac{N_2}{(1 - q)} \quad (\text{A.15})$$

Given that

$$N_1 = k \times N_2 \quad (\text{A.16})$$

The final number of subjects to recruit to perform the diagnostic test number 1, n_1 , is:

$$n_1 = \frac{N_1}{(1 - q)} \quad (\text{A.17})$$

The final total number of subjects to recruit is:

$$N = n_1 + n_2 \quad (\text{A.18})$$

Compare accuracy of two tests and correction factor The allocation ratio is the ratio between the number of subjects recruited to perform the diagnostic test number 1 and the diagnostic test number 2:

$$k = \frac{n_1}{n_2}$$

$$p = \frac{kp_1 + p_2}{1 + k} \quad (\text{A.19})$$

Sample size computed using conditional approach [237]:

$$N_2 = \frac{[Z_{\frac{\alpha}{2}} \sqrt{(1 + \frac{1}{k})p(1 - p)} + Z_{\beta} \sqrt{\frac{p_1(1 - p_1)}{k} + p_2(1 - p_2)}]^2}{(p_1 - p_2)^2} \quad (\text{A.20})$$

Sample size computed using unconditional approach [242]:

$$N_2 = \frac{(Z_{\frac{\alpha}{2}} + Z_{\beta})^2}{(p_1 - p_2)^2} \left[\frac{p_1(1 - p_1)}{k} + p_2(1 - p_2) \right] \quad (\text{A.21})$$

Continuity correction factor [243]:

$$\mathbf{N}_2 = \frac{N_2}{4} \left[1 + \sqrt{1 + \frac{2(k + 1)}{kN_2|p_1 - p_2|}} \right]^2 \quad (\text{A.22})$$

$$n_2 = \frac{\mathbf{N}_2}{(1 - q)} \quad (\text{A.23})$$

$$N_1 = k \times \mathbf{N}_2 \quad (\text{A.24})$$

$$n_1 = \frac{N_1}{(1 - q)} \quad (\text{A.25})$$

$$N = n_1 + n_2 \quad (\text{A.26})$$

A.1.6 Results and Discussion

The latest version of the sample size calculator to date is available at <https://power-app2.web.app> [154, 155], and a screenshot of the main page is shown in Fig. A.1. The calculations performed by sample size calculator for estimating accuracy were verified against the original journal article that contained the formulas, Tables 3 and 4 in [245], and against Tables 1, 2

Sample Size Calculator

This sample size calculator identifies the required sample size for evaluating the accuracy of a diagnostic test. Diagnostic accuracy can be expressed as sensitivity, specificity, likelihood ratio (LR) or area under the ROC curve (AUC), and it assesses the ability of a diagnostic test to detect the target condition of interest. According to your study purpose, you can choose two ways to estimate the proper sample size needed. You can either be interested in estimating the accuracy of a diagnostic test, or testing a hypothesis to compare the accuracy of a diagnostic test with another test, or with a specific value. The goal of this calculator is to enable you to calculate the required sample size base on any of these parameters. You can select '[Estimating accuracy of a single test](#)' if you want to meet prespecified accuracy goals, e.g., you want to recruit a certain number of subjects to achieve an expected level of sensitivity. You can select '[Compare two values of accuracy](#)' if you either want to [compare the accuracy of two diagnostic tests](#) or [compare your test with a minimally acceptable prespecified accuracy](#).

Choose the purpose of your study:

Estimate accuracy of a
single test

Compare two values of
accuracy

Figure A.1: **Main page of the sample size calculator web-interface, 'powerapp'**. The main page of the web-interface is the first page that user visualise. It provides a description of the options and the user can choose if compute the sample size either to estimate the accuracy of a new test (button: Estimate accuracy of a single test) or compare the accuracy with a new test with the accuracy of a reference or a second test (button: Compare two values of accuracy).

and 5 in [237]. The final validation of the hypothesis testing part was carried out against [242]. To make the sample size calculator complete, a few more features could be added, such as estimating accuracy based on the likelihood ratio or comparing two diagnostic tests based on AUC. However, the current sample size calculator offers a valuable tool that our research group can use to design future diagnostic studies.

In the future, it would be interesting to develop a web interface that allows to generate a ROC curve in a simple way. This would prevent the users to learn new programming languages and provide an accessible and robust platform for the ROC curve.

A.2 Pressure Applied to the PMMA Stack to Create the 3D Structure of Point-Of-Care Device

The pressure applied onto the PMMA stack was derived from the the pressure formula, Eq. A.27a, as described below.

$$\vec{Pressure} = \frac{\vec{Force}}{Area} = \frac{mass \times \vec{g}}{Area} \quad (\text{A.27a})$$

$$Pressure = \frac{mass \times g}{Area} \quad (\text{A.27b})$$

$$Pressure = \frac{(1.72 + 0.84) \text{ kg} \times 9.81 \text{ m/s}^2}{(4.1 \times 5.5) \times 10^{-4} \text{ m}^2} = 26.16 \text{ kPa} \quad (\text{A.27c})$$

Where \vec{g} is the gravitational acceleration, m is the mass of the weights applied onto the PMMA stack. The two metal blocks weighted 1.72 kg and 0.84 kg. $Area$ is the area of the device onto which the weights were applied (as shown in Fig. 2.22); not all the area of the PMMA is covered by the weights. The area covered was approximated to the width of the PMMA layers (4.1 cm) times the shortest edge of the metal block (5.5 cm). The dimensions of the first metal block were $5.5 \times 8.7 \times 14.8 \text{ cm}^3$ and the dimensions of the black metal block were $3.9 \times 7.6 \times 12.4 \text{ cm}^3$.

A.3 Enzyme-free Amplification Strategies Materials and Methods

A.3.1 Oligonucleotide Sequences

Table A.3: Oligonucleotide sequences used in the CHA biosensor developed by Zhou *et al.* [128].

Name	Sequence
EC1	5'-TGTCGAGACCTGCGACAGGAAGACTACACACAGTTGTGTG-3'
DNA2	5'-TCTTGATCGAACCAATACAGACGAAC-3'
DNA 3 (RDS1)	5'-ACTCTTCCTAGCFRQGGTTCGATCAAGA-3'
DNA 6	5'-ATTATCTTTCTCTAACCCACAGCTAGGAAGAGT-3'
DNA 7	5'-GTTTCGTCTGTATGTGGGTTAGAGA-3'
H1	5'-GTGGGTTAGAGAAAGATAAATTGGGTGGGTGGATTATCTTTCTCTA-3'
H2	5'-AGATAATCCACCCACCCAATTATCTTTCTCTATGGGTGGGTGG-3'

A.3.2 Polyacrylamide Gel Electrophoresis (PAGE)

For each of the individual reaction (DRC, ASR, CHA, SGR), the DNA solutions were mixed with 6X loading buffer (15% ficoll, 0.25% bromophenol blue, 0.25% xylene cyanol in NFW) and analysed by using 10% denaturing polyacrylamide gel electrophoresis (dPAGE) or 15% native polyacrylamide gel electrophoresis (nPAGE) ((v/v) 29:1 bisacrylamide:acrylamide). The electrophoresis was conducted in 1X TBE (pH 8.0) at a constant voltage as specified in each experiment.

The gels were scanned using a Typhoon 9200 variable mode imager (GE Healthcare) to image either FAM labelled DNA species or after staining with SYBRTMGold (Invitrogen, ThermoFisher Scientific) to image non-labelled DNA species. Imaging parameters were set as follows: emission filter: 526 SP Fluorescein, Cy2, AlexaFluor488; laser: blue (488nm); PMT: 400; Focal plane: +3; 100 pixels.

A.3.3 Preparation of Crude Extracellular Matrix and Crude Intracellular Mixture from *E. coli* K12

Crude extracellular matrix (CEM) and crude intracellular mixture (CIM) were used in the cleavage experiments.

In both the preparation of CEM and CIM from *E. coli* K12 the bacteria were anaerobically grown as described in the previous section until the optical density at 260 nm of the culture reached approximately 1, corresponding to $\sim 10^8$ CFU/mL.

CEM from *E. coli* K12 was prepared as follow: The cells were precipitated by centrifugation at 11000 g for 5 min at 4 °C. The supernatant was collected, filtered with a 0.2 μ m filter disc, aliquoted and stored at -20 °C until needed.

CIM from *E. coli* K12 was prepared as follow: 1 mL aliquots of the bacterial culture were created and centrifuged at 15000 g for 10 min at 4 °C. The supernatant was discarded, and the cells were suspended in 500 μ L of a reaction buffer (HEPES 50 mM, NaCl 150 mM, MgCl₂ 15 mM, Tween 20 0.01%, pH 7.5). This suspension was heated at 90 °C for 5 min before leaving it at room temperature for further 10 min. A second centrifugation at 15000 g for 10 min was performed. The supernatant was then collected, filtered through a 0.2 μ m filter disc, aliquoted and stored at -20 °C until use.

A.3.4 Cleavage Reactions and Activity

The DRC reaction was stopped with 2X Quenching Buffer (QB) (60 mM EDTA, 7 M urea and loading dye solution) after the incubation period. The DNazyme cleaved the substrate (RDS1) and the products were separated by 10% dPAGE. The gels were imaged as explained above and ImageJ was used to analyse the images and calculate the cleavage percentage (Clv%) of the DNazyme. The cleavage activity was computed as indicated by Rothenbroker *et al.* [246] and described in Eq. A.28. I is the band intensity derived from the gel using ImageJ. An example of gel is provided in Fig. A.2.

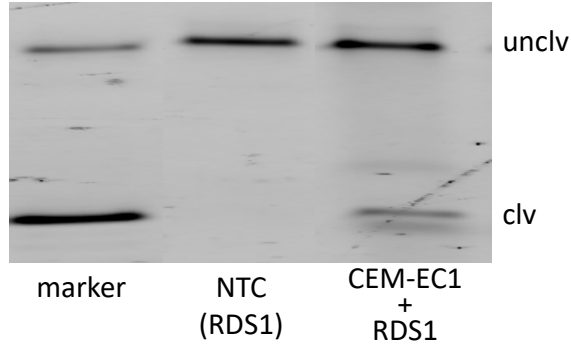


Figure A.2: **10% dPAGE analysis of the DNazyme cleavage reaction.** DNazyme-mediated RNA cleavage (DRC) involving a DNA molecule (EC1) and its substrate (RDS1). RDS1 is a DNA strand that contains a single RNA linkage surrounded by nucleotides with a fluorophore (FAM) and a quencher. FAM labelled DNA species were imaged. CEM = crude extracellular matrix. NTC = non-target control, containing only the substrate RDS1. clv = cleaved, RDS1 is cleaved. Unclv = un-cleaved.

The quencher molecule in the substrate can quench the fluorophore's fluorescence only when it is close enough [246]. However, some fluorescence can still be measured when the quencher is next to the fluorophore. To account for this imperfect interaction, the intensity of the cleaved band was divided by 6 as determined experimentally before [247].

$$I_{Clv_Adj} = (I_{Clv} - I_{Background})/6 \quad (\text{A.28a})$$

$$I_{Unclv_Adj} = (I_{Unclv} - I_{Background}) \quad (\text{A.28b})$$

$$Clv\% = \frac{I_{Clv_Adj}}{I_{Clv_Adj} + I_{Unclv_Adj}} \times 100 \quad (\text{A.28c})$$

A.3.5 Conditions for DNazyme Mediated Enzyme-Free Amplification Method

The methodology followed was inspired from Zhou *et al.* [128] as shown below. All reactions were performed in a reaction buffer (pH 8) that contains 5 mM Tris-HCl, 0.5 mM EDTA, 100 mM NaCl, 20 mM KCl and 50 mM MgCl₂.

DNazyme mediated RNA cleavage (DRC) reactions The reactions (30 μ L) were performed at room temperature using 0.5 μ M EC1 DNazyme and 40 nM of RDS1 substrate in reaction buffer. CEM or CIM from *E. coli* cells (10⁷-10⁹ CFU/mL) were incubated with the EC1 and RDS1 mixture for 15-120 min. Table A.4 provides the volumes used.

Table A.4: **Volumes needed for DNazyme mediated RNA cleavage (DRC) reactions.** For the negative control 15 μL of Luria broth were added instead of the *E. coli* CEM/CIM.

	Volume (μL)
EC1 (10 μM)	1.5
RDS1 (1 μM)	1.2
Water	6.3
E. coli CEM/CIM	15
Reaction Buffer (5X)	6
Final volume	30

Assembly-mediated strand release reaction (ASR), turn-on mode To perform the ASR reaction (30 μL), DNA strands 2, 6, 7 (40 nM each) and RDS1 (40 nM) were mixed in reaction buffer and incubated at room temperature for 10 min. Different concentrations of DNA strand 6 were trialled. The assembly of the four-way junction complex, with the four DNA strands, blocks the DNA6 from being released and stops the CHA reaction from happening.

Coupling of CHA and Lateral Flow Assay Steps followed to carry out the CHA reaction are given below, and the volumes used are shown in Table A.5

1. Hairpin structure folding: DNA hairpins H1 and H2 were separately heated at 90 $^{\circ}\text{C}$ for 10 min then cooled on ice for 10 min and then incubated at room temperature for another 15 min or at 4 $^{\circ}\text{C}$ overnight.
2. H1 and H2 were then mixed in reaction buffer to achieve a final concentration of 60 nM for each hairpin, and DNA6 was added in a concentration of 15 nM. The final volume of the reaction was 80 μL .
3. The CHA reaction was incubated at room temperature for 1 h.

Table A.5: **Volumes needed in CHA reactions.** When DNA6 was not included, reaction buffer was added to reach the final volume of 80 μL .

	Volume (μL)
H1 (1 μM)	4.8
H2 (1 μM)	4.8
DNA 6 (1 μM)	1.2
Water	53.2
Reaction Buffer (5X)	16
Final volume	80

A.4 Hairpins details for CHA

Hairpins details for CHA

Original Hairpin Sequences

DNA sequences used in the CHA reaction introduced by Zhou *et al.* (2020) ('Original'), performed in a reaction buffer with pH 8 and 5 mM Tris-HCl, 0.5 mM EDTA, 100 mM NaCl, 20 mM KCl and 50 mM MgCl₂.

DNA6	5'-ATTATCTTTCTCTA ACCCACAGCTAGGAAGAGT -3'
H1	5'- GTGGGT TAGAGAAAGATAATT GGGTGGGTGG ATTATCTTTCTCTA-3'
H2	5'-AGATAATCCACCCACCCAATTATCTTTCTCTAT GGGTGGGTGG -3'

The bold elements in H1 and H2 are split G-quadruples sequences. The sequence in italics in DNA6 is the initiator sequence for CHA.

The Gibbs free energy (ΔG) and melting temperatures were computed for each hairpin and hairpins combination using OligoAnalyzerTM. The parameters entered are: [Na⁺] = 100mM, and [Mg⁺⁺] = 50 mM. The ΔG for the hybridised hairpins (H1/H2) is -56.66 kcal/mole (32 base pairs interacting), and the ΔG for the hybridised catalyst and H1 (H1/DNA6) is -32.95 kcal/mole, with 20 interacting base pairs.

Moreover, it was estimated that the stability of H1 and H2 hairpins decrease with increasing temperatures, as demonstrated by increasing ΔG values:

	ΔG (kcal/mole)					
	25 °C	30 °C	37 °C	40 °C	45 °C	50 °C
H1	-13.73	-12.24	-10.16	-7.78	-7.78	-6.29
H2	-15.86	-14.63	-12.9	-12.16	-10.92	-9.69

H1

Results from the OligoAnalyzer™ Tool for 25 °C and 37 °C. ΔH is the change in enthalpy, and ΔS the change in entropy.

25 °C

Nucleotide type: DNA, Na Concentration: 100 mM, Mg Concentration: 50 mM, Suboptimality: 50 %

Sequence type: Linear, Temperature: 25 °C, Max Foldings: 20, Start Position: 0, Stop Position: 0

Structures

structure	Image	ΔG (kcal.mole ⁻¹)	T_m (°C)	ΔH (kcal.mole ⁻¹)	ΔS (cal.K ⁻¹ .mole ⁻¹)	Output
1		-13.73	71.2	-102.4	-297.41	<input type="button" value="Ct"/> <input type="button" value="Det"/>
2		-11.15	65	-94.3	-278.87	<input type="button" value="Ct"/> <input type="button" value="Det"/>
3		-11.04	61.4	-101.4	-303.05	<input type="button" value="Ct"/> <input type="button" value="Det"/>
4		-9.25	58.6	-91.2	-274.87	<input type="button" value="Ct"/> <input type="button" value="Det"/>
5		-9.23	59.7	-88.6	-266.2	<input type="button" value="Ct"/> <input type="button" value="Det"/>
6		-8.81	57.2	-90.4	-273.65	<input type="button" value="Ct"/> <input type="button" value="Det"/>
7		-8.63	58.7	-84.9	-255.82	<input type="button" value="Ct"/> <input type="button" value="Det"/>
8		-8.19	59.4	-79.2	-238.18	<input type="button" value="Ct"/> <input type="button" value="Det"/>
9		-7.98	56.8	-82.7	-250.63	<input type="button" value="Ct"/> <input type="button" value="Det"/>
10		-7.84	57.8	-79.2	-239.34	<input type="button" value="Ct"/> <input type="button" value="Det"/>
11		-7.82	55.2	-85.1	-259.2	<input type="button" value="Ct"/> <input type="button" value="Det"/>

37 °C

Nucleotide type: DNA, Na Concentration: 100 mM, Mg Concentration: 50 mM, Suboptimality: 50 %

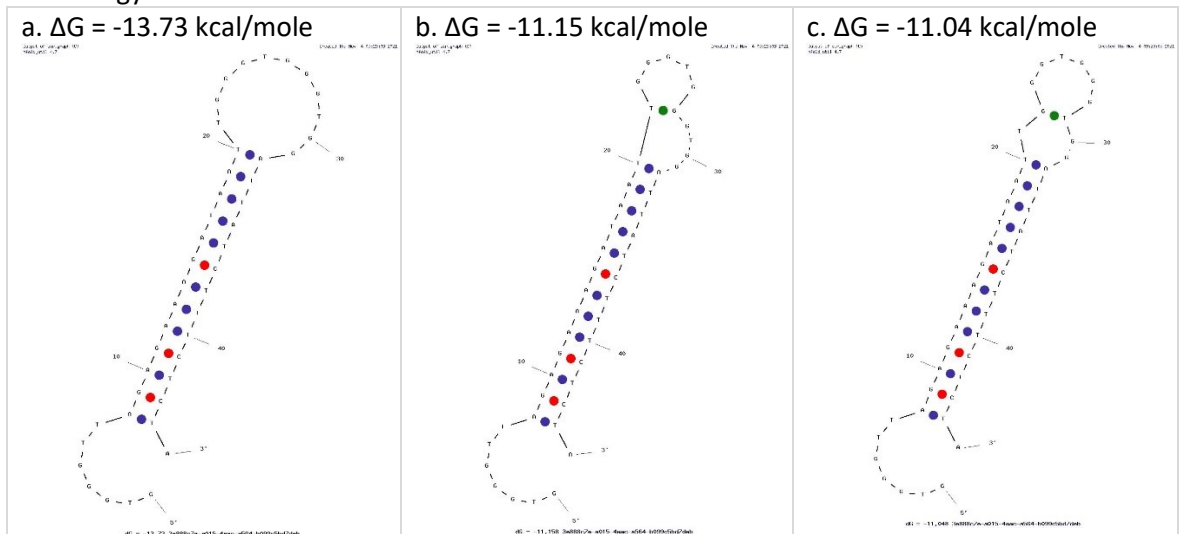
Sequence type: Linear, Temperature: 37 °C, Max Foldings: 20, Start Position: 0, Stop Position: 0

Warning: if there is very little or no secondary structure, using a temperature higher than the default may give odd results.

Structures

structure	Image	ΔG (kcal.mole ⁻¹)	T_m (°C)	ΔH (kcal.mole ⁻¹)	ΔS (cal.K ⁻¹ .mole ⁻¹)	Output
1		-10.16	71.2	-102.4	-297.41	<input type="button" value="Ct"/> <input type="button" value="Det"/>
2		-7.81	65	-94.3	-278.87	<input type="button" value="Ct"/> <input type="button" value="Det"/>
3		-7.41	61.4	-101.4	-303.05	<input type="button" value="Ct"/> <input type="button" value="Det"/>
4		-6.04	59.7	-88.6	-266.2	<input type="button" value="Ct"/> <input type="button" value="Det"/>
5		-5.95	58.6	-91.2	-274.87	<input type="button" value="Ct"/> <input type="button" value="Det"/>
6		-5.56	58.7	-84.9	-255.82	<input type="button" value="Ct"/> <input type="button" value="Det"/>
7		-5.53	57.2	-90.4	-273.65	<input type="button" value="Ct"/> <input type="button" value="Det"/>
8		-5.33	59.4	-79.2	-238.18	<input type="button" value="Ct"/> <input type="button" value="Det"/>
9		-5.12	59.4	-75.9	-228.22	<input type="button" value="Ct"/> <input type="button" value="Det"/>

The first three secondary structures that H1 forms at 25 °C, from the lowest (a) to the highest (c) free energy values:



The three secondary structures with the lowest ΔG remain the same when the temperature of the reaction is increased to 37 °C.

H2

Results from the OligoAnalyzer™ Tool for 25 °C and 37 °C. ΔH is the change in enthalpy, and ΔS the change in entropy.

25 °C

Nucleotide type: DNA, Na Concentration: 100 mM, Mg Concentration: 50 mM, Suboptimality: 50 %

Sequence type: Linear, Temperature: 25 °C, Max Foldings: 20, Start Position: 0, Stop Position: 0

[UPDATE](#) [ADD TO ORDER](#)

Structures

structure	Image	ΔG (kcal.mole ⁻¹)	T_m (°C)	ΔH (kcal.mole ⁻¹)	ΔS (cal.K ⁻¹ .mole ⁻¹)	Output
1		-15.86	89.2	-89.5	-246.98	Ct Det
2		-13.48	76.3	-91.9	-263.01	Ct Det
3		-12.81	78.1	-84.7	-241.12	Ct Det
4		-12.41	72	-91.1	-263.94	Ct Det
5		-12.1	73.9	-85.9	-247.53	Ct Det
6		-9.6	67.1	-77.6	-228.09	Ct Det
7		-9.57	68.5	-75.1	-219.8	Ct Det
8		-9.03	65.7	-75.1	-221.61	Ct Det
9		-8.4	74	-59.5	-171.4	Ct Det
10		-8.21	64.7	-69.8	-206.58	Ct Det
11		-8.05	68.9	-62.7	-183.3	Ct Det

37 °C

Nucleotide type: DNA, Na Concentration: 100 mM, Mg Concentration: 50 mM, Suboptimality: 50 %

Sequence type: Linear, Temperature: 37 °C, Max Foldings: 20, Start Position: 0, Stop Position: 0

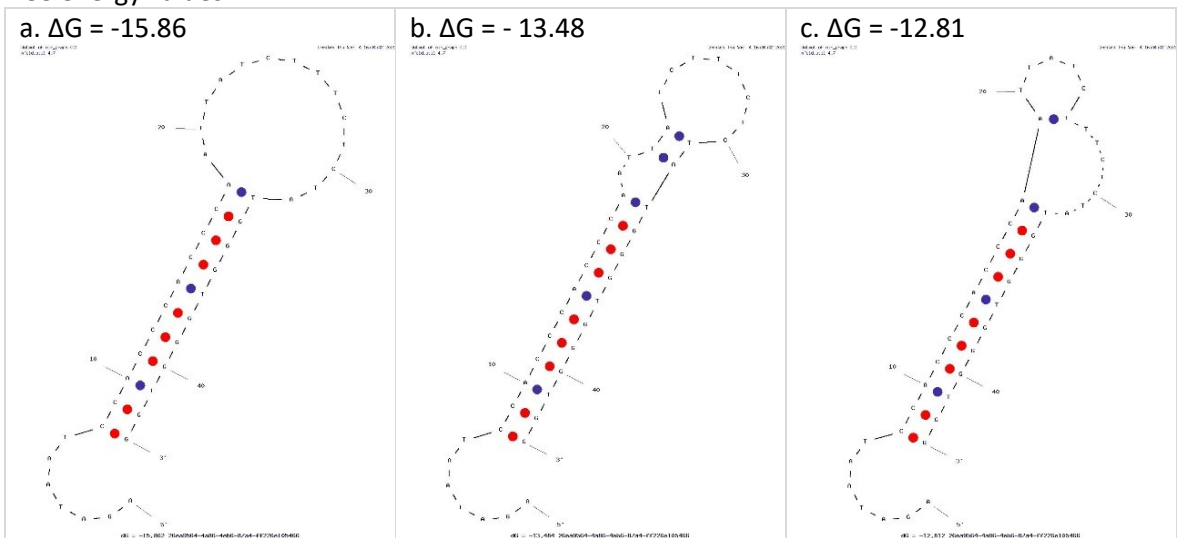
[UPDATE](#) [ADD TO ORDER](#)

Warning: if there is very little or no secondary structure, using a temperature higher than the default may give odd results.

Structures

structure	Image	ΔG (kcal.mole ⁻¹)	T_m (°C)	ΔH (kcal.mole ⁻¹)	ΔS (cal.K ⁻¹ .mole ⁻¹)	Output
1		-12.9	89.2	-89.5	-246.98	Ct Det
2		-10.33	76.3	-91.9	-263.01	Ct Det
3		-9.92	78.1	-84.7	-241.12	Ct Det
4		-9.34	76.8	-82.2	-234.92	Ct Det
5		-9.13	73.9	-85.9	-247.53	Ct Det
6		-6.93	68.5	-75.1	-219.8	Ct Det
7		-6.86	67.1	-77.6	-228.09	Ct Det

The first three secondary structures that H1 forms at 25 °C, from the lowest (a) to the highest (c) free energy values:



Additional Hairpin Sequences

The ΔG and melting temperatures were computed for each hairpin and hairpins combination using OligoAnalyzer™. The parameters entered are: $[Na^+] = 100mM$, and $[Mg^{++}] = 50 mM$. Temperature was set at 25 °C.

Each pair was named as Option 1, 2, 3, etc. To ensure that H2 can effectively compete with H1 for binding to DNA6, we designed the hairpin pairs such that the free energy of H1/DNA6 interaction is less negative than that of H1/H2 interaction.

Summary of the results for each combination:

	ΔG (kcal/mole)			
	H1	H2	H1/H2	H1/DNA6
Original	-13.73	-15.86	-56.66	-32.95
Option 1	-13.73	-14.41	-50.98	-32.95
Option 2	-13.73	-14.33	-52.7	-32.95
Option 3	-13.73	-14.33	-52.7	-32.95
Option 4	-13.73	-14.24	-54.41	-32.95
Option 5	-13.73	-14.33	-52.7	-32.95
Option 6	-13.73	-13.43	-53.29	-32.95
Option 7	-13.73	-13.43	-53.29	-32.95

The highlighted rows are the hairpins combinations chosen for further study. They are the hairpins pairs with the most negative ΔG .




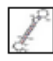



The DNA sequences used for different pairs of hairpins are in the sections below, along with details OligoAnalyzer™ Tool results. The letters in red are the changed base pairs compared to the sequence used in Zhou *et al.* (2020) ('Original').

Option 1

H1	5'- GTGGG TTAGAGAAAGATAATT GTGTGTGG ATTATCTTTCTCTA-3'
H2	5'-AGATAATCCAC ACACA CAATTATCTTTCTCTAT GTGTGTGG -3'

H1/H2: $\Delta G = -50.98$ kcal/mole; Base pairs interacting: 32

H1/DNA6: $\Delta G = -32.95$ kcal/mole; Base pairs interacting: 20







OligoAnalyzer™ Tool results:							
H1				H2			
structure	Image	ΔG (kcal.mole ⁻¹)	T _m (°C)	structure	Image	ΔG (kcal.mole ⁻¹)	T _m (°C)
1		-13.73	71.2	1		-14.41	80.9
2		-11.64	62.8	2		-12.03	68.9
3		-11.12	60.9	3		-11.36	70.1
4		-10.85	62.3				

Option 2

H1	5'-GTGGGTTAGAGAAAGATAAATTGGTTGTGGATTATCTTTCTCTA-3'
H2	5'-AGATAATCCACACAACCAATTATCTTTCTCTATGGTTGTGG-3'

H1/H2: $\Delta G = -52.7$ kcal/mole; Base pairs interacting: 32

H1/DNA6: $\Delta G = -32.95$ kcal/mole; Base pairs interacting: 20


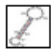

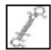


OligoAnalyzer™ Tool results:							
H1				H2			
structure	Image	ΔG (kcal.mole ⁻¹)	T _m (°C)	structure	Image	ΔG (kcal.mole ⁻¹)	T _m (°C)
1		-13.73	71.2	1		-14.33	81.2
2		-11.15	65	2		-11.95	69.1
3		-11.04	61.4	3		-11.28	70.3

Option 3

H1	5'-GTGGGTTAGAGAAAGATAAATTGGTGTGGATTATCTTTCTCTA-3'
H2	5'-AGATAATCCACACACCAATTATCTTTCTCTATGGTGTGG-3'

H1/H2: $\Delta G = -52.7$ kcal/mole; Base pairs interacting: 32

H1/DNA6: $\Delta G = -32.95$ kcal/mole; Base pairs interacting: 20


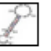

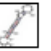

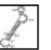
OligoAnalyzer™ Tool results:							
H1				H2			
structure	Image	ΔG (kcal.mole ⁻¹)	T _m (°C)	structure	Image	ΔG (kcal.mole ⁻¹)	T _m (°C)
1		-13.73	71.2	1		-14.33	81.2
2		-12.83	71.2	2		-11.95	69.1
3		-10.28	58.5	3		-11.28	70.3

Option 4

H1	5'-GTGGGTTAGAGAAAGATAAATTGGTGGTGGATTATCTTTCTCTA-3'
H2	5'-AGATAATCCACCAACCAATTATCTTTCTCTATGGTGGTGG-3'

H1/H2: $\Delta G = -54.41$ kcal/mole; Base pairs interacting: 32

H1/DNA6: $\Delta G = -32.95$ kcal/mole; Base pairs interacting: 20




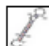

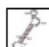
OligoAnalyzer™ Tool results:							
H1				H2			
structure	Image	ΔG (kcal.mole ⁻¹)	T _m (°C)	structure	Image	ΔG (kcal.mole ⁻¹)	T _m (°C)
1		-13.73	71.2	1		-14.24	81.6
2		-12.83	71.2	2		-11.86	69.3
3		-11.23	64.4	3		-11.19	70.5

Option 5

H1	5'- GTGGG TTAGAGAAAGATAA TTGGTG TGGATTATCTTTCTCTA-3'
H2	5'-AGATAATCCACACACCAAATTATCTTTCTCTAT TTGGTG TGGG-3'

H1/H2: $\Delta G = -52.7$ kcal/mole; Base pairs interacting: 32

H1/DNA6: $\Delta G = -32.95$ kcal/mole; Base pairs interacting: 20

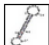



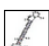

OligoAnalyzer™ Tool results:							
H1				H2			
structure	Image	ΔG (kcal.mole ⁻¹)	T _m (°C)	structure	Image	ΔG (kcal.mole ⁻¹)	T _m (°C)
1		-13.73	71.2	1		-14.33	81.2
2		-12.83	71.2	2		-11.95	69.1
3		-10.28	58.5	3		-11.28	70.3

Option 6

H1	5'- GTGGG TTAGAGAAAGATAA TTGGTTT TGGATTATCTTTCTCTA-3'
H2	5'-AGATAATCCACAAACCAAATTATCTTTCTCTAT TTGGTTT TGGG-3'

H1/H2: $\Delta G = -53.29$ kcal/mole; Base pairs interacting: 32

H1/DNA6: $\Delta G = -32.95$ kcal/mole; Base pairs interacting: 20

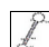
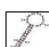




H1				H2			
structure	Image	ΔG (kcal.mole ⁻¹)	T _m (°C)	structure	Image	ΔG (kcal.mole ⁻¹)	T _m (°C)
1		-13.73	71.2	1		-13.43	77.8
2		-12.83	71.2	2		-11.05	65.9
3		-11.23	64.4	3		-10.38	66.8

Option 7

H1	5'- GTGGG TTAGAGAAAGATAA TTGGTTG TGGATTATCTTTCTCTA-3'
H2	5'-AGATAATCCAACAACC AAATTATCTTTCTCTAT TTGGTTG TGG-3'

H1/H2: $\Delta G = -53.29$ kcal/mole; Base pairs interacting: 32

H1/DNA6: $\Delta G = -32.95$ kcal/mole; Base pairs interacting: 20

H1				H2			
structure	Image	ΔG (kcal.mole ⁻¹)	T _m (°C)	structure	Image	ΔG (kcal.mole ⁻¹)	T _m (°C)
1		-13.73	71.2	1		-13.43	77.8
2		-12.91	70.4	2		-11.05	65.9
3		-11.23	64.4	3		-10.38	66.8

A.5 Proof of Copyright Permissions

Proof of copyright permissions are listed in Tables A.6, and A.7.

Table A.6: **Copyright permissions.**

No.	Type of work	Name of work	Source of work	Copyright holder and contact	Permission requested on	I have permission (yes /no)	Permission note
1.3	figure	Figure 5	Fu, Elain, <i>et al.</i> “Transport in two-dimensional paper networks.” Microfluid Nanofluidics. 2011, 10(1):29-35.	Springer-Verlag Copyright clearance center, Inc. customercare@copyright.com	28/11/2023	yes	Licence number: 5677850167649 Copyright 2010
1.3	figure	Figure 2	Shin, Joong Ho <i>et al.</i> “Programmed sample delivery on a pressurized paper.” Biomicrofluidics, 2014, 8: 054121.	AIP Publishing Copyright clearance center, Inc. customercare@copyright.com	28/11/2023	yes	Licence number: 5677871158706
1.3	figure	Figure 3.B	Shin, Joong Ho <i>et al.</i> “Programmed sample delivery on a pressurized paper.” Biomicrofluidics, 2014, 8: 054121.	AIP Publishing Copyright clearance center, Inc. customercare@copyright.com	28/11/2023	yes	Licence number: 5677870862504
1.4	figure	Figure 1	Byrnes, S. A. <i>et al.</i> “One-step purification and concentration of DNA in porous membranes for point-of-care applications.” Lab chip, 2015, 15:2647.	Royal Society of Chemistry Copyright clearance center, Inc. customercare@copyright.com	29/11/2023	yes	Licence ID: 1421725-1 ISSN: 1473-0189

Table A.7: Copyright permissions.

No.	Type of work	Name of work	Source of work	Copyright holder and contact	Permission requested on	I have permission (yes /no)	Permission note
1.5	figure	Figure 3. Sample-to-answer HPV16 and HPV18 test process on NATflow.	Kundrod, Kathryn A., <i>et al.</i> “An integrated isothermal nucleic acid amplification test to detect HPV16 and HPV18 DNA in resource-limited settings” Sci. Transl. Med. 15 (2023), eabn4768.	American Association for the Advancement of Science Copyright clearance center, Inc. customercare@copyright.com	29/11/2023	yes	Licence ID: 1421667-1 ISSN: 1946-6234 Copyright 2023
1.5	figure	Graphical abstract and Figure 2(b).	Rodriguez-Mateos, Pablo, <i>et al.</i> “A lab-on-a-chip platform for integrated extraction and detection of SARS-CoV-2 RNA in resource-limited settings.” Analytica chimica acta, 1177(2021):338758.	Elsevier Copyright clearance center, Inc. customercare@copyright.com	29/11/2023	yes	ELSEVIER LICENSE Licence number: 5678291090410 Copyright 2021
1.5	figure	Figure 2	Zhou, Zhixue, <i>et al.</i> “Integrated Nucleic Acid Testing System to Enable TB Diagnosis in Peripheral Settings.” Lab chip, 2020, 20(21):4071.	Royal Society of Chemistry Copyright clearance center, Inc. customercare@copyright.com	29/11/2023	yes	Licence ID: 1421656-1 ISSN: 1473-0189
4.6	figure	Figure 2. Loop-mediated isothermal amplification (LAMP).	Alhassan, Andy, <i>et al.</i> “Expanding the MDx toolbox for filarial diagnosis and surveillance.” Trends in parasitology 31.8(2015):391-400.	Elsevier Copyright clearance center, Inc. customercare@copyright.com	10/11/2023	yes	ELSEVIER LICENSE Licence number: 5665360923434
6.1	figure	Figure 5. A turn-on sensor design.	Zhou, Zhixue, <i>et al.</i> “A Multi-component All-DNA Biosensing System Controlled by a DNzyme.” Angew. Chem. 132(2020):1-6.	John Wiley & Sons - Books Copyright clearance center, Inc. customercare@copyright.com	14/11/2023	yes	Licence ID: 1416460-1 ISSN: 1433-7851

Appendix B

MATLAB[®] Scripts

B.1 MATLAB[®] Script Used to Compute Time-to-Positive Values in Real Time LAMP

Function Varycolor

This function produces colors with maximum variation on plots with multiple lines. This was gently provided by Alice Garrett, former member of the research group, and created by Daniel Helmick (8 December 2008).

Listing B.1: varycolor funcion.m

```
1 function ColorSet=varycolor(NumberOfPlots)
2 % VARYCOLOR Produces colors with maximum variation on plots with multiple
3 % lines.
4 %
5 %VARYCOLOR(X) returns a matrix of dimension X by 3. The matrix may be
6 %used in conjunction with the plot command option 'color' to vary the
7 %color of lines.
8 %
9 %Yellow and White colors were not used because of their poor
10 %translation to presentations.
11
12 %Created by Daniel Helmick 8/12/2008
13
14 error(nargchk(1,1,nargin))%correct number of input arguements??
15 error(nargoutchk(0, 1, nargout))%correct number of output arguements??
16
17 %Take care of the anomolies
18 if NumberOfPlots<1
19     ColorSet=[];
20 elseif NumberOfPlots==1
21     ColorSet=[0 1 0];
22 elseif NumberOfPlots==2
23     ColorSet=[0 1 0; 0 1 1];
24 elseif NumberOfPlots==3
25     ColorSet=[0 1 0; 0 1 1; 0 0 1];
26 elseif NumberOfPlots==4
27     ColorSet=[0 1 0; 0 1 1; 0 0 1; 1 0 1];
28 elseif NumberOfPlots==5
29     ColorSet=[0 1 0; 0 1 1; 0 0 1; 1 0 1; 1 0 0];
30 elseif NumberOfPlots==6
31     ColorSet=[0 1 0; 0 1 1; 0 0 1; 1 0 1; 1 0 0; 0 0 0];
32
33 else %default and where this function has an actual advantage
34
35     %we have 5 segments to distribute the plots
36     EachSec=floor(NumberOfPlots/5);
37
38     %how many extra lines are there?
39     ExtraPlots=mod(NumberOfPlots,5);
40
41     %initialize our vector
42     ColorSet=zeros(NumberOfPlots,3);
43
44     %This is to deal with the extra plots that don't fit nicely into the
45     %segments
46     Adjust=zeros(1,5);
47     for m=1:ExtraPlots
48         Adjust(m)=1;
49     end
50
51     SecOne =EachSec+Adjust(1);
52     SecTwo =EachSec+Adjust(2);
53     SecThree =EachSec+Adjust(3);
54     SecFour =EachSec+Adjust(4);
```



```

55     SecFive =EachSec;
56
57     for m=1:SecOne
58         ColorSet(m,:)= [0 1 (m-1)/(SecOne-1)];
59     end
60
61     for m=1:SecTwo
62         ColorSet(m+SecOne,:)= [0 (SecTwo-m)/(SecTwo) 1];
63     end
64
65     for m=1:SecThree
66         ColorSet(m+SecOne+SecTwo,:)= [(m)/(SecThree) 0 1];
67     end
68
69     for m=1:SecFour
70         ColorSet(m+SecOne+SecTwo+SecThree,:)= [1 0 (SecFour-m)/(SecFour)];
71     end
72
73     for m=1:SecFive
74         ColorSet(m+SecOne+SecTwo+SecThree+SecFour,:)= [(SecFive-m)/(SecFive) 0 0];
75     end
76
77 end

```

TTP values detection

Listing B.2: LAMPDataAnalysis.m

```

1 %% Initialisings
2 clear
3 close all
4 clc
5 %% Initial settings
6 %Manually add path of the folder containing the saved excel data
7 filename = 'example.xls'; %This takes the exported file from
8 %QuantStudio Design & Analysis Software
9 %Read from a worksheet
10 RawData = xlsread(filename,'Raw Data');
11 [wells_num1,Results_data] = xlsread(filename,'Results');
12
13 [row,column]=find(~isnan(wells_num1));
14 row=row(find(column==1));
15 column=column(find(column==1));
16 idx = sub2ind(size(wells_num1),row,column);
17 wells_num=wells_num1(idx);
18
19 Wells=cell(size(wells_num,1),3);
20 for i=1:size(wells_num,1)
21     Wells{i,1}=wells_num(i,1); %number of the 96 wells plate
22     Wells{i,2}=Results_data(44+i,2); %name of the well (A1, A2, etc.)
23     Wells{i,3}=Results_data(44+i,4); %sample name given by the user
24 end
25
26 %% For QS3 qPCR Machines
27 %Structure of the excel data saved when using QS3
28 %Col 1: Well number
29 %Col 2: Well name
30 %Col 3: Cycle number
31 %Col 4: Filter 1 value
32
33 %Finding the number of cycles
34 nb_cycle=max(RawData(:,3)); %This includes melting curve
35 %The number of cycles (minutes) for LAMP has been decided prior
36 %the experiment=60
37 cycle=60;
38 %Defining the sample size (96 for the 96 well plate)
39 nb_sample=size(RawData,1)/nb_cycle; %rows of RawData/#cycles
40 nb_test=size(RawData,2)-2;
41
42 %Take all the fluorescence values from 'column 4'
43 % of the data set corresponding to Filter 1
44 PC.data=RawData(:,4);
45 %re-shape to get all values for A1, A2 etc grouped together
46 %Z is all the RFU values for each well, time sequential
47 Z=reshape(PC.data, [nb_sample nb_cycle]);
48 %Rows: 96 wells - row 1 =A1, row 2=A2, etc.
49 %Columns: value of RFU taken for each cycle.
50
51 %% Select number of biological samples to analyse
52 nb_assay_c = inputdlg('Enter the no. of samples you want to analyse (not the no. of wells)', 'Number of assays');
53 nb_assay=str2double(nb_assay_c{:});
54 %% Automatic identification of replicates for the same sample
55 find_triplicates=Wells;
56 contend=size(wells_num,1);
57 stivalues=[];
58 jvalues=[];
59 sti=1;
60 while sti<=nb_assay
61     assays(sti).name=find_triplicates{1,3};
62     assays(sti).well_num=[find_triplicates{1,1}];

```

```

63     assays(sti).RFU=[Z(find_triplicates{1,1},:)]];
64     stivalues=[stivalues sti];
65     rep_num=1; %replicate number
66     samesamplepos=[];
67     if contend>1
68         for j=2:size(wells_num,1)
69             jvalues=[jvalues j];
70             a=strcmp(find_triplicates{1,3},find_triplicates{j,3});
71             if a
72                 rep_num=rep_num+1;
73                 assays(sti).well_num=[assays(sti).well_num find_triplicates{j,1}];
74                 assays(sti).RFU=[assays(sti).RFU; Z(find_triplicates{j,1},:)]];
75                 samesamplepos=[samesamplepos j];
76                 %find_triplicates(j,:)=[];
77                 %contend=contend-1;
78             end
79             if j==contend
80                 break
81             end
82         end
83     elseif contend==1
84         break
85     end
86     find_triplicates([1 samesamplepos],:)=[];
87     contend=contend-rep_num;
88     sti=sti+1;
89 end
90
91 %% Interpolation of fluorescent values
92 %choose number of interpolation point between each minute
93 time=1:1:nb_cycle;
94 intv=10;
95 timeq=1:(1/intv):nb_cycle;
96 cycleq=find(timeq==cycle); %
97
98 for i=1:nb_assay
99     assays(i).RFUint=spline(time,assays(i).RFU,timeq);
100 end
101 %% Definition of colours for plots
102 ColorSet=varycolor(nb_assay);
103
104 %% Computation of time-to-positive (TTP) values through 1st & 2nd derivatives
105 %Computation of first derivative of fluorescent signal
106 % and storage of values in the cell
107 for i=1:nb_assay
108     matzeros=zeros(size(assays(i).well_num,2),length(time));
109     for j=1:size(assays(i).well_num,2)
110         matzeros(j,:)=gradient(assays(i).RFU(j,:),time);
111     end
112     assays(i).firstder=matzeros;
113 end
114 %Computation of second derivative of fluorescent signal
115 % and storage of values in the cell
116 for i=1:nb_assay
117     matzeros=zeros(size(assays(i).well_num,2),length(time));
118     for j=1:size(assays(i).well_num,2)
119         matzeros(j,:)=gradient(assays(i).firstder(j,:),time);
120     end
121     assays(i).secder=matzeros;
122 end
123
124 %Interpolation of the second derivative of the fluorescent signal
125 % and storage of values in the cell
126 for i=1:nb_assay
127     for j=1:size(assays(i).well_num,2)
128         assays(i).secderInt(j,:)=spline(time,assays(i).secder(j,:),timeq);
129     end
130 end
131
132 %% Second derivative control plot
133 %NB: Before time=5 min to time=56 min the interpolated signal
134 % is very noisy.
135 %Therefore, spline is not a good interpolation method
136 figure()
137 hold on;
138 p=zeros(1,nb_assay);
139 cont1=1;
140 posLeg=[];
141 %constant to determine where to analyse the signal to avoid noisy edges.
142 %Insert minutes
143 FIRST=4*intv; % mins
144 LAST=4*intv; % mins
145
146 for i=1:nb_assay
147     for j=1:size(assays(i).RFUint, 1)
148         p(cont1)=plot(timeq(FIRST:cycleq-LAST),assays(i).secderInt(j,(FIRST:cycleq-LAST)), 'color', ColorSet(i,:),
149             'DisplayName',assays(i).name{1});
150         if j==1
151             posLeg=[posLeg cont1];
152         end
153         cont1=cont1+1;
154     end
155 end
156 legend(p(posLeg),'Location','northeast')

```

```

156 title('Second derivatives plot')
157 hold off
158
159 %% Determine TTP values, based on the second derivative max value of the Negative Controls
160 %%This additional control is necessary to avoid the identification of TTPs
161 %%in negative controls (NTCs)
162
163 %Select the row number where the NTCs are located inside the variable
164 %'assays' from the workspace
165 NTCcon = inputdlg('Enter the row number in the variable assays that contains the negative control', 'Negative
Control');
166 NTCc=str2double(NTCcon{:});
167
168 %Creation of a separate structure containing the values of fluorescence
169 % that can be used to plot TTP values
170 for i=1:nb_assay
171     assays_fluor(i).name=assays(i).name;
172     assays_fluor(i).well_num=assays(i).well_num;
173 end
174 %column vector containing the maximum value of each row:
175 %if there are more than 1 negative controls
176 maxRFUNTC=max(assays(NTCc).secderInt(:,FIRST:cycleq-LAST), [], 2);
177 threshNTC=max(maxRFUNTC);
178
179 for i=1:nb_assay
180     M=max(assays(i).secderInt(:,FIRST:cycleq-LAST), [], 2);%column vector containing the maximum value of each row.
181     %I look for the max from time=FIRST/10 min to time= (cycleq-LAST)/10 mins because the signal is very noisy in
the edges.
182     %Spline is not a good interpolation method
183     assays_fluor(i).maxSecdev=M;
184
185     %col_max will contain the column number where the max value of secdevInt is found
186     col_max=zeros(length(M),1);
187     Ct=zeros(length(M),1);
188     for k=1:length(M)
189         col_max(k)=find(assays(i).secderInt(k,:)==M(k)); %Index position of the x-axis where the max value is found
190         Ct(k)=timeq(col_max(k));
191         %I want to consider only those values of the second derivatives that are greater than the ones from the
negative control
192         if M(k)<=threshNTC
193             Ct(k)=nan;
194         end
195
196         %Additional control with the classic threshold from the
197         %baseline
198         thresh=10*std(assays(i).RFUint(k,1:col_max(k)-FIRST));
199         if assays(i).RFUint(k,col_max(k))<thresh
200             Ct(k)= nan;
201         end
202     end
203     assays(i).Ctvalues=Ct;
204     assays(i).Mean_Ct=nanmean(Ct);
205     assays(i).SD_Ct=nanstd(Ct);
206     assays_fluor(i).Ctindex=col_max;
207 end
208
209 %% Table containing the original TTP values detected, exported into an excel sheet
210 for i=1:nb_assay
211     assaystoex(i).Sample=assays(i).name;
212     rep=length(assays(i).Ctvalues)-sum(isnan(assays(i).Ctvalues));
213     assaystoex(i).Rep=rep;
214     assaystoex(i).Ct_values=assays(i).Ctvalues(1:size(assays(i).Ctvalues, 1)); %Single Ct values
215     assaystoex(i).Mean_Ct=assays(i).Mean_Ct; %Mean Ct value
216     assaystoex(i).SD_Ct=assays(i).SD_Ct;
217 end
218 excname=strcat(filename(1:(length(filename)-4)), '_summary_results_original.xlsx');
219 writetable(struct2table(assaystoex), excname)
220 %% -----
221 % This part serves to plot the amplification plots with the variable
222 % names and order preferred,
223 % Possibility to modify the initial detected TTP values in case
224 % the algorithm could not find the appropriate values.
225 %To do so:
226 %In the workspace right click on the variable assays and Duplicate it -->
227 %This action creates a variable called 'assaysCopy'. You could modify the
228 %TTP values in this variable. 'assaysCopy' can also be used to re-order
229 %samples in the plot and re-save the desired plot.
230 %When modifying TTP values, remember to re compute the mean and std with
231 %the following commands in the Command Window:
232 % assaysCopy(2).Mean_Ct=nanmean(assaysCopy(2).Ctvalues);
233 % assaysCopy(2).SD_Ct=nanstd(assaysCopy(2).Ctvalues);
234
235 %% Control plot with amplification plot with interpolated data, and TTP values shown
236 ampplotcopy=figure();
237 for i=1:size(assaysCopy,2)
238     ss_nomistring(i)=string(assaysCopy(i).name);
239 end
240 nb_assay2=size(assaysCopy,2);
241 ColorSet=varycolor(nb_assay2); %For this I can use varycolor
242 hold on;
243 p=zeros(1,nb_assay2);
244 cont1=1;
245 posLeg=[];
246 for i=1:nb_assay2

```

```

247     for j=1:size(assaysCopy(i).RFUint, 1)
248         p(cont1)=plot(timeq(2:cycleq-1),assaysCopy(i).RFUint(j,(2:cycleq-1)), 'color', ColorSet(i,:), 'DisplayName'
                ,ss_nomistring(i),'linewidth', 1.5);
249         if j==1
250             posLeg=[posLeg cont1];
251         end
252         cont1=cont1+1;
253     end
254 end
255 legend(p(posLeg),'Location','eastoutside')
256
257 hTitle=title('Amplification plot');
258 hXLabel=xlabel('Time');
259 hYLabel=ylabel('Fluorescence (RFU)');
260 set(gca,'fontsize',20)
261 hold off
262
263 %Control for Ct values
264 hold on
265 for i=1:nb_assay2
266     for j=1:size(assays(i).Ctvalues, 1)
267         scatter(assays(i).Ctvalues(j),assays(i).RFUint(j,assays_fluor(i).Ctindex(j)));
268     end
269 end
270 hold off
271
272 %% Amplification Plot
273 amplotcopy=figure();
274 for i=1:size(assaysCopy,2)
275     ss_nomistring(i)=string(assaysCopy(i).name);
276 end
277 nb_assay2=size(assaysCopy,2);
278 ColorSet=varycolor(nb_assay2); %For this I can use varycolor or
279 hold on; % add new plot lines on top of previous ones
280 p=zeros(1,nb_assay2);
281 cont1=1;
282 posLeg=[];
283 for i=1:nb_assay2
284     %plot(timeq(1:cycleq-1),assays(i).RFUint(:,(1:cycleq-1)), 'color', ColorSet(i,:), 'DisplayName',assays(i).name
                {i});
285     %legend(assays(i).name)
286     for j=1:size(assaysCopy(i).RFU, 1)
287         p(cont1)=plot(time(1:cycle),assaysCopy(i).RFU(j,(1:cycle)), 'color', ColorSet(i,:), 'DisplayName',
                ss_nomistring(i),'linewidth', 1.5);
288         if j==1
289             posLeg=[posLeg cont1];
290         end
291         cont1=cont1+1;
292     end
293 end
294 legend(p(posLeg),'Location','eastoutside')
295
296 hTitle=title('Amplification plot');
297 hXLabel=xlabel('Time [min]');
298 hYLabel=ylabel('Fluorescence [RFU]');
299 set(gca,'fontsize',20)
300 hold off
301
302 %Save plot in different format files
303 filename=strcat(filename(1:(length(filename)-4)),'.fig');
304 epsname=strcat(filename(1:(length(filename)-4)),'.eps');
305 pngname=strcat(filename(1:(length(filename)-4)),'.png');
306 savefig(amplotcopy,filename) %save as fig
307 saveas(gcf,epsname,'epsc') %save as eps
308 saveas(gcf,pngname) %save as png
309
310 %% Create and save table containing the TTP values manually selected
311 % Table exported into an excel sheet
312 for i=1:nb_assay2
313     assaystoex(i).Sample=assaysCopy(i).name;
314     rep=length(assaysCopy(i).Ctvalues)-sum(isnan(assaysCopy(i).Ctvalues));
315     assaystoex(i).Rep=rep;
316     assaystoex(i).Ct_values=assaysCopy(i).Ctvalues(1:size(assaysCopy(i).Ctvalues, 1)); %Single Ct values
317     assaystoex(i).Mean_Ct=assaysCopy(i).Mean_Ct; %Mean Ct value
318     assaystoex(i).SD_Ct=assaysCopy(i).SD_Ct;
319 end
320 excname=strcat(filename(1:(length(filename)-4)),'_summary_results.xlsx');
321 writetable(struct2table(assaystoex), excname)

```

B.2 MATLAB[®] Script Used to Compute ANOVA

Listing B.3: ANOVA.m

```
1 %% Initialising
2 clear
3 close all
4 clc
5 %% Instructions
6 %In the excel file created with LAMP_DataAnalysis, create an empty sheet
7 %Called 'ANOVA-Matlab'
8 %In this sheet copy the following:
9 % Column 1: Name of Biological samples
10 % Column 2: Mean TTP value of technical replicates for that sample
11 % Column 3: Std of TTP values of technical replicates for that sample
12 %% Import the table created via LAMP_DataAnalysis
13 filename = 'example_summary_results.xlsx';
14 %Read from a worksheet
15 DataAnova = readtable(filename,'Sheet','ANOVA-Matlab');
16 CellAnova = table2cell(DataAnova); %convert to cell
17
18 %% Creation of a structure (AnovaMatrix) that groups biological samples
19 find_triplicates=CellAnova;
20 contend=size(DataAnova,1);
21 stivalues=[];
22 jvalues=[];
23 sti=1;
24 while sti<=size(DataAnova,1)
25     AnovaMatrix(sti).name=find_triplicates{1,1};
26     AnovaMatrix(sti).Means=[find_triplicates{1,2}];
27     AnovaMatrix(sti).STD=[find_triplicates{1,3}];
28     stivalues=[stivalues sti];
29     rep_num=1; %replicate number
30     samesamplepos=[];
31     if contend>1
32         for j=2:size(DataAnova,1)
33             jvalues=[jvalues j];
34             a=strncmp(find_triplicates{1,1},find_triplicates{j,1});
35             if a
36                 rep_num=rep_num+1;
37                 AnovaMatrix(sti).Means=[AnovaMatrix(sti).Means find_triplicates{j,2}];
38                 AnovaMatrix(sti).STD=[AnovaMatrix(sti).STD; find_triplicates{j,3}];
39                 samesamplepos=[samesamplepos j];
40             end
41             if j==contend
42                 break
43             end
44         end
45     elseif contend==1
46         break
47     end
48     find_triplicates([1 samesamplepos],:)=[];
49     contend=contend-rep_num;
50     sti=sti+1;
51 end
52
53 %In certain occasions, the number of PCs and NTCs is lower than the number
54 %of biological samples for the other conditions
55 %In order to use anova1 and multcompare, all the biological samples
56 %need to have the same sample size.
57 % Therefore, PCs and NTCs are populated with NaN values to fill
58 % the missing values.
59 for i=2:size(AnovaMatrix,2)
60     if length(AnovaMatrix(i).Means)<length(AnovaMatrix(1).Means)
61         AnovaMatrix(i).Means = [AnovaMatrix(i).Means NaN];
62         AnovaMatrix(i).STD = [AnovaMatrix(i).STD NaN];
63     end
64 end
65
66 %% Compute variance analysis, ANOVA and Tukey-Kramer
67 %Groups in the columns:
68 manova=[];
69 for i=1:size(AnovaMatrix,2)
70     manova=[manova , AnovaMatrix(i).Means'];
71 end
72 [pvalue,tbl,stats]=anova1(manova); %tbl gives the anova analysis in a table format
73 writetable(cell2table(tbl),filename,'Sheet','Res-ANOVA-Mat','WriteVariableNames',false);
74 tukeykramer=multcompare(stats); %the last column is p-value for the groups indicated in columns 1 and 2.
75 %Save the file on the same excel file, in a different sheet:
76 writetable(array2table(tukeykramer),filename,'Sheet','Res-ANOVA-Mat','WriteVariableNames',false, 'Range', 'A7');
77 %tukey-kramer default
```

B.3 MATLAB[®] Script Used to Study Pullulan Tablets Dissolution Rate

The scripts in this section were kindly provided by Olivia McGleish.

B.3.1 Script Used to Identify the Colour Difference detected by the Camera

The user uploaded the image of the wells (Fig. 2.25A) and selected the wells of interest in the image. The software could not detect the wells automatically due to the lens curvature and the 96-well plate transparency. A mask was applied to analyse the chosen regions. Each ‘mixed’ well was compared with both the red and blue control by computing ΔE for each pixel in each pair of wells, e.g., ‘mixed’ well vs blue control and ‘mixed’ well vs red control. The mean of the ΔE for each pair of wells was calculated and plotted on a graph for each well.

Listing B.4: MixTesting.m

```
1 %% Initial settings
2 clc
3 clear all
4 close all
5
6 fontSize = 18;
7 binaryThreshold = 0.3;
8 circSmall = 20;
9 circBig = 200;
10 %%
11 % User selects image
12 disp('Loading mixing image')
13 % Read the video
14 mixImage = imread('MixingTest.png');
15
16 %% Circle ROIs
17 figure(1) % Open a new figure
18 set(gcf, 'Color', 'w') % Set the background of the figure to white (instead of grey)
19 imshow(mixImage) % Show the loaded image
20 axis('image') % Set the axis to be equal to the number of pixels (prevents image stretching)
21 title('Control Image', 'FontSize', fontSize) % Title
22 set(gca, 'FontSize', fontSize-2); % Scaling axes text to match chosen font size
23
24 % Max figure size to aid ROI selection
25 g = gcf;
26 g.WindowState = 'maximized';
27 % Ask user to draw circle ROIs for each control colour
28 uiwait(helpdlg('Draw circle ROI (Click and Drag)'));
29
30 % Circle ROI Drawing - forcing matlab to wait until user completes all ROIs
31 for nCircs = 1:1:35
32     clear control
33     if nCircs <= 5
34         circCol = 'b';
35     elseif (nCircs > 5) && (nCircs <= 10)
36         circCol = 'r';
37     else
38         circCol = 'y';
39     end
40     control.Radius = 0;
41     while control.Radius == 0
42         control = drawcircle('Color', circCol, 'FaceAlpha', 0.4);
43         if control.Radius == 0
44             uiwait(helpdlg('You need to single click, then drag, then single click again.'));
45         end
46         radii(nCircs, 1) = control.Radius;
47         centers(nCircs, 1) = control.Center(1);
48         centers(nCircs, 2) = control.Center(2);
49     end
50 end
51
52 %% Calculating the circle coordinates
53 for nCircs = 1:1:35
54     angles = linspace(0, 2*pi, 10000);
55     x_control(nCircs,:) = cos(angles) * radii(nCircs, 1) + centers(nCircs, 1);
56     y_control(nCircs,:) = sin(angles) * radii(nCircs, 1) + centers(nCircs, 2);
57 end
58
59 % Show circles over image.
60 figure
61 set(gcf, 'Color', 'w')
62 imshow(mixImage);
63 axis('image');
```

```

64 hold on;
65 for nCircs = 1:1:35
66     plot(x_control(nCircs,:), y_control(nCircs,:), 'w-', 'LineWidth', 2);
67 end
68 hold off
69 title('Individual controls image with ROI overlaid', 'FontSize', fontSize);
70
71 %% Control Masks
72 % Get circle masks
73 [imRows, imCols, imChans] = size(mixImage);
74 %
75 for nCircs = 1:1:35
76     mask(:,:,nCircs) = poly2mask(x_control(nCircs,:), y_control(nCircs,:), imRows, imCols);
77     interimMask = poly2mask(x_control(nCircs,:), y_control(nCircs,:), imRows, imCols);
78
79     % if nCircs == 1
80     %     mask = interimMask;
81     % else
82     %     mask = mask + interimMask;
83     % end
84 end
85
86 %%
87 % Mask with the user selected circles
88 for nCircs = 1:1:35
89     interimMask = bsxfun(@times, mixImage, cast(mask(:,:,nCircs), class(mixImage)));
90     maskedImage(:,:,nCircs) = interimMask;
91     % if mod(nCircs, 5) == 0
92     %     figure
93     %     set(gcf, 'Color', 'w')
94     %     imshow(maskedImage(:,:,nCircs));
95     %     title('Mask', 'FontSize', FontSize);
96     % end
97 end
98 %% Crop the images to the bounding box.
99 for nCircs = 1:1:35
100     clearvars rgbList
101     props_mask = regionprops(mask(:,:,nCircs), 'BoundingBox');
102     maskedImageFinal = imcrop(maskedImage(:,:,nCircs), props_mask.BoundingBox);
103     [rows, cols, channels] = size(maskedImageFinal);
104     nPix = rows*cols;
105     rgbValsInterim = zeros(1, 3);
106     pixCount = 1;
107     for iter = 1:1:nPix
108         rgbList(:,1) = reshape(maskedImageFinal(:, :, 1), [], 1);
109         rgbList(:,2) = reshape(maskedImageFinal(:, :, 2), [], 1);
110         rgbList(:,3) = reshape(maskedImageFinal(:, :, 3), [], 1);
111         if (sum(rgbList(iter, :), 2) > 0)
112             %     rgbValsInterim(iter, :) = NaN;
113             % else
114             %     rgbValsInterim(pixCount, :) = rgbList(iter, :);
115             %     pixCount = pixCount + 1;
116             % end
117         end
118     if nCircs == 1
119         rgbVals = rgbValsInterim;
120     else
121         rgbVals = [rgbVals; rgbValsInterim];
122     end
123     nPixGroups(nCircs, 1) = pixCount;
124     if nCircs == 1
125         pixSums(nCircs, 1) = pixCount;
126     else
127         pixSums(nCircs, 1) = pixSums(nCircs-1, 1) + pixCount;
128     end
129     % MixRGB(:,:,nCircs) = [rM(:,:,nCircs), gM(:,:,nCircs), bM(:,:,nCircs)];
130 end
131 %% Delta E - Blue
132 nControls = 5;
133 nWells = 25;
134 loopVal = 1;
135 blueControlVal = 1;
136
137 for iter = 1:nWells
138     if blueControlVal == 1
139         blueDE = rgbVals(1:pixSums(1), :);
140     elseif blueControlVal == 2
141         clearvars blueDE
142         blueDE = rgbVals(pixSums(1):pixSums(2), :);
143     elseif blueControlVal == 3
144         clearvars blueDE
145         blueDE = rgbVals(pixSums(2):pixSums(3), :);
146     elseif blueControlVal == 4
147         clearvars blueDE
148         blueDE = rgbVals(pixSums(3):pixSums(4), :);
149     elseif blueControlVal == 5
150         clearvars blueDE
151         blueDE = rgbVals(pixSums(4):pixSums(5), :);
152     end
153
154     % if loopVal == 1
155     mix = rgbVals(pixSums(9+iter):(pixSums(9+iter)+nPixGroups(10+iter)), :);
156     %     maxPixels = min(length(blueDE), length(mix));
157     maxPixels = 500;

```

```

158     dEblue(:,iter) = deltaE(mix(1:maxPixels,:), blueDE(1:maxPixels,:), 'isInputLabel', 0);
159 %     end
160
161
162     loopVal = loopVal + 1;
163     if loopVal > 5
164         loopVal = 1;
165         blueControlVal = blueControlVal + 1;
166     end
167 end
168 %% DeltaE - Red
169 nControls = 5;
170 nWells = 25;
171 loopVal = 1;
172 redControlVal = 1;
173
174 for iter = 1:nWells
175     if redControlVal == 1
176         redDE = rgbVals(pixSums(5):pixSums(6),:);
177     elseif redControlVal == 2
178         clearvars blueDE
179         redDE = rgbVals(pixSums(6):pixSums(7),:);
180     elseif redControlVal == 3
181         clearvars blueDE
182         redDE = rgbVals(pixSums(7):pixSums(8),:);
183     elseif redControlVal == 4
184         clearvars blueDE
185         redDE = rgbVals(pixSums(8):pixSums(9),:);
186     elseif redControlVal == 5
187         clearvars blueDE
188         redDE = rgbVals(pixSums(9):pixSums(10),:);
189     end
190
191 %     if loopVal == 1
192     mix = rgbVals(pixSums(9+iter):(pixSums(9+iter)+nPixGroups(10+iter)),:);
193 %     maxPixels = min(length(blueDE), length(mix));
194     maxPixels = 500;
195     dERed(:,iter) = deltaE(mix(1:maxPixels,:), redDE(1:maxPixels,:), 'isInputLabel', 0);
196 %     end
197
198     redControlVal = redControlVal + 1;
199     loopVal = loopVal + 1;
200     if redControlVal > 5
201         redControlVal = 1;
202 %         redControlVal = redControlVal + 1;
203     end
204 end
205 %% Plot the DeltaE blue and Red for each mixing well
206
207 meanDEblue = mean(dEblue, 1);
208 sdDEblue = std(dEblue, 1);
209 meanDERed = mean(dERed, 1);
210 sdDERed = std(dERed, 1);
211
212 mixes = (1:1:24)';
213
214 figure
215 set(gcf, 'Color', 'w')
216 hold on
217 plot(mixes, meanDEblue, 'b', 'LineWidth', 2)
218 plot(mixes, meanDERed, 'r', 'LineWidth', 2)
219 hold off
220 xlim([11 20])
221 grid on
222 set(gca, 'FontSize', 16)
223
224 figure
225 set(gcf, 'Color', 'w')
226 plot(mixes, meanDEblue+meanDERed, 'k', 'LineWidth', 2)
227 xlim([11 20])
228 grid on
229 set(gca, 'FontSize', 16)

```

B.3.2 Script Used for Image and Statistical Analysis of Pul- lulan Tablets Dissolution Rate

The first control image was used to automatically identify all the wells position in the image (Control 1, Fig. B.1A). First, a binary image was created with automatic thresholding [248] (Fig. B.1B), and circular region-of-interests (ROIs) were identified (Fig. B.1C). A wells' mask was created so that it was possible to analyse only the part of the image that was not 'covered' by the mask itself. These areas corresponded to the wells content (Fig. B.1D). All the images taken every 30 seconds were uploaded and masked, so that the number of pixels of interest in each well could be derived. All the wells were numbered as indicated in Fig. B.1E. The 'well controls' were numbered

as (1) pullulan tablet only, (2) pullulan tablet dissolved in 100 μL of 0.2 g/L of xylene cyanol solution, and (3) 100 μL of 0.02 g/L of xylene cyanol solution, and the triplicates of pullulan tablets dissolving were numbered from 4 to 6 ($n = 3$). Each well, 4 to 6, was compared to each ‘well control’, 1, 2 or 3, by computing the colour difference (ΔE) for each pixel in each pair of wells, e.g., Well 4 vs Control 1, Well 4 vs Control 2, Well 4 vs Control 3, etc. The mean of the ΔE for each pair of wells was computed ($\mu_{\Delta E}$), and this was done for all the loaded images, to understand how ΔE changed over time. For the first pullulan tablets studied, the information provided by comparing the wells with each ‘well control’ were observed to understand which comparison/ ΔE was providing the most meaningful information. It was then decided to compute the ΔE between each well containing the dissolving pullulan tablet and the already dissolved tablet in xylene cyanol solution. The mean of the ΔE for wells 4, 5, 6 compared to ‘well control 2’ was plotted for each image over time, and this resulting signal (mean- ΔE signal) was used to derive the time at which we considered the pullulan tablet completely dissolved in the solution (time-to-plateau).

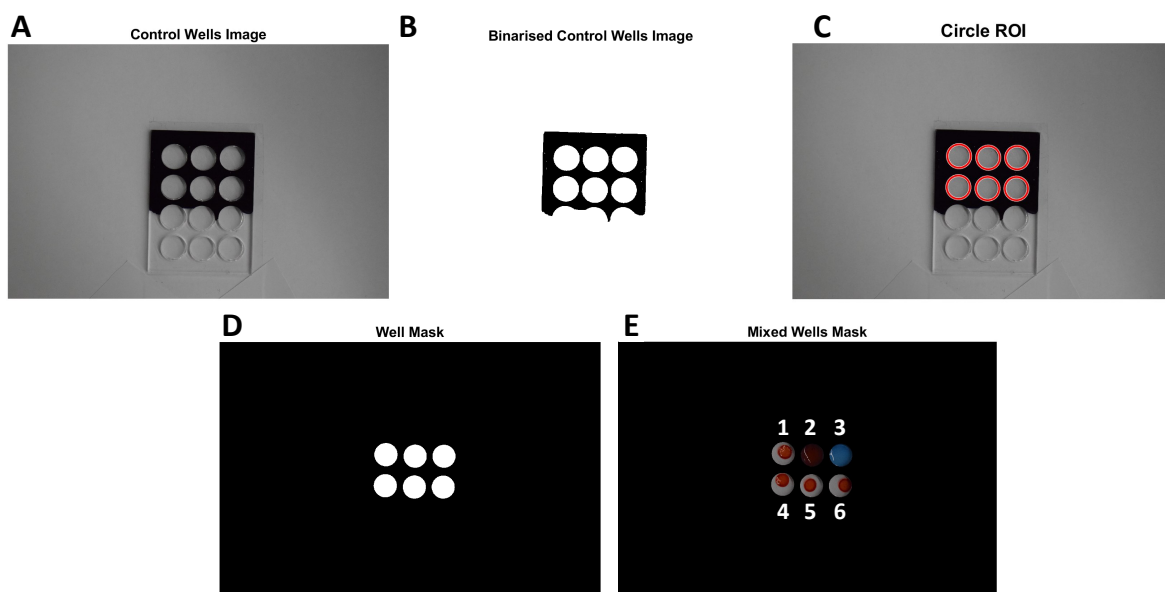


Figure B.1: **Wells identification process in PMMA mould for pullulan dissolution rate study.** **A.** Control 1. **B.** Binary image [248] of (A). **C.** Identification of circular region-of-interest (ROI) thanks to (B). **D.** Well’s mask derived from (C). **E.** Wells numbered for further processing and colour change analysis.

Listing B.5: Wellanalysis.m

```

1 %% Ignoring warnings
2 % Ignoring im2bw change to imbinarise warning > im2bw can be swapped of
3 % imbinarise in the future only slight editing of the code will be required
4 %#ok<*IM2BW>
5 % ----- %
6 %   TO-DO   %
7 % fileList needs to be sorted based on the image number (DONE)
8 % Variance of the individual wells (DONE)
9 % Mean DeltaE of all pixels together (PROBLEM WITH CONTROL WELLS IN THE MEAN)
10 %% Initialisings
11 disp('Clearing all variables')
12 clearvars
13 clc
14 disp('-----')
15 close all
16 %% Initial settings
17 % Opening figure for tab group
18 disp('Setting initial variables and opening figures')
19 h1 = figure; hold all;
20 set(h1, 'defaultUITabBackgroundColor', [1 1 1])
21 % set(gcf, 'BackgroundColor', 'w')
22 tg = uitabgroup('Parent', h1); % tab group
23 % Variables
24 InitVars.fontSize = 18; % Fontsize for plots
25 InitVars.binaryThreshold = 0.1; % 0.1 works | 0.2 finds 6 circles

```

```

26 InitVars.Polarity = 'bright'; % 'bright' | 'dark'
27 InitVars.circSmall = 50; % Smallest circles
28 InitVars.circBig = 400; % Largest circles
29 InitVars.circleMaxLinespace = 10000; % Maximum circle points for plotting
30 pixRad = 10; % Reducing circle radius by n pixels
31 disp('-----')
32 %% Time between images input
33 disp('Input the time between image acquisitions (s)')
34 TimePrompt = {'Enter the time between image acquisitions (s)'};
35 dlgtitle = 'Time between images';
36 dims = [1 40];
37 defaultInput = {'30'};
38 imageSepInput = inputdlg(TimePrompt, dlgtitle, dims, defaultInput);
39 InitVars.timeSep = str2double(imageSepInput{1,1});
40 clearvars TimePrompt dlgtitle dims defaultInput
41 clear imageSepInput
42 disp('-----')
43 %% Select folder containing all images
44 disp('Saving current path')
45 originalPath = dir;
46 disp('Select folder of images to load')
47 pause(1);
48 folderDir = uigetdir;
49 % Adding path
50 addpath(folderDir);
51 cd(folderDir);
52 disp('-----')
53 %% Well control image
54 % Select the control image of the wells
55 disp('Loading control image of the wells')
56 controlImages.controlWellsFilePath = uigetfile('*.JPG');
57 controlImages.controlWellsImage = imread(controlImages.controlWellsFilePath);
58 disp('-----')
59 %% Mixed controls loading
60 % Select the control image of the wells
61 disp('Loading control image of the mixes')
62 controlImages.controlImageFilePath = uigetfile('*.JPG');
63 controlImages.controlImage = imread(controlImages.controlImageFilePath);
64 disp('-----')
65 %% Calculating number of files to skip in the folder
66 ReadMeAnswer = questdlg('Does a "Readme" file exist in the directory?', ...
67     'Readme?', ...
68     'Yes', 'No', 'Yes');
69 % Handle 'ReadMe' response
70 switch ReadMeAnswer
71     case 'Yes'
72         InitVars.ReadMe = 1;
73         disp(['ReadMe = ' num2str(InitVars.ReadMe)]);
74     case 'No'
75         InitVars.ReadMe = 0;
76         disp(['ReadMe = ' num2str(InitVars.ReadMe)]);
77 end
78 ControlsLoadedAnswer = questdlg('How many control images were loaded?', ...
79     'Control images', ...
80     '0', '1', '2', '2');
81 % Handle 'ReadMe' response
82 switch ControlsLoadedAnswer
83     case '0'
84         InitVars.controlImageNumber = 0;
85         disp(['Control images = ' num2str(InitVars.controlImageNumber)]);
86     case '1'
87         InitVars.controlImageNumber = 1;
88         disp(['Control images = ' num2str(InitVars.controlImageNumber)]);
89     case '2'
90         InitVars.controlImageNumber = 2;
91         disp(['Control images = ' num2str(InitVars.controlImageNumber)]);
92 end
93 clearvars ControlsLoadedAnswer ReadMeAnswer
94 disp('-----')
95 %% Number of images to analyse and loading images into structure
96 disp('Calculating number of files to load')
97 fileList = dir(folderDir);
98 InitVars.auxFiles = 0;
99 for iter = 1:length(fileList)
100     if fileList(iter).isdir == 1
101         InitVars.auxFiles = InitVars.auxFiles + 1;
102     end
103 end
104 clearvars iter
105
106 InitVars.ImagesToLoad = length(fileList) - (InitVars.controlImageNumber + ...
107     InitVars.ReadMe + InitVars.auxFiles);
108 InitVars.otherFiles = InitVars.controlImageNumber + InitVars.ReadMe ...
109     + InitVars.auxFiles;
110
111 strId = '\d*\d';
112
113 for fileNumber = 1:1:InitVars.ImagesToLoad
114     fileVal = InitVars.otherFiles + fileNumber;
115     fileName = fileList(fileVal).name;
116     loadedImages.OriginalImages{fileNumber,1} = imread(fileName);
117     extractedFileNumber = regexp(fileName, strId, 'match');
118     loadedImages.OriginalImages{fileNumber,2} = str2double(extractedFileNumber{1,1});
119 end

```

```

120 % Sorting based on image number
121 loadedImages.OriginalImages = sortrows(loadedImages.OriginalImages, 2);
122 clearvars fileName fileNumber strId extractedFileNumber
123 disp('All images loaded')
124 disp('-----')
125 %% Plot control wells image
126 disp('Plotting well control image')
127 tab = uitab(tg, 'Title', 'Well Control Image'); % Open a new tab
128 axes('Parent', tab);
129 imshow(controlImages.controlWellsImage)
130 title('Control Wells Image', InitVars.fontSize + 2)
131 set(gca, 'FontSize', InitVars.fontSize)
132 disp('-----')
133 %% Binary image of wells control
134 disp('Calculating binary image of wells and plotting')
135 tab = uitab(tg, 'Title', 'Binary Circle Mask');
136 axes('Parent', tab);
137 imshow(im2bw(controlImages.controlWellsImage, InitVars.binaryThreshold))
138 title('Binarised Control Wells Image', InitVars.fontSize + 2)
139 set(gca, 'FontSize', InitVars.fontSize)
140 disp('-----')
141 %% Circle well mask
142 disp('Circle finding')
143 % Circle finding
144 % Median filter (NEW)
145 [wells.centers, wells.radii, wells.metric] = imfindcircles(medfilt2(im2bw(controlImages.controlWellsImage, InitVars
    .binaryThreshold), [9 9]),[InitVars.circSmall InitVars.circBig], 'ObjectPolarity', InitVars.Polarity);
146
147 % Sorting circles from top left to bottom right
148 wells.circleID = (1:length(wells.centers))';
149 wells.centersWithIDs = [wells.centers, wells.radii, wells.circleID];
150 wells.iCentersWithIDs = sortrows(wells.centersWithIDs, 2);
151 wells.totCircs = length(wells.centers);
152 mat1 = sortrows(wells.iCentersWithIDs(1:(wells.totCircs/2),:), 1);
153 mat2 = sortrows(wells.iCentersWithIDs((wells.totCircs/2)+1:end,:), 1);
154 wells.sortCentersWithIDs = [mat1; mat2];
155 clearvars mat1 mat2
156 wells.centers = wells.sortCentersWithIDs(:,1:2);
157 wells.radii = wells.sortCentersWithIDs(:,3) - pixRad;
158 wells.circleIDs = wells.sortCentersWithIDs(:,4);
159 % plot
160 tab = uitab(tg, 'Title', 'Highlighted Circles');
161 axes('Parent', tab);
162 hold on
163 imshow(controlImages.controlWellsImage)
164 viscircles(wells.centers, wells.radii, 'EdgeColor', 'r');
165 hold off
166 title('Circle ROI', InitVars.fontSize + 2)
167 set(gca, 'FontSize', InitVars.fontSize)
168 disp('-----')
169 %% Circle coordinates & Control Mask
170 disp('Calculating well mask')
171 [imParams.Rows, imParams.Cols, imParams.Channels] = size(controlImages.controlWellsImage);
172 wells.x_controlCircles = zeros([length(wells.centers) InitVars.circleMaxLinespace]);
173 wells.y_controlCircles = zeros([length(wells.centers) InitVars.circleMaxLinespace]);
174 wells.WellMask = zeros([imParams.Rows, imParams.Cols, length(wells.centers)]);
175 for nCircs = 1:length(wells.centers)
176     wells.angles = linspace(0, 2*pi, InitVars.circleMaxLinespace);
177     wells.x_controlCircles(nCircs,:) = cos(wells.angles) * wells.radii(nCircs, 1) + wells.centers(nCircs, 1);
178     wells.y_controlCircles(nCircs,:) = sin(wells.angles) * wells.radii(nCircs, 1) + wells.centers(nCircs, 2);
179     wells.WellMask(:, :, nCircs) = poly2mask(wells.x_controlCircles(nCircs,:), ...
180         wells.y_controlCircles(nCircs,:), imParams.Rows, imParams.Cols);
181 end
182 clearvars nCircs
183 disp('-----')
184 %% Final Well Mask
185 disp('Summing to final well mask')
186 wells.fullMask = sum(wells.WellMask, 3);
187 tab = uitab(tg, 'Title', 'Well Mask'); % Open a new tab
188 axes('Parent', tab);
189 imshow(wells.fullMask)
190 title('Well Mask', InitVars.fontSize + 2)
191 set(gca, 'FontSize', InitVars.fontSize)
192 disp('-----')
193 %% This section needs to be done for each individual well -> not the summed mask
194 % Plotting
195 disp('Masking control image wells')
196 % WellMaskNaNs = zeros(imRows, imCols, length(centers));
197 controlImages.controlImageMaskedFull = uint8(zeros(imParams.Rows, imParams.Cols, imParams.Channels));
198 controlImages.controlImageMasked = uint8(zeros(imParams.Rows, imParams.Cols, imParams.Channels, length(wells.
    centers)));
199 for nCircs = 1:length(wells.centers)
200     for chnls = 1:imParams.Channels
201         controlImages.controlImageMaskedFull(:, :, chnls) = uint8(controlImages.controlImage(:, :, chnls)) .* (uint8(
            wells.fullMask));
202         controlImages.controlImageMasked(:, :, chnls, nCircs) = uint8(controlImages.controlImage(:, :, chnls)) .* (uint8
            (wells.WellMask(:, :, nCircs)));
203     end
204 end
205 disp('Plotting control image')
206 tab = uitab(tg, 'Title', 'Control Image'); % Open a new tab
207 axes('Parent', tab);
208 imshow(controlImages.controlImageMaskedFull)
209 title('Mixed Wells Mask', InitVars.fontSize + 2)

```

```

210 set(gca, 'FontSize', InitVars.fontSize)
211 disp('-----')
212 %% Masking all loaded images
213 disp('Masking all images')
214 MaskedFullImages = uint8(zeros(imParams.Rows, imParams.Cols, imParams.Channels));
215 MaskedImagesPerWell = uint8(zeros(imParams.Rows, imParams.Cols, imParams.Channels, length(wells.centers)));
216 for nImage = 1:1:InitVars.ImagesToLoad
217     image = loadedImages.OriginalImages{nImage,1};
218     for nCircs = 1:1:length(wells.centers)
219         for chnls = 1:imParams.Channels
220             MaskedFullImages(:,:,chnls) = uint8(image(:,:,chnls)) .* (uint8(wells.fullMask));
221             MaskedImagesPerWell(:,:,chnls,nCircs) = uint8(image(:,:,chnls)) .* (uint8(wells.WellMask(:,:,nCircs)));
222         end
223     end
224     loadedImages.MaskedFullImages(nImage,1) = {MaskedFullImages};
225     loadedImages.MaskedImagesPerWell(nImage,1) = {MaskedImagesPerWell};
226 end
227 clearvars MaskedImagesPerWell MaskedFullImages nCircs nImage
228 disp('-----')
229 %% Calculating number of pixels in each well
230 disp('Calculating number of pixels in each well')
231 wells.WellPixels = zeros(6,1);
232 for nCircs = 1:1:length(wells.centers)
233     wells.WellPixels(nCircs,1) = sum(wells.WellMask(:,:,nCircs),'all');
234 end
235 wells.minWellPixels = min(wells.WellPixels);
236 clearvars nCircs
237 disp('-----')
238 %% Reshaping images as column matrices
239 disp('Reshaping images into column matrices')
240 interimMat2 = uint8(zeros((imParams.Rows*imParams.Cols), imParams.Channels, length(wells.centers)));
241 for nCircs = 1:1:6
242     rgb.controlColumns(:,:,nCircs) = reshape(controlImages.controlImageMasked(:,:,nCircs), [], 1, 3);
243 end
244 for nImage = 1:1:InitVars.ImagesToLoad
245     interimMat = cell2mat(loadedImages.MaskedImagesPerWell(nImage,1));
246     for nCircs = 1:1:6
247         interimMat2(:,:,nCircs) = reshape(interimMat(:,:,nCircs), [], 1, 3);
248     end
249     rgb.imagesColumns(nImage,1) = {interimMat2};
250 end
251 clearvars interimMat interimMat2 nCircs nImage
252 disp('-----')
253 %% Number of non-zero pixels
254 disp('Calculating the number of non-zero pixels')
255 for nCircs = 1:1:6
256     interimMatrix = rgb.controlColumns(:,:,nCircs);
257     interimMatrix(all(~interimMatrix,2), :) = [];
258     rgb.pixelNumbersNonZero(nCircs,1) = length(interimMatrix);
259 end
260 for nImage = 1:1:InitVars.ImagesToLoad
261     interimMatrix1 = cell2mat(rgb.imagesColumns(nImage,1));
262     for nCircs = 1:1:6
263         interimMatrix = interimMatrix1(:,:,nCircs);
264         interimMatrix(all(~interimMatrix,2), :) = [];
265         rgb.pixelNumbersNonZero(nCircs,1 + nImage) = length(interimMatrix);
266     end
267 end
268 clearvars nCircs nImage interimMatrix interimMatrix1
269 disp('-----')
270 %% Short matrices of RGBs
271 disp('Obtaining RGB values within the wells')
272 rgb.minPixelsNonZero = min(rgb.pixelNumbersNonZero, [], 'all');
273 for nImage = 1:1:(InitVars.ImagesToLoad + 1)
274     clearvars interimMatrix
275     if nImage == 1
276         interimMatrix = rgb.controlColumns;
277     else
278         interimMatrix = cell2mat(rgb.imagesColumns(nImage - 1,1));
279     end
280     for nCircs = 1:1:6
281         interimMatrixCircs = interimMatrix(:,:,nCircs);
282         interimMatrixCircs(~any(interimMatrixCircs(:,2),:)) = [];
283         rgb.allRGB(:, :, nCircs, nImage) = interimMatrixCircs(1:rgb.minPixelsNonZero,:);
284     end
285 end
286 clearvars interimMatrixCircs interimMatrix nCircs nImage
287 disp('-----')
288 %% DeltaE Values
289 disp('Calculating DeltaE values compared to each control well')
290 for nImage = 1:1:(InitVars.ImagesToLoad)
291     for nCircs = 1:1:6
292         dE.versusControl1(:, nCircs, nImage) = deltaE(rgb.allRGB(:, :, 1, 1), rgb.allRGB(:, :, nCircs, (1+nImage)))
293         ;
294         dE.versusControl2(:, nCircs, nImage) = deltaE(rgb.allRGB(:, :, 2, 1), rgb.allRGB(:, :, nCircs, (1+nImage)))
295         ;
296         dE.versusControl3(:, nCircs, nImage) = deltaE(rgb.allRGB(:, :, 3, 1), rgb.allRGB(:, :, nCircs, (1+nImage)))
297         ;
298         dE.meanVersusControl1(nCircs, nImage) = mean(dE.versusControl1(:, nCircs, nImage));
299         dE.meanVersusControl2(nCircs, nImage) = mean(dE.versusControl2(:, nCircs, nImage));
300         dE.meanVersusControl3(nCircs, nImage) = mean(dE.versusControl3(:, nCircs, nImage));
301         dE.sdVersusControl1(nCircs, nImage) = std(dE.versusControl1(:, nCircs, nImage), 0);

```

```

301         dE.sdVersusControl2(nCircs, nImage) = std(dE.versusControl2(:, nCircs, nImage), 0);
302         dE.sdVersusControl3(nCircs, nImage) = std(dE.versusControl3(:, nCircs, nImage), 0);
303     end
304 end
305 disp('-----')
306 %% All DeltaE Values Combined > to obtain mean of all wells
307 disp('Obtaining the mean DeltaE and standard deviation')
308 for nImage = 1:1:(InitVars.ImagesToLoad)
309     interimMat1 = dE.versusControl1(:,4:end,nImage);
310     interimMat2 = dE.versusControl2(:,4:end,nImage);
311     interimMat3 = dE.versusControl3(:,4:end,nImage);
312
313     dE.allWellsMeanVersusC1(1, nImage) = mean(interimMat1, 'all');
314     dE.allWellsMeanVersusC2(1, nImage) = mean(interimMat2, 'all');
315     dE.allWellsMeanVersusC3(1, nImage) = mean(interimMat3, 'all');
316
317     dE.allWellsSdVersusC1(1, nImage) = std(interimMat1, 0, 'all');
318     dE.allWellsSdVersusC2(1, nImage) = std(interimMat2, 0, 'all');
319     dE.allWellsSdVersusC3(1, nImage) = std(interimMat3, 0, 'all');
320 end
321 disp('-----')
322 %% Error bounds plot
323 images = (1:1:length(loadedImages.OriginalImages))';
324 xvals = images.*InitVars.timeSep;
325 disp('Plotting DeltaE plots')
326 figure(1)
327 tab = uitab(tg, 'Title', 'DeltaE V Control 1'); % Open a new tab
328 axes('Parent', tab);
329 for nCircs = 4:1:6 % From Control wells + 1 to max number of wells
330     for nControl = 1:1:3
331         % Calculating standard deviation bounds
332         subplot(3,3,((nCircs - 4)*3) + nControl)
333         if nControl == 1
334             lo = (dE.meanVersusControl1(nCircs,:) - dE.sdVersusControl1(nCircs,:));
335             hi = (dE.meanVersusControl1(nCircs,:) + dE.sdVersusControl1(nCircs,:));
336             hold on
337             hp1 = patch([xvals; xvals(end:-1:1); xvals(1)], [lo; hi(end:-1:1); lo(1)], 'r');
338             p1 = plot(xvals, dE.meanVersusControl1(nCircs,:), 'r', 'LineWidth', 2);
339             set(hp1, 'edgecolor', 'none', 'FaceAlpha', 0.2);
340             hold off
341             xlim([min(xvals) max(xvals)])
342             ylim([0 100])
343             deL = [p1(1); hp1(1)];
344             legend(deL, '\mu', '\sigma')
345             title(['Well ' num2str(nCircs) ' - Control ' num2str(nControl)], 'FontSize', InitVars.fontSize + 2)
346         elseif nControl == 2
347             lo = (dE.meanVersusControl2(nCircs,:) - dE.sdVersusControl2(nCircs,:));
348             hi = (dE.meanVersusControl2(nCircs,:) + dE.sdVersusControl2(nCircs,:));
349             hold on
350             hp2 = patch([xvals; xvals(end:-1:1); xvals(1)], [lo; hi(end:-1:1); lo(1)], 'k');
351             p2 = plot(xvals, dE.meanVersusControl2(nCircs,:), 'k', 'LineWidth', 2);
352             set(hp2, 'edgecolor', 'none', 'FaceAlpha', 0.2);
353             hold off
354             xlim([min(xvals) max(xvals)])
355             ylim([0 100])
356             deL = [p2(1); hp2(1)];
357             legend(deL, '\mu', '\sigma')
358             title(['Well ' num2str(nCircs) ' - Control ' num2str(nControl)], 'FontSize', InitVars.fontSize + 2)
359         elseif nControl == 3
360             lo = (dE.meanVersusControl3(nCircs,:) - dE.sdVersusControl3(nCircs,:));
361             hi = (dE.meanVersusControl3(nCircs,:) + dE.sdVersusControl3(nCircs,:));
362             hold on
363             hp3 = patch([xvals; xvals(end:-1:1); xvals(1)], [lo; hi(end:-1:1); lo(1)], 'b');
364             p3 = plot(xvals, dE.meanVersusControl3(nCircs,:), 'b', 'LineWidth', 2);
365             set(hp3, 'edgecolor', 'none', 'FaceAlpha', 0.2);
366             hold off
367             xlim([min(xvals) max(xvals)])
368             ylim([0 100])
369             deL = [p3(1); hp3(1)];
370             legend(deL, '\mu', '\sigma')
371             title(['Well ' num2str(nCircs) ' - Control ' num2str(nControl)], 'FontSize', InitVars.fontSize + 2)
372         end
373         %
374         ylabel('\DeltaE')
375         xlabel('Time (s)')
376         set(gca, 'FontSize', InitVars.fontSize)
377     end
378 end
379 disp('-----')
380 %% Plots for Mean of all wells !!! Has to be based on control numbers
381
382 dE.allWellsMeanVersusC3(1, nImage) = mean(dE.versusControl3(:,nImage), 'all');
383
384 dE.allWellsSdVersusC1(1, nImage) = std(dE.versusControl1(:,nImage), 0, 'all');
385
386 images = (1:1:length(loadedImages.OriginalImages))';
387 xvals = images.*InitVars.timeSep;
388
389 disp('Plotting mean DeltaE across the wells')
390 figure(1)
391 tab = uitab(tg, 'Title', 'Mean DeltaE'); % Open a new tab
392 axes('Parent', tab);
393 subplot(3,1,1)
394 lo = (dE.allWellsMeanVersusC1 - dE.allWellsSdVersusC1)';

```

```

395 hi = (dE.allWellsMeanVersusC1 + dE.allWellsSdVersusC1)';
396 hp = patch([xvals; xvals(end:-1:1); xvals(1)], [lo; hi(end:-1:1); lo(1)], 'k');
397 hold on
398 p1 = plot(xvals, dE.allWellsMeanVersusC1, 'k', 'LineWidth', 2);
399 hold off
400 set(hp, 'edgecolor', 'none', 'FaceAlpha', 0.2);
401 xlim([min(xvals) max(xvals)])
402 ylim([0 100])
403 ylabel('\DeltaE')
404 xlabel('Time (s)')
405 deL = [p1(1); hp(1)];
406 legend(deL, '\mu', '\sigma')
407 set(gca, 'FontSize', InitVars.fontSize)
408 title('Control 1', 'FontSize', InitVars.fontSize + 2)
409
410 subplot(3,1,2)
411 lo = (dE.allWellsMeanVersusC2 - dE.allWellsSdVersusC2)';
412 hi = (dE.allWellsMeanVersusC2 + dE.allWellsSdVersusC2)';
413 hp = patch([xvals; xvals(end:-1:1); xvals(1)], [lo; hi(end:-1:1); lo(1)], 'k');
414 hold on
415 p1 = plot(xvals, dE.allWellsMeanVersusC2, 'k', 'LineWidth', 2);
416 hold off
417 set(hp, 'edgecolor', 'none', 'FaceAlpha', 0.2);
418 % set(p1, 'Marker', 'o', 'LineStyle', 'none')
419 xlim([min(xvals) max(xvals)])
420 ylim([0 100])
421 ylabel('\DeltaE')
422 xlabel('Time (s)')
423 deL = [p1(1); hp(1)];
424 legend(deL, '\mu', '\sigma')
425 set(gca, 'FontSize', InitVars.fontSize)
426 title('Control 2', 'FontSize', InitVars.fontSize + 2)
427
428 subplot(3,1,3)
429 lo = (dE.allWellsMeanVersusC3 - dE.allWellsSdVersusC3)';
430 hi = (dE.allWellsMeanVersusC3 + dE.allWellsSdVersusC3)';
431 hp = patch([xvals; xvals(end:-1:1); xvals(1)], [lo; hi(end:-1:1); lo(1)], 'k');
432 hold on
433 p1 = plot(xvals, dE.allWellsMeanVersusC3, 'k', 'LineWidth', 2);
434 hold off
435 set(hp, 'edgecolor', 'none', 'FaceAlpha', 0.2);
436 xlim([min(xvals) max(xvals)])
437 ylim([0 100])
438 ylabel('\DeltaE')
439 xlabel('Time (s)')
440 deL = [p1(1); hp(1)];
441 legend(deL, '\mu', '\sigma')
442 set(gca, 'FontSize', InitVars.fontSize)
443 title('Control 3', 'FontSize', InitVars.fontSize + 2)
444 disp('-----')
445 %% Plot Mean dE of each well versus Control 2
446 disp('Plots of MeandE for each well compared to Well control 2')
447 TimesfromImages=loadedImages.OriginalImages(:,2);
448 xvals=zeros(nImage,1);
449 for i=1:nImage
450     xvals(i,1) = TimesfromImages{i};
451 end
452 clearvars i
453 time = cell2mat(TimesfromImages);
454 dEvsControl2Matrix = zeros([nCircs-nControl, nImage]);
455 for iter = 1:3
456     dEvsControl2Matrix (iter, :) = dE.meanVersusControl2(iter+nControl,:);
457 end
458 DeltaEvsC2 = figure();
459 hold on
460 set(gcf, 'color', 'w')
461 plot(time,dEvsControl2Matrix, 'LineWidth', 2)
462 legend('Well 4', 'Well 5', 'Well 6')
463 hold off
464 minvalue=0;
465 xlim([minvalue max(xvals)])
466 ylabel('\DeltaE')
467 xlabel('Time [s]')
468 set(gca, 'FontSize', 24)
469 set(gca, 'TickDir', 'out');
470 set(get(gca(),'XAxis'),'MinorTick', 'on', 'MinorTickValues',[0:50:max(xvals)])
471 %set(get(gca(),'YAxis'),'MinorTick', 'on')
472 disp('-----')
473
474 %% Plot Mean dE of each well versus Control 1
475 time = cell2mat(TimesfromImages);
476 disp('Plots of MeandE for each well compared to Well control 1')
477 dEvsControl1Matrix = zeros([nCircs-nControl, nImage]);
478 for iter = 1:3
479     dEvsControl1Matrix (iter, :) = dE.meanVersusControl1(iter+nControl,:);
480 end
481 DeltaEvsC1 = figure();
482 hold on
483 set(gcf, 'color', 'w')
484 plot(time,dEvsControl1Matrix, 'LineWidth', 2)
485 legend('Well 4', 'Well 5', 'Well 6')
486 hold off
487 minvalue=0;
488 xlim([minvalue max(xvals)])

```

```

489 ylabel('\DeltaE')
490 xlabel('Time [s]')
491 set(gca, 'FontSize', 24)
492 set(gca, 'TickDir', 'out');
493 set(get(gca(), 'XAxis'), 'MinorTick', 'on', 'MinorTickValues', [0:50:max(xvals)])
494 %set(get(gca(), 'YAxis'), 'MinorTick', 'on')
495 disp('-----')
496 %% Plot Mean dE of each well versus Control 3
497 time = cell2mat(TimesfromImages);
498 disp('Plots of MeandE for each well compared to Well control 3')
499 dEvsControl3Matrix = zeros([nCircs-nControl, nImage]);
500 for iter = 1:3
501     dEvsControl3Matrix (iter, :) = dE.meanVersusControl3(iter+nControl,:);
502 end
503 DeltaEvsC3 = figure();
504 hold on
505 set(gcf, 'color', 'w')
506 plot(time, dEvsControl3Matrix, 'LineWidth', 2)
507 legend('Well 4', 'Well 5', 'Well 6')
508 minvalue=0;
509 xlim([minvalue max(xvals)])
510 ylabel('\DeltaE')
511 xlabel('Time [s]')
512 set(gca, 'FontSize', 24)
513 set(gca, 'TickDir', 'out');
514 set(get(gca(), 'XAxis'), 'MinorTick', 'on', 'MinorTickValues', [0:50:max(xvals)])
515 %set(get(gca(), 'YAxis'), 'MinorTick', 'on')
516 hold off
517 disp('-----')
518
519 %% Signal variation - standard deviation
520 PlateauIndex = zeros(nCircs-nControl,1);
521 PlateauTime = zeros(nCircs-nControl,1);
522 PlateauValue = zeros(nCircs-nControl,1);
523 for iter = 1 : (nCircs-nControl)
524     y = dEvsControl2Matrix(iter,:);
525     filteredSignal = stdfilt(y, ones(3, 3));
526     % Find out where the standard deviation is less than 0.15
527     PlateauIndex(iter) = find(filteredSignal(2:end) < 0.15, 1, 'first');
528     % Find out the time at which the standard deviation is less than 0.15
529     PlateauTime(iter) = time(PlateauIndex(iter));
530     % Find out the DeltaE value at which the plateau starts
531     PlateauValue(iter) = dEvsControl2Matrix(iter, PlateauIndex(iter));
532 end
533
534 %% Plot the point at which the Plateau starts
535 DeltaEvsC2Plateau = figure();
536 hold on
537 set(gcf, 'color', 'w')
538 plot(time, dEvsControl2Matrix, 'LineWidth', 2)
539 mycolors = [0 0.4470 0.7410; 0.9290 0.6940 0.1250; 0.8500 0.3250 0.0980];
540 colororder(mycolors)
541 thresh1 = yline(PlateauValue(1), '--', 'LineWidth', 1.5);
542 thresh1.Color = '#0072BD';
543 thresh2 = yline(PlateauValue(2), '--', 'LineWidth', 1.5);
544 thresh2.Color = '#EDB120';
545 thresh3 = yline(PlateauValue(3), '--', 'LineWidth', 1.5);
546 thresh3.Color = '#D95319';
547 sz = 60;
548 PVP = scatter(PlateauTime, PlateauValue, sz, mycolors, "filled", 'MarkerEdgeColor', 'k');
549 legend('Well 4', 'Well 5', 'Well 6')
550 hold off
551 % minvalue=0;
552 % ylim([minvalue inf])
553 ylabel('\DeltaE')
554 xlabel('Time [s]')
555 set(gca, 'FontSize', InitVars.fontSize)
556 set(gca, 'TickDir', 'out');
557 set(get(gca(), 'XAxis'), 'MinorTick', 'on', 'MinorTickValues', [0:50:max(xvals)])
558 disp('-----')
559
560 %% RGB values over Time of Well Control 2
561 test1 = rgb.allRGB(:, :, 2, :); %Well control 2
562 test2 = squeeze(test1); %RGB values of Well control 2 over time (each Image)
563 for imIter = 1:1:size(test2,3)
564     test3(:, imIter) = uint8(mean(test2(:, :, imIter), 1));
565     test3_sd(:, imIter) = uint8(std(double(test2(:, :, imIter)))); %LOOP
566 end
567
568 % Plot of RGB values
569 figure()
570 hold on
571 plot(time, test3(1,2:end)', 'r', 'LineWidth', 1.5)
572 plot(time, test3(2,2:end)', 'g', 'LineWidth', 1.5)
573 plot(time, test3(3,2:end)', 'b', 'LineWidth', 1.5)
574 errorbar(time, test3(1,2:end)', test3_sd(1,2:end)', 'r')
575 errorbar(time, test3(2,2:end)', test3_sd(2,2:end)', 'g')
576 errorbar(time, test3(3,2:end)', test3_sd(3,2:end)', 'b')
577 %legend('Red', 'Green', 'Blue')
578 minvalue=0;
579 xlim([minvalue max(xvals)])
580 ylabel('RGB value')
581 xlabel('Time [s]')
582 set(gca, 'FontSize', 24)

```

```
583 set(gca, 'TickDir', 'out');
584 set(get(gca(),'XAxis'),'MinorTick', 'on', 'MinorTickValues',[0:50:max(xvals)])
585 %set(get(gca(),'YAxis'),'MinorTick', 'on')
586 hold off
```